55F

FRACTURE ANALYSIS AND CORROSION FATIGUE IN PIPELINES

by

F. Erdogan and R.P. Wei
Department of Mechanical Engineering and Mechanics
Lehigh University, Bethlehem, PA 18015

FINAL REPORT

October 1982 - August 1985

Prepared for
U.S. Department of Transportation
Research and Special Programs Administration
Office of University Research
and
U.S. Department of Interior
Minerals Management Service
Technology Assessment and Research Branch
Under the Contract DTRS 56 82-C-00014

METRIC CONVERSION FACTORS

Approximate Conversions to Metric Measures

Symbol	When You Know	Multiply by	To Find	Symbol
	LENGTH			
in	inches	*2.5	centimeters	cm
ft	feet	30	centimeters	cm
yd	yards	0.9	meters	m
mi	miles	1.6	kilometers	km
	AREA			
in^2	square inches	6.5	square centimeters	cm^2
ft^2	square feet	0.09	square meters	m^2
yd^2	square yards	0.8	square meters	m^2
mi^2	square miles	2.6	square kilometers	km^2
	acres	0.4	hectares	ha
	MASS (weight)			
oz	ounces	28	grams	g
lb	pounds	0.45	kilograms	kg
	short tons (2000 lb)	0.9	tonnes	t
	VOLUME			
tsp	teaspoons	5	milliliters	ml
Tbsp	tablespoons	15	milliliters	ml
fl oz	fluid ounces	30	milliliters	ml
c	cups	0.24	liters	l
pt	pints	0.47	liters	l
qt	quarts	0.95	liters	l
gal	gallons	3.8	liters	l
ft^3	cubic feet	0.03	cubic meters	m^3
yd^3	cubic yards	0.76	cubic meters	m^3
	TEMPERATURE (exact)			
°F	Fahrenheit temperature	5/9 (after subtracting 32)	Celsius temperature	°C

*1 in = 2.54 (exactly). For other exact conversions and more detailed tables, see NBS Misc. Publ. 286, Units of Weights and Measures, Price $2.25, SD Catalog No. C13.10:286.

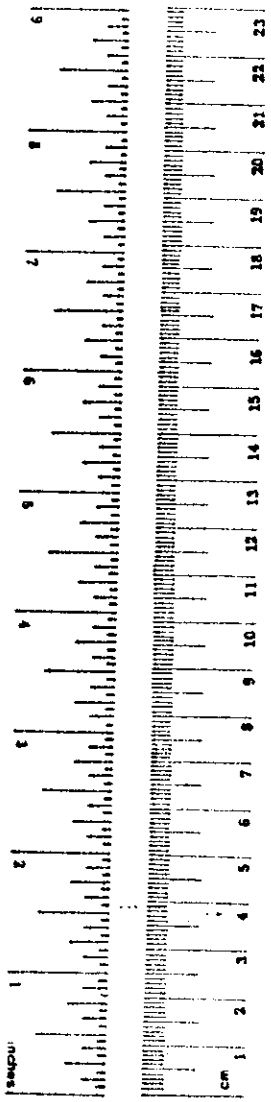

Approximate Conversions from Metric Measures

Symbol	When You Know	Multiply by	To Find	Symbol
	LENGTH			
mm	millimeters	0.04	inches	in
cm	centimeters	0.4	inches	in
m	meters	3.3	feet	ft
m	meters	1.1	yards	yd
km	kilometers	0.6	miles	mi
	AREA			
cm^2	square centimeters	0.16	square inches	in^2
m^2	square meters	1.2	square yards	yd^2
km^2	square kilometers	0.4	square miles	mi^2
ha	hectares (10,000 m^2)	2.6	acres	
	MASS (weight)			
g	grams	0.035	ounces	oz
kg	kilograms	2.2	pounds	lb
t	tonnes (1000 kg)	1.1	short tons	
	VOLUME			
ml	milliliters	0.03	fluid ounces	fl oz
l	liters	2.1	pints	pt
l	liters	1.06	quarts	qt
l	liters	0.26	gallons	gal
m^3	cubic meters	35	cubic feet	ft^3
m^3	cubic meters	1.3	cubic yards	yd^3
	TEMPERATURE (exact)			
°C	Celsius temperature	9/5 (then add 32)	Fahrenheit temperature	°F

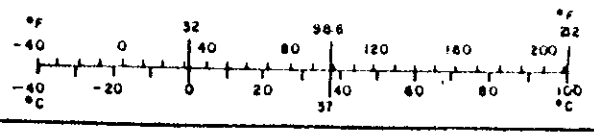

FRACTURE ANALYSIS AND

CORROSION FATIGUE IN PIPELINES

PREFACE

This report presents the theoretical and experimental results of a two year study on the analysis of cracks and inclusions simulating various types of weld and other defects in pipelines and on some fundamental aspects of corrosion fatigue process in pipeline steels. The research program was supported by the U.S. Department of Interior Minerals Management Service and by the U.S. Department of Transportation, Office of University Research.

The primary objectives of the program have been (a) classification and assessment of the relative importance of various types of weld defects, (b) development of analytical models to simulate part-through cracks and inclusions in plate and shell structures, (c) an in-depth study of the problem of interaction between two flaws or between flaws and free surfaces, (d) the effect of crack orientation on the fracture strength of pipes with possible applications to 45 degree seam-welded pipes and to pipes under nonsymmetric loading such as torsion, (e) the study aimed at a quantitative understanding of the early stage of chemical reactions in relation to the corrosion fatigue crack initiation and propagation, (f) elucidating the mechanisms for corrosion fatigue crack initiation and propagation, including the influence of chemical, mechanical and metallurgical variables in pipeline steels, and (g) the formulation and evaluation of models for predicting cracking response and service performance by using a combined fracture mechanics, surface chemistry and materials science approach.

In Part I of the report first a general review of the common types of flaws that may be found in pipelines and other welded structures is given and some relevant results for various flaw-inclusion-free surface interaction problems are presented. Then the basic models simulating part-through cracks and flat inclusions are developed and some sample results are given. The results of the experimental studies on the corrosion fatigue of the pipeline steels are presented in Part II. The Appendices include extensive results

obtained from individual studies on the variety of the crack and inclusion problems which may have relevance to the fracture problems in pipelines.

The research program led to following publications:

- "A Cylindrical Shell with an Arbitrarily Oriented Crack" (O.S. Yahsi and F. Erdogan) Int. J. Solids Structures, Vol. 19, pp. 955-972, 1983.
- "Surface Cracks in a Plate of Finite Width under Extension and Bending" (F. Erdogan and H. Boduroglu), J. Theoretical and Applied Fracture Mechanics, Vol. 2, pp. 197-216, 1984.
- "The Crack-Inclusion Interaction Problem" (X-H. Liu and F. Erdogan) J. Engng. Fracture Mechanics, 1986 (to appear).
- "The Line Spring Model" (F. Erdogan) Computational Methods in Fracture Mechanics, North Holland, 1986 (to appear)

and the thesis

"Interaction of Part-Through Cracks in a Flat Plate" (B. Aksel) Lehigh University, 1985.

The experimental part of the research program was carried out by Professor R.P. Wei who was assisted by Mr. Chiou Song. Mr. B. Aksel, Dr. X-H. Liu, Dr. H. Boduroglu and Dr. O.S. Yahsi who made major contributions to the theoretical part of the program. Dr. Liu was a visiting scholar from the People's Republic of China and Drs. Boduroglu and Yahsi were partially supported by grants from NSF and NASA.

The Project Monitor was Mr. Doughlas B. Chisholm from the Department of Transportation Research and Special Programs Administration, Office of Pipeline Safety Regulation. Dr. Charles E. Smith, Research Program Manager, Technology Assessment and Research Branch, Minerals Management Service was the Department of Interior technical representative.

F. Erdogan
Professor of Mechanics
ME-Mech. Dept.
Lehigh University
Bethlehem, PA 18015

TABLE OF CONTENTS

(Table of Contents - cont.)

(Table of Contents - cont.)

FRACTURE ANALYSIS AND CORROSION FATIGUE IN PIPELINES

PART I

ANALYSIS OF CRACK AND INCLUSION PROBLEMS

This report consists of two parts. Part I and the appendices deal with the theoretical studies of crack and inclusion problems simulating various kinds of weld defects and other flaws in pipes. Particular emphasis in the study is placed on the question of interaction between flaws and free surfaces. After an introductory review of the background material, first a broad classification of possible defects is made. One of the primary objectives of this study is to prepare the necessary engineering science basis and to develop the necessary tools that may be used in fitness for purpose type investigations in pipelines. Therefore in classifying the defects as well as in the subsequent investigations the emphases have been on the fracture mechanics aspects of the problem. In Section 3 of Part I the problem of interaction between cracks and elastic solid inclusions or pores is considered and relevant results are presented. Section 4 deals with exact solutions of the corresponding plane strain approximations of multiple crack problems. This includes multiple surface or internal cracks perpendicular or parallel to the plate surface.

The general problem of planar cracks of finite dimensions is discussed in Section 5. In this section the treatment of the related three-dimensional crack problem is based on the "line spring model". The underlying principle of the model and the general method of its solution are described and some comparisons of the result with the available finite element solutions are given to establish its validity. Also included are some examples from plates and shells to show the range of application of the technique. Section 6 deals with the general interaction problem for cracks and flat inclusions of finite thickness.

The detailed results of the individual problems studied are given in the appendices. Appendices A and B deal with the application of the line

spring model to plates containing multiple surface, corner or internal cracks. The problem of interaction between flat elastic inclusions and cracks is described in Appendix C. The limiting case in which the inclusion and the crack intersect is studied in Appendix D. Appendix E gives the solution and some extensive results for an arbitrarily oriented crack in a cylinder.

The results of the experimental investigation of the corrosion fatigue process in line pipe steels are presented in Part II.

1. INTRODUCTION

The standards of acceptability of welds in pipelines are generally based on certain empirical criteria in which primary importance is placed on flaw length. Specifically for girth welds such standards are described in API STANDARD 1104 prepared by the "American Petroleum Institute - American Gas Association Joint Committee on Oil and Gas Pipeline Field Welding Practices". However, the API Standard also recognizes fitness for purpose criteria based on fracture mechanics methodology as an alternative technique for flaw evaluation. The advantage of the fracture mechanics approach is that since it takes into account all factors which may be relevant to the failure of the pipe such as the type and the relative size, shape, orientation and location of the flaw, the effect of multiple flaws, the nature of the applied stresses, and the environmental conditions, it could be somewhat more precise than the empirical rules which are largely based on the flaw length.

In fracture mechanics approach to flaw evaluation it is implicitly assumed that the material contains some macroscopic flaws which may form the nucleus of fracture initiation. Generally, these flaws may be mapped by using an appropriate nondestructive flaw detection technique. Aside from the weld defects the pipe may also have flaws which may be external

in origin. Generally the initial phase of the failure in a pipe is the rupture of the net ligament adjacent to the critical flaw in the pipe wall. In most cases the resulting through crack is arrested and the pipe is repaired before further damage. However, in some cases the resulting through crack, after some stable growth, may become unstable leading to circumferential pipe break or dynamic propagation of an axial crack. The initial rupture of the net ligament in the pipe wall is usually preceded by some subcritical crack growth due to fatigue, corrosion fatigue, or stress corrosion cracking and the actual net ligament rupture is generally a ductile fracture process.

Therefore, it is seen that in order to apply fracture mechanics analysis to welded pipes, first one needs to characterize the material itself (the base metal, the weld material and the material in the heat affected zone) with regard to fatigue and corrosion fatigue crack propagation, stress corrosion cracking, fracture toughness and ductile fracture. Next, for a given flaw geometry and loading conditions one has to solve the related mechanics problem to calculate the appropriate fracture mechanics parameter such as the stress intensity factor, the crack tip opening displacement, or the J-integral. The third step in the process would be the selection or development of a proper failure theory and the application of the related quantitative failure criterion. The type of analysis and the experimental work to be performed and the particular criterion to be used are clearly dependent on the expected or the most likely mode of failure.

Even though the primary applied load in the pipelines is the internal pressure which is largely time-independent, there may be some small variations in pressure and some vibrations particularly near the pumping stations which may add a fluctuating component to the static stresses just high enough to cause concern. There are also secondary stresses which are mainly time-varying in nature and therefore would enhance the subcritical crack propagation. Some of the sources of these secondary stresses are misalignment and fit-up, daily, seasonal and other thermal fluctuations, ground settlement and possible earthquakes, axial constraint,

and gross bending in offshore piping due to buoyancy and other hydroelastic effects. It should be added that the "stress transients" may also play a major role in the subcritical crack propagation and particularly in the final phase of the fracture process, if one takes place. These stresses are generally caused by the pressure waves resulting from changes in flow rate due to partially or fully closing of the valves. In the case of pipes carrying liquids such as petroleum pipelines this is known as the "water hammer" effect due to which the peak pressure may be as high as multiples of the then operating pressure in the pipe. In the natural gas pipelines, this increase in the peak pressure may be somewhat more moderate. Nevertheless, in either case, such sudden surges of pressure are probably responsible in most cases for the final stage of the net ligament failure in the pipe wall resulting in leaks or in a catastrophic failure.

A detailed description and classification of weld discontinuities (including "flaws" which are considered to be undesirable) and a critical review of the literature as well as very extensive references on the subject up to 1976 may be found in [1]. The problem of interaction between two (planar) cracks and some empirical rules to define a single equivalent crack are discussed in [2]. The procedures dealing with the subcritical crack propagation by using the tools of linear elastic fracture mechanics (LEFM) is highly standardized and may be found, for example, in [3] or [4]. Similarly, the process of brittle or quasi-brittle fracture is relatively well-understood and is easily dealt with techniques based on LEFM and the concept of fracture toughness. The process which is not well-understood and not standardized, however, is the ductile fracture. The Appendix in the API Standard 1104 concerning the fracture mechanics applications is based on the critical crack tip opening displacement concept, whereas the J-integral seems to be more widely used in pressure vessel technology. The description, some applications of and extensive references on the crack opening displacement approach to fracture may be found in [5]-[7]. Application of a general fracture instability concept based on the crack opening displacement to shells and plates with a part-through crack is described in [8].

In this report the emphasis is on the flaw evaluation based on fracture mechanics techniques. In particular this part of the study is concerned with the effect flaw-flaw and flaw-boundary interaction on the fracture mechanics parameters. After classifying possible flaws which may be found in welds from a viewpoint of their importance in fracture mechanics applications, some of the more important flaw interaction problems have been identified, their method of solution is briefly discussed and some typical and useful results are given.

2. TYPES OF FLAWS

In this report our primary interest in flaws is from a viewpoint of their influence on enhancing or inhibiting fracture initiation and propagation in the pipe. Generally a flaw may be defined as a discontinuity in material constants or geometry. Variety of inclusions come under first and notches, pores and cracks come under the second group of flaws. A common feature of all flaws is that they disturb or perturb the stress field around them. Generally this perturbation gives rise to a stress concentration around the flaw. However, for certain types of flaws there may also be a reduction in key components of the stresses. With their importance in the application of fracture mechanics analysis in mind, in this study we will, therefore, introduce a somewhat unconventional classification of flaws.

2.1 Pores and Solid Inclusions

Pores are the holes or voids in the material having entirely smooth surfaces (Fig. 1.a1). If σ_o refers to the magnitude of the uniform stress field outside the perturbation region of the pore, then the pore leads to a stress concentration which is of the form

$$\sigma_{max} = K\sigma_o \quad , \quad K = \frac{A}{\sqrt{\rho}} \quad , \tag{1}$$

where K is the "stress concentration factor", A is a (finite) constant which depends on the geometry of the medium and ρ is radius of curvature

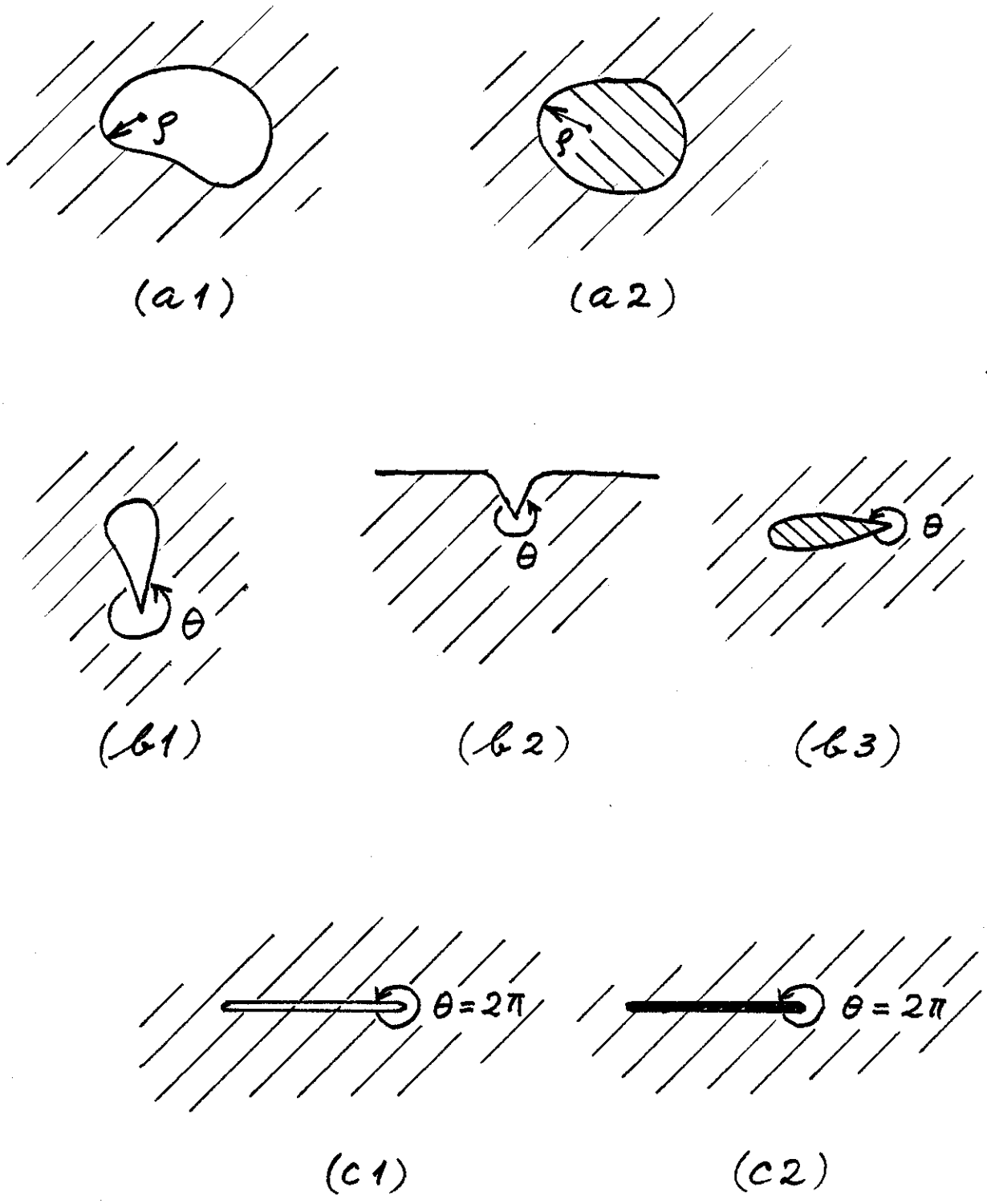

Fig. 1 Types of Flaws

of the pore. Generally K is greater than one. We note that surface notches with finite radius of curvature ρ would also come under this category.

Solid inclusions are the second phase materials in the medium also having entirely smooth surfaces. The modulus E_i of the inclusion may be greater or less than the modulus E of the matrix or the base material, the two limiting cases being the rigid inclusion ($E_i=\infty$) and the hole ($E_i=0$). If $E_i<E$, qualitatively the perturbed stress field of the inclusion is similar to that of a pore, meaning that there would be a stress concentration around the inclusion. On the other hand, if $E_i>E$ there would be a reduction in the net section stress. However, in this case there would also be a stress concentration in other planes perpendicular to the applied stress. For example, Fig. 2 shows the stress distribution in a medium containing a circular inclusion under plane strain or plane stress conditions. Note that for c>R around the inclusion there is indeed some stress concentration. In this figure, μ is the shear modulus, $\kappa = 3-4\nu$ for plane strain, and $\kappa = (3-\nu)/(1+\nu)$ for plane stress, ν being the Poisson's ratio.

2.2 Pores, Notches and Solid Inclusions with Sharp Corners

From Eq. (1) and Fig. 2 it may be seen that from a viewpoint of failure analysis a distinguishing feature of the pores, notches and solid inclusions with smooth surfaces is that the stress state around such flaws is always bounded. Eq. (1) also indicates that as the root radius ρ of the notch tends to zero, the stress state around notch tip would tend to infinity. Particularly in problems concerning brittle fracture and fatigue crack initiation such flaws may have to be treated differently. In these nonplanar flaw problems it is said that the inclusion or the notch tip is a point of stress singularity around which the stress state would have the following behavior:

$$\sigma_{ij} = \frac{k}{r^{\lambda}} \quad , \quad 0 < \mathrm{Re}(\lambda) \leq 1/2 \ , \tag{2}$$

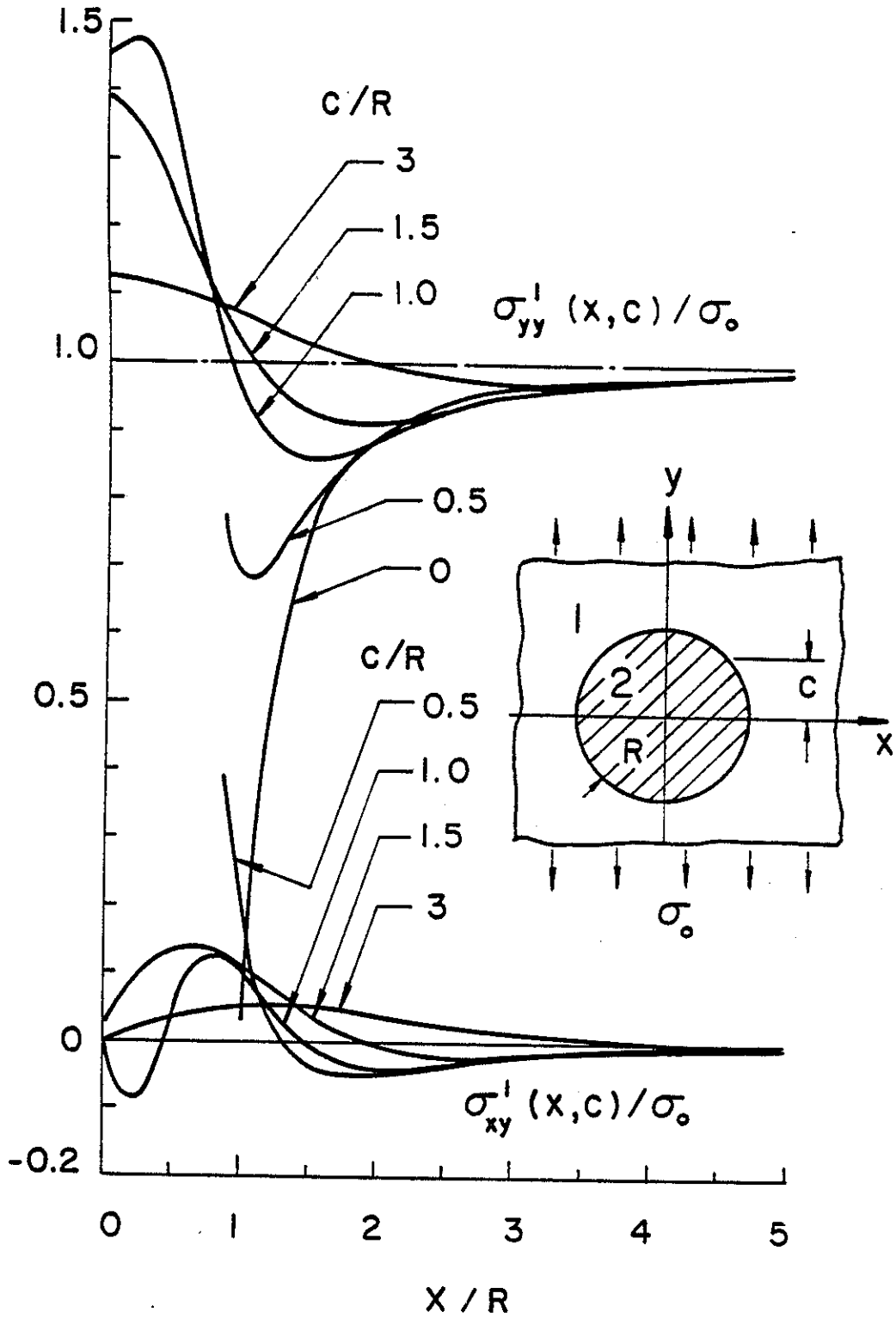

Figure 2. The stress distribution in a plate with a circular elastic inclusion ($\mu_2 = 23\mu_1$, $\kappa_1 = 1.6$, $\kappa_2 = 1.8$).

where k and λ are constants representing the strength and the power of the stress singularity and r is a (small) distance from the notch tip. Generally, Eq. (2) is valid for values of the material angle $\theta > \pi$ (Fig. 1 b1, b2, b3). Even though the term "stress intensity factor" is commonly used in relation with crack problems for which $\lambda = 0.5$, in the more general problem leading to an expression such as (2) k is also called the "stress intensity factor".

In the case of notches with a material angle $\pi < \theta < 2\pi$ the power of singularity λ is dependent on θ only and may be obtained from (see, for example, [9] where the general problem of bimaterial wedge under variety of boundary conditions are discussed)

$$\cos[2(\lambda-1)\theta] - 1 + (\lambda-1)^2(1-\cos 2\theta) = 0 \quad . \tag{3}$$

Fig. 3 shows the solution of (3) in the relevant range.

2.3 Cracks and Flat Inclusions

These are simply the planar flaws in which the material angle θ (theoretically) is 2π (Fig. 1 c1, c2). Again, the inclusion may be elastic or rigid, the crack being a limiting case with zero modulus. In all planar inclusion as well as crack problems eq. (2) is valid with $\lambda = 0.5$.

The bulk of the material in this report is devoted to the problem of interaction between two flaws or a flaw and a boundary. Since the initial phase of the fracture problem is invariably a subcritical crack growth and since the stress intensity factor is the primary fracture mechanics parameter used in analyzing the subcritical crack growth process, the quantitative results in the interaction problems considered are mostly the stress intensity factors.

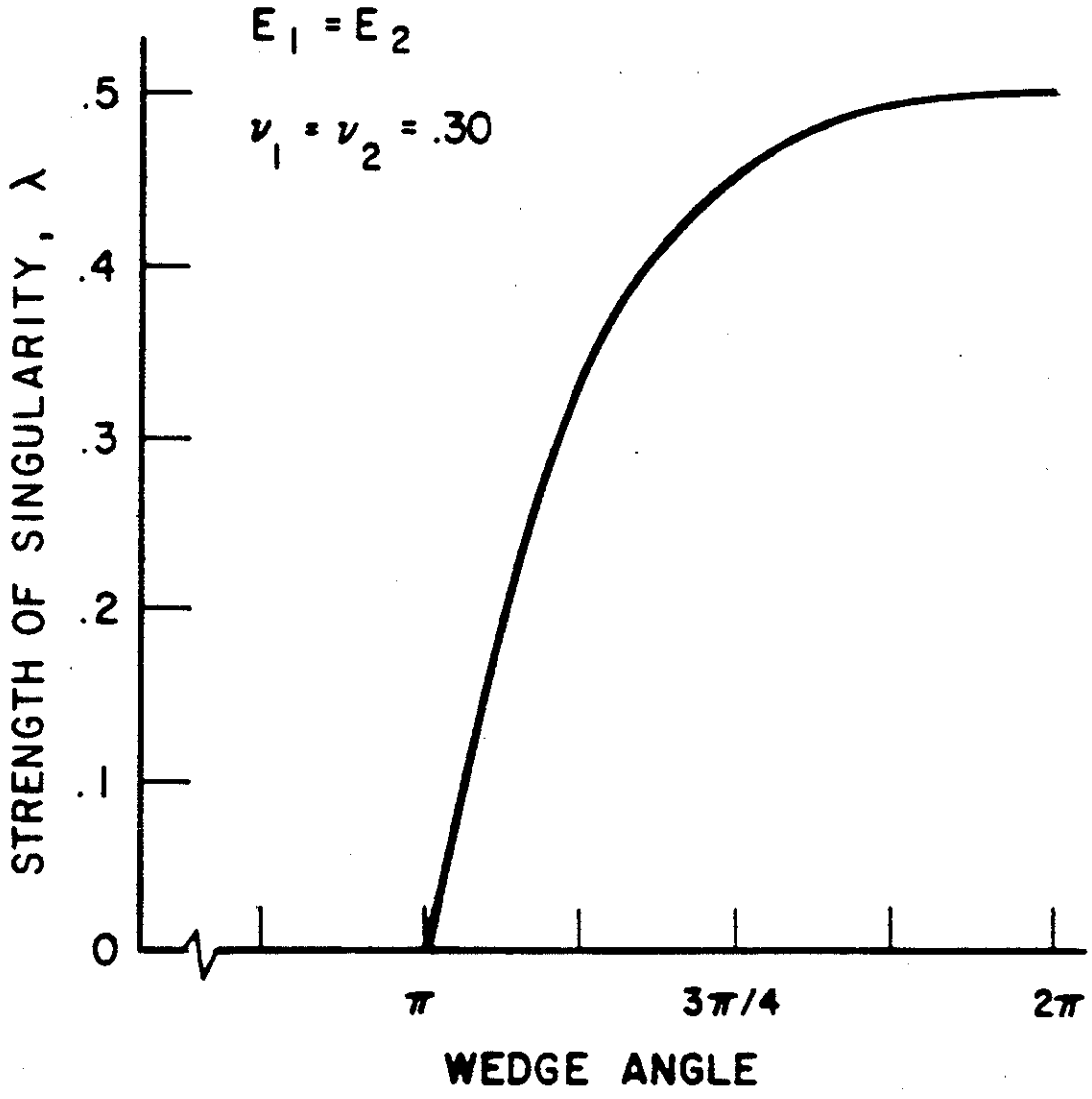

Fig. 3 STRENGTH OF STRESS SINGULARITY ($\sigma_{ij} \propto r^{-\lambda}$)

3. INTERACTION BETWEEN A CRACK AND A SOLID INCLUSION OR A PORE

In this section we will consider the problem of the interaction between a solid elastic inclusion and a line crack. It will be assumed that the inclusion and the crack are sufficiently close to each other so that their perturbed stress fields interact with each other. It will also be assumed that the crack-inclusion region is sufficiently far away from the boundaries so that their combined perturbed stress field does not interact with the boundaries. Consequently, for the purpose of calculating the perturbed stress state and the stress intensity factors it may be assumed that the domain is infinite.

3.1 Plane Strain Problem for a Circular Inclusion or Pore

Consider the general crack-inclusion problem described in Fig. 4. Assume that the composite medium is under plane strain or generalized plane stress conditions, with μ_i and κ_i, (i=1,2) referring to the elastic constants (μ_i the shear modulus, $\kappa_i = 3-4\nu_i$ for plane strain, and $\kappa_i = (3-\nu_i)/(1+\nu_i)$ for plane stress, ν_i being the Poisson's ratio). Let u_t and u_w be the displacement components in t and w directions shown in Fig. 4(b). By defining

$$g_1(t) = \frac{\partial}{\partial t}\,(u_t^+ - u_t^-)\ ,\quad g_2(t) = \frac{\partial}{\partial t}\,(u_w^+ - u_w^-)\ , \tag{4}$$

and by referring to [10] for details, the problem may be formulated in terms of a pair of singular integral equations of the following form:

$$\frac{1}{\pi}\int_{t_2}^{t_1} \sum_{j=1}^{2} k_{ij}(t,t_o)g_j(t_o)dt_o = \frac{1+\kappa_1}{2\mu_1}\,p_i(t)\ ,\quad (i=1,2) \tag{5}$$

where the kernels k_{ij} are known functions and have a Cauchy type singularity. The known input functions p_1 and p_2 are given by

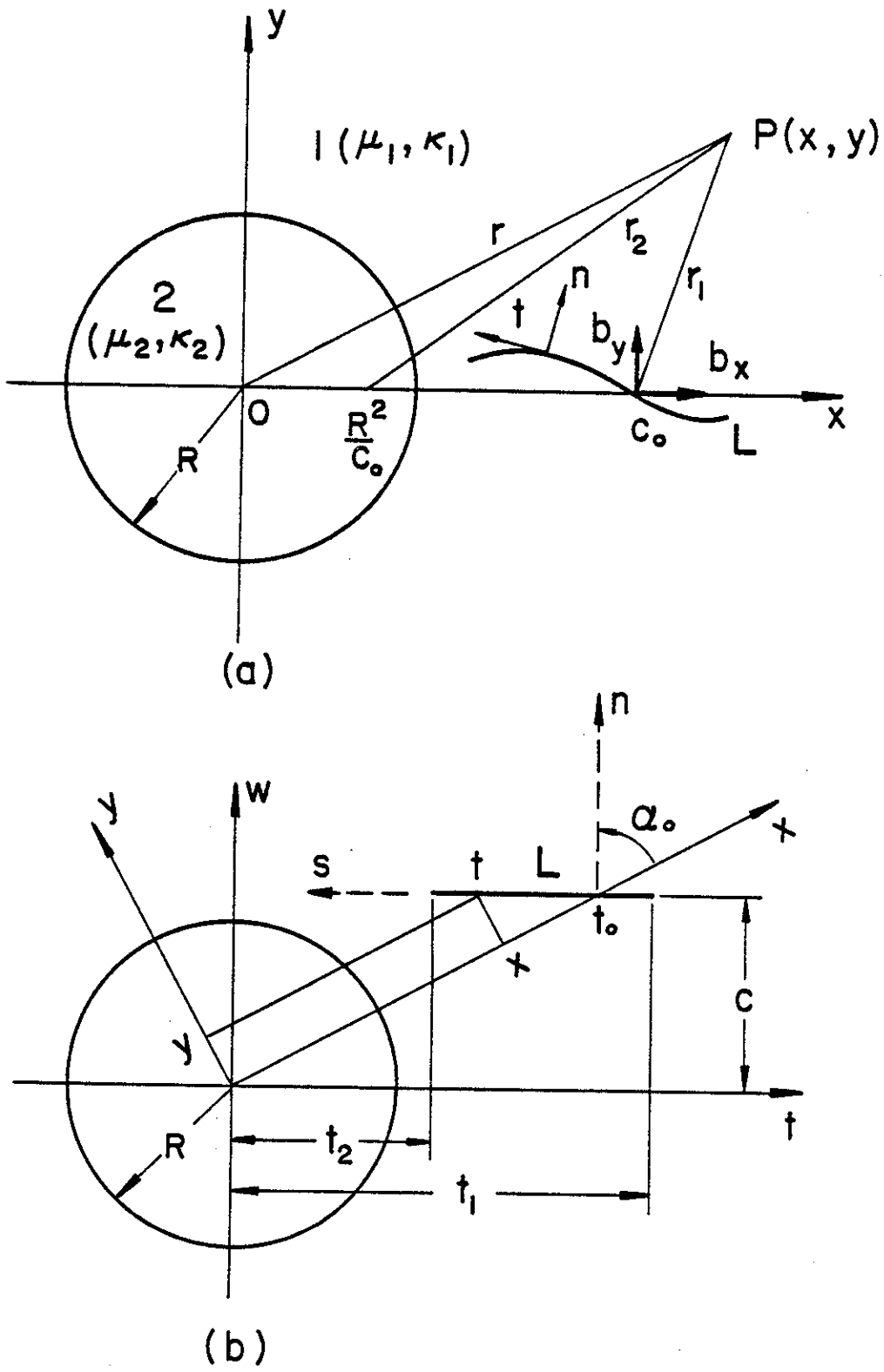

Figure 4. Geometry showing the dislocations b_x and b_y, and the crack L in the neighborhood of the inclusion 2.

$$p_1(t) = -\sigma_{ww}(t,c) \ , \ p_2(t) = -\sigma_{wt}(t,c) \ , \ (t_2<t<t_1) \ , \qquad (6)$$

σ_{ww} and σ_{wt} being the stress components at the point (t,c) in the plane with inclusion but without a crack. For example, for a plane under uniform tension σ_o away from the inclusion these stresses are given by Fig. 2. The solution of (5) is of the following form

$$g_j(t) = G_j(t)/\sqrt{(t-t_2)(t_1-t)} \ , \quad (j=1,2) \qquad (7)$$

where G_1 and G_2 are unknown bounded functions. After solving the integral equations the Modes I and II stress intensity factors at the crack tips t_1 and t_2 may be defined by and obtained from the following expressions:

$$k_1(t_1) = \lim_{t\to t_1} \sqrt{2(t-t_1)} \ \sigma_{ww}(t,c) = -\frac{2\mu_1}{1+\kappa_1} \lim_{t\to t_1} \sqrt{2(t_1-t)} \ g_2(t) \ ,$$

$$k_2(t_1) = \lim_{t\to t_1} \sqrt{2(t-t_1)} \ \sigma_{wt}(t,c) = -\frac{2\mu_1}{1+\kappa_1} \lim_{t\to t_1} \sqrt{2(t_1-t)} \ g_1(t) \ ,$$

$$k_1(t_2) = \lim_{t\to t_2} \sqrt{2(t_2-t)} \ \sigma_{ww}(t,c) = \frac{2\mu_1}{1+\kappa_1} \lim_{t\ t_2} \sqrt{2(t-t_2)} \ g_2(t) \ ,$$

$$k_2(t_2) = \lim_{t\to t_2} \sqrt{2(t_2-t)} \ \sigma_{wt}(t,c) = \frac{2\mu_1}{1+\kappa_1} \lim_{t\to t_2} \sqrt{2(t-t_2)} \ g_1(t).$$

(8a-d)

In the absence of a crack the stress components on a line perpendicular to the loading direction are shown in Fig. 2 for an elastic inclusion. Similar results for a circular hole (i.e., for μ_2=0) are shown in Fig. 5.

The stress intensity factors calculated at the crack tips t_1 and t_2 are shown in Figures 6-13. The results shown in the figures are normalized with respect to $\sigma_o\sqrt{a}$ where σ_o is the tensile stress acting on the plane away from and perpendicular to the crack and a is the half crack length. Thus, the normalized stress intensity factors k_{ij} shown in the

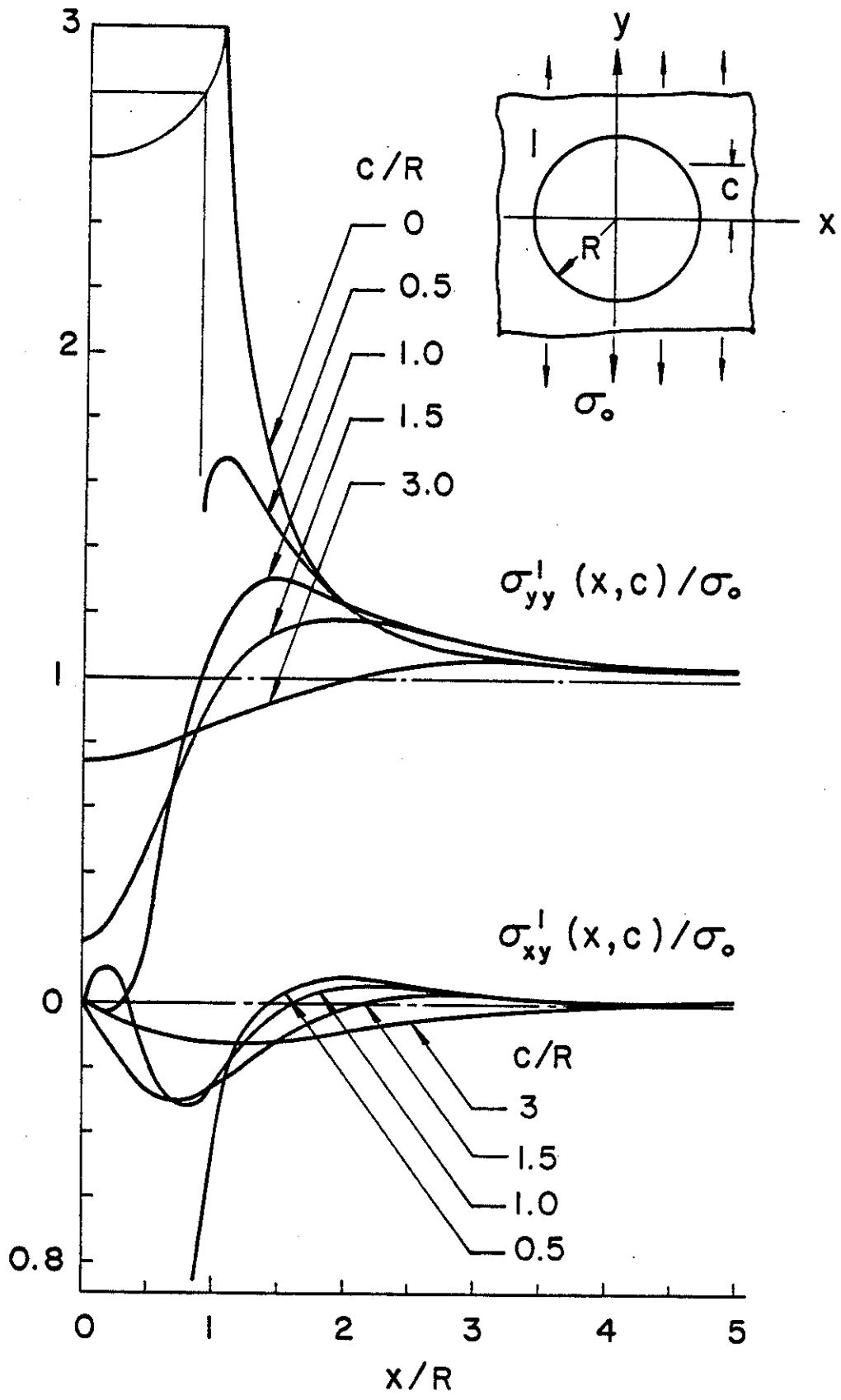

Figure 5. The stress distribution in a plate with a circular hole.

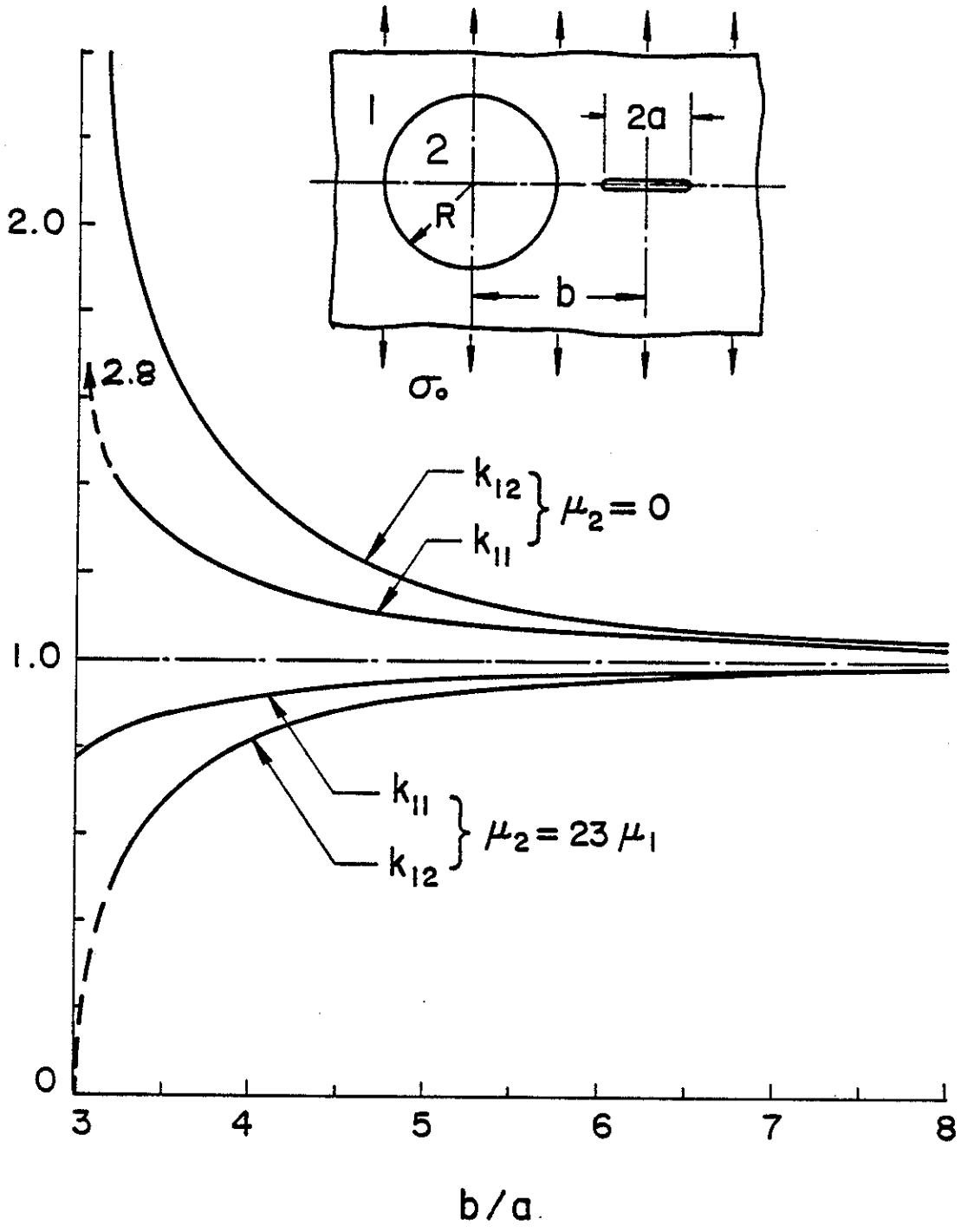

Figure 6. The stress intensity factors for a symmetrically located radial crack (R/a = 2, c = 0).

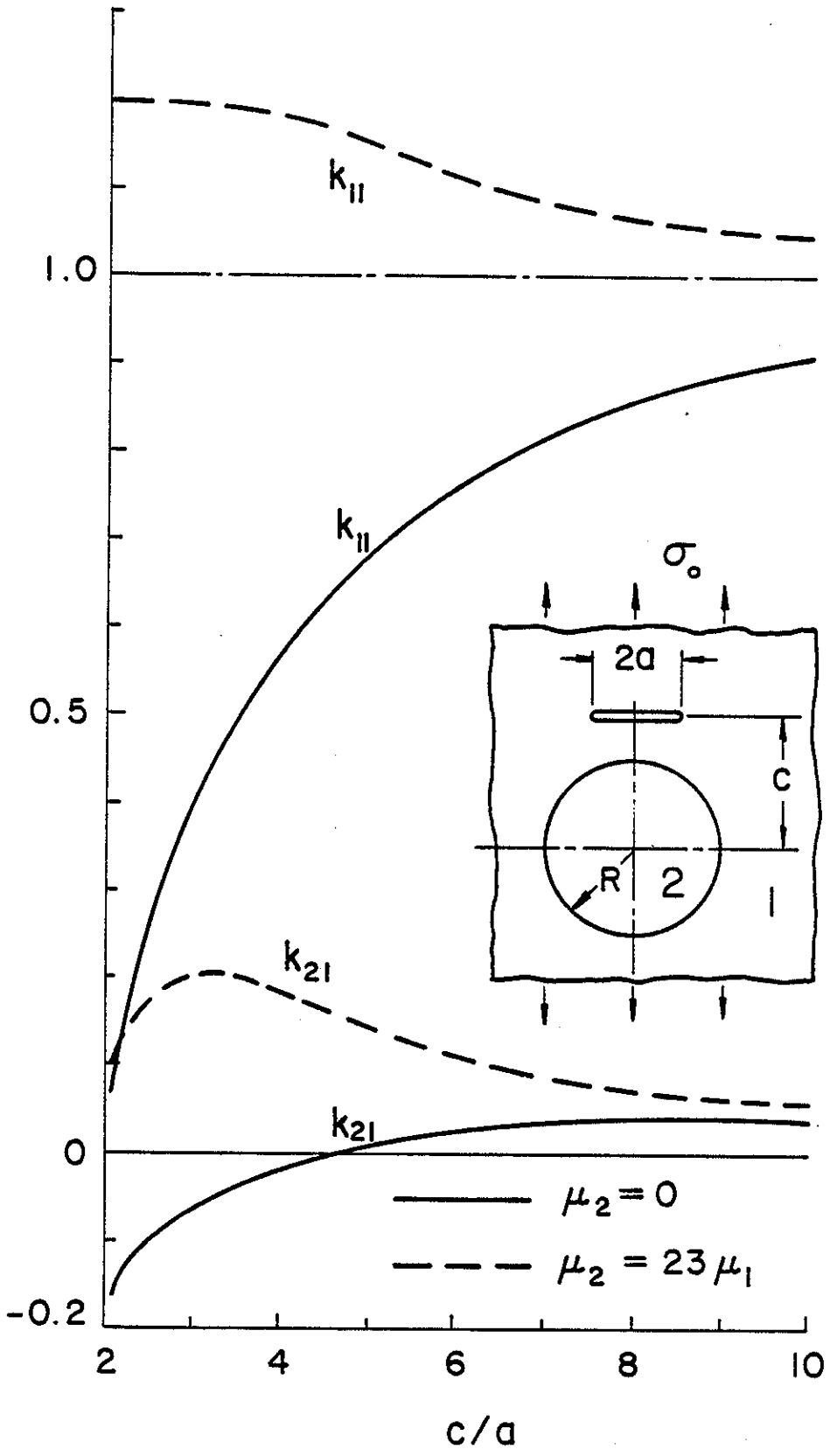

Figure 7. The stress intensity factors for a symmetrically located "tangential crack" perpendicular to the load (b = 0, R = 2a).

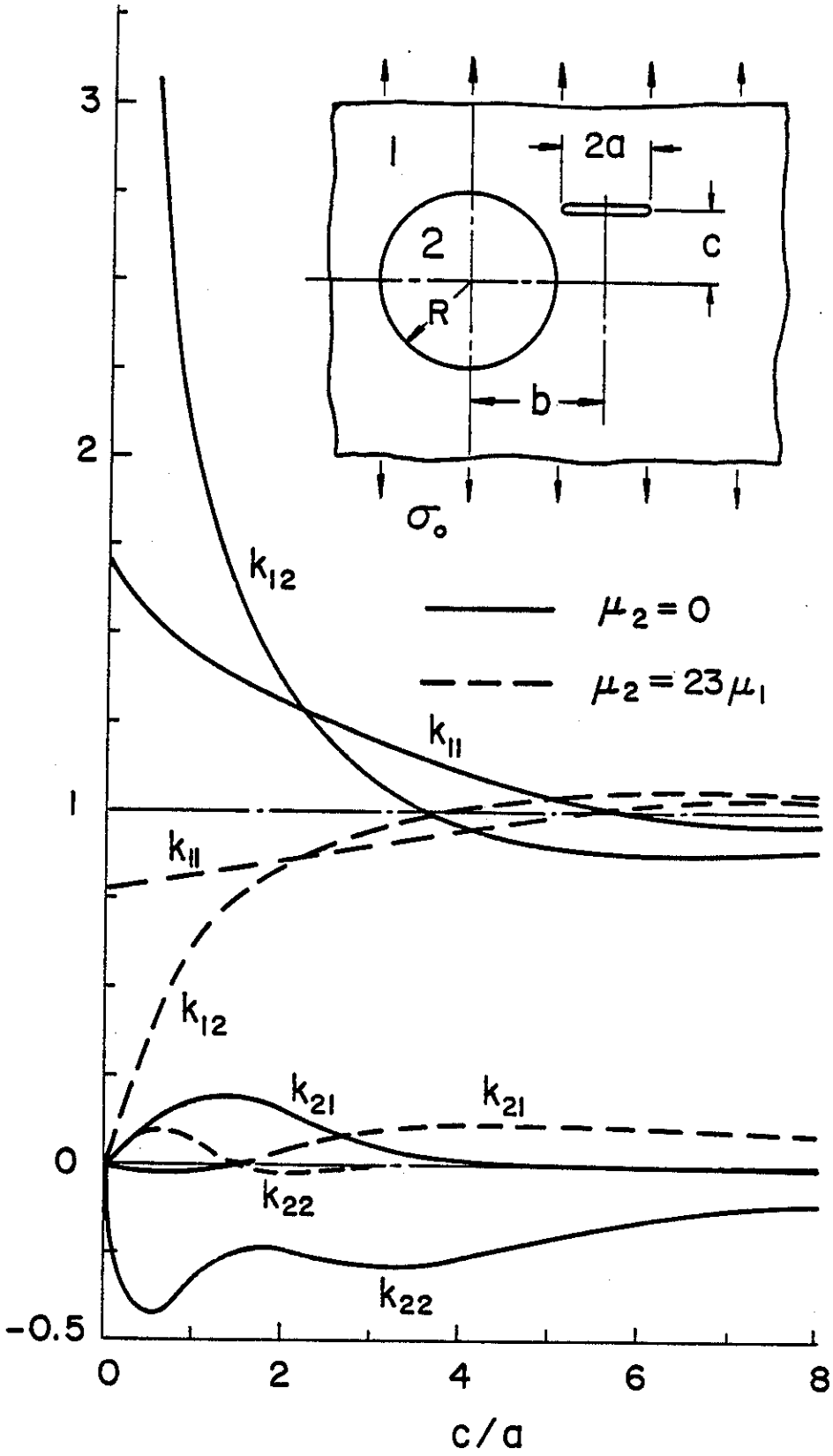

Figure 8. Stress intensity factors for a crack perpendicular to the external load (R = 2a, b = 3a).

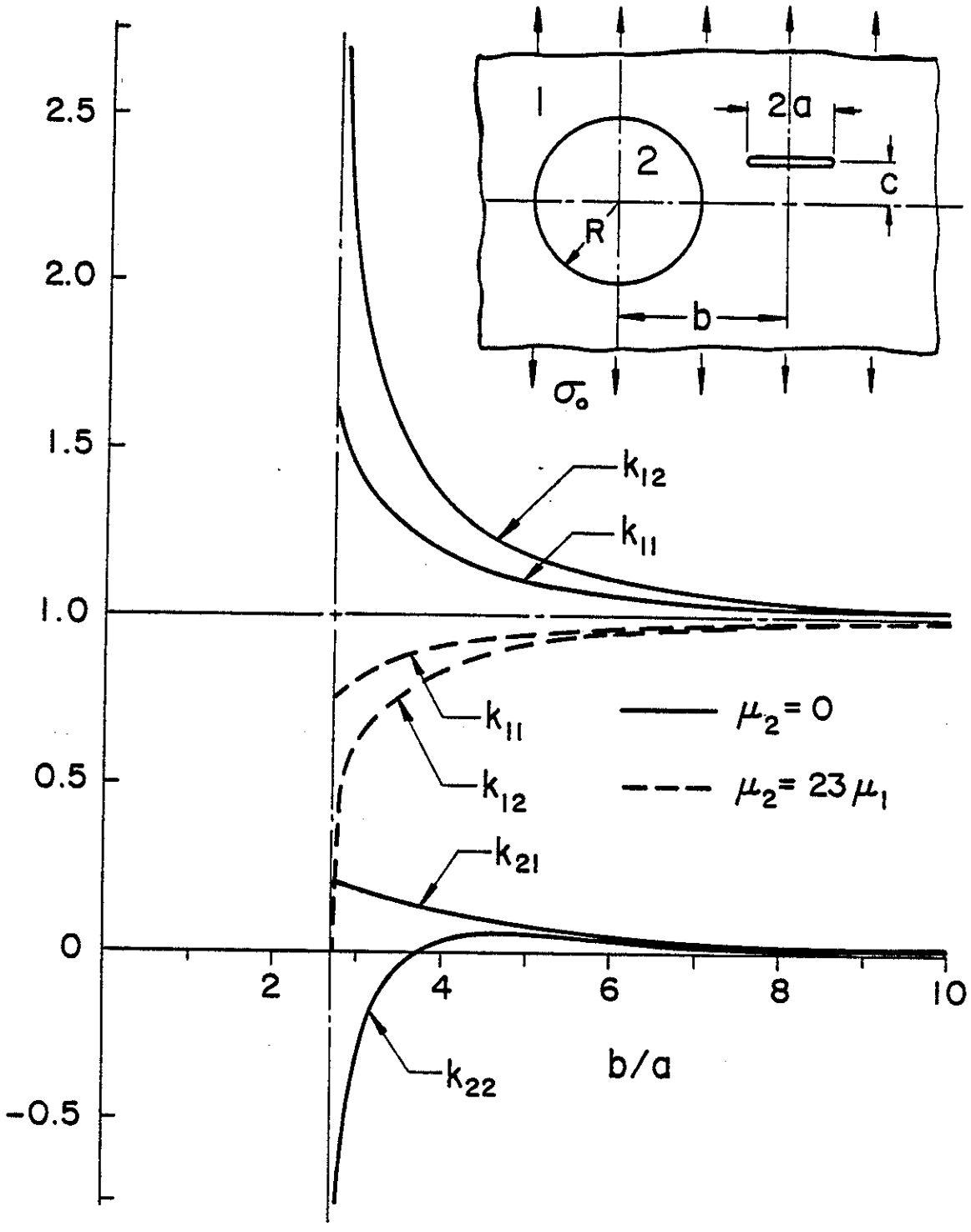

Figure 9. Stress intensity factors for a crack perpendicular to the external load (R = 2a, c = a).

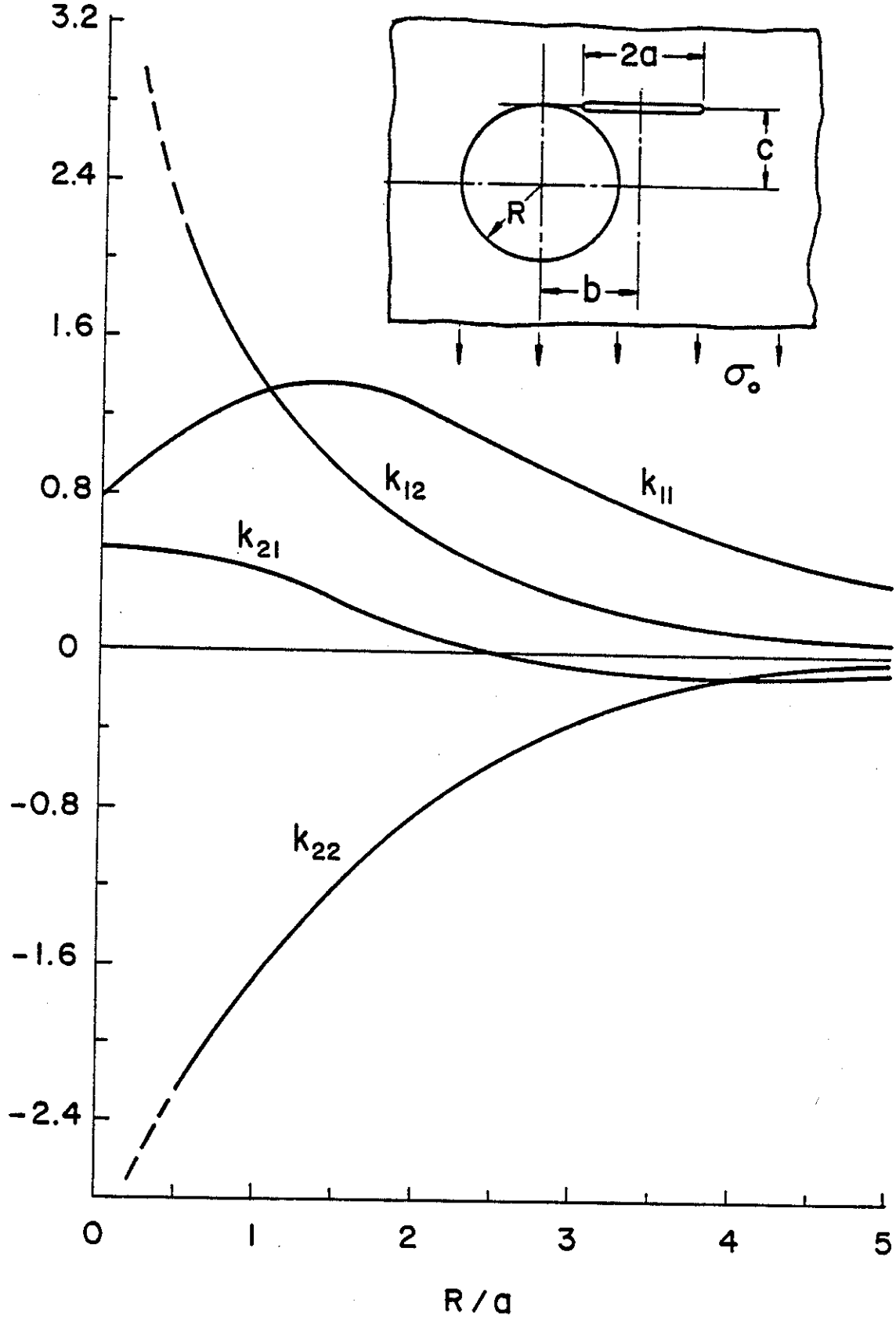

Figure 10. Stress intensity factors for a crack in the matrix containing a circular hole ($\mu_2 = 0$, $c = R$, $b-a = 0.2R$, a = constant).

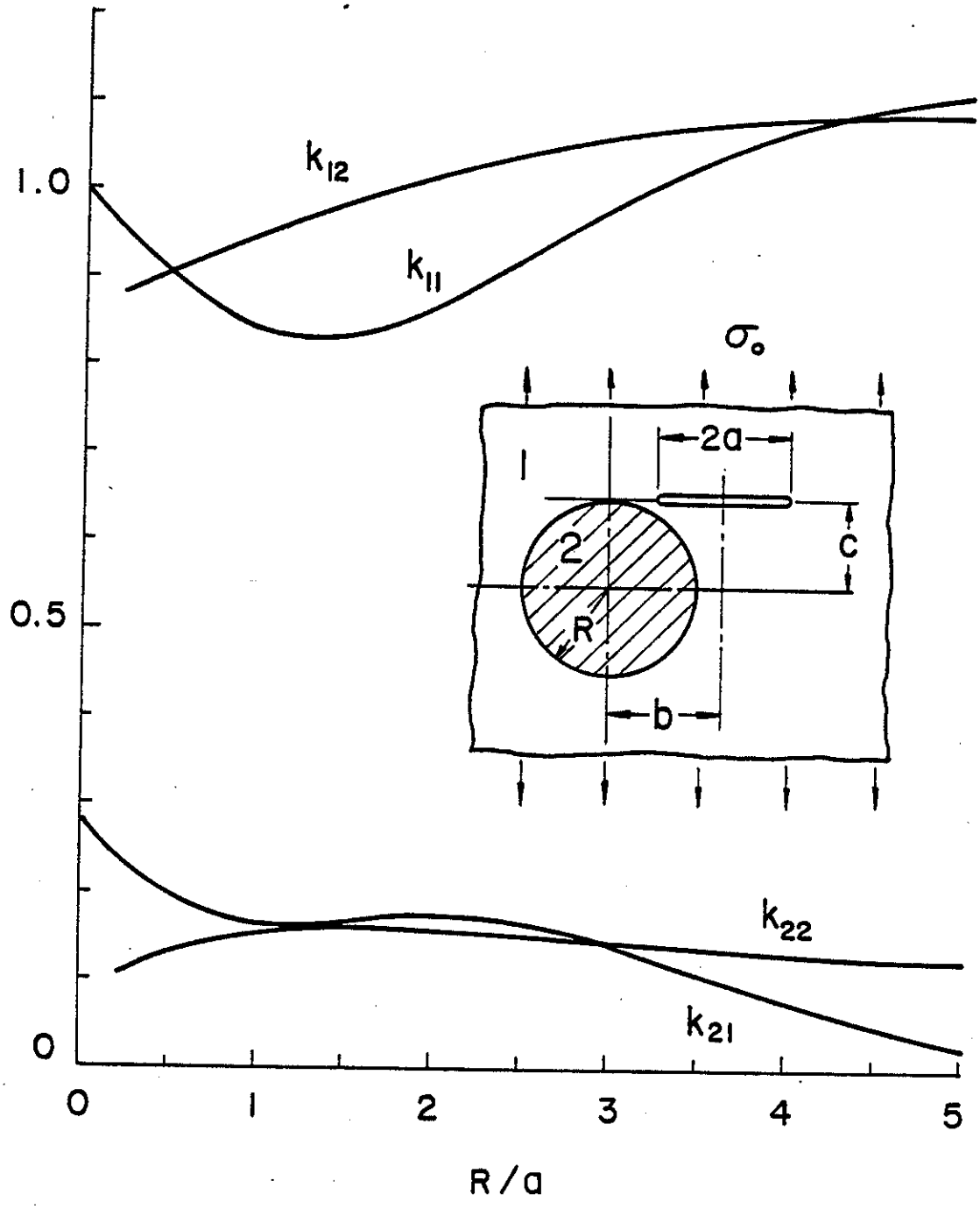

Figure 11. Stress intensity factors for a crack in the matrix containing an elastic inclusion ($\mu_2 = 23\mu_1$, c = R, b-a = 0.2R, a = constant).

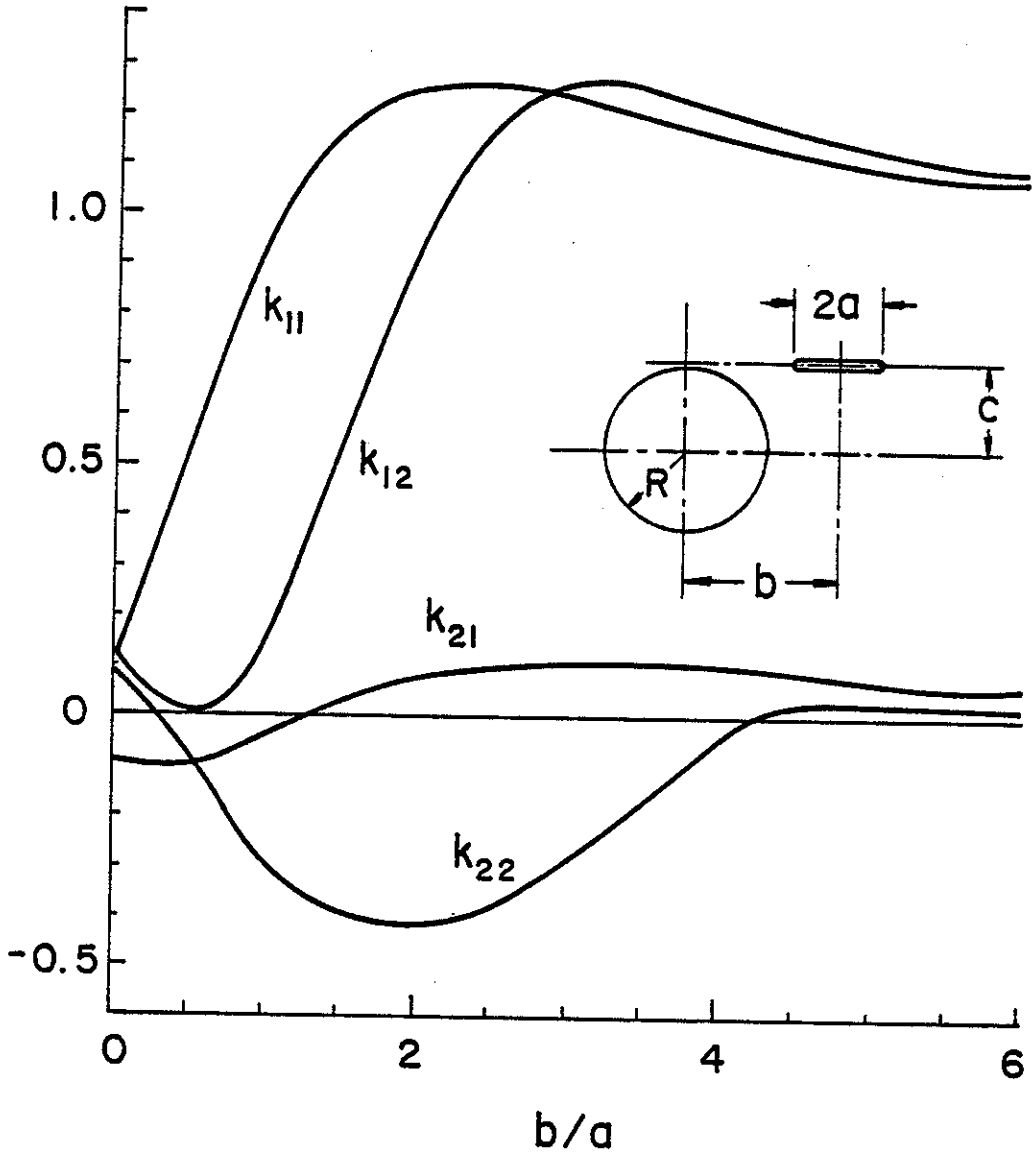

Figure 12. Stress intensity factors for a crack in the matrix containing a circular hole ($\mu_2 = 0$, $c = 2.2a$, $R = 2a$).

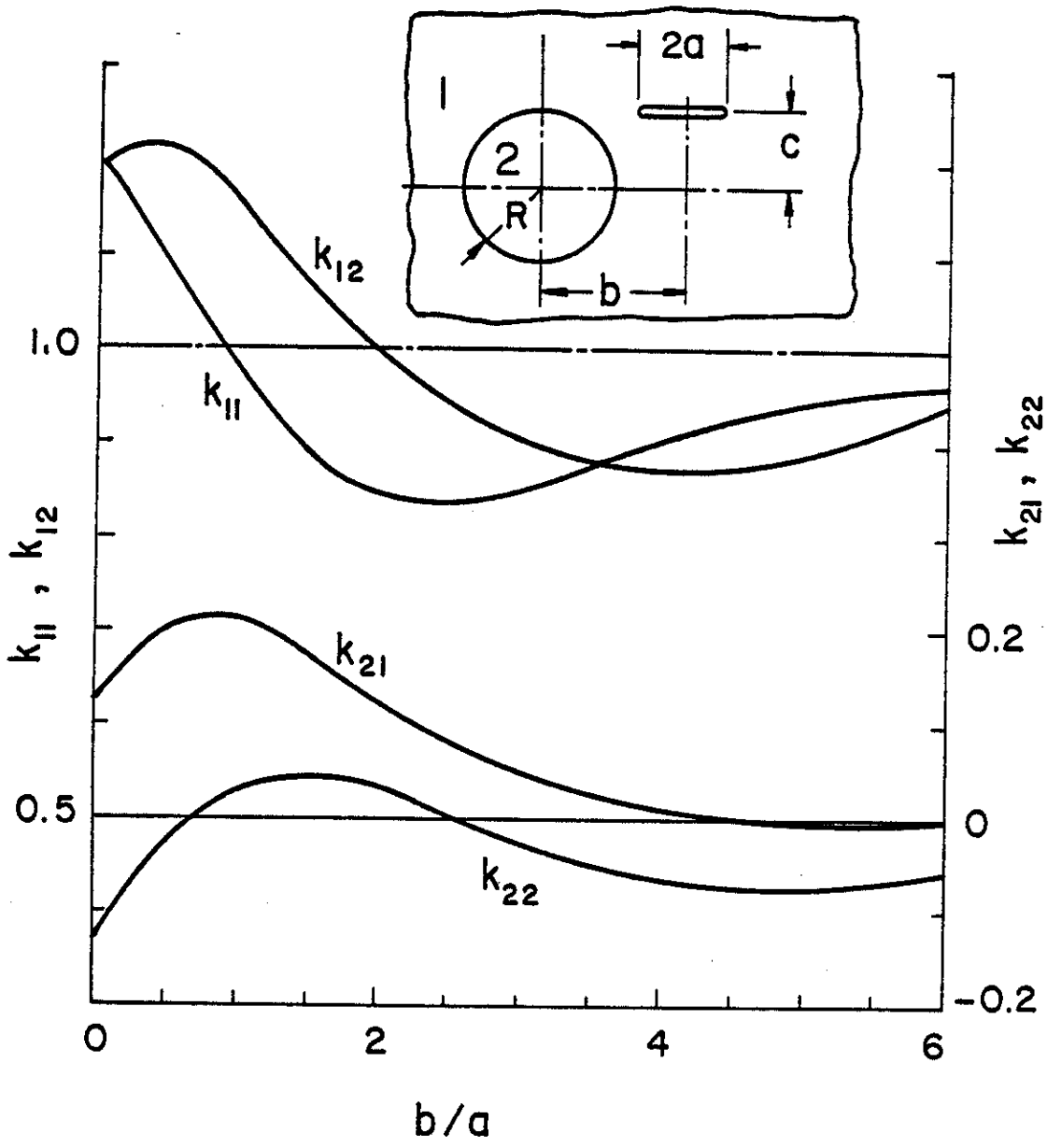

Figure 13. Stress intensity factors for a crack in the matrix containing an elastic inclusion ($\mu_2 = 23\mu_1$, c = 2.2a, R = 2a).

figures are defined by

$$k_{ij} = \frac{k_i(t_j)}{\sigma_o\sqrt{a}} \quad , \quad (i,j = 1,2) \tag{9}$$

where $k_i(t_j)$ are given in (8). Figures show the results for only two cases, namely a circular hole (i.e., μ_2=0) and a stiffer elastic inclusion with elastic constants

$$(\mu_2/\mu_1) = 23 \quad , \quad \kappa_1 = 1.6 \ , \ \kappa_2 = 1.8 \quad . \tag{10}$$

Fig. 6 shows the results for a symmetrically located radial crack. Note that as the (inner) crack tip t_2 approaches the boundary (i.e., for $b \to R+a$) the stress intensity factor $k_1(t_2)$ tends to infinity for the case of hole and to zero for the case of inclusion. Qualitatively the results given in this figure are very general, that is if the perturbed stress fields of a crack and a hole (or a pore) interact, then the stress intensity factors at the crack tips would be greater than those which would be obtained for the cracked medium without the hole. For example, note that in Fig. 6 the stress intensity factors for μ_2=0 are greater than $\sigma_o\sqrt{a}$, the value for the cracked plane without a hole, and approach this value as the crack moves away from the hole (i.e., as $b \to \infty$). Similar trend would be observed for an inclusion the stiffness of which is less than that of the cracked medium (i.e., for $\mu_2 < \mu_1$). On the other hand, if the plane contains a stiffer inclusion (i.e., for $\mu_2 > \mu_1$), then the stress intensity factors are smaller than $\sigma_o\sqrt{a}$.

The results shown in Figures 7-13 are self-explanatory. Depending on the location of the crack, one may observe some trends in these results which are opposite to that observed for the symmetric radial crack shown in Fig. 6. These trends, however, may easily be explained by examining the stress fields perturbed by an inclusion or a hole which are shown in figures 2 and 5. By examining the signs of the Modes I and II stress intensity factors, from the results given in these figures one may easily conclude that generally for the crack tip near the matrix-inclusion boundary the crack would propagate towards the boundary if

$\mu_2=0$ or $\mu_2<\mu_1$, and away from the boundary if $\mu_2>\mu_1$. This conclusion is based on the analysis giving the plane of the maximum cleavage stress at the crack tip. The details of the analysis and its experimental verification may be found in [12].

In another class of crack-inclusion interaction problems both the inclusion and the matrix material may contain a crack. For symmetrically located radial cracks the general problem is described by Fig. 14. The details of the analysis of this problem may be found in [11]. Figures 15-21 show some calculated results. In this problem the formulation given in [11] and Fig. 14 allow the consideration of the special cases of a crack terminating at the interface (i.e., $b=R+a$, $\mu_2\neq 0$ in Fig. 6 or $a_2=b_2$, $a_1=a$ in Fig. 14), and the crack going through the interface (i.e., $b_2=a=a_1$ in Fig. 14). In these special cases it is shown that [11] the point ($x=a$, $y=0$) (Fig. 14) is a point of stress singularity and the stress state in a close neighborhood of it has the following form:

$$\sigma_{ij}(r,\theta) = \frac{k}{r^{\beta}} g_{ij}(\theta) \quad , \quad (i,j=x,y) \ , \ (0<\beta<1) \tag{11}$$

where r and θ are the polar coordinates centered at the singular point, g_{ij} is a bounded function and the stress intensity factor k is a constant. The stress intensity factors $k = k(a)$ given in this section are defined in terms of the related cleavage stresses as follows (Fig. 14):

(i) crack in the matrix ($-a<a_2<b_2<a = a_1<b_1$):

$$k(a) = \lim_{x\to a} \sqrt{2}\,(a-x)^{\beta}\sigma_{2yy}(x,0) \ , \tag{12}$$

(ii) crack in the inclusion ($-a<a_2<b_2 = a<a_1<b_1$):

$$k(a) = \lim_{x\to a} \sqrt{2}\,(x-a)^{\alpha}\sigma_{1yy}(x,0) \tag{13}$$

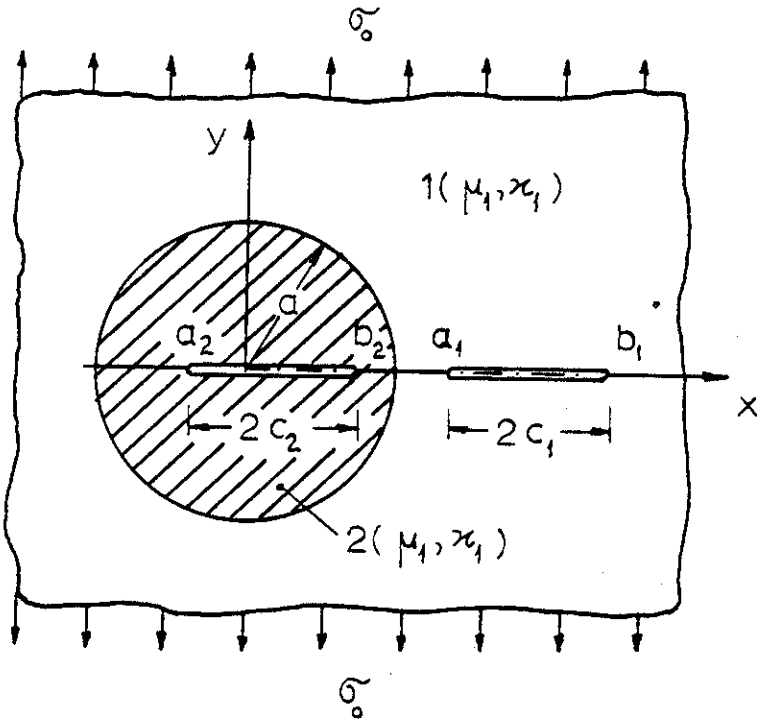

Figure 14. Inclusion-crack geometry.

(iii) crack crossing the boundary ($-a<a_2<b_2 = a = a_1<b_1$):

In this case for simplicity we define the following normal and shear cleavage stress intensity factors

$$k_{xx}(a) = \lim_{y\to 0} \; y^{\gamma} \, \sigma_{1xx}(a,y) \;, \text{ (normal cleavage)} \;, \tag{14}$$

$$k_{xy}(a) = \lim_{y\to 0} \; y^{\gamma} \, \sigma_{1xy}(a,y) \;, \text{ (shear cleavage)} \;. \tag{15}$$

The first special problem (i) with $a_2=b_2$ corresponds to the limiting case of the problem considered in Fig. 6. In the problem of a crack terminating at the bimaterial interface such as the cases (i) and (ii) mentioned above, the power of the stress singularity (α or β) is highly dependent on the stiffness ratio μ_2/μ_1 and is relatively insensitive to the Poisson's ratios (or κ_1 and κ_2). For the crack geometry $a_2=b_2$, $a_1=a$, $b_1>a$, Fig. 14, Table 1 shows the effect of μ_2/μ_1 on β. It may be seen that for $(\mu_2/\mu_1)<1$ the power β is greater than 0.5, meaning that if the stiffness of the inclusion is less than that of the matrix, then the stress singularity is stronger than the corresponding homogeneous case. Similarly, if $\mu_2>\mu_1$ then $\beta<0.5$. This is the reason for the asymptotic trends observed in Fig. 6 for the stress intensity factor k(a) as $b\to R+a$. Table 1 also gives the corresponding stress intensity factors calculated from (12).

For this problem, to give some idea about the nature and the relative magnitude of the crack surface displacement, Fig. 15 shows some calculated results. Here v(x,0) is the crack surface displacement in y direction.

Figures 16 and 17 show the stress intensity factors for a crack located in the inclusion. The limiting values of the stress intensity factors shown in these figures for the crack length $2c_2$ approaching zero are obtained from uniformly loaded "infinite" plane solution with the applied stress state away from the crack region given by the uncracked

Table 1. The effect of modulus ratio on the stress intensity factors for a crack terminating at the interface ($a_1 = a$, $b_1/a = 2$, $\kappa_1 = \kappa_2 = 1.8$, $c_1 = (b_1-a)/2$).

$m = \frac{\mu_2}{\mu_1}$	β	$\frac{k(b_1)}{\sigma_o\sqrt{c_1}}$	$\frac{k(a)}{\sigma_o c_1^{\beta}}$
0		2.808	
0.05	0.81730	1.615	1.053
1/3	0.62049	1.229	0.5836
1.0	0.5	1.000	1.000
3.0	0.40074	0.8610	1.299
10.0	0.33277	0.7969	1.389
23.0	0.30959	0.7796	1.375
100	0.29387	0.7691	1.345
300	0.28883	0.7667	1.348

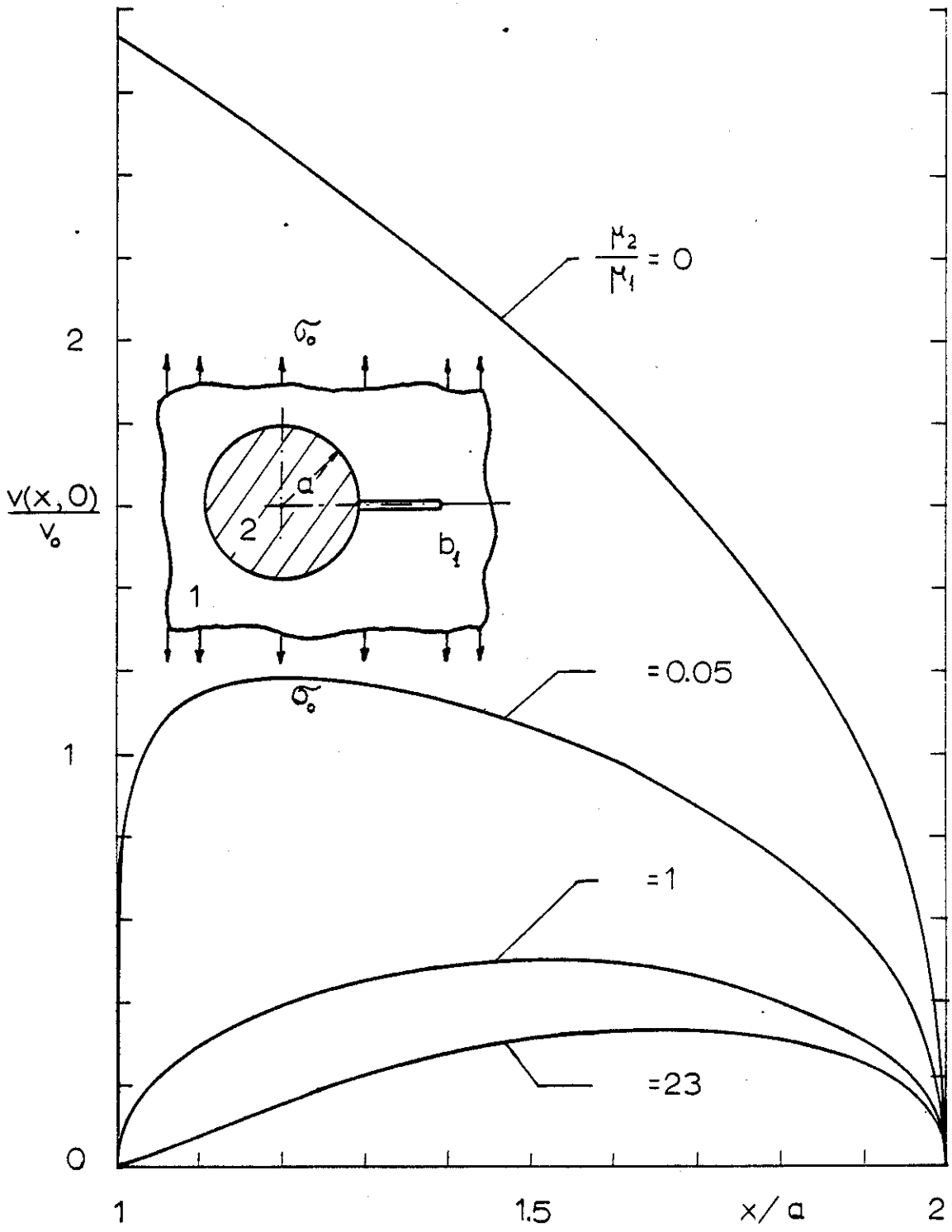

Figure 15. Crack surface displacement for a crack in the matrix with one tip on the interface ($\kappa_1 = \kappa_2 = 1.8$, $b_1/a = 2$, $v_0 = (1+\kappa_1)a\sigma_0/\mu_1$).

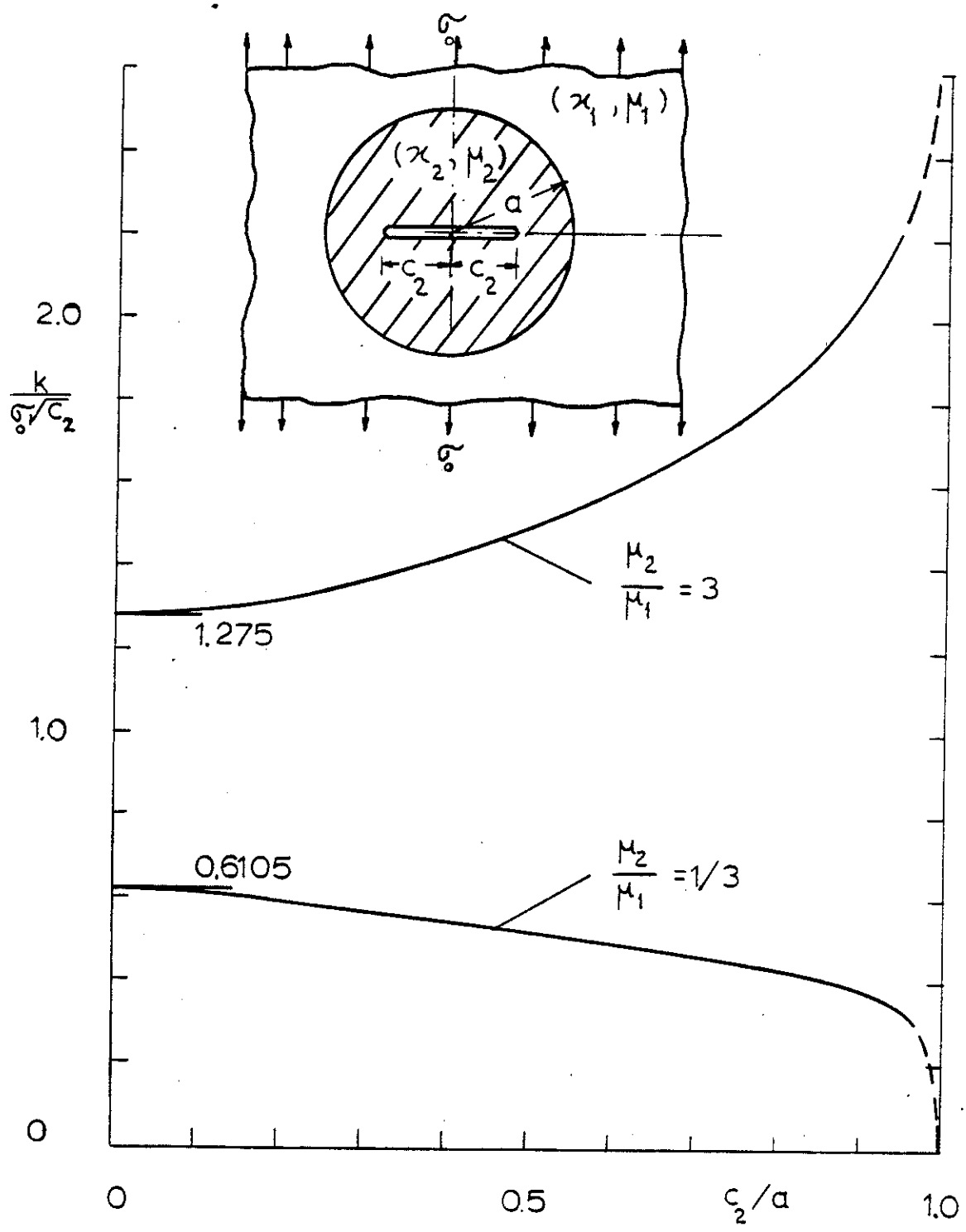

Figure 16. Stress intensity factor for a symmetrically located crack in the inclusion ($\kappa_1 = \kappa_2 = 1.8$).

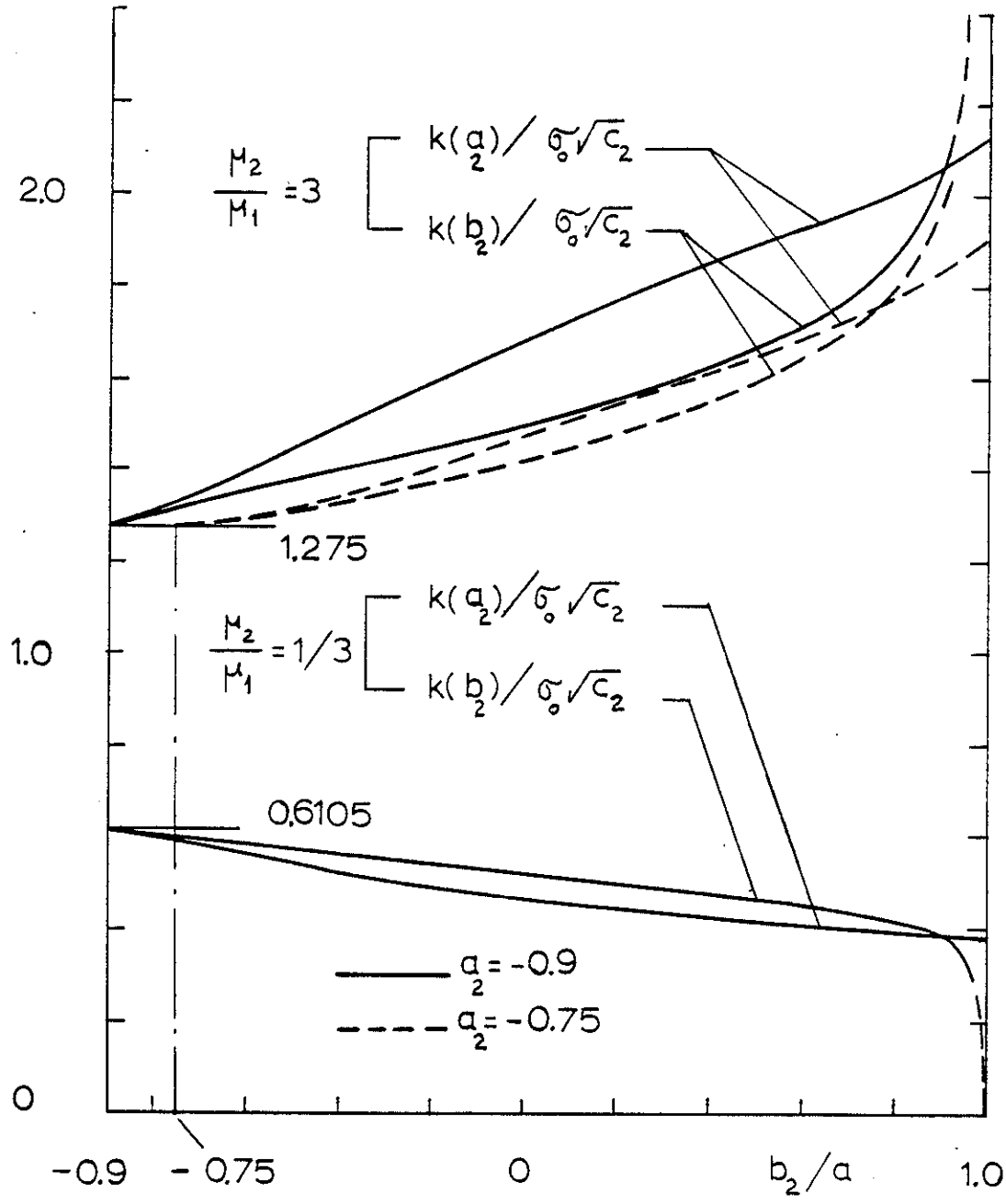

Figure 17. Stress intensity factors for a crack located in the inclusion ($\kappa_1 = \kappa_2 = 1.8$, one tip fixed at $a_2 = -0.9a$ or $a_2 = -0.75a$, b_2 variable, $c_2 = (b_2 - a_2)/2$).

inclusion solution [13], namely

$$\sigma^a_{2yy}(x,0) = \sigma_o \frac{(1+\kappa_1)\mu_2}{2\mu_1}\left(\frac{1}{\kappa_2-1+2\mu_2/\mu_1} + \frac{1}{1+\kappa_1\mu_2/\mu_1}\right) , \quad |x|<a , \tag{16}$$

$$\sigma^a_{1yy}(x,0) = \sigma_o\left[1 - \frac{a^2}{2x^2}\frac{\mu_2(\kappa_1-1)-\mu_1(\kappa_2-1)}{2\mu_2+\mu_1(\kappa_2-1)} - \frac{a^4}{x^4}\frac{3(\mu_2-\mu_1)}{2(\mu_1+\kappa_1\mu_2)}\right], \quad |x|>a ,$$

(17)

$$\sigma^a_{1xy}(x,0) = 0 \quad , \quad \sigma^a_{2xy}(x,0) = 0 \quad . \tag{18}$$

By using (16) it may be shown that for the crack in the inclusion the stress intensity factor has the following limit:

$$\lim_{c_2\to 0} \frac{k}{\sigma_o\sqrt{c_2}} = \frac{\mu_2(\kappa_1+1)}{2\mu_1}\left(\frac{\mu_1}{2\mu_2+\mu_1(\kappa_2-1)} + \frac{\mu_1}{\mu_1+\kappa_1\mu_2}\right) \quad . \tag{19}$$

Fig. 16 shows the results for a symmetrically located crack. The results for an eccentric crack are shown in Fig. 17 (see Fig. 14 for notation).

Some typical results for the case in which both the inclusion and the matrix or base material contain a crack are shown in Fig. 18.

The stress intensity factor for a completely cracked inclusion (i.e., for $a_2=-a$, $b_2=a$, $a_1=b_1$) is given in Table 2. The stress intensity factor k(a) given in this table is defined by (13) where α is the power of stress singularity.

The stress intensity factors for a crack crossing the interface are given by figures 19 and 20. In these figures $x=a_2$ and $x=b_1$ are conventional crack tips for which the stress state has square-root singularity (i.e., $\alpha'=\beta'=0.5$). For the point of the intersection of the crack with the boundary (x=a) the normal and shear cleavage components of the stress intensity factor k_{xx} and k_{xy} are defined by (14) and (15). The asymptotic trends of the stress intensity factors observed in these figures as a crack tip approaches the boundary x=a are again due to the change in the

Table 2. Stress intensity factor for a completely cracked inclusion.

$\frac{\mu_2}{\mu_1}$	$\kappa_1 = \kappa_2 = 1.8$		$\kappa_1=2.2,\ \kappa_2=1.8$		$\kappa_1=1.8,\ \kappa_2=2.2$		$\kappa_1 = \kappa_2 = 2.2$	
	α	$\frac{k(a)}{\sigma_0 a^{\alpha}}$	α	$\frac{k(a)}{\sigma_0 a^{\alpha}}$	α	$\frac{k(a)}{\sigma_0 a^{\alpha}}$	α	$\frac{k(a)}{\sigma_0 a^{\alpha}}$
0.2	0.36621	0.7890	0.38087	0.7848	0.32027	1.046	0.33845	1.010
0.6	0.45025	1.014	0.47028	0.9456	0.42123	1.174	0.44466	1.068
1.0	0.5	1.0	0.51991	0.9209	0.47724	1.107	0.5	1.0
2.0	0.57451	0.8843	0.59188	0.8165	0.55687	0.9465	0.57624	0.8613
5.0	0.67885	0.6555	0.69124	0.6194	0.66380	0.6940	0.67733	0.6500

power of stress singularity. For example, in Fig. 19 for $b_1 > a$ the stress components around the singular point (x=a, y=0) are (see (14) and (15))

$$\sigma_{xx}(a,y) \cong \frac{k_{xx}(a)}{y^{\gamma}} \quad , \quad \sigma_{xy}(a,y) \cong \frac{k_{xy}(a)}{y^{\gamma}} \quad , \quad \gamma = 0.27326. \tag{20}$$

On the other hand, for $b_1 = a$ (i.e., the case of a crack in the inclusion terminating at the boundary) the stress state around (x=a, y=0) is given by (see eq. (13))

$$\sigma_{ij} = \frac{k(a)}{\sqrt{2}\, r^{\alpha}} f_{ij}(\theta) \quad , \quad \alpha = 0.82580 \ , \tag{21}$$

where r and θ are the polar coordinates centered at the point (x=a, y=0) (i.e., $r=y$ for $\theta = \pi/2$). Thus, as $b_1 \to a$ from (20) and (21) it follows that

$$\sigma_{xx}(a,y) \cong \frac{k_{xx}(a)}{y^{\gamma}} \to \frac{k(a)}{\sqrt{2}\, y^{\alpha}} f_{xx}(\tfrac{\pi}{2}) \tag{22}$$

or

$$\sigma_{xx}(a,y) \to \frac{1}{y^{\gamma}} \left[\frac{k(a)}{\sqrt{2}\, y^{\alpha-\gamma}} f_{xx}(\pi/2) \right] , \tag{23}$$

and

$$k_{xx}(a) \to \frac{k(a)}{\sqrt{2}\, y^{\alpha-\gamma}} f_{xx}(\pi/2) \quad . \tag{24}$$

Since k(a) and f_{xx} are bounded and $\alpha > \gamma$, for y=0 (at which, by (14), k_{xx} must be calculated) $k_{xx}(a)$ would become unbounded. Similarly, it is seen that for $b_1 \to a$, k_{xy} tends to (negative) infinity. Also, since α (for the terminating crack tip) is greater than 0.5 (at b_1 for the embedded crack tip), by following a similar argument it may be shown that as $b_1 \to a$, $k(b_1)$ becomes unbounded.

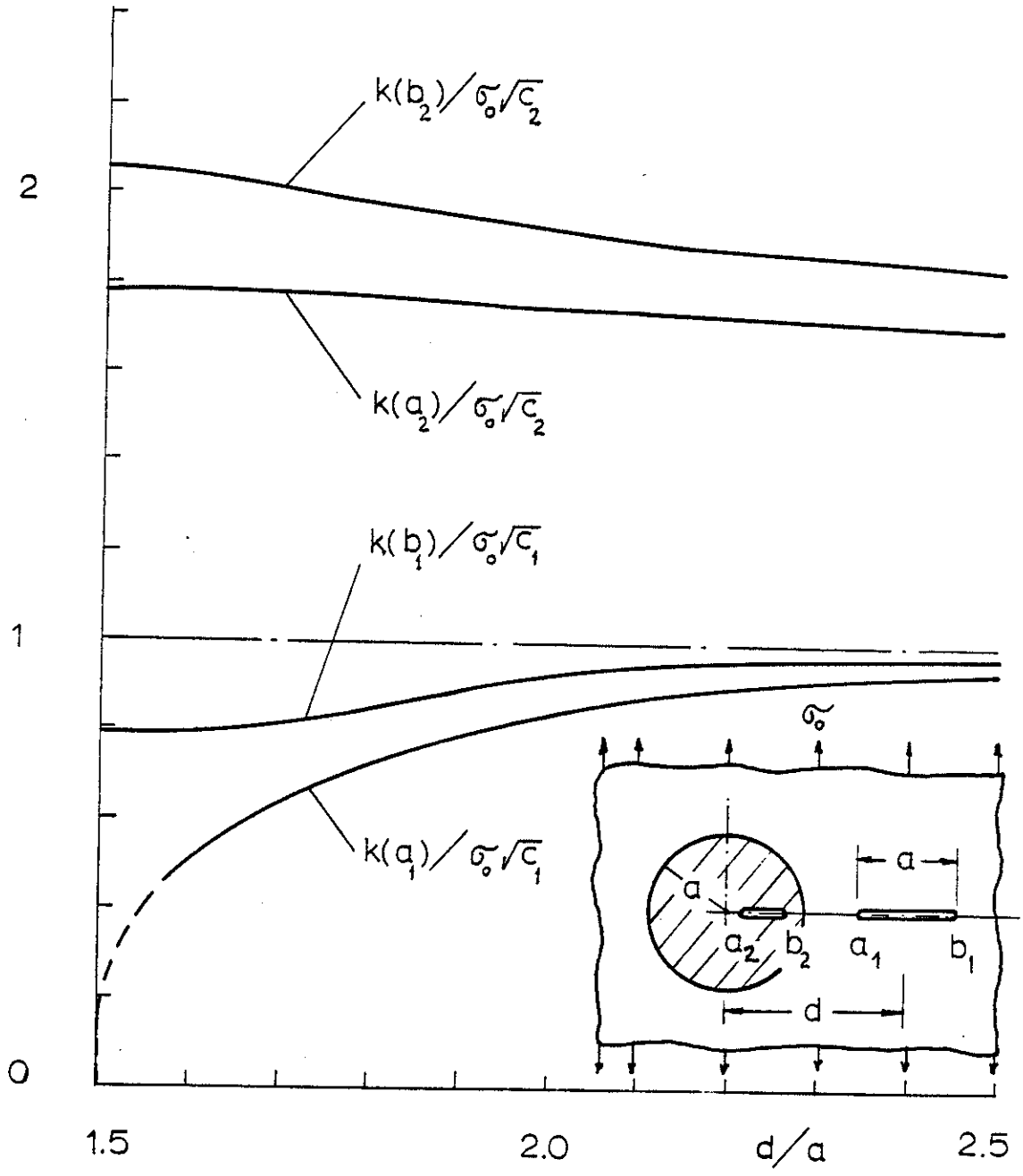

Figure 18. Stress intensity factors for a crack in the matrix (epoxy) and a crack in the inclusion (aluminum) ($\kappa_1 = 1.6$, $\kappa_2 = 1.8$, $\mu_2/\mu_1 = 23.077$; $a_2 = 0.3a$, $b_2 = 0.8a$, $2c_1 = (b_1 - a_1) = a$ fixed, $d = (b_1 + a_1)/2$ variable).

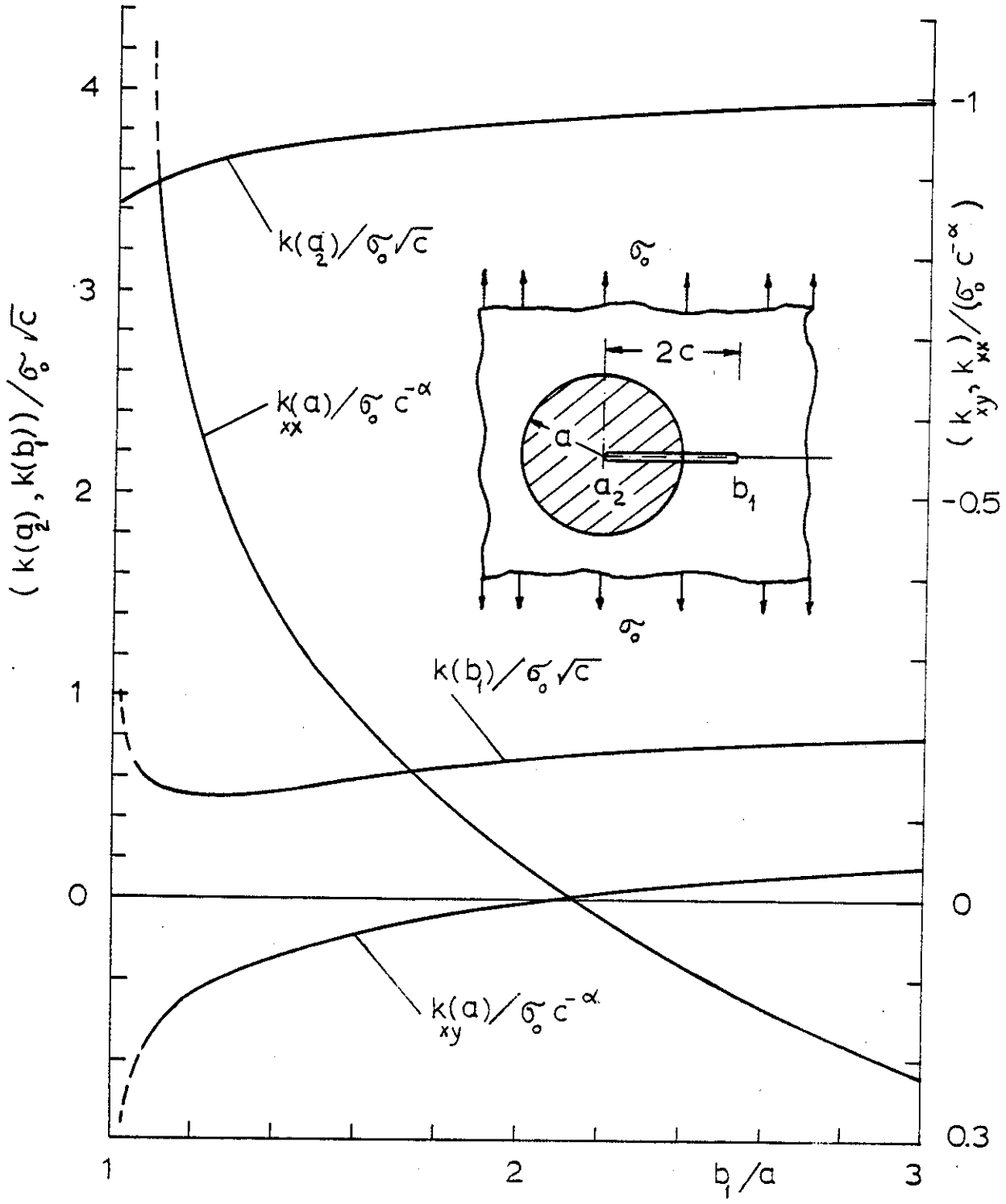

Figure 19. Stress intensity factors for a crack going through the matrix-inclusion interface ($\kappa_1 = 1.6$, $\kappa_2 = 1.8$, $\mu_2/\mu_1 = 23.077$, $\alpha' = \beta' = -0.5$, $\alpha = \beta = 0.27326$, $c = (b_1 - a_2)/2$, $a_2 = 0$ fixed, b_1 variable).

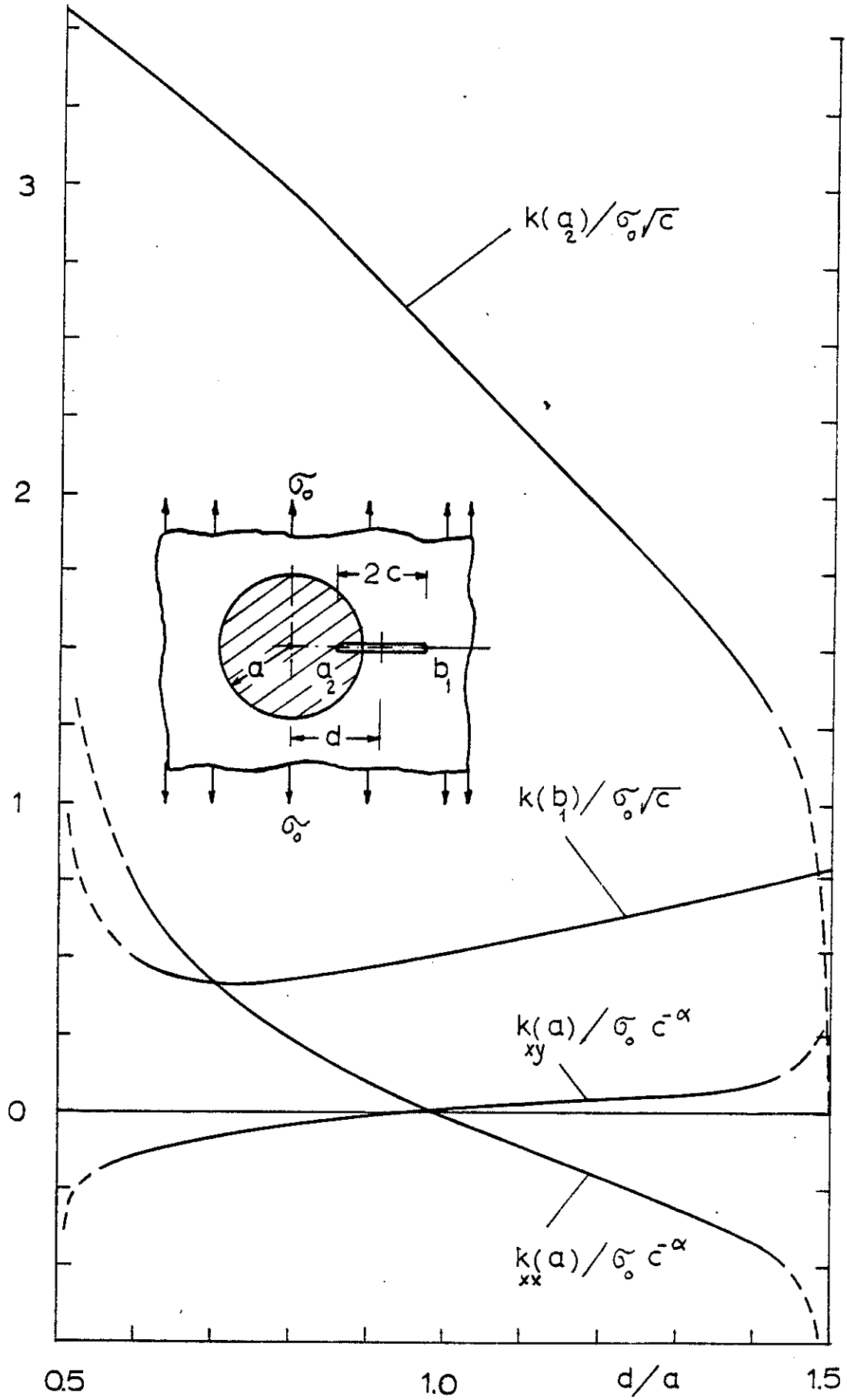

Figure 20. Stress intensity factors for a crack going through the interface ($\kappa_1 = 1.6$, $\kappa_2 = 1.8$, $\mu_2/\mu_1 = 23.077$, $\gamma = \alpha = \beta = 0.27326$, $2c = (b_1 - a_2) = a$ fixed, $d = (b_1 + a_2)/2$ variable).

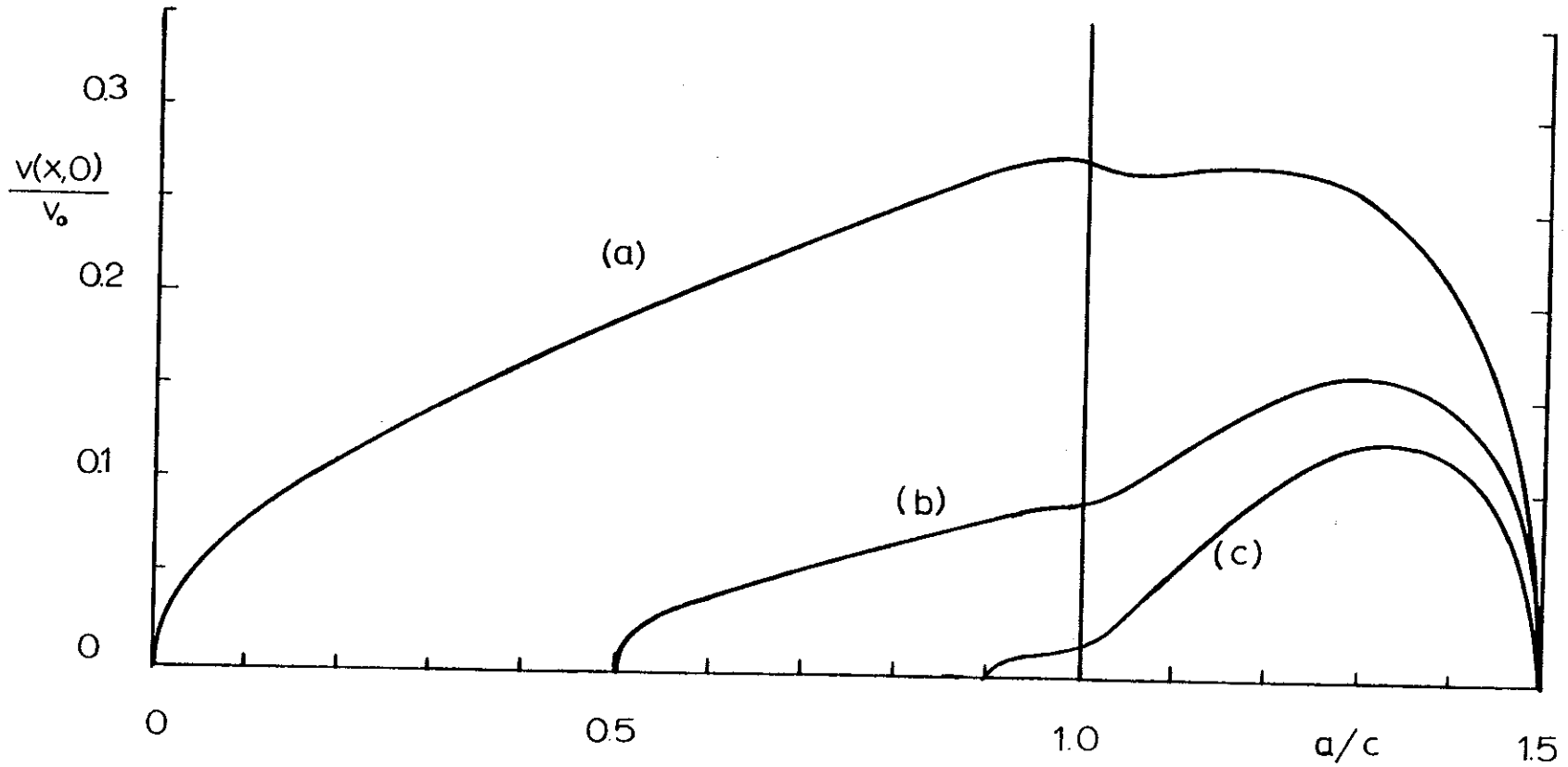

Figure 21. Crack surface displacement for cracks going through the interface ($\kappa_1 = 1.6$, $\kappa_2 = 1.8$, $\mu_2/\mu_1 = 23.077$, $v_0 = (1+\kappa_1)a\sigma_0/\mu_1$, $b_2 = a$ fixed, a_2 variable: (a) $a_2 = 0$, (b) $a_2 = a/2$, (c) $a_2 = 0.9a$).

The asymptotic trends in Fig. 20 can be explained by observing that $\gamma=\alpha=0.27326$ for the crack crossing the boundary ($a_2<b_2=a=a_1<b_1$), $\alpha=0.5$ for the crack tip embedded in the matrix, $\beta=0.33811$ for the crack in the matrix terminating at the boundary ($a_1=a$, $d/a=1.5$) and $\alpha=0.82580$ for the crack in the inclusion terminating at the boundary ($b_2=a$, $d/a = 0.5$).

Figure 21 shows some sample results for the crack surface displacements of a crack crossing the boundary.

For a crack terminating at the boundary to study the further crack propagation the details of the angular variation of the stresses, that is the functions $f_{ij}(\theta)$ in (21) may be needed. Sample results giving the distribution of these functions are shown in Figures 22-24. From the definitions (12), (13) and (21) we note that $f_{\theta\theta}(0) = 1$. The functions G_{ij} shown in Figures 22-24 are obtained from

$$\sigma_{ij}(r,\theta) \cong \frac{G_{ij}(\theta)}{\sqrt{2}\, r^{\alpha}} \quad , \quad (i,j=r,\theta),\ (-\pi<\theta<\pi). \tag{25}$$

Thus, $G_{\theta\theta}(0) = k(a)$ and $f_{ij}(\theta)$ is given by

$$f_{ij}(\theta) = \frac{G_{ij}(\theta)}{G_{\theta\theta}(0)} \ , \ (i,j=r,\theta) \ , \ (-\pi<\theta<\pi) \quad . \tag{26}$$

The analytical details of a crack terminating at and crossing the boundary in a two-phase nonhomogeneous elastic medium may be found in [14] and [15].

3.2 Anti-Plane Shear Problem for a Crack Interacting with a Circular Inclusion

The simpler problem for a medium containing a crack and a circular elastic inclusion or a hole shown in Fig. 4 and subjected to a uniform anti-plane shear loading

$$\sigma_{yz}(x, \mp \infty) = p_o \tag{27}$$

can also be treated in a manner similar to the plane strain problem

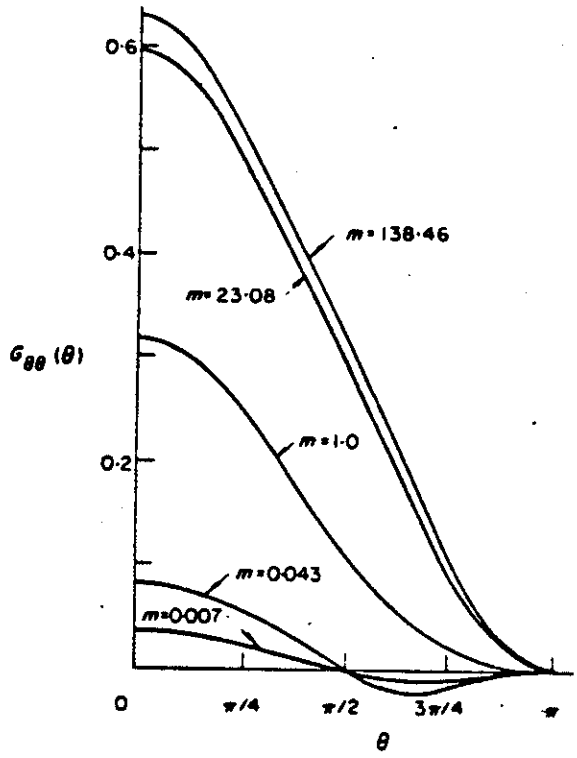

Fig. 22. Angular variation of $\sigma_{\theta\theta}$ around a crack tip touching the interface.

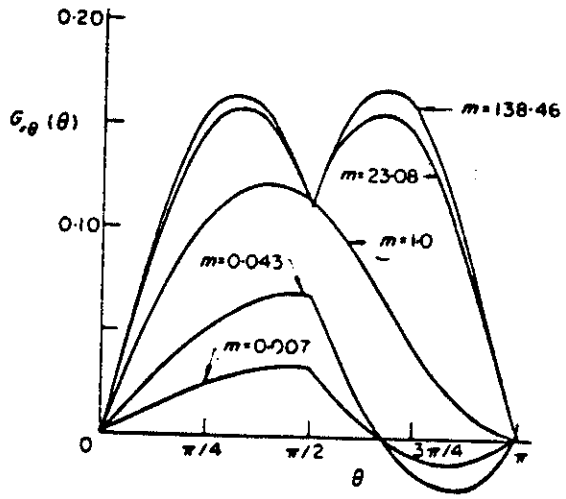

Fig. 23. Angular variation of $\sigma_{r\theta}$ around a crack tip touching the interface.

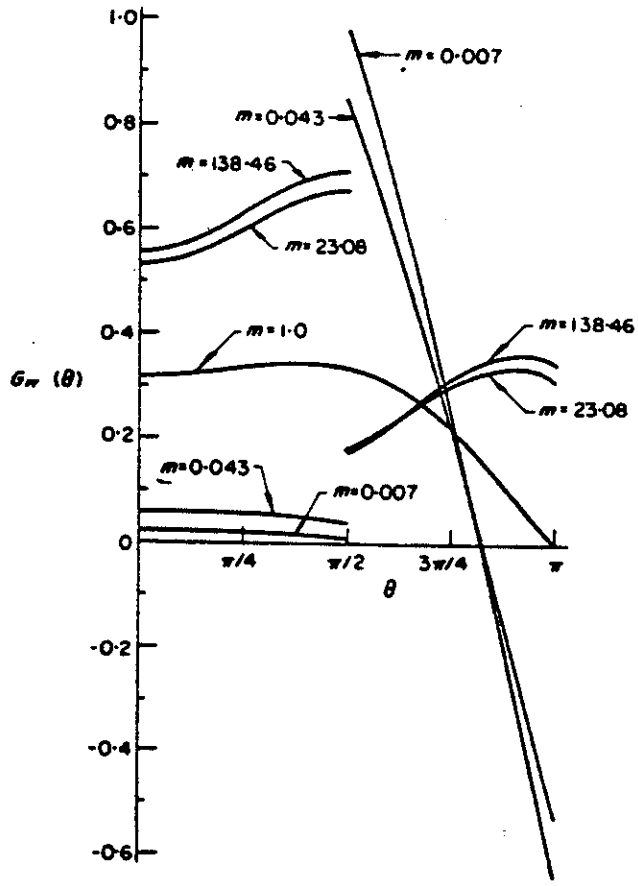

Fig. 24. Angular variation of σ_{rr} around a crack tip touching the interface.

discussed in the previous section. In this case the crack surface tractions for the perturbation problem are obtained by solving the problem of inclusion or hole without a crack. Some sample results giving the stress distribution $\sigma_{yz}(x,y)$ (for various fixed values of y) are shown in Figures 25 and 26. Again note that qualitatively these results are very similar to the plane strain results shown in figures 2 and 5. For this problem some sample results giving the Mode III stress intensity factors k_3 at the crack tips $x = \mp a$ are defined by

$$k(a)p_0\sqrt{a} = k_3(a) = \lim_{x\to a} \sqrt{2(x-a)}\, \sigma_{1yz}(x,c) \ , \tag{28}$$

$$k(-a)p_0\sqrt{a} = k_3(-a) = \lim_{x\to -a} \sqrt{2(x+a)}\, \sigma_{1yz}(x,c) \ . \tag{29}$$

Figure 27 shows the results for the radial crack in a medium containing an inclusion or a hole. Similar results for an arbitrarily located crack are shown in Figures 28 and 29. Figure 30 gives some comparative results showing the influence of the crack length-to-radius ratio on the stress intensity factors where m is the modulus ratio $m = \mu_2/\mu_1$ and $k(\mp a) = k_3(\mp a)/p_0\sqrt{R}$. For $m = 1$ we have a homogeneous plane with a crack of length 2a for which $k_3(\mp a) = p_0\sqrt{a}$. Consequently

$$k(\mp a) = \frac{k_3(\mp a)}{p_0\sqrt{R}} = \frac{p_0\sqrt{a}}{p_0\sqrt{R}} = \sqrt{a/R} \ , \tag{30}$$

giving the straight line shown in the figure. For m=0, m=1 and m=23.3 the slopes of $k(\mp a)$ vs. $\sqrt{a/R}$ curves as $(a/R)\to 0$ are 1.47, 1 and 0.57, respectively. The results for m=0 and m>0 are obtained from the solution of an "infinite" plane with a central crack subjected to the crack surface tractions $\sigma_{yz}(x,0)$ which are equal and opposite to the corresponding stresses given in figures 25 and 26 at x=b=1.5R.

The singular behavior of the stresses terminating at and crossing the boundary is discussed in [16] and [17].

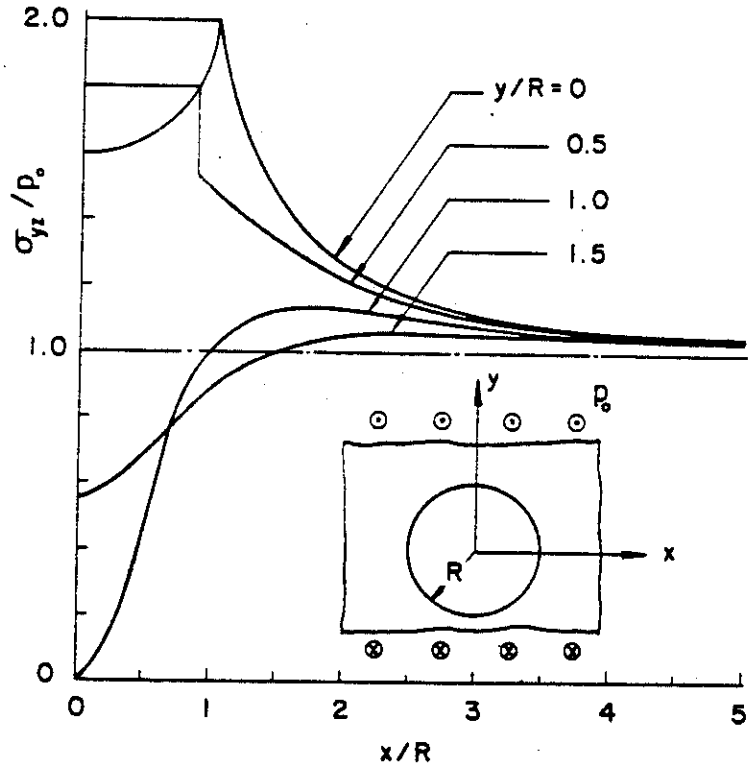

Fig. 25. The shear stress τ_{yz} in a matrix with a circular hole.

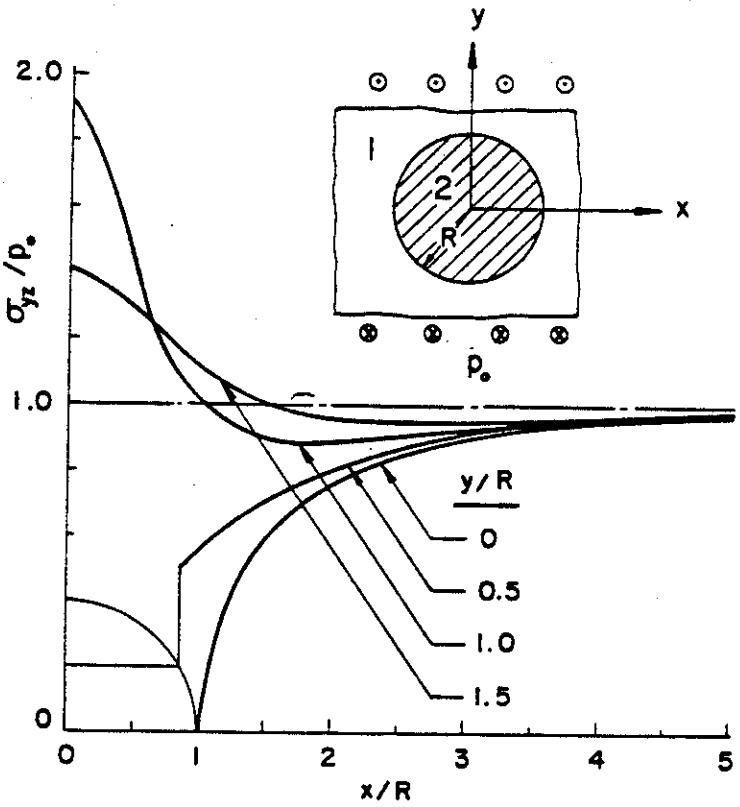

Fig. 26. The shear stress τ_{yz} in a matrix with a circular inclusion ($\mu_2 = 23.3\ \mu_1$).

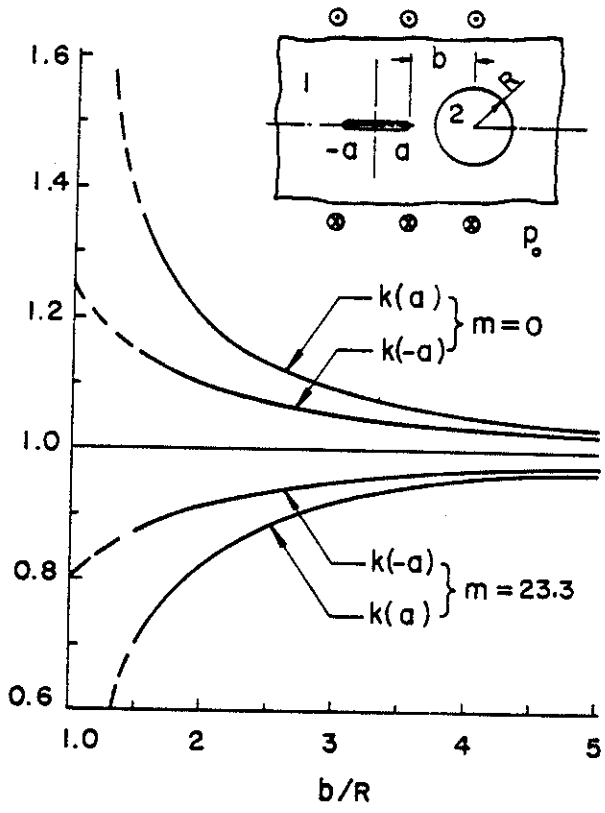

Fig. 27. Stress intensity factors for the antiplane shear problem ($k = k_3/p_o\sqrt{a}$, $R = a$).

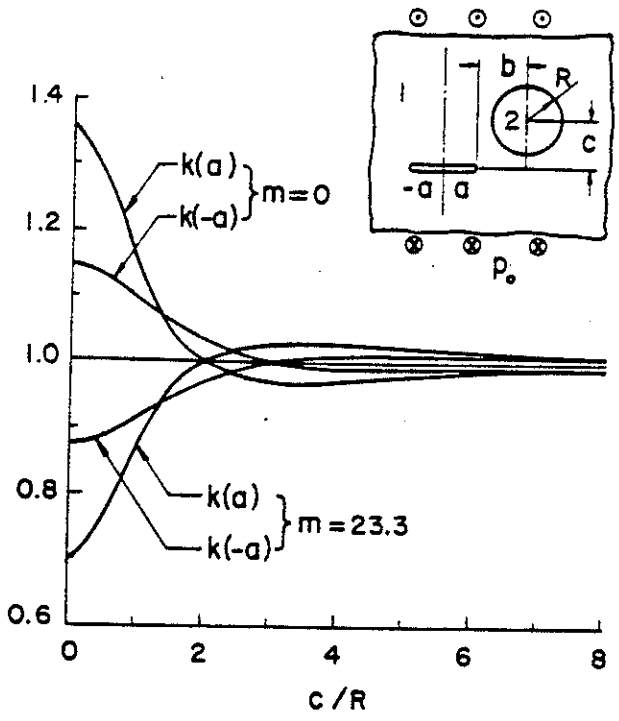

Fig. 28. Stress intensity factors for the antiplane shear problem ($k=k_3/p_o\sqrt{a}$, R=a, b=1.5R).

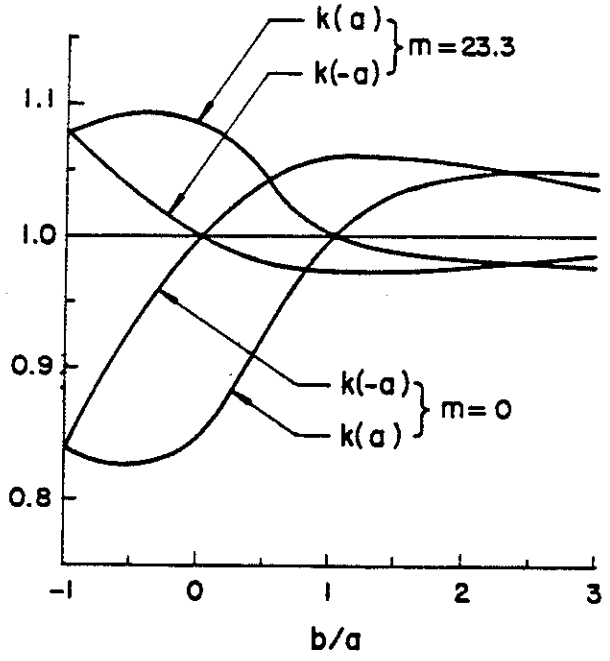

Fig. 29. Stress intensity factors for the antiplane shear problem ($k=k_3/p_o\sqrt{a}$, R=a, c=1.5R).

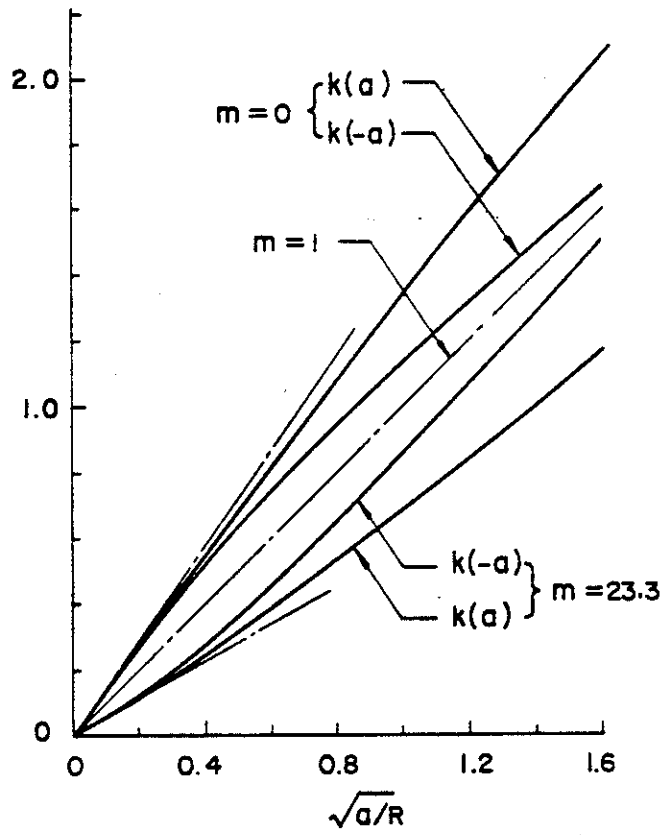

Fig. 30. Stress intensity factors for the antiplane shear problem ($k=k_3/p_0\sqrt{R}$, c=0, b=1.5R).

4. INTERACTION BETWEEN CRACKS

In this section the problem of interaction between cracks on the surface and inside a plate with finite thickness is considered.

4.1 Interaction Between Parallel Internal Cracks

The basic geometry of the problem is shown in Fig. 31. In this section we will consider various special cases relating two or three cracks on the surface of a plate under uniform tension.

For two symmetrically located parallel cracks the stress intensity factors are given in Table 3. Referring to Fig. 31, for this problem we have a=b (i.e., no crack on x axis) c = H-d, P = 0 (no concentrated force) 2B is the distance between the cracks, 2ℓ is the crack length and $\sigma_{yy} = \sigma_0$ for $y \to \mp\infty$. In this section too the Modes I and II stress intensity factors k_1 and k_2 are defined by

$$k_1 = \lim_{r\to 0} \sqrt{2r}\, \sigma_{yy}(r,0) \ , \quad k_2 = \lim_{r\to 0} \sqrt{2r}\, \sigma_{xy}(r,0) \ , \tag{31}$$

where r,ϕ are the polar coordinates at the crack tip, the crack being along $\phi = \pi$. Note that as the distance 2B between the cracks decreases k_1 also decreases and k_2 becomes more significant. The angle θ shown in this table is an (approximate) direction of a probable crack growth which is obtained from a simple assumption that along this radial line at the crack tip the cleavage stress $\sigma_{\theta\theta}(r,\theta)$ is maximum [12], where $r<<H-d$. Here $\theta>0$ indicates that the cracks would grow away from each other.

4.2 Interaction Between Parallel Surface Cracks

The stress intensity factors and the angle of probable crack growth direction in a plate containing two parallel and equal surface cracks under uniform tension or pure bending are shown in Figures 32-35. In this problem we have a=b, c=0 and d<H. The figures also show the Mode I

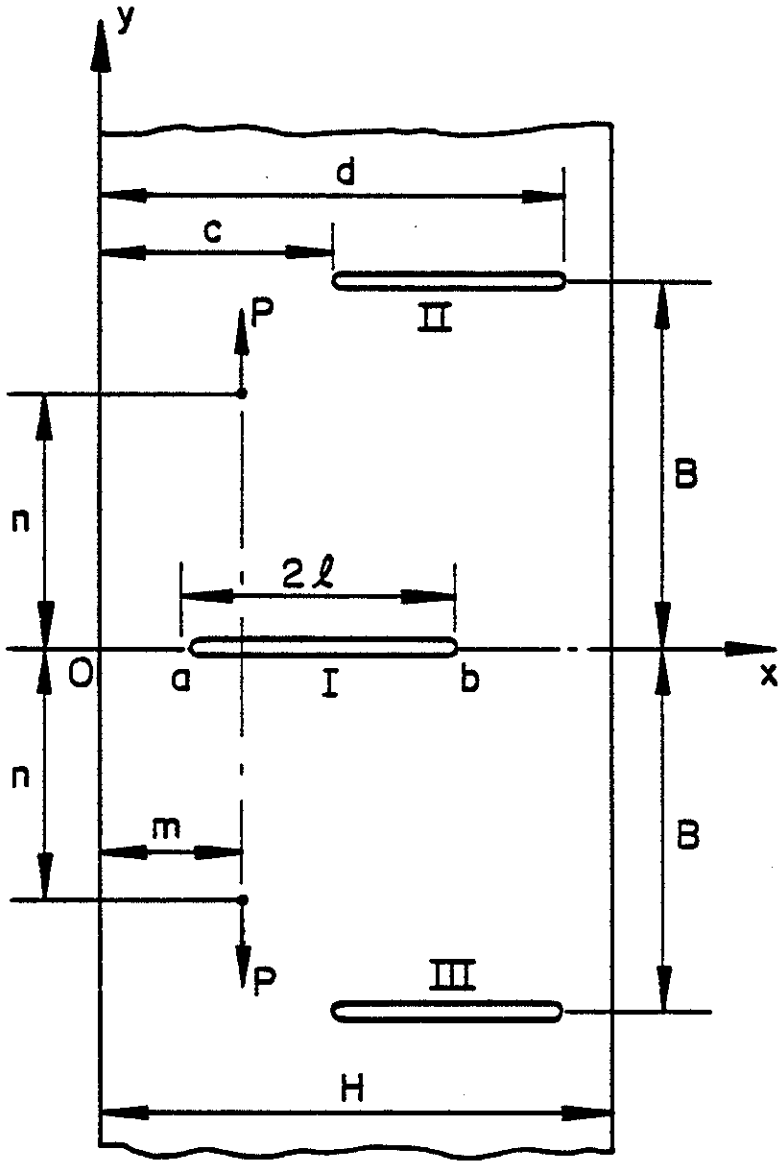

Figure 31. The basic crack geometry.

Table 3. Stress intensity factors in a strip containing two symmetric internal cracks, $\ell=(d-c)/2$.

ℓ/H	B/ℓ	$k_1/\sigma_0\sqrt{\ell}$	$k_2/\sigma_0\sqrt{\ell}$	$\theta(°)$
0.05	0.5	0.7797	-0.1175	16.430
	1.0	0.8512	-0.0616	8.194
	1.5	0.9052	-0.0308	3.887
	2.0	0.9395	-0.0163	1.992
	5.0	0.9953	-0.0001	0.157
	10.0	1.0053	-0.00001	0.014
	20.0	1.0060	0.0000	0.000
0.1	0.5	0.7992	-0.1199	16.363
	1.0	0.8749	-0.0624	8.076
	1.5	0.9310	-0.0307	3.774
	2.0	0.9660	-0.0162	1.920
	5.0	1.0219	-0.0001	0.106
	10.0	1.0247	-0.00001	0.003
	20.0	1.0248	0.0000	0.000
0.2	0.5	0.8846	-0.2570	15.578
	1.0	0.9749	-0.0656	7.634
	1.5	1.0437	-0.0330	3.648
	2.0	1.0839	-0.0155	1.641
	5.0	1.1096	-0.0001	0.019
	10.0	1.1097	0.0000	0.000

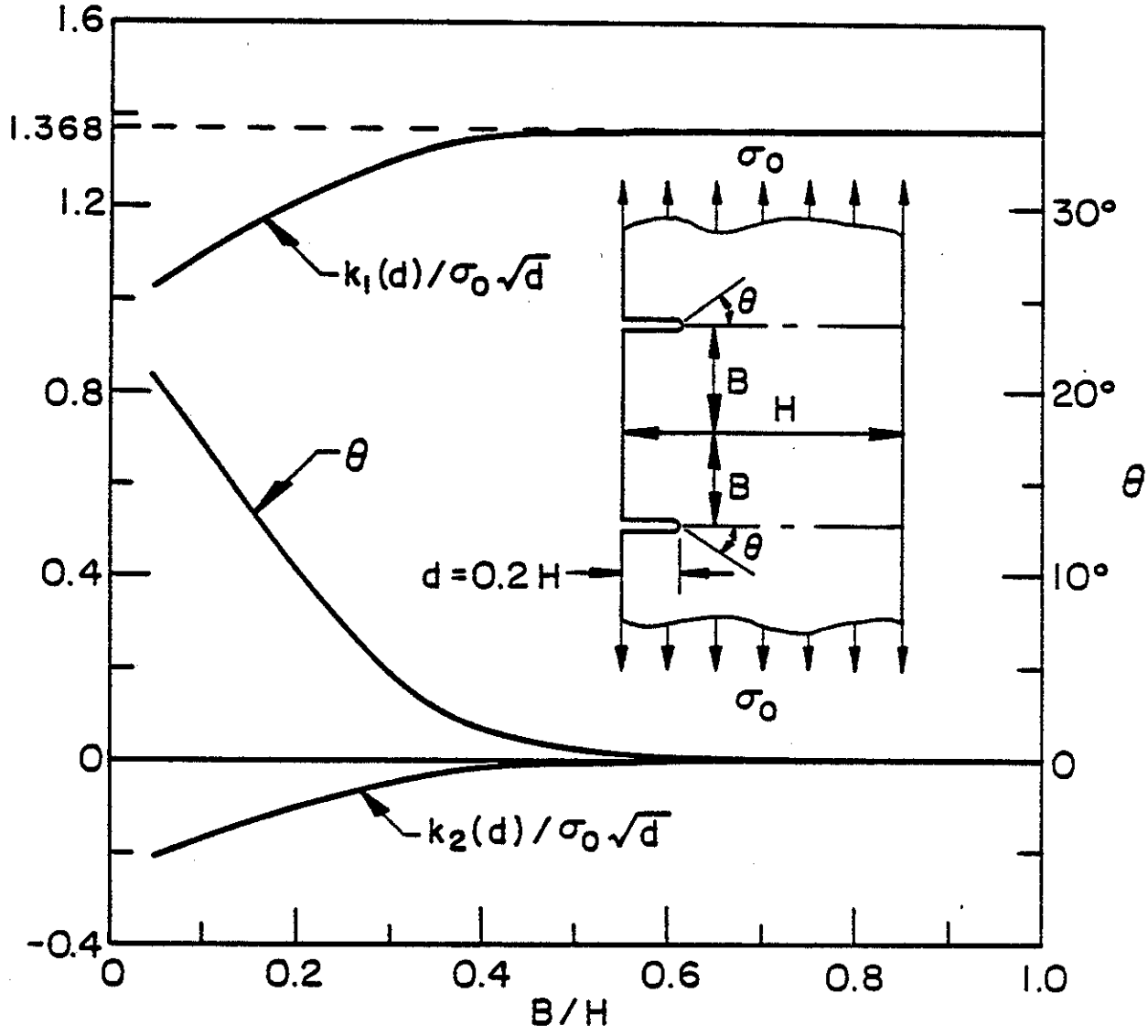

Figure 32. Stress intensity factors and probable crack propagation angle in an infinite strip containing two edge cracks under uniform tension, d=0.2H.

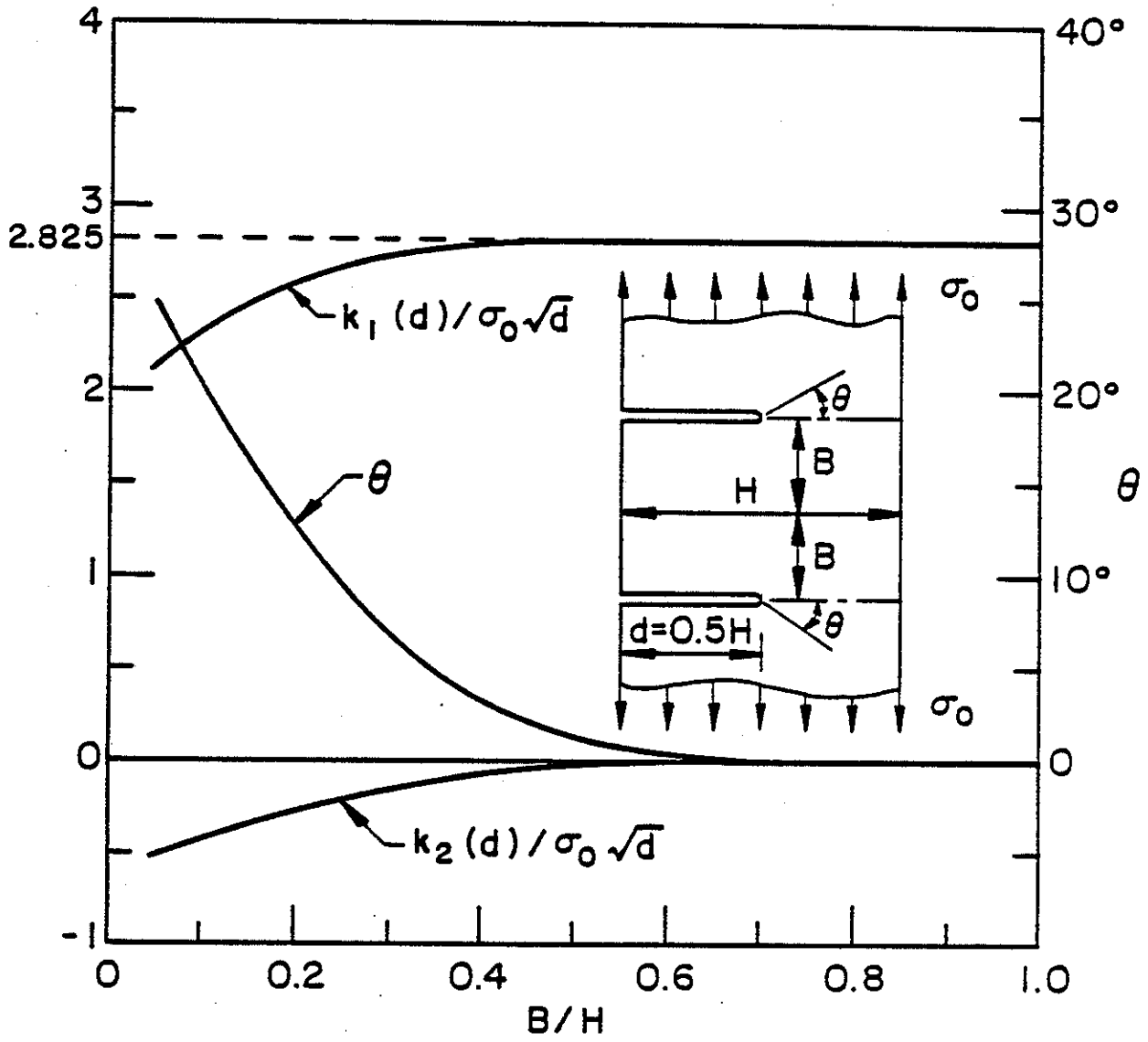

Figure 33. Same as Figure 2, d=0.5H.

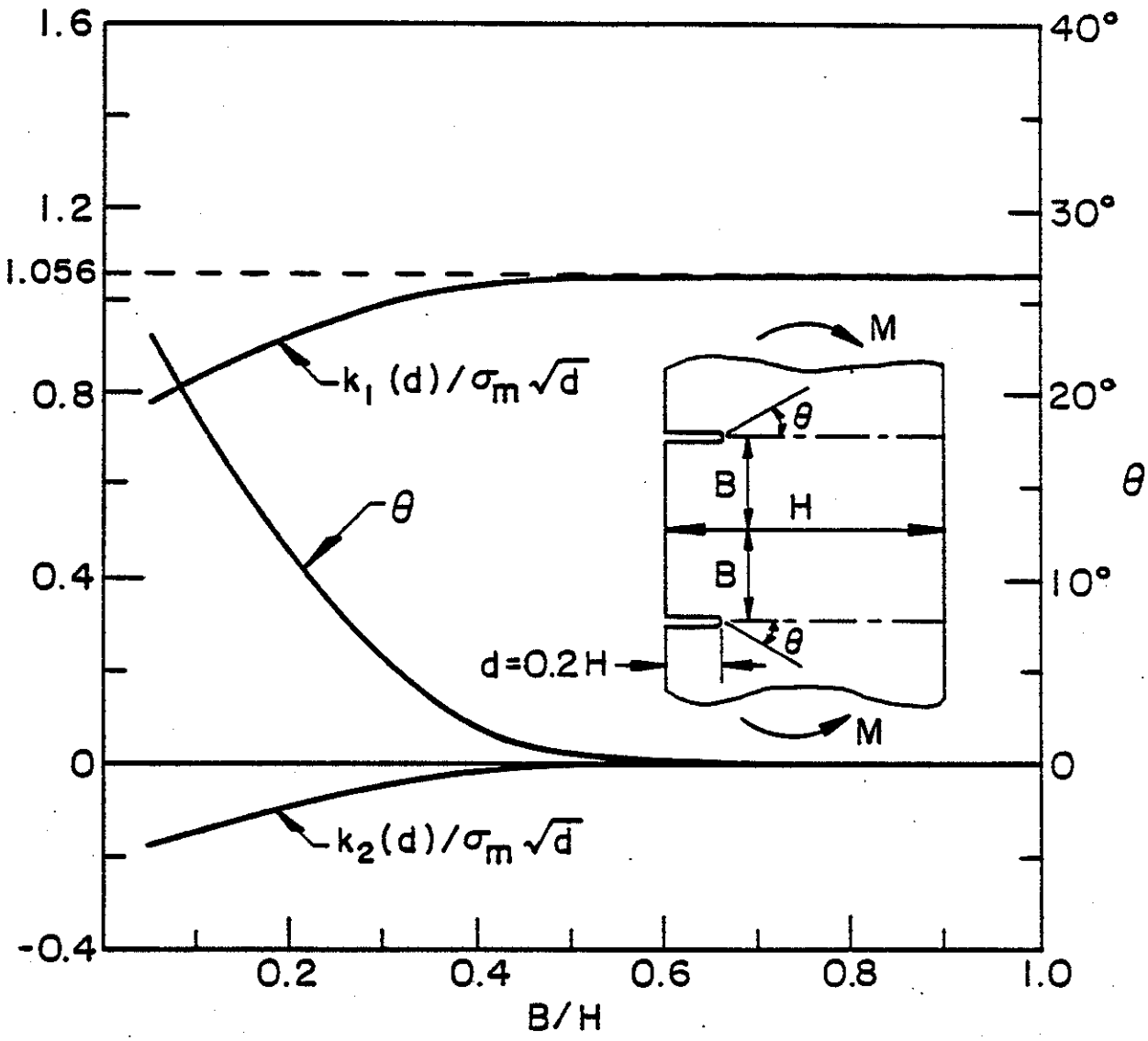

Figure 34. Stress intensity factors and probable crack propagation angle in an infinite strip with two edge cracks under bending, d=0.2H.

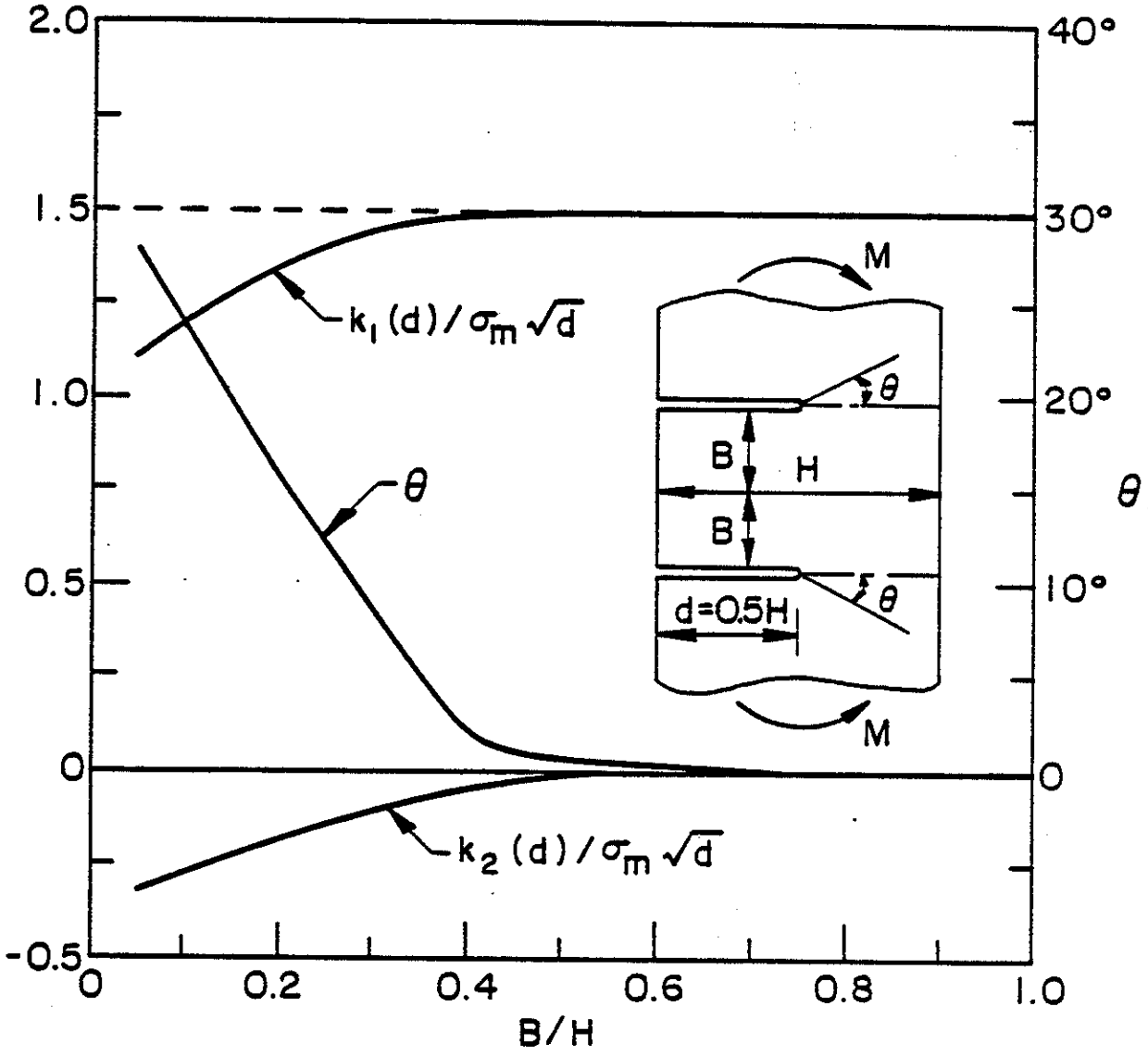

Figure 35. Same as Figure 4, d=0.5H.

stress intensity factor k_1 for a single surface crack for comparison (the dashed line). For the single crack k_2 is 0. Again note that k_1 is smaller than the corresponding single crack value, k_2 becomes more significant as B decreases, and cracks would tend to propagate away from each other. For the bending problem shown in Figures 34 and 35 the normalizing stress σ_m is given by

$$\sigma_m = \frac{6M}{H^2} \tag{32}$$

where M is the moment for unit thickness.

Figures 36-41 show the results for a plate containing three parallel surface cracks under uniform tension or bending. In this case, too, $k_2<0$, meaning that the outside cracks would grow away from the middle crack. Comparison of the two and three crack results shows that the introduction of the middle crack "relaxes" the stress intensity factors in the outer cracks. Fig. 40 shows that for short cracks the interaction and for longer cracks the back surface effect would dominate. Figure 41 shows the results for three point bending. In this problem, too, σ_m is the surface stress in the plate under bending, namely

$$\sigma_m = \frac{6M}{H} = \frac{24P}{H} \quad . \tag{33}$$

The stress intensity factor k(d) for the outer cracks approaches zero as $B \to 4H$ (for which the moment is zero).

4.3 Cracks Parallel to the Boundary

The basic geometry for the plate containing a crack parallel to the boundary is shown by the insert in Fig. 42. The problem considered in this section also takes into account the material orthotropy. Thus, the material constants shown in Fig. 42 are related to the elastic constants of an orthotropic plate as follows:

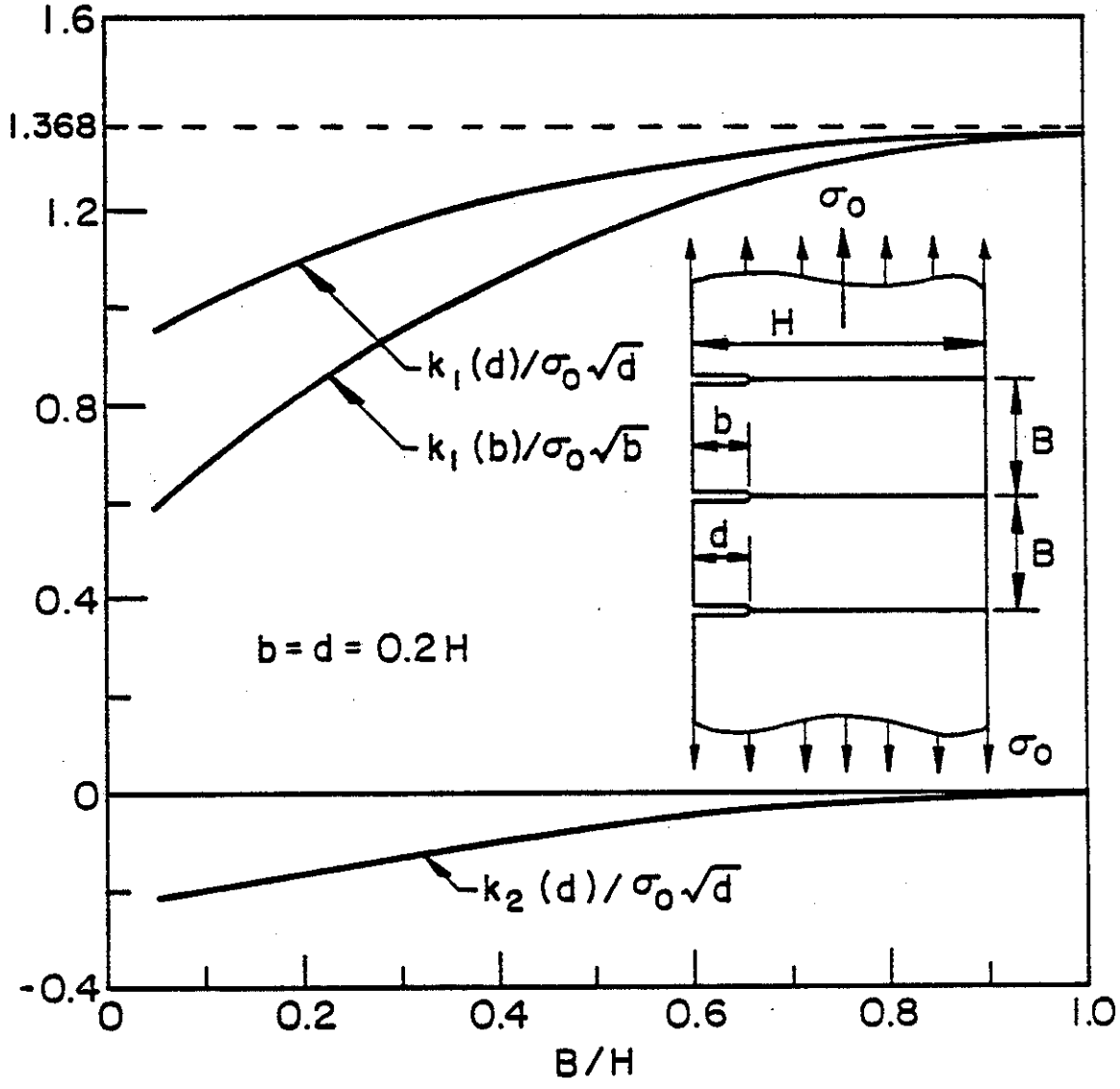

Figure 36. Stress intensity factors in an infinite strip containing three edge cracks under uniform tension, d=b=0.2H.

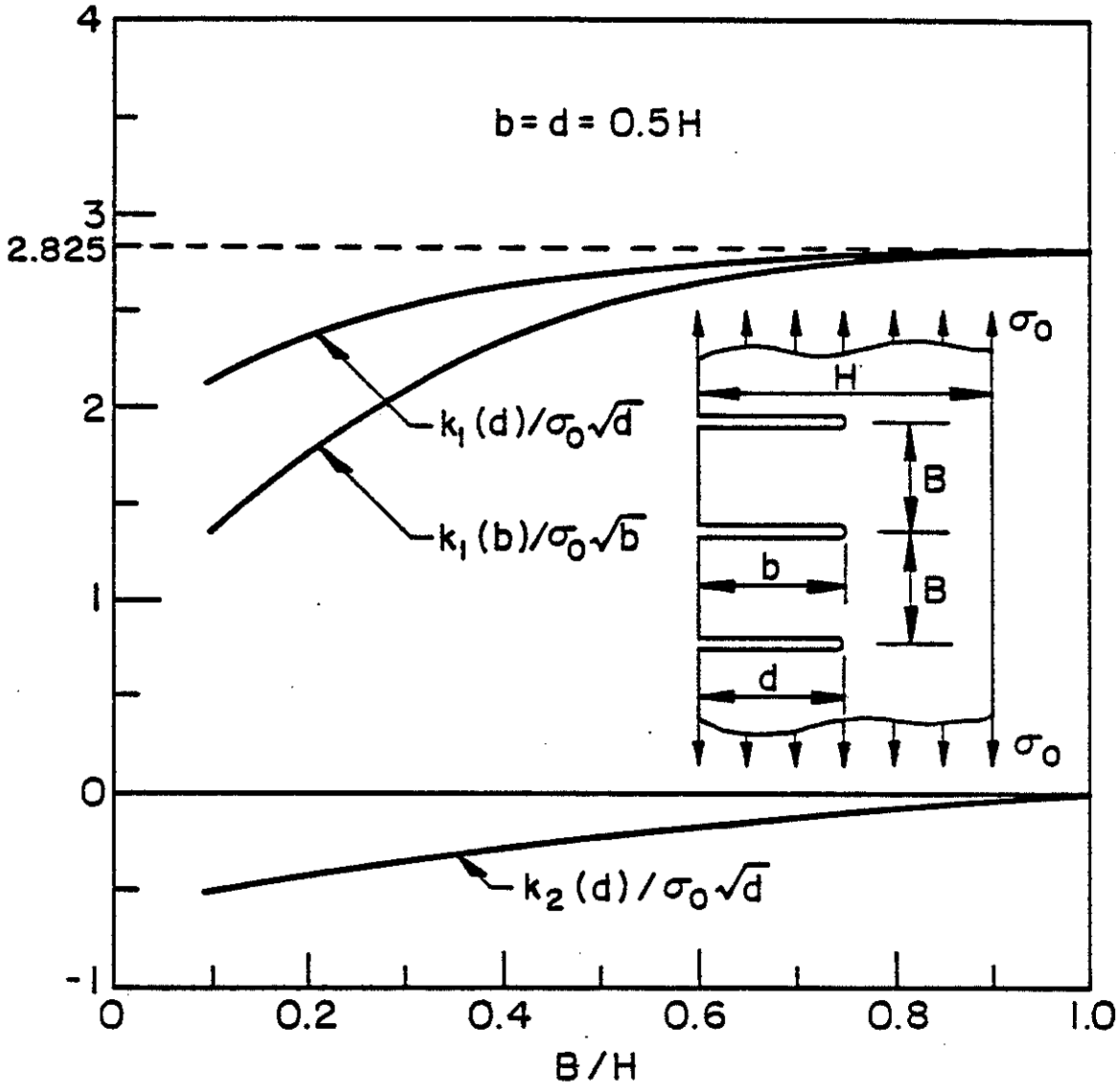

Figure 37. Same as Figure 6, d=b=0.5H.

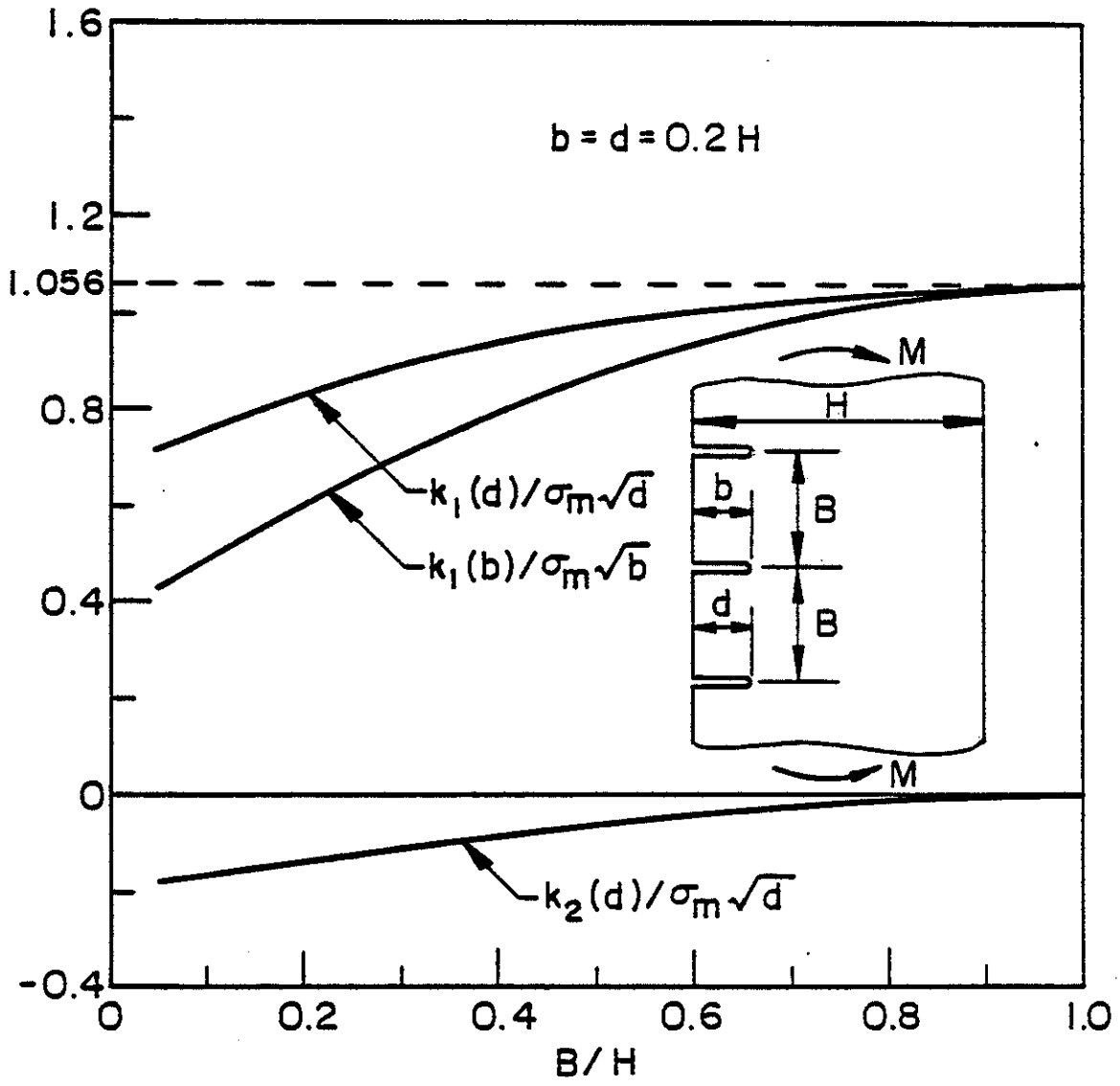

Figure 38. Stress intensity factors in an infinite strip containing three edge cracks under bending, d=b=0.2H, $\sigma_m=6M/H^2$.

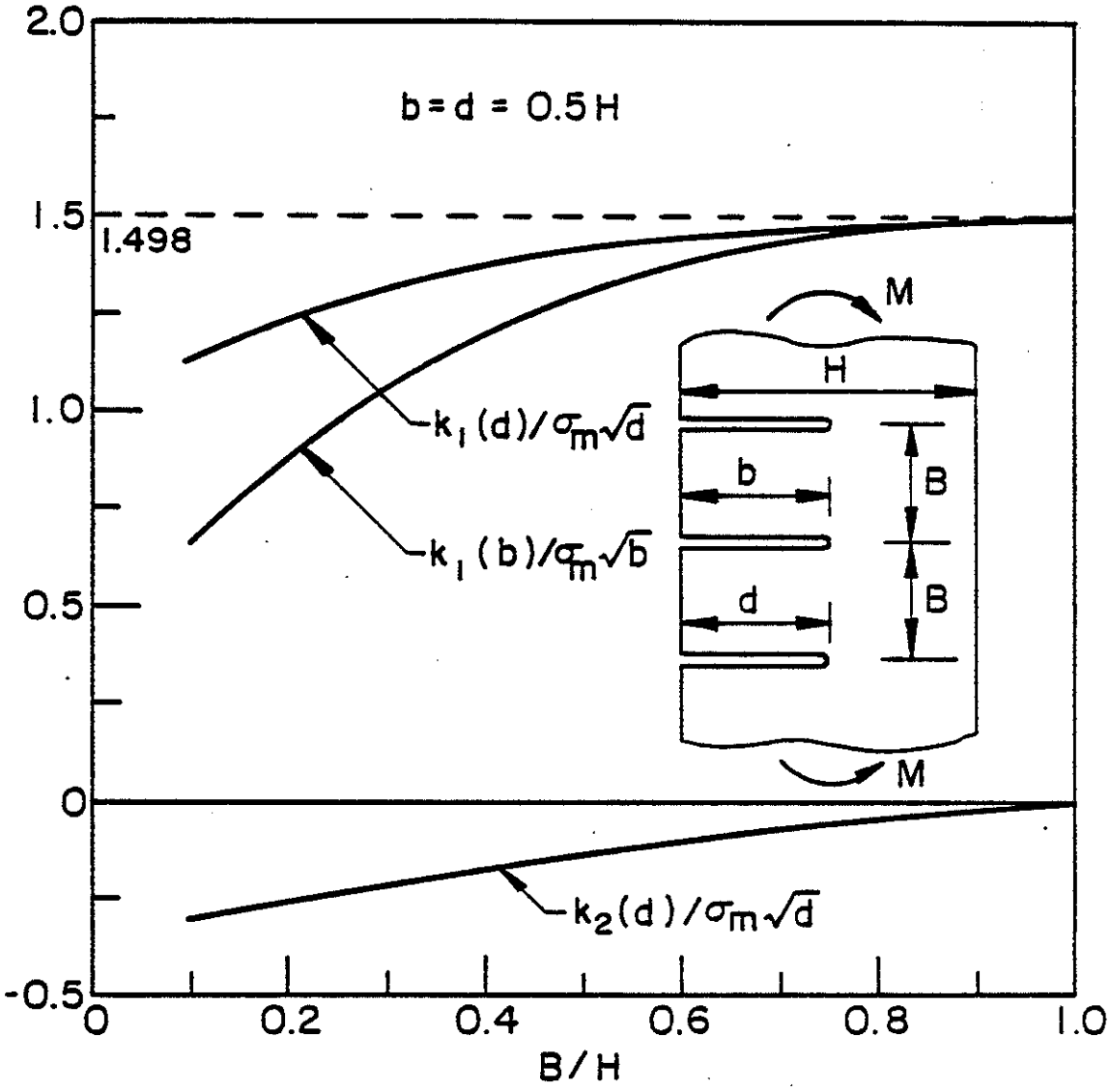

Figure 39. Same as Figure 8, d=b=0.5H, $\sigma_m=6M/H^2$.

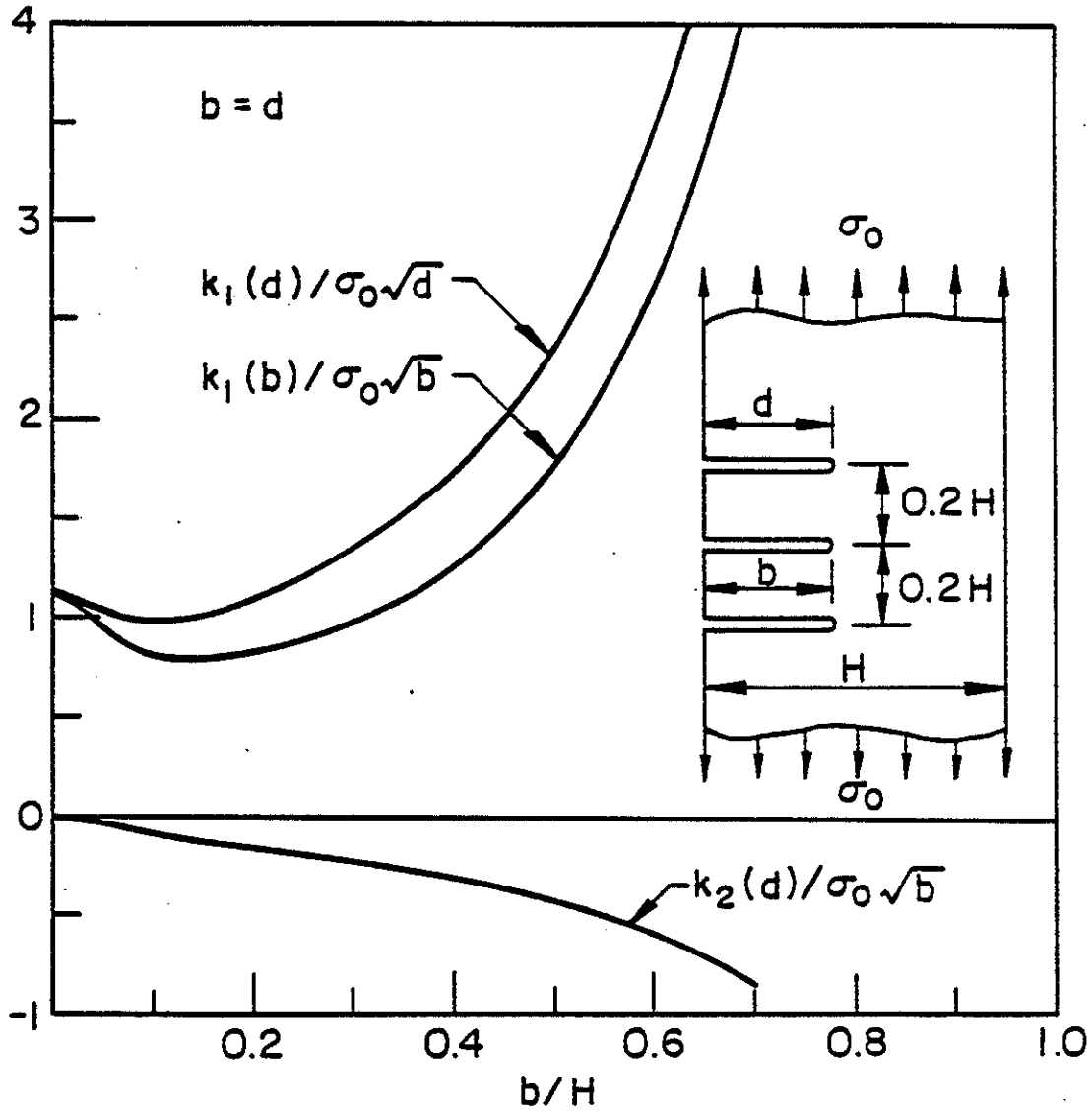

Figure 40. The effect of the crack depth on the stress intensity factors in an infinite strip under tension, B=0.2H.

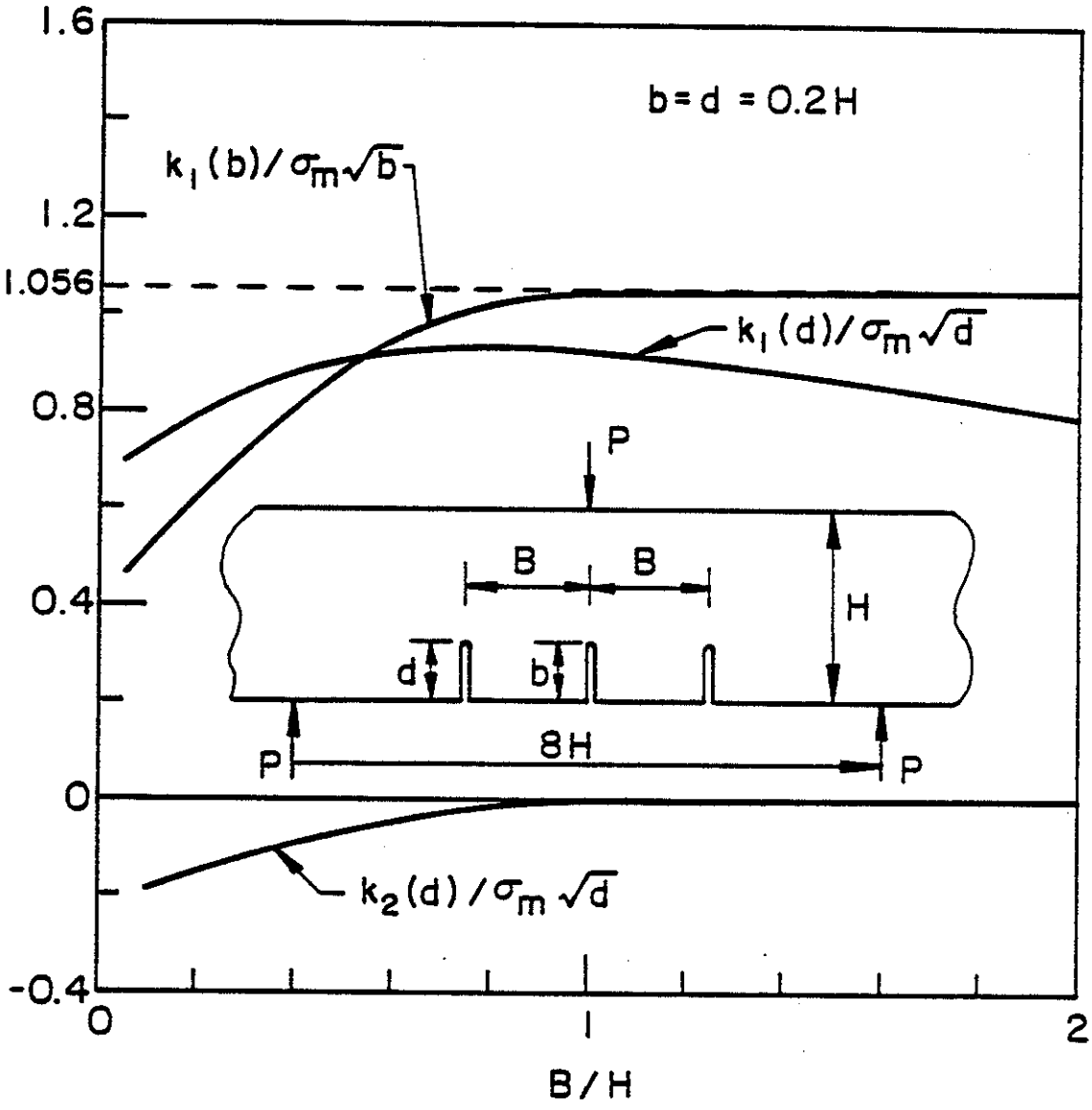

Figure 41. Stress intensity factors in an infinite strip containing edge cracks and subjected to three point bending, $\sigma_m = 6M/H^2 = 24P/H$.

$$\delta^4 = E_{11}/E_{22} \quad , \quad \kappa = \frac{\sqrt{E_{11}E_{22}}}{2G_{12}} - \sqrt{\nu_{12}\nu_{21}} \quad . \tag{34}$$

The engineering material constants which appear in (34) are defined by the following stress-strain relations

$$\begin{aligned} \varepsilon_{11} &= \frac{1}{E_{11}} (\sigma_{11} - \nu_{12}\sigma_{22} - \nu_{13}\sigma_{33}) \ , \ \cdots \\ 2\varepsilon_{12} &= \frac{1}{G_{12}} \sigma_{12} \ , \ \cdots \end{aligned} \tag{35}$$

In Fig. 42 and the subsequent figures the coordinate axes 1 and 2 are respectively parallel and are perpendicular to the crack. The main result of Fig. 42 is that as the crack approaches the boundary the stress intensity factors become unbounded. Also, the analysis of the mixed mode stress state at the crack tip would indicate that the direction along which the cleavage stress is maximum is inclined toward the nearest boundary, meaning that any further propagation of the crack would be toward the nearest boundary. The corresponding results for a crack loaded under pure shear are shown in Fig. 43. The peculiarity of these results is that the Mode II stress intensity factor is relatively insensitive to the location of the crack, in fact it somewhat decreases as the crack approaches the boundary before becoming unbounded.

Figures 44 and 45 show the effect of the relative crack length for a symmetrically located crack under Modes I and II loading conditions.

The results for two collinear cracks loaded under Mode I conditions are shown in Fig. 46. The figure also shows the stress intensity factors for an infinite plate ($H=\infty$) which are given by

$$k_1(b) = p\sqrt{(b-a)/2} \left(\frac{2b}{b-a}\right)^{1/2} \left[1 - \frac{E(k)}{K(k)}\right]/k \tag{36}$$

$$k_1(a) = p\sqrt{(b-a)/2} \left(\frac{2b^2}{a(b-a)}\right)^{1/2} \left[\frac{E(k)}{K(k)} - \left(\frac{a}{b}\right)^2\right]/k \tag{37}$$

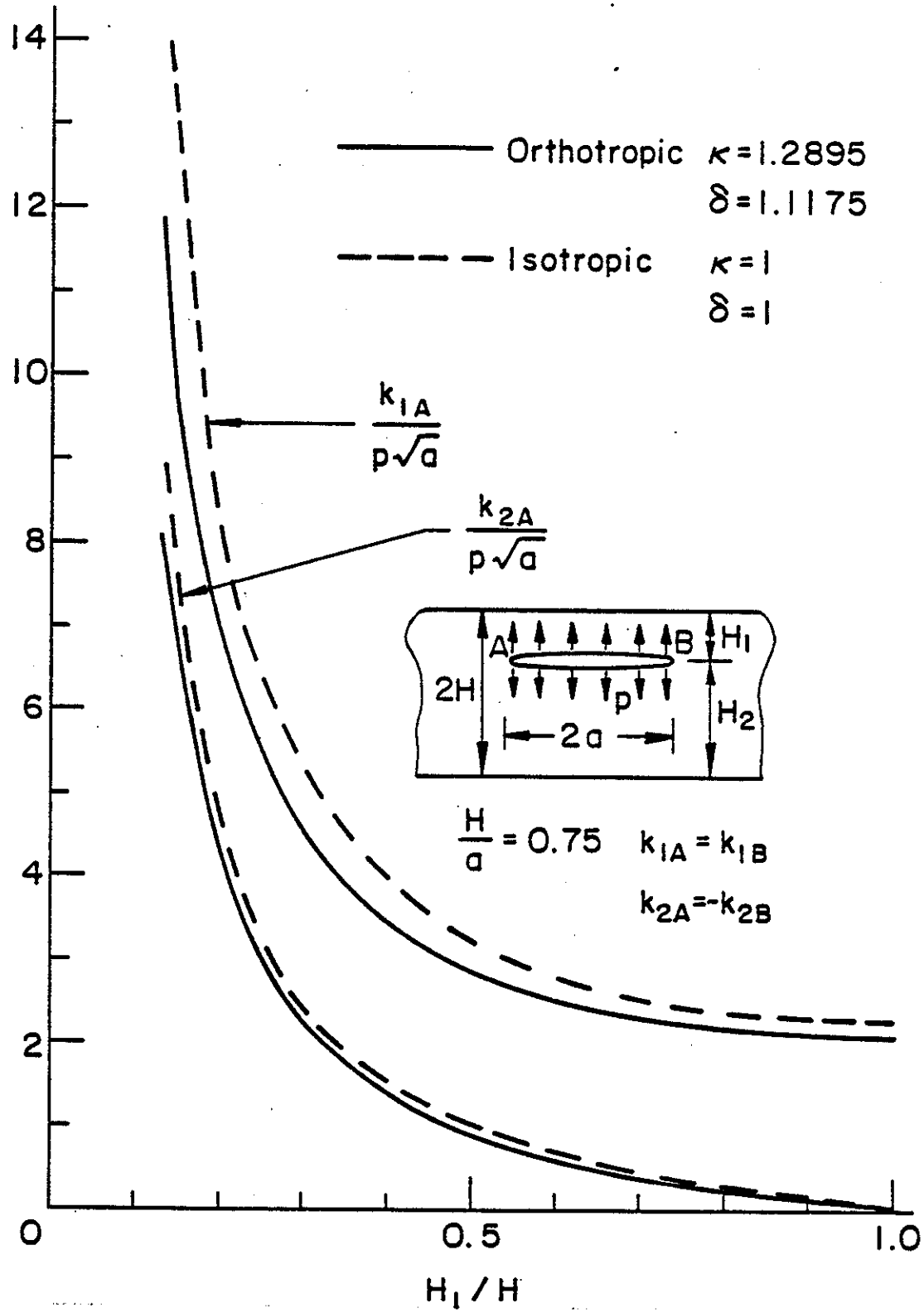

Figure 42. The effect of the crack location on the stress intensity factors for uniform surface pressure. $H = 0.75a$, $\delta = 1 = \kappa$ for the isotropic materials and $\delta = 1.1175$, $\kappa = 1.2895$ for the orthotropic material (yellow birch).

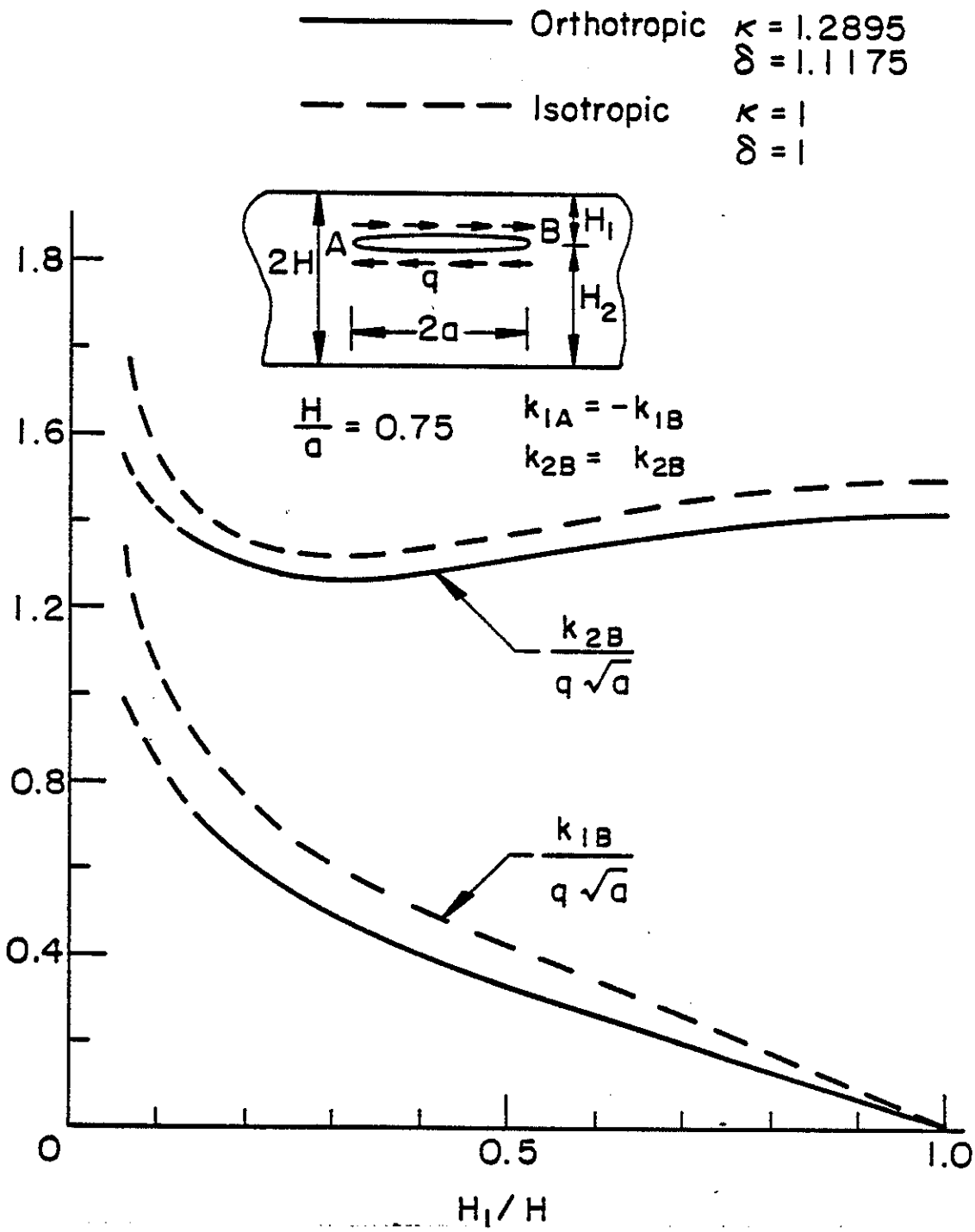

Figure 43. Same as figure 2 for uniform shear applied to the crack surface.

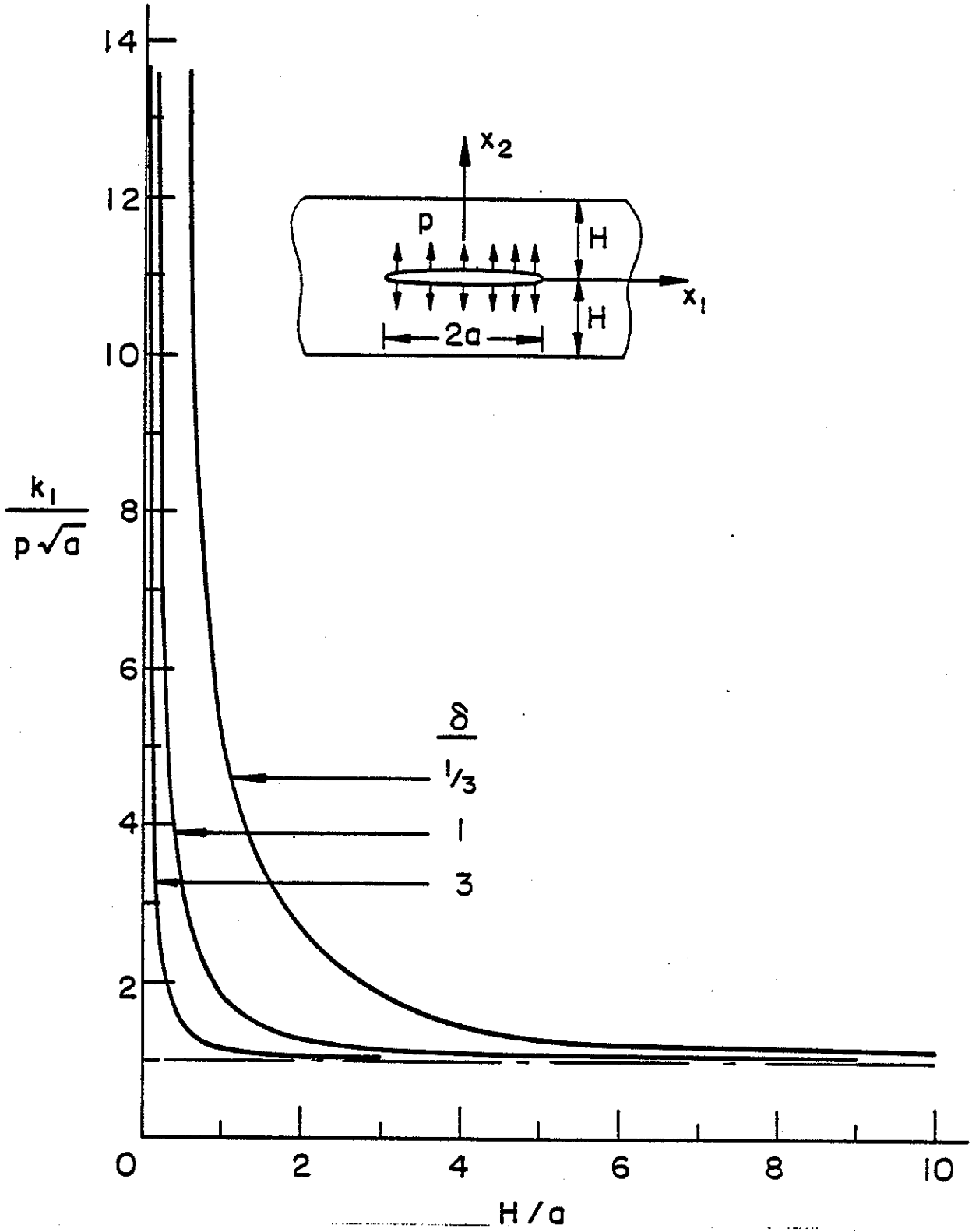

Figure 44. Effect of the crack length on the stress intensity factor for a symmetrically located crack under uniform pressure, $\kappa = 1$.

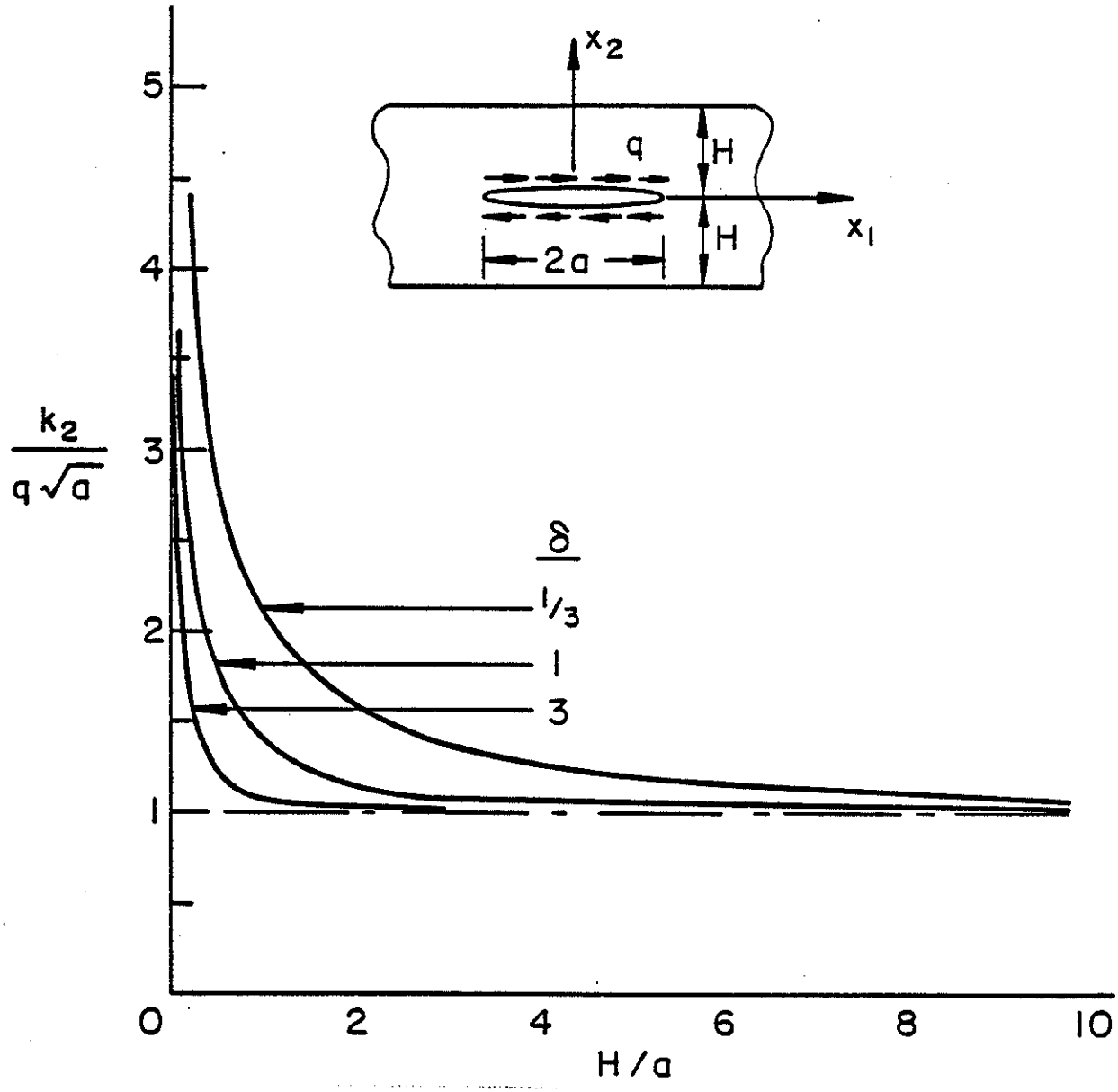

Figure 45. Same as figure 4 for uniform shear applied to crack surface.

where K(k) and E(k) are complete elliptic integrals of respectively first and second kind, and the modulus k is defined by

$$k = \sqrt{1-a^2/b^2} \quad . \tag{37}$$

For convenience a table giving the elliptic integrals (Table 4) is included in this report where the angle α is related to k by $\sin\alpha=k$.

Further results for collinear cracks under Mode II loading condition are given in Table 5. In these results the half crack length (b-a)/2 is used in normalizing stress intensity factor. (a/b) = 0 and (a/b) = 1 correspond to the two limiting cases of a single crack of length 2b and b-a, respectively. As expected $k_1(a)$ becomes unbounded for $a\to 0$ and both $k_1(a)$ and $k_1(b)$ approach the corresponding single crack value for $(a/b)\to 1$ (i.e., for $a\to\infty$). An interesting result observed in Fig. 46 and Table 5, however, is that generally for smaller plate thicknesses as a approaches zero the stress intensity factor $k_1(a)$ goes through a minimum before becoming unbounded. This reduction is apparently due to the interaction of the stress fields of the two cracks as the distance 2a decreases. For example, from Fig. 47 it may clearly be seen that even though the cleavage stress $\sigma_{22}(x_1,0)$ perpendicular to and on the line of the crack is tensile near the crack and becomes unbounded at the crack tip, it becomes compressive in a certain interval away from the crack. This is largely due to the "bending" effect of the two halves of the plate. Thus after the interaction of stress fields of the two cracks it is seen that the inner crack tips would be in compressive region and consequently there would be some decrease in the stress intensity factor.

4.4 Collinear Cracks Perpendicular to the Boundary

From a viewpoint of interaction between two cracks or between cracks and free boundaries another geometry of great deal of practical interest is that of collinear cracks perpendicular to the plate boundary described in Fig. 48. A special case of this problem is the two surface

4. Tables of Complete Elliptic Integrals K(k) and E(k), k = sinα.

V. Vollständige elliptische Integrale.
V. Complete elliptic integrals.

α	K	E	α	K	E	α	K	E
0°	1,5708	1,5708	50°	1,9356	1,3055	82° 0′	3,3699	1,0278
1°	1,5709	1,5707	51°	1,9539	1,2963	82° 12′	3,3946	1,0267
2°	1,5713	1,5703	52°	1,9729	1,2870	82° 24′	3,4199	1,0256
3°	1,5719	1,5697	53°	1,9927	1,2776	82° 36′	3,4460	1,0245
4°	1,5727	1,5689	54°	2,0133	1,2682	82° 48′	3,4728	1,0234
5°	1,5738	1,5678	55°	2,0347	1,2587	83° 0′	3,5004	1,0223
6°	1,5751	1,5665	56°	2,0571	1,2492	83° 12′	3,5288	1,0213
7°	1,5767	1,5650	57°	2,0804	1,2397	83° 24′	3,5581	1,0202
8°	1,5785	1,5632	58°	2,1047	1,2301	83° 36′	3,5884	1,0192
9°	1,5805	1,5611	59°	2,1300	1,2206	83° 48′	3,6196	1,0182
10°	1,5828	1,5589	60°	2,1565	1,2111	84° 0′	3,6519	1,0172
11°	1,5854	1,5564	61°	2,1842	1,2015	84° 12′	3,6853	1,0163
12°	1,5882	1,5537	62°	2,2132	1,1921	84° 24′	3,7198	1,0153
13°	1,5913	1,5507	63°	2,2435	1,1826	84° 36′	3,7557	1,0144
14°	1,5946	1,5476	64°	2,2754	1,1732	84° 48′	3,7930	1,0135
15°	1,5981	1,5442	65°	2,3088	1,1638	85° 0′	3,8317	1,0127
16°	1,6020	1,5405	66°	2,3439	1,1546	85° 12′	3,8721	1,0118
17°	1,6061	1,5367	67°	2,3809	1,1454	85° 24′	3,9142	1,0110
18°	1,6105	1,5326	68°	2,4198	1,1362	85° 36′	3,9583	1,0102
19°	1,6151	1,5283	69°	2,4610	1,1273	85° 48′	4,0044	1,0094
20°	1,6200	1,5238	70° 0′	2,5046	1,1184	86° 0′	4,0528	1,0087
21°	1,6252	1,5191	70° 30′	2,5273	1,1140	86° 12′	4,1037	1,0079
22°	1,6307	1,5142	71° 0′	2,5507	1,1096	86° 24′	4,1574	1,0072
23°	1,6365	1,5090	71° 30′	2,5749	1,1053	86° 36′	4,2142	1,0065
24°	1,6426	1,5037	72° 0′	2,5998	1,1011	86° 48′	4,2746	1,0059
25°	1,6490	1,4981	72° 30′	2,6256	1,0968	87° 0′	4,3387	1,0053
26°	1,6557	1,4924	73° 0′	2,6521	1,0927	87° 12′	4,4073	1,0047
27°	1,6627	1,4864	73° 30′	2,6796	1,0885	87° 24′	4,4812	1,0041
28°	1,6701	1,4803	74° 0′	2,7081	1,0844	87° 36′	4,5609	1,0036
29°	1,6777	1,4740	74° 30′	2,7375	1,0804	87° 48′	4,6477	1,0031
30°	1,6858	1,4675	75° 0′	2,7681	1,0764	88° 0′	4,7427	1,0026
31°	1,6941	1,4608	75° 30′	2,7998	1,0725	88° 12′	4,8479	1,0022
32°	1,7028	1,4539	76° 0′	2,8327	1,0686	88° 24′	4,9654	1,0017
33°	1,7119	1,4469	76° 30′	2,8669	1,0648	88° 36′	5,0988	1,0014
34°	1,7214	1,4397	77° 0′	2,9026	1,0611	88° 48′	5,2527	1,0010
35°	1,7313	1,4323	77° 30′	2,9397	1,0574	89° 0′	5,4349	1,0008
36°	1,7415	1,4248	78° 0′	2,9786	1,0538	89° 6′	5,5402	1,0006
37°	1,7522	1,4171	78° 30′	3,0192	1,0502	89° 12′	5,6579	1,0005
38°	1,7633	1,4092	79° 0′	3,0617	1,0468	89° 18′	5,7914	1,0005
39°	1,7748	1,4013	79° 30′	3,1064	1,0434	89° 24′	5,9455	1,0003
40°	1,7868	1,3931	80° 0′	3,1534	1,0401	89° 30′	6,1278	1,0002
41°	1,7992	1,3849	80° 12′	3,1729	1,0388	89° 36′	6,3506	1,0001
42°	1,8122	1,3765	80° 24′	3,1928	1,0375	89° 42′	6,6385	1,0001
43°	1,8256	1,3680	80° 36′	3,2132	1,0363	89° 48′	7,0440	1,0000
44°	1,8396	1,3594	80° 48′	3,2340	1,0350	89° 54′	7,7371	1,0000
45°	1,8541	1,3506	81° 0′	3,2553	1,0338	90°	∞	1,0000
46°	1,8692	1,3418	81° 12′	3,2771	1,0326			
47°	1,8848	1,3329	81° 24′	3,2995	1,0313			
48°	1,9011	1,3238	81° 36′	3,3223	1,0302			
49°	1,9180	1,3147	81° 48′	3,3458	1,0290			

Jahnke & Emde, "Tables of Functions"

Table 5. Stress intensity factors in an orthotropic strip containing two identical collinear cracks loaded by uniform crack surface pressure p or shear q; $H_1=H_2=H$, $\kappa=1$, $H\delta/(b-a)/2 = 0.4$.

$\frac{2a}{b-a}$	$\sigma_{22}(x_1,0)=-p$		$\sigma_{12}(x_1,0)=-q$	
	$\frac{k_1(b)}{p(\frac{b-a}{2})^{1/2}}$	$\frac{k_1(a)}{p(\frac{b-a}{2})^{1/2}}$	$\frac{k_2(b)}{q(\frac{b-a}{2})^{1/2}}$	$\frac{k_2(a)}{q(\frac{b-a}{2})^{1/2}}$
0	9.376	∞	2.629	∞
.01	3.693	6.996	2.106	5.837
.1	3.788	2.837	1.952	2.300
.2	3.962	3.113	1.935	1.989
.3	4.074	3.642	1.933	1.939
.4	4.124	3.971	1.933	1.933
.5	4.138	4.103	1.933	1.932
.6	4.141	4.138	1.933	1.933
.7	4.140	4.143	1.933	1.933
.8	4.140	4.142	1.933	1.933
.9	4.139	4.140	1.933	1.933
1	4.139	4.140	1.933	1.933
2	4.142	4.142	1.933	1.933

cracks simulating weld defects on both surfaces.

Some sample results for the stress intensity factors k(a) and k(b) for two symmetrically located collinear cracks are given in Table 6. Fig. 49 shows the results for two (collinear) surface cracks. For very shallow surface cracks (i.e., for a→h), as seen from the figure k(a) approaches the stress intensity factor in a semi-infinite plane containing an edge crack of depth $2a_0$, namely

$$k_1(a) \to 1.586\ \sigma_0\sqrt{a_0} \quad . \tag{38}$$

In the other limiting case for which a→0, k(a) approaches the stress intensity factor in a symmetrically loaded infinite plane containing

Table 6. Stress intensity factors for collinear internal cracks in a strip (Figure 1, $a_0 = (b-a)/2$).

a/h	b/h	$\frac{k(a)}{\sigma_0\sqrt{a_0}}$	$\frac{k(b)}{\sigma_0\sqrt{a_0}}$
0	0.4	(→ ∞)	1.5690
0.1	0.5	1.1746	1.1169
0.2	0.6	1.1102	1.0961
0.4	0.8	1.0984	1.1250
0.5	0.9	1.1290	1.2278
0.6	1.0	1.6080	(→ ∞)
0	0.8	(→ ∞)	2.5680
0.1	0.9	1.6730	1.7451
0.2	1.0	2.1769	(→ ∞)
0.5	0.95	1.1960	1.4711
0.5	0.98	1.2713	1.9008
0.5	1.0	1.6228	(→ ∞)

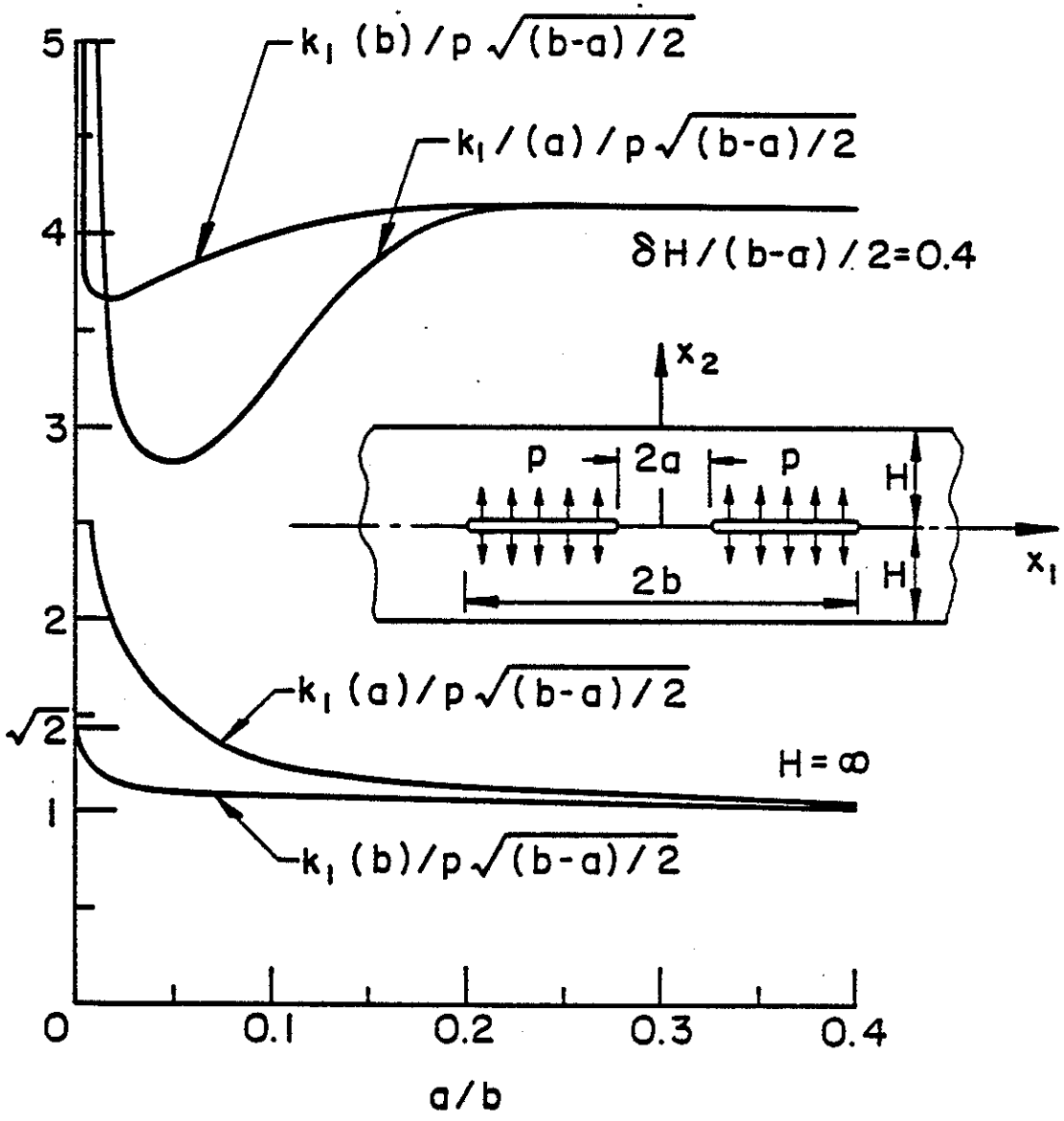

Figure 46. Stress intensity factors for two collinear cracks in an orthotropic strip.

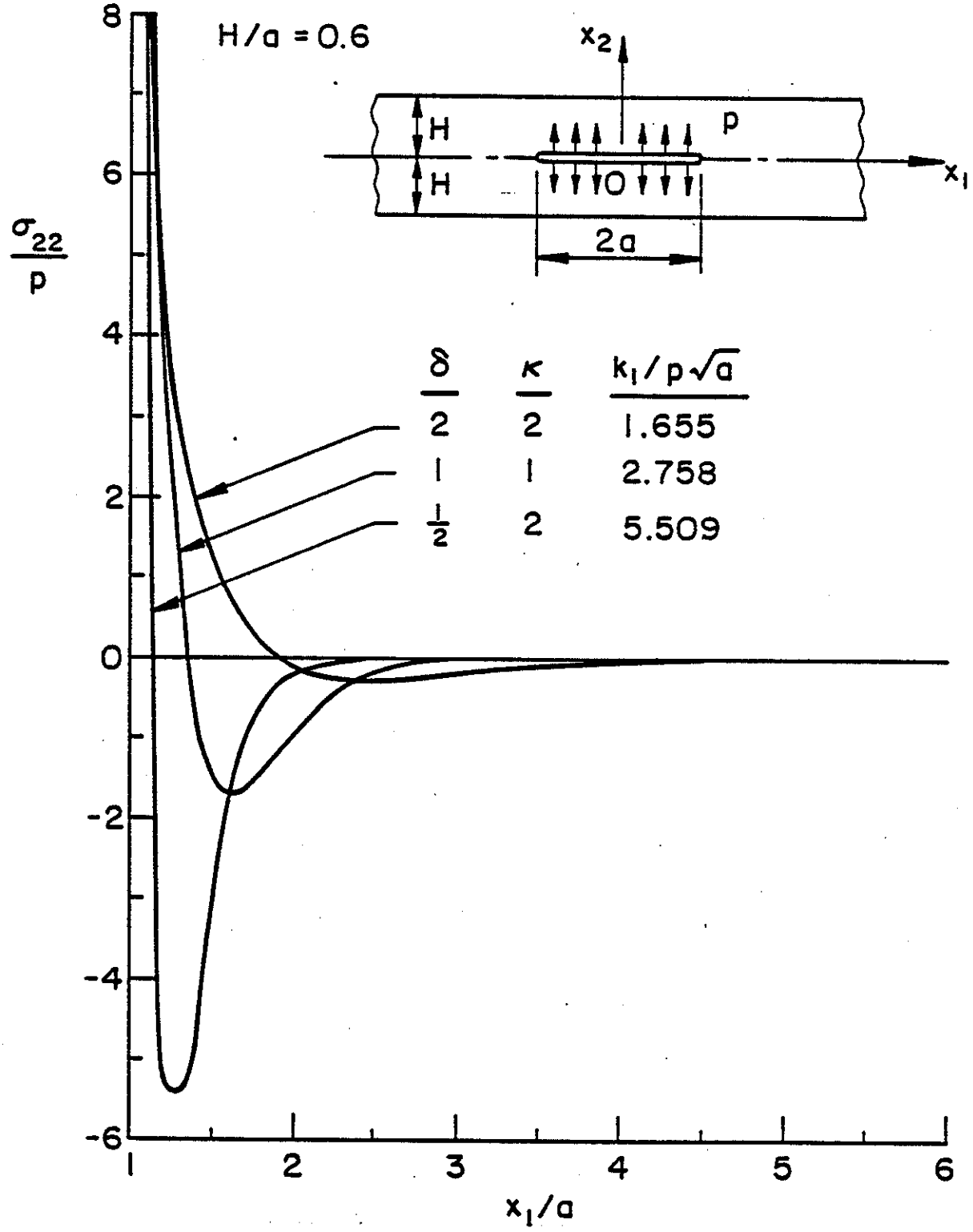

Figure 47. The effect of material orthotropy on the normal stress $\sigma_{22}(x_1,0)$ in a strip containing a pressurized crack ($\delta=\kappa=1$ isotropic strip).

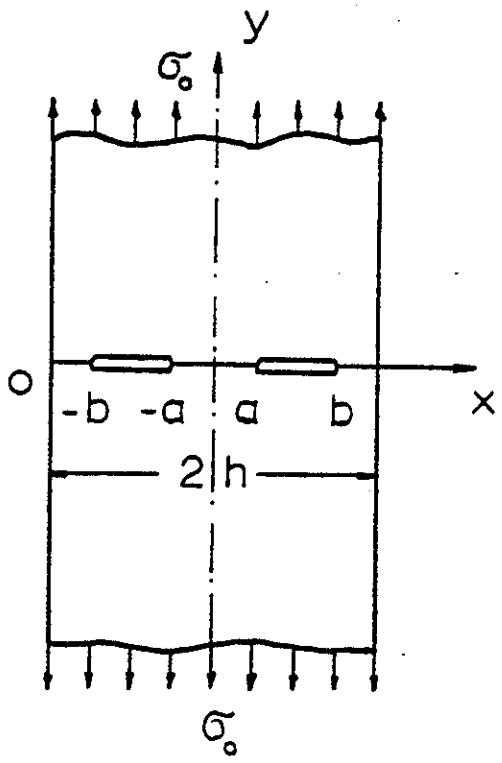

Figure 48. Infinite strip with two internal cracks.

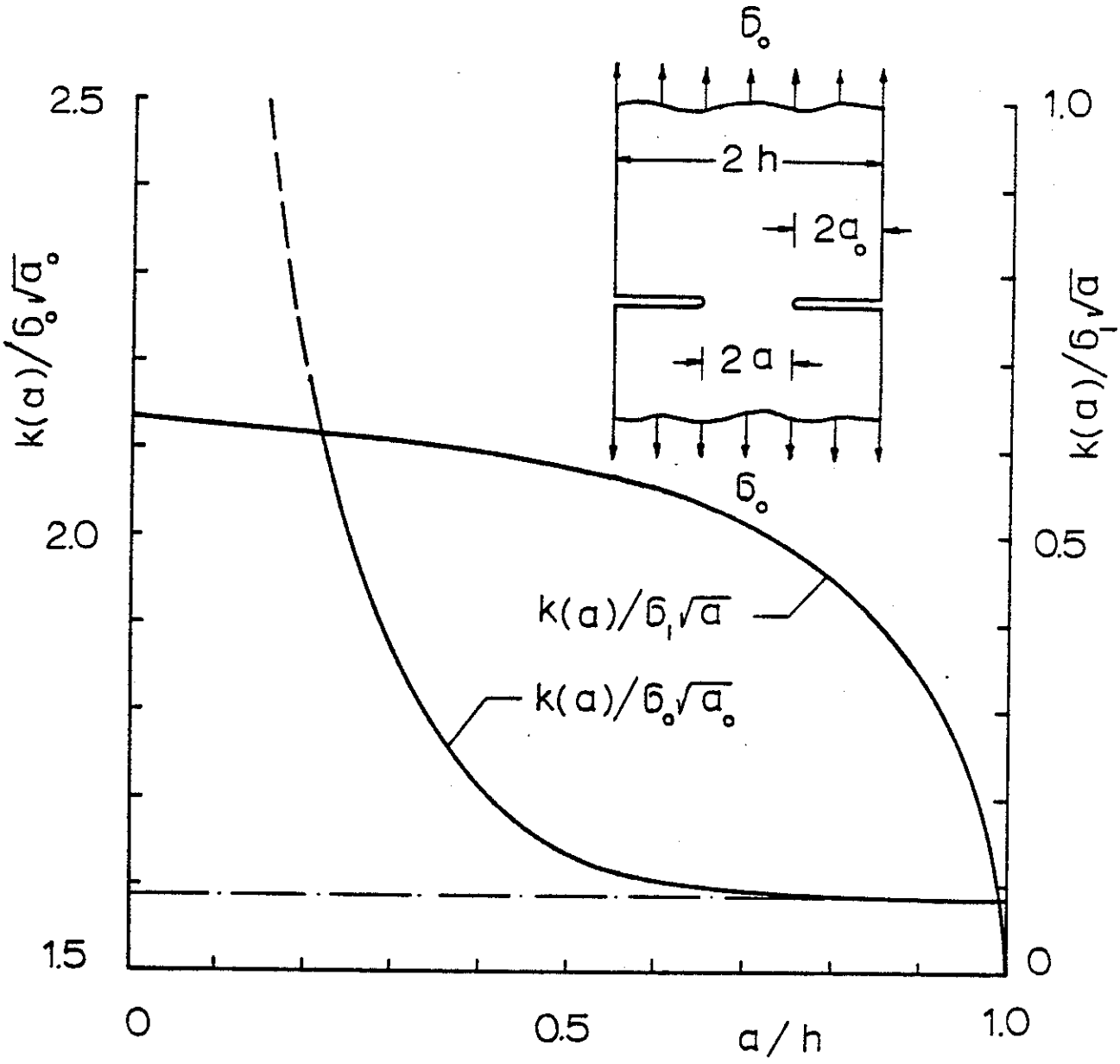

Figure 49. The stress intensity factor for the edge cracks in an infinite strip ($\sigma_1 = \sigma_0 h/a$).

two edge cracks. In this case, if the resultant force perpendicular to the cracks is P, and the length of the net ligament is 2a, it can be shown that the stress state in the net ligament is given by

$$\sigma_{yy}(x,0) = \frac{P}{\pi\sqrt{a^2-x^2}} \quad , \quad \sigma_{xy}(x,0) = 0 \quad . \tag{39}$$

Thus, by observing that

$$P = 2h\sigma_o = 2a\sigma_1 \tag{40}$$

and

$$k(x) = \lim_{x\to a} \sqrt{2(a-x)}\ \sigma_{yy}(x,0) \ , \tag{41}$$

we obtain

$$k(a) = \frac{2}{\pi}\sigma_1\sqrt{a} \quad . \tag{42}$$

These two limiting results are also shown in Fig. 49.

5. PLANAR CRACKS OF FINITE SIZE - THE LINE SPRING MODEL

Figure 50 which is reproduced from API Standard 1104 describes a set of empirical rules for the interaction of coplanar cracks of finite size. Quite clearly the actual problem is a very highly complicated three-dimensional multiple crack problem which does not lend itself to any kind of rigorous analytical treatment. On the other hand the problem is a very practical one and, therefore, requires a somewhat more quantitative and reliable solution. Such a solution may of course be obtained by using a finite element technique. However, highly reliable analytical solutions may also be obtained by using the so-called line-spring model in conjunction with a transverse shear theory of plates or shells. In this section the general theory of the model is redeveloped by generalizing it to embedded cracks of arbitrary location. Some comparisons of the results with the existing finite element solutions are made to show the validity and various examples are given to demonstrate the range of applicability of the technique. Extensive results for the multiple internal and surface cracks are given in Appendices A and B.

5.1 Introduction

From the viewpoint of practical applications the analysis of a part-through crack in a structural component which may locally be represented by a "plate" or a "shell" is certainly one of the most important problems in fracture mechanics. In its general form the problem is a three-dimensional crack problem in a bounded geometry where the stress field perturbed by the crack interacts very strongly with the surfaces of the solid. At present even for the linearly elastic solids a neat analytical treatment of the problem appears to be intractable. Consequently, as indicated in reference [18], the available solutions of the problem very heavily rely on some kind of numerical technique, most notably on the finite element method. The renewed interest in recent years in the so-called "line-spring model" first described in [19] has been due partly to the desire of providing simpler and less expensive solutions to the part-through crack problem and partly to the fact that for certain important crack geometries the model seems to give results that have an acceptable degree of accuracy.

In a plate or a shell containing a part-through crack and subjected to membrane and bending loads, the net ligament(s) around the crack would generally have a constraining effect on the crack surface displacements. The basic idea underlying the "line-spring model" consists of approximating the three-dimensional crack problem by a two-dimensional coupled bending-membrane problem through the reduction of the net ligament stresses to the neutral surface of the plate or shell as a membrane load N and a bending moment M. In the resulting two-dimensional

		INTERACTION EXISTS IF:	IF INTERACTION EXISTS EFFECTIVE FLAW SIZE IS:
CASE 1	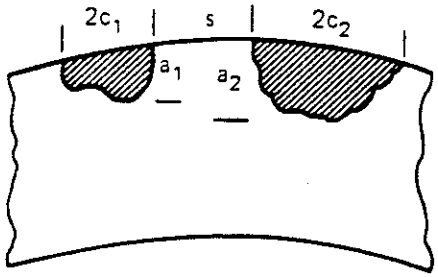	$s < c_1 + c_2$	$a_e = a_2$ $2c_e = 2c_1 + s + 2c_2$
CASE 2	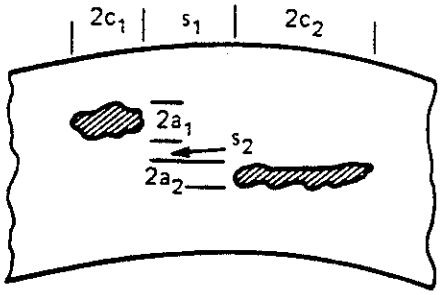	$s_1 < c_1 + c_2$ and $s_2 < a_1 + a_2$	$2a_e = 2a_1 + s_2 + 2a_2$ $2c_e = 2c_1 + s_1 + 2c_2$
CASE 3	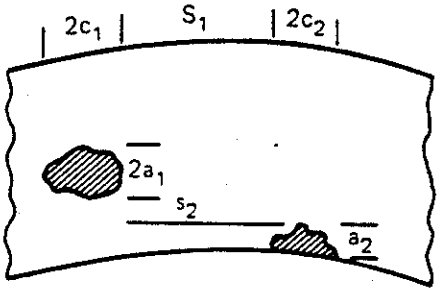	$s_1 < c_1 + c_2$ and $s_2 < a_1 + \frac{a_2}{2}$	$a_e = 2a_1 + s_2 + a_2$ $2c_e = 2c_1 + s_1 + 2c_2$
CASE 4	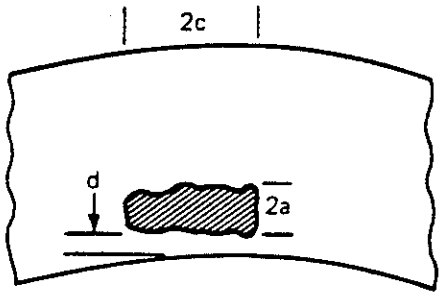	$d < a$	$a_e = d + 2a$ $2c_e = 2c$
CASE 5	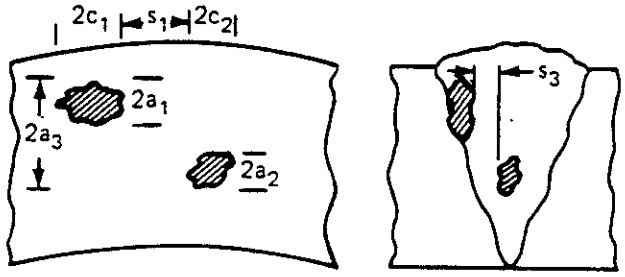	$s_1 < c_2 + c_2$ and $s_3 < a_1 + a_2$	$2a_e = 2a_3$ $2c_e = 2c_1 + s_1 + 2c_2$

Fig. 50. RULES FOR EVALUATION OF FLAW INTERACTION

problem the crack surface displacements are represented by a crack opening displacement δ and a crack surface rotation θ, referred to, again, the neutral surface. The quantities N, M, δ and θ are assumed to be functions of a single variable, namely the coordinate x_1 along the crack in the neutral surface (Fig. 51). The pair of functions (δ,θ) or (N,M) are determined from the corresponding mixed boundary value problem for the "plate" or the "shell" having a through crack in which N and M are treated as unknown crack surface loads. Once N and M are determined the stress intensity factors are evaluated from the two-dimensional elasticity solution of a strip under the membrane force N and the bending moment M (Fig. 51b).

The model introduced in [19] is based on the classical plate bending theory. There is no need here to go into a detailed discussion on the necessity of using a higher order plate (or shell) theory in studying the crack problems (see, for example, [20]-[22]). It is, however, sufficient to point out that the asymptotic stress field around the crack tip given by the classical plate bending theory is not consistent with the elasticity solutions, whereas a transverse shear theory (such as that of Reissner's [23], [24]) which can accommodate all stress and moment resultants on the crack surface separately (i.e., three boundary conditions in plates, five in shells) give results which are identical to the asymptotic solutions obtained from the plane strain and anti-plane shear crack problems [25], [26]. The line spring model was later used in [27] and [28] to treat the longitudinal part-through crack problem in a cylinder by using, again, the classical shell theory. The solution obtained by using a transverse shear theory in plates and shells may be found in [29] and [30] (see also [31] for more extensive results in line pipes). Rather extensive results for corner cracks and for collinear surface cracks in a plate having a finite width are given in [32].

The concept of "line spring" may be used to treat also the problem of plastic deformations in the net ligament [33], [27], [28]. For materials without any strain hardening a simpler fully-plastic version of the model was used in [34] and [35] to calculate the crack opening displacement (see also [31] for the application to pipes containing a circumferential part-through crack).

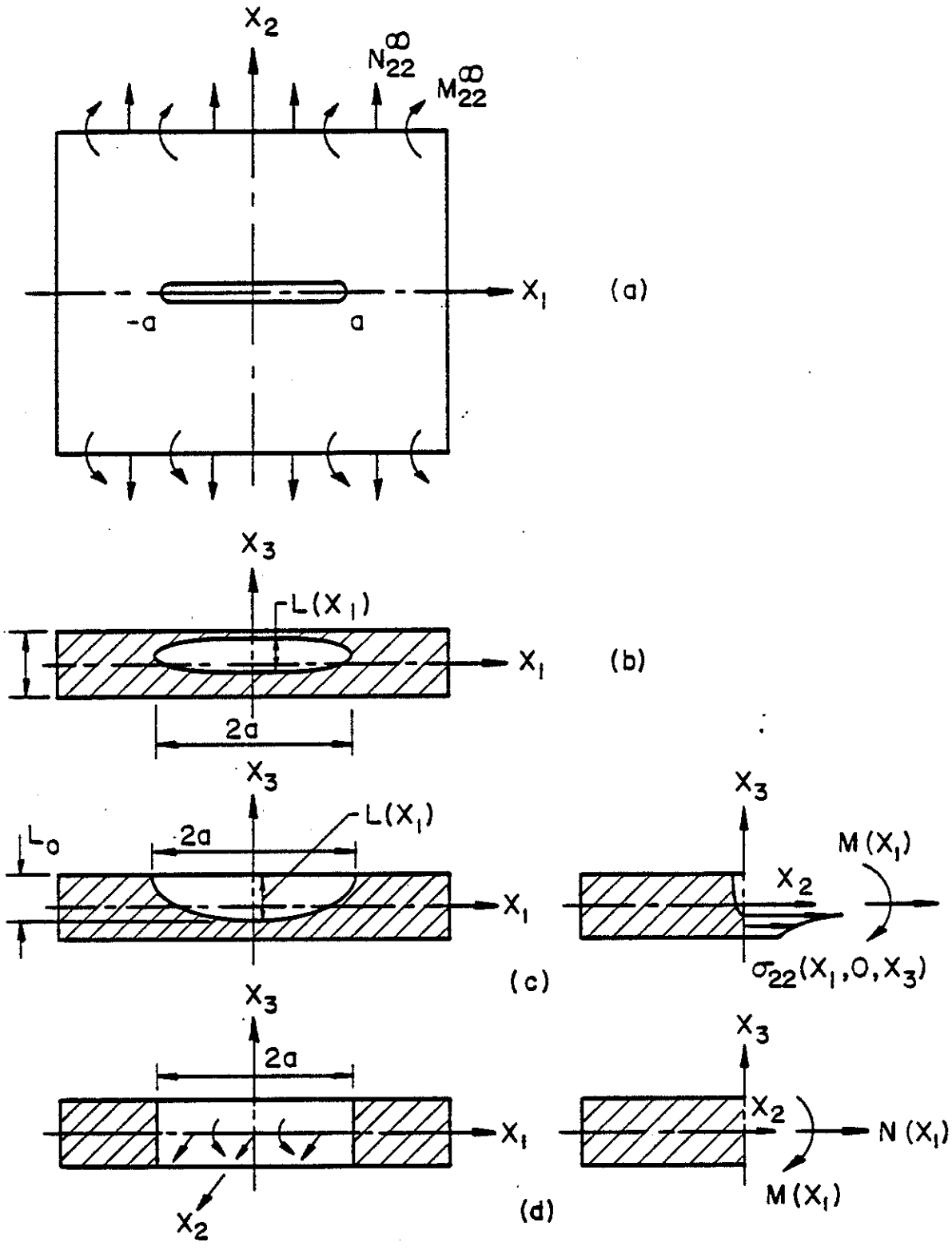

Fig. 51 Notation for the part-through crack problem.

5.2 Description of the Model

The problem under consideration is a surface or an internal crack problem for a relatively thin-walled structural component which is solved basically as a plate or shell problem. In the usual notation it will therefore be assumed that referred to the local coordinate system shown in Fig.5l; u_1, u_2, u_3 are the components of the displacement vector, β_1 and β_2 are the angles of rotation of the normal to the neutral surface in x_1x_3 and x_2x_3 planes, respectively, and N_{ij}, M_{ij} and V_i, $(i,j=1,2)$ are respectively the membrane, moment and transverse shear resultants. It will further be assumed that the <u>through crack</u> problem for the plate or the shell has already been formulated and has been reduced to a system of integral equations. In the solutions given in [29]-[32] the derivatives of the crack surface displacement and the crack surface rotation on the neutral surface are assumed to be the unknown functions in the integral equations. This comes quite naturally out of the formulation of the related mixed boundary value problem for the plate or the shell. For a symmetric problem of a through crack (located in one of the principal planes of curvature) along $-a<x_1<a$ in a plate or shell under Mode I loading conditions, invariably the integral equations are of the following form:

$$\frac{a(1-\nu^2)}{2\pi h\lambda^4}\int_{-1}^{1}\left[\frac{3+\nu}{1+\nu}\,\frac{1}{t-x}+k_{11}(x,t)\right]g_1(t)dt+\int_{-1}^{1}k_{12}(x,t)g_2(t)dt$$

$$=-\frac{m_\infty}{6E}+\frac{m(x)}{6E}\,,\quad -1<x<1\,, \tag{43}$$

$$\frac{1}{2\pi}\int_{-1}^{1}\frac{g_2(t)}{t-x}\,dt+\int_{-1}^{1}\left[k_{21}(x,t)g_1(t)+k_{22}(x,t)g_2(t)\right]dt$$

$$=-\frac{\sigma_\infty}{E}+\frac{\sigma(x)}{E}\,,\quad -1<x<1\,, \tag{44}$$

where the unknown functions are defined by

$$g_1(x)=\frac{\partial}{\partial x}\beta_y(x,+0)\,,\quad g_2(x)=\frac{\partial}{\partial x}v(x,+0)\,,\quad \beta_y=\beta_2\,,\quad v=\frac{u_2}{a}\,. \tag{45}$$

The external loads

$$\sigma_\infty = N^\infty_{22}/h \ , \ m_\infty = 6M^\infty_{22}/h^2 \tag{46}$$

represent uniform membrane and bending resultant applied to the plate or the shell away from the crack region (Fig. 51a) and σ and m which are defined by

$$\sigma(x) = N(x_1,0)/h \ , \ m(x) = 6M(x_1,0)/h^2 \ , \ (-1<x<1, \ x = x_1/a) \tag{47}$$

are the membrane and bending loads applied to the crack surfaces (Fig.51d), 2a is the length and $L(x_1)$ the depth of the part-through crack(*). The thickness h and the principal radii of curvature R_1 and R_2 are the other length parameters of the structure. The formulation is given in terms of the dimensionless quantities defined in Table 7. E and ν are the elastic constants of the material. The integral equations are obtained from the following mixed boundary conditions in $x_2 = 0$ plane (Fig. 51d):

$$N_{22}(x_1,0) = -N^\infty_{22} + N(x_1) \ , \ -a<x_1<a \ , \tag{48a}$$

$$u_2(x_1,0) = 0, \quad |x_1| > a \ , \tag{48b}$$

$$M_{22}(x_1,0) = -M^\infty_{22} + M(x_1) \ , \ -a<x_1<a, \tag{49a}$$

$$\beta_2(x_1,0) = 0 \ , \ |x_1|>a \ , \tag{49b}$$

where the general principle of superposition is used to account for the loading N^∞_{22} and M^∞_{22} applied to the structure away from the crack region. From $v = u_2/a$, $\beta_y = \beta_2$ and the definitions(45) it follows that the unknown functions g_1 and g_2 must satisfy the single-valuedness conditions given by

$$\int_{-1}^{1} g_1(t)dt = 0 \ , \ \int_{-1}^{1} g_2(t)dt = 0 \ . \tag{50}$$

(*) Clearly any additional known external loads may be accommodated by using the notion of superposition and thereby adding appropriate functions to the right hand sides of (43) and (44).

Table 7. The dimensionless quantities used in plate and shell problems.

$x = x_1/a,\ y = x_2/a,\ z = x_3/a$,

$u = u_1/a,\ v = u_2/a,\ w = u_3/a$,

$\beta_x = \beta_1,\ \beta_y = \beta_2$,

$\lambda_1^4 = 12(1-\nu^2)\ \frac{a^4}{h^2R_1^2}$, $\lambda_2^4 = 12(1-\nu^2)\ \frac{a^4}{h^2R_2^2}$,

$\lambda^4 = 12(1-\nu^2)\ \frac{a^2}{h^2}$, $\kappa = \frac{h^2}{5(1-\nu)a^2}$

R_1, R_2: principal radii of curvature

In all Mode I plate and shell problems the dominant part of the kernels in (43)and (44)namely, the terms having the Cauchy singularity $1/(t-x)$ are the same. The Fredholm kernels k_{ij}, $(i,j=1,2)$ represent the details of the plate or shell geometry. For the through crack problem in plates the integral equations (43)and (44)are uncoupled, i.e., $k_{12}=0$, $k_{21}=0$. Thus, the through crack problem for the plate under membrane and bending loads can be solved separately. As will be shown below, in the case of a part-through crack the equations are coupled through the loading terms $\sigma(x)$ and $m(x)$ (which are also unknown). For example, for an infinite plate (43)(44)may be expressed as [20-22], [29]

$$\frac{a(1-\nu^2)}{2\pi h\lambda^4}\int_{-1}^{1}\left[\frac{3+\nu}{1+\nu}\frac{1}{t-x}-\frac{4\kappa(1-\nu)}{1+\nu}\frac{1}{(t-x)^3}\right.$$

$$\left.+\frac{4}{1+\nu}\frac{1}{t-x}K_2(\alpha|t-x|)\right]g_1(t)dt=-\frac{m_\infty}{6E}+\frac{m(x)}{6E}\ ,\ -1<x<1\ , \qquad (51)$$

$$\frac{1}{2\pi}\int_{-1}^{1}\frac{1}{t-x}g_2(t)dt=-\frac{\sigma_\infty}{E}+\frac{\sigma(x)}{E}\ ,\ -1<x<1\ , \qquad (52)$$

$$\alpha=[2/\kappa(1-\nu)]^{1/2}\ , \qquad (53)$$

where K_2 is the modified Bessel function of the second kind and the constants λ and κ are defined in Table 7. In shells the kernels k_{ij}, $(i,j=1,2)$ are always nonzero.

Let us now assume that the local plate or shell geometry is represented by Fig. 51 and for simplicity we also assume that the structure contains only a single surface crack as shown in Fig.51c. Let $N(x_1)$ and $M(x_1)$ be the membrane and bending resultants acting on the neutral surface which are statically equivalent to the net ligament stress $\sigma_{22}(x_1,0,x_3)$, $(-a<x_1<a,-h/2<x_3<h/2-L(x_1))$ (Fig. 51c). The first approximating assumption made in introducing the line spring model is that the crack may now be assumed as being a through crack of length 2a (Fig.51d) and the constraint caused by the net ligament stress $\sigma_{22}(x_1,0,x_3)$ (tending to prevent the crack faces from opening and rotating) may be accounted for by applying the membrane and bending resultants $N(x_1)$ and $M(x_1)$ on the crack surfaces. Note that N and M tend to close the crack surfaces whereas the external loads N^∞_{22} and M^∞_{22} tend to open them.

The second major assumption made in developing the model is that the stress intensity factor at a location x_1 along the crack front may be approximated by the corresponding plane strain value obtained from a plate which contains an edge crack of (uniform) depth $L(x_1)$ and which is subjected to uniform bending moment $M(x_1)$ and uniform tension $N(x_1)$ away from the crack region (Fig. 51c). This assumption makes it possible to express $N(x_1)$ and $M(x_1)$ in terms of the unknown functions g_1 and g_2 in (43) and (44) which may then be solved in a straightforward manner. It should again be emphasized that it is because of these two rather gross approximating assumptions that a basically intractable three-dimensional problem is reduced to a relatively straightforward plate or shell problem.

In order to obtain N and M in terms of g_1 and g_2 the energy available for fracture along the crack front is expressed in two different ways, namely as the crack closure energy and as the product of load-load point displacement. In a plate with an edge crack subjected to a uniform tension N and uniform bending moment M(Fig. 52a), if K_1 is the stress intensity factor given by the plane strain solution, from the crack closure energy the energy (per unit width) available for fracture may be obtained as

$$G = \frac{\partial}{\partial L}(U-V) = \frac{1-\nu^2}{E} K_1^2 \qquad (54)$$

where U is the work done by the external loads and V is the strain energy.

Now, let δ and θ be the load line "displacements" corresponding to N and M as shown in Fig. 52a. Let $d\delta$ and $d\theta$ be the changes in δ and θ as the crack length goes from L to L+dL under "fixed load" conditions. Then referring to Fig. 52b the changes in U and V may be expressed as

$$dU = Nd\delta + Md\theta \ , \qquad (55)$$

$$dV = \frac{1}{2}[N(\delta+d\delta)+M(\theta+d\theta)] - \frac{1}{2}(N\delta+M\theta) = \frac{1}{2}(Nd\delta+Md\theta) \ . \qquad (56)$$

Equations (52) and (53) give the energy available for a crack growth dL as follows:

$$d(U-V) = \frac{1}{2}(Nd\delta+Md\theta) \ . \qquad (57)$$

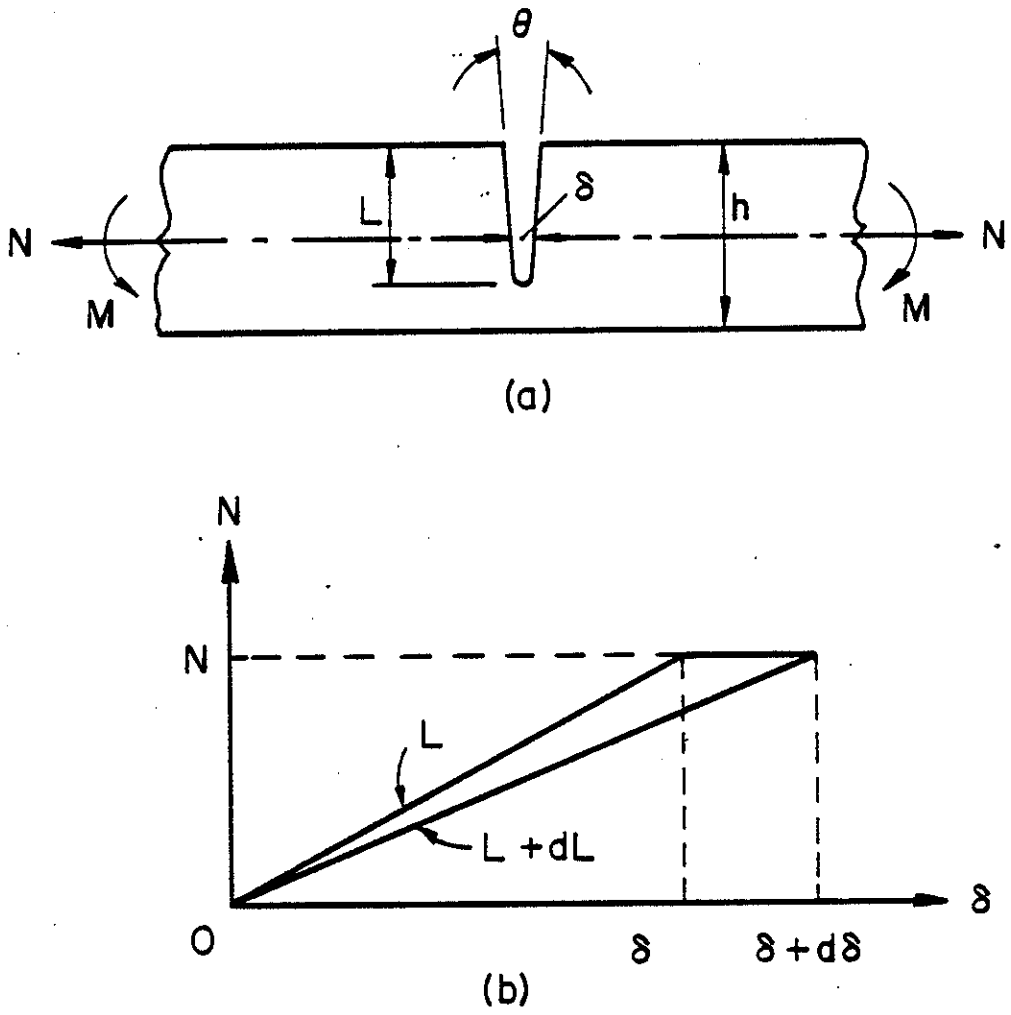

Fig.52 Notation for the related plane strain problem.

On the other hand for constant N and M and for a change of dL in the crack length we have

$$d\delta = \frac{\partial \delta}{\partial L} dL \ , \ d\theta = \frac{\partial \theta}{\partial L} dL \ . \tag{58}$$

Thus, from (54) and (55) it follows that

$$\frac{\partial}{\partial L} (U-V) = G = \frac{1}{2} \left(N \frac{\partial \delta}{\partial L} + M \frac{\partial \theta}{\partial L}\right) , \tag{59}$$

and, by using (51) we find

$$\frac{1}{2} \left(N \frac{\partial \delta}{\partial L} + M \frac{\partial \theta}{\partial L}\right) = \frac{1-\nu^2}{E} K_1^2 \ . \tag{60}$$

Let us now define the membrane and bending stresses by

$$\sigma = N/h \ , \ m = 6M/h^2 \tag{61}$$

and assume that the solution of the plane strain problem shown in Fig. 52a give the stress intensity factor as follows:

$$K_1 = \sqrt{h} \ [\sigma g_t(s) + m g_b(s)] \ , \ s = L/h \ , \tag{62}$$

where g_t and g_b are known functions. If we also define the following matrices

$$\tau = (\tau_i) = \begin{bmatrix} m \\ \sigma \end{bmatrix} \ , \ \omega = (\omega_i) = \begin{bmatrix} \frac{h}{6} \theta \\ \delta \end{bmatrix} \ , \ G(s) = (g_{ij}) = \begin{bmatrix} g_b^2 & g_t g_b \\ g_t g_b & g_t^2 \end{bmatrix} , \tag{63}$$

from (54) and (62) we obtain

$$G = \frac{1-\nu^2}{E} K_1^2 = \left(\frac{1-\nu^2}{E} h\right) \tau^T G \tau \ . \tag{64}$$

Similarly, from (59), (61) and (63) we find

$$G = \frac{1}{2}\left(h\tau_2 \frac{\partial \omega_2}{\partial L} + \frac{h^2}{6}\tau_1 \frac{6}{h}\frac{\partial \omega_1}{\partial L}\right) = \frac{h}{2}\tau^T \frac{\partial \omega}{\partial L} \quad . \tag{65}$$

From (64) and (65) it is seen that

$$\frac{\partial \omega}{\partial L} = \frac{2}{E}(1-\nu^2)G\tau \quad . \tag{66}$$

By observing that G is a function of L, τ is independent of L and $\omega=0$ for L=0, from (66) we find

$$\omega = \frac{2}{E}(1-\nu^2)\left(\int_0^L GdL\right)\tau = \frac{2}{E}(1-\nu^2)A\tau, \; A = \int_0^L GdL \quad . \tag{67}$$

If we also define

$$B = \begin{bmatrix} h/6 & 0 \\ 0 & a \end{bmatrix}, \; \eta = \begin{bmatrix} \beta_y(x,+0) \\ v(x,+0) \end{bmatrix} \tag{68}$$

from $\delta = 2u_2(x_1,0) = 2av(x,0)$, $\theta = 2\beta_2(x_1,0) = 2\beta_y(x,0)$ and (67), (68), and (45) it may be seen that

$$\tau = \frac{E}{1-\nu^2}A^{-1}B\eta \; , \; C(x) = \frac{1}{1-\nu^2}A^{-1}B, \; \tau = EC\begin{bmatrix} \int_{-1}^{x} g_1(t)dt \\ \int_{-1}^{x} g_2(t)dt \end{bmatrix} . \tag{69}$$

Note that since $L = L(x_1) = L(ax)$ is a known function of x the matrix A and consequently $C = (1-\nu^2)^{-1}A^{-1}B$ consist of also known functions of x.

Substituting now from (69) into (43) and (44) we obtain

$$\frac{a(1-\nu^2)}{2\pi h\lambda^4}\int_{-1}^{1}\left[\frac{3+\nu}{1+\nu}\frac{1}{t-x} + k_{11}(x,t)\right]g_1(t)dt + \int_{-1}^{1}k_{12}(x,t)g_2(t)dt$$
$$- \frac{c_{11}(x)}{6}\int_{-1}^{x}g_1(t)dt - \frac{c_{12}(x)}{6}\int_{-1}^{x}g_2(t)dt = -\frac{m_\infty}{6E}, \; -1<x<1, \tag{70}$$

$$\frac{1}{2\pi}\int_{-1}^{1}\frac{1}{t-x}g_2(t)dt + \int_{-1}^{1}[k_{21}(x,t)g_1(t) + k_{22}(x,t)g_2(t)]dt$$
$$- c_{21}(x)\int_{-1}^{x}g_1(t)dt - c_{22}(x)\int_{-1}^{x}g_2(t)dt = -\frac{\sigma_\infty}{E}, \; -1<x<1 \; , \tag{71}$$

where the functions c_{ij} are the elements of C which is defined by (69).

The functions g_t and g_b giving the stress intensity factor in an edge-notched strip as defined by (62) (see Fig.52a), and the elements of the matrix A defined by (67) are given in [29]. The functions g_t and g_b valid for $0<L/h\leq 0.8$ were obtained as follows [29]:

$$g_t(s) = \sqrt{\pi s}\,(1.1215 + 6.5200s^2 - 12.3877s^4 + 89.0554s^6$$

$$- 188.6080s^8 + 207.3870s^{10} - 32.0524s^{12}),\ s = L/h\ , \qquad (72)$$

$$g_b(s) = \sqrt{\pi s}\,(1.1202 - 1.8872s + 18.0143s^2 - 87.3851s^3$$

$$+ 241.9124s^4 - 319.9402s^5 + 168.0105s^6),\ s = L/h\ . \qquad (73)$$

The dominant part of the system of integral equations (70) and (71) has only a Cauchy kernel and, therefore, the solution is of the following form:

$$g_i(t) = \frac{f_i(t)}{\sqrt{1-t^2}}\ ,\ i = 1,2 \qquad (74)$$

where the functions f_1 and f_2 are bounded in the closed interval $-1\leq t\leq 1$. Even in the simplest case (of the infinte plate considered in [29]) the system has no closed form solution. However, the unknown functions f_1 and f_2 may be determined numerically within any desired degree of accuracy by using the quadrature formulas given, for example, in [36]. After determining f_1 and f_2 the net ligament resultants m and σ are obtained from (66) and the stress intensity factor from (62).

5.3 Internal Cracks

The line spring model described in the previous section may easily be extended to internal cracks such as that, for example, shown in Fig. 51b. In this case the basic integral equations for a through crack in a plate or shell under membrane or bending loads remain the same and are again given by (43) and (44). The major difference is in expressing the resultants $\sigma(x)$ and $m(x)$ of the net ligament stress $\sigma_{22}(x_1,0,x_3)$ in terms of δ and θ or

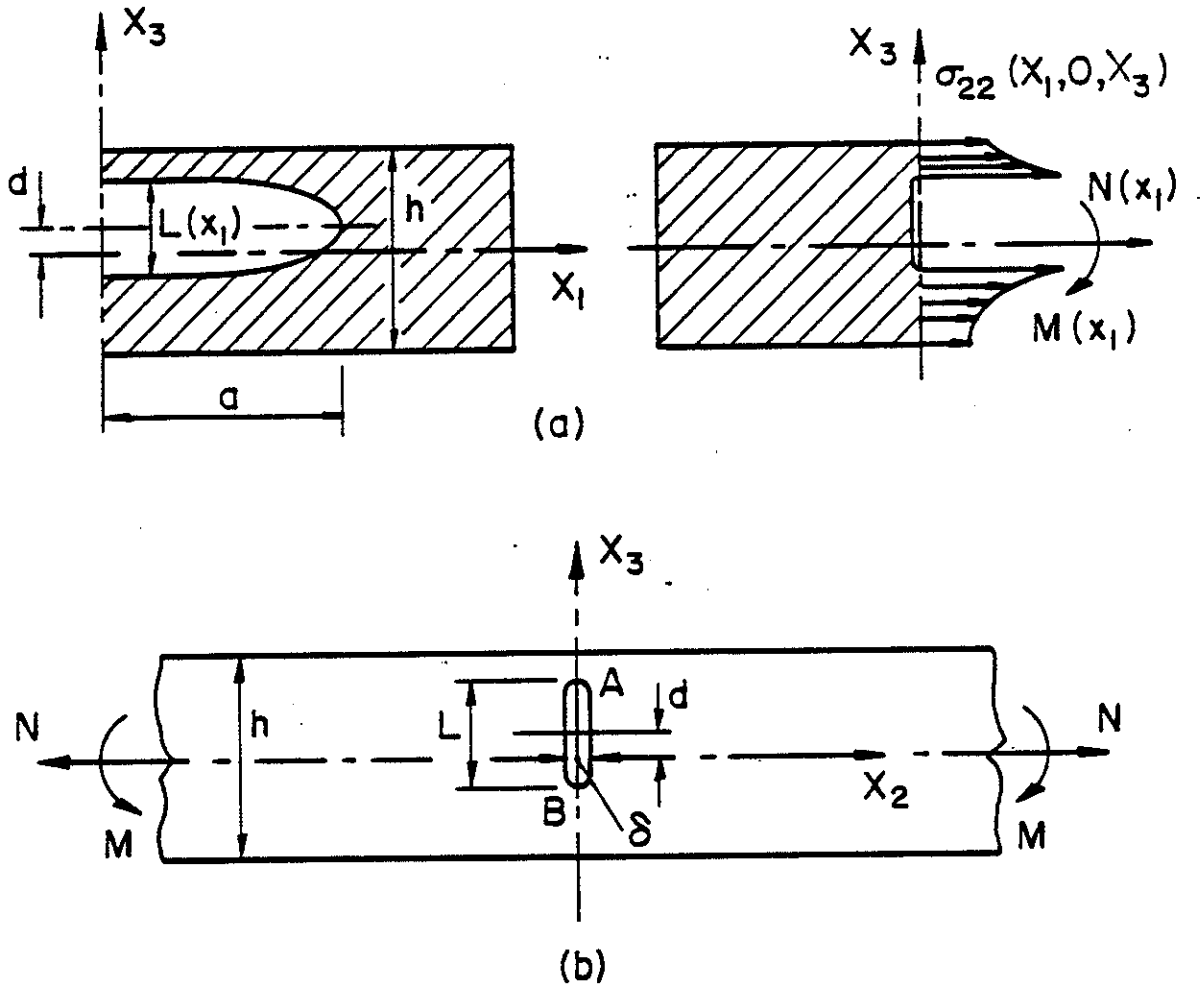

Fig. 53 Geometry and notation for an internal crack.

$v(x)$ and $\beta_y(x)$ which represent the crack opening displacement and rotation on the load line (Fig. 53). Let the plane internal crack be defined by

$$-a<x_1<a,\ x_2 = 0,\ d - \frac{L(x_1)}{2} < x_3 < d + \frac{L(x_1)}{2} \tag{75}$$

where, for simplicity, d is assumed to be constant. Thus, if K_A and K_B are the stress intensity factors at the crack tips A and B in the corresponding plane strain problem shown in Fig.53b, as L increases by dL the energy increment available for fracture may be expressed as

$$d(U-V) = \frac{1-\nu^2}{E}\left[K_A{}^2 d(L/2) + K_B{}^2 d(L/2)\right] \tag{76}$$

giving

$$G = \frac{\partial}{\partial L}(U-V) = \frac{1-\nu^2}{2E}\left(K_A{}^2 + K_B{}^2\right) \tag{77}$$

which replaces (54). The rate of energy available for fracture as expressed in terms of load line "displacements" and "forces" remains the same and is given by (59).

Let us now assume that the stress intensity factors for the plane strain problem shown in Fig.53b are known as follows:

$$K_A = \sqrt{h}\left[\sigma\, g_{At}(s) + m\, g_{Ab}(s)\right],\ s = L/h, \tag{78}$$

$$K_B = \sqrt{h}\left[\sigma\, g_{Bt}(s) + m\, g_{Bb}(s)\right],\ s = L/h \tag{79}$$

where σ and m are again given by (61). The solution of the problem is given in [37] from which the functions g_{At}, g_{Ab}, g_{Bt} and g_{Bb} are obtained by a suitable curve-fitting. It is clear that the derivation given in the previous section, particularly the integral equations (70) and (71) will remain unchanged and the only change will be in the matrix G(s) defined by (63). For the internal crack problem shown in Fig.53 the matrix G now becomes

$$G(s) = \frac{1}{2}\begin{bmatrix} g_{Ab}^2 + g_{Bb}^2 & g_{Ab}g_{At}+g_{Bb}g_{Bt} \\ g_{Ab}g_{At}+g_{Bb}g_{Bt} & g_{At}^2 + g_{Bt}^2 \end{bmatrix}, \tag{80}$$

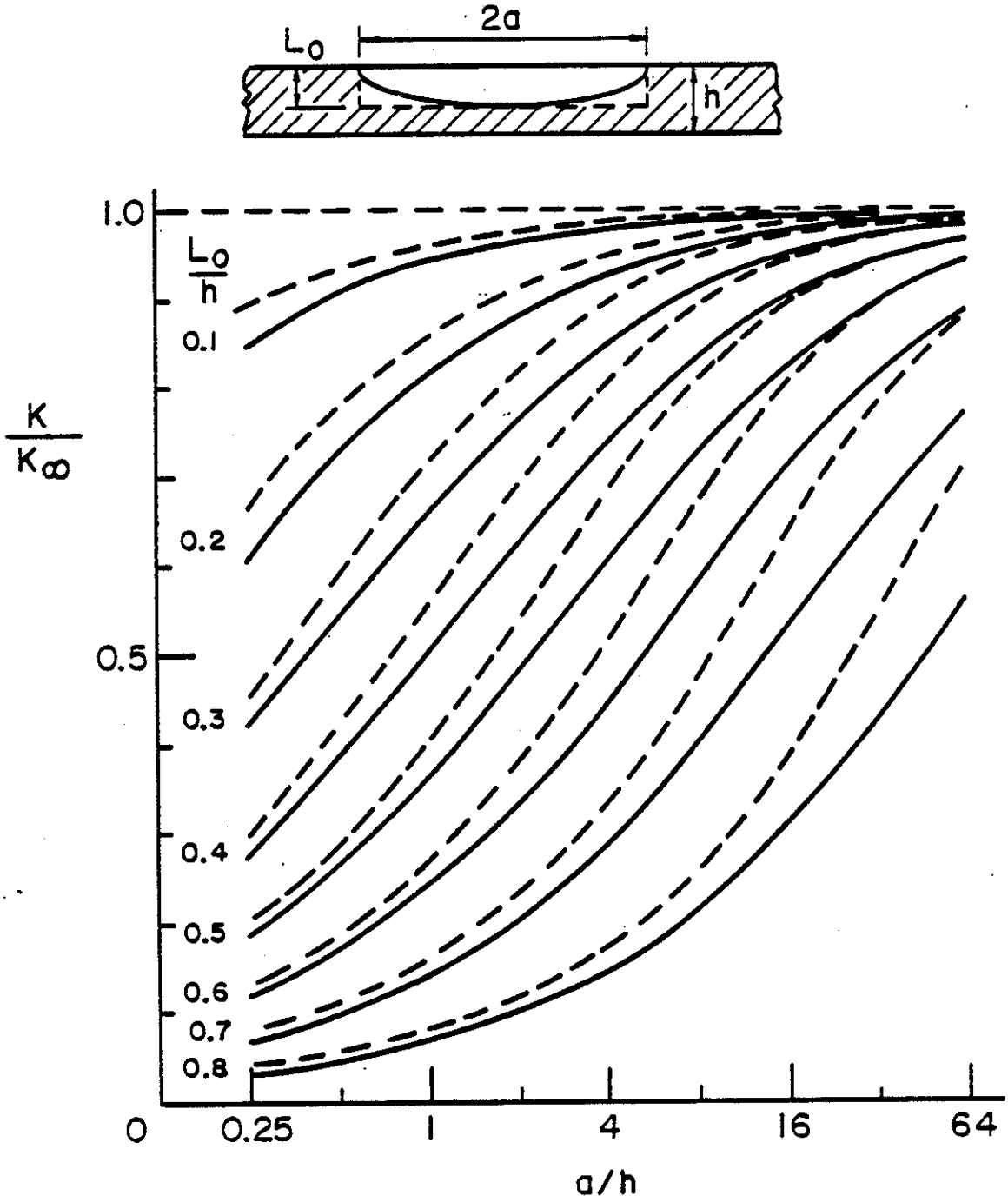

Fig. 54 Stress intensity factors for a semi-elliptic (full lines) and a rectangular (dashed lines) surface crack in a plate under uniform tension (ν=0.3).

and the matrices τ, A and C are again defined by (66)-(69). After solving the integral equations (70) and (71) for g_1 and g_2, σ and m are obtained from (63) and (69) and the stress intensity factors from (78) and (79).

From the derivation of the model given in this report it is clear that the technique can be used to estimate the stress intensity factors in any plate or shell containing part-through cracks provided the integral equations for the corresponding through crack problem is available and the related plane strain crack problem has a reliable solution which can be properly parametrized. Thus, extending the method to such problems as the corner cracks [32], collinear surface or internal cracks [32], part-through cracks in reinforced plates and shells, and other crack-crack and crack-boundary interaction problems becomes quite straightforward.

5.4 Some Results

As noted before for the application of the line spring model the contour of the part-through crack can be any reasonable curve provided the crack is relatively long (i.e., a>h). Figure 6 shows the stress intensity factor in an infinite plate containing a surface crack and subjected to uniform membrane loading N_{22}^{∞} away from the crack region. The normalizing stress intensity factor K_∞ which is defined by

$$K_\infty = \left(\frac{N_{22}^{\infty}}{h}\right) \sqrt{h}\, g_t(s_o) \ , \ s_o = L_o/h \tag{81}$$

is the corresponding plane strain value for an edge-cracked strip (see eq. 72). The figure shows the stress intensity factor at the midsection (i.e., at x_1=0) of a semi-elliptic and a rectangular crack respectively defined by

$$L(x_1) = L_o\sqrt{1-(x_1/a)^2} = L_o\sqrt{1-x^2} \ , \ L(x_1) = L_o, \ -a<x_1<a \ . \tag{82}$$

Note that the limiting values of the stress intensity factor are

$$K \to 0 \ \text{ for } \ a/h \to 0 \ ; \ K \to K_\infty \ \text{ for } \ a/h \to \infty \ . \tag{83}$$

As one may expect, the stress intensity factor for the rectangular crack is somewhat greater than that for the semi-elliptic crack and converges faster to the asymptotic value K_∞ as $a/h \to \infty$.

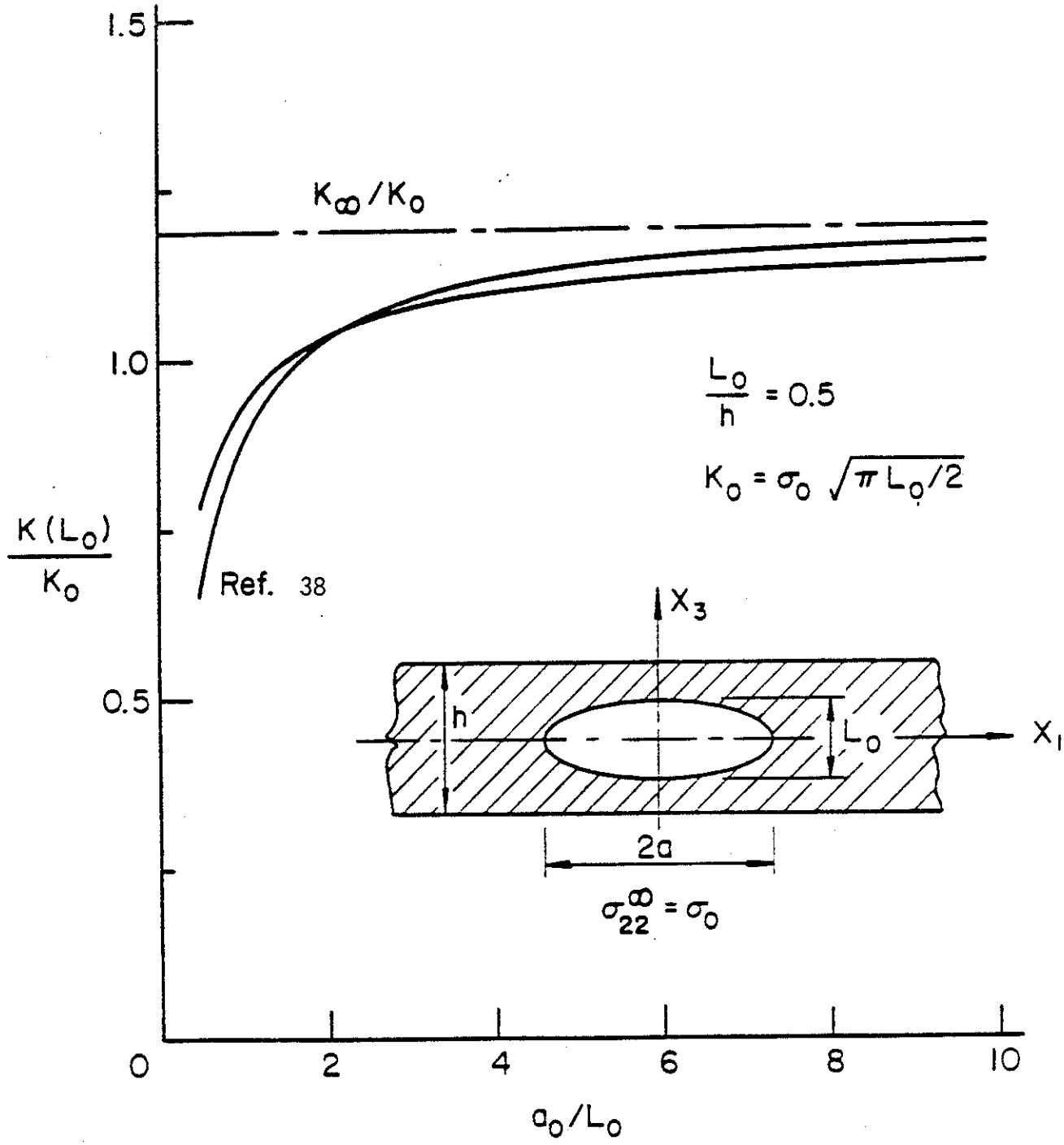

Fig. 55 Stress intensity factor at the mid section of a symmetrically located elliptic crack in a plate under uniform tension; $\sigma_{22}^{\infty}=\sigma_0$, $L_0/h=0.5$, $K_0=\sigma_0\sqrt{\pi L_0/2}$; K_∞ is the corresponding plane strain value in a strip (i.e., for $a_0=\infty$).

From a viewpoint of applying the line spring model perhaps the simplest part- through crack problem is that of a symmetrically located internal crack in an infinite plate under uniform tension (see the insert in Fig.55). In this case since there is no bending the problem is reduced to a simple integral equation given by (71) in which k_{21}, k_{22} and c_{21} are zero. In (80) $g_{At} = g_{Bt}$ and G(s) reduces to g_{At}^2 and the function c_{22} becomes

$$c_{22}(x) = a[(1-\nu^2)\int_0^{L(x)} g_{At}^2(L/h)dL]^{-1} . \tag{84}$$

Figure 55 shows the result of a simple example which is compared with that given in [38] for a plate containing a symmetrically located elliptic crack and subjected to uniform tension $\sigma_o = N_{22}^{\infty}/h$.

If the plate is also subjected to uniform bending moment M_{22}^{∞}, then in (80) $g_{Ab} = -g_{Bb}$ and $g_{At} = g_{Bt}$ and the integral equations (70) and (71) would be uncoupled. It should, however, be noted that because of crack closure on the compression side, in this case taken separately the bending results are meaningless. They may be used together with tension results which are sufficiently large so that the stress intensity factors on both sides of the crack are positive. The functions g_{At} and g_{Ab} are obtained from the results given in [37] as follows:

$$g_{At}(s) = \sqrt{\pi s} \sum_1^n b_j s^{2(j-1)} , \; s = L/h , \tag{85}$$

$$g_{Ab}(s) = \sqrt{\pi s} \sum_1^n c_j s^{j-1} , \; s = L/h \tag{86}$$

where the constants b_j and c_j are given in Table 8 which is based on the stress intensity ratios shown in Table 9 (see [37]). Extensive results for multiple part-through cracks of various configurations are given in Appendices A and B.

Table 8. The coefficients b_j and c_j for the shape functions g_{At} and g_{Ab} (eqs. 42 and 43).

j	bj	cj
1	0.7071	0.1013
2	0.4325	-2.7775
3	-0.1091	90.3734
4	7.3711	-862.4307
5	-57.7894	4843.4692
6	271.1551	-17069.1142
7	-744.4204	38813.4897
8	1183.9529	-56865.3055
9	-1001.4920	51832.6941
10	347.9786	-26731.2995
11		5959.4888

Table 9. Stress intensity factors for a centrally cracked plate subjected to tension (N) or bending (M) under plane strain conditions, (σ=N/h, m=6M/h^2; Fig. 3b).

L/h	$\frac{K_N}{\sigma\sqrt{\pi L/2}}$	$\frac{K_M}{m\sqrt{\pi L/2}}$
0.05		0.0250
0.1	1.0060	0.0500
0.2	1.0246	0.1001
0.3	1.0577	0.1505
0.4	1.1094	0.2023
0.5	1.1867	0.2573
0.6	1.3033	0.3197
0.7	1.4884	0.3986
0.8	1.8169	0.5186
0.9	2.585	0.7776
0.95	4.252	1.1421

The problem of a plate having a finite width with the emphasis on collinear part-through cracks and corner cracks was considered in [32]. Figures 56 and 57 show some sample results for central and corner cracks. Figure 56 shows the comparison of the stress intensity factors along the crack front for a symmetrically located, semi-elliptic and a rectangular surface crack in a plate under uniform tension. The normalizing stress intensity factors K_{to} and K_{bo} shown in Figures 56 and 57 are defined by

$$K_{to} = \left(\frac{N^{\infty}_{22}}{h}\right)\sqrt{h}\, g_t(s_o)\ ,\ K_{bo} = \left(\frac{6M^{\infty}_{22}}{h^2}\right)\sqrt{h}\, g_b(s_o)\ ,\ s_o = \frac{L_o}{h} \qquad (87)$$

and are the corresponding plane strain values for an edge-cracked strip under tension or bending. Figure 57 shows the stress intensity factor at the free surfaces of the plate $x_1 = \mp b$ in a plate containing two symmetric corner cracks under uniform tension or bending with crack length being the variable.

The form of the integral equations such as that given by (70) and (71) is quite general and is applicable to a great variety of part-through crack problems in plates and shells. The details of the problem influence only the kernels k_{ij}. The analysis and extensive results for collinear surface cracks and for corner cracks in a plate of finite width are given in Appendix A of this report.

Extensive results for an infinite cylindrical shell containing an external or internal, axial or circumferential part-through crack under local membrane loading or bending moment may be found in [18] (see, also [31] for some of the results). Tables 10 and 11 show some sample results for a 24 in. diameter pipe. The crack profile is again semi-elliptic which is defined by (82). The normalizing stress intensity factor K_o used in these tables is the corresponding edge crack plane strain value and is defined by (87a) for $N^{\infty}_{22} = N_{\infty} \neq 0$, $M^{\infty}_{22} = M_{\infty} = 0$ and by (87b) $N^{\infty}_{22} = N_{\infty} = 0$, $M^{\infty}_{22} = M_{\infty} \neq 0$.

5.5 Conclusions

Despite its simplicity, if carefully applied the line spring model may give very useful results for certain group of three-dimensional surface and internal cracks which are otherwise analytically intractable. The application of the model to the plasticity problems in plates and shells appears to be

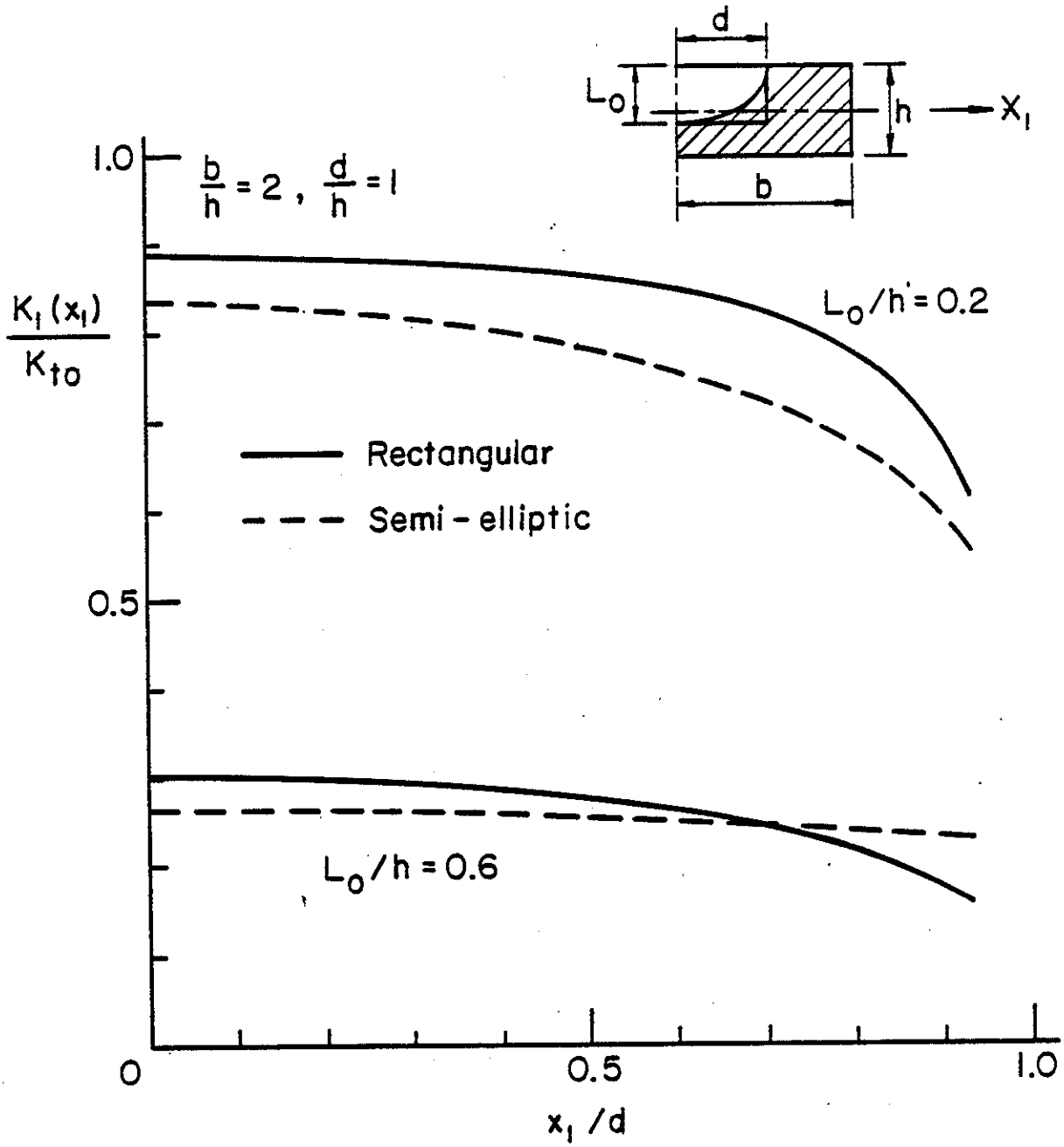

Fig. 56 Stress intensity factors for a semi-elliptic (dashed lines) and a rectangular (full lines) surface crack in a plate of finite width under uniform tension N_{22}^{∞}.

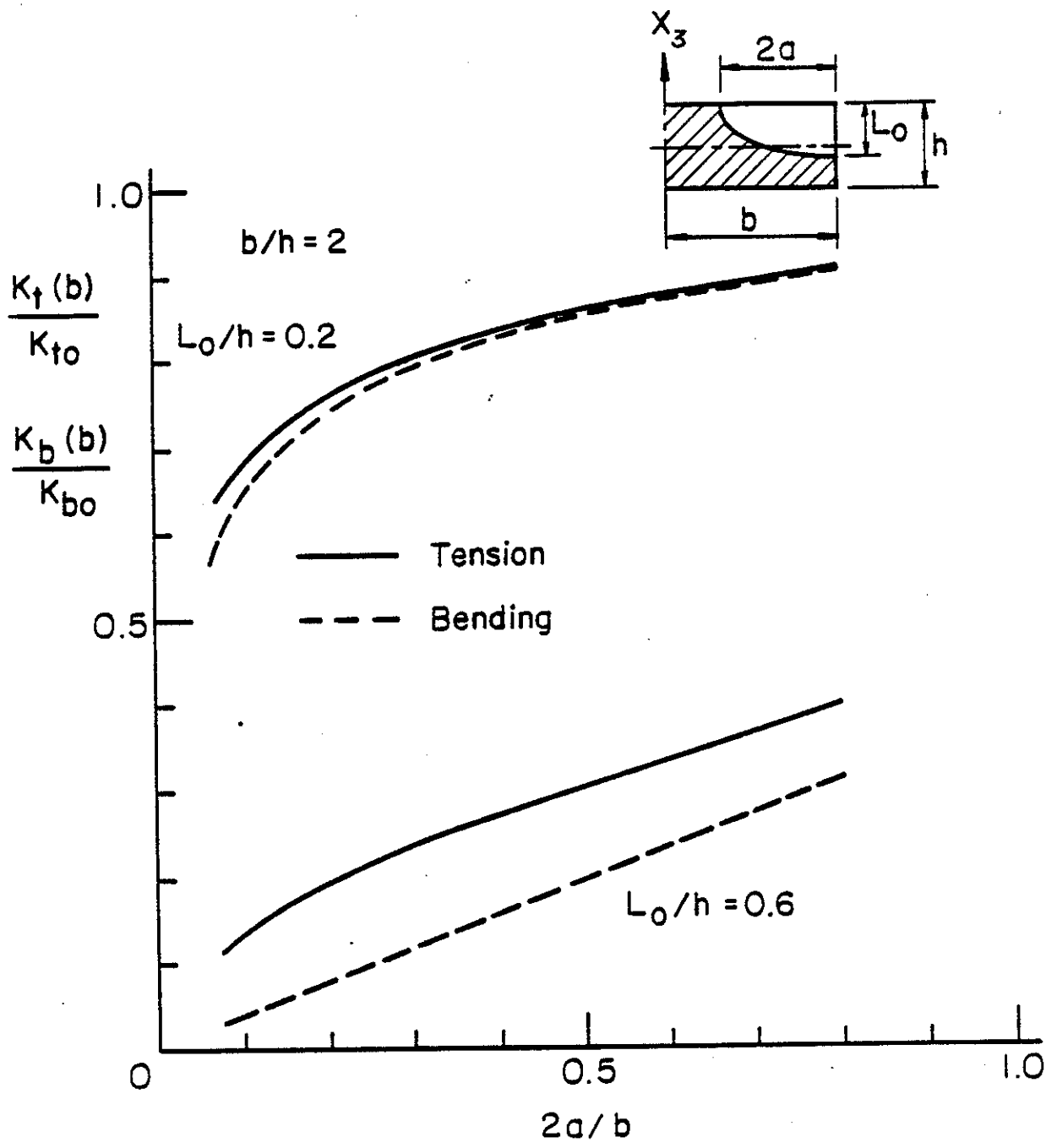

Fig. 57 Stress intensity factors in a plate of finite width containing two symmetrically located quarter elliptic corner cracks and subjected to uniform tension N_{22}^{∞} or bending M_{22}^{∞}.

also highly promising [27], [28], [33]. If the material has no strain hardening, then the plastic line spring reduces to some version of the Dugdale model which can be analyzed in a relatively straightforward manner [18],[31], [34]. The extension of the model to mixed mode part-through crack problems in plates and shells is being studied and appears to be quite feasible.

Table 10. K/K_0 in a line pipe with OD = 24 in., h = 0.344 in.

L_0/h →	0.1	0.2	0.3	0.4	0.5	0.6	0.7	0.8	0.9
a/h↓	Outer circumferential crack, $N_\infty \neq 0$, $M_\infty = 0$								
1.0	0.945	0.817	0.664	0.508	0.366	0.247	0.147	0.073	0.033
2.0	0.967	0.882	0.766	0.628	0.481	0.340	0.210	0.106	0.048
3.0	0.976	0.911	0.817	0.695	0.553	0.405	0.257	0.132	0.060
4.0	0.980	0.928	0.847	0.739	0.604	0.455	0.297	0.155	0.070
5.0	0.983	0.938	0.868	0.769	0.642	0.493	0.329	0.175	0.080
6.0	0.985	0.945	0.882	0.791	0.670	0.524	0.357	0.193	0.088
7.0	0.987	0.950	0.892	0.807	0.692	0.549	0.380	0.209	0.097
8.0	0.987	0.953	0.899	0.819	0.709	0.570	0.400	0.223	0.104
	Outer circumferential crack, $N_\infty = 0$, $M_\infty \neq 0$								
1.0	0.944	0.805	0.627	0.443	0.273	0.133	0.040	-0.011	-0.034
2.0	0.966	0.874	0.741	0.581	0.407	0.242	0.109	0.020	-0.028
3.0	0.975	0.905	0.798	0.657	0.492	0.318	0.164	0.048	-0.021
4.0	0.980	0.923	0.832	0.707	0.551	0.376	0.209	0.072	-0.012
5.0	0.983	0.934	0.854	0.741	0.594	0.421	0.246	0.094	-0.004
6.0	0.985	0.941	0.869	0.765	0.626	0.457	0.277	0.114	0.005
7.0	0.986	0.946	0.880	0.783	0.651	0.485	0.303	0.131	0.013
8.0	0.987	0.950	0.888	0.797	0.670	0.508	0.325	0.146	0.020
	Inner circumferential crack, $N_\infty \neq 0$, $M_\infty = 0$								
1.0	0.944	0.814	0.659	0.503	0.361	0.243	0.145	0.073	0.033
2.0	0.965	0.877	0.756	0.615	0.467	0.327	0.201	0.102	0.048
3.0	0.974	0.904	0.803	0.675	0.530	0.383	0.241	0.124	0.058
4.0	0.978	0.919	0.831	0.714	0.573	0.423	0.271	0.141	0.066
5.0	0.981	0.929	0.849	0.740	0.604	0.453	0.296	0.156	0.074
6.0	0.983	0.935	0.862	0.759	0.628	0.477	0.316	0.168	0.080
7.0	0.984	0.940	0.871	0.773	0.646	0.497	0.332	0.179	0.086
8.0	0.985	0.943	0.878	0.784	0.660	0.513	0.347	0.189	0.091
	Inner circumferential crack, $N_\infty = 0$, $M_\infty \neq 0$								
1.0	0.943	0.801	0.621	0.436	0.267	0.129	0.037	-0.012	-0.034
2.0	0.964	0.868	0.729	0.565	0.390	0.226	0.099	0.015	-0.030
3.0	0.973	0.897	0.782	0.634	0.463	0.291	0.143	0.037	-0.024
4.0	0.977	0.914	0.813	0.677	0.513	0.337	0.177	0.055	-0.018
5.0	0.980	0.924	0.833	0.706	0.548	0.372	0.204	0.070	-0.012
6.0	0.982	0.931	0.846	0.728	0.575	0.399	0.227	0.084	-0.007
7.0	0.983	0.936	0.856	0.743	0.595	0.421	0.246	0.095	-0.002
8.0	0.984	0.939	0.864	0.755	0.611	0.439	0.261	0.105	0.003

Table 11. K/K_o in a line pipe with OD = 24 in., h = 0.344 in.

L_o/h →	0.1	0.2	0.3	0.4	0.5	0.6	0.7	0.8	0.9
a/h↓				Outer axial crack, $N_\infty \neq 0$, $M_\infty = 0$					
1.0	0.946	0.820	0.668	0.512	0.370	0.250	0.149	0.074	0.033
2.0	0.968	0.887	0.774	0.639	0.492	0.350	0.217	0.110	0.050
3.0	0.977	0.917	0.829	0.712	0.574	0.425	0.273	0.142	0.063
4.0	0.983	0.935	0.863	0.762	0.634	0.485	0.323	0.171	0.077
5.0	0.986	0.947	0.886	0.797	0.679	0.535	0.367	0.200	0.090
6.0	0.988	0.955	0.902	0.824	0.715	0.577	0.406	0.227	0.103
7.0	0.990	0.961	0.914	0.844	0.744	0.611	0.441	0.253	0.117
8.0	0.991	0.965	0.924	0.860	0.767	0.640	0.472	0.277	0.130
				Outer axial crack, $N_\infty = 0$, $M_\infty \neq 0$					
1.0	0.944	0.807	0.631	0.448	0.278	0.137	0.042	-0.010	-0.034
2.0	0.967	0.879	0.750	0.593	0.421	0.255	0.118	0.025	-0.027
3.0	0.977	0.912	0.811	0.678	0.517	0.343	0.183	0.059	-0.016
4.0	0.982	0.931	0.849	0.734	0.586	0.415	0.241	0.092	-0.005
5.0	0.985	0.944	0.875	0.775	0.639	0.473	0.292	0.124	0.008
6.0	0.988	0.952	0.893	0.805	0.681	0.521	0.338	0.155	0.022
7.0	0.989	0.959	0.907	0.828	0.713	0.562	0.378	0.183	0.036
8.0	0.991	0.963	0.917	0.845	0.740	0.595	0.413	0.210	0.050
				Inner axial crack, $N_\infty \neq 0$, $M_\infty = 0$					
1.0	0.944	0.815	0.660	0.504	0.362.	0.244	0.145	0.073	0.034
2.0	0.966	0.879	0.760	0.620	0.472	0.332	0.205	0.104	0.049
3.0	0.975	0.908	0.810	0.685	0.542	0.394	0.250	0.130	0.060
4.0	0.980	0.925	0.842	0.730	0.593	0.443	0.288	0.151	0.071
5.0	0.983	0.937	0.864	0.762	0.632	0.483	0.321	0.172	0.081
6.0	0.985	0.945	0.880	0.787	0.664	0.517	0.351	0.191	0.090
7.0	0.987	0.951	0.892	0.807	0.690	0.546	0.378	0.209	0.099
8.0	0.988	0.956	0.902	0.823	0.713	0.572	0.402	0.226	0.108
				Inner axial crack, $N_\infty = 0$, $M_\infty \neq 0$					
1.0	0.943	0.802	0.622	0.437	0.268	0.129	0.038	-0.012	-0.034
2.0	0.965	0.871	0.734	0.570	0.396	0.232	0.103	0.017	-0.029
3.0	0.974	0.902	0.790	0.646	0.478	0.305	0.154	0.043	-0.022
4.0	0.979	0.920	0.825	0.696	0.537	0.362	0.198	0.066	-0.014
5.0	0.983	0.932	0.850	0.733	0.583	0.409	0.236	0.090	-0.005
6.0	0.985	0.941	0.868	0.762	0.620	0.449	0.270	0.110	0.004
7.0	0.987	0.948	0.882	0.784	0.650	0.484	0.301	0.131	0.013
8.0	0.988	0.953	0.893	0.803	0.676	0.514	0.330	0.150	0.022

6. THE INTERACTION BETWEEN FLAT INCLUSIONS OF FINITE THICKNESS AND CRACKS

6.1 Introduction

In studying the strength and fracture of welded components it is often necessary to take into account, among other factors, the effect of the imperfections in the material. Generally such imperfections are in the form of either geometric discontinuities or material inhomogeneities. For example, in welded joints, various shapes of voids, cracks, notches and regions of lack of fusion may be mentioned as examples for the former and variety of inclusions for the latter. From a viewpoint of fracture mechanics two important classes of imperfections are the planar flaws which may be idealized as cracks and relatively thin inhomogeneities which may be represented by flat inclusions.

Few unusual results aside, the problem of interaction between two cracks is relatively well-understood in the sense that the resulting stress field or the stress intensity factors would either be amplified or reduced as the distance between the cracks decreases. Almost in all cases the qualitative nature of the result could be predicted intuitively. For example, if the cracks are parallel then they would be in each other's shadow and there would be a reduction in the stress intensity factors. On the other hand if the cracks are co-planar then one would expect an amplification in the stress intensity factors. The exception or the unusual result in this case is the reduction in the stress intensity factors at the inner crack tips for certain relative crack locations in plates with relatively smaller thicknesses. Some specific problems relating to interaction between cracks were discussed in sections 4 and 5.

Intuitively what is not as well understood is the problem of interaction between cracks and flat inclusions. Separately both flaws have singular stresses and consequently are locations for potential fracture initiation. However, the inclusions are also "stiffeners" and therefore, properly oriented, they should tend to arrest crack propagation. For this reason in this study it is found to be worthwhile to undertake a detailed investigation of the problem on which the technical literature seems to be extremely weak. Particularly interesting in this problem is the behavior of the stress state around the ends

of the inclusions and at the points of intersection between inclusions and cracks. The details of the analysis of this crack-inclusion interaction problem and very detailed results are given in Appendix C of this report. Additional results on the special case of the inclusion intersecting the crack are given in Appendix D of this report. The interesting problem in this case is the peculiar stress singularities at the end of the inclusion which terminates at the crack surface rather than the crack tip which is discussed in Appendix C.

The correct way of modeling an inclusion would perhaps be to consider it as an elastic continuum fully bonded to the surrounding matrix. In this case, however, the crack-inclusion problems are generally difficult and only simple geometries and orientations can be treated analytically (see, for example, [39], [40]). A simple feature of such crack-inclusion interaction problems is that generally the stress intensity factors are magnified if the stiffness of the inclusion is less than that of the matrix and are diminished if the inclusion is stiffer than the matrix. For certain types of "flat" inclusions a simpler way of modeling may be to represent them as either a membrane with no bending stiffness or a perfectly rigid plane stiffener with negligible thickness. In these problems one may use the basic body force solution as the Green's function to derive the related integral equations. On the other hand, since the flat inclusion with an elastic modulus smaller than that of the matrix would itself have a behavior similar to a crack, it needs to be modeled basically as a "cavity" rather than a "stiffener".

Even though the technical literature on cracks, voids and inclusions which exist in the material separately is quite extensive, the problems of interaction between cracks and inclusions do not seem to be as widely studied. Such problems may be important in studying, for example, the micromechanics of fatigue and the fracture in welded joints. In this section a simple model for flat elastic inclusions is presented and the crack-inclusion interaction problem is considered for various relative orientations.

6.2 Integral Equations of the Problem

The plane strain or the generalized plane stress interaction problem under consideration is described in Fig.58. It is assumed that the boundaries of the medium are sufficiently far away from the crack-inclusion region so that

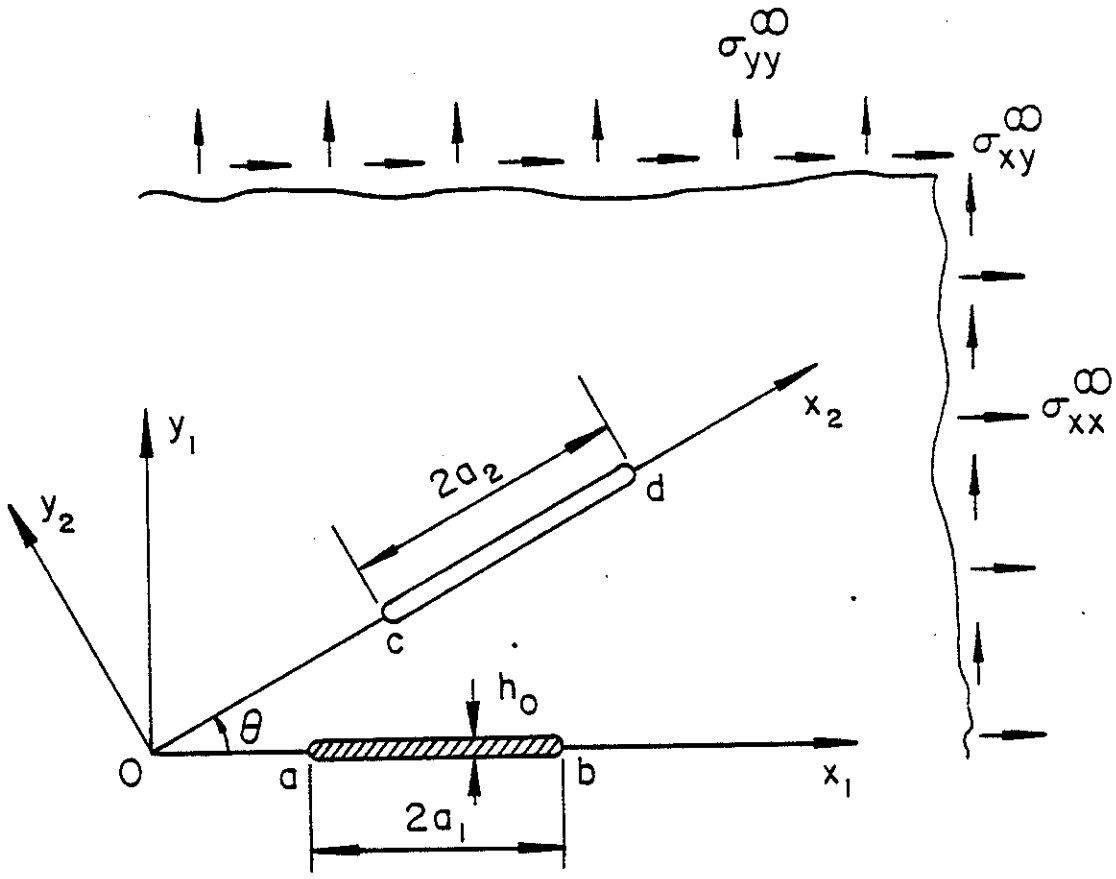

Fig. 58 The geometry of the crack-inclusion problem

their effect on the stress state perturbed by the crack and the inclusion may be neglected and the plane may be considered as being infinite.

Referring to Fig.58 we define the following unknown functions

$$g_1(x_1) = \frac{\partial}{\partial x_1}\,[v_1(x_1,+0)-v_1(x_1,-0)]\ ,\ (a<x_1<b)\ , \tag{88}$$

$$h_1(x_1) = \frac{\partial}{\partial x_1}\,[u_1(x_1,+0)-u_1(x_1,-0)]\ ,\ (a<x_1<b)\ , \tag{89}$$

$$g_2(x_2) = \frac{\partial}{\partial x_2}\,[v_2(x_2,+0)-v_2(x_2,-0)]\ ,\ (c<x_2<d)\ , \tag{90}$$

$$h_2(x_2) = \frac{\partial}{\partial x_2}\,[u_2(x_2,+0)-u_2(x_2,-0)]\ ,\ (c<x_2<d) \tag{91}$$

where u and v are, respectively, x and y components of the displacement vector in the coordinate systems shown in the figure. It is assumed that the inclusion fills a flat cavity the initial thickness of which is $h_o(x)$ which is "small" compared to its length $2a_1$. It is also assumed that the thickness variation of the stresses and the strain ε^i_{xx} in the inclusion are negligible. Thus, for the plane strain case, from the Hooke's Law we obtain the following stress-strain relations in the inclusion

$$\varepsilon^i_{yy}(x_1) = \frac{1-\nu_o-2\nu_o^2}{E_o(1-\nu_o)}\,\sigma^i_{yy}(x_1)\ ,\ \varepsilon^i_{xy}(x_1) = \frac{1}{2\mu_o}\,\sigma^i_{xy}(x_1)\ , \tag{92}$$

where E_o, ν_o, μ_o are the elastic constants of the inclusion. Now, by observing that

$$\varepsilon^i_{yy}(x_1) \cong [v_1(x_1,+0)-v_1(x_1,-0)]/h_o(x_1)\ , \tag{93}$$

$$2\varepsilon^i_{xy}(x_1) \cong [u_1(x_1,+0)-u_1(x_1,-0)]/h_o(x)\ , \tag{94}$$

and

$$E_o = 2\mu_o(1+\nu_o)\ ,\ \kappa_o = 3-4\nu_o\ , \tag{95}$$

from (1), (2) and (5)-(8) we find

$$\sigma^i_{yy}(x_1) = \frac{\kappa_o+1}{\kappa_o-1}\,\frac{\mu_o}{h_o(x_1)}\int_a^{x_1} g_1(t)dt\ , \tag{96}$$

$$\sigma_{xy}^{i}(x_1) = \frac{\mu_o}{h_o(x_1)} \int_a^{x_1} h_1(t)dt \quad . \tag{97}$$

If we let the medium to be uniformly loaded away from the crack-inclusion region as shown in Fig.58, for the stress components along the x_1 and x_2 axes we obtain

$$\sigma_{yy}^{1\infty}(x_1,0) = \sigma_{yy}^{\infty} \ , \ \sigma_{xy}^{1\infty}(x_1,0) = \sigma_{xy}^{\infty} \ , \tag{98}$$

$$\sigma_{yy}^{2\infty}(x_2,0) = \sigma_{yy}^{\infty}\cos^2\theta + \sigma_{xx}^{\infty}\sin^2\theta - 2\sigma_{xy}^{\infty}\sin\theta\cos\theta \ , \tag{99}$$

$$\sigma_{xy}^{2\infty}(x_2,0) = (\sigma_{yy}^{\infty}-\sigma_{xx}^{\infty})\sin\theta\cos\theta + \sigma_{xy}^{\infty}(\cos^2\theta-\sin^2\theta) \ . \tag{100}$$

From the basic dislocation solution given in, for example, [41], referred to the coordinate system x_1,y_1 the stress state at a point (x_1,y_1) in the plane due to the displacement derivatives g_1,h_1 defined by (88) and (89) may be expressed as

$$\sigma_{xx}^{11}(x_1,y_1) = \int_a^b [G_{xx}(x_1,y_1,t)g_1(t) + H_{xx}(x_1,y_1,t)h_1(t)]dt \ , \tag{101}$$

$$\sigma_{yy}^{11}(x_1,y_1) = \int_a^b [G_{yy}(x_1,y_1,t)g_1(t) + H_{yy}(x_1,y_1,t)h_1(t)]dt \ , \tag{102}$$

$$\sigma_{xy}^{11}(x_1,y_1) = \int_a^b [G_{xy}(x_1,y_1,t)g_1(t) + H_{yy}(x_1,y_1,t)h_1(t)]dt \ , \tag{103}$$

where

$$G_{xx}(x,y,t) = A(t-x)[(t-x)^2-y^2] ,$$

$$G_{yy}(x,y,t) = A(t-x)[3y^2+(t-x)^2] ,$$

$$G_{xy}(x,y,t) = Ay[y^2-(t-x)^2] ,$$

$$H_{xx}(x,y,t) = Ay[y^2+3(t-x)^2] , \qquad (104)$$

$$H_{yy}(x,y,t) = Ay[y^2-(t-x)^2] ,$$

$$H_{xy}(x,y,t) = A(t-x)[(t-x)^2-y^2] ,$$

$$A(x,y,t) = \frac{2\mu}{(1+\kappa)} \frac{1}{[(t-x)^2+y^2]^2} ,$$

and μ and κ are the elastic constants of the medium ($\mu=E/2(1+\nu)$, $\kappa=3-4\nu$ for plane strain and $\kappa=(3-\nu)/(1+\nu)$ for generalized plane stress). Similarly, referred to the axes x_2,y_2 the stress state σ_{ij}^{22}, $(i,j=x,y)$ in the plane due to g_2,h_2 may be obtained from (101)-(105) by substituting (c,d) for (a,b) and (x_2,y_2) for (x_1,y_1) and (g_2,h_2) for (g_1,h_1).

The integral equations to determine the unknown functions g_1,h_1,g_2, and h_2 may be obtained from the following traction boundary conditions along $(y_1=0,\ a<x_1<b)$ and $(y_2=0,\ c<x_2<d)$:

$$\sigma_{yy}^{11}(x_1,0) + \sigma_{yy}^{12}(x_1,0) + \sigma_{yy}^{1\infty}(x_1,0) = \sigma_{yy}^{i}(x_1) , \ (a<x_1<b) , \qquad (105)$$

$$\sigma_{xy}^{11}(x_1,0) + \sigma_{xy}^{12}(x_1,0) + \sigma_{xy}^{1\infty}(x_1,0) = \sigma_{xy}^{i}(x_1) , \ (a<x_1<b) , \qquad (106)$$

$$\sigma_{yy}^{22}(x_2,0) + \sigma_{yy}^{21}(x_2,0) + \sigma_{yy}^{2\infty}(x_2,0) = 0 , \ (c<x_2<d) , \qquad (107)$$

$$\sigma_{xy}^{22}(x_2,0) + \sigma_{xy}^{21}(x_2,0) + \sigma_{xy}^{2\infty}(x_2,0) = 0 , \ (c<x_2<d) , \qquad (108)$$

where all except the coupling stresses in the second column are given by (96)-(104). The coupling stresses have the following meaning: $\sigma_{yy}^{12}(x_1,0)$ is

the normal stress on $y_1=0$ plane due to the displacement derivatives $g_2(x_2)$ and $h_2(x_2)$ and $\sigma_{yy}^{21}(x_2,0)$ is the normal stress on $y_2=0$ plane due to g_1, h_1, etc. Thus, after making the necessary stress transformations similar to (99) and (100) we obtain

$$\sigma_{yy}^{12}(x_1,0) = \int_c^d [G_{yy}^{12}(x_1,t)g_2(t) + H_{yy}^{12}(x_1,t)h_2(t)]dt \ , \tag{109}$$

$$\sigma_{xy}^{12}(x_1,0) = \int_c^d [G_{xy}^{12}(x_1,t)g_2(t) + H_{xy}^{12}(x_1,t)h_2(t)]dt \ , \tag{110}$$

$$\sigma_{yy}^{21}(x_2,0) = \int_a^b [G_{yy}^{21}(x_2,t)g_1(t) + H_{yy}^{21}(x_2,t)h_1(t)]dt \ , \tag{111}$$

$$\sigma_{xy}^{21}(x_2,0) = \int_a^b [G_{xy}^{21}(x_2,t)g_1(t) + H_{xy}^{21}(x_2,t)h_1(t)]dt \ , \tag{112}$$

where from

$$\sigma_{yy}^{12}(x_1,0) = \sigma_{yy}^{22}(x_2,y_2)\cos^2\theta + \sigma_{xx}^{22}\sin^2\theta + \sigma_{xy}^{22}\sin 2\theta \tag{113}$$

calculated at $x_2=x_1\cos\theta$, $y_2=-x_1\sin\theta$ we have

$$G_{yy}^{12}(x_1,t) = G_{yy}(x_1\cos\theta,-x_1\sin\theta,t)\cos^2\theta + G_{xx}(x_1\cos\theta,-x_1\sin\theta,t)$$
$$+ G_{xy}(x_1\cos\theta,\ x_1\sin\theta,t)\sin 2\theta \ , \tag{114}$$

$$H_{yy}^{12}(x_1,t) = H_{yy}(x_1\cos\theta,-x_1\sin\theta,t)\cos^2\theta + H_{xx}(x_1\cos\theta,-x_1\sin\theta,t)$$
$$+ H_{xy}(x_1\cos\theta,-x_1\sin\theta,t)\sin 2\theta \ . \tag{115}$$

Similar expressions for the remaining kernels in (110)-(112) are obtained by using the stress transformations

$$\sigma_{xy}^{12}(x_1,0) = [\sigma_{xx}^{22}(x_2,y_2)-\sigma_{yy}^{22}(x_2,y_2)]\sin\theta\cos\theta$$

$$+ \sigma_{xy}^{22}(x_2,y_2)(\cos^2\theta-\sin^2\theta) \ , \ (x_2=x_1\cos\theta, \ y_2=-x_1\sin\theta) \ , \qquad (116)$$

$$\sigma_{yy}^{21}(x_2,0) = \sigma_{yy}^{11}(x_1,y_1)\cos^2\theta + \sigma_{xx}^{11}(x_1,y_1)\sin^2\theta$$

$$- \sigma_{xy}^{11}(x_1,y_1)\sin2\theta, \ (x_1=x_2\cos\theta, \ y_1=x_2\sin\theta) \ , \qquad (117)$$

$$\sigma_{xy}^{21}(x_2,0) = [\sigma_{yy}^{11}(x_1,y_1)-\sigma_{xx}^{11}(x_1,y_1)]\sin\theta\cos\theta$$

$$+ \sigma_{xy}^{11}(x_1,y_1)(\cos^2\theta-\sin^2\theta), \ (x_1=x_2\cos\theta, \ y_1=x_2\sin\theta) \ . \qquad (118)$$

Thus, from (101)-(112) and (116)-(118) it follows that

$$G_{xy}^{12}(x_1,t) = [G_{xx}(x,y,t)-G_{yy}(x,y,t)]\sin\theta\cos\theta$$

$$+ G_{xy}(x,y,t)\cos2\theta, \ (x=x_1\cos\theta, \ y=-x_1\sin\theta) \ , \qquad (119)$$

$$H_{xy}^{12}(x_1,t) = [H_{xx}(x,y,t)-H_{yy}(x,y,t)]\sin\theta\cos\theta$$

$$+ H_{xy}(x,y,t)\cos2\theta, \ (x=x_1\cos\theta, \ y=-x_1\sin\theta) \ , \qquad (120)$$

$$G_{yy}^{21}(x_2,t) = G_{yy}(x,y,t)\cos^2\theta + G_{xx}(x,y,t)\sin^2\theta$$

$$- G_{xy}(x,y,t)\sin2\theta \ , \ (x=x_2\cos\theta, \ y=x_2\sin\theta) \ , \qquad (121)$$

$$H_{yy}^{21}(x_2,t) = H_{yy}(x,y,t)\cos^2\theta + H_{xx}(x,y,t)\sin^2\theta$$

$$- H_{xy}(x,y,t)\sin2\theta \ , \ (x=x_2\cos\theta, \ y=x_2\sin\theta) \ , \qquad (122)$$

$$G^{21}_{xy}(x_2,t) = [G_{yy}(x,y,t)-G_{xx}(x,y,t)]\sin\theta\cos\theta$$

$$+ G_{xy}(x,y,t)\cos 2\theta \ , \ (x=x_2\cos\theta,\ y=x_2\sin\theta) \ , \tag{123}$$

$$H^{21}_{xy}(x_2,t) = [H_{yy}(x,y,t)-H_{xx}(x,y,t)]\sin\theta\cos\theta$$

$$+ H_{xy}(x,y,t)\cos 2\theta \ , \ (x=x_2\cos\theta,\ y=x_2\sin\theta) \ . \tag{124}$$

From (105)-(108) the integral equations of the problem may then be obtained as

$$\frac{1}{\pi}\int_a^b \frac{1}{t-x_1} g_1(t)dt + \int_a^{x_1} G(x_1)g_1(t)dt + c_o\int_c^d G^{12}_{yy}(x_1,t)g_2(t)dt$$

$$+ c_o\int_c^d H^{12}_{yy}(x_1,t)h_2(t)dt = -c_o\sigma^{\infty}_{yy} \ , \ (a<x_1<b) \ , \tag{125}$$

$$\frac{1}{\pi}\int_a^b \frac{1}{t-x_1} h_1(t)dt + \int_a^{x_1} H(x_1)h_1(t)dt + c_o\int_c^d G^{12}_{xy}(x_1,t)g_2(t)dt$$

$$+ c_o\int_c^d H^{12}_{xy}(x_1,t)h_2(t)dt = -c_o\sigma^{\infty}_{xy}, \ (a<x_1<b) \ , \tag{126}$$

$$c_o\int_a^b G^{21}_{yy}(x_2,t)g_1(t)dt + c_o\int_a^b H^{21}_{yy}(x_2,t)h_1(t)dt + \frac{1}{\pi}\int_c^d \frac{1}{t-x_2} g_2(t)dt$$

$$= -c_o(\sigma^{\infty}_{yy}\cos^2\theta+\sigma^{\infty}_{xx}\sin^2\theta-\sigma^{\infty}_{xy}\sin 2\theta), \ (c<x_2<d) \ , \tag{127}$$

$$c_o \int_a^b G_{xy}^{21}(x_2,t)g_1(t)dt + c_o \int_a^b H_{xy}^{21}(x_2,t)h_1(t)dt + \frac{1}{\pi}\int_c^d \frac{1}{t-x_2} h_2(t)dt$$

$$= -c_o[(\sigma_{yy}^{\infty}-\sigma_{xx}^{\infty})\sin\theta\cos\theta + \sigma_{xy}^{\infty}\cos 2\theta], \quad (c<x_2<d) \ , \tag{128}$$

where

$$c_o = \frac{1+\kappa}{2\mu} \ , \ G(x_1) = -\frac{\mu_o(\kappa+1)(\kappa_o+1)}{2\mu(\kappa_o-1)} \frac{1}{h_o(x_1)} \ ,$$

$$H(x_1) = -\frac{\mu_o(\kappa+1)}{2\mu} \frac{1}{h_o(x_1)} \ . \tag{129}$$

If there is no crack in the medium, $g_2=0=h_2$, the integral equations uncouple and (125) and (126) give the unknown functions g_1 and h_1. For example, if the inclusion has an elliptic cross-section given by

$$h_o(x) = b_o\sqrt{1-x^2} \ , \tag{130}$$

(125) becomes

$$\frac{1}{\pi}\int_{-1}^{1} \frac{g_1(t)}{t-x} dt - \int_{-1}^{x} \frac{c_1}{\sqrt{1-x^2}} g_1(t)dt = -c_o \sigma_{yy}^{\infty} \tag{131}$$

where

$$c_1 = \frac{\mu_o(1+\kappa)(1+\kappa_o)}{2\mu b_o(\kappa_o-1)} \ , \tag{132}$$

and without any loss in generality it is assumed that $a=-1$, $b=1$, $x_1=x$. The solution of (131) is found to be

$$g_1(t) = -\frac{c_o \sigma_{yy}^{\infty}}{1+c_1} \frac{t}{\sqrt{1-t^2}} \ , \quad (-1<t<1) \tag{133}$$

which, for $\mu_o=0$ reduces to the well-known crack solution. By using the following definition of the stress intensity factor

$$k_1(t) = -\lim_{x\to 1} \frac{2\mu}{1+\kappa} \sqrt{2(1-x)}\, g_1(x) \ , \tag{134}$$

from (133) it follows that

$$k_1(1) = \frac{\sigma^{\infty}_{yy}}{1+c_1} \quad . \tag{135}$$

Similarly, in the absence of a crack from (126), (129) and (130) it may be shown that

$$h_1(t) = -\frac{c_o \sigma^{\infty}_{xy}}{1+c_2} \frac{t}{\sqrt{1-t^2}} \quad , \quad (-1<t<1) \tag{136}$$

$$k_2(1) = \frac{\sigma^{\infty}_{xy}}{1+c_2} \quad , \quad c_2 = \frac{\mu_o(1+\kappa)}{2\mu b_o} \quad . \tag{137}$$

As another special case if we assume that the stiffness of the inclusion $\mu_o=0$, then the functions G and H defined by (129) vanish and the integral equations (125)-(128) reduce to that of two arbitrarily oriented cracks shown in Fig. 58.

6.3 Stress Intensity Factors

In the linearly elastic medium under consideration the intensity of the stress state around the end points of the crack and the inclusion is governed by the singular behavior of the displacement derivatives g_1, g_2, h_1 and h_2 which are defined by (88)-(91). If we assume the following standard definition of Modes I and II stress intensity factors

$$k_1(a) = \lim_{x_1 \to a} \sqrt{2(a-x_1)}\ \sigma^1_{yy}(x_1,0) \quad , \tag{138}$$

$$k_2(a) = \lim_{x_1 \to a} \sqrt{2(a-x_1)}\ \sigma^1_{yy}(x_1,0) \quad , \tag{139}$$

$$k_1(c) = \lim_{x_2 \to c} \sqrt{2(c-x_2)}\ \sigma^2_{yy}(x_2,0) \quad , \text{ etc.} \quad , \tag{140}$$

and observe that the system of integral equations (125)-(128) which has simple Cauchy type kernels has a solution of the form

$$g_i(t) = \frac{G_i(t)}{\sqrt{(b-t)(t-a)}} , \quad h_i(t) = \frac{H_i(t)}{\sqrt{(d-t)(t-c)}} , \quad (i=1,2) , \tag{141}$$

from (125)-(128) and (138)-(141) it can be shown that

$$k_1(a) = \frac{2\mu}{1+\kappa} \lim_{x_1 \to a} \sqrt{2(x_1-a)}\, g_1(x_1) , \tag{142}$$

$$k_1(b) = -\frac{2\mu}{1+\kappa} \lim_{x_1 \to b} \sqrt{2(b-x_1)}\, g_1(x_1) , \tag{143}$$

$$k_2(a) = \frac{2\mu}{1+\kappa} \lim_{x_1 \to a} \sqrt{2(x_1-a)}\, h_1(x_1) , \tag{144}$$

$$k_2(b) = -\frac{2\mu}{1+\kappa} \lim_{x_1 \to b} \sqrt{2(b-x_1)}\, h_1(x_1) \quad . \tag{145}$$

The stress intensity factors $k_i(c)$ and $k_i(d)$, $(i=1,2)$ may be expressed in terms of g_2 and h_2 by means of equations similar to (142)-(145).

6.4 Results

The integral equations (125)-(128) are solved by using the technique described in [36] and the stress intensity factors are calculated from (142)-(145) and from similar expressions written for the crack. For various crack-inclusion geometries and stiffness ratios μ_0/μ (μ_0 being the shear modulus of the inclusion) the calculated results are given in Tables 12-17. The main interest in this paper is in relatively "thin" and flat inclusions. Hence in the numerical analysis it is assumed that the thickness h_0 is constant. Table 12 shows the normalized stress intensity factors in a plane which contains a crack equal in size and coplanar with an inclusion and subjected to uniform tension and shear away from the crack-inclusion region (Fig.59a). The inclusion model used in this analysis is basically a crack the surfaces of which are held together by an elastic medium of shear modulus μ_0. Thus, for $\mu_0=0$ one recovers the two crack solution. It may be observed that for $\mu_0>0$ there is a significant reduction in the stress intensity factors around the end points $x_1=a$ and $x_1=b$ (Fig.59a). In Table 12 the variables are the

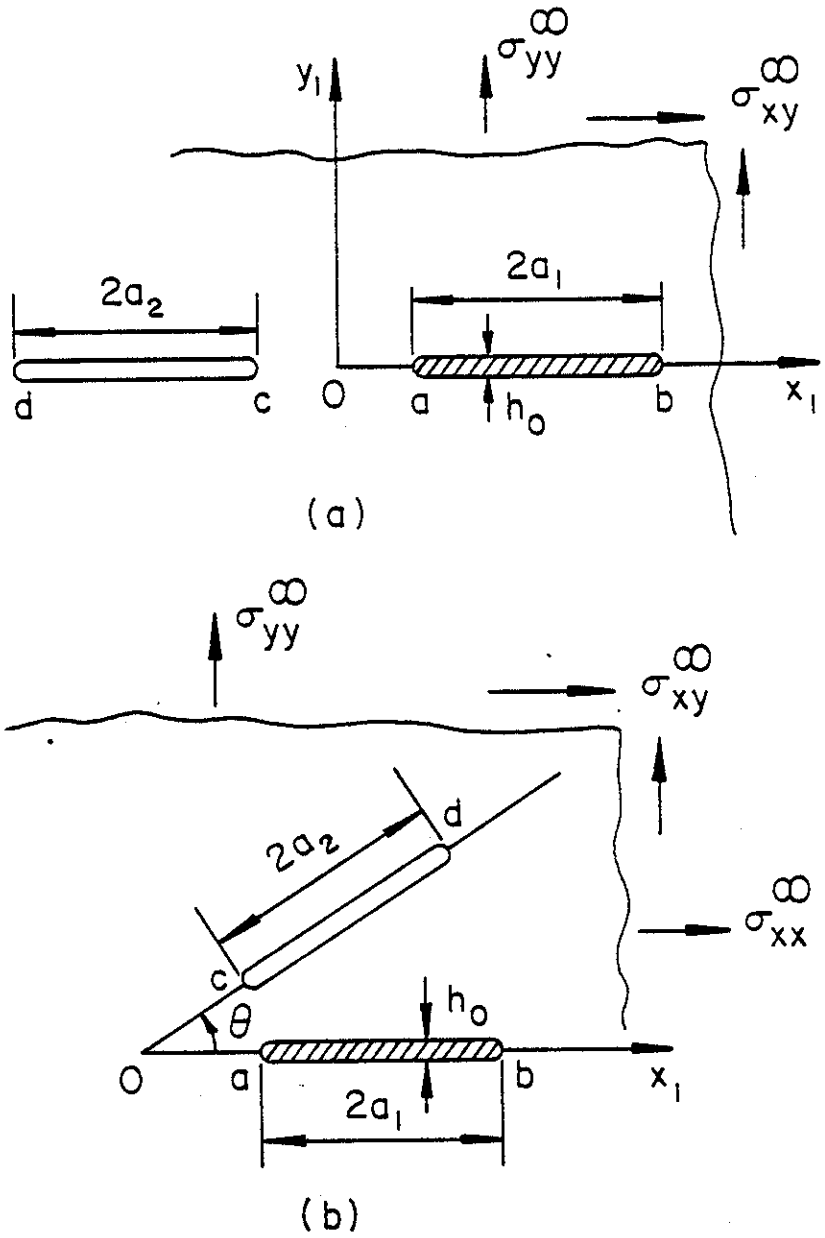

Fig. 59 Special crack-inclusion geometries used in numerical analysis

stiffness ratio μ_o/μ and the thickness of the inclusion h_o/a_1 with the spacing $a/a_1 = 0.01$ being constant, where $2a_1$ is the length of the inclusion (Fig.59a). Similar results calculated by assuming that $h_o/a_1 = 1/20$ and a/a_1 is variable are shown in Table 13.

For various values of the stiffness ratio μ_o/μ and fixed values of the inclusion thickness ($h_o/a_1=1/20$) and the distance a ($a/a_1=0.1$), the effect of the angle θ on the crack tip stress intensity factors are given in Table 14. The geometry and the loading condition away from the crack-inclusion region are shown in Fig.59b. In this example, too, it is assumed that the inclusion and the crack are of equal length ($a_2=a_1$). For the special case of $\mu_o=0$, that is, for the case of two cracks of equal lengths oriented at an angle θ the stress intensity factors are given in Table 15.

The stress intensity factors for the symmetric crack-inclusion geometries shown in Figures 60a and 60b are given in Table 16 where the length ratio a_2/a_1 is assumed to be the variable. In both examples the inclusion (half) length a_1 is used as the normalizing length parameter and the relative distance c/a_1 (Fig.60a) or a/a_1 (Fig.60b) is assumed to be constant.

Table 17 gives the stress intensity factors for a crack perpendicular to the inclusion where, referring to Fig.58, $\theta=\pi/2$, $a=0$, $\mu_o=\mu/20$ and $c/a_1=0.05$ are fixed and a_2 is variable.

It should be noted that since the superposition is valid, the tables give the stress intensity factors for the most general homogeneous loading conditions away from the crack-inclusion region. Also, the tables give the stress intensity factors which are normalized with respect to $\sigma^{\infty}_{ij}\sqrt{a_1}$ where $2a_1$ is the length of the inclusion and $(i,j)=(x,y)$, (Fig.58). The notation used in the tables is

$$k_{1a} = \frac{k_1(a)}{\sigma^{\infty}_{ij}\sqrt{a_1}}, \quad k_{2a} = \frac{k_2(a)}{\sigma^{\infty}_{ij}\sqrt{a_1}}, \quad k_{1c} = \frac{k_1(c)}{\sigma^{\infty}_{ij}\sqrt{a_1}}, \text{ etc.} \tag{146}$$

where k_1 and k_2 are, respectively, Modes I and II stress intensity factors defined by equations such as (138)-(140) and calculated from the expressions such as (142)-(145).

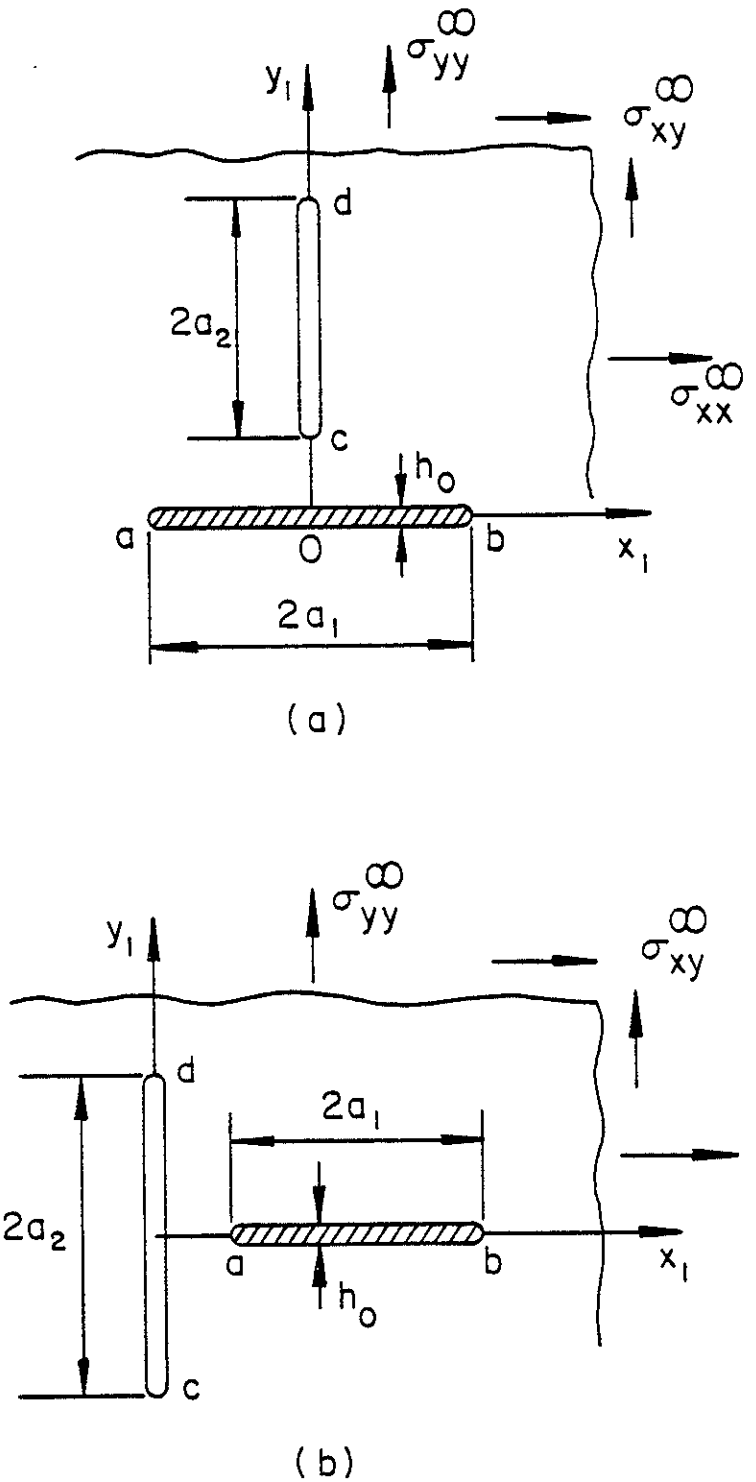

Fig. 60 Special crack-inclusion geometries used in numerical analysis

Table 12. Modes I and II stress intensity factors for the case of a crack located in the plane of the inclusion in a medium subjected to σ^{∞}_{yy} or σ^{∞}_{xy} away from the crack-inclusion region (Fig. 11); c=-a, d=-b, a/a_1=0.01, $k_{1c}=k_1(c)/\sigma^{\infty}_{yy}\sqrt{a_1}$, $k_{1d}=k_1(d)/\sigma^{\infty}_{yy}\sqrt{a_1}$, $k_{2c}=k_2(c)/\sigma^{\infty}_{xy}\sqrt{a_1}$, $k_{2d}=k_2(d)/\sigma^{\infty}_{xy}\sqrt{a_1}$, $k_{1a}=k_1(a)/\sigma^{\infty}_{yy}\sqrt{a_1}$, $k_{2a}=k_2(a)/\sigma^{\infty}_{xy}\sqrt{a_1}$, $k_{1b}=k_1(b)/\sigma^{\infty}_{yy}\sqrt{a_1}$, $k_{2b}=k_2(b)/\sigma^{\infty}_{xy}\sqrt{a_1}$, $a_1=(b-a)/2$.

	$\frac{2h_o}{b-a}$	μ_o/μ							
		0	0.05	0.1	0.25	0.5	1.0	2.0	5.0
k_{1b}	0.01	1.2063	.1578	.1031	.0535	.0303	.0163	.0085	.0035
	0.02	1.2063	.2320	.1578	.0888	.0535	.0303	.0163	.0068
	0.1	1.2063	.5146	.3713	.2320	.1578	.1031	.0634	.0303
	0.2	1.2063	.6836	.5146	.3323	.2320	.1578	.1031	.0535
k_{1a}	0.01	2.9642	.5725	.3908	.2104	.1207	.0654	.0342	.0140
	0.02	2.9642	.7941	.5725	.3404	.2104	.1207	.0654	.0276
	0.1	2.9642	1.5036	1.1620	.7941	.5725	.3908	.2478	.1207
	0.2	2.9642	1.8803	1.5036	1.0636	.7941	.5725	.3908	.2104
k_{1c}	0.01	2.9642	1.1795	1.1045	1.0479	1.0255	1.0132	1.0067	1.0027
	0.02	2.9642	1.2952	1.1795	1.0870	1.0480	1.0255	1.0132	1.0054
	0.1	2.9642	1.7825	1.5321	1.2952	1.1795	1.1045	1.0583	1.0255
	0.2	2.9642	2.0764	1.7825	1.4645	1.2952	1.1795	1.1045	1.0479
k_{1d}	0.01	1.2063	1.0116	1.0063	1.0027	1.0014	1.0007	1.0004	1.0001
	0.02	1.2063	1.0211	1.0116	1.0051	1.0027	1.0014	1.0007	1.0003
	0.1	1.2063	1.0693	1.0432	1.0211	1.0116	1.0063	1.0033	1.0014
	0.2	1.2063	1.1019	1.0693	1.0366	1.0211	1.0116	1.0063	1.0027
k_{2b}	0.01	1.2063	.3106	.2159	.1275	.0810	.0482	.0269	.0117
	0.02	1.2063	.4368	.3106	.1910	.1275	.0810	.0482	.0221
	0.1	1.2063	.8214	.6500	.4368	.3106	.2159	.1459	.0810
	0.2	1.2063	.9673	.8214	.5946	.4368	.3106	.2159	.1275
k_{2a}	0.01	2.9642	1.0075	.7480	.4743	.3122	.1900	.1076	.0470
	0.02	2.9642	1.3214	1.0075	.6747	.4743	.3122	.1900	.0885
	0.1	2.9642	2.1749	1.8071	1.3214	1.0075	.7480	.5345	.3122
	0.2	2.9642	2.4785	2.1749	1.6847	1.3214	1.0075	.7480	.4743
k_{2c}	0.01	2.9642	1.4272	1.2691	1.1366	1.0778	1.0425	1.0225	1.0093
	0.02	2.9642	1.6463	1.4272	1.2298	1.1366	1.0778	1.0425	1.0182
	0.1	2.9642	2.3136	2.0183	1.6463	1.4272	1.2691	1.1622	1.0778
	0.2	2.9642	2.5619	2.3136	1.9221	1.6463	1.4272	1.2691	1.1366
k_{2d}	0.01	1.2063	1.0330	1.0188	1.0085	1.0045	1.0023	1.0012	1.0005
	0.02	1.2063	1.0549	1.0330	1.0156	1.0085	1.0045	1.0023	1.0010
	0.1	1.2063	1.1292	1.0954	1.0549	1.0330	1.0188	1.0103	1.0045
	0.2	1.2063	1.1583	1.1292	1.0846	1.0549	1.0330	1.0188	1.0085

Table 13. Modes I and II stress intensity factors for the case of a crack located in the plane of the inclusion in a medium subjected to σ^{∞}_{yy} or σ^{∞}_{xy} away from the crack-inclusion region (Fig. 11); c=-a, d=-b, h_o/a_1=1/20.

	$\frac{2a}{b-a}$	μ_o/μ							
		0	0.05	0.1	0.25	0.5	1.0	2.0	5.0
k_{1b}	0.01	1.2063	.3713	.2611	.1578	.1031	.0635	.0366	.0163
	0.5	1.0517	.3544	.2513	.1527	.0998	.0615	.0354	.0158
	1	1.0280	.3493	.2479	.1508	.0986	.0607	.0350	.0156
	2	1.0125	.3453	.2452	.1492	.0976	.0601	.0347	.0154
k_{1a}	0.01	2.9642	1.1620	.8751	.5725	.3908	.2478	.1454	.0654
	0.5	1.1125	.3877	.2768	.1693	.1110	.0685	.0395	.0176
	1	1.0480	.3604	.2564	.1563	.1023	.0630	.0364	.0162
	2	1.0176	.3481	.2474	.1506	.0985	.0607	.0350	.0156
k_{1c}	0.01	2.9642	1.5321	1.3433	1.1795	1.1045	1.0583	1.0313	1.0132
	0.5	1.1125	1.0229	1.0130	1.0057	1.0030	1.0015	1.0008	1.0003
	1	1.0480	1.0096	1.0054	1.0024	1.0012	1.0006	1.0003	1.0001
	2	1.0176	1.0035	1.0020	1.0009	1.0004	1.0002	1.0001	1.0000
k_{1d}	0.01	1.2063	1.0432	1.0253	1.0116	1.0063	1.0033	1.0017	1.0007
	0.5	1.0517	1.0104	1.0058	1.0026	1.0013	1.0007	1.0003	1.0001
	1	1.0280	1.0056	1.0031	1.0014	1.0007	1.0004	1.0002	1.0001
	2	1.0125	1.0025	1.0014	1.0006	1.0003	1.0002	1.0001	1.0000
k_{2b}	0.01	1.2063	.6500	.4845	.3106	.2159	.1459	.0943	.0481
	0.5	1.0517	.6031	.4576	.2979	.2084	.1412	.0914	.0467
	1	1.0280	.5925	.4503	.2938	.2057	.1395	.0903	.0461
	2	1.0125	.5849	.4449	.2905	.2035	.1380	.0893	.0456
k_{2a}	0.01	2.9642	1.8071	1.4340	1.0075	.7480	.5345	.3601	.1900
	0.5	1.1125	.6498	.4971	.3272	.2302	.1567	.1017	.0520
	1	1.0480	.6081	.4636	.3035	.2129	.1446	.0937	.0479
	2	1.0176	.5889	.4483	.2930	.2053	.1393	.0902	.0461
k_{2c}	0.01	2.9642	2.0183	1.7299	1.4272	1.2691	1.1623	1.0937	1.0425
	0.5	1.1125	1.0523	1.0344	1.0172	1.0095	1.0050	1.0026	1.0011
	1	1.0480	1.0222	1.0145	1.0072	1.0040	1.0021	1.0011	1.0004
	2	1.0176	1.0081	1.0053	1.0026	1.0014	1.0008	1.0004	1.0002
k_{2d}	0.01	1.2063	1.0954	1.0637	1.0330	1.0188	1.0104	1.0055	1.0023
	0.5	1.0517	1.0239	1.0157	1.0078	1.0043	1.0023	1.0012	1.0005
	1	1.0280	1.0129	1.0084	1.0042	1.0023	1.0012	1.0006	1.0003
	2	1.0125	1.0057	1.0038	1.0019	1.0010	1.0005	1.0003	1.0001

Table 14. The effect of angular orientation θ and the modulus ratio μ_o/μ on the stress intensity factors in a medium under general in-plane loading (Fig. 10); c=a, d=b, $2h_o/(b-a)=1/20$, $2a/(b-a)=0.1$.

σ^∞	k	θ°					
		30	60	90	120	150	180
		$\mu_o/\mu = 0.05$					
σ^∞_{xx}	k_{1c}	0.2624	0.8047	1.0961	0.8097	0.2654	0
	k_{2c}	-0.4711	-0.4636	0.0163	0.4737	0.4585	0
	k_{1d}	0.2560	0.7618	1.0106	0.7562	0.2518	0
	k_{2d}	-0.4378	-0.4253	0.0122	0.4432	0.4383	0
σ^∞_{yy}	k_{1c}	0.6402	0.2232	-0.0311	0.2749	0.8366	1.1094
	k_{2c}	0.4596	0.4217	-0.0483	-0.5019	-0.4771	0
	k_{1d}	0.7052	0.2221	-0.0109	0.2568	0.7702	1.0250
	k_{2d}	0.4105	0.3981	-0.0386	-0.4636	-0.4493	0
σ^∞_{xy}	k_{1c}	-0.5020	-0.5895	0.2839	1.1440	1.0302	0
	k_{2c}	0.3394	-0.5681	-1.0010	-0.3793	0.7098	1.2367
	k_{1d}	-0.9072	-0.8566	0.0354	0.9049	0.8903	0
	k_{2d}	0.4353	-0.5284	-0.9911	-0.4631	0.5521	1.0567
		$\mu_o/\mu = 0.1$					
σ^∞_{xx}	k_{1c}	0.2552	0.7786	1.0613	0.7908	0.2608	0
	k_{2c}	-0.4593	-0.4546	0.0095	0.4610	0.4512	0
	k_{1d}	0.2534	0.7570	1.0066	0.7540	0.2512	0
	k_{2d}	-0.4366	-0.4291	0.0072	0.4395	0.4366	0
σ^∞_{yy}	k_{2c}	0.6535	0.2334	-0.0181	0.2628	0.8003	1.0643
	k_{2c}	0.4533	0.4238	-0.0293	-0.4758	-0.4605	0
	k_{1d}	0.7248	0.2350	-0.0058	0.2540	0.7615	1.0143
	k_{2d}	0.4219	0.4145	-0.0215	-0.4506	-0.4425	0
σ^∞_{xy}	k_{1c}	-0.6023	-0.6717	0.1849	1.0482	0.9749	0
	k_{2c}	0.3956	-0.5401	-0.9996	-0.4197	0.6414	1.1599
	k_{1d}	-0.8892	-0.8588	0.0230	0.8910	0.8817	0
	k_{2d}	0.4617	-0.5172	-0.9943	-0.4762	0.5343	1.0374

Table 15 - cont.

		$\mu_o/\mu = 0.5$					
σ^{∞}_{xx}	k_{1c}	0.2478	0.7537	1.0157	0.7622	0.2535	0
	k_{2c}	-0.4414	-0.4405	0.0019	0.4418	0.4391	0
	k_{1d}	0.2509	0.7517	1.0017	0.7511	0.2503	0
	k_{2d}	-0.4341	-0.4322	0.0017	0.4347	0.4341	0
σ^{∞}_{yy}	k_{1c}	0.7013	0.2427	-0.0045	0.2523	0.7620	1.0158
	k_{2c}	0.4381	0.4288	-0.0078	-0.4448	-0.4407	0
	k_{1d}	0.7446	0.2469	-0.0012	0.2510	0.7527	1.0033
	k_{2d}	0.4312	0.4292	-0.0048	-0.4371	-0.4353	0
	k_{1c}	-0.7657	-0.8011	0.0517	0.9166	0.8971	0
	k_{2c}	0.4738	-0.5057	-0.9981	-0.4766	0.5420	1.0479
	k_{1d}	-0.8712	-0.8639	0.0061	0.8726	0.8702	0
	k_{2d}	0.4910	-0.5046	-0.9987	-0.4938	0.5094	1.0105
		$\mu_o/\mu = 2$					
σ^{∞}_{xx}	k_{1c}	0.2484	0.7504	1.0041	0.7535	0.2510	0
	k_{2c}	-0.4356	-0.4354	0.0003	0.4356	0.4349	0
	k_{1d}	0.2503	0.7505	1.0004	0.7503	0.2501	0
	k_{2d}	-0.4333	-0.4328	0.0004	0.4335	0.4333	0
σ^{∞}_{yy}	k_{1c}	0.7317	0.2473	-0.0012	0.2505	0.7531	1.0042
	k_{2c}	0.4330	0.4314	-0.0022	-0.4363	-0.4352	0
	k_{1d}	0.7487	0.2492	-0.0003	0.2503	0.7507	1.0009
	k_{2d}	0.4326	0.4321	-0.0012	-0.4341	-0.4336	0
σ^{∞}_{xy}	k_{1c}	-0.8318	-0.8460	0.0146	0.8801	0.8748	0
	k_{2c}	0.4947	-0.5001	-0.9989	-0.4932	0.5122	1.0139
	k_{1d}	-0.8674	-0.8655	0.0016	0.8678	0.8672	0
	k_{2d}	0.4976	-0.5013	-0.9997	-0.4983	0.5026	1.0029

Table 16. Interaction of two cracks (Fig. 11b); $\mu_0/\mu_1=0$, c=a, d=b, 2a/(b-a) = 0.1.

		θ°					
		30	60	90	120	150	180
σ^{∞}_{xx}	k_{1a}	0.1834	-0.0122	-0.1604	-0.1271	-0.0361	0
	k_{2a}	0.1293	0.0928	0.2122	0.2877	0.1946	0
	k_{1b}	-0.1471	-0.1373	-0.0666	-0.0113	0.0024	0
	k_{2b}	0.1825	0.2323	0.2104	0.1371	0.0588	0
	k_{1c}	0.3637	1.0032	1.2370	0.8684	0.2790	0
	k_{2c}	-0.5576	-0.4950	0.0577	0.5191	0.4810	0
	k_{1d}	0.3073	0.8057	1.0308	0.7633	0.2536	0
	k_{2d}	-0.3956	-0.3708	0.0477	0.4591	0.4441	0
σ^{∞}_{yy}	k_{1a}	0.5843	0.9140	1.2370	1.3954	1.4643	1.4914
	k_{2a}	-0.1912	-0.0242	-0.0577	-0.1080	-0.0730	0
	k_{1b}	0.9210	1.0081	1.0308	1.0567	1.0994	1.1220
	k_{2b}	0.0215	-0.0427	-0.0477	-0.0168	0.0054	0
	k_{1c}	0.4051	-0.1004	-0.1604	0.3999	1.1491	1.4914
	k_{2c}	0.6195	0.4264	-0.2122	-0.6987	-0.6027	0
	k_{1d}	0.4666	0.0652	-0.0666	0.2821	0.8481	1.1220
	k_{2d}	0.1916	0.1811	-0.2104	-0.5795	-0.5082	0
σ^{∞}_{xy}	k_{1a}	0.1842	0.7402	0.6381	0.3381	0.1384	0
	k_{2a}	1.1741	1.1315	1.0152	1.1777	1.4058	1.4914
	k_{1b}	0.4327	0.1938	0.0748	0.0610	0.0532	0
	k_{2b}	0.5851	0.7960	0.9950	1.1104	1.1305	1.1220
	k_{1c}	-0.4402	-0.4311	0.6381	1.4876	1.2302	0
	k_{2c}	0.3095	-0.6671	-1.0152	-0.2462	0.9347	1.4914
	k_{1d}	-1.1414	-0.8951	0.0748	0.9554	0.9234	0
	k_{2d}	0.1531	-0.6362	-0.9950	-0.4219	0.6115	1.1220

Table 17. Stress intensity factors for the case of a crack perpendicular to the inclusion, $\mu_o/\mu=1/20$, $h_o/a_1=1/20$.

	σ^∞	k	a_2/a_1			
			0.1	0.5	1.0	5.0
Fig. 3a $a=-b=-a_1$ $c/a_1=0.1$	σ^∞_{xx}	$k_{1a}=k_{1b}$	-0.0088	-0.0479	-0.0938	-0.1449
		$k_{2a}=-k_{2b}$	-0.0058	-0.0820	-0.1428	-0.2729
		k_{1c}	+1.0636	1.1611	1.1572	1.1256
		k_{1d}	1.0320	1.0245	1.0109	1.0029
	σ^∞_{yy}	$k_{1a}=k_{1b}$	0.3424	0.3441	0.3441	0.3438
		$k_{2a}=-k_{2b}$	0.0006	0.0039	0.0039	0.0033
		k_{1c}	-0.1220	-0.0896	-0.0632	-0.0255
		k_{1d}	-0.0988	-0.0116	0.0067	0.0021
	σ^∞_{xy}	$k_{1a}=-k_{1b}$	-0.0004	-0.0162	-0.0850	-0.5164
		$k_{2a}=k_{2b}$	0.5703	0.5162	0.4502	0.4199
		k_{2c}	-0.7288	-0.9533	-1.0730	-1.2431
		k_{2d}	-0.7856	-1.0338	-1.0638	-1.0200
Fig. 3b $c=-d=-a_2$ $a/a_1=0.1$	σ^∞_{xx}	k_{1a}	0.0208	-0.1238	-0.2149	-0.2773
		k_{1b}	0.0006	0.0100	0.0234	-0.1170
		$k_{1c}=k_{1d}$	1.0037	1.0053	1.0101	1.0026
		$k_{2c}=-k_{2d}$	-0.0011	-0.0074	-0.0107	-0.0045
	σ^∞_{yy}	k_{1a}	0.3476	0.3543	0.3764	0.3057
		k_{1b}	0.3416	0.3418	0.3416	0.3469
		$k_{1c}=k_{1d}$	0.1584	-0.0186	-0.0324	-0.0048
		$k_{2c}=-k_{2d}$	-0.0353	0.0460	0.0406	0.0073
	σ^∞_{xy}	k_{2a}	0.6514	0.5903	0.4304	0.0544
		k_{2b}	0.5808	0.6066	0.6315	0.3702
		$k_{1c}=-k_{1d}$	-0.4813	-0.2431	-0.1012	-0.0010
		$k_{2c}=k_{2d}$	-1.3694	-0.9632	-0.9372	-0.9946

Table 18. Stress intensity factors for a crack perpendicular to the inclusion (Fig. 1); $\theta=\pi/2$, $a=0$, $2c/(b-a)=0.05$, $\mu_o/\mu=1/20$, $2h_o/(b-a)=0.05$.

σ^∞	k	a_2/a_1			
		0.1	0.5	1.0	5.0
σ^∞_{xx}	k_{1a}	.0399	.2055	.3675	1.1277
	k_{2a}	.0128	.0418	.0555	.1125
	k_{1b}	.0005	.0035	-.0081	-.0715
	k_{2b}	.0021	.0402	.1107	.3050
	k_{1c}	1.0762	1.1674	1.1729	1.1435
	k_{2c}	.0162	-.0056	-.0311	-.0740
	k_{1d}	1.0310	1.0274	1.0143	1.0018
	k_{2d}	.0207	.0212	.0115	-.0015
σ^∞_{yy}	k_{1a}	.3574	.3716	.3791	.3884
	k_{2a}	.0092	.0283	.0390	.0533
	k_{1b}	.3414	.3411	.3418	.3456
	k_{2b}	.0001	-.0010	-.0036	-.0062
	k_{1c}	-.0490	-.0607	-.0514	-.0250
	k_{2c}	-.3157	-.2298	-.1863	-.0933
	k_{1d}	-.0468	-.0250	-.0084	-.0009
	k_{2d}	-.1943	-.0830	-.0464	-.0048
σ^∞_{xy}	k_{1a}	.0887	.3231	.4952	1.1795
	k_{2a}	.6265	.7947	.9710	1.9112
	k_{1b}	.0002	.0001	.0079	.2709
	k_{2b}	.5805	.5910	.5713	.4743
	k_{1c}	1.1620	.6411	.4373	.1825
	k_{2c}	-1.0423	-1.1380	-1.1889	-1.2670
	k_{1d}	.6504	.1454	.0426	.0045
	k_{2d}	-.9292	-.9710	-1.0075	-1.0117

7. REFERENCES FOR PART I

1. C.D. Lundin, "The Significance of Weld Discontinuities - A Review of Current Literature", W.R.C. Bulletin, No. 222, Dec. 1976.

2. "Proposed Assessment Methods for Flaws with Respect to Failure by Brittle Fracture", Welding in the World, Vol. 13, No. 1/2, 1975.

3. S.T. Rolfe and J.M. Barsom, Fracture and Fatigue Control in Structures, Prentice Hall, 1977.

4. Fatigue Crack Propagation, ASTM-STP 415, 1967.

5. M.S. Kamath, "The COD Design Curve: An Assessment of Validity Using Wide Plate Tests", The Welding Institute Research Report 71/1978/E, Sept. 1978.

6. J.D. Harrison, "The 'State-of-the-Art' in Crack Tip Opening Displacement Testing and Analysis", the Welding Institute Research Report 108/1980, April 1980.

7. J.D. Harrison, M.G. Dawes, G.L. Archer, and M.S. Kamath, "The COD Approach and Its Application to Welded Structures", ASTM-STP668, 1979.

8. F. Erdogan, "Theoretical and Experimental Study of Fracture in Pipelines Containing Circumferential Flaws", Final Report, DOT-RSPA-DMA-50/83/3, Sept. 1982.

9. V.L. Hein and F. Erdogan, "Stress Singularities in a Two-Material Wedge", Int. J. of Fracture Mechanics, Vol. 7, pp. 317-330, 1971.

10. F. Erdogan, G.D. Gupta and M. Ratwani, "Interaction Between a Circular Inclusion and an Arbitrarily Oriented Crack", J. Appl. Mech., Vol. 41, Trans. ASME, pp. 1007-1013, 1974.

11. F. Erdogan and G.D. Gupta, "The Inclusion Problem with a Crack Crossing the Boundary", Int. J. of Fracture, Vol. 11, pp. 13-27, 1975.

12. F. Erdogan and G.C. Sih, "On the Crack Extension in Plates Under Plane Loading and Transverse Shear", J. Basic Engng., Trans. ASME, Vol. 85, pp. 519-526, 1963.

13. N.I. Muskhelishvili, Some Basic Problems of the Mathematical Theory of Elasticity, P. Noordhoff Ltd. Groningen-Holland, 1953.

14. T.S. Cook and F. Erdogan, "Stresses in Bonded Materials with a Crack Perpendicular to the Interface", Int. J. Engng. Sci., Vol. 10, pp. 667-697, 1972.

15. F. Erdogan and V. Biricikoglu, "Two Bonded Half Planes with a Crack Going Through the Interface", Int. J. Engng. Sci., Vol. 11, pp. 745-766, 1973.

16. F. Erdogan and T.S. Cook, "Antiplane Shear Crack Terminating at and Going Through a Bimaterial Interface", Int. J. of Fracture, Vol. 10, pp. 227-240, 1974.

17. J.L. Bassani and F. Erdogan, "Stress Intensity Factors in Bonded Half Planes Containing Inclined Cracks and Subjected to Antiplane Shear Loading", Int. J. Fracture, Vol. 15, pp. 145-158, 1979.

18. F. Erdogan, "Theoretical and Experimental Study of Fracture in Pipelines Containing Circumferential Flaws", Final Report, DOT-RSPA-DMA-50/83/3, Sept. 1982.

19. J.R. Rice and N. Levy, "The Part-Through Surface Crack in an Elastic Plate", J. Appl. Mech., Vol. 39, Trans. ASME, pp. 185-194, 1972.

20. J.K. Knowles and N.M. Wang, "On the Bending of an Elastic Plate Containing a Crack", J. of Mathematics and Physics, Vol. 39, p. 223, 1960.

21. N.M. Wang, "Effects of Plate Thickness on the Bending of an Elastic Plate Containing a Crack" J. of Mathematics and Physics, Vol. 47, p. 371, 1968.

22. R.J. Hartranft and G.C. Sih, "Effect of Plate Thickness on the Bending Stress Distribution around Through Cracks", J. of Mathematics and Physics, Vol. 47, p. 276, 1968.

23. E. Reissner, "On Bending of Elastic Plates", Quarterly of Applied Mathematics, Vol. 5, p. 55, 1947.

24. E. Reissner and F.Y.M. Wan, "On the Equations of Linear Shallow Shell Theory", Studies in Applied Mathematics, Vol. 48, p. 132, 1969.

25. F. Delale and F. Erdogan, "Transverse Shear Effect in a Circumferentially Cracked Cylindrical Shell", Quarterly of Applied Mathematics, Vol. 37, p. 239, 1979.

26. F. Delale and F. Erdogan, "The Effect of Transverse Shear in a Cracked Plate under Skewsymmetric Loading", J. Appl. Mech., Vol. 46, Trans. ASME, p.

27. D.M. Parks, "The Inelastic Line Spring: Estimates of Elastic-Plastic Fracture Prarmeters for Surface Cracked Plates and Shells", Paper 80/C2/PVP-109, ASME, 1980.

28. D.M. Parks, "Inelastic Analysis of Surface Flaws Using the Ling Spring Model", Proceedings of the 5th Int. Conf. on Fracture, Cannes, France, 1981.

29. F. Delale and F. Erdogan, "Line Spring Model for Surface Cracks in a Reissner Plate", Int. J. Engng. Sci., Vol. 19, p. 1331, 1981.

30. F. Delale and F. Erdogan, "Application of the Line Spring Model to a Cylindrical Shell Containing a Circumferential or an Axial Part-Through Crack", J. Appl. Mech., Vol. 49, p. 97, Trans. ASME, 1982.

31. F. Erdogan and H. Ezzat, "Fracture of Pipelines Containing a Circumferential Crack", Welding Research Council Bulletin 288, WRC, 1983.

32. F. Erdogan and H. Boduroglu, "Surface Cracks in a Plate of Finite Width under Extension or Bending", Theoretical and Applied Fracture Mechanics, Vol. 1, 1985 (to appear).

33. J.R. Rice, "The Line Spring Model for Surface Flaws", The Surface Crack, Physical Problems and Computational Solutions, J.L. Swedlow, ed. p. 171, ASME, New York, 1972.

34. F. Erdogan, G.R. Irwin and M. Ratwani, "Ductile Fracture of Cylindrical Vessels Containing a Large Flaw", ASTM-STP601, p. 191, 1976.

35. F. Erdogan and F. Delale, "Ductile Fracture of Pipes and Cylindrical Containers with a Circumferential Flaw", J. Pressure Vessel Technology, Trans. ASME, Vol. 103, p. 160, 1981.

36. F. Erdogan, "Mixed Boundary Value Problems in Mechanics", Mechanics Today, S. Nemat-Nasser, ed. Vol. 4, p. 1, Pergamon Press, Oxford, 1978.

37. A.C. Kaya and F. Erdogan, "Stress Intensity Factors and COD in an Orthotropic Strip", Int. Journal of Fracture, Vol. 16, p. 171, 1980.

38. T.C. Newman and T.S. Raju, "Stress Intensity Factor Equations for Cracks in Three-Dimensional Finite Bodies", ASTM STP 791, 1983.

39. F. Erdogan and G.D. Gupta, "The Inclusion Problem with a Crack Crossing the Boundary", Int. J. of Fracture, Vol. 11, pp. 13-27, 1975.

40. F. Erdogan, G.D. Gupta and M. Ratwani, "Interaction Between a Circular Inclusion and an Abitrarily Oriented Crack", J. Appl. Mech., Vol. 41, Trans. ASME, pp. 1007-1013, 1974.

41. J. Dundurs, "Elastic Interaction of Dislocations with Inhomogeneities", Mathematical Theory of Dislocations, T. Mura, ed., pp. 70-115, ASME, New York, 1969.

PART II

MECHANISMS OF CORROSION FATIGUE IN LINEPIPE STEELS

In this part, results of studies, designed for developing mechanistic understanding of corrosion fatigue, are described. These studies provide the scientific bases for guiding the development of methodology for assessing the safety and durability of pipelines in service, and for guiding the development of improved materials and protection systems. The results are not intended for use directly in design and rule-making.

1. INTRODUCTION

Transmission and distribution pipelines are exposed to a broad range of chemical environments, both in terms of corrosive species that are present in soils (such as carbonates, chlorides and nitrates) and of deleterious species that may be transported within the lines (such as hydrogen and ammonia, and hydrogen sulfide and water/water vapor as impurities in natural gas and oil). These environments, acting in concert with operating stresses (both static and cyclic stresses) and residual stresses, can cause cracks to initiate and grow, and result in subsequent failure (leakage or rupture). In addition to these external environments, hydrogen that might be present in the steel (introduced during fabrication, processing or field installation, or by corrosion or cathodic charging during service) can also lead to cracking. Quantitative information and understanding are needed, therefore, to assess the safety, durability and reliability of pipelines during service, and to guide in the development of improved materials and protection systems.

Although a considerable amount of research has been devoted to the problem of environmentally assisted cracking in linepipe steels, most of this effort, however, has been directed to the study of stress corrosion cracking (or cracking under static loading) and of corrosion per se. For a range of reasons, quantitative understanding of the phenomenological and mechanistic aspects of environmentally assisted cracking is yet to be fully developed. Results during recent years, at Lehigh University and elsewhere [1-7], have shown that environmentally assisted cracking results from the interaction of

clean metal surfaces (produced by cracking or by deformation) with the environment, and that the very early stages (i.e., the first few milliseconds to several seconds) of reactions are responsible for the enhanced cracking. Fatigue (associated with cyclic loading from a variety of sources), being a proficient mechanical process for creating new surfaces, acting in concert with corrosion, therefore, may be a more serious failure mechanism than stress corrosion cracking.

The need to consider corrosion fatigue as a potentially significant failure mechanism in pipelines is based on the recognition that operating pressures (or stresses) do not remain truly constant and that minor fluctuations in stresses can significantly alter cracking response [8-11]. Indeed it has been difficult to reconcile service failures and laboratory stress corrosion cracking data without allowing for the possibility for corrosion fatigue [11,12]. To properly address the problems of corrosion fatigue, it is essential to recognize the multi-faceted nature of the phenomenon which reflects the synergism of chemistry/electrochemistry, mechanics and metallurgy. The cracking response reflects both the nature and the kinetics of chemical reactions between the environment and the fresh crack surfaces, and the interactions of hydrogen that is produced by these reactions with the microstructure [6]. Significant advances in understanding and in placing corrosion fatigue analysis on a fundamentally sound and quantitative basis depend on the understanding of the mechanisms of the various processes that control corrosion fatigue.

2. PROGRAM OBJECTIVE AND SCOPE

In this part of the program, a multi-disciplinary research was undertaken to investigate the mechanisms of corrosion fatigue crack initiation and propagation in linepipe steels exposed to aqueous environments. The program is directed at (1) the development of quantitative understanding of the early stages of chemical reactions in relation to crack initiation and growth, (2) elucidating the mechanisms for corrosion fatigue crack initiation and growth, including the influences of chemical, mechanical and metallurgical variables, and (3) the formulation and evaluation of models for predicting cracking response and service performance. A combined fracture mechanics,

surface chemistry and materials science approach was used. The specific areas of planned research were as follows:

(1) Determination of the kinetics of passivation (viz., initial reactions) as functions of pH, ion concentration, and other factors.

(2) Determination of the kinetics of fatigue crack initiation as a function of temperature for selected environmental conditions, and correlation with the chemical data.

(3) Determination of the kinetics of fatigue crack growth as a function of temperature for selected environmental conditions, and correlation with the chemical data.

(4) Examination of the influences of loading variables (such as cyclic load frequency, waveform, and load ratio) on corrosion fatigue crack initiation and growth.

(5) Synthesis of chemical, mechanical and metallurgical data to develop quantitative understanding of the mechanisms for corrosion fatigue crack initiation and growth. Formulation and verification of models for predicting cracking response and service performance.

The research program was planned for a period of three (3) years, and complemented an ongoing study on the mechanisms for corrosion fatigue in high-strength steels and titanium alloys sponsored by the Office of Naval Research. Because of funding constraints, the program has been restricted to studies of the kinetics of passivation and the kinetics of fatigue crack growth in X-70 steel. Results from the first two (2) years are summarized in this final technical report.

3. MATERIAL AND EXPERIMENTAL WORK

A X-70 steel, obtained as 5/8-inch-thick plate, was used in this study. Passivation measurements and corrosion fatigue crack growth studies were carried out over a range of temperatures from about 0°C to 90° C (273 to 363 K). Procedures for the electrochemical and crack growth experiments are described separately in the following subsections.

3.1 Electrochemical Measurements

Two electrochemical measurement techniques were considered [13,14]. The first one (the potential step technique) involved cathodically polarizing a "clean" surface at a suitable potential in the electrolyte of interest, suddenly switching to another potential, and monitoring the current transient under potentiostatic conditions at the new potential. In the second (galvanic current) technique, the galvanic current between a cathodically "cleaned" surface and a surface that had been "oxidized" in the electrolyte was measured. The current flow in each of these two cases was expected to contain information on the reactions of a clean surface with the electrolyte. Because the second technique was believed to more closely simulate the reactions at the crack tip, under open circuit conditions, it was selected. A schematic diagram showing the essential elements of this technique is given in Fig. 1.

Galvanic current measurements were made on X-70 steel in a deaerated electrolyte, consisting of an equivolume mixture of 1N Na_2CO_3-1N $NaHCO_3$ at pH = 9.7 (at room temperature), at temperatures from about 0° to 90°C (or 273 to 363 K). The desired test temperature was obtained by immersing the corrosion cell in a constant-temperature bath, and was maintained constant to ± 1°C. To minimize contamination of the electrolyte, the cleaning electrode was placed in a separate cell, and was connected to the main cell through a salt bridge. The specimen was mechanically polished, rinsed with acetone and methanol, and was cleaned ultrsonically in distilled water. It was then introduced into the galvanic cell and cleaned electrochemically at -1700 mV SCE for at least 10 minutes before starting the galvnic current experiment. Current transients and the associated electrode potential were recorded digitally and were analyzed.

3.2 Fatigue Crack Growth Measurements

Fatigue crack growth experiments were carried out on the X-70 steel, as a function of frequency, in distilled water and in an 1N Na_2CO_3-1N $NaHCO_3$ solution at temperatures ranging from 23° to 90°C (296 to 363 K). A limited number of tests were also carried out in a 0.6N NaCl solution at room temperature. Compact tension (CT) specimens, with thickness of 12.7 mm (0.50 in.) and width of 63.5 mm (2.5 in.), were used, and were tested in the LT orienta-

tion; that is, with the crack plane perpendicular to the principal rolling direction and crack growth in the long-transverse direction of the plate. Tests were carried out under constant-K conditions, at ΔK = 40 MPa-$m^{1/2}$ (36.4 ksi-$in.^{1/2}$) and a load ratio R = 0.1, in an automated electrohydraulic testing machine. Crack growth was monitored by the compliance method [15]. The calibration relationship given by Hudak and Saxena [16] was checked experimentally and was used. Crack growth rate measurements were estimated to be better than 10%, and specimen-to-specimen variation in rates was estimated to be about 20%.

The experiments were first conducted in static (quiescent), deaerated solutions. It was recognized that the chemical conditions in the crack may be different in the absence of forced flow, and additional experiments were then carried out with the deaerated solution flowing at a rate of about 0.1 ml/min. (or about 1.6 x 10^{-3} gal/h). The solutions were deaerated by continuous purging with pure nitrogen.

4. RESULTS AND DISCUSSIONS

4.1 Fatigue Crack Growth Response

Fatigue crack growth rate data for X-70 steel are shown as a function of the effective time for reactions (1/2f, where f is the cyclic load frequency) at different temperatures in Fig. 2, for quiescent distilled water, and in Fig. 3, for flowing distilled water, respectively. A comparison between room temperature data in quiescent and flowing (0.1 ml/min.) distilled water is given in Fig. 4.

At a given temperature (Figs. 2 and 3), crack growth rates increased with decreasing frequency. This increase in rate is consistent with the increased time for chemical/electrochemical reactions at the lower frequencies. Increases in temperature shifted the entire crack growth rate versus inverse frequency response curves in the direction of higher frequencies (i.e., to the left or to shorter times), while leaving the form of the response curve sensibly unchanged. The observed shift with temperature indicated that at least one of the reaction steps, responsible for crack growth enhancement, is thermally activated. The constancy in form of the response curve suggested

that the responsible reaction remained unchanged over the temperature range used in the investigation. These results are consistent with those observed in a modified HY130 steel in distilled water and in acetate buffer solution [6,13,14], and suggested that the behavior may be representative of corrosion fatigue of steels in aqueous environments.

From Fig. 4, it may be seen that the crack growth rates in flowing water were slower (by about 50%) than those in quiescent water; (compare also Figs. 2 and 3). This difference may be attributed to changes in pH at the crack tip. Brown and coworkers [7] have shown that, under freely corroding conditions, crack-tip pH can be highly acidic even when the pH of the bulk solution is neutral. Acidification of the crack tip region resulted from hydrolysis of the anodic dissolution products, as follows:

$$Fe^{++} + 2H_2O = Fe(OH)^{+} + H_3O^{+}$$

Solution flow tended to minimize this acidification process by flushing hydrogen ions out of the crack tip region, and both the anodic dissolution and the hydrogen reduction rates are expected to be reduced. The observed decrease in crack growth rates with solution flow is therefore consistent with control by the rates of electrochemical reactions at the crack tip.

Fatigue crack growth behavior of X-70 steel in 1N Na_2CO_3-1N $NaHCO_3$ solution (pH = 9.7 at 296 K) was found to be more complex and more difficult to explain. A comparison of crack growth rate data in quiescent and in flowing 1N Na_2CO_3-1N $NaHCO_3$ solution (pH = 9.7) at room temperature (296 K) is given in Fig. 5. The frequency dependence of fatigue crack growth rates in the flowing solution is consistent with that observed in distilled water. In the quiescent solution, on the other hand, the growth rates were essentially independent of frequency from 0.03 to 10 Hz. This difference in behavior cannot be readily explained in terms of crack tip pH, since the solution was well buffered. Measurement of crack tip pH for the quiescent case, using Brown's indicator method, indeed showed no change in pH between the crack tip and the bulk solution. Addition work is required to understand this phenomenon.

Since the response in flowing solution was well behaved, principal attention was directed towards the study of fatigue crack growth response for this

case. Fatigue crack growth data in 1N Na_2CO_3-1N $NaHCO_3$ solution at different temperatures are shown in Fig. 6. The characteristic shift of crack growth rate response towards the higher frequencies (or to the left) with increases in temperature (as was observed in distilled water) is again apparent, and is indicative of control of fatigue crack growth by thermally activated reaction processes.

At a given temperature, the overall fatigue crack growth rate response in 1N Na_2CO_3-1N $NaHCO_3$ solution is slower than that in distilled water. In other words, the crack growth rate curve is displaced in the lower frequency direction (or to the right), such that the growth rate at any given frequency would tend to be slower than the corresponding rate in distilled water. In fact, the addition of any foreign ions into (pure) distilled water tended to retard crack growth rate response. This phenomenon is illustrated in Fig. 7 where the room-temperature fatigue crack growth data in three different environments are compared. It may be noted that, at a given frequency, the crack growth rate is highest in distilled water; followed by 0.6N NaCl solution, and then 1N Na_2CO_3-1N $NaHCO_3$ solution. The fact that the crack growth rate is faster in 0.6N NaCl solution than in 1N Na_2CO_3-1N $NaHCO_3$ solution is not surprising, because the NaCl solution is deemed to be more corrosive; (interpreted here as having faster reaction kinetics). What is surprising, however, is the observation of slower fatigue crack growth rates in 0.6N NaCl solution relative to that in distilled water, because the presence of chloride ions is known to accelerate metal dissolution in occluded regions (such as pits, crevices and cracks) [18]. Apparently the presence of foreign ions, including chloride ions, moderates and slows (and may alter the mechanisms for) the metal-electrolyte reactions that are responsible for the enhancement of fatigue crack growth. The ions, however, do not appear to inhibit the extent of or to prevent the completion of such reactions. The nature of the reactions and the mechanisms for the ionic influences are not known at the present time, but are important to the understanding of corrosion fatigue crack growth response.

The overall crack growth response (Figs. 2 to 6) and the similarity of this response to that of other steels [5,6,13,19] strongly suggest that fatigue crack growth of X-70 steel in aqueous environment is controlled by electrochemical reactions at the crack tip. A modified superposition model

has been proposed to analyze the contribution by electrochemical reactions [6], and may be used to correlate the crack growth and chemical reaction data. According to this model, the observed crack growth rate in an aqueous environment, $(da/dN)_e$, is expressed as the sum of two rates [6]:

$$(da/dN)_e = (da/dN)_r^* + (da/dN)_{cf} \quad (1)$$

In Eqn. (1), $(da/dN)_r^*$ is a modified reference crack growth rate which incorporates the inert environment crack growth rate and the contribution by the extremely fast initial chemical reaction, and $(da/dN)_{cf}$ is the contribution associated with electrochemical reactions [4-7,20]. Actually, Eqn. (1) is to be viewed as a condensed form of a more correct representation of concurrent micromechanisms for crack growth, which is described in detail in [20]. The common plateau rate at the higher frequencies (greater than about 5 Hz) in Figs. 2 and 6 corresponds to $(da/dN)_r^*$. Increases in crack growth rate beyond this base level are considered to be electrochemical in nature and correspond to $(da/dN)_{cf}$.

Reaction controlled fatigue crack growth response in aqueous environments is assumed to be analogous to that in a gaseous environment [19]. As a first order approximation, first-order or Langmuir reaction kinetics may be assumed, and the reaction controlled model for crack growth may be expressed in the following simple form [19]:

$$(da/dN)_{cf} = (da/dN)_{cf,s} [1 - \exp(-t/\tau)]$$

or

$$(da/dN)_{cf} = (da/dN)_{cf,s} [1 - \exp(-\frac{1}{2f\tau})] \quad (2)$$

where $(da/dN)_{cf,s}$ is the saturation crack growth rate, τ is the reaction time constant, and f is the frequency.

By using estimated values of $(da/dN)_r^* = 3 \times 10^{-7}$ m/c and $(da/dN)_{cf,s} = 1.4 \times 10^{-6}$ m/c, approximate time constants were estimated from Figs. 3 and 6 by "fitting" Eqn. (2) to the crack growth data. The crack growth response based on Eqn. (2) are shown as dashed curves in these figures. The time constants ranged from about 1.5 to 10 s for distilled water, corresponding to temperatures from 336 to 296 K, and from about 2.5 to 35 s for the 1N Na_2CO_3-1N $NaHCO_3$ solution from 355 to 296 K, respectively. These time constants

correspond to an apparent activation energy of about 37 kJ/mol. The time constants from the 1N Na_2CO_3-1N $NaHCO_3$ solution may be compared to those observed in the simulation electrochemical experiments to probe the correlation between crack growth rates and electrochemical reaction kinetics.

4.2 Electrochemical Reaction Kinetics and Correlation with Crack Growth

Typical current transients obtained from the electrochemical experiments at different temperatures are shown in Fig. 8. The change in reaction rates with temperature can be clearly seen. The nonlinear nature of the log i versus time data indicated that the current transients represented the operation of more than one process. Assuming that the electrochemical reactions on the fresh metal surface proceeded by two or more parallel first-order processes, an approximate time constant may be then determined for each reaction step by the using the following equation [21]:

$$i = i_o + \sum_k i_k \exp(-t/\tau_k) \qquad (3)$$

where i is the observed current, i_o is the base level (or steady state) current, i_k and τ_k are respectively the initial current and the time constant for the k-th reaction, and t is time. The time constants, τ_k, may be determined from the experimental data by using a suitable nonlinear regression analysis method, or estimated graphically from the log i vs. t curves.

Three (3) sources of current have been identified [14], namely (i) the discharge of the double layer (or electrons), (ii) oxidation of adsorbed hydrogen (and perhaps hydrogen gas) that have been deposited on the specimen surface during cathodic cleaning, and (iii) anodic reactions of the clean surface with the electrolyte. The initial current decay is believed to reflect principally electron transfer from the first two sources. Based on this recognition, time constants were estimated graphically and were found to range from 1 to 80 seconds. Recognizing that the longer time constants may correspond to the formation of higher order reaction products or may be attributed to slow eqilibriation in the galvanic current experiment, the range of time constants may be reduced to about 1 to 40 s. This range overlapped that of the crack growth results, which strongly suggests the correlation between crack growth and electrochemical reactions at the crack tip.

A more careful examination of the galvanic cell experiment revealed, however, that there is one important difference between this simulation experiment and the real crack tip condition [14]. In the galvanic cell experiment the clean metal surface was obtained by cathodic cleaning, which caused an accumulation of extraneous charges on the working electrode. These extra charges would not be present on the fresh metal surface at the crack tip under open circuit condition. During the galvanic cell experiment, the extra charges would be transferred and contribute to the total current. Therefore, depending on the relative contribution of these extra charges to the whole reaction process, the galvanic cell experiment may or may not be a proper simulation of the crack tip condition, and provide usable information on the electrochemical reaction kinetics.

The experimental results now suggest that the extraneous charges due to cathodic cleaning may have been excessive [14]. Although the galvanic cell experiment may be considered adequate for obtaining information on hydrogen evolution kinetics, the results could not be used at this time to make an unequivocal correlation between the electrochemical kinetics and the crack growth kinetics, particularly with respect to the rate controlling process. Resolution of this uncertainty must be made to arrive at a more complete understanding of the rate of electrochemical reactions in corrosion fatigue.

Since the extra charges were introduced by cathodic cleaning, an obvious way of resolving the problem is to produce the clean metal surface by mechanical means. A modified scratching electrode method may be used, whereby a masked working electrode is coupled to the freely corroding cathode and then scratched to expose fresh metal surfaces. The resultant current and potential transients may then be analyzed by the same way as was discussed previously. Another possibility may be in situ breaking of a specimen in the electrochemical cell to generate the requisite clean surfaces. The in situ fracture technique is being examined under another program, and may be adopted for use in further studies of X-70 steel under internal funding.

5. SUMMARY

Corrosion fatigue crack growth behavior of a X-70 linepipe steel in deaerated distilled water and 1N Na_2CO_3-1N $NaHCO_3$ solution was examined as a function of frequency and temperature at ΔK of 40 MPa-$m^{1/2}$ and R = 0.1. The frequency and temperature ranges were 0.03 to 10 Hz and 296 to 355 K, respectively. Room temperature tests were also carried out in deaerated 0.6N NaCl solution to provide for comparison.

In these environments, corrosion fatigue crack growth rates were shown to depend strongly upon frequency and temperature. The dependence was consistent with a model for surface reaction controlled fatigue crack growth, and was thermally activated, with an apparent activation energy of about 40 kJ/mol. This dependence was reflected by a shift of the entire crack growth response curve to higher frequencies with increasing temperature, while leaving the growth rates within the response curve (or the form of the response curve) sensibly unchanged. Crack growth response in deaerated distilled water was found to be the fastest, followed by deaerated 0.6N NaCl solution, and then deaerated 1N Na_2CO_3-1N $NaHCO_3$ solution. The highest (or "saturation") growth rates in the three electrolytes, however, were essentially the same.

The crack growth results also showed a strong influence of solution flow, particularly for the deaerated 1N Na_2CO_3-1N $NaHCO_3$ solution. Crack gowth rates tended to be faster in quiescent distilled water as compared to water flowing at 0.1 liter per minute. For the deaerated 1N Na_2CO_3-1N $NaHCO_3$ solution, on the other hand, crack growth rates became essentially independent of frequency from about 10 Hz downward to 0.3 Hz, while the response in the flowing solution appeared "normal".

Efforts were made to obtain independent measurements of the rates of electrochemical reactions of X-70 steel with the deaerated 1N Na_2CO_3-1N $NaHCO_3$ solution to provide for a direct correlation between corrosion fatigue crack growth rates and electrochemical reaction kinetics. A new electrochemical measurement technique was used, whereby a "clean" surface of X-70 steel was suddenly coupled to an "oxidized" surface of the same steel in the electrolyte. The time constants of the resulting galvanic current transient were expected to serve as a measure of the reaction rate constant. The results

showed that the time constants (ranging from about 1 to 40 s) and the apparent activation energy (of about 40 kJ/mol) compared well with those obtained from the fatigue crack growth experiments. Because of uncertainty introduced by the accumulated charges during cathodic cleaning in the simulation experiment, however, it was not possible to make a definitive connection between these measurements and corrosion fatigue cracking response, and to make a positive identification of the rate controlling (anodic or cathodic) process. To alleviate the difficulty associated with cathodic cleaning, in-situ breaking of a specimen inside the electrochemical cell and the use of a modified version of the scratching electrode method are being considered as alternate means of creating clean metal surfaces.

Nevertheless, it is clear that corrosion fatigue cracking response can be complex. The frequency and temperature dependence must be recognized and incorporated in the acquisition of design data and in the design of pipelines and offshore structures. These factors are of particular concern when it becomes necessary to make extrapolation beyond the range of existing data, and in the development of "accelerated" tests. Identification of the electrochemical reactions that control corrosion fatigue crack growth will facilitate data analysis and the formulation of rational design procedures. Additional (or continued) research in this area is to be encouraged.

6. REFERENCES FOR PART II

1. O. Devereux, A. J. McEvily and R. W. Staehle, eds., Corrosion Fatigue: Chemistry, Mechanics and Microstructure, NACE-2, Nat. Assoc. Corro. Engrs., Houston, Texas, 1973.

2. R. P. Gangloff, ed., Embrittlement by the Localized Crack Environment, The Metallurgical Society of AIME, Warrendale, Pennsylvania, 1984.

3. R. P. Wei, "On Understanding Environment-Enhanced Fatigue Crack Growth — A Fundamental Approach", in Fatigue Mechanisms, ASTM STP 675, J. T. Fong, ed.; Am. Soc. Testing & Mater., Philadelphia, PA, 1979, pp. 816-840.

4. T. W. Weir, G. W. Simmons, R. G. Hart, and R. P. Wei, "A Model for Surface Reaction and Transport Controlled Fatigue Crack Growth", Scripta Met., 14(1980) pp. 357-364.

5. R. P. Wei and G. W. Simmons, "Surface Reactions and Fatigue Crack Growth", in FATIGUE: Environment and Temperature Effects, John J. Burke and Volker Weiss, eds.; Sagamore Army Materials Research Conference Proceedings, 27, 1983, pp. 59-70.

6. R. P. Wei and Gunchoo Shim, "Fracture Mechanics and Corrosion Fatigue," in Corrosion Fatigue, ASTM STP 801, T. W. Crooker and B. N. Leis, eds.; Am. Soc. Testing & Mater., Philadelphia, Pennsylvania, 1983, pp. 5-25.

7. R. P. Wei, Gunchoo Shim and K. Tanaka, "Corrosion Fatigue and Modeling", in Embrittlement by the Localized Crack Environment, R. P. Gangloff, ed.; The Metallurgical Society of AIME, Warrendale, Pennsylvania, 1984, pp. 243-263.

8. R. R. Fessler and T. J. Barlo, "The Effect of Cyclic Loading on the Threshold Stress for Stress Corrosion Cracking in Mild and HSLA Steels", presented at the ASME Third National Congress on Pressure Vessel and Piping Technology, San Francisco, 1979.

9. O. Vosikovsky and R. J. Cooke, "An Analysis of Crack Extension by Corrosion Fatigue in a Crude Oil Pipeline", Int. J. Pres. Ves. & Piping, Vol. 6, 1978, pp. 113-129.

10. R. N. Parkins and B. S. Greenwell, "The Interface Between Corrosion Fatigue and Stress Corrosion Cracking", Metal Science, Vol. 11, Aug.-Sept. 1977, pp. 405-413.

11. "Environmentally Induced Cracking of Natural Gas and Liquid Pipelines", Vols. 1 & 2, Final Report, Contract #DOT-OS-60519, ASL Engineering, Inc., 495 South Fairview Ave., Goleta, CA 33017, Dec. 1977.

12. "Proceedings - 5th Symposium on Line Pipe Research", American Gas Association, Cat. No. L30174, 1974.

13. Gunchoo Shim, "Corrosion Fatigue and Electrochemical Reactions in Modified HY130 Steel," Ph.D. Dissertation, Department of Metallurgy and Materials Engineering, Lehigh University, 1983.

14. G. Shim, Y. Nakai and R. P. Wei, "Corrosion Fatigue and Electrochemical Reactions in Steels", Proceedings of ASTM Symposium on Fundamental Questions and Critical Experiments on Fatigue, Oct. 22-23, 1984, Dallas-Fort Worth, Texas, to be published.

15. G. R. Yoder, L. A. Cooley, and T. W. Crooker, "Procedures for Precision Measurement of Fatigue Crack Growth Rate Using Crack-Opening Displacement Techniques", in Fatigue Crack Growth Measurement and Data Analysis, ASTM STP 738, 1981, pp. 85-102.

16. A. Saxena and S. J. Hudak, "Review and Extension of Compliance Information for Common Crack Growth Specimens", Intn. J. of Fracture, 15, (5), 1978, pp. 453-468.

17. B. F. Brown, C. T. Fujii, and E. P. Dahlberg, "Methods of Studying the Solution Chemistry Within Stress Corrosion Cracks", J. Electrochem. Soc., 116, (2), February 1969, p. 218.

18. A. Turnbull, "Progress in the Understanding of the Electrochemistry in Cracks", in Embrittlement by the Localized Crack Environment, R. P. Gangloff, ed.; The Metallurgical Society of AIME, Warrendale, PA, 1984, pp. 3-31.

19. R. P. Wei, "Electrochemical Reactions and Fatigue Crack Growth Response", in Corrosion in Power Generation Equipment, Markus O. Speidel and Andrejs Atrens, eds.; Brown Boveri Symposia Series, Plenum Publishing Corp., New York, 1984, pp. 169-174.

20. R. P. Wei and Ming Gao, "Reconsideration of the Superposition Model for Environmentally Assisted Fatigue Crack Growth," Scripta Met., 17, 1983 pp. 959-962.

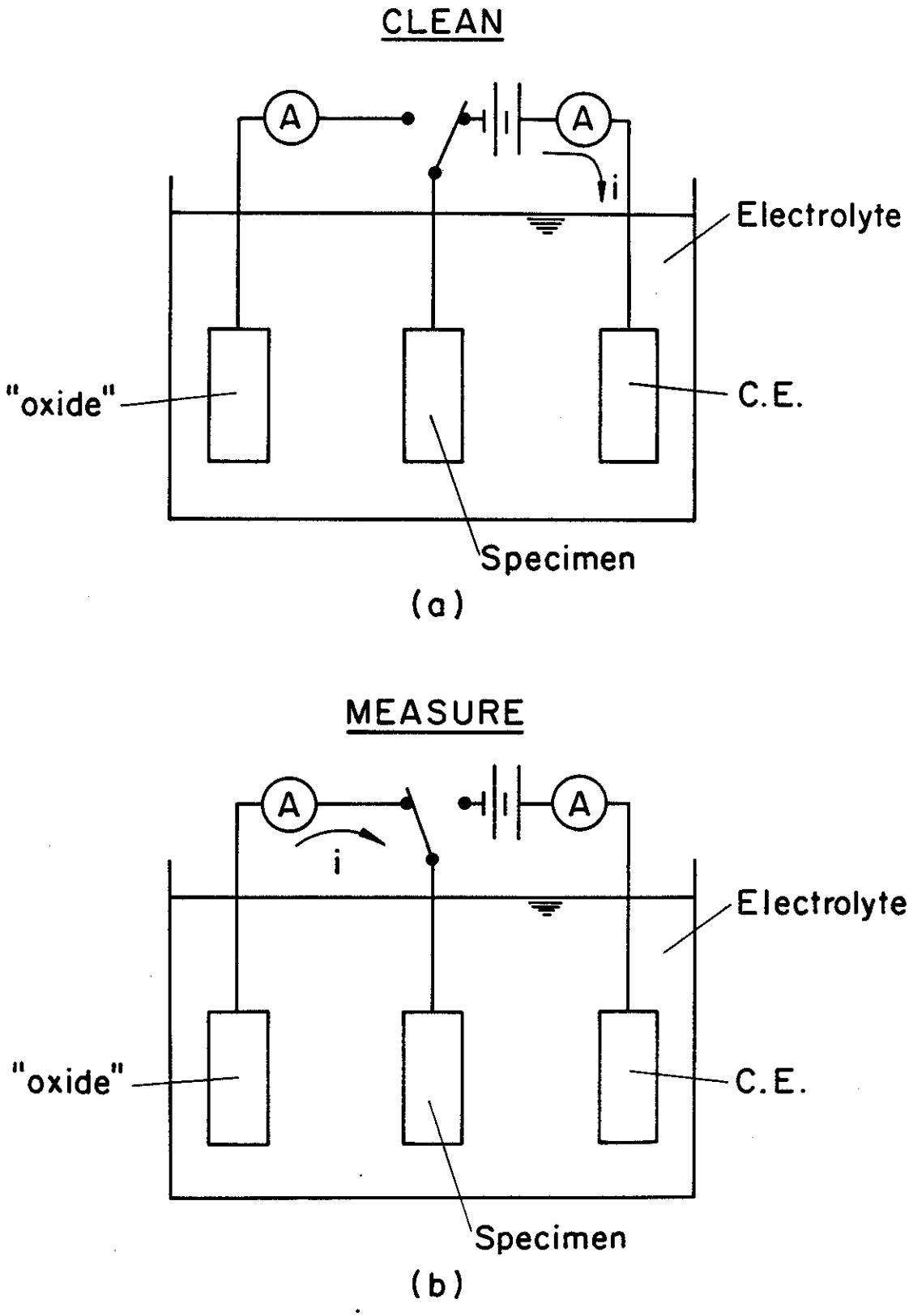

Fig. 1: Schematic illustration of technique for measuring galvanic current transient between "clean" and "oxidized" metal surfaces.

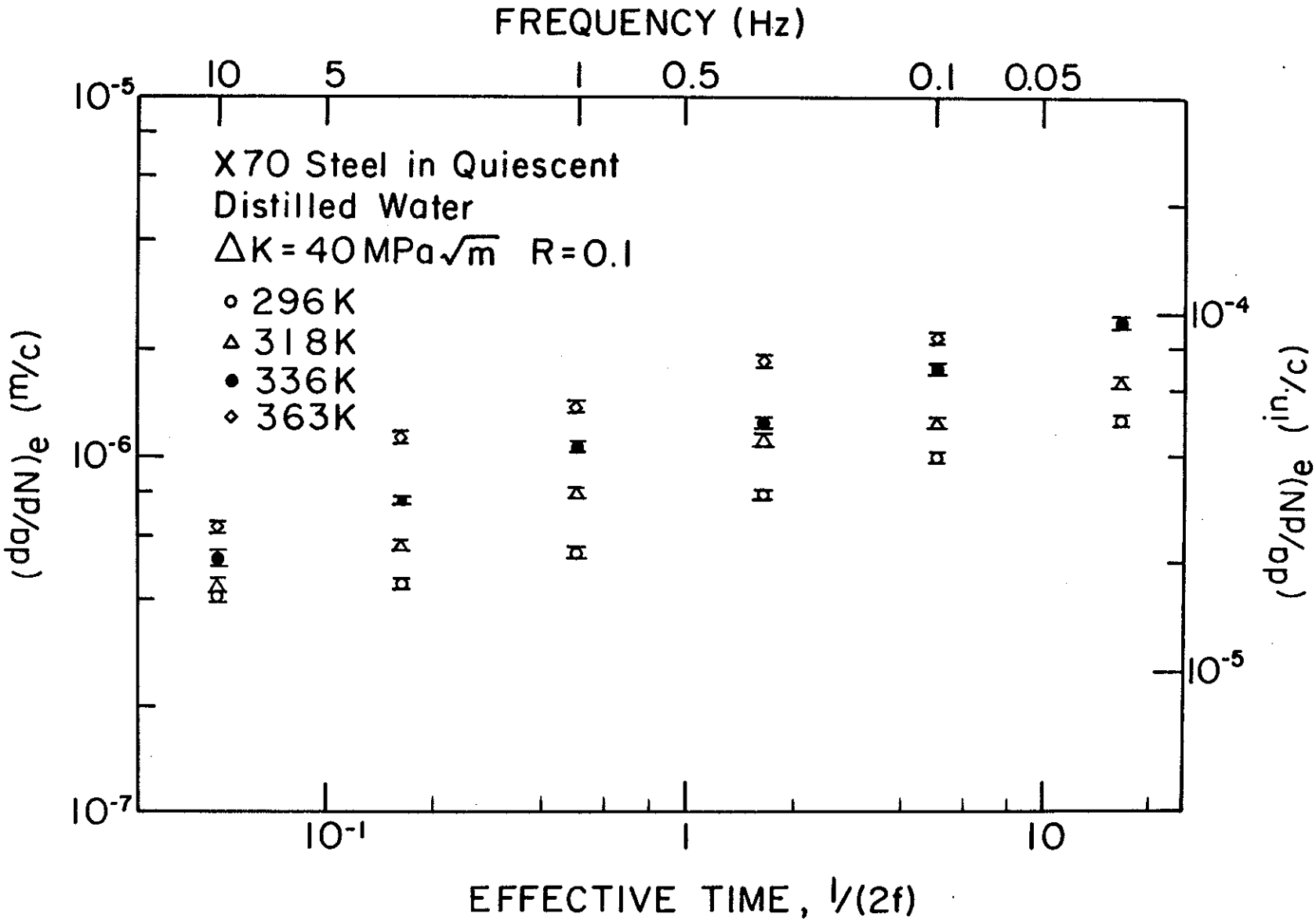

Fig. 2: The influence of frequency on fatigue crack growth for an X-70 line-pipe steel in quiescent, deaerated distilled water at different temperatures (K = 40 MPa-$m^{1/2}$, R = 0.1).

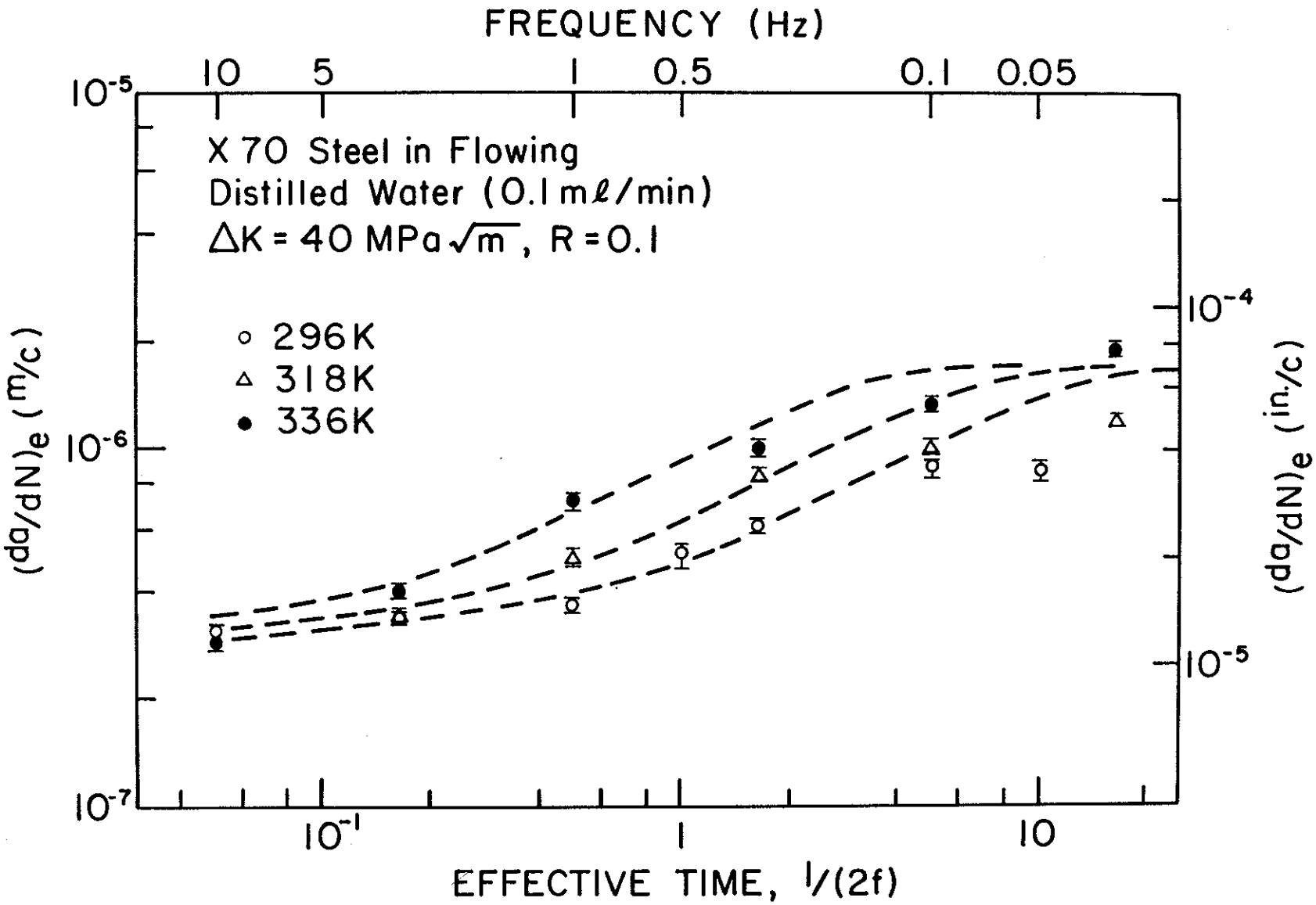

Fig. 3: The influence of frequency on fatigue crack growth for an X-70 linepipe steel in flowing, deaerated distilled water (0.1 ℓ/min.) at different temperatures (K = 40 MPa-$m^{1/2}$, R = 0.1). (Dashed curves represent Eqn. (2).)

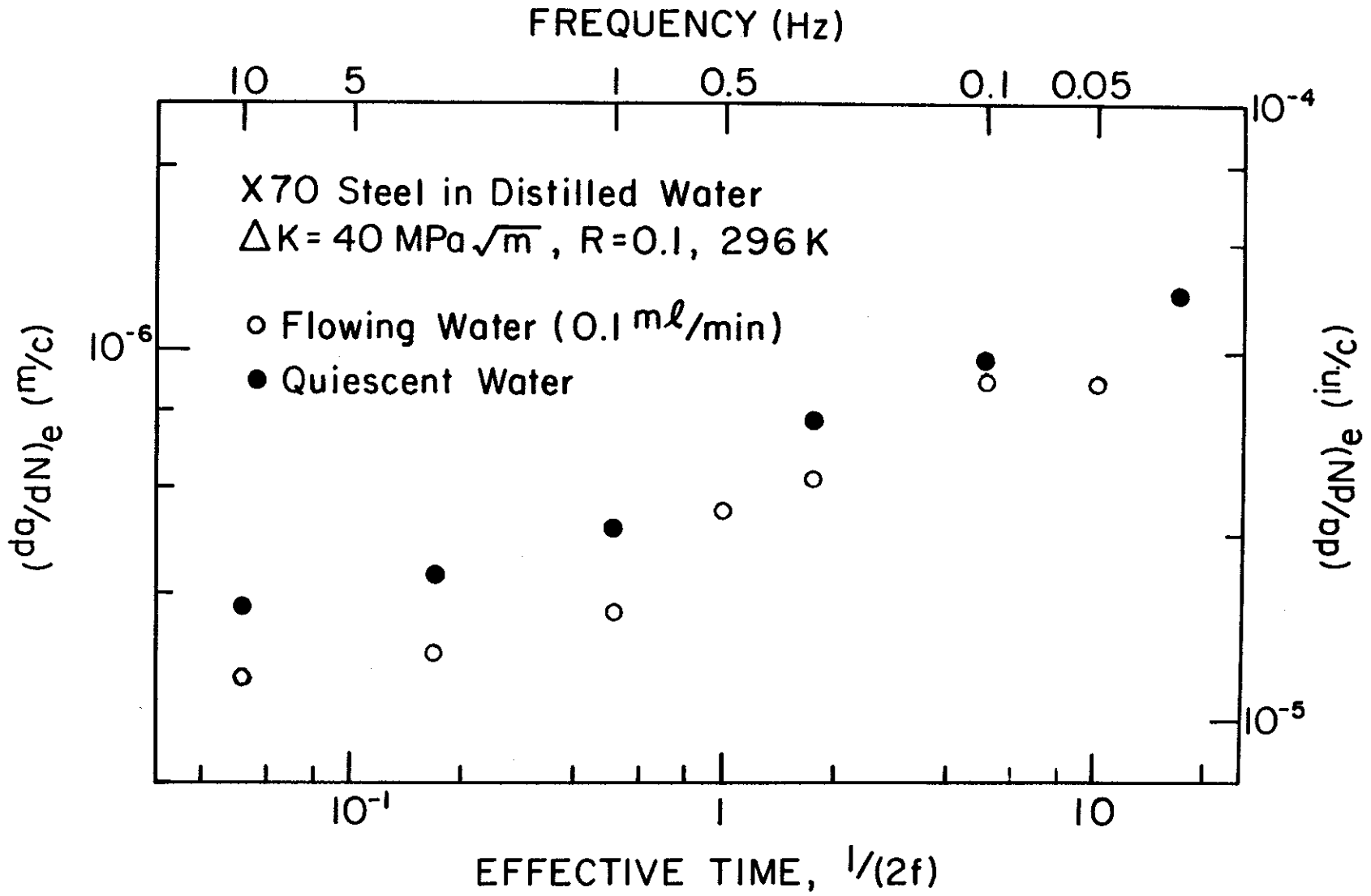

Fig. 4: Comparison between the fatigue crack growth response in quiescent and flowing, deaerated distilled water at room temperature (296 K).

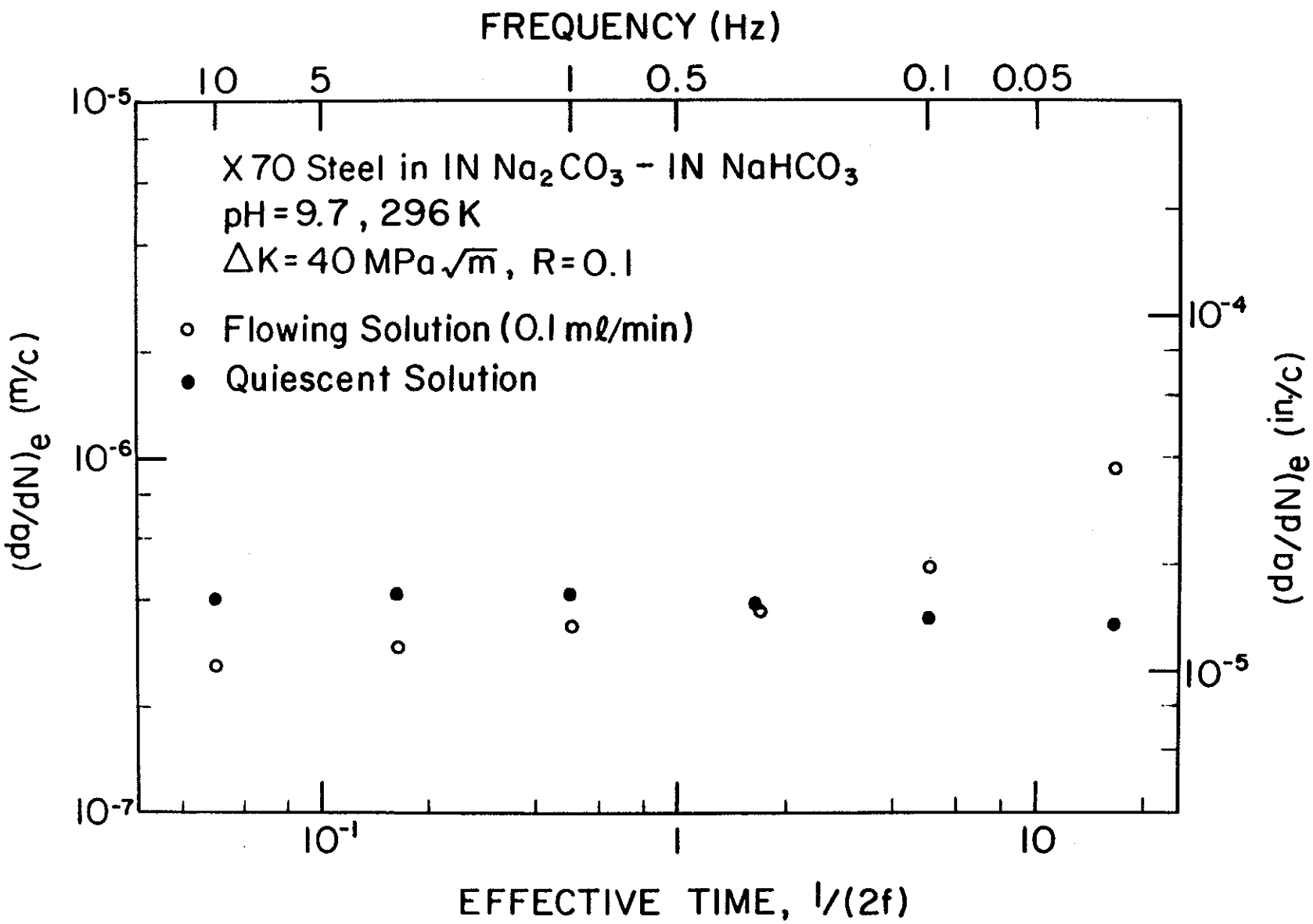

Fig. 5: Comparison between the fatigue crack growth response in quiescent and flowing, deaerated 1N Na_2CO_3-1N $NaHCO_3$ solution at room temperature (296 K).

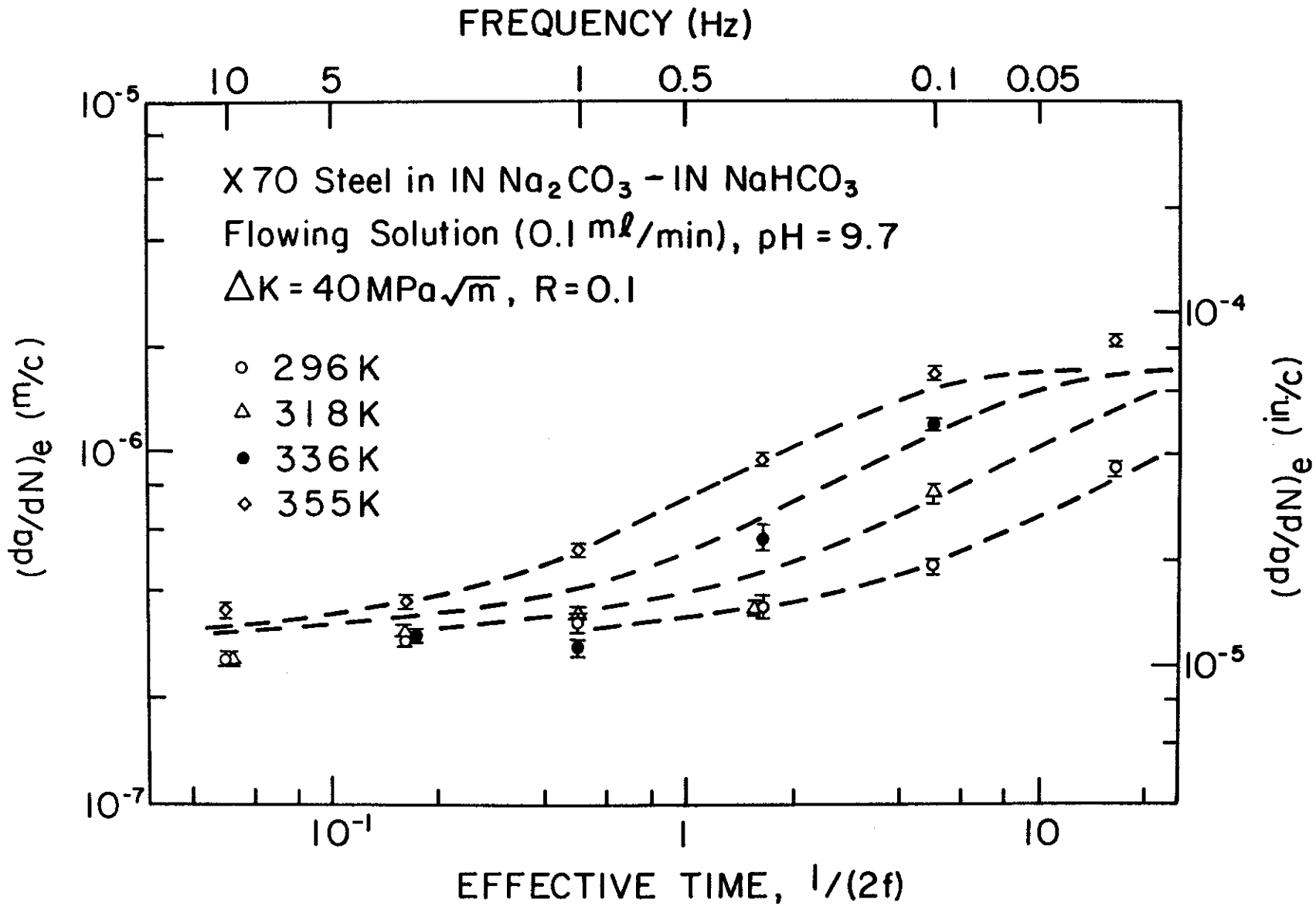

Fig. 6: The influence of frequency on fatigue crack growth for an X-70 line-pipe steel in quiescent and in flowing, deaerated 1N Na_2CO_3-1N $NaHCO_3$ solution (0.1 /min., with pH = 9.7 at 296 K) at different temperatures (K = 40 MPa-$m^{1/2}$, R = 0.1). (Dashed curves represent Eqn. (2).)

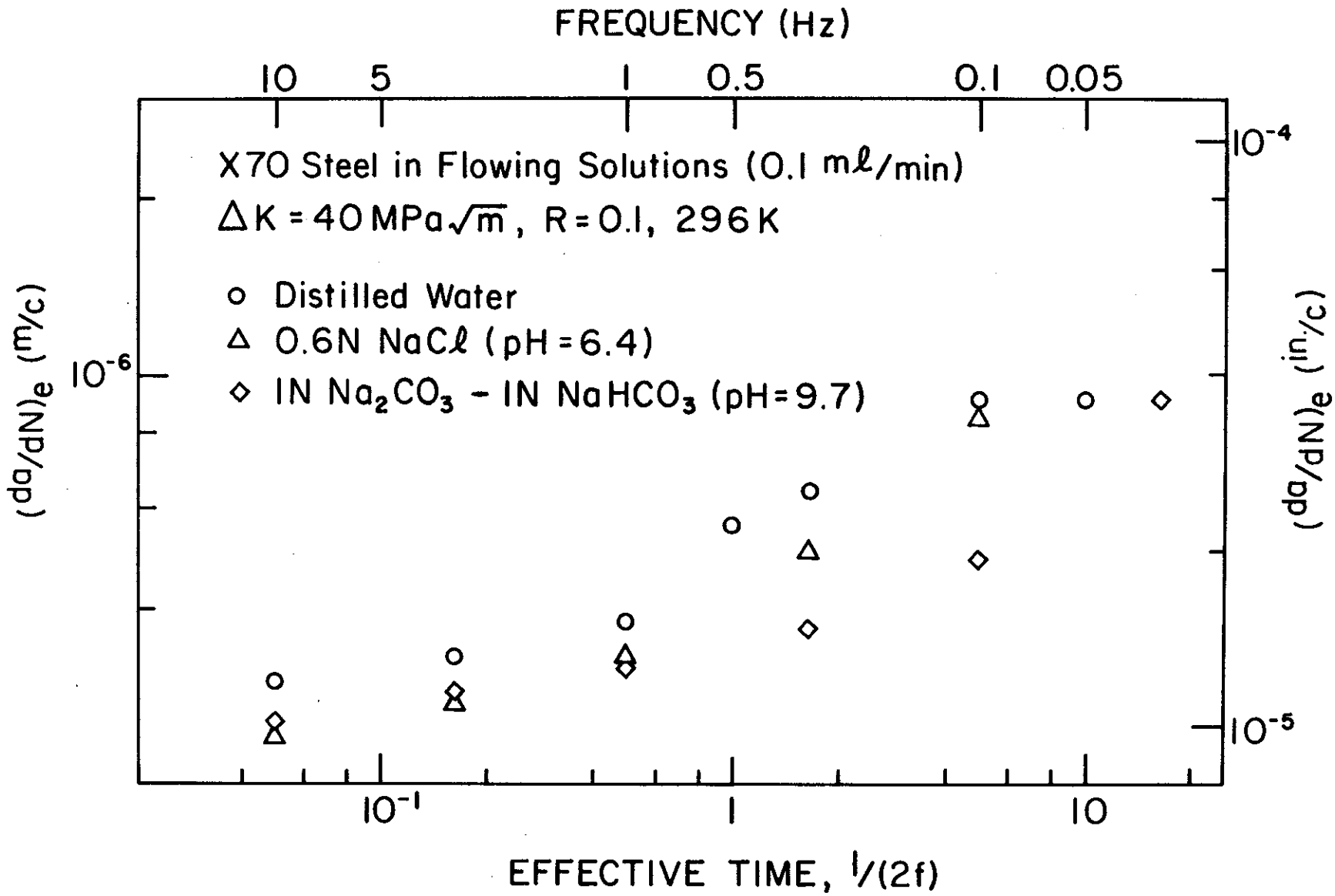

Fig. 7: Comparison of the fatigue crack growth response in flowing, deaerated distilled water, and 0.6N NaCl and 1N Na_2CO_3-1N $NaHCO_3$ solutions at room temperature (296 K).

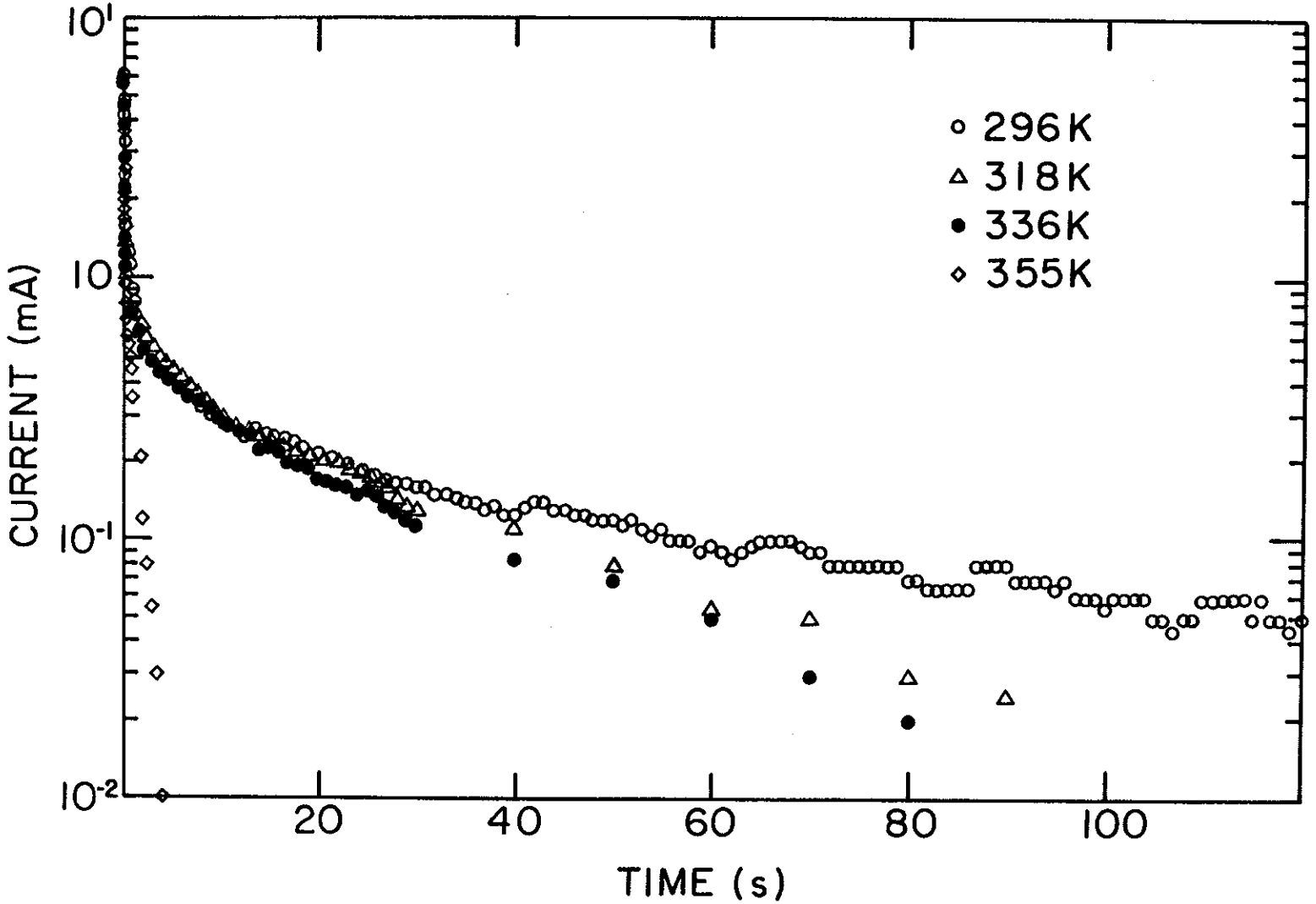

Fig. 8: Typical galvanic current transient between a cathodically cleaned and an oxidized surface of X-70 steel in deaerated 1N Na_2CO_3-1N $NaHCO_3$ solution at different temperatures.

APPENDIX A

SURFACE CRACKS IN A PLATE OF FINITE WIDTH UNDER EXTENSION OR BENDING

F. Erdogan and H. Boduroglu

Lehigh University, Bethlehem, PA

ABSTRACT

In this paper the problem of a finite plate containing collinear surface cracks is considered. The problem is solved by using the line spring model with plane elasticity and Reissner's plate theory. The main purpose of the study is to investigate the effect of interaction between two cracks or between cracks and stress-free plate boundaries on the stress intensity factors and to provide extensive numerical results which may be useful in applications. First, some sample results are obtained and are compared with the existing finite element results. Then the problem is solved for a single (internal) crack, two collinear cracks and two corner cracks for wide range of relative dimensions. Particularly in corner cracks the agreement with the finite element solution is surprisingly very good. The results are obtained for semi-elliptic and rectangular crack profiles which may, in practice, correspond to two limiting cases of the actual profile of a subcritically growing surface crack.

1. Introduction

Surface cracks are among the most common flaws in structural components, particularly in welded structures. Under cyclic loading or under static loading in the presence of corrosive environment any surface flaw has the potential of subcritically growing into a surface crack. Analysis of the structure containing such flaws is needed for modeling and prediction of the corresponding crack propagation rate. A review of the subject and a number of articles dealing with the analysis of the surface crack problem in plates may be found in [1]. At this

point the analytical treatment of the problem appears to be intractable. Therefore, the reliable solutions of the problem seem to be based on numerical techniques, most notably on the finite element method (see, for example, [2] for the solution of a wide plate containing a semi-elliptic surface crack). In recent years, however, there has been some renewed interest in the application of the line spring model which was first described in [3] to the analysis of surface crack problems. The method was used in [4] in conjunction with Reissner's plate theory and the stress intensity factors for a semi-elliptic and a rectangular surface crack were calculated for a wide plate under tension or bending. The semi-elliptic crack results described in [4] compare very favorably with the finite element solution given in [2].

In this paper the general problem is considered for a plate having a finite width. Analytically, it is known that if the stress fields of more than one crack or that of a crack and a stress-free boundary of the plate interact, there would be some magnification in the stress intensity factors. The problem may therefore be important in plate structures having more than one initial surface flaw or having a flaw near or at the boundary. Extensive finite element results for a single central or corner surface crack in a plate of finite width are given in [5] and [6]. Empirically developed expressions for stress intensity factors based on the results given in [5] are also described in [7]. The present study was undertaken partly to show that the line spring model may be used for cracks in finite plates, particularly for corner cracks just as effectively as the infinite plate and partly to supplement the results given in [5] and [6] by, for example, considering the cases of a rectangular crack profile and collinear surface cracks.

2. The General Formulation of the Problem

The problem under consideration is described in Fig. 1. It is assumed that x_1x_3 and x_2x_3 planes are planes of symmetry with respect to loading and geometry and the length of the plate in x_2 direction is relatively long compared to the width 2b so that in formulating the

perturbation problem one may assume the plate to be infinitely long. Even though the numerical results are given for uniform tension in x_2 direction and cylindrical bending in x_2x_3 plane applied to the plate away from the crack region, as will be seen from the formulation of the problem, there is no restriction on the external loads provided in the absence of any cracks the membrane and bending resultants in x_1x_3 plane can be obtained for the given plate geometry and the applied loads.

The problem is formulated for the collinear cracks shown in Fig. 1. The single central crack and the edge or the corner cracks are then considered as the special cases. One of the advantages of the line spring model is that the crack profile (as described by the function $L(x_1)$ giving the crack depth) can be arbitrary. However, the actual crack morphology studies indicate that for a given length 2a and a depth L_o the crack profile may be bounded by a semi-ellipse and a rectangle. Hence, in this paper the calculated results will be given only for these two limiting crack shapes.

Ordinarily, the problems of in-plane loading (as expressed as a generalized plane stress problem) and bending of a plate are uncoupled. Consequently, the corresponding through crack problems can be solved independently. For the plate geometry shown in Fig. 1 the plane elasticity and plate bending solutions are given in [8] and [9], respectively. In the case of surface cracks, because of the absence of symmetry in thickness direction, the membrane and bending problems are clearly coupled. As in [9] in this paper, too, a transverse shear theory is used to formulate the bending component of the problem. The particular theory used is that of Reissner's [10] which is a sixth order theory and accounts for all three boundary conditions on the crack surfaces separately.

Referring to Appendix A for normalized quantities and, for example, to [11] for the general formulation, the basic equations of the plate problem may be expressed as follows:

$$\nabla^4\phi = 0 , \tag{1}$$

$$\nabla^4 w = 0 , \tag{2}$$

$$\kappa\nabla^2\psi - \psi - w = 0 \quad , \tag{3}$$

$$\kappa \frac{1-\nu}{2} \nabla^2\Omega - \Omega = 0 \quad , \tag{4}$$

$$\sigma_{xx} = \frac{\partial^2}{\partial y^2} (h\phi) \quad , \quad \sigma_{yy} = \frac{\partial^2}{\partial x^2} (h\phi) \quad , \quad \sigma_{xy} = - \frac{\partial^2}{\partial x \partial y} (h\phi) \tag{5}$$

$$\beta_x = \frac{\partial \psi}{\partial x} + \frac{1-\nu}{2} \kappa \frac{\partial \Omega}{\partial y} \quad , \quad \beta_y = \frac{\partial \psi}{\partial y} - \frac{1-\nu}{2} \kappa \frac{\partial \Omega}{\partial x} \quad , \tag{6}$$

$$M_{xx} = \frac{a}{h\lambda^4} \left[\frac{\partial^2 \psi}{\partial x^2} + \nu \frac{\partial^2 \psi}{\partial y^2} + \frac{\kappa}{2} (1-\nu)^2 \frac{\partial^2 \Omega}{\partial x \partial y} \right] \quad , \tag{7}$$

$$M_{yy} = \frac{a}{h\lambda^4} \left[\frac{\partial^2 \psi}{\partial y^2} + \nu \frac{\partial^2 \psi}{\partial x^2} - \frac{\kappa}{2} (1-\nu)^2 \frac{\partial^2 \Omega}{\partial x \partial y} \right] \quad , \tag{8}$$

$$M_{xy} = \frac{a(1-\nu)}{2h\lambda^4} \left[2 \frac{\partial^2 \psi}{\partial x \partial y} + \frac{\kappa}{2} (1-\nu) \left(\frac{\partial^2 \Omega}{\partial y^2} - \frac{\partial^2 \Omega}{\partial x^2} \right) \right] \quad , \tag{9}$$

$$V_x = \frac{\partial w}{\partial x} + \frac{\kappa}{2} (1-\nu) \frac{\partial \Omega}{\partial y} + \frac{\partial \psi}{\partial x} \quad , \tag{10}$$

$$V_y = \frac{\partial w}{\partial y} - \frac{\kappa}{2} (1-\nu) \frac{\partial \Omega}{\partial x} + \frac{\partial \psi}{\partial y} \tag{11}$$

where, in the usual notation, F (or ϕ) is the Airy stress function, N_{ij}, M_{ij}, and V_i, (i,j=1,2) are the membrane, bending, and transverse shear resultants, β_1 and β_2 are the components of the rotation vector, u_1, u_2 and u_3 are the components of the displacement vector, a^* is a length parameter representing the crack size ($a^*=a$ for $0<c<d\leq b$ and $a^*=d$ for $c=0$, $d<b$, Fig. 1), E and ν are the elastic constants, the constants κ and λ are defined in Appendix A, ψ and Ω are auxiliary functions defined in [11], and the dimensions h, a, b, c, and d are shown in Fig. 1.

Because of symmetry, it is sufficient to consider the problem for $0\leq x_1<b$, $0\leq x_2<\infty$ only. Thus, the membrane and bending problems of the plate must be solved under the following boundary and symmetry conditions stated in terms of the normalized quantities (Fig. 1 and Appendix A):

$$u(0,y) = 0, \; N_{xy}(0,y) = 0, \; 0\leq y<\infty \quad , \tag{12}$$

$$N_{xx}(b',y) = 0, \; N_{xy}(b',y) = 0, \; 0\leq y<\infty \quad , \tag{13}$$

$$N_{xy}(x,0) = 0, \quad 0 \leq x < b', \tag{14}$$

$$N_{yy}(x,0) = \frac{1}{E}\left[-\sigma_\infty(x) + \sigma(x)\right], \quad c' < x < d', \tag{15a}$$

$$v(x,0) = 0, \quad 0 \leq x < c', \quad d' < x < b'; \tag{15b}$$

$$\beta_x(0,y) = 0, \quad M_{xy}(0,y) = 0, \quad V_x(0,y) = 0, \quad 0 \leq y < \infty, \tag{16}$$

$$M_{xx}(b',y) = 0, \quad M_{xy}(b',y) = 0, \quad V_x(b',y) = 0, \quad 0 \leq y < \infty, \tag{17}$$

$$M_{xy}(x,0) = 0, \quad V_y(x,0) = 0, \quad 0 \leq x < b', \tag{18}$$

$$M_{yy}(x,0) = \frac{1}{6E}\left[-m_\infty(x) = m(x)\right], \quad c' < x < d', \tag{19a}$$

$$\beta_y(x,0) = 0, \quad 0 \leq x < c', \quad d' < x < b'. \tag{19b}$$

The conditions stated above refer to the perturbation problem in which the crack surface tractions are the only nonzero external loads. Consequently, in addition to (12)-(19) it is required that

$$N_{yy}(x,\infty) = 0, \quad N_{xy}(x,\infty) = 0, \quad 0 \leq x < b', \tag{20}$$

$$M_{yy}(x,\infty) = 0, \quad M_{xy}(x,\infty) = 0, \quad V_y(x,\infty) = 0, \quad 0 \leq x < b'. \tag{21}$$

The input functions σ_∞ and m_∞ which appear in (15a) and (19a) are defined by

$$\sigma_\infty(x) = N^\infty_{22}(x_1,0)/h, \quad m_\infty(x) = 6M^\infty_{22}(x_1,0)/h^2 \tag{22}$$

where $N^\infty_{ij}(x_1,x_2)$ and $M^\infty_{ij}(x_1,x_2)$, $(i,j=1,2)$ are the membrane and moment resultants in the plate under the actual applied loads in the absence of any cracks. The functions $\sigma(x)$ and $m(x)$ are unknown and are defined by

$$\sigma(x) = \frac{N(x_1)}{h} = \frac{N(a^*x)}{h}, \quad m(x) = \frac{6M(x_1)}{h^2} = \frac{6M(a^*x)}{h^2} \tag{23}$$

where the membrane load $N(x_1)$ and the bending moment $M(x_1)$ represent the stress component $\sigma_{22}(x_1,0,x_3)$ in the net ligament $c < x_1 < d$, $-\frac{h}{2} < x_3 < \frac{h}{2} - L$.

In the bending problem the solution of the differential equations (2)-(4) satisfying the symmetry conditions (16) and the regularity conditions (21) may be expressed as follows [9]:

$$w(x,y) = \frac{2}{\pi}\int_0^\infty (A_1+yA_2)e^{-\alpha y}\cos\alpha x\, d\alpha + \frac{2}{\pi}\int_0^\infty (C_1\cosh\beta x + C_2 x\sinh\beta x)\cos\beta y\, d\beta , \tag{24}$$

$$\Omega(x,y) = \frac{2}{\pi}\int_0^\infty B_1 e^{-r_1 y}\sin\alpha x\, d\alpha + \frac{2}{\pi}\int_0^\infty B_2 \sinh r_2 x \sin\beta y\, d\beta , \tag{25}$$

$$\psi(x,y) = \frac{2}{\pi}\int_0^\infty [-A_1+(2\kappa\alpha-y)A_2]e^{-\alpha y}\cos\alpha x\, d\alpha + \frac{2}{\pi}\int_0^\infty [-(C_1+2\kappa\beta C_2)\cosh\beta x - C_2 x\sinh\beta x]\cos\beta y\, d\beta , \tag{26}$$

where $A_i(\alpha)$, $B_i(\alpha)$ and $C_i(\beta)$, $(i=1,2)$ are unknown functions and

$$r_1 = \left[\alpha^2 + \frac{2}{\kappa(1-\nu)}\right]^{\frac{1}{2}} , \quad r_2 = \left[\beta^2 + \frac{2}{\kappa(1-\nu)}\right]^{\frac{1}{2}} . \tag{27}$$

By substituting from (24)-(26) into (7), (9)-(11) and by using five homogeneous conditions (17) and (18) five of the six unknown functions may be eliminated. The mixed boundary condition (19) would then determine the sixth.

Similarly from the plane stress solution of the plate satisfying the conditions (12), (14) and (20) the stresses and the y-component of the displacement may be expressed as [8]

$$N_{xx}(x,y) = -\frac{2}{\pi}\int_0^\infty h_1(\alpha)(1-\alpha y)e^{-\alpha y}\cos\alpha x\, d\alpha - \frac{2}{\pi}\int_0^\infty [h_2(\beta)\cosh\beta x+\beta x h_3(\beta)\sinh\beta x]\cos\beta y\, d\beta , \tag{28}$$

$$N_{yy}(x,y) = -\frac{2}{\pi}\int_0^\infty h_1(\alpha)(1+\alpha y)e^{-\alpha y}\cos\alpha x\, d\alpha$$

$$+\frac{2}{\pi}\int_0^\infty [(h_2+2h_3)\cosh\beta x+\beta x h_3\sinh\beta x]\cos\beta y\, d\beta, \qquad (29)$$

$$N_{xy}(x,y) = -\frac{2}{\pi}\int_0^\infty \alpha y h_1(\alpha)e^{-\alpha y}\sin\alpha x\, d\alpha$$

$$+\frac{2}{\pi}\int_0^\infty [(h_2+h_3)\sinh\beta x + \beta x h_3\cosh\beta x]\sin\beta y\, d\beta\ , \qquad (30)$$

$$\frac{E}{1+\nu}v(x,y) = \frac{2}{\pi}\int_0^\infty \frac{h_1}{\alpha}\left(\frac{1+\kappa}{2}+\alpha y\right)e^{-\alpha y}\cos\alpha x\, d\alpha$$

$$+\frac{2}{\pi}\int_0^\infty [(\frac{h_2}{\beta}+\frac{1+\kappa}{2}h_3)\cosh\beta x + x h_3\sinh\beta x]\sin\beta y\, d\beta\ . \qquad (31)$$

In this case the unknown functions h_1, h_2 and h_3 are determined from the remaining boundary conditions (13) and (15).

3. The Integral Equations

If we now replace the mixed boundary conditions (15) and (19) respectively by

$$\frac{\partial}{\partial x}v(x,0) = g_1(x)\ ,\ 0\leq x<b\ , \qquad (32)$$

$$\frac{\partial}{\partial x}\ \beta_y(x,0) = g_2(x)\ ,\ 0\leq x<b\ , \qquad (33)$$

it is seen that by using (17), (18), (13), (32) and (33) all nine unknown functions A_i, B_i, C_i, (i=1,2) and h_j, (j=1,2,3) which appear in the formulation of the problem given in the previous section may be expressed in terms of the new unknown functions g_1 and g_2. From the definitions (32) and (33) it also follows that conditions (15b) and (19b) are equivalent to

$$g_i(x) = 0 \ , \ 0 \le x < c' \ , \ d' < x < b' , \ (i=1,2) \ , \tag{34}$$

$$\int_{c'}^{d'} g_i(x)dx = 0 \ , \ (i=1,2) \ . \tag{35}$$

The functions g_1 and g_2 may now be determined from the two remaining conditions (15a) and (19a). Referring to [8] and [9] for details, the following integral equations may be obtained from these two conditions:

$$\frac{\sigma(x)}{E} - \frac{1}{2\pi}\int_{c'}^{d'} \left[\frac{1}{t-x} + \frac{1}{t+x} + k_1(x,t) - k_1(x,-t)\right] g_1(t)dt = \frac{\sigma_\infty(x)}{E} \ , \tag{36}$$

$$\frac{m(x)}{6E} - \frac{a^*(1-\nu^2)}{2\pi h\lambda^4}\int_{c'}^{d'} \left\{\left[\frac{3+\nu}{1+\nu}\left(\frac{1}{t-x} + \frac{1}{t+x}\right) - \frac{4\kappa(1-\nu)}{1+\nu}\left[\frac{1}{(t-x)^3} + \frac{1}{(t+x)^3}\right]\right.\right.$$

$$+ \frac{4}{1+\nu}\left[\frac{1}{t-x}K_2(\gamma|t-x|) + \frac{1}{t+x}K_2(\gamma|t+x|)\right] + k_2(x,t)$$

$$\left.\left. - k_2(x,-t)\right\} g_2(t)dt = \frac{m_\infty(x)}{6E} \ , \ c' < x < d' \ , \tag{37}$$

where K_2 is the modified Bessel function of the second kind, the Fredholm kernels $k_1(x,t)$ and $k_2(x,t)$ are given in Appendix B and the constant γ is given by

$$\gamma = \frac{h}{12(1-\nu^2)a^*} \ . \tag{38}$$

The functions $\sigma(x)$ and $m(x)$ which appear in (36) and (37) are defined by (23) and represent the membrane and moment resultants of the tensile stress σ_{22} in the net ligament $c' < x < d'$. By using the plane strain solution for an edge crack occupying $(h/2)-L < x_3 \le h/2$ in a strip of thickness h (Fig. 1) under membrane load $N(x_1)$ and bending moment $M(x_1)$ (applied in x_2x_3 plane) and by expressing the rate of change of the potential energy in terms of crack closure energy and the change of compliance, $\sigma(x)$ and $m(x)$ may be expressed in terms of the crack opening

displacement $2v(x,0,0)$ and the crack opening angle $2\beta_y(x,0)$ as follows (see [1] and [4] for details):

$$\sigma(x) = E[\gamma_{tt}(x)v(x) + \gamma_{tb}(x)\beta_y(x)] \quad , \tag{39}$$

$$m(x) = 6E[\gamma_{bt}(x)v(x) + \gamma_{bb}(x)\beta_y(x)] \quad , \tag{40}$$

where the functions γ_{ij}, $(i,j=t,b)$ depend on the local crack depth $L(x)$ and hence are implicit functions of x. The algebraic expressions of these functions are given in [4] . From (32), (33) and (34) by observing that

$$v(x,+0) = \int_{c'}^{x} g_1(t)dt \quad , \quad \beta_y(x,+0) = \int_{c'}^{x} g_2(t)dt \quad , \tag{41}$$

and by using (39) and (40), the integral equations (36) and (37) may then be expressed as

$$\gamma_{tt}(x)\int_{c'}^{x} g_1(t)dt - \frac{1}{2\pi}\int_{c'}^{d'}\left[\frac{1}{t-x} + \frac{1}{t+x} + k_1(x,t) - k_1(x,-t)\right]g_1(t)dt$$

$$+ \gamma_{tb}(x)\int_{c'}^{x} g_2(t)dt = \frac{1}{E}\sigma_\infty(x) \quad , \quad c'<x<d' \quad , \tag{42}$$

$$\gamma_{bt}(x)\int_{c'}^{x} g_1(t)dt + \gamma_{bb}(x)\int_{c'}^{x} g_2(t)dt - \frac{a^*(1-\nu^2)}{2\pi h\,\lambda^4}\int_{c'}^{d'}\left\{\frac{3+\nu}{1+\nu}\left(\frac{1}{t-x}\right.\right.$$

$$\left. + \frac{1}{t+x}\right) - \frac{4\kappa(1-\nu)}{1+\nu}\left[\frac{1}{(t-x)^3} + \frac{1}{(t+x)^3}\right] + \frac{4}{1+\nu}\left[\frac{1}{t-x}K_2(\gamma|t-x|)\right.$$

$$\left.\left. + \frac{1}{t+x}K_2(\gamma|t+x|)\right] + k_2(x,t) - k_2(x,-t)\right\}g_2(t)dt$$

$$= \frac{1}{6E}m_\infty(x) \quad , \quad c'<x<d' \quad . \tag{43}$$

From the following asymptotic behavior of the Bessel function $K_2(z)$ for small values of z

$$K_2(z) = \frac{2}{z^2} - \frac{1}{2} + 0(z^2 \log z) \tag{44}$$

it can be shown that, as in (42), the integral equation (43) has a simple Cauchy type singular kernel. We also note that the system of singular integral equations (42) and (43) must be solved under the additional conditions (35).

After solving the integral equations (42) and (43) for g_1 and g_2 the Mode I stress intensity factor K at the leading edge of the crack may be obtained by substituting from (39)-(41) into the following expression giving K in a strip containing an edge crack of depth L and subjected to the membrane load σ and bending moment m [4]:

$$K(x) = \sqrt{h}\ [\sigma(x) g_t + m(x) g_b] \tag{45}$$

where g_t and g_b are functions of L/h and are obtained from the corresponding plane strain solution. From the results given in [12] the expressions for g_t and g_b valid in $0<L/h\leq 0.8$ may be obtained as follows:

$$g_t(s) = \sqrt{\pi s}\ (1.1216 + 6.5200s^2 - 12.3877s^4 + 89.0554s^6 - 188.6080s^4 + 207.3870s^{10} - 32.0524s^{12}) , \tag{46a}$$

$$g_b(s) = \sqrt{\pi s}\ (1.1202 - 1.8872s + 18.0143s^2 - 87.3851s^3 + 241.9124s^4 - 319.9402s^5 + 168.0105s^6) , \tag{46b}$$

where $s = L(x)/h$.

We now note that for $0<c'<d'<b$ the solution of the system of singular integral equations is of the form

$$g_i(x) = \frac{G_i(x)}{(x-c')^{\frac{1}{2}}(d'-x)^{\frac{1}{2}}} , \quad c'<x<d' , \ (i=1,2) , \tag{47}$$

where the bounded unknown functions G_1 and G_2 may easily be obtained by using the technique described, for example, in [13] .

The general crack geometry shown in Fig. 1 has two special cases. The first is the case of a symmetrically located single crack along $-d'<x<d'$, (i.e., $c'=0$, $d'<b'$). In this problem by using the symmetry considerations and by observing that $g_i(t) = -g_i(-t)$, $(i=1,2)$, the integral equations (42) and (43) may be somewhat simplified as follows:

$$\gamma_{tt}(x)\int_{-d'}^{x} g_1(t)dt - \frac{1}{2\pi}\int_{-d'}^{d'}\left[\frac{1}{t-x} + k_1(x,t)\right]g_1(t)dt$$

$$+ \gamma_{tb}(x)\int_{-d'}^{x} g_2(t)dt = \frac{1}{E}\sigma_\infty(x) \quad , \quad -d'<x<d' \quad , \tag{48}$$

$$\gamma_{bt}(x)\int_{-d'}^{x} g_1(t)dt + \gamma_{bb}(x)\int_{-d'}^{x} g_2(t)dt - \frac{d(1-\nu^2)}{2\pi h\,\lambda^4}\int_{-d'}^{d'}\left[\frac{3+\nu}{1+\nu}\frac{1}{t-x}\right.$$

$$\left. - \frac{4\kappa(1-\nu)}{1+\nu}\frac{1}{(t-x)^3} + \frac{4}{1+\nu}\frac{1}{t-x}K_2(\gamma|t-x|) + k_2(x,t)\right]g_2(t)dt$$

$$= \frac{1}{6E}m_\infty(x) \quad , \quad -d'<x<d \quad . \tag{49}$$

By using (44) it may again be shown that (49) has a simple Cauchy kernel and the solution of the integral equations is of the following form:

$$g_i(x) = \frac{F_i(x)}{(d'^2-x^2)^{\frac{1}{2}}} \quad , \quad -d'<x<d' \quad , \quad (i=1,2) \quad . \tag{50}$$

The second special case is that of corner cracks for which $0<c'<d'=b'$. In this case it may be shown that as x and t approach the end point b' simultaneously, the kernels k_1 and k_2 in (42) and (43) become unbounded. As shown in [8] and [9] the singular part of these kernels may be separated and may be shown to be

$$k_{1s}(x,t) = k_{2s}(x,t) = \frac{1}{2b'-x-t} - \frac{6(b'-x)}{(2b'-x-t)^2} + \frac{4(b'-x)^2}{(2b'-x-t)^3} \quad , \tag{51}$$

where

$$k_i(x,t) = k_{is}(x,t) + k_{if}(x,t) \ , \ (i=1,2) \tag{52}$$

and k_{1f} and k_{2f} are bounded. Together with the Cauchy kernel $1/(t-x)$ in (42) and (43), (51) constitutes a generalized Cauchy kernel. It may be observed that the generalized Cauchy kernel $k_g(x,t) = 1/(t-x)+k_{is}(x,t)$ has the property that $k_g(x,b') = 0$, $k_g(b',t) = 0$ and consequently $g_1(t)$ and $g_2(t)$ are nonsingular at $t=b'$ [8] . Also, in this case the single-valuedness conditions (35) are not valid and, as pointed out in [8] , are not needed for a unique solution of the integral equations.

4. The Results

First, some sample problems are solved in order to compare the results obtained from the line spring model in this paper with that obtained from the finite element solutions given in [5] and [6] . In [5] the single symmetric semi-elliptic surface crack problem is considered for a finite plate under uniform tension or cylindrical bending (i.e., $c=0$, $d<b$, Fig. 1). It is assumed that the half length of the plate is $\ell=5d$. Figures 2 and 3 show the comparison of the normalized stress intensity factors calculated along the crack front by the two methods. The normalizing stress intensity factor K_N shown in these figures is defined by

$$K_N = \sigma_\infty \sqrt{\pi L_o}/E(k) \ , \ k = \sqrt{1-L_o^2/d^2} \tag{53}$$

and is the stress intensity factor at the location $x_1 = 0$, $x_2 = 0$, $x_3 = L_o$, (i.e., the end points of the minor axis) of a flat elliptic crack (with semi axes d and L_o) in an infinite solid subjected to uniform tension $\sigma_{22} = \sigma_\infty$ in x_2 direction ($c=0$, Fig. 1). Note that, considering the simplicity of the line spring model, the agreement is not bad. One may also note that at the intersection point of the crack and the plate surface $x = x_1/d = 1$ the results based on the line spring model would not be expected to be very good. Furthermore, at the singular point on the free surface the power of the stress singularity seems to be less

than 1/2 [14] . Hence, theoretically the stress intensity factor defined on the basis of conventional 1/2 power should tend to zero as the point on the crack front approaches the free surface at an angle of $\pi/2$. Thus, strictly speaking, the bounded nonzero stress intensity factor given by the finite element solution at the surface do not seem to be correct either.

Figures 4 and 5 show the comparison of the stress intensity factors for a corner crack having the profile of a quarter ellipse and obtained from the line spring model and the finite element solution given in [6] . It should be noted that the finite element results are obtained for a finite plate in which the half length is equal to the total width of the plate and the crack is only on one corner (see the insert in Fig. 4). However, since the crack length-to plate width ratio in both cases is relatively small (2a/2b = 1/10 in line spring and 2a/b = 1/5 in finite element solution), the stress intensity factors for the two geometries should be approximately equal. The figures again show that the agreement is quite good.

The calculated stress intensity factors are given in Tables 1-11. All stress intensity factors were calculated as a function of $x = x_1/a^*$, ($a^*=d$ for a single crack, $a^*=a$ for two cracks, Fig. 1) defining the location along the crack front and of the relative dimensions of the crack and the plate. The following notation and normalizing stress intensity factors are used in presenting the results:

$$\sigma_{b22}(r,0,x_1) \tilde{=} \frac{K_b(x)}{\sqrt{2\pi r}} \quad , \; x = x_1/a^* \quad , \tag{54}$$

$$\sigma_{t22}(r,0,x_1) \tilde{=} \frac{K_t(x)}{\sqrt{2\pi r}} \quad , \; x = x_1/a^* \tag{55}$$

where supscripts b and t correspond to plates under bending and tension, respectively, σ_{22} is the cleavage stress around the crack front, r and θ are the usual polar coordinates at the crack front in x_2x_3 plane (Fig. 1) and K_b and K_t are the corresponding Mode I stress intensity factors. The results are given for uniform membrane load $N_{22} = N_\infty$ and cylindrical

bending moment $M_{22} = M_\infty$ away from the crack region. The normalized stress intensity factors shown in the tables are defined by

$$k_b(x) = \frac{K_b(x)}{K_{bo}} , \quad k_t(x) = \frac{K_t(x)}{K_{to}} , \tag{56}$$

$$K_{to} = \left(\frac{N_\infty}{h}\right) \sqrt{h} \; g_t(s_o) \quad , \quad s_o = L_o/h \quad , \tag{57}$$

$$K_{bo} = \left(\frac{6M_\infty}{h^2}\right) \sqrt{h} \; g_b(s_o) \quad , \quad s_o = L_o/h \tag{58}$$

where L_o is the maximum crack depth and the functions g_t and g_b are given by (45) and (46). One may note that $g_t(s_o)$ and $g_b(s_o)$ are the shape factors obtained from the corresponding plane strain solution of a plate with an edge crack of depth L_o and, for the values of L_o/h shown in the tables, are given by [12] .

$s_o = L_o/h$	0.2	0.4	0.6	0.8
$g_t(s_o)/\sqrt{\pi s_o}$	1.3674	2.1119	4.035	11.988
$g_b(s_o)/\sqrt{\pi s_o}$	1.0554	1.2610	1.915	4.591

Table 1 shows the normalized stress intensity factors at the deepest penetration point of a centrally located single semielliptic surface crack (i.e., c=0, d<b, Fig. 1) in a plate under uniform tension N_∞ or bending M_∞. Here the crack profile is given by

$$\frac{L^2}{L_o^2} + \frac{x_1^2}{d^2} = 1 \tag{59}$$

or

$$L(x) = L_o\sqrt{1-x^2} \quad , \quad (x = x_1/a^* \; , \; a^* = d) \tag{60}$$

and hence x=0 is the deepest point on the crack front. This is also the point where k_t assumes its maximum value. For b/h = 10 relatively complete and for other plate dimensions some sample results showing the variation of the stress intensity factors along the crack front are shown in Tables 2 and 3. Similar results are shown in Tables 4 and 5 for a single surface crack with a rectangular profile (i.e., for $L(x) = L_o$, $-1<x<1$). One may observe that, as expected, generally the stress intensity factors for the rectangular crack are higher than that for the semi-elliptic crack.

The results for two collinear semi-elliptic surface cracks (Fig. 1) are shown in tables 6 and 7. Here the crack profile is defined by (Fig. 1)

$$L(\bar{x}) = L_o\sqrt{1-\bar{x}^2}\ ,\ \bar{x} = \frac{x_1-(c+a)}{a}\ ,\ -1<\bar{x}<1\ . \tag{61}$$

Table 6 shows the value $k_i(x^*)$, (i=b,t) and the location $\bar{x} = x^*$ of the maximum stress intensity factor for various crack geometries in a plate for which b = 10h and a = h. The factor D = a/(a+c) determines the crack location. Table 7 shows some sample results giving the distribution of the stress intensity factors along the crack front for two extreme crack locations considered. The skewness in this distribution does not seem to be very significant.

The results for a plate containing two corner cracks having a profile of a quarter ellipse are shown in Tables 8 and 9 (Fig. 1). In this case the crack profile (or the crack depth) L is defined by

$$L(\bar{x}) = L_o\sqrt{1-\left(\frac{1-\bar{x}}{2}\right)^2}\ ,\ \bar{x} = \frac{x_1-(c+a)}{a}\ ,\ -1<\bar{x}<1\ . \tag{62}$$

Table 8 shows the normalized Mode I stress intensity factors at the maximum penetration point of the crack which is on the plate boundary x = b' (i.e., for $x_1 = b$ or $\bar{x} = 1$ or $L = L_o$). Some results showing the distribution of the stress intensity factors are given in Table 9. The results were similar for all crack geometries in that for plates under

tension and for those having shallow cracks under bending the maximum stress intensity factor was on the boundary $x = b'$, whereas for deep cracks in plates under bending K was maximum at the surface $x_1 = c$ or $x = c'$ (Fig. 1). For corner cracks with a rectangular profile results similar to those shown in Tables 8 and 9 are given in Tables 10 and 11. For this crack geometry too one may note that generally the stress intensity factors for rectangular cracks are higher than those for the elliptic cracks.

From the formulation of the problem it may be seen that all results in the surface crack problem are dependent on the Poisson's ratio ν of the plate. The stress intensity factors given in this paper are calculated for $\nu = 0.3$, However, as shown [9] , since the stress intensity factors are not very sensitive to the Poisson's ratio, the results given in Tables 1-11 should be valid for nearly all structural materials.

References

1. The Surface Crack: Physical Problems and Computational Solutions, J.L. Swedlow, ed. ASME, New York, 1972.

2. I.S. Raju and J.C. Newman, "Stress Intensity Factors for a Wide Range of Semi-Elliptical Surface Cracks in Finite Thickness Plates", Journal of Engineering Fracture Mechanics, Vol. 11, pp. 817-829, 1979.

3. J.R. Rice and N. Levy, "The Part-Through Surface Crack in an Elastic Plate", J. Applied Mechanics, Vol. 39, pp. 185-194, Trans. ASME, 1972.

4. F. Delale and F. Erdogan, "Line Spring Model for Surface Cracks in a Reissner Plate", Int. J. Engng. Science, Vol. 19, pp. 1331-1340, 1981.

5. J.C. Newman, Jr. and I.S. Raju, Analysis of Surface Cracks in Finite Plates Under Tension or Bending Loads", NASA Technical Paper 1578, 1979.

6. J.C. Newman, Jr. and I.S. Raju, "Stress Intensity Factor Equations for Cracks in Three-Dimensional Finite Bodies", ASTM, STP791, 1983.

7. J.C. Newman, Jr. and I.S. Raju, "An Empirical Stress Intensity Factor Equation for the Surface Crack", Journal of Engineering Fracture Mechanics, Vol. 15, pp. 185-192, 1981.

8. G.D. Gupta and F. Erdogan, "The Problem of Edge Cracks in an Infinite Strip", J. Appl. Mech., Vol. 41, pp. 1001-1006, Trans. ASME, 1974.

9. H. Boduroglu and F. Erdogan, "Internal and Edge Cracks in a Plate of Finite Width Under Bending", J. Appl. Mech., Vol. 50, Trans. ASME, pp. 621-629, 1983.

10. E. Reissner, "On Bending of Elastic Plates", Quarterly of Applied Mathematics, Vol. 5, pp. 55-68, 1947-48.

11. F. Delale and F. Erdogan, "Transverse Shear Effect in a Circumferentially Cracked Cylindrical Shell", Quarterly of Applied Mathematics, Vol. 37, pp. 239-258, 1979.

12. A.C. Kaya and F. Erdogan, "Stress Intensity Factors and COD in an Orthotropic Strip", Int. Journal of Fracture, Vol. 16, pp. 171-190, 1980.

13. F. Erdogan, "Mixed Boundary Value Problems in Mechanics", Mechanics-Today, S. Nemat-Nasser, ed. Vol. 4, pp. 1-86, Pergamon Press, Oxford, 1978.

14. J.P. Benthem, "The Quarter Infinite Crack in a Half Space: Alternative and Additional Solutions", Int. J. Solids Structures, Vol. 16, pp. 119-130, 1980.

Appendix A

The definition of normalized quantities

$$x = x_1/a^* \ , \ y = x_2/a^* \ , \ z = x_3/a^* \ , \tag{A.1}$$

$$u = u_1/a^* \ , \ v = u_2/a^* \ , \ w = u_3/a^* \ , \tag{A.2}$$

$$\phi = \frac{F}{a^{*2}hE} \ , \ \beta_x = \beta_1 \ , \ \beta_y = \beta_2 \ , \tag{A.3}$$

$$\sigma_{xx} = \sigma_{11}/E \ , \ \sigma_{yy} = \sigma_{22}/E \ , \ \sigma_{xy} = \sigma_{12}/E \ , \tag{A.4}$$

$$N_{\alpha\beta} = \frac{N_{ij}}{hE} \ , \ M_{\alpha\beta} = \frac{M_{ij}}{h^2E} \ , \ (\alpha,\beta) = (x,y) \ , \ (i,j) = (1,2) \ , \tag{A.5}$$

$$V_x = V_1/hB \ , \ V_y = V_2/hB \ , \tag{A.6}$$

$$B = \frac{5}{6}\frac{E}{2(1+\nu)} \ , \ \kappa = \frac{E}{B\lambda^4} \ , \ \lambda^4 = 12(1-\nu^2)a^{*2}/h^2 \ . \tag{A.7}$$

$$b' = b/a^* \ , \ c' = c/a^* \ , \ d' = d/a^*$$

In the problem described by Fig. 1, $a^* = a = (d-c)/2$ for $0<c<d\leq b$ and $a^* = d$ for $c = 0$, $d<b$.

Appendix B

The Fredholm kernels k_1 and k_2 which appear in the integral equations (36) and (37)

$$k_1(x,t) = \int_0^\infty \frac{e^{-(2b'-t)\beta}}{1+4\beta b' e^{-2\beta b'} - e^{-4\beta b'}} \{-[1+(3+2\beta b')e^{-2\beta b'}]\cosh\beta x$$

$$-2\beta x e^{-2\beta b'} \sinh\beta x - [2\beta x \sinh\beta x + (3-2\beta b'$$

$$+e^{-2\beta b'})\cosh\beta x][1-2\beta(b'-t)]\}d\beta \,, \qquad (B.1)$$

$$k_2(x,t) = \int_0^\infty \{[-\frac{3+\nu}{1+\nu} - \frac{1-\nu}{1+\nu}\beta(b'-t)] \frac{1+e^{-2\beta x}}{1-e^{-2\beta b'}} e^{-(2b'-t-x)\beta}$$

$$- \frac{2\kappa(1-\nu)}{1+\nu} \frac{1+e^{-2r_2 x}}{1-e^{-2r_2 b'}} (\beta^2 e^{-(b'-t)r_2} - \beta r_2 e^{-(b'-t)\beta}) e^{-(b'-x)r_2}$$

$$+ [(\frac{2\beta}{1-\nu} - \frac{2b'\beta^2}{1+\nu}\frac{1+e^{-2b'\beta}}{1-e^{-2b'\beta}})(1+e^{-2\beta x}) + \frac{4}{1+\nu}\{\kappa\beta^3(1+e^{-2\beta x})$$

$$+ \frac{\beta^2}{2} x(1-e^{-2\beta x}) - \frac{\nu}{1-\nu}\beta(1+e^{-2\beta x})\}] \frac{1}{D} D_1 e^{-(2b'-t-x)\beta}$$

$$+ D_2 e^{-(b'-x)\beta} e^{-(b'-t)r_2}] - \frac{4\kappa}{1+\nu}\beta^2 r_2(1+e^{-2r_2 x}) \frac{1}{D}[D_1 e^{-(b'-t)\beta}$$

$$+ D_2 e^{-(b'-t)r_2}] \frac{1-e^{-2b'\beta}}{1-e^{-2b'r_2}} e^{-(b'-x)r_2}\}d\beta \,, \qquad (B.2)$$

$$D_1 = \frac{2\beta}{\gamma^2} r_2(1-e^{-2b'\beta}) \frac{1+e^{-2b'r_2}}{1-e^{-2b'r_2}} - 2(1+e^{-2b'\beta})$$

$$+ \frac{1+e^{-2b'\beta}}{\kappa\gamma^2}[1-(b'-t)\beta] - (1-\nu)[\frac{\beta}{2}(b'-t) - \kappa\beta^2](1-e^{-2b'\beta}) \,,$$

$$(B.3)$$

$$D_2 = -\frac{2\beta^2}{\gamma^2}\frac{1+e^{-2b'r_2}}{1-e^{-2b'r_2}}(1-e^{-2b'\beta}) - \kappa\beta^2(1-\nu)(1-e^{-2b'\beta}) \quad , \qquad (B.4)$$

$$D = 4b'\beta^2 e^{-2b'\beta} - (\frac{3+\nu}{1-\nu}\beta + 2\kappa\beta^3)(1-e^{-4b'\beta})$$

$$+ 2\beta^2\kappa r_2 \frac{1+e^{-2b'r_2}}{1-e^{-2b'r_2}}(1-e^{-2b'\beta})^2 \quad . \qquad (B.5)$$

Table 1. The normalized stress intensity factors at the maximum penetration point (x=0) of a symmetrically located single semi-elliptic surface crack in a plate under uniform tension or bending (ν=0.3).

$\frac{b}{h}$	$\frac{d}{h}$	L_o = 0.2h		L_o = 0.4h		L_o = 0.6h		L_o = 0.8h	
		$k_b(0)$	$k_t(0)$	$k_b(0)$	$k_t(0)$	$k_b(0)$	$k_t(0)$	$k_b(0)$	$k_t(0)$
10	0.5	.709	.729	.308	.390	.0518	.175	-.0290	0.0503
	0.6	.737	.755	.342	.421	.0705	.192	-.0257	.0555
	0.8	.777	.792	.398	.470	.104	.221	-.0188	.0648
	1	.805	.818	.443	.508	.132	.246	-.0121	.0730
	4/3	.837	.848	.501	.559	.174	.282	-.0014	.0848
	2	.876	.884	.584	.630				
	4	.930	.934	.723	.752	.390	.464	.0726	.155
	6	.953	.956	.800	.819	.499	.556	.127	.203
	8	.967	.969	.853	.865	.592	.634	.190	.256
	9.5	.975	.976	.885	.893	.659	.689	.249	.305
	9.61	.976	.977	.887	.894	.664	.693	.254	.310
	9.8	.977	.978	.891	.898	.672	.700	.264	.318
8	0.5	.709	.729	.308	.390	.0519	.175	-.0290	.0503
	0.6	.738	.755	.342	.421	.0706	.192	-.0256	.0556
	0.8	.778	.792	.399	.470	.104	.221	-.0188	.0649
	1	.805	.818	.444	.509	.133	.247	-.0120	.0731
	2	.877	.885	.586	.632	.246	.341	.0189	.105
	4	.932	.936	.730	.758	.400	.472	.0774	.159
	6	.957	.959	.814	.830	.525	.576	.144	.216
	7.69	.971	.972	.867	.876	.626	.660	.223	.282
	7.84	.972	.973	.872	.880	.635	.667	.233	.290
6	0.5	.710	.729	.307	.391	.0521	.176	-.0289	.0503
	0.6	.738	.756	.343	.422	.0710	.192	-.0256	.0556
	0.9	.794	.807	.424	.492	.122	.235	-.0152	.0693
	1.2	.827	.839	.483	.543	.160	.270	-.0051	.0807
	1.5	.851	.861	.530	.583	.196	.301	.0046	.0910
	3	.915	.920	.681	.715	.341	.423	.0531	.137
	4	.930	.934	.723	.752	.390	.464	.0726	.155
	5	.953	.955	.802	.818	.507	.560	.136	.208
	5.77	.963	.964	.839	.850	.576	.616	.187	.250
	5.88	.964	.965	.844	.855	.587	.625	.197	.258

Table 1 (cont)

$\frac{b}{h}$	$\frac{d}{h}$	$L_o = 0.2h$		$L_o = 0.4h$		$L_o = 0.6h$		$L_o = 0.8h$	
		$k_b(0)$	$k_t(0)$	$k_b(0)$	$k_t(0)$	$k_b(0)$	$k_t(0)$	$k_b(0)$	$k_t(0)$
4	0.5	.711	.730	.309	.392	.0528	.176	-.0289	.0504
	0.666	.755	.771	.366	.441	.0839	.204	-.0231	.0591
	0.8	.780	.795	.403	.474	.106	.223	-.0184	.0653
	1	.809	.821	.450	.514	.137	.250	-.0112	.0738
	1.33	.843	.853	.512	.568	.183	.289	.0006	.0866
	1.5	.856	.865	.540	.591	.204	.307	.0068	.0929
	2	.886	.893	.608	.650	.265	.358	.0257	.111
	3.92	.951	.953	.800	.815	.519	.565	.152	.218
2	0.5	.716	.735	.316	.398	.0557	.179	-.0287	.0508
	0.6	.747	.763	.355	.431	.0768	.197	-.0249	.0564
	0.8	.791	.804	.421	.488	.117	.232	-.0166	.0671
	0.9	.808	.820	.450	.513	.136	.248	-.0121	.0722
	1.0	.823	.843	.477	.537	.156	.265	-.0072	.0774
	4/3	.864	.872	.561	.608	.224	.321	.0118	.0961
	1.9	.916	.919	.701	.726	.385	.450	.0754	.150
	1.96	.920	.924	.718	.740	.411	.471	.0903	.162

Table 2. Distribution of the stress intensity factors along the crack front in a plate containing a single symmetric semi-elliptic surface crack (b/h = 10, ν = 0.3, $x = x_1/d$).

	k_b	k_t	k_b	k_t	k_b	k_t	k_b	k_t
L_o/h	0.2		0.4		0.6		0.8	
x	b/h = 10 , d/h = 0.5 , ν = 0.3							
0.929	0.628	.547	.428	.340	.191	.152	.0486	.444
0.828	.672	.609	.392	.349	.154	.156	.0314	.472
0.688	.694	.656	.361	.364	.123	.162	.0113	.510
0.516	.704	.691	.336	.376	.0924	.169	-.0061	.512
0.319	.708	.715	.318	.385	.0672	.173	-.0187	.502
0.108	.709	.727	.308	.390	.0535	.175	-.0276	.503
0	.709	.729	.307	.390	.0518	.175	-.0290	.503
	b/h = 10 , d/h = 1 , ν = 0.3							
0.929	.631	.545	.505	.391	.272	.205	.0809	.0649
0.828	.709	.639	.496	.426	.239	.215	.0621	.0677
0.688	.756	.710	.480	.457	.209	.226	.0396	.0718
0.516	.783	.762	.464	.482	.177	.236	.0183	.0729
0.319	.798	.798	.451	.499	.149	.243	.0163	.0724
0.108	.804	.816	.444	.507	.134	.246	-.0103	.0728
0	.805	.818	.443	.508	.132	.246	-.0121	.0730
	b/h = 10 , d/h = 4 , ν = 0.3							
0.929	.623	.535	.561	.420	.402	.285	.168	.121
0.828	.739	.661	.626	.517	.420	.339	.163	.137
0.688	.819	.763	.666	.601	.426	.387	.144	.150
0.516	.875	.844	.695	.671	.418	.425	.120	.156
0.319	.910	.901	.713	.722	.402	.451	.0953	.156
0.108	.927	.930	.722	.748	.391	.463	.0756	.155
0	.930	.934	.723	.752	.390	.464	.0726	.155
	b/h = 10 , d/h = 8 , ν = 0.3							
0.929	.622	.533	.571	.423	.453	.316	.238	.170
0.828	.747	.667	.665	.542	.513	.403	.260	.209
0.688	.837	.778	.735	.653	.560	.487	.261	.240
0.516	.901	.868	.791	.749	.586	.558	.245	.256
0.319	.944	.931	.830	.821	.593	.607	.219	.259
0.108	.965	.965	.850	.860	.592	.631	.194	.256
0	.967	.969	.853	.865	.592	.634	.190	.256

Table 2 (cont.)

	k_b	k_t	k_b	k_t	k_b	k_t	k_b	k_t
L_o/h	0.2		0.4		0.6		0.8	
x	b/h = 10 , d/h = 9.8 , ν = 0.3							
0.929	.629	.538	.597	.442	.508	.355	.312	.225
0.828	.753	.673	.692	.562	.572	.446	.341	.270
0.688	.844	.784	.763	.675	.626	.536	.345	.305
0.516	.909	.875	.822	.775	.658	.614	.328	.323
0.319	.952	.939	.865	.851	.670	.669	.298	.324
0.108	.974	.973	.888	.892	.672	.697	.268	.319
0	.977	.978	.891	.898	.672	.700	.264	.318

Table 3. Distribution of the stress intensity factors along the crack front in a plate containing a single symmetric semi-elliptic surface crack (b/h = 2,4,6; ν=0.3).

	k_b	k_t	k_b	k_t	k_b	k_t	k_b	k_t
L_o/h	0.2		0.4		0.6		0.8	
x	b/h = 2, d/h = 1, ν = 0.3							
0.929	.646	.559	.542	.421	.306	.232	.0941	0.0752
0.828	.726	.654	.533	.456	.271	.240	.0736	.0768
0.688	.774	.726	.517	.487	.238	.249	.0492	.0796
0.516	.801	.779	.500	.511	.204	.257	.0261	.0793
0.319	.816	.814	.486	.527	.174	.262	.0077	.0777
0.108	.823	.832	.478	.536	.158	.264	-.0053	.0774
0	.823	.834	.477	.537	.156	.265	-.0072	.0774
	b/h = 4, d/h = 1, ν = 0.3							
0.929	.634	.548	.512	.397	.278	.210	.0833	.0668
0.828	.713	.642	.504	.432	.245	.220	.0642	.0694
0.688	.760	.713	.488	.463	.214	.230	.0414	.0733
0.516	.787	.766	.471	.488	.182	.240	.0198	.0741
0.319	.802	.801	.458	.505	.154	.246	.0028	.0734
0.108	.808	.819	.451	.513	.139	.249	-.0094	.0737
0	.809	.821	.450	.514	.137	.250	-.0112	.0738
	b/h = 6, d/h = 1.2, ν = 0.3							
0.929	.632	.545	.522	.402	.296	.221	.0921	.0723
0.828	.717	.645	.523	.446	.266	.234	.0732	.0754
0.688	.770	.722	.513	.483	.237	.247	.0501	.0796
0.516	.801	.778	.501	.512	.206	.258	.0277	.0808
0.319	.819	.817	.490	.532	.178	.266	.0096	.0802
0.108	.827	.836	.474	.541	.162	.270	-.0032	.0806
0	.827	.839	.483	.543	.160	.270	-.0051	.0807

Table 4. The normalized stress intensity factors at the center (x=0) of a single symmetric rectangular surface crack in a plate under tension or bending ($\nu = 0.3$).

$\frac{b}{h}$	$\frac{d}{h}$	$L_o = 0.2h$		$L_o = 0.4h$		$L_o = 0.6h$		$L_o = 0.8h$	
		$k_b(0)$	$k_t(0)$	$k_b(0)$	$k_t(0)$	$k_b(0)$	$k_t(0)$	$k_b(0)$	$k_t(0)$
10	0.5	.765	.784	.340	.429	.0607	.194	-.0316	.0599
	2	.915	.922	.652	.699	.284	.388	.0261	.122
	5	.970	.973	.847	.868	.544	.611	.134	.222
	9.8	.999	.999	.987	.989	.914	.927	.557	.603
8	0.5	.766	.785	.340	.429	.0608	.194	-.0316	.0599
	1	.853	.865	.496	.563	.154	.276	-.0105	.0851
	4	.963	.966	.814	.840	.487	.562	.104	.195
	7.84	.998	.998	.982	.985	.892	.907	.503	.554
6	0.5	.766	.785	.341	.429	0.0610	.194	-.0316	.0600
	1	.855	.867	.498	.566	.155	.277	-.0103	.0854
	3	.951	.955	.767	.797	.414	.500	.0721	.165
	5.88	.997	.998	.975	.978	.857	.878	.434	.491
4	0.5	.768	.787	.343	.431	0.0619	.195	-.0315	.0602
	1	.859	.870	.505	.571	.159	.281	-.0095	.0863
	2	.930	.936	.690	.732	.320	.419	.0370	.133
	3.92	.996	.996	.959	.965	.797	.826	.341	.408
2	0.5	.776	.794	.352	.439	.0655	.198	-.0312	.0609
	1	.880	.890	.545	.606	.186	.304	-.0041	.0923
	1.5	.941	.945	.710	.749	.334	.432	.0395	.135
	1.96	.990	.991	.916	.927	.666	.715	.205	.285

Table 5. Distribution of the stress intensity factors along the crack front in a plate containing a single symmetric rectangular surface crack, $x = x_1/d$.

	k_b	k_t	k_b	k_t	k_b	k_t	k_b	k_t
L_o/h	0.2		0.4		0.6		0.8	
x	b/h = 2, d/h = 1, ν = 0.3							
0.929	.585	.618	.233	.334	.0289	.159	-.0295	0.0458
0.828	.737	.759	.354	.440	.0798	.209	-.0261	.0619
0.688	.814	.829	.439	.514	.122	.248	-.0190	.0741
0.516	.852	.864	.495	.562	.154	.276	-.0120	.0831
0.319	.871	.881	.528	.591	.174	.294	-.0070	.0890
0.108	.879	.889	.543	.605	.184	.302	-.0044	.0920
0	.880	.890	.545	.606	.186	.304	-.0041	.0923
	b/h = 6, d/h = 1, ν = 0.3							
0.929	.566	.601	.210	.314	.0181	.149	-.0302	.0439
0.828	.715	.738	.321	.411	.0623	.194	-.0283	.0586
0.688	.789	.806	.399	.480	.0996	.228	-.0227	.0694
0.516	.827	.841	.451	.524	.127	.253	-.0169	.0773
0.319	.846	.858	.482	.551	.145	.269	-.0127	.0825
0.108	.854	.866	.496	.564	.154	.276	-.0105	.0851
0	.855	.867	.498	.566	.155	.277	-.0103	.0854
	b/h = 10, d/h = 1, ν = 0.3							
0.929	.423	.470	.112	.228	-.0172	.108	-.0293	.0309
0.828	.574	.609	.191	.298	.0038	.138	-.0343	.0417
0.688	.667	.694	.252	.352	.0250	.160	-.0350	.0492
0.516	.721	.744	.297	.390	.0421	.177	-.0339	.0545
0.319	.751	.771	.325	.415	.0539	.188	-.0325	.0580
0.108	.764	.783	.339	.427	.0599	.193	-.0317	.0597
0	.765	.784	.340	.429	.0607	.194	-.0316	.0599

Table 6. The location $x=x^*$ and magnitude $k_b(x^*)$ and $k_t(x^*)$ of the normalized stress intensity factors in a plate containing two collinear semi-elliptic surface cracks, $D=a/(a+c)$.

D		L_o = 0.2h		L_o = 0.4h		L_o = 0.6h		L_o = 0.8h	
		$k_b(x^*)$	$k_t(x^*)$	$k_b(x^*)$	$k_t(x^*)$	$k_b(x^*)$	$k_t(x^*)$	$k_b(x^*)$	$k_t(x^*)$
0.112	x^*	0.2	0.05	.929	.319	.929	.929	.929	.929
	$k(x^*)$	.831	.839	.649	.554	.409	.308	.138	.107
0.125	x^*	0	0	.929	.040	.929	.108	.929	.516
	$k(x^*)$	.812	.824	.522	.518	.287	.523	.867	.756
.250	x^*	0	0	$\mp$.929	0	.929	0	.929	$\mp$.516
	$k(x^*)$	.807	.820	.509	.512	.275	.248	.0822	.735
0.5	x^*	0	0	-.929	0	-.929	0	-.828	.516
	$k(x^*)$	.811	.823	.521	.517	.285	.251	.0858	.0744
0.75	x^*	-0.50	0	-.929	-.050	-.929	-.108	-.929	-.688
	$k(x^*)$	.818	.829	.550	.528	.310	.259	.0951	.786

Table 7. Distribution of the normalized stress intensity factors along the crack front in a plate containing two collinear semi-elliptic surface cracks, $\bar{x} = [x_1-(c+a)]/a$ (Fig. 1).

	k_b	k_t	k_b	k_t	k_b	k_t	k_b	k_t
L_o/h	0.2		0.4		0.6		0.8	
$\bar{x}$	b/h = 10, d/h = 1, D = a/(c+a)=0.112, ν=0.3							
0.929	.688	.596	.649	.505	.409	.308	.138	.107
0.828	.766	.689	.623	.527	.351	.300	.106	.102
0.688	.805	.754	.584	.541	.297	.294	.0720	.0975
0.516	.824	.798	.548	.550	.246	.289	.0411	.0915
0.319	.831	.827	.519	.554	.204	.285	.0175	.0858
0.108	.831	.839	.500	.553	.178	.280	.0013	.0829
0	.829	.839	.494	.550	.173	.278	-.0016	.0821
-0.108	.826	.835	.491	.546	.172	.275	-.0004	.0814
-0.319	.816	.814	.492	.532	.184	.269	.0117	.0809
-0.516	.799	.776	.500	.512	.209	.261	.0293	.0818
-0.688	.769	.721	.513	.484	.240	.250	.0516	.0814
-0.828	.720	.649	.526	.450	.270	.239	.0751	.0780
-0.929	.640	.553	.533	.413	.303	.229	.0949	.0758
	b/h = 10, d/h = 1, D = a/(c+a)=0.75, ν = 0.3							
0.929	.637	.551	.521	.404	.288	.217	.0872	.0698
0.828	.716	.645	.514	.440	.254	.227	.0678	.0721
0.688	.764	.717	.499	.472	.224	.237	.0446	.0757
0.516	.793	.771	.484	.498	.192	.247	.0225	.0763
0.319	.809	.807	.472	.516	.164	.254	.0050	.0753
0.108	.816	.826	.467	.526	.149	.258	-.0075	.0754
0	.818	.829	.467	.528	.148	.258	-.0093	.0755
-0.108	.818	.828	.469	.528	.151	.259	-.0073	.0755
-0.319	.814	.812	.480	.522	.169	.258	.0057	.0760
-0.516	.801	.778	.497	.509	.200	.253	.0243	.0778
-0.688	.776	.727	.517	.488	.236	.247	.0481	.0786
-0.828	.730	.657	.538	.460	.272	.240	.0735	.0766
-0.929	.651	.563	.550	.427	.310	.235	.0951	.0757

Table 8. The normalized intensity factors on the edges ($x=\pm b'$) of a plate containing two symmetric corner cracks having a profile of a quarter ellipse (Fig. 1).

tension and for those having shallow cracks under bending the maximum stress intensity factor was on the boundary $x = b'$, whereas for deep cracks in plates under bending K was maximum at the surface $x_1 = c$ or $x = c'$ (Fig. 1). For corner cracks with a rectangular profile results similar to those shown in Tables 8 and 9 are given in Tables 10 and 11. For this crack geometry too one may note that generally the stress intensity factors for rectangular cracks are higher than those for the elliptic cracks.

From the formulation of the problem it may be seen that all results in the surface crack problem are dependent on the Poisson's ratio ν of the plate. The stress intensity factors given in this paper are calculated for $\nu = 0.3$, However, as shown [9] , since the stress intensity factors are not very sensitive to the Poisson's ratio, the results given in Tables 1-11 should be valid for nearly all structural materials.

References

1. The Surface Crack: Physical Problems and Computational Solutions, J.L. Swedlow, ed. ASME, New York, 1972.

2. I.S. Raju and J.C. Newman, "Stress Intensity Factors for a Wide Range of Semi-Elliptical Surface Cracks in Finite Thickness Plates", Journal of Engineering Fracture Mechanics, Vol. 11, pp. 817-829, 1979.

3. J.R. Rice and N. Levy, "The Part-Through Surface Crack in an Elastic Plate", J. Applied Mechanics, Vol. 39, pp. 185-194, Trans. ASME, 1972.

4. F. Delale and F. Erdogan, "Line Spring Model for Surface Cracks in a Reissner Plate", Int. J. Engng. Science, Vol. 19, pp. 1331-1340, 1981.

5. J.C. Newman, Jr. and I.S. Raju, Analysis of Surface Cracks in Finite Plates Under Tension or Bending Loads", NASA Technical Paper 1578, 1979.

Table 8 - cont.

$\frac{b}{h}$	$\frac{a}{h}$	$L_o = 0.2h$		$L_o = 0.4h$		$L_o = 0.6h$		$L_o = 0.8h$	
		$k_b(b')$	$k_t(b')$	$k_b(b')$	$k_t(b')$	$k_b(b')$	$k_t(b')$	$k_b(b')$	$k_t(b')$
10	0.25	.772	.787	.376	.452	.0967	.218	-.0165	.0684
	0.75	.873	.882	.576	.625	.249	.349	.0307	.118
	1	.895	.902	.630	.672	.299	.391	.0483	.135
	1.5	.922	.927	.704	.736	.378	.457	.0786	.163
	2	.939	.943	.755	.780	.440	.510	.106	.188
	2.5	.951	.953	.793	.813	.494	.555	.133	.211
	3.0	.959	.961	.823	.840	.541	.594	.160	.234
	3.5	.966	.968	.848	.861	.584	.630	.188	.258
	4.0	.972	.973	.869	.880	.624	.664	.218	.283
	4.5	.976	.977	.888	.896	.664	.696	.252	.312
20	1	.895	.901	.629	.671	.298	.390	.0483	.135

Table 9. Distribution of the normalized stress intensity factors along the crack front in a plate containing two (elliptic) corner cracks, $\bar{x} = [x_1-(c+a)]/a$ (Fig. 1).

	k_b	k_t	k_b	k_t	k_b	k_t	k_b	k_t
L_o/h	0.2		0.4		0.6		0.8	
$\bar{x}$	b/h = 2, a/h = 0.5, ν = 0.3							
0.999	.852	.862	.522	.577	.197	.303	.0089	.0963
0.936	.846	.856	.515	.571	.191	.297	.0073	.0936
0.784	.834	.843	.503	.557	.182	.286	.0050	.0883
0.558	.824	.828	.493	.543	.177	.274	.0064	.0834
0.279	.813	.808	.492	.528	.184	.266	.0138	.0805
-0.026	.799	.777	.498	.510	.204	.257	.0263	.0798
-0.329	.776	.732	.511	.488	.231	.248	.0450	.0794
-0.600	.736	.669	.526	.460	.261	.240	.0679	.0768
-0.815	.668	.583	.537	.427	.294	.231	.0882	.0748
-0.953	.549	.460	.532	.390	.336	.232	.112	.0772
	b/h = 8, a/h = 0.8, ν = 0.3							
0.999	.879	.887	.589	.636	.260	.358	.0343	.122
0.936	.874	.882	.582	.630	.253	.351	.0317	.118
0.784	.866	.872	.570	.617	.242	.339	.0277	.112
0.558	.857	.859	.561	.602	.237	.326	.0281	.105
0.279	.844	.836	.557	.583	.243	.314	.0357	.101
-0.026	.825	.800	.557	.559	.259	.302	.0489	.0990
-0.329	.793	.746	.558	.525	.282	.286	.0677	.0966
-0.600	.741	.671	.558	.481	.304	.269	.0896	.0917
-0.815	.658	.573	.547	.428	.326	.249	.108	.0869
-0.953	.521	.434	.502	.361	.345	.231	.127	.0850

Table 10. The normalized stress intensity factors at the edges $x = \pm b'$ of a plate containing two symmetric rectangular corner cracks.

$\frac{b}{h}$	$\frac{a}{h}$	$L_o = 0.2h$		$L_o = 0.4h$		$L_o = 0.6h$		$L_o = 0.8h$	
		$k_b(b')$	$k_t(b')$	$k_b(b')$	$k_t(b')$	$k_b(b')$	$k_t(b')$	$k_b(b')$	$k_t(b')$
2	0.25	.821	.835	.415	.494	.108	.238	-.0185	.0773
	0.5	.895	.903	.581	.638	.223	.337	-.0119	.109
	0.8	.954	.958	.754	.787	.388	.477	.0620	.156
4	0.26	.820	.835	.419	.497	.112	.242	-.0163	.0797
	0.4	.860	.871	.507	.574	.174	.295	.0014	.0985
	1	.937	.942	.716	.755	.359	.453	.0595	.154
	1.6	.976	.978	.856	.876	.550	.617	.139	.227
6	0.27	.823	.838	.426	.504	.117	.246	-.0149	0.0812
	0.6	.891	.900	.589	.645	.240	.353	.0227	.120
	1.6	.956	.960	.788	.817	.453	.534	.0983	.190
	2.4	.984	.985	.902	.915	.648	.700	.202	.283
8	0.28	.827	.841	.433	.510	.122	.250	-.0136	.0826
	0.8	.912	.919	.648	.696	.294	.399	.0409	.138
	2	.967	.970	.833	.856	.525	.595	.133	.222
	3.2	.988	.989	.927	.937	.714	.756	.255	.331
10	0.27	.823	.837	.425	.503	.117	.246	-.0150	.0811
	1	.927	.933	.692	.734	.341	.439	.0573	.153
	2.5	.974	.976	.864	.882	.581	.643	.165	.251
	4	.991	.992	.943	.951	.761	.796	.302	.374

Table 11. Distribution of the normalized stress intensity factors in a plate with rectangular corner cracks, $\bar{x} = [x_1-(c+a)]/a$.

	k_b	k_t	k_b	k_t	k_b	k_t	k_b	k_t
L_o/h	0.2		0.4		0.6		0.8	
$\bar{x}$	b/h = 2, a/h = 0.5, ν = 0.3							
0.999	.895	.903	.581	.638	.223	.337	.0119	.109
0.936	.892	.901	.576	.634	.218	.332	.0102	.107
0.784	.887	.896	.564	.623	.207	.323	.0059	.103
0.558	.879	.889	.548	.609	.193	.310	.0003	.0967
0.279	.868	.879	.525	.589	.175	.295	-.0057	.0902
-0.026	.851	.863	.493	.561	.153	.275	-.0122	.0828
-0.329	.818	.833	.444	.518	.124	.249	-.0195	.0739
-0.600	.756	.776	.370	.454	.0852	.214	-.0268	.0626
-0.815	.630	.660	.262	.359	.0373	.168	-.0314	.0481
-0.953	.385	.434	.115	.229	-.0098	.107	-.0260	.0284
	b/h = 8, a/h = 0.8, ν = 0.3							
0.999	.912	.919	.648	.696	.294	.399	.0409	.138
0.936	.911	.918	.643	.692	.289	.394	.0383	.135
0.784	.907	.915	.633	.683	.277	.384	.0322	.129
0.558	.902	.910	.619	.671	.261	.370	.0249	.121
0.279	.894	.902	.598	.652	.242	.353	.0172	.114
-0.026	.880	.890	.567	.625	.217	.331	.0086	.105
-0.329	.856	.868	.520	.584	.183	.301	-.0015	.0934
-0.600	.809	.824	.446	.520	.137	.260	-.0133	.0792
-0.815	.705	.729	.331	.420	.0759	.205	-.0245	.0610
-0.953	.462	.505	.160	.270	.0073	.131	-.0263	.0367

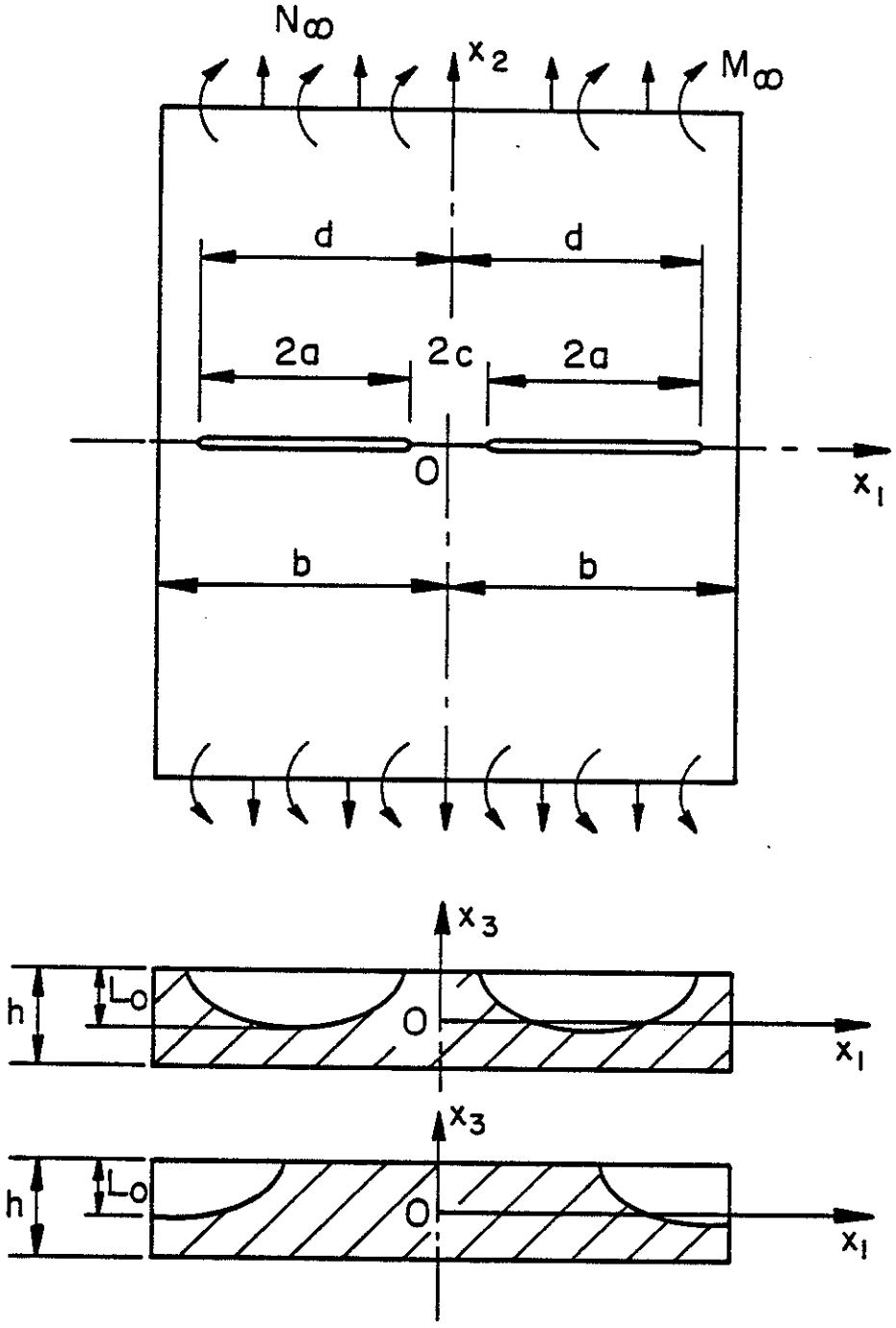

Fig. 1 The geometry of the plate with surface cracks

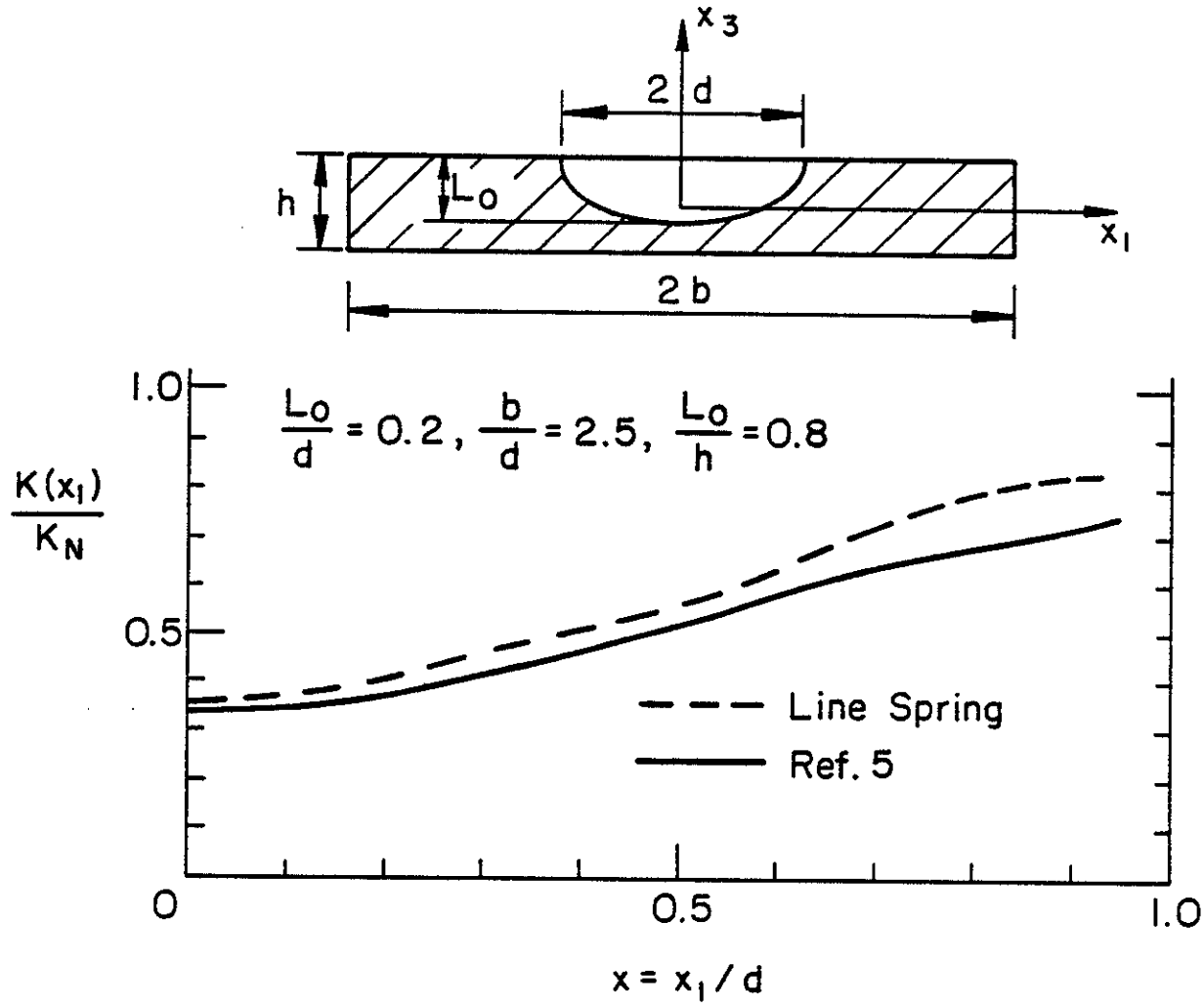

Fig. 2 Comparison of stress intensity factors calculated by the finite element and line spring methods in a plate containing a symmetrically located semi-elliptic surface crack and subjected to uniform tension.

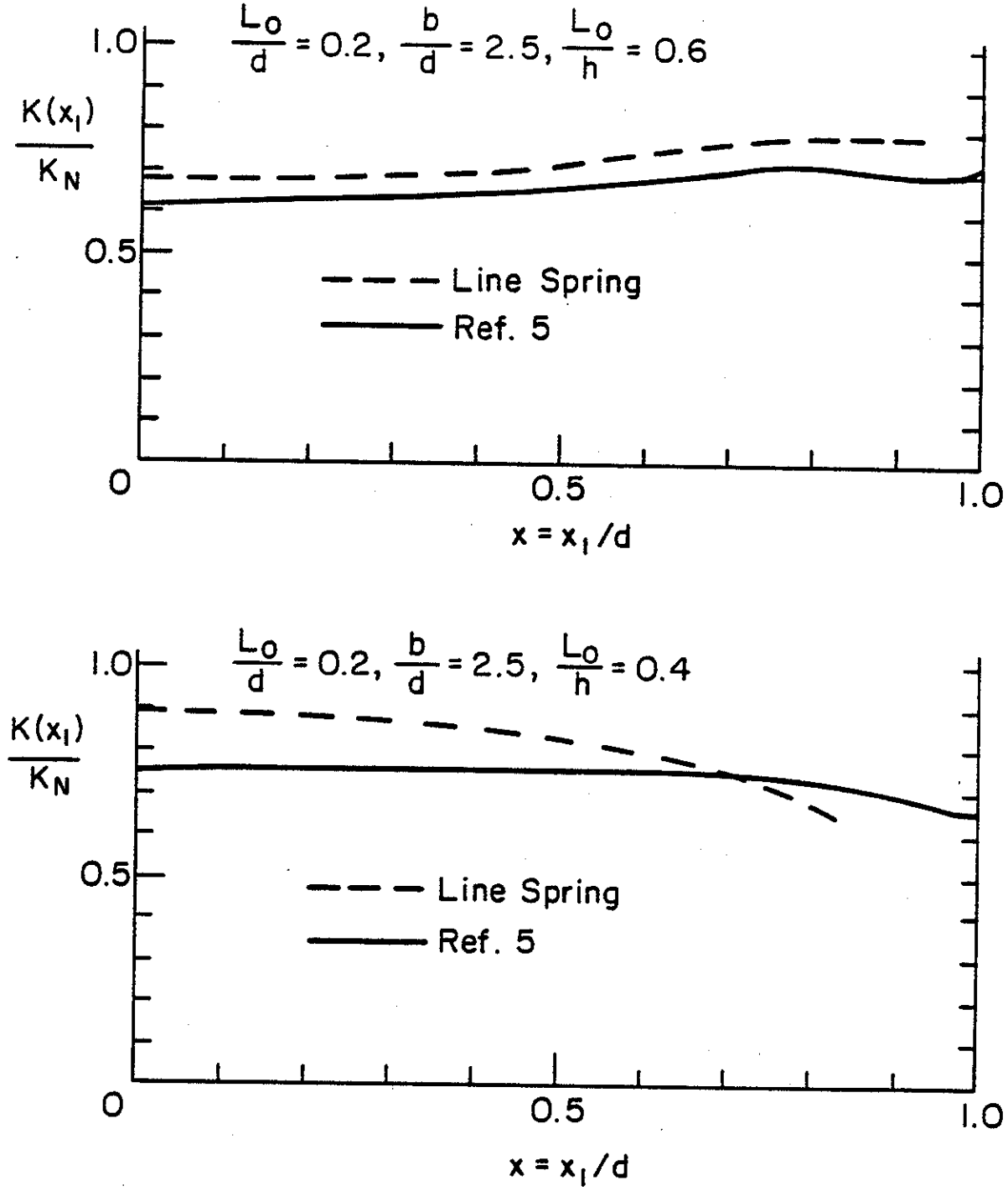

Fig. 3 Comparison of the stress intensity factors calculated by the finite element and line spring methods in a plate containing a single symmetric semi-elliptic surface crack and subjected to uniform bending.

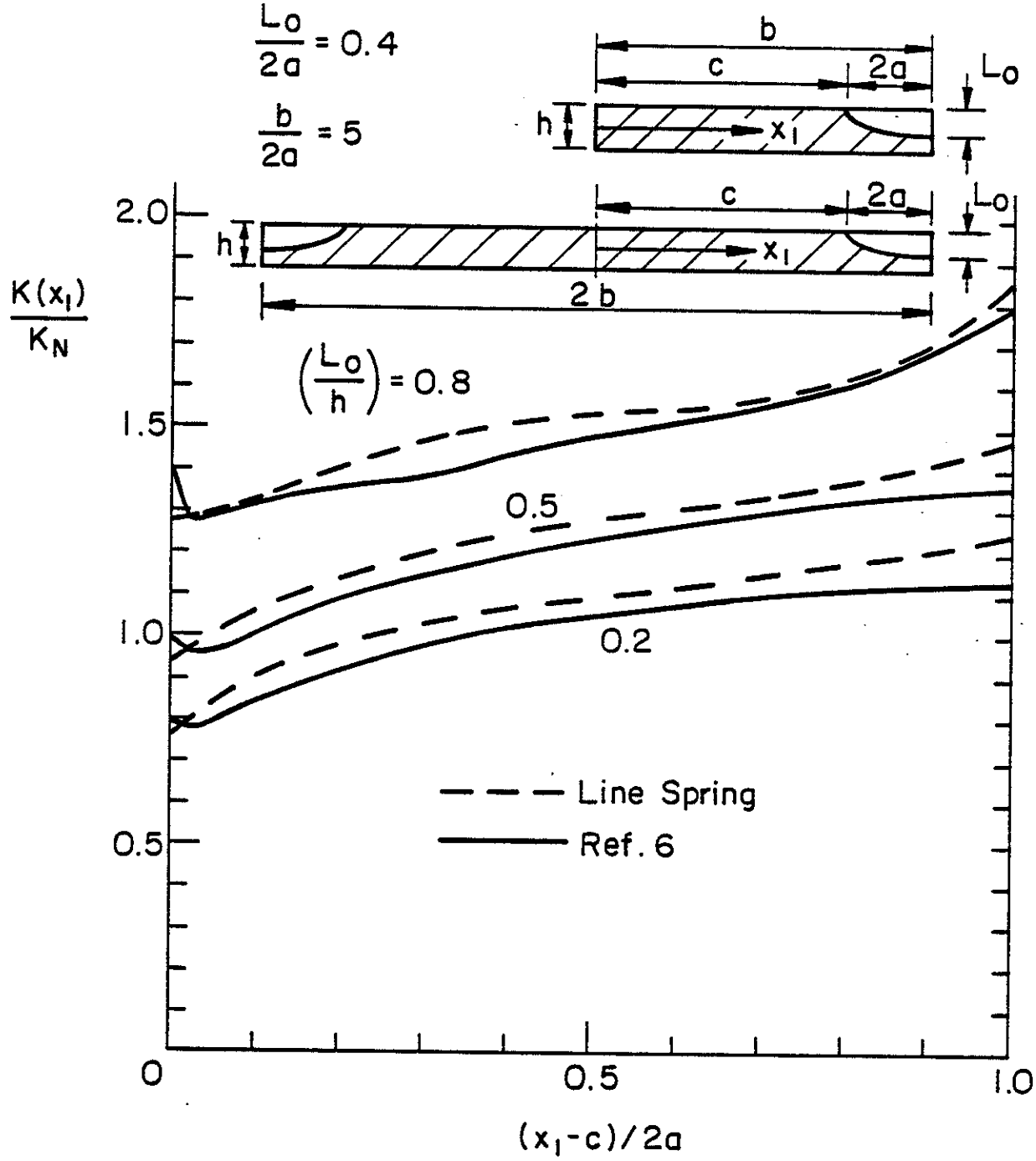

Fig. 4 Comparison of the stress intensity factors calculated by the finite element and line spring methods in a plate containing elliptic corner cracks and subjected to uniform tension, $L_o/2a = 0.4$, $b/2a = 5$.

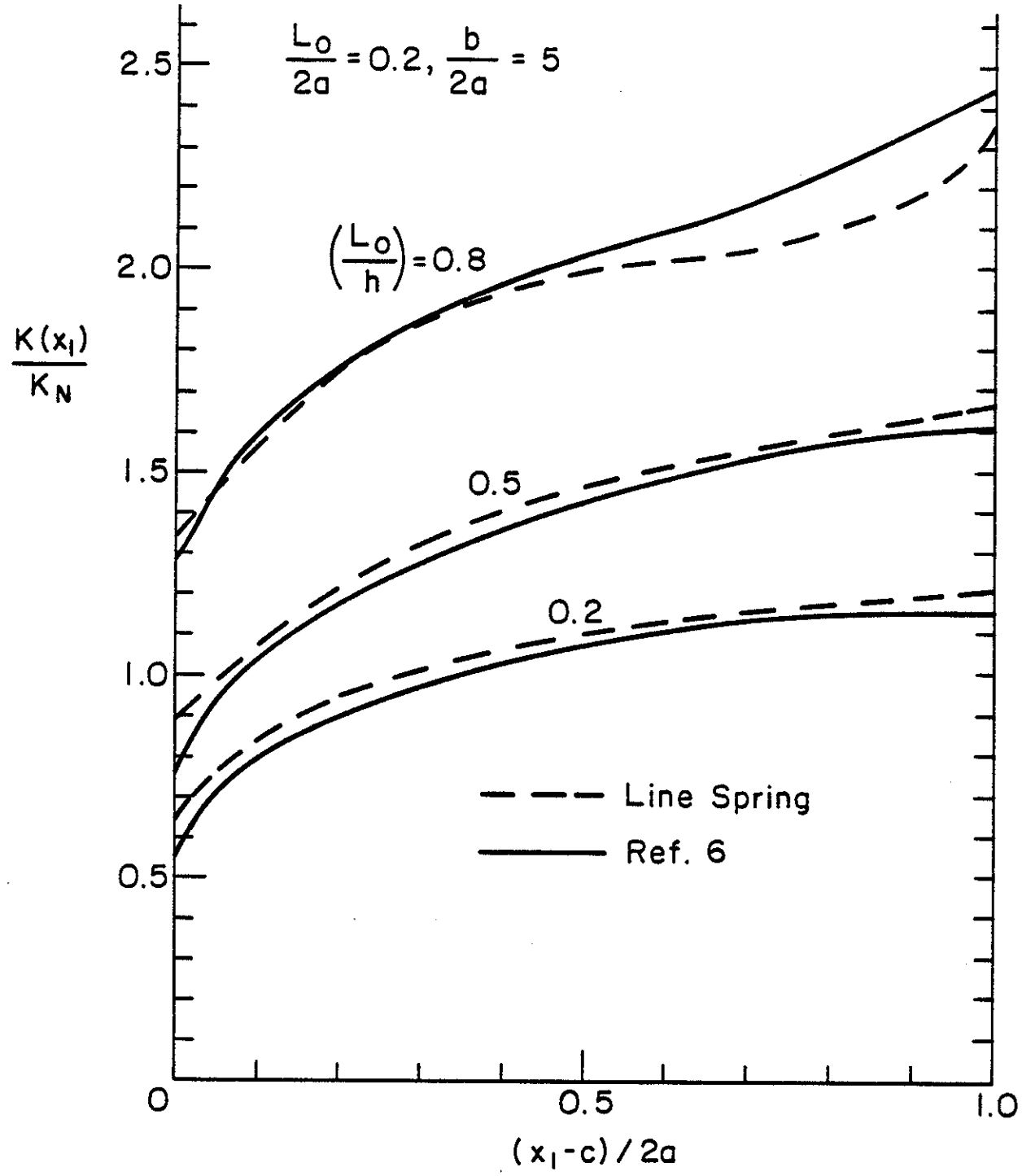

Fig. 5 Comparison of the stress intensity factors calculated by the finite element and line spring methods in a plate containing elliptic corner cracks and subjected to uniform tension, $L_o/2a = 0.2$, $b/2a = 5$.

APPENDIX B

INTERACTION OF PART-THROUGH CRACKS IN A FLAT PLATE

B. Aksel and F. Erdogan

Lehigh University, Bethlehem, PA

ABSTRACT

Main purpose of this study is to determine the accuracy of the line spring model, to investigate the effect of interaction between two and three cracks, and to provide extensive numerical results which may be useful in applications. Line spring model with Reissner's plate theory is formulated to be used for any number and configurations of cracks provided that there is symmetry. This model is used to find stress intensity factors for elliptic internal cracks, elliptic edge cracks and two opposite elliptic edge cracks. Unfortunately, because of the unavailability of previous work done on the cases considered, only stress intensity factors for central elliptic crack could be compared with other methods. Despite the simplicity of the line spring model, the results are found to be surprisingly close.

1. INTRODUCTION

From the viewpoint of practical applications, the analysis of a part through crack in a structural component which may locally be represented by a "plate" or a "shell" is certainly one of the most important problems in fracture mechanics. In its general form, the problem is a three-dimensional crack problem in a bounded geometry where the stress fields perturbed by the crack interacts very strongly with the surfaces of the solid. At present, even for the linearly elastic solids, a neat analytical treatment of the problem very heavily rely on some kind of numerical technique, such as alternating method, [5], [6], or boundary integral equation method, [7]; but most notably on the finite element method, [8]-[10]. The renewed interest in recent years in the so called "line-spring model" first described in [3] has been due partly to the desire of providing simpler and less expensive solutions to the part-through crack problem and partly to the fact that for certain important crack geometries, the model seems to give results that have an acceptable degree of accuracy.

In a plate or shell containing a part-through crack and subjected to membrane and bending loads, the net ligament(s) around the crack would generally have a constraining effect on the crack surface displacements and rotations. The basic idea underlying the "line-spring model" consists of approximating the three-dimensional

crack problem by a two-dimensional coupled bending-membrane problem through the reduction of the net ligament stresses to the neutral surface of the plate or shell as a membrane load N and a bending moment M. In the resulting two-dimensional problem, the crack surface displacements are represented by a crack opening displacement δ and a crack surface rotation θ, referred to, again, the neutral surface. The quantities N, M, δ and θ are assumed to be functions of a single variable, namely the coordinate x_1, along the crack in the neutral surface (Fig. 1). The pair of functions (δ,θ) or (N,M) are determined from the corresponding mixed boundary value problem for the plate or the shell having a through crack in which N and M are treated as unknown crack surface loads. Once N and M are determined, the stress intensity factors are evaluated from the two-dimensional elasticity solution of a strip under the membrane force N and the bending moment M.

The model introduced in [3] is based on the classical theory. However, the asymptotic stress field around the crack tip given by classical plate bending theory is not consistant with the elasticity solutions, whereas a transverse shear theory (such as that of Reissner's) which can accomodate all stress and moment resultants on the crack surface seperately (i.e., three boundary conditions in plates, five in shells) give results which are identical to the asymptotic solutions obtained from the plane strain and anti-plane shear crack problems [2], [11]. The line spring model was later used

in [12], [13] to treat the longitudinal part-through crack problem in a cylinder by using the classical shell theory and in [1], [14] by using transverse shear theory. Rather extensive results for corner cracks and for collinear surface cracks in a plate having a finite width are given in [15]. The similar problem of surface crack-boundary interaction in a cylindrical shell with a free or a fixed boundary is considered in [16] and [17].

In this study, stress intensity factors for elliptic internal cracks under pure bending and tension, and for collinear elliptic edge cracks under pure tension will be studied by using the line-spring model with Reissner's plate bending theory. Interaction of two and three identical elliptic edge and internal crcaks will also be studied by using the same method.

2. FORMULATION OF THE PROBLEM

2.1 Governing Integral Equations

The problem under consideration is a surface or an internal crack problem for a relatively thin-walled structural component which is solved basically as a plate or shell problem. In the usual notation u_1, u_2, u_3 are the components of the displacement vector, β_1 and β_2 are the angles of rotation of the normal to the neutral surface in x_1x_3 and x_2x_3 planes, respectively, and N_{ij}, M_{ij} and $V_i(i,j=1,2)$ are respectively the membrane, moment and transverse shear resultants (Fig. 1).

Related mixed boundary value problem for any number of cracks has been formulated in [15] by using Reissner's plate bending theory. The derivatives of the crack surface displacement and the crack surface rotation on the neutral surface are chosen as the unknown functions. Fredholm kernels $k_1(x,t)$ and $k_2(x,t)$ in [15] represent the effect of finite length of the plate in x_1 direction. They will vanish in this case since the plate has an infinite length in x_1 direction. Integral equations are written for only half of the infinite plate ($x_1 > 0$) and are only valid when symmetry with respect to the x_2x_3 plane exists. D represents the normalized cracked region on the x_1 axis, which means that if there is a crack in the region (b,c), D represents the region (b/a , c/a) where "a"

is the half crack length and equals to (c-b)/2. x is also normalized parameter on x_1 axis which is $x=x_1/a_i$, where a_i the half crack length for the corresponding crack(i subscript is needed because general formulation is done for more than one crack).

From [15], integral equations are as follows:

$$\frac{\sigma(x)}{E} - \frac{1}{2\pi}\int_D \left[\frac{1}{t-x} + \frac{1}{t+x}\right] G_1(t)\, dt = \frac{\sigma_o(x)}{E}, \qquad x \in D, \qquad (1)$$

$$\frac{m(x)}{6E} - R_1\int_D \left[R_2\left[\frac{1}{t-x} + \frac{1}{t+x}\right] - R_3\left[\frac{1}{(t-x)^3} + \frac{1}{(t+x)^3}\right] + R_4\left[\frac{1}{t-x} K_2(p|t-x|) + \frac{1}{t+x} K_2(p|t+x|)\right]\right] G_2(t)\, dt = \frac{m_o(x)}{6E}, \qquad x \in D, \qquad (2)$$

where K_2 is the modified Bessel function of the second kind and the constants R_1, R_2, R_3, R_4 and p are defined in Appendix I. h is the thickness of the plate, 2a is the length and $L(x_1)$ is the depth of the crack (Fig. 1). E is the modulus of elasticity and ν is the Poisson's ratio of the material. The unknown functions are defined by

$$G_1(x) = \frac{\partial}{\partial x} \beta_y(x,+0) , \qquad G_2(x) = \frac{\partial}{\partial x} v(x,+0) , \qquad (3)$$

$$\beta_y = \beta_2 , \qquad v = u_2/a .$$

The external loads

$$\sigma_o = \frac{N_{22}^o}{h} , \qquad m_o = \frac{6M_{22}^o}{h^2} , \qquad (4)$$

represent uniform membrane and bending resultants applied to the plate away from the crack region and σ and m which are defined by

$$\sigma(x) = \frac{N(x,0)}{h} , \qquad m(x) = \frac{6M(x,0)}{h^2} , \qquad x \in D , \qquad (5)$$

are the membrane and bending loads applied to the crack surfaces (Fig. 1). The integral equations are obtained from the following mixed boundary conditions in $x_2=0$ plane

$$N_{22}(x,0) = -N^{o}_{22} + N(x) \quad , \quad x \in D \ , \qquad (6a)$$

$$u_2(x,0) = 0 \quad , \quad x \in D \ , \qquad (6b)$$

$$M_{22}(x,0) = -M^{o}_{22} + M(x) \quad , \quad x \in D \ , \qquad (7a)$$

$$\beta_2(x,0) = 0 \quad , \quad x \in D \ , \qquad (7b)$$

where the general principle of superposition is used to account for the loading N^{o}_{22}, and M^{o}_{22} applied to the structure away from the crack region.

2.2 Line-Spring Model for an Edge Crack

Edge crack is chosen for introductory purposes because of the simplicity of its formulation. Modifications will be made as more complicated crack geometries are examined.

The configuration studied here is an "infinite" elastic plate of thickness h, which contains a surface crack of length 2a and depth $L(x_1)$ penetrating part through the thickness (Fig. 1). For general purposes $L(x_1)$can be any function which enables us to treat any crack geometry. At remote distances from the crack site, the plate is subjected to loads equipollent to a uniform simple tension in the x_2 direction and to pure bending about the x_1 axis. The first

assumption in the line-spring analysis is that the stress intensity factor at a point along the crack front with coordinate x_1 is identical to the stress intensity factor for an edge cracked strip in plane strain (Fig. 2), subjected to an axial force and moment equal, respectively, to $N_{22}(x_1,0)$ and $M_{22}(x_1,0)$, and having a crack depth equal to $L(x_1)$. In [1], [3], mode I stress intensity factor for the plane strain problem is given as

$$K(s) = \sqrt{h}\,[\sigma g_t(s) + m g_b(s)] \,, \qquad (8)$$

$$s(x_1) = L(x_1)/h \,, \qquad (9)$$

where functions $g_t(s)$ and $g_b(s)$ are called shape functions for tension and bending respectively, and given as

$$g_t(s) = \sqrt{\pi s}\sum_{i=1}^{n} b_i s^{2(i-1)} \,, \qquad (10a)$$

$$g_b(s) = \sqrt{\pi s}\sum_{i=1}^{n} c_i s^{(i-1)} \,. \qquad (10b)$$

The value of n is chosen according to the desired accuracy. The coefficients b_i and c_i can be found by a suitable curve fitting (Appendix II). Coefficients of the shape functions for a number of crack geometries are given in Tables 2, 4, 6, 8, 10, 12, 14, 16, 17.

In order to obtain $N(x_1)$ and $M(x_1)$ in terms of G_1 and G_2, the energy available for fracture along the crack front is expressed in two different ways, namely as the crack closure energy and as the product of load-load point displacement. In a plate with an edge crack subjected to uniform tension N and uniform bending moment M (Fig. 2), if K is the stress intensity factor given by the plane strain solution, from the crack closure energy, the energy (per unit width) available for fracture may be obtained as

$$G = \frac{\partial}{\partial L}(U-V) = \frac{1-\nu^2}{E} K^2 \quad , \tag{11}$$

where U is the work done by the external loads and V is the strain energy.

Let δ and θ be the load line displacements corresponding to N and M shown in Fig. 2 and $d\delta$ and $d\theta$ be the changes in δ and θ as the crack length goes from L to L+dL under fixed load conditions. Then referring to Fig. 2, the changes in U and V may be expressed as

$$dU = N d\delta + M d\theta \quad , \tag{12}$$

$$dV = (1/2)\,[N(\delta+d\delta) + M(\theta+d\theta) - (1/2)\,(N\delta + M\theta) =$$

$$= (1/2)\,(N d\delta + M d\theta) \quad , \tag{13}$$

Equations (12) and (13) give the energy available for a crack growth dL as follows:

$$d(U-V) = (1/2)\,(N d\delta + M d\theta) \quad . \tag{14}$$

On the other hand for constant N and M, and for a change of dL in the crack length, we have

$$d\delta = \frac{\partial \delta}{\partial L} dL \,, \qquad d\theta = \frac{\partial \theta}{\partial L} dL \quad . \tag{15}$$

Thus, from (14) and (15) it follows that

$$\frac{\partial}{\partial L}(U-V) = G = \frac{1}{2}\left[N\frac{\partial \delta}{\partial L} + M\frac{\partial \theta}{\partial L}\right], \tag{16}$$

and, by using (11) we find

$$\frac{1}{2}\left[N\frac{\partial \delta}{\partial L} + M\frac{\partial \theta}{\partial L}\right] = \frac{1-\nu^2}{E} K^2 \quad . \tag{17}$$

From (5) and (8), we may rewrite (17) in terms of σ and m as

follows:

$$\frac{1}{2}\left[\sigma h\frac{\partial\delta}{\partial L}+m\frac{h^2}{6}\frac{\partial\theta}{\partial L}\right]=h\frac{1-\nu^2}{E}(g_t^2\sigma^2+2g_tg_b\sigma m+g_b^2m^2)\ . \tag{18}$$

In order to solve σ and m in terms of δ and θ or vice versa we introduce the so called compliance coefficients. In a cracked strip, displacement and rotation are functions of both the applied stress and bending moment. This relation may be expressed as

$$h\delta = A_{tt}\sigma + A_{tb}m\ , \tag{19a}$$

$$h^2\theta/6 = A_{bt}\sigma + A_{bb}m\ , \tag{19b}$$

where (with proper normalizations) $A_{tb}=A_{bt}$ by elastic reciprocity. The compliance coefficients A_{ij} depend only on L and vanish when L=0. If we substitute (19) into (18) and equate common coefficients in the quadratic forms of both sides, we get

$$\frac{dA_{tt}}{dL}=\frac{2(1-\nu^2)h}{E}g_t^2\ , \tag{20a}$$

$$\frac{dA_{tb}}{dL} = \frac{dA_{bt}}{dL} = \frac{2(1-\nu^2)h}{E} g_t g_b \ , \qquad (20b)$$

$$\frac{dA_{bb}}{dL} = \frac{2(1-\nu^2)h}{E} g_b^2 \ . \qquad (20c)$$

By defining

$$\alpha_{ij} = h^{-1} \int_0^L g_i g_j \, dL \quad , \quad (i,j = b,t) \ , \qquad (21)$$

and knowing that $A_{ij}=0$ at $L=0$, we may write

$$A_{tt} = \frac{2h^2(1-\nu^2)}{E} \alpha_{tt} \quad , \qquad (22a)$$

$$A_{tb} = A_{bt} = \frac{2h^2(1-\nu^2)}{E} \alpha_{tb} \ , \qquad (22b)$$

$$A_{bb} = \frac{2h^2(1-\nu^2)}{E} \alpha_{bb} \ . \qquad (22c)$$

Substitution of (22) into (19) gives

$$\delta = \frac{2h(1-\nu^2)}{E} (\alpha_{tt}\sigma + \alpha_{tb}m) , \tag{23}$$

$$\theta = \frac{12(1-\nu^2)}{E} (\alpha_{bt}\sigma + \alpha_{bb}m) , \tag{24}$$

where $\alpha_{tb}=\alpha_{bt}$. From (3), δ and θ may be expressed in terms of the unknown functions G_1 and G_2 as

$$\theta = 2\beta_2(x,+0) = 2\int_{-1}^{x} G_1(t)\,dt , \tag{25}$$

$$\delta = 2au_2(x,+0) = 2a\int_{-1}^{x} G_2(t)\,dt . \tag{26}$$

If we solve (23) and (24) for $\sigma(x)$ and $m(x)$ and substitute (25) and (26) for δ and θ, we can determine $\sigma(x)$ and $m(x)$ in terms of the unknown functions G_1 and G_2 as follows:

$$\sigma(x) = E\left[\gamma_{tt}(x)\int_{-1}^{x} G_2(t)\,dt + \gamma_{tb}(x)\int_{-1}^{x} G_1(t)\,dt\right] , \tag{27}$$

$$m(x) = 6E\left[\gamma_{bt}(x)\int_{-l}^{x} G_2(t)\,dt + \gamma_{bb}(x)\int_{-l}^{x} G_1(t)\,dt\right], \quad (28)$$

where

$$\gamma_{tt} = \frac{a}{h(1-\nu^2)}\frac{\alpha_{bb}}{\Delta}, \quad (29a)$$

$$\gamma_{tb} = -\frac{1}{6(1-\nu^2)}\frac{\alpha_{tb}}{\Delta}, \quad (29b)$$

$$\gamma_{bt} = -\frac{1}{6h(1-\nu^2)}\frac{\alpha_{bt}}{\Delta}, \quad (29c)$$

$$\gamma_{bb} = \frac{1}{36(1-\nu^2)}\frac{\alpha_{tt}}{\Delta}, \quad (29d)$$

$$\Delta = \alpha_{tt}\alpha_{bb} - \alpha_{tb}^2 . \quad (29e)$$

We should keep in mind that α_{ij} is a function of L(x)/h, which means α_{ij} is also a function of x.

For a single crack shown in Fig. 1, the normalized cracked region on x_1 axis (called D in (1) and (2)) is defined as (0,1). (1) and (2) then become

$$\frac{\sigma(x)}{E} - \frac{1}{2\pi}\int_0^1 \left[\frac{1}{t-x} + \frac{1}{t+x}\right] G_1(t)\, dt = \frac{\sigma_o}{E}, \quad 0 < x < 1, \tag{30}$$

$$\frac{m(x)}{6E} - R_1 \int_0^1 \left[R_2 \left[\frac{1}{t-x} + \frac{1}{t+x}\right] - R_3 \left[\frac{1}{(t-x)^3} + \frac{1}{(t+x)^3}\right] + R_4 \left[\frac{1}{t-x} K_2(p|t-x|) + \frac{1}{t+x} K_2(p|t+x|)\right]\right] G_2(t)\, dt$$

$$= \frac{m_o}{6E}, \qquad 0 < x < 1. \tag{31}$$

For convenience in the numerical solution of integral equations we need to convert the integrals calculated over (0,1) to (-1,1). Because of that the geometry and loading conditions are symmetric with respect to the x_2x_3 plane, $u_2(x,+0)$ and $\beta_2(x,+0)$ should also be symmetric with respect to the same plane. In mathemathical form

$$u_2(-x,+0) = u_2(x,+0), \tag{32a}$$

$$\beta_2(-x,+0) = \beta_2(x,+0) \quad . \tag{32b}$$

Observing that derivative of a symmetric function is antisymmetric, we may write

$$G_1(-t) = -G_1(t) \quad , \tag{33a}$$

$$G_2(-t) = -G_2(t) \quad . \tag{33b}$$

By applying the above properties, integrand of (30) can be rewritten as

$$\int_0^1 \left[\frac{1}{t-x} + \frac{1}{t+x}\right] G_1(t)\, dt = \int_0^1 \frac{1}{t-x} G_1(t)\, dt + \int_0^1 \frac{1}{t_1+x} G_1(t_1)\, dt_1 \quad . \tag{34}$$

By a change of variable $t_1 = -t$ and from (33a), we can write

$$\int_0^1 \frac{1}{t_1+x}\, G_1(t_1)\, dt_1 = \int_0^{-1} \frac{1}{-t+x}\,[-G_1(t)]\,(-dt)$$

$$= \int_{-1}^{0} \frac{1}{t-x}\, G_1(t)\, dt \quad . \qquad (35)$$

Substituting (35) in (34)

$$\int_0^1 \left[\frac{1}{t-x} + \frac{1}{t+x}\right] G_1(t)\, dt = \int_{-1}^{1} \frac{1}{t-x}\, G_1(t)\, dt \quad . \qquad (36)$$

After applying the same procedure to (31) and substituting (27) and (28) for $\sigma(x)$ and $m(x)$, integral equations take the following final form

$$\gamma_{bb}(x) \int_{-1}^{x} G_1(t)\, dt - R_1 \int_{-1}^{1} \left[R_2 \frac{1}{t-x} - R_3 \frac{1}{(t-x)^3}\right.$$

$$\left. + R_4 \frac{1}{t-x} K_2(p|t-x|)\right] G_1(t)\, dt + \gamma_{bt}(x) \int_{-1}^{x} G_2(t)\, dt$$

$$= \frac{m_o}{6E} \quad , \quad -1 < x < 1 \quad , \qquad (37a)$$

$$\gamma_{tb}(x)\int_{-1}^{x} G_1(t)\,dt + \gamma_{tt}(x)\int_{-1}^{x} G_2(t)\,dt - \frac{1}{2\pi}\int_{-1}^{1}\frac{G_2(t)}{t-x}dt = \frac{\sigma_o}{E}\,, \quad -1 < x < 1\,. \tag{37b}$$

From (3) it follows that the unknown functions G_1 and G_2 must satisfy the single valuedness conditions given by

$$\int_{-1}^{1} G_1(t)\,dt = 0\,, \qquad \int_{-1}^{1} G_2(t)\,dt = 0\,. \tag{38}$$

After solving (37) and (38) by using Gauss-Chebyshev closed type integration formula which is defined in Appendix III, a backward procedure is applied to find the stress intensity factors along the crack front. Unknown functions are integrated (Appendix IV) from -1 to the value of x at which the stress intensity factor is desired. Then those integrals are substituted to (27) and (28) with the functions $\gamma_{ij}(x)$, (i, j=t, b) evaluated at that particular point to get corresponding σ and m. Once σ and m are found, (8) gives the stress intensity factor at a specific point on the crack front.

2.3 Internal Cracks

The line-spring model described in the previous section may easily be extended to internal cracks such as that shown in Fig. 3. In this case the basic integral equations remain the same and again are given by (1) and (2). However, there are two crack tips (shown as A and B in Fig. 3) which create two different stress intensity factors for each cross-section taken perpendicular to x_1 direction. Previous assumptions regarding the stress intensity factors will also remain the same; however, they are now defined seperately, i.e.,

$$K_A = \sqrt{h}\,[\sigma g_{At}(s) + m g_{Ab}(s)] \quad , \qquad (39a)$$

$$K_B = \sqrt{h}\,[\sigma g_{Bt}(s) + m g_{Bb}(s)] \quad , \qquad (39b)$$

where g_{At}, g_{Ab}, g_{Bt}, g_{Bb} are the shape functions corresponding to crack tips A and B. Unlike the edge crack case, these shape functions are now functions of both $L(x_1)/h$ and d/h where d is the distance from the center of the crack to the neutral plane. Two way

parametrization is needed in order to define the shape functions which are valid for any kind of internal crack. Since elliptic cracks whose major axis are parallel to the free surface are the main concern in the present study, parametrization can be simplified by observing that the distance between the center of any crack obtained by taking cross-sections perpendicular to the major axis and the center line of the plate is fixed. In other words, d is constant for any elliptic crack whose major axis is parallel to the free surface. Because of this property, as in the previous case, we may again define the shape functions for each crack as a function of only one variable, which is $L(x_1)/h$, as

$$g_{At} = \sqrt{\pi s} \sum_{i=1}^{n} b_{Ai} s^{2(i-1)} \quad , \qquad (40a)$$

$$g_{Ab} = \sqrt{\pi s} \sum_{i=1}^{n} c_{Ai} s^{i-1} \quad , \qquad (40b)$$

$$g_{Bt} = \sqrt{\pi s} \sum_{i=1}^{n} b_{Bi} s^{2(i-1)} \quad , \qquad (40c)$$

$$g_{Bb} = \sqrt{\pi s} \sum_{i=1}^{n} c_{Bi} s^{i-1} \quad . \qquad (40d)$$

Keep in mind that coefficients are different for each value of d.

The next step is the representation of the energy available for fracture in terms of both stress intensity factors and product of load-load point displacement. As L increases by dL, the energy

increment available for fracture may be expressed as

$$d(U-V) = \frac{1-\nu^2}{E}\left[K_A^2\, d(L/2) + K_B^2\, d(L/2)\right] \quad , \tag{41}$$

giving

$$G = \frac{\partial}{\partial L}(U-V) = \frac{1-\nu^2}{2E}(K_A^2 + K_B^2) \quad , \tag{42}$$

which replaces (11). The rate of energy available for fracture as expressed in terms of the load line displacements and forces remains the same and is given by (16). If the same procedure as in the previous section is followed, the functions $\alpha(ij)$ may be found as

$$\alpha_{tt} = h^{-1} \int_0^L (g_{At}^2 + g_{Bt}^2)/2 \, dL \quad , \tag{43a}$$

$$\alpha_{bb} = h^{-1} \int_0^L (g_{Ab}^2 + g_{Bb}^2)/2 \, dL \quad , \tag{43b}$$

$$\alpha_{tb} = \alpha_{bt} = h^{-1} \int_0^L (g_{At}g_{Ab} + g_{Bt}g_{Bb})/2 \, dL \quad . \tag{43c}$$

After this point, everything, including the resulting integral

equations and the solution method, is exactly the same as explained in Section 2.2. After solving the equations, the functions G_1 and G_2 are again substituted to (27) and (28) to find σ and m, which are then substituted to (39) to find the two stress intensity factors at the corresponding value of x.

2.4 Symmetric Internal Crack

This is a special case of an internal crack where d=0. Due to the fact that simple tension cannot create any crack surface rotation and simple bending cannot create any crack opening displacement (on the neutral plane), from (23) and (24) one can write

$$\alpha_{tb} = \alpha_{bt} = 0 \quad , \qquad (44)$$

which gives

$$\gamma_{tb} = \gamma_{bt} = 0 \quad . \qquad (45)$$

Substitution of (45) into (37) would decouple the integral equations

(only unknown in (37a) is G_1 while the only unknown in (37b) is G_2) which would in turn enable us to solve them seperately. This property reduces both the computer time and memory space needed in the numerical solution.

2.5 Two Opposite Elliptic Edge Cracks

Two opposite edge cracks shown in Fig. 4 has exactly the same properties as symmetric internal cracks except for the coefficients of the shape functions. Once the shape functions are established by a suitable curve fitting, the same procedure that is applied to symmetric internal cracks is applied to find the stress intensity factors.

2.6 Interaction Between Two Identical Cracks

All the crack geometries that we considered up to now were single cracks lying in the region (-a,a) on the x_1 axis. Only difference among them was their configuration in the thickness

direction. Shape functions, energy available for fracture and functions α_{ij} and γ_{ij} are all sensitive to this configuration, while the form of the integral equation is independent of it. In this section, we will modify (1) and (2) for two identical cracks which is shown in Fig. 5. In this case D is defined as (b/a , c/a). With the new definition of D, (1) and (2) will take the following form.

$$\frac{\sigma(x')}{E} - \frac{1}{2\pi}\int_{b'}^{c'}\left[\frac{1}{z-x'} + \frac{1}{z+x'}\right]G_1(z)\,dz = \frac{\sigma_o}{E}, \quad b' < x' < c' , \tag{46}$$

$$\frac{m(x')}{E} - R_1\int_{b'}^{c'}\left[R_2\left[\frac{1}{z-x'} + \frac{1}{z+x'}\right] - R_3\left[\frac{1}{(z-x')^3} + \frac{1}{(z+x')^3}\right] + R_4\left[\frac{1}{z-x'}K_2(p|z-x'|) + \frac{1}{z+x'}K_2(p|z+x'|)\right]\right]G_2(z)\,dz$$

$$= \frac{m_o}{6E} \quad , \quad b' < x' < c' \quad , \tag{47}$$

where

$$x' = x_1/a, \qquad b' = b/a, \qquad c' = c/a .$$

Again we have to convert the limits of integrals to (-1,1) for

numerical solution purposes. By introducing the following parameters (keep in mind that from Fig. 5, $(c'-b')/2 = 1$)

$$x = (2x'-c'-b') / (c'-b') \quad , \tag{48}$$

$$x' = [(c'-b')x+c'+b'] / 2 = x + [(c'+b') / 2] \quad , \tag{49}$$

$$dx' = dx \quad ,$$

and

$$t = (2z-c'-b') / (c'-b') \quad , \tag{50}$$

$$z = [(c'-b')t+c'+b'] / 2 = t + [(c'+b') / 2] \quad , \tag{51}$$

$$dz = dt \quad ,$$

and substituting (27) and (28) for $\sigma(x)$ and $m(x)$ respectively, (46) and (47) can be rewritten as follows:

$$\gamma_{bb}(x) \int_{-1}^{x} G_1(t)\, dt - R_1 \int_{-1}^{1} \left[R_2\left[\frac{1}{y_1} + \frac{1}{y_2}\right] - R_3\left[\frac{1}{y_1^3} + \frac{1}{y_2^3}\right] \right.$$

$$\left. + R_4\left[\frac{1}{y_1} K_2(p|y_1|) + \frac{1}{y_2} K_2(p|y_2|)\right] \right] G_1(t)\, dt + \gamma_{bt}(x) \int_{-1}^{x} G_2(t)\, dt$$

$$= \frac{m_o}{6E} \quad , \quad -1 < x < 1 \quad , \tag{52}$$

$$\gamma_{tb}(x) \int_{-1}^{x} G_1(t)\, dt + \gamma_{tt}(x) \int_{-1}^{x} G_2(t)\, dt - \frac{1}{2\pi} \int_{-1}^{1} \left[\frac{1}{y_1} + \frac{1}{y_2}\right] G_2(t)\, dt$$

$$= \frac{\sigma_o}{E} \quad , \quad -1 < x < 1 \quad , \tag{53}$$

where

$$y_1 = t - x \quad ,$$

$$y_2 = t + x + b' + c' \quad . \tag{54}$$

Integral equations (52) and (53) will again be solved by Gauss-Chebyshev closed form integration formula with the additional conditions

$$\int_{-1}^{1} G_1(t)\, dt = 0 \quad ,$$

$$\int_{-1}^{1} G_2(t)\, dt = 0 \quad ,$$

and the same backward procedure defined in Section 2.2 is used to find stress intensity factors at any point on the crack defined in

the region (b,c). Due to symmetry with respect to the x_2x_3 plane, stress intensity factors on the two cracks are also symmetric with respect to the same plane. Integral equations are valid for any two identical crack (edge, internal, two opposite) problem providing the corresponding γ functions defined in Section 2.2 .

2.7 Interaction of Three Identical Cracks

As stated earlier integral equations for general case given in (1) and (2) are valid for any number of cracks provided there is symmetry with respect to the x_2x_3 plane. This means that any three crack system composed of a symmetric crack surrounded by two identical cracks (not needed to be identical with the third one) can be solved by using (1) and (2). But in this study, for simplification purposes, all of them are chosen identical. Configuration and parameters are shown in Fig. 6. D is defined as (0,1), (b/a , c/a). Because of the nature of the problem, we expect that crack surface displacements and rotations be symmetric with respect to the x_2x_3 plane. This suggests that two outer cracks should have the same rotation and displacement at the equidistant points from the origin, while the third one undergoes completely different displacement and rotation. For this reason G functions

should be defined seperately for inner crack and two outer cracks. Let

G_{11} : Crack surface rotation derivative for the inner crack, (-a,a),

G_{12} : Crack opening displacement derivative for the inner crack, (-a,a),

G_{21} : Crack surface rotation derivative for the outer crack, (b,c),

G_{22} : Crack opening displacement derivative for the outer crack, (b,c).

Also $\sigma(x)$ and $m(x)$ for the inner and outer cracks should be defined seperately as follows,

$\sigma_1(x)$: $\sigma(x)$ for inner crack,

$m_1(x)$: $m(x)$ for inner crack,

$\sigma_2(x)$: $\sigma(x)$ for outer crack,

$m_2(x)$: $m(x)$ for outer crack.

(1) and (2) can be written for inner crack

$$\frac{\sigma_1(x')}{E} - \frac{1}{2\pi}\int_0^1 \left[\frac{1}{z-x'} + \frac{1}{z+x'}\right] G_{11}(z)\,dz - \frac{1}{2\pi}\int_b^c \left[\frac{1}{z-x'}\right.$$

$$+\frac{1}{z+x'}\Big]\,G_{12}(z)\,dz=\frac{\sigma_o}{E}\quad,\quad 0<x'<1\,,\qquad(55)$$

$$\frac{m_1(x')}{6E}-R_1\int_0^1\Big[R_2\Big[\frac{1}{z-x'}+\frac{1}{z+x'}\Big]-R_3\Big[\frac{1}{(z-x')^3}+\frac{1}{(z+x')^3}\Big]$$

$$+R_4\Big[\frac{1}{z-x'}K_2(p\,z-x')+\frac{1}{z+x'}K_2(p\,z+x')\Big]\Big]G_{12}(z)\,dz$$

$$-R_1\int_{b'}^{c'}\Big[R_2\Big[\frac{1}{z-x'}+\frac{1}{z+x'}\Big]-R_3\Big[\frac{1}{(z-x')^3}+\frac{1}{(z+x')^3}\Big]$$

$$+R_4\Big[\frac{1}{z-x'}K_2(p|z-x'|)+\frac{1}{z+x'}K_2(p|z+x'|)\Big]\Big]G_{22}(z)\,dz$$

$$=\frac{m_o}{6E}\quad,\quad 0<x'<1\,,\qquad(56)$$

and for outer crack

$$\frac{\sigma_2(x')}{E}-\frac{1}{2\pi}\int_0^1\Big[\frac{1}{z-x'}+\frac{1}{z+x'}\Big]G_{11}(z)\,dz-\frac{1}{2\pi}\int_{b'}^{c'}\Big[\frac{1}{z-x'}$$

$$+\frac{1}{z+x'}\Big]G_{12}(z)\,dz=\frac{\sigma_o}{E},\quad b'<x'<c'\,,\qquad(57)$$

$$\frac{m_2(x')}{6E} - R_1 \int_0^1 \left[R_2\left[\frac{1}{z-x'} + \frac{1}{z+x'}\right] - R_3\left[\frac{1}{(z-x')^3} + \frac{1}{(z+x')^3}\right] \right.$$

$$\left. + R_4\left[\frac{1}{z-x'} K_2(p|z-x'|) + \frac{1}{z+x'} K_2(p|z+x'|)\right] \right] G_{12}(z)\, dz$$

$$- R_1 \int_{b'}^{c'} \left[R_2\left[\frac{1}{z-x'} + \frac{1}{z+x'}\right] - R_3\left[\frac{1}{(z-x')^3} + \frac{1}{(z+x')^3}\right] \right.$$

$$\left. + R_4\left[\frac{1}{z-x'} K_2(p|z-x'|) + \frac{1}{z+x'} K_2(p|z+x'|)\right] \right] G_{22}(z)\, dz$$

$$= \frac{m_o}{6E} \quad , \quad b' < x' < c' \, , \tag{58}$$

where $x' = x/a$, $b' = b/a$, $c' = c/a$.

From (36), we may write

$$\int_0^1 \left[\frac{1}{z-x'} + \frac{1}{z+x'}\right] G_{11}(z)\, dz = \int_{-1}^1 \frac{1}{z-x'} G_{11}(z)\, dz \quad , \tag{59}$$

$$\int_0^1 \left[R_2\left[\frac{1}{z-x'} + \frac{1}{z+x'} - R_3\left[\frac{1}{(z-x')^3} + \frac{1}{(z+x')^3}\right] + R_4\left[\frac{1}{z-x'} K_2(p|z-x'|)\right.\right.\right.$$

$$+\frac{1}{z+x'}\,K_2(p|z+x'|)\Big]\Big]\,G_{12}(z)\,dz = \int_{-1}^{1}\Big[R_2\,\frac{1}{z-x'} - R_3\,\frac{1}{(z-x')^3}$$

$$+\,R_4\,\frac{1}{z-x'}\,K_2(p|z-x'|)\Big]\,G_{12}(z)\,dz \quad . \qquad (60)$$

Same expressions as (59) and (60) can also be written for G_{21} and G_{22}.

If we define

$$x' = x \quad \text{for} \quad -1 < x' < 1 \quad ,$$

$$z = t \quad \text{for} \quad -1 < z < 1 \quad ,$$

and use (49) and (51) for $b' < x' < c'$ and $b' < z < c'$ respectively, and substitute (27), (28) for $\sigma(x)$ and $m(x)$, (55), (56), (57), (58) will take the following final form.

$$\gamma_{bb}(x)\int_{-1}^{x} G_{21}(t)\,dt - R_1\int_{-1}^{1}\Big[R_2\Big[\frac{1}{y_1}+\frac{1}{y_2}\Big] - R_3\Big[\frac{1}{y_1^3}+\frac{1}{y_2^3}\Big]$$

$$+\,R_4\Big[\frac{1}{y_1}K_2(p|y_1|)+\frac{1}{y_2}K_2(p|y_2|)\Big]\Big]\,G_{21}(t)\,dt - R_1\int_{-1}^{1}\Big[R_2\,\frac{1}{y_3}$$

$$- R_3 \frac{1}{y_3^3} + R_4 \frac{1}{y_3} K_2(p|y_3|) \Big] G_{11}(t)\, dt + \gamma_{bt}(x) \int_{-1}^{x} G_{22}(t)\, dt$$

$$= \frac{m_o}{6E} \quad , \quad -1 < x < 1 \, , \tag{61}$$

$$\gamma_{tb}(x) \int_{-1}^{x} G_{21}(t)\, dt + \gamma_{tt}(x) \int_{-1}^{x} G_{22}(t)\, dt - \frac{1}{2\pi} \int_{-1}^{1} \Big[\frac{1}{y_1}$$

$$+ \frac{1}{y_2} \Big] G_{22}(t)\, dt - \frac{1}{2\pi} \int_{-1}^{1} \frac{1}{y_3} G_{12}(t)\, dt = \frac{\sigma_o}{E} \, , \quad -1 < x < 1, \tag{62}$$

$$\gamma_{bb}(x) \int_{-1}^{x} G_{11}(t)\, dt - R_1 \int_{-1}^{1} \Big[R_2 \Big[\frac{1}{y_4} + \frac{1}{y_5} \Big] - R_3 \Big[\frac{1}{y_4^3} + \frac{1}{y_5^3} \Big]$$

$$+ R_4 \Big[\frac{1}{y_4} K_2(p\, y_4) + \frac{1}{y_5} K_2(p\, y_5) \Big] \Big] G_{21}(t)\, dt - R_1 \int_{-1}^{1} \Big[R_2 \frac{1}{y_1}$$

$$- R_3 \frac{1}{y_1^3} + R_4 \frac{1}{y_1} K_2(p\, y_1) \Big] G_{11}(t)\, dt + \gamma_{bt}(x) \int_{-1}^{x} G_{12}(t)\, dt$$

$$= \frac{m_o}{6E} \quad , \quad -1 < x < 1 \, , \tag{63}$$

$$\gamma_{tb}(x) \int_{-1}^{x} G_{11}(t)\, dt + \gamma_{tt}(x) \int_{-1}^{x} G_{12}(t)\, dt - \frac{1}{2\pi} \int_{-1}^{1} \Big[\frac{1}{y_4}$$

$$+\frac{1}{y_5}\Big]\, G_{22}(t)\, dt - \frac{1}{2\pi}\int_{-1}^{1}\frac{1}{y_1}\, G_{12}(t)\, dt = \frac{\sigma_o}{E}\ , \quad -1 < x < 1\ , \quad (64)$$

where

$$y_1 = t-x \quad ,$$

$$y_2 = t+x+b'+c' \quad ,$$

$$y_3 = t-x - [(b'+c') / 2] \quad ,$$

$$y_4 = t+x + [(b'+c') / 2] \quad ,$$

$$y_5 = t-x + [(b'+c') / 2] \quad .$$

This problem has four integral equations, (61), (62), (63), (64), with four unknown functions, G_{11}, G_{12}, G_{21}, G_{22}, which will be solved by Gauss-Chebyshev closed type integration formula under the following single-valuedness conditions.

$$\int_{-1}^{1} G_{11}(t)\, dt = 0 \quad ,$$

$$\int_{-1}^{1} G_{12}(t)\, dt = 0 \quad ,$$

$$\int_{-1}^{1} G_{21}(t)\, dt = 0 \quad ,$$

$$\int_{-1}^{1} G_{22}(t)\, dt = 0 \quad .$$

After solving for the unknown functions, the same backward procedure

defined in Section 2.2 will be used for each crack seperately in order to find stress intensity factors.

Provided the corresponding Ψ functions, equations (61), (62), (63), (64) can be applied to any type(edge, internal, collinear) of identical cracks. The only reason for considering identical cracks to demonstrate interaction of three cracks in this section is simplicity. Line-spring model can also be applied to any three crack system which has two outer identical cracks with another symmetric(with respect to the x_2x_3 plane) crack in the middle. In this case, Ψ functions and crack length will be defined seperately for both(outer ones and inner one) cracks. One should keep in mind that crack length is a parameter in the coefficients of (61), (62), (63), (64). Attention must be paid to redifine the coefficients in such case.

3. RESULTS AND DISCUSSION

There are two main objectives in this study:

1. Assess the accuracy of line spring model,
2. Provide extensive numerical results which may be useful in application.

Due to unavailability of the solutions for the cases that we are interested in, the first objective can only be reached for the central (d/h=0) elliptic internal crack under pure tension. Extensive results for central, eccentric internal cracks and two opposite edge cracks as well as the interaction among two and three cracks are tabulated. In all cases it was assumed that $\nu=0.3$. However, the effect of ν on the stress intensity factors does not seem to be significant.

First step for the application of line spring model is to represent the SIFs as a polynomial in L/h. For this purpose, extensive information about plane strain (a/L_o) stress intensity factors are needed. These results are obtained from previous materials for internal cracks, from [18] for two opposite edge cracks and are tabulated in Tables 1,3,5,7,9,11,13,15. Corresponding coefficients of shape functions are tabulated in Tables 2,4,6,8,10,12,14,16. Coefficients of shape functions for the edge crack case are directly taken from [1] and tabulated in Table 17.

As noted before, for the application of the line spring model, the contour of the part-through crack can be any reasonable curve. Elliptic cracks are studied here since it is believed that ellipse is the closest contour for the actual shape of the crack which may be encountered in practical applications. Thus, crack length for any cross section is defined by,

$$L(x_1) = L_o\sqrt{1 - (x_1/a)^2} = L_o\sqrt{1 - x^2}$$

L_o being the total crack length at the midsection (x=0) . Note that the limiting values of the SIF are

$$K \to 0 \quad \text{for} \quad a/h \to 0 \quad ; \quad K \to K_\infty \quad \text{for} \quad a/h \to \infty$$

The first case that is studied is the central internal elliptic crack (d/h=0). Extensive results and formulas developed from a finite element method for this case are given in [19]. Table 18 and Figs. 19,20 show the comparision of the SIFs obtained from this study with those generated from the formulas given in [19]. SIFs obtained from [19] are represented as K^r while the normalizing SIF is $K_o = \sigma_o\sqrt{\pi L_o/2}$ where $\sigma_o = N_{22}^{\infty}/h$. Both values and the percent differences between them are given for various parameters at x=0 and x=1/2 . As expected, the SIFs $K(L_o)$ for the elliptic crack are

consistently smaller than the plane strain values. The table shows that with the exception of relatively small values of a/L_o at small L_o/h (for which the line spring is really not a suitable model) the agreement is surprisingly good. From the results, one may conclude that line spring can be used with some confidence for any central internal elliptic crack which has an a/L_o ratio larger than 2.

SIFs for the same geometry, but under pure bending are given in Table 20 (Fig. 21). This time, normalizing SIF is defined as $K_o = m_o(\pi L_o/2)^{1/2}$ where $m_o = 6M_{22}^{\infty}/h$. The results given are for the tension side. On the compression side the stress intensity factors have the same values with a negative sign. Under pure bending, since the crack faces on the compression side of the plate would close, the results given in the table cannot be used seperately. The results are, of course, useful and valid if the plate is subjected to tension, as well as bending, in such a way that the superimposed SIF is positive everywhere.

From Table 20, by excluding the case of a/L_o=0.5 which proved to be unreliable, it may be concluded that SIF are independent of a/L_o ratio for $L_o/h < 0.5$. For $L_o/h > 0.5$, SIF begins to increase with increasing L_o/h ratio, which is expected. Though we are unable to confirm the accuracy of the line spring model in this case, we could say that there is no unusual behaviour in the results. Results are asymptotically approaching to plane strain values as a/L_o is

increased except for large L_o/h values.

Another comparision with the previous finite element results [20] is shown in Table 19 (Fig. 23). It should be noted that in the results given in Table 19 a/L_o=1.25 is relatively small for the line spring model to be effective. Despite that, the relative error does not seem to be very high.

After symmetric internal cracks, nonsymmetrically located internal cracks are studied both under pure tension and pure bending conditions. Extensive results which scan almost all possible configurations are given in Tables 21-32 (Figs. 7-18). Normalizing SIFs are the same as that defined in the previous case for both tension and bending. Again we are unable to verify in which region the line spring results are reliable because of the lack of previous work done on this kind of problem. Asymptotic convergence to plane strain results is fairly good. A close observation of the tension results would show that for small a/L_o ratios SIFs first decrease, then increase with increasing L_o/h. This is mainly due to the fact that tabulated results are normalized with respect to $\sigma_o\sqrt{\pi L_o/2}$. Thus, even though the normalized SIF is decreasing, the real SIF may increase (which indeed happens in this case) but with a lower rate than the rate of increase of L_o . Also, again for small L_o/h and a/L_o values SIF on the inside part of the crack front turns out to be greater than that on the other part of the crack border which is

closer to the free surface.

Two opposite elliptic edge cracks have been studied only under pure tension. Normalizing stress intensity factor is again $\sigma_o (\pi L_o/2)^{1/2}$ with $\sigma_o = N_{22}^{\infty}/h$. Decreasing-increasing behaviour of the SIFs is again observed here. Same explanation which is given earlier is also valid for this case. Plane strain results are very close to each other in the region that we observe the slight decrease in SIFs. For this reason, a small uncertainity in the calculations can easily result with a slight decrease while we are expecting a slight increase. Except this behaviour, everything is as expected in Table 33 (Fig. 22).

Results for the interaction of two identical elliptic internal cracks under pure bending and pure tension have been tabulated in Tables 34 and 35 respectively. It can be seen that there is almost no interaction between two identical elliptic edge cracks if the distance between them (Fig.5) is larger than 8 times the half crack length, a. Another result which may be observed is that the interaction is more effective for the cracks having large L_o/h ratios.

SIFs for the two identical central internal elliptic cracks are tabulated in Table 36. Results are given only for tension case because it has been observed that there is no appreciable

interaction for the crack geometries given in Table 36 under pure bending. SIF deviates not more than 1% from the single crack value for b/a=0.1 in bending. It is seen that as the distance between the two cracks is increased the single crack solution is easily recovered. There is almost no interaction for $b/a \geq 0.1$ for the cracks $L_o/h < 0.5$. If $L_o/h > 0.5$, no interaction region can be defined for $b/a \geq 4$.

Interaction results for any two identical elliptic internal cracks are given in Table 37. Some erratic results are observed for small a/L_o ratios at small L_o/h ratios. Clearly, for these crack geometries line spring is not a suitable model.

As the last example, SIFs for the three identical internal elliptic cracks under pure tension are calculated and are given in Table 38. The only conclusion one may draw from these results is that the SIFs on the middle crack are slightly higher than the SIFs on the outer crack. But the difference is so small that they may be regarded as equal.

Table 1. Stress intensity factors for centrally cracked plate subjected to tension N or bending M under plane strain conditions.

L/h	$(K/K_o)_N$	$(K/K_o)_M$
0.05		0.0250
0.1	1.0060	0.0500
0.2	1.0246	0.1001
0.3	1.0577	0.1505
0.4	1.1094	0.2023
0.5	1.1867	0.2573
0.6	1.3033	0.3197
0.7	1.4884	0.3986
0.8	1.8169	0.5186
0.9	2.585	0.7776
0.95	4.252	1.1421

Table 2. The coefficients b_i and c_i for the shape functions g_t and g_b for symmetric internal (d/h=0) crack.

i	b_i	c_i
1	0.7070	0.0169
2	0.4325	-0.4629
3	-0.1091	15.0622
4	7.3711	-143.7384
5	-57.7894	807.2449
6	271.1551	-2844.8525
7	-744.4204	6468.9152
8	1183.9529	-9477.5512
9	-1001.4920	8638.7826
10	347.9786	-4455.2167
11		993.2482

Table 3. Stress intensity factors for the plate which has an internal crack with d/h=0.05 subjected to uniform tension N or bending M under plane strain conditions.

L/h	$(K_A/K_o)_N$	$(K_B/K_o)_N$	$(K_A/K_o)_M$	$(K_B/K_o)_M$
0.0001			0.1001	0.1000
0.09	1.0053	1.0050	0.1455	0.0555
0.18	1.0221	1.0200	0.1923	0.0120
0.27	1.0530	1.0452	0.2409	-0.0305
0.36	1.1021	1.0823	0.2925	-0.0722
0.45	1.1769	1.1340	0.3497	-0.1134
0.54	1.2909	1.2053	0.4175	-0.1547
0.63	1.4731	1.3053	0.5068	-0.1973
0.72	1.7983	1.4518	0.6467	-0.2430
0.81	2.5631	1.6887	0.9525	-0.2923
0.855	3.6610	1.8858	1.3814	-0.3125

Table 4. The coefficients of b_i and c_i for the shape functions g_t and g_b for internal crack with d/h=0.05.

i	b_{Ai}	b_{Bi}	c_{Ai}	c_{Bi}
1	0.7071	0.7071	0.0708	0.0707
2	0.4597	0.4347	-0.0623	-0.3701
3	0.7671	-0.0915	13.1229	0.5654
4	0.1552	2.6973	-166.4280	-6.6423
5	-9.3017	-14.1195	1145.8217	45.7189
6	97.3172	54.9653	-4762.0914	-189.9515
7	-413.9673	-135.3432	12511.5152	498.8463
8	936.4719	205.3051	-20927.0019	-834.5704
9	-1078.2322	-173.3480	21613.9362	862.1672
10	504.0555	62.8847	-12568.0268	-501.4354
11			3148.4879	125.5869

Table 5. Stress intensity factors for the plate which has an internal crack with d/h=0.10 subjected to uniform tension N or bending M under plane strain conditions.

L/h	$(K_A/K_o)_N$	$(K_B/K_o)_N$	$(K_A/K_o)_M$	$(K_B/K_o)_M$
0.0001			0.2001	0.2000
0.08	1.0050	1.0046	0.2410	0.1609
0.16	1.0212	1.0179	0.2843	0.1236
0.24	1.0513	1.0399	0.3308	0.0881
0.32	1.0998	1.0709	0.3821	0.0545
0.40	1.1743	1.1126	0.4410	0.0231
0.48	1.2887	1.1677	0.5136	-0.0059
0.56	1.4722	1.2418	0.6123	-0.0313
0.64	1.8002	1.3465	0.7701	-0.0504
0.72	2.5705	1.5167	1.1183	-0.0519
0.76	3.6693	1.6727	1.6050	-0.0280

Table 6. The coefficients of b_i and c_i for the shape functions g_t and g_b for internal crack with d/h=0.10.

i	b_{Ai}	b_{Bi}	c_{Ai}	c_{Bi}
1	0.7071	0.7072	0.1415	0.1414
2	0.5498	0.5043	-0.1734	-0.3871
3	1.5235	-0.5779	18.7434	1.2936
4	-2.2395	7.6480	-266.7713	-17.0715
5	-5.2844	-52.8793	2066.4692	132.0282
6	226.0267	257.2074	-9661.5218	-617.3023
7	-1423.2887	-799.7410	28556.2764	1826.3191
8	4348.1446	1530.8314	-53734.1216	-3441.9797
9	-6553.5540	-1634.0240	62435.9340	4007.6642
10	3959.2116	749.0673	-40844.2364	-2628.6642
11			11511.5912	743.3343

Table 7. Stress intensity factors for the plate which has an internal crack with d/h=0.15 subjected to uniform tension N or bending M under plane strain conditions.

L/h	$(K_A/K_o)_N$	$(K_B/K_o)_M$	$(K_A/K_o)_M$	$(K_B/K_o)_M$
0.0001			0.3001	0.3000
0.07	1.0049	1.0045	0.3365	0.2663
0.14	1.0208	1.0172	0.3763	0.2352
0.21	1.0506	1.0380	0.4206	0.2066
0.28	1.0988	1.0671	0.4714	0.1807
0.35	1.1729	1.1057	0.5319	0.1580
0.42	1.2868	1.1561	0.6089	0.1395
0.49	1.4693	1.2235	0.7164	0.1271
0.56	1.7938	1.3197	0.8909	0.1259
0.63	2.5476	1.4829	1.2760	0.1533
0.665	3.6065	1.6426	1.8090	0.2032

Table 8. The coefficients of b_i and c_i for the shape functions g_t and g_b for internal crack with d/h=0.15.

i	b_{Ai}	b_{Bi}	c_{Ai}	c_{Bi}
1	0.7071	0.7072	0.2122	0.2121
2	0.7028	0.6376	-0.2929	-0.4042
3	2.7653	-1.2331	26.3239	2.2494
4	-7.2036	19.0057	-427.2558	-33.6757
5	9.1384	-173.8407	3782.9591	297.4990
6	667.4954	1108.9410	-20214.1250	-1590.1109
7	-6105.7233	-4517.1019	68285.5344	5378.6049
8	25260.2847	11317.3469	-146859.5866	-11588.2217
9	-50586.0954	-15802.5485	195038.2341	15425.1699
10	40325.8388	9475.7480	-145833.6228	-11566.8288
11			46980.5243	3740.3538

Table 9. Stress intensity factors for the plate which has an internal crack with d/h=0.20 subjected to uniform tension N or bending M under plane strain conditions.

L/h	$(K_A/K_o)_N$	$(K_B/K_o)_N$	$(K_A/K_o)_M$	$(K_B/K_o)_M$
0.0001			0.4001	0.4000
0.06	1.0048	1.0044	0.4319	0.3718
0.12	1.0205	1.0170	0.4682	0.3468
0.18	1.0497	1.0374	0.5102	0.3252
0.24	1.0968	1.0660	0.5601	0.3070
0.30	1.1691	1.1034	0.6216	0.2930
0.36	1.2799	1.1535	0.7020	0.2844
0.42	1.4562	1.2202	0.8162	0.2839
0.48	1.7668	1.3161	1.0031	0.2981
0.54	2.4756	1.4806	1.4127	0.3482
0.57	3.4498	1.6422	1.9674	0.4165

Table 10. The coefficients of b_i and c_i for the shape functions g_t and g_b for internal crack with d/h=0.20.

i	b_{Ai}	b_{Bi}	c_{Ai}	c_{Bi}
1	0.7071	0.7072	0.2829	0.2828
2	0.9394	0.8534	-0.4105	-0.4192
3	5.0186	-2.2518	36.3675	3.4524
4	-19.6345	47.2610	-686.9924	-59.3848
5	76.1489	-589.3736	7097.1745	611.7194
6	2376.8770	5125.5432	-44245.1037	-3814.7743
7	-32402.0663	-28413.7181	174386.6733	15058.0019
8	187563.3073	96818.0664	-437594.1661	-37860.2290
9	-517758.7465	-183743.9141	678087.6506	58816.9514
10	566112.6482	149736.5141	-591607.7634	-51479.6217
11			222394.8277	19433.7456

Table 11. Stress intensity factors for the plate which has an internal crack with d/h=0.25 subjected to uniform tension N or bending M under plane strain conditions.

L/h	$(K_A/K_o)_N$	$(K_B/K_o)_N$	$(K_A/K_o)_M$	$(K_B/K_o)_M$
0.0001			0.5001	0.5000
0.05	1.0046	1.0042	0.5273	0.4771
0.10	1.0197	1.0165	0.5598	0.4583
0.15	1.0476	1.0364	0.5991	0.4434
0.20	1.0925	1.0644	0.6473	0.4327
0.25	1.1610	1.1016	0.7084	0.4270
0.30	1.2652	1.1505	0.7900	0.4277
0.35	1.4295	1.2160	0.9074	0.4380
0.40	1.7151	1.3099	1.0996	0.4649
0.45	2.3529	1.4684	1.5149	0.5310
0.475	3.2077	1.6192	2.0658	0.6085

Table 12. The coefficients of b_i and c_i for the shape functions g_t and g_b for internal crack with d/h=0.25.

i	b_{Ai}	b_{Bi}	c_{Ai}	c_{Bi}
1	0.7071	0.7071	0.3536	0.3536
2	1.3041	1.1918	-0.5246	-0.4284
3	9.6510	-4.1793	50.2589	4.8592
4	-57.8163	129.7358	-1136.1027	-97.6558
5	450.7761	-2325.3551	14085.0245	1206.5210
6	10351.8621	29069.6053	-105370.0173	-9029.9162
7	-227973.9193	-231101.0011	498386.1475	42788.3389
8	1960136.6080	1128028.3541	-1500844.1305	-129153.3052
9	-7899243.5583	-3063223.0225	2791092.0497	240895.9775
10	12538854.7550	3568834.5097	-2922538.2779	-253169.5873
11			1318591.9416	114779.2965

Table 13. Stress intensity factors for the plate which has an internal crack with d/h=0.30 subjected to uniform tension N or bending M under plane strain conditions.

L/h	$(K_A/K_o)_N$	$(K_B/K_o)_N$	$(K_A/K_o)_M$	$(K_B/K_o)_M$
0.001			0.6001	0.6000
0.04	1.0043	1.0040	0.6226	0.5824
0.08	1.0183	1.0155	0.6510	0.5686
0.12	1.0442	1.0343	0.6867	0.5607
0.16	1.0855	1.0608	0.7320	0.5568
0.20	1.1481	1.0959	0.7909	0.5584
0.24	1.2425	1.1419	0.8708	0.5669
0.28	1.3898	1.2031	0.9866	0.5855
0.32	1.6423	1.2895	1.1755	0.6209
0.36	2.1937	1.4309	1.5773	0.6939
0.38	2.9157	1.5591	2.0992	0.7709

Table 14. The coefficients of b_i and c_i for the shape functions g_t and g_b for internal crack with d/h=0.30.

i	b_{Ai}	b_{Bi}	c_{Ai}	c_{Bi}
1	0.7071	0.7071	0.4244	0.4243
2	1.9027	1.7480	-0.6553	-0.4321
3	20.8636	-8.9087	72.3179	6.6403
4	-197.8895	440.7103	-2037.1553	-160.0429
5	2675.1513	-12390.9668	31569.7505	2468.7747
6	71601.3880	241718.2677	-295202.5115	-23090.8486
7	-2639273.5314	-2989605.6659	1745346.7908	136788.4159
8	35994016.1511	22618755.1306	-6570139.7052	-516213.4074
9	-227958779.2155	-94950523.9757	15273818.2302	1203928.2026
10	567162515.8604	170542044.2578	-19993047.6604	-1582260.0614
11			11276922.9053	897240.7983

Table 15. Stress intensity factors for the plate with collinear edge cracks subjected to uniform tension N under plane strain conditions.

L/h	$(K/K_o)_N$
0.0001	1.1221
0.1	1.1231
0.2	1.1254
0.3	1.1292
0.4	1.1370
0.5	1.1546
0.6	1.2117
0.7	1.3254
0.8	1.5393
0.9	2.0836

Table 16. The coefficients of b_i for the shape function g_t for collinear edge crack.

i	b_i
1	0.7934
2	0.0775
3	-0.7542
4	7.5825
5	-12.1712
6	-186.5011
7	1236.2858
8	-3043.6190
9	3350.3456
10	-1374.8426

Table 17. The coefficients of b_i and c_i for the shape functions g_t and g_b for edge crack.

i	b_i	c_i
1	1.1216	1.1202
2	6.5200	-1.8872
3	-12.3877	18.0143
4	89.0554	-87.3851
5	-188.6080	241.9124
6	207.3870	-319.9402
7	-32.0524	168.0105

Table 18. Comparison of the stress intensity factors K(x) calculated in this study at x=0 and x=1/2 ($x=x_1/a$) for an internal planar elliptic crack in a plate under uniform tension N with the corresponding values $K^r(x)$ given in Ref.[19] . $\%D=100(K^r-K)/K^r$.

L_o/h	a/L_o	x	$K(x)/K_o$	$K^r(x)/K_o$	%D
0.1	0.5	0	0.916	0.637	43.7
0.1	0.5	1/2	0.868	0.637	36.2
0.1	1.0	0	0.955	0.827	15.5
0.1	1.0	1/2	0.896	0.785	14.2
0.1	2.0	0	0.976	0.935	4.3
0.1	2.0	1/2	0.911	0.875	4.1
0.1	3.0	0	0.983	0.967	1.7
0.1	3.0	1/2	0.916	0.902	1.6
0.1	4.0	0	0.987	0.980	0.6
0.1	4.0	1/2	0.919	0.914	0.5
0.1	10.0	0	0.993	0.999	-0.6
0.1	10.0	1/2	0.923	0.930	-0.7
0.2	0.5	0	0.862	0.638	35.1
0.2	0.5	1/2	0.827	0.638	29.6
0.2	1.0	0	0.931	0.830	12.2
0.2	1.0	1/2	0.880	0.788	11.6
0.2	2.0	0	0.971	0.942	3.1
0.2	2.0	1/2	0.908	0.881	3.1
0.2	3.0	0	0.986	0.976	1.0
0.2	3.0	1/2	0.918	0.910	0.9
0.2	4.0	0	0.993	0.991	0.2
0.2	4.0	1/2	0.923	0.923	0.0
0.2	10.0	0	1.007	1.013	-0.6
0.2	10.0	1/2	0.933	0.942	-1.0

Table 18- Cont.

L_o/h	a/L_o	x	$K(x)/K_o$	$K^r(x)/K_o$	%D
0.3	0.5	0	0.824	0.641	28.6
0.3	0.5	1/2	0.796	0.640	24.4
0.3	1.0	0	0.920	0.837	9.9
0.3	1.0	1/2	0.871	0.794	9.8
0.3	2.0	0	0.979	0.957	2.3
0.3	2.0	1/2	0.914	0.893	2.3
0.3	3.0	0	1.001	0.996	0.5
0.3	3.0	1/2	0.930	0.927	0.3
0.3	4.0	0	1.012	1.014	-0.2
0.3	4.0	1/2	0.937	0.942	-0.5
0.3	10.0	0	1.034	1.041	-0.7
0.3	10.0	1/2	0.952	0.966	-1.5
0.4	0.5	0	0.798	0.645	23.6
0.4	0.5	1/2	0.775	0.644	20.3
0.4	1.0	0	0.920	0.851	8.1
0.4	1.0	1/2	0.871	0.804	8.3
0.4	2.0	0	1.000	0.984	1.6
0.4	2.0	1/2	0.929	0.915	1.6
0.4	3.0	0	1.030	1.031	-0.1
0.4	3.0	1/2	0.950	0.955	-0.4
0.4	4.0	0	1.047	1.054	-0.7
0.4	4.0	1/2	0.961	0.974	-1.3
0.4	10.0	0	1.078	1.091	-1.2
0.4	10.0	1/2	0.982	1.005	-2.3

Table 18- Cont.

L_o/h	a/L_o	x	$K(x)/K_o$	$K^r(x)/K_o$	%D
0.5	0.5	0	0.783	0.654	19.8
0.5	0.5	1/2	0.761	0.650	17.2
0.5	1.0	0	0.932	0.874	6.7
0.5	1.0	1/2	0.880	0.821	7.3
0.5	2.0	0	1.036	1.030	0.6
0.5	2.0	1/2	0.956	0.949	0.7
0.5	3.0	0	1.078	1.090	-1.1
0.5	3.0	1/2	0.984	0.998	-1.4
0.5	4.0	0	1.101	1.121	-1.8
0.5	4.0	1/2	0.998	1.023	-2.4
0.5	10.0	0	1.145	1.172	-2.4
0.5	10.0	1/2	1.025	1.063	-3.5
0.6	0.5	0	0.779	0.667	16.9
0.6	0.5	1/2	0.756	0.658	14.9
0.6	1.0	0	0.960	0.911	5.4
0.6	1.0	1/2	0.901	0.846	6.4
0.6	2.0	0	1.095	1.103	-0.8
0.6	2.0	1/2	0.997	0.999	-0.2
0.6	3.0	0	1.151	1.183	-2.7
0.6	3.0	1/2	1.033	1.061	-2.6
0.6	4.0	0	1.183	1.225	-3.5
0.6	4.0	1/2	1.052	1.092	-3.6
0.6	10.0	0	1.245	1.298	-4.0
0.6	10.0	1/2	1.088	1.143	-4.7

Table 18- Cont.

L_o/h	a/L_o	x	$K(x)/K_o$	$K^r(x)/K_o$	%D
0.7	0.5	0	0.788	0.687	14.7
0.7	0.5	1/2	0.760	0.671	13.3
0.7	1.0	0	1.009	0.968	4.3
0.7	1.0	1/2	0.935	0.882	6.0
0.7	2.0	0	1.187	1.213	-2.2
0.7	2.0	1/2	1.058	1.067	-0.8
0.7	3.0	0	1.266	1.322	-4.2
0.7	3.0	1/2	1.106	1.144	-3.3
0.7	4.0	0	1.310	1.381	-5.1
0.7	4.0	1/2	1.132	1.183	-4.4
0.7	10.0	0	1.403	1.483	-5.4
0.7	10.0	1/2	1.179	1.242	-5.1
0.8	0.5	0	0.818	0.717	14.1
0.8	0.5	1/2	0.777	0.686	12.9
0.8	1.0	0	1.096	1.051	4.3
0.8	1.0	1/2	0.991	0.930	6.6
0.8	2.0	0	1.341	1.372	-2.3
0.8	2.0	1/2	1.152	1.152	0.0
0.8	3.0	0	1.457	1.521	-4.3
0.8	3.0	1/2	1.218	1.245	-2.2
0.8	4.0	0	1.525	1.603	-4.9
0.8	4.0	1/2	1.253	1.290	-2.9
0.8	10.0	0	1.674	1.747	-4.2
0.8	10.0	1/2	1.318	1.349	-2.3

Table 18- Cont.

L_o/h	a/L_o	x	$K(x)/K_o$	$K^r(x)/K_o$	%D
0.9	0.5	0	0.905	0.759	19.3
0.9	0.5	1/2	0.813	0.709	14.7
0.9	1.0	0	1.284	1.167	10.0
0.9	1.0	1/2	1.086	0.987	10.1
0.9	2.0	0	1.661	1.594	4.2
0.9	2.0	1/2	1.310	1.246	5.1
0.9	3.0	0	1.858	1.799	3.3
0.9	3.0	1/2	1.405	1.347	4.2
0.9	4.0	0	1.981	1.912	3.6
0.9	4.0	1/2	1.456	1.392	4.6

Table 19. Comparison of the stress intensity factors $K(L_o)$ calculated in this study at the midsection of a symmetrically located internal(d/h=0) planar crack in a plate under uniform tension N with the corresponding results K^r given in [20]. $L_o/h=.75$, $a/L_o=1.25$, $x=x_1/a=\cos\theta$, $\%D=100(K-K^r)/K^r$.

θ	x	K^r/K_o	K/K_o	%D
90°	0	0.985	1.120	13.7
80°	0.174	0.971	1.103	13.6
70°	0.342	0.944	1.052	11.4
60°	0.500	0.898	0.973	8.4
45°	0.707	0.810	0.832	2.7
40°	0.766	0.770	0.742	-3.6

Table 20. Normalized stress intensity factors calculated at the midsection of a symmetrically located (d/h=0) internal planar elliptic crack in a plate under uniform bending M.

L_0/h \ $a/L_0 \rightarrow$	0.5	2.0	3.0	4.0	5.0	10.0	Plane Strain
0.1	.050	.050	.050	.050	.050	.050	.050
0.2	.099	.099	.099	.099	.099	.099	.100
0.3	.148	.149	.149	.149	.149	.149	.151
0.4	.195	.199	.199	.199	.200	.200	.202
0.5	.240	.250	.251	.252	.253	.254	.257
0.6	.285	.305	.308	.310	.311	.313	.320
0.7	.332	.369	.375	.379	.382	.387	.399
0.8	.387	.457	.470	.478	.483	.496	.519
0.9	.476	.619	.650	.670	.683	.717	.778

Table 21. Normalized stress intensity factors calculated at the midsection of an internal planar elliptic crack with d/h=.05 in a plate under uniform tension N.

K_A/K_o

L_o/h \ a/L_o →	0.5	1.0	2.0	3.0	4.0	7.0	10.0	Plane Strain
.05	0.954	0.975	0.987	0.990	0.992	0.995	0.996	1.002
.15	0.887	0.944	0.976	0.988	0.994	1.001	1.004	1.015
.25	0.838	0.926	0.979	0.998	1.008	1.022	1.028	1.045
.35	0.804	0.921	0.996	1.025	1.040	1.061	1.070	1.096
.45	0.782	0.931	1.032	1.073	1.095	1.126	1.139	1.177
.55	0.775	0.959	1.096	1.153	1.185	1.231	1.251	1.307
.65	0.786	1.018	1.204	1.288	1.336	1.407	1.439	1.529
.75	0.828	1.134	1.407	1.539	1.619	1.742	1.799	1.970
.85	0.994	1.479	1.987	2.268	2.452	2.761	2.921	3.481

K_B/K_o

L_o/h \ a/L_o →	0.5	1.0	2.0	3.0	4.0	7.0	10.0	Plane Strain
.05	0.955	0.976	0.987	0.991	0.993	0.995	0.996	1.002
.15	0.891	0.946	0.977	0.988	0.993	1.001	1.003	1.014
.25	0.847	0.929	0.978	0.996	1.006	1.018	1.023	1.039
.35	0.817	0.923	0.991	1.017	1.031	1.049	1.056	1.078
.45	0.798	0.928	1.017	1.051	1.070	1.095	1.105	1.134
.55	0.789	0.944	1.056	1.102	1.127	1.161	1.176	1.215
.65	0.788	0.972	1.115	1.176	1.210	1.257	1.277	1.333
.75	0.797	1.017	1.201	1.284	1.332	1.401	1.432	1.517
.85	0.822	1.088	1.334	1.455	1.529	1.643	1.697	1.859

Table 22. Normalized stress intensity factors calculated at the midsection of an internal planar elliptic crack with d/h=0.10 in a plate under uniform tension N.

K_A/K_o

L_o/h \ a/L_o →	0.5	1.0	2.0	3.0	4.0	7.0	10.0	Plane Strain
.05	0.950	0.974	0.986	0.990	0.992	0.995	0.996	1.002
.15	0.878	0.940	0.975	0.988	0.994	1.003	1.006	1.018
.25	0.825	0.921	0.980	1.002	1.013	1.029	1.036	1.056
.35	0.789	0.919	1.004	1.037	1.055	1.081	1.092	1.124
.45	0.770	0.937	1.056	1.105	1.132	1.172	1.189	1.240
.55	0.770	0.986	1.152	1.226	1.268	1.331	1.360	1.444
.65	0.805	1.093	1.342	1.462	1.534	1.646	1.699	1.860
.75	0.961	1.426	1.900	2.159	2.329	2.615	2.764	3.291

K_B/K_o

L_o/h \ a/L_o →	0.5	1.0	2.0	3.0	4.0	7.0	10.0	Plane Strain
.05	0.952	0.974	0.986	0.990	0.993	0.995	0.996	1.002
.15	0.886	0.943	0.976	0.988	0.993	1.001	1.005	1.016
.25	0.843	0.927	0.979	0.998	1.007	1.021	1.026	1.043
.35	0.815	0.923	0.993	1.020	1.034	1.054	1.062	1.085
.45	0.798	0.928	1.019	1.055	1.075	1.102	1.113	1.145
.55	0.789	0.944	1.059	1.107	1.133	1.171	1.187	1.231
.65	0.788	0.970	1.116	1.181	1.218	1.272	1.296	1.363
.75	0.795	1.010	1.203	1.297	1.355	1.445	1.488	1.625

Table 23. Normalized stress intensity factors calculated at the midsection of an internal planar elliptic crack with d/h=0.15 in a plate under uniform tension N.

K_A/K_o

L_o/h \ a/L_o→	0.5	1.0	2.0	3.0	4.0	7.0	10.0	Plane Strain
.05	0.944	0.971	0.985	0.989	0.992	0.995	0.996	1.002
.15	0.864	0.934	0.974	0.988	0.996	1.006	1.010	1.024
.25	0.808	0.916	0.984	1.009	1.022	1.041	1.049	1.076
.35	0.773	0.921	1.020	1.060	1.083	1.115	1.129	1.173
.45	0.761	0.956	1.101	1.164	1.200	1.254	1.279	1.354
.55	0.784	1.051	1.273	1.378	1.441	1.540	1.588	1.733
.65	0.926	1.362	1.789	2.021	2.172	2.427	2.560	3.033

K_B/K_o

L_o/h \ a/L_o→	0.5	1.0	2.0	3.0	4.0	7.0	10.0	Plane Strain
.05	0.964	0.972	0.985	0.990	0.992	0.995	0.996	1.002
.15	0.876	0.939	0.975	0.988	0.994	1.003	1.007	1.020
.25	0.833	0.923	0.979	1.000	1.012	1.027	1.033	1.054
.35	0.806	0.920	0.997	1.027	1.044	1.067	1.077	1.106
.45	0.791	0.929	1.028	1.070	1.093	1.126	1.141	1.182
.55	0.784	0.947	1.076	1.134	1.167	1.216	1.238	1.303
.65	0.783	0.976	1.152	1.239	1.293	1.379	1.422	1.561

Table 24. Normalized stress intensity factors calculated at the midsection of an internal planar elliptic crack with d/h=0.20 in a plate under uniform tension N.

K_A/K_o

L_o/h \ a/L_o→	0.5	1.0	2.0	3.0	4.0	7.0	10.0	Plane Strain
.05	0.964	0.967	0.983	0.989	0.991	0.995	0.996	1.003
.15	0.848	0.928	0.974	0.990	0.999	1.011	1.016	1.033
.25	0.790	0.914	0.992	1.022	1.039	1.062	1.073	1.107
.35	0.761	0.933	1.054	1.104	1.133	1.176	1.196	1.258
.45	0.770	1.019	1.202	1.289	1.342	1.424	1.463	1.587
.55	0.896	1.293	1.666	1.863	1.990	2.204	2.316	2.710

K_B/K_o

L_o/h \ a/L_o→	0.5	1.0	2.0	3.0	4.0	7.0	10.0	Plane Strain
.05	0.939	0.968	0.984	0.989	0.992	0.995	0.996	1.003
.15	0.863	0.933	0.974	0.988	0.996	1.006	1.011	1.026
.25	0.818	0.918	0.982	1.006	1.020	1.038	1.046	1.072
.35	0.793	0.918	1.007	1.043	1.063	1.092	1.105	1.144
.45	0.779	0.931	1.049	1.102	1.132	1.178	1.199	1.263
.55	0.770	0.955	1.121	1.204	1.256	1.340	1.382	1.524

Table 25. Normalized stress intensity factors calculated at the midsection of an internal planar elliptic crack with d/h=0.25 in a plate under uniform tension N.

K_A/K_o

L_o/h \ a/L_o →	0.5	1.0	2.0	3.0	4.0	7.0	10.0	Plane Strain
.05	0.927	0.962	0.981	0.988	0.991	0.995	0.997	1.005
.15	0.831	0.922	0.976	0.995	1.006	1.020	1.026	1.048
.25	0.776	0.919	1.013	1.051	1.071	1.101	1.115	1.161
.35	0.768	0.977	1.133	1.201	1.241	1.303	1.333	1.429
.45	0.876	1.228	1.540	1.698	1.798	1.964	2.051	2.353

K_B/K_o

L_o/h \ a/L_o →	0.5	1.0	2.0	3.0	4.0	7.0	10.0	Plane Strain
.05	0.930	0.964	0.982	0.988	0.991	0.995	0.997	1.004
.15	0.847	0.926	0.973	0.991	1.000	1.012	1.017	1.036
.25	0.801	0.913	0.989	1.018	1.034	1.057	1.068	1.102
.35	0.775	0.919	1.026	1.072	1.098	1.138	1.157	1.216
.45	0.758	0.938	1.095	1.172	1.220	1.297	1.336	1.468

Table 26. Normalized stress intensity factors calculated at the midsection of an internal planar elliptic crack with d/h=0.30 in a plate under uniform tension N.

K_A/K_o

L_o/h \ a/L_o→	0.5	1.0	2.0	3.0	4.0	7.0	10.0	Plane Strain
.05	0.917	0.958	0.980	0.987	0.991	0.996	0.998	1.007
.15	0.816	0.921	0.985	1.008	1.021	1.038	1.046	1.073
.25	0.780	0.951	1.070	1.119	1.146	1.187	1.207	1.273
.35	0.869	1.170	1.420	1.537	1.610	1.727	1.787	1.996

K_B/K_o

L_o/h \ a/L_o→	0.5	1.0	2.0	3.0	4.0	7.0	10.0	Plane Strain
.05	0.919	0.959	0.980	0.987	0.991	0.996	0.997	1.006
.15	0.829	0.920	0.976	0.997	1.008	1.023	1.030	1.053
.25	0.783	0.914	1.005	1.042	1.063	1.093	1.108	1.156
.35	0.753	0.927	1.071	1.138	1.178	1.243	1.276	1.387

Table 27. Normalized stress intensity factors calculated at the midsection of an internal planar elliptic crack with d/h=0.05 in a plate under uniform bending M.

K_A/K_o

L_o/h \ a/L_o →	1.0	2.0	3.0	4.0	7.0	10.0	Plane Strain
.05	0.118	0.119	0.120	0.120	0.120	0.120	0.121
.15	0.170	0.173	0.174	0.175	0.176	0.176	0.177
.25	0.217	0.222	0.224	0.225	0.227	0.228	0.230
.35	0.266	0.274	0.278	0.279	0.282	0.283	0.287
.45	0.316	0.329	0.335	0.338	0.342	0.344	0.350
.55	0.371	0.391	0.400	0.405	0.412	0.416	0.426
.65	0.436	0.469	0.484	0.493	0.506	0.513	0.532
.75	0.528	0.586	0.614	0.631	0.659	0.673	0.716
.85	0.753	0.889	0.963	1.013	1.099	1.144	1.313

K_B/K_o

L_o/h \ a/L_o →	1.0	2.0	3.0	4.0	7.0	10.0	Plane Strain
.05	0.073	0.074	0.074	0.074	0.074	0.075	0.075
.15	0.020	0.023	0.024	0.025	0.025	0.026	0.026
.25	-0.032	-0.027	-0.025	-0.024	-0.023	-0.022	-0.021
.35	-0.082	-0.075	-0.073	-0.072	-0.070	-0.069	-0.068
.45	-0.130	-0.123	-0.120	-0.118	-0.116	-0.115	-0.113
.55	-0.178	-0.170	-0.167	-0.165	-0.162	-0.161	-0.159
.65	-0.226	-0.219	-0.215	-0.213	-0.210	-0.209	-0.207
.75	-0.278	-0.272	-0.269	-0.267	-0.264	-0.262	-0.259
.85	-0.339	-0.338	-0.334	-0.331	-0.325	-0.322	-0.311

Table 28. Normalized stress intensity factors calculated at the midsection of an internal planar elliptic crack with d/h=0.10 in a plate under uniform bending M.

K_A/K_o

L_o/h \ a/L_o →	1.0	2.0	3.0	4.0	7.0	10.0	Plane Strain
.05	0.216	0.218	0.219	0.219	0.220	0.220	0.221
.15	0.263	0.270	0.273	0.274	0.276	0.276	0.279
.25	0.308	0.321	0.325	0.328	0.331	0.332	0.337
.35	0.357	0.376	0.383	0.387	0.393	0.395	0.403
.45	0.412	0.440	0.451	0.457	0.467	0.471	0.484
.55	0.477	0.520	0.538	0.549	0.566	0.574	0.598
.65	0.571	0.642	0.676	0.697	0.730	0.746	0.797
.75	0.804	0.959	1.045	1.101	1.199	1.251	1.441

K_B/K_o

L_o/h \ a/L_o →	1.0	2.0	3.0	4.0	7.0	10.0	Plane Strain
.05	0.170	0.172	0.173	0.173	0.174	0.174	0.175
.15	0.114	0.120	0.123	0.124	0.125	0.126	0.128
.25	0.061	0.071	0.075	0.077	0.080	0.081	0.084
.35	0.010	0.024	0.030	0.033	0.037	0.038	0.043
.45	-0.038	-0.020	-0.013	-0.009	-0.004	-0.001	0.005
.55	-0.084	-0.062	-0.053	-0.048	-0.040	-0.037	-0.028
.65	-0.128	-0.102	-0.089	-0.082	-0.071	-0.066	-0.052
.75	-0.171	-0.137	-0.117	-0.105	-0.083	-0.073	-0.037

Table 29. Normalized stress intensity factors calculated at the midsection of an internal planar elliptic crack with d/h=0.15 in a plate under uniform bending M.

K_A/K_o

L_o/h \ $a/L_o \rightarrow$	1.0	2.0	3.0	4.0	7.0	10.0	Plane Strain
.05	0.313	0.317	0.319	0.319	0.320	0.321	0.323
.15	0.355	0.367	0.371	0.373	0.376	0.378	0.382
.25	0.399	0.420	0.428	0.432	0.438	0.440	0.449
.35	0.450	0.482	0.495	0.502	0.512	0.517	0.532
.45	0.514	0.563	0.584	0.596	0.614	0.623	0.650
.55	0.610	0.689	0.727	0.750	0.786	0.804	0.860
.65	0.846	1.015	1.106	1.167	1.270	1.325	1.524

K_B/K_o

L_o/h \ $a/L_o \rightarrow$	1.0	2.0	3.0	4.0	7.0	10.0	Plane Strain
.05	0.266	0.270	0.272	0.273	0.273	0.274	0.275
.15	0.207	0.218	0.221	0.223	0.226	0.227	0.231
.25	0.152	0.169	0.176	0.179	0.184	0.186	0.191
.35	0.101	0.125	0.134	0.139	0.146	0.149	0.158
.45	0.055	0.085	0.098	0.105	0.116	0.120	0.133
.55	0.011	0.051	0.069	0.080	0.096	0.104	0.125
.65	-0.028	0.028	0.058	0.077	0.108	0.123	0.176

Table 30. Normalized stress intensity factors calculated at the midsection of an internal planar elliptic crack with d/h=0.20 in a plate under uniform bending M.

K_A/K_o

L_o/h \ $a/L_o \rightarrow$	1.0	2.0	3.0	4.0	7.0	10.0	Plane Strain
.05	0.410	0.417	0.419	0.420	0.421	0.422	0.425
.15	0.445	0.464	0.471	0.474	0.479	0.481	0.488
.25	0.490	0.522	0.534	0.541	0.551	0.555	0.569
.35	0.549	0.600	0.621	0.633	0.651	0.660	0.687
.45	0.642	0.725	0.764	0.787	0.823	0.841	0.897
.55	0.875	1.050	1.142	1.202	1.303	1.357	1.549

K_B/K_o

L_o/h \ $a/L_o \rightarrow$	1.0	2.0	3.0	4.0	7.0	10.0	Plane Strain
.05	0.362	0.368	0.370	0.372	0.373	0.373	0.376
.15	0.298	0.315	0.321	0.324	0.328	0.329	0.336
.25	0.242	0.268	0.278	0.283	0.291	0.294	0.304
.35	0.193	0.229	0.244	0.252	0.264	0.269	0.285
.45	0.148	0.197	0.219	0.232	0.252	0.261	0.289
.55	0.109	0.181	0.218	0.242	0.280	0.299	0.365

Table 31. Normalized stress intensity factors calculated at the midsection of an internal planar elliptic crack with d/h=0.25 in a plate under uniform bending M.

K_A/K_o

L_o/h \ $a/L_o \rightarrow$	1.0	2.0	3.0	4.0	7.0	10.0	Plane Strain
.05	0.506	0.516	0.519	0.520	0.523	0.523	0.527
.15	0.535	0.563	0.573	0.578	0.585	0.589	0.599
.25	0.585	0.633	0.652	0.662	0.677	0.685	0.708
.35	0.670	0.751	0.787	0.808	0.840	0.856	0.907
.45	0.895	1.066	1.152	1.206	1.298	1.346	1.515

K_B/K_o

L_o/h \ $a/L_o \rightarrow$	1.0	2.0	3.0	4.0	7.0	10.0	Plane Strain
.05	0.457	0.466	0.469	0.471	0.473	0.473	0.477
.15	0.388	0.412	0.421	0.425	0.431	0.434	0.443
.25	0.332	0.370	0.385	0.393	0.405	0.410	0.427
.35	0.285	0.340	0.363	0.377	0.398	0.407	0.438
.45	0.305	0.332	0.369	0.395	0.437	0.459	0.513

Table 32. Normalized stress intensity factors calculated at the midsection of an internal planar elliptic crack with d/h=0.30 in a plate under uniform bending M.

K_A/K_o

L_o/h \ a/L_o →	1.0	2.0	3.0	4.0	7.0	10.0	Plane Strain
.05	0.600	0.614	0.618	0.621	0.624	0.625	0.630
.15	0.627	0.666	0.680	0.688	0.698	0.703	0.720
.25	0.698	0.771	0.801	0.817	0.842	0.855	0.895
.35	0.910	1.067	1.141	1.187	1.261	1.300	1.432

K_B/K_o

L_o/h \ a/L_o →	1.0	2.0	3.0	4.0	7.0	10.0	Plane Strain
.05	0.550	0.563	0.567	0.570	0.572	0.574	0.579
.15	0.477	0.511	0.524	0.530	0.539	0.543	0.557
.25	0.423	0.479	0.501	0.514	0.533	0.542	0.570
.35	0.381	0.471	0.513	0.538	0.579	0.600	0.669

Table 33. Normalized stress intensity factors calculated at the midsection of two opposite planar elliptic edge cracks in a plate under uniform tension N.

L_o/h \ a/L_o →	1.0	2.0	3.0	4.0	10.0	100.0	Plane Strain
0.1	1.060	1.089	1.099	1.104	1.113	1.119	1.123
0.2	1.009	1.062	1.081	1.091	1.109	1.121	1.125
0.3	0.966	1.028	1.065	1.079	1.106	1.124	1.129
0.4	0.929	1.019	1.053	1.072	1.108	1.131	1.137
0.5	0.902	1.008	1.050	1.073	1.118	1.148	1.155
0.6	0.902	1.038	1.080	1.108	1.165	1.203	1.212
0.7	0.929	1.082	1.149	1.186	1.262	1.315	1.325
0.8	0.997	1.195	1.284	1.336	1.445	1.524	1.539

Table 34. Maximum normalized stress intensity factors for two planar elliptic edge cracks in a plate under pure tension N.

L_o/h	a/L_o	b/a → 0.1	1.0	4.0	20.0	Single Crack
0.1	2	0.996	0.986	0.982	0.981	0.981
0.1	4	1.072	1.065	1.062	1.062	1.062
0.1	10	1.127	1.122	1.121	1.120	1.120
0.2	2	0.979	0.959	0.951	0.949	0.949
0.2	4	1.107	1.090	1.084	1.082	1.082
0.2	10	1.221	1.210	1.207	1.206	1.206
0.3	2	1.007	0.975	0.963	0.961	0.961
0.3	4	1.189	1.160	1.151	1.149	1.149
0.3	10	1.382	1.364	1.359	1.358	1.358
0.4	2	1.051	1.006	0.991	0.989	0.989
0.4	4	1.299	1.255	1.243	1.240	1.240
0.4	10	1.600	1.571	1.563	1.562	1.562
0.5	2	1.106	1.048	1.032	1.030	1.030
0.5	4	1.430	1.370	1.354	1.352	1.352
0.5	10	1.879	1.836	1.824	1.822	1.821
0.6	2	1.230	1.096	1.080	1.077	1.077
0.6	4	1.568	1.491	1.472	1.469	1.469
0.6	10	2.208	2.141	2.124	2.121	2.121
0.7	2	1.370	1.120	1.100	1.097	1.097
0.7	4	1.694	1.575	1.553	1.550	1.550
0.7	10	2.532	2.434	2.409	2.405	2.405

Table 35. Maximum normalized stress intensity factors for two planar elliptic edge cracks in a plate under uniform bending M.

L_o/h	a/L_o	b/a → 0.1	1.0	4.0	20.0	Single Crack
0.1	2	0.874	0.864	0.861	0.860	0.860
0.1	4	0.943	0.936	0.934	0.933	0.933
0.1	10	0.992	0.988	0.987	0.986	0.986
0.2	2	0.766	0.728	0.719	0.718	0.718
0.2	4	0.847	0.830	0.825	0.824	0.824
0.2	10	0.940	0.930	0.927	0.927	0.927
0.3	2	0.751	0.665	0.651	0.650	0.650
0.3	4	0.803	0.755	0.745	0.744	0.744
0.3	10	0.915	0.900	0.896	0.896	0.895
0.4	2	0.792	0.677	0.659	0.658	0.656
0.4	4	0.801	0.726	0.713	0.711	0.711
0.4	10	0.923	0.902	0.896	0.895	0.895
0.5	2	0.826	0.684	0.663	0.661	0.659
0.5	4	0.834	0.719	0.703	0.701	0.700
0.5	10	0.950	0.910	0.902	0.901	0.901
0.6	2	0.855	0.686	0.662	0.660	0.659
0.6	4	0.909	0.743	0.724	0.722	0.721
0.6	10	0.995	0.925	0.912	0.910	0.910
0.7	2	0.874	0.683	0.658	0.655	0.654
0.7	4	0.989	0.784	0.761	0.759	0.757
0.7	10	1.064	0.956	0.939	0.937	0.936

Table 36. Normalized stress intensity factors calculated at the midsection of symmetrically located(d=0) two identical planar internal elliptic cracks in a plate under uniform tension N.

L_o/h	a/L_o	b/a → 0.1	1.0	4.0	20.0	Single Crack
0.1	2	0.977	0.976	0.976	0.976	0.967
0.1	4	0.987	0.987	0.987	0.986	0.987
0.1	10	0.994	0.993	0.993	0.993	0.993
0.2	2	0.975	0.972	0.971	0.971	0.971
0.2	4	0.995	0.994	0.993	0.993	0.993
0.2	10	1.008	1.007	1.007	1.007	1.007
0.3	2	0.980	0.980	0.979	0.979	0.979
0.3	4	1.015	1.013	1.012	1.012	1.012
0.3	10	1.035	1.034	1.034	1.034	1.034
0.4	2	1.007	1.002	1.000	1.000	1.000
0.4	4	1.051	1.048	1.047	1.047	1.047
0.4	10	1.080	1.078	1.078	1.078	1.078
0.5	2	1.046	1.039	1.037	1.036	1.036
0.5	4	1.106	1.102	1.101	1.101	1.101
0.5	10	1.147	1.145	1.145	1.145	1.145
0.6	2	1.108	1.098	1.095	1.095	1.095
0.6	4	1.190	1.185	1.183	1.183	1.183
0.6	10	1.248	1.246	1.245	1.245	1.245
0.7	2	1.205	1.192	1.188	1.187	1.187
0.7	4	1.321	1.313	1.311	1.310	1.310
0.7	10	1.407	1.404	1.403	1.403	1.403
0.8	2	1.367	1.348	1.342	1.341	1.341
0.8	4	1.541	1.529	1.526	1.525	1.525
0.8	10	1.681	1.676	1.674	1.674	1.674
0.9	2	1.703	1.672	1.662	1.661	1.661
0.9	4	2.007	1.988	1.982	1.981	1.981
0.9	10	2.285	2.275	2.272	2.272	

Table 37. Normalized stress intensity factors calculated at the midsection of two identical planar internal elliptic cracks in a plate under uniform tension N.

			K_A/K_o			
			b/a → 0.1	1.0	4.0	20.0
d	L_o/h	a/L_o				
0.1	0.1	2	0.957	0.821	0.981	0.979
0.1	0.1	4	1.002	0.994	0.992	0.991
0.1	0.1	10	1.000	0.999	0.999	0.999
0.1	0.2	2	1.027	0.986	0.977	0.976
0.1	0.2	4	1.005	1.002	1.001	1.001
0.1	0.2	10	1.018	1.018	1.018	1.018
0.1	0.3	2	1.012	0.995	0.990	0.989
0.1	0.3	4	1.034	1.032	1.031	1.031
0.1	0.3	10				
0.1	0.35	2	1.021	1.010	1.005	1.004
0.1	0.35	4	1.058	1.056	1.055	1.055
0.1	0.35	10				
0.2	0.1	2	0.947	0.783	0.979	0.976
0.2	0.1	4	1.006	0.995	0.992	0.992
0.2	0.1	10	1.003	1.002	1.002	1.002
0.2	0.2	2	1.052	0.993	0.981	0.979
0.2	0.2	4	1.020	1.016	1.014	1.014
0.2	0.2	10	1.039	1.038	1.038	1.038
0.2	0.25	2	1.056	1.003	0.994	0.992
0.2	0.25	4	1.044	1.040	1.040	1.039
0.2	0.25	10	1.073	1.073	1.073	1.073
0.3	0.1	2	0.933	0.760	0.980	0.975
0.3	0.1	4	1.018	1.003	0.999	0.998
0.3	0.1	10	1.014	1.013	1.013	1.013
0.3	0.15	2	0.814	0.985	0.988	0.985
0.3	0.15	4	1.033	1.024	1.022	1.021
0.3	0.15	10	1.047	1.046	1.046	1.046

Table 37- Cont.

K_B/K_o

d	L_o/h	a/L_o	b/a → 0.1	1.0	4.0	20.0
0.1	0.1	2	0.959	0.830	0.982	0.979
0.1	0.1	4	1.002	0.993	0.991	0.991
0.1	0.1	10	0.999	0.999	0.999	0.999
0.1	0.2	2	1.020	0.984	0.978	0.976
0.1	0.2	4	1.002	1.000	0.999	0.999
0.1	0.2	10	1.014	1.014	1.014	1.014
0.1	0.3	2	1.004	0.989	0.985	0.984
0.1	0.3	4	1.021	1.020	1.019	1.019
0.1	0.3	10				
0.1	0.35	2	1.006	0.997	0.993	0.993
0.1	0.35	4	1.036	1.035	1.034	1.034
0.1	0.35	10				
0.2	0.1	2	0.950	0.799	0.979	0.976
0.2	0.1	4	1.004	0.994	0.992	0.991
0.2	0.1	10	1.001	1.001	1.001	1.001
0.2	0.2	2	1.038	0.987	0.977	0.976
0.2	0.2	4	1.010	1.007	1.006	1.005
0.2	0.2	10	1.026	1.026	1.026	1.026
0.2	0.25	2	1.034	0.990	0.983	0.982
0.2	0.25	4	1.023	1.021	1.020	1.019
0.2	0.25	10	1.046	1.046	1.046	1.046
0.3	0.1	2	0.935	0.778	0.978	0.974
0.3	0.1	4	1.013	0.999	0.996	0.995
0.3	0.1	10	1.009	1.009	1.008	1.008
0.3	0.15	2	0.829	0.977	0.979	0.977
0.3	0.15	4	1.019	1.011	1.008	1.008
0.3	0.15	10	1.030	1.030	1.030	1.030

Table 38. Normalized stress intensity factors calculated at the midsection of three identical planar internal elliptic cracks in a plate under uniform tension N.

K_A/K_o for the middle crack

d	L_o/h	a/L_o	b/a → 0.1	1.0	4.0	20.0
0.1	0.1	2	0.983	0.981	0.979	0.979
0.1	0.1	4	0.994	0.992	0.992	0.991
0.1	0.2	2	0.985	0.980	0.977	0.976
0.1	0.2	4	1.007	1.004	1.002	1.001
0.1	0.3	2	1.006	0.997	0.991	0.989
0.1	0.3	4	1.040	1.035	1.032	1.031
0.2	0.1	2	0.981	0.978	0.976	0.975
0.2	0.1	4	0.995	0.994	0.992	0.992
0.2	0.2	2	0.993	0.986	0.981	0.979
0.2	0.2	4	1.023	1.018	1.015	1.014
0.3	0.1	2	0.983	0.979	0.976	0.975
0.3	0.1	4	1.003	1.001	0.999	0.998

K_B/K_o for the middle crack

0.1	0.1	2	0.984	0.981	0.980	0.979
0.1	0.1	4	0.993	0.992	0.991	0.991
0.1	0.2	2	0.984	0.980	0.977	0.976
0.1	0.2	4	1.003	1.001	0.999	0.999
0.1	0.3	2	0.997	0.990	0.986	0.984
0.1	0.3	4	1.026	1.022	1.020	1.019
0.2	0.1	2	0.981	0.978	0.977	0.976
0.2	0.1	4	0.994	0.993	0.992	0.991
0.2	0.2	2	0.987	0.981	0.977	0.976
0.2	0.2	4	1.012	1.009	1.006	1.005
0.3	0.1	2	0.981	0.977	0.975	0.974
0.3	0.1	4	0.999	0.997	0.996	0.995

Table 38-Cont.

K_A/K_o for outer crack

d	L_o/h	a/L_o	b/a → 0.1	1.0	4.0	20.0
0.1	0.1	2	0.982	0.980	0.979	0.979
0.1	0.1	4	0.993	0.992	0.991	0.991
0.1	0.2	2	0.982	0.978	0.976	0.976
0.1	0.2	4	1.005	1.003	1.002	1.001
0.1	0.3	2	0.999	0.994	0.991	0.989
0.1	0.3	4	1.037	1.034	1.032	1.031
0.2	0.1	2	0.979	0.977	0.976	0.975
0.2	0.1	4	0.994	0.993	0.992	0.992
0.2	0.2	2	0.988	0.983	0.980	0.979
0.2	0.2	4	1.019	1.016	1.014	1.014
0.3	0.1	2	0.980	0.978	0.976	0.975
0.3	0.1	4	1.001	1.000	0.999	0.998

K_B/K_o for outer crack

0.1	0.1	2	0.982	0.980	0.980	0.979
0.1	0.1	4	0.993	0.992	0.991	0.991
0.1	0.2	2	0.981	0.978	0.976	0.976
0.1	0.2	4	1.002	1.000	0.999	0.999
0.1	0.3	2	0.992	0.988	0.985	0.984
0.1	0.3	4	1.023	1.021	1.020	1.019
0.2	0.1	2	0.979	0.978	0.976	0.976
0.2	0.1	4	0.993	0.992	0.991	0.991
0.2	0.2	2	0.983	0.979	0.977	0.976
0.2	0.2	4	1.010	1.007	1.006	1.005
0.3	0.1	2	0.978	0.976	0.974	0.974
0.3	0.1	4	0.998	0.996	0.995	0.995

Table 39. Normalized stress intensity factors on the crack front for an internal elliptic crack with $d/h=0.20$, $L_o/h=0.45$, $a/L_o=4$.

x	$(K_A/K_o)_N$	$(K_B/K_o)_N$	$(K_B/K_o)_M$	$(K_B/K_o)_M$
0.99	0.426	0.411	0.186	0.151
0.90	0.723	0.707	0.357	0.218
0.80	0.865	0.831	0.454	0.229
0.70	0.974	0.916	0.531	0.233
0.60	1.065	0.980	0.595	0.233
0.50	1.143	1.028	0.649	0.233
0.40	1.211	1.068	0.697	0.233
0.30	1.266	1.096	0.735	0.233
0.20	1.307	1.116	0.763	0.233
0.10	1.333	1.128	0.781	0.233
0.00	1.342	1.132	0.787	0.232

Table 40. Normalized stress intensity factors on the crack front for an internal elliptic crack with $d/h=0.10$, $L_o/h=0.45$, $a/L_o=4$.

x	$(K_A/K_o)_N$	$(K_B/K_o)_N$	$(K_B/K_o)_M$	$(K_B/K_o)_M$
0.99	0.411	0.393	0.097	0.065
0.90	0.692	0.686	0.205	0.072
0.80	0.816	0.804	0.269	0.057
0.70	0.902	0.883	0.318	0.041
0.60	0.967	0.941	0.357	0.028
0.50	1.018	0.984	0.388	0.016
0.40	1.061	1.019	0.414	0.007
0.30	1.092	1.044	0.433	0.000
0.20	1.114	1.061	0.446	-0.005
0.10	1.128	1.072	0.455	-0.008
0.00	1.132	1.075	0.457	-0.009

Table 41. Normalized stress intensity factors on the crack front for an elliptic edge crack with $L_o/h=0.45$, $a/L_o=4$.

x	(K_N/K_o)	(K_M/K_o)
0.99	0.762	0.646
0.90	0.920	0.696
0.80	1.027	0.711
0.70	1.084	0.701
0.60	1.130	0.695
0.50	1.166	0.689
0.40	1.197	0.686
0.30	1.214	0.680
0.20	1.227	0.676
0.10	1.237	0.675
0.00	1.240	0.675

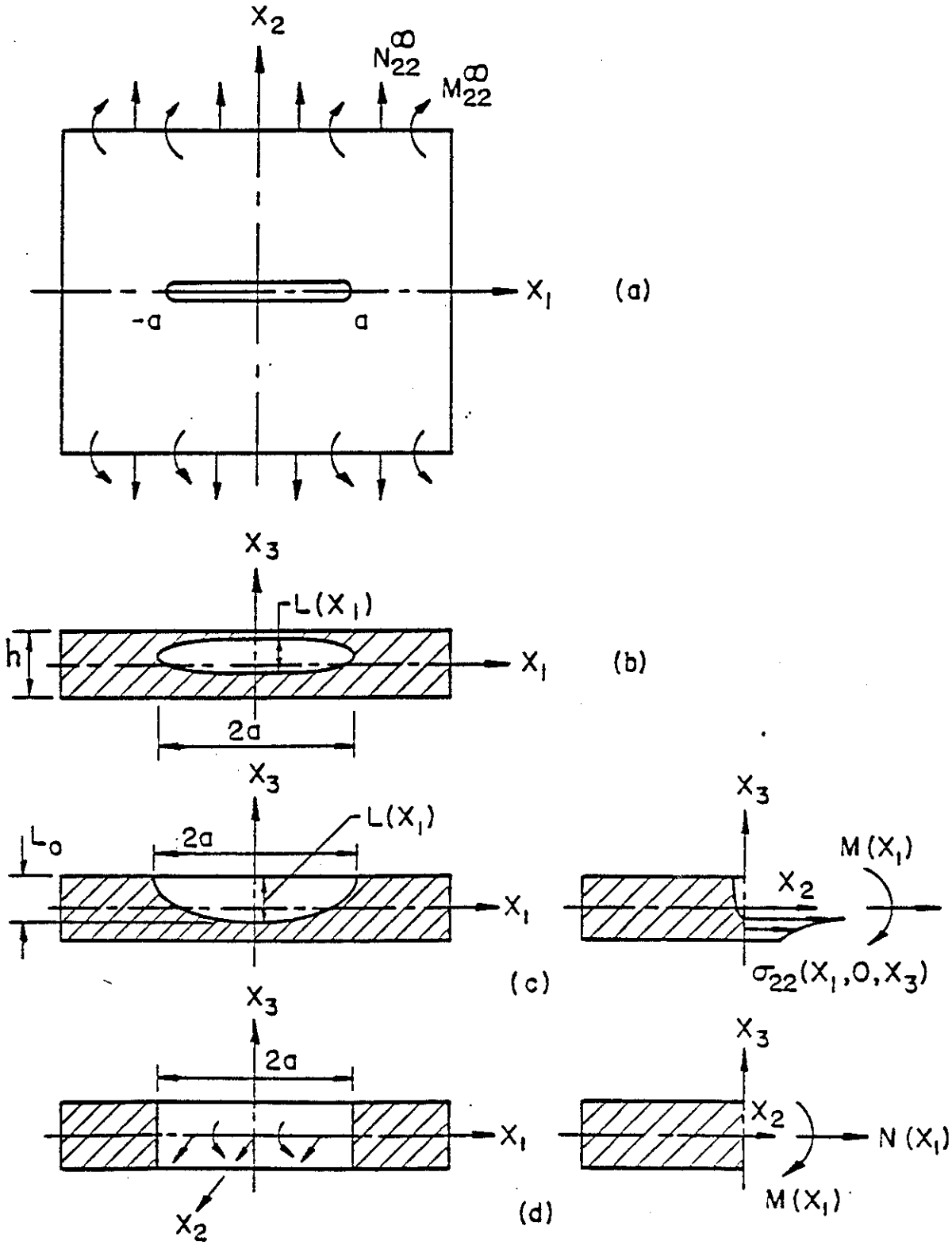

Figure 1. Notation for the part-through crack problem.

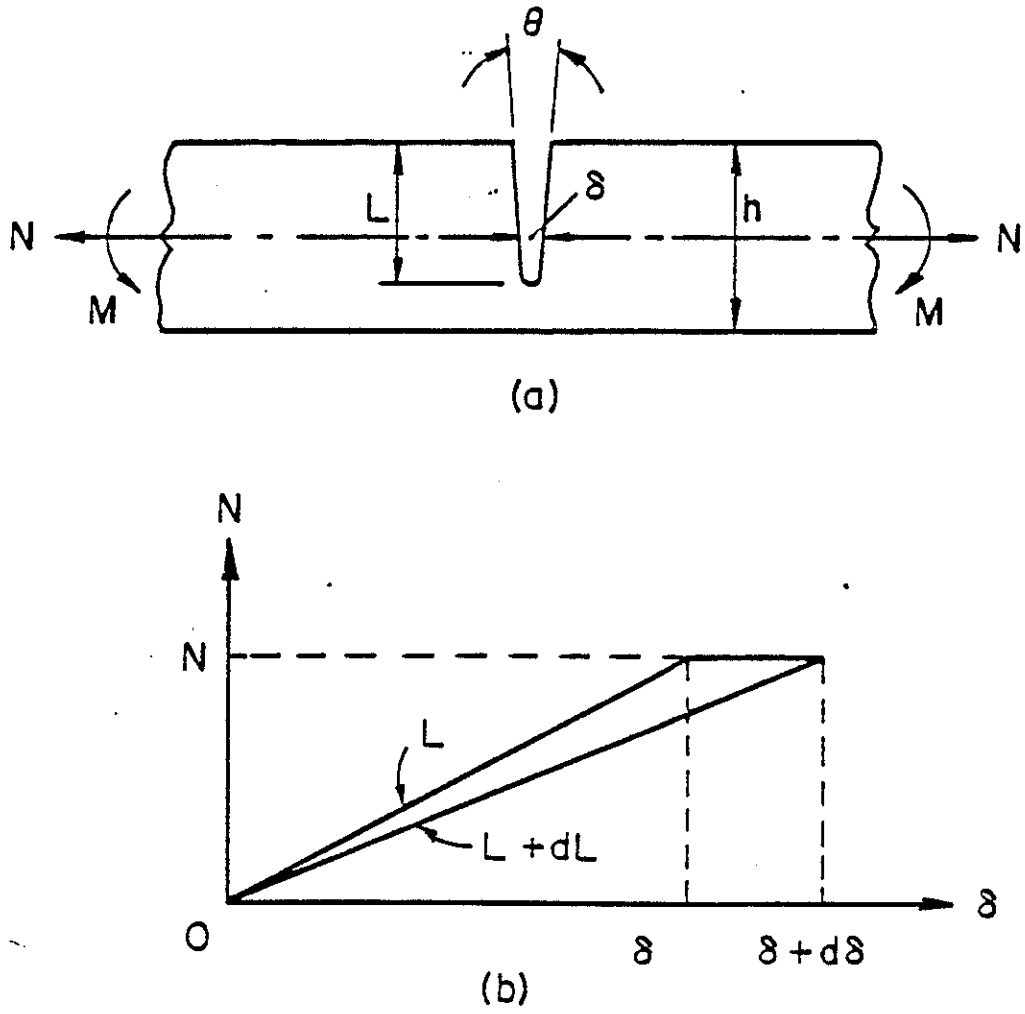

Figure 2. Notation for the related plane strain problem.

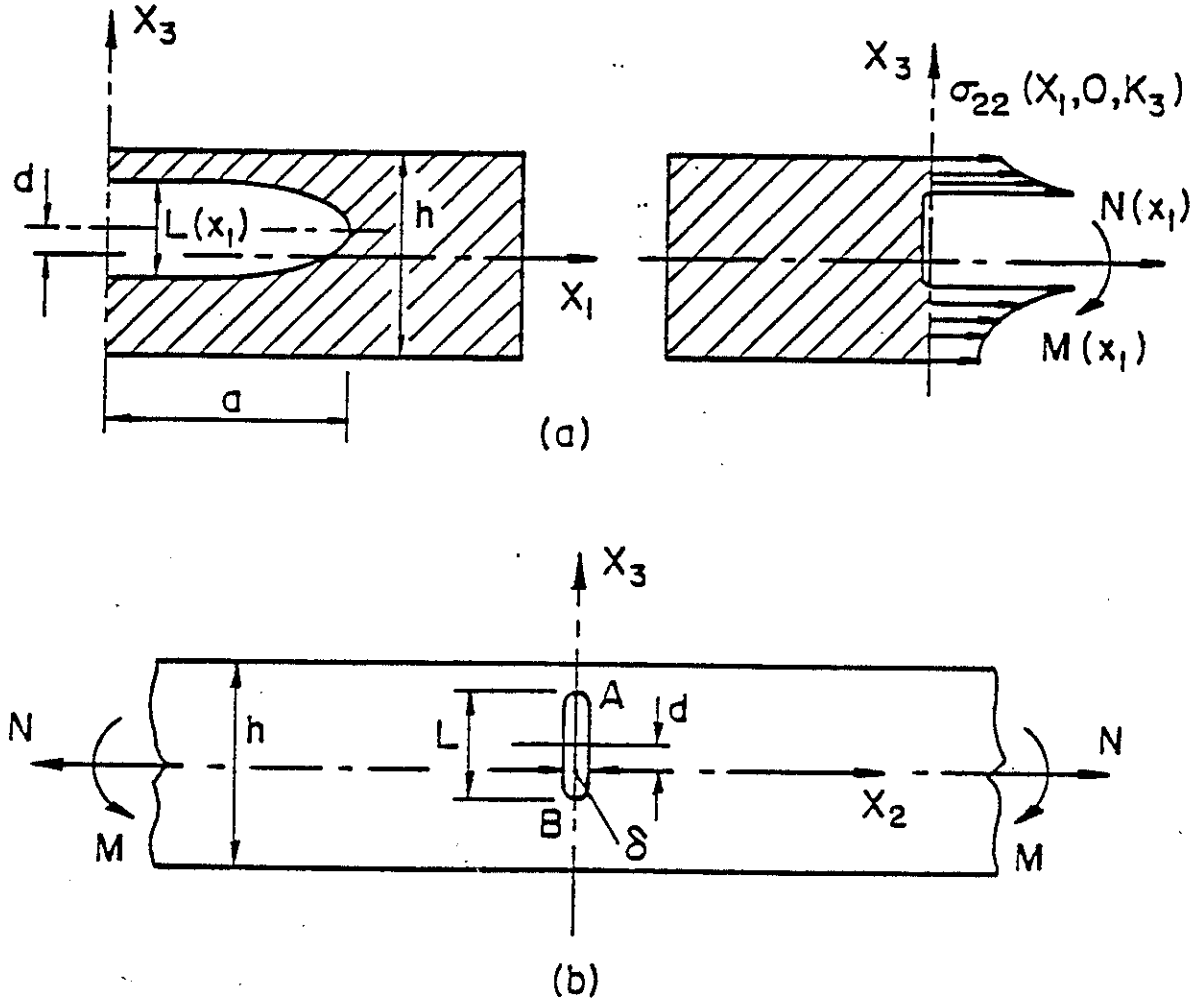

Figure 3. Geometry and notation for an internal crack.

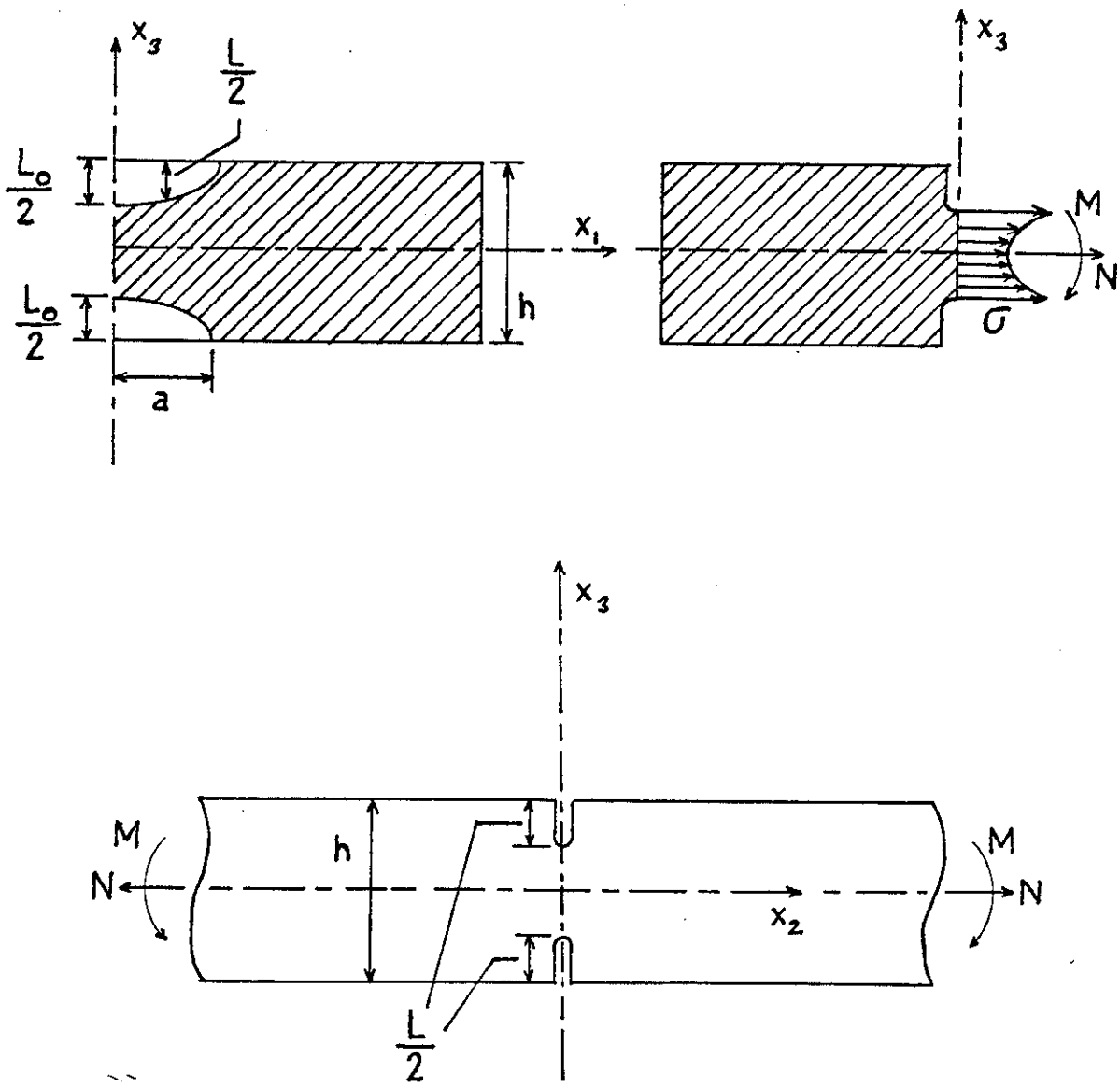

Figure 4. Geometry and notation for two opposite elliptic edge cracks.

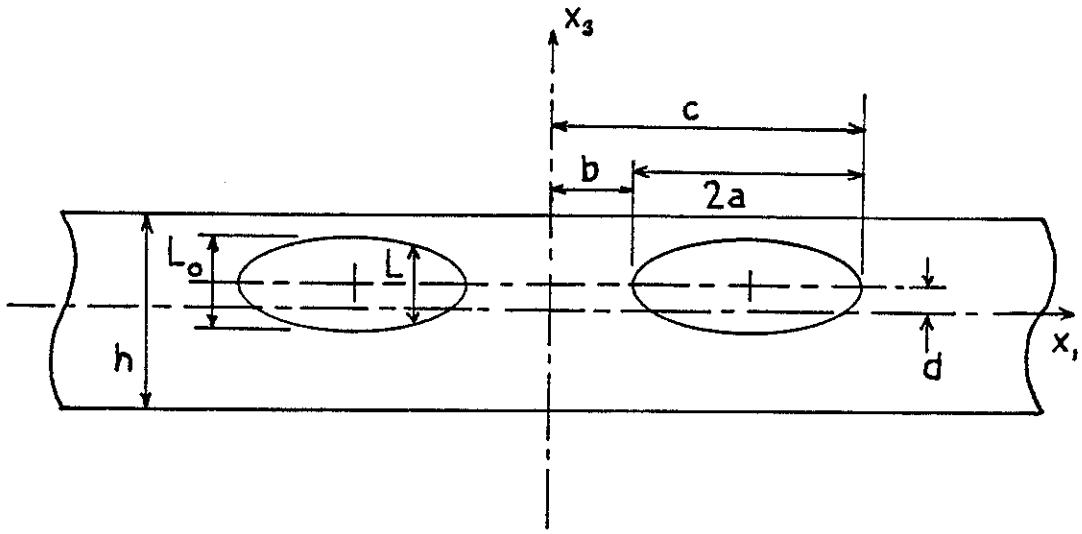

Figure 5. Geometry and notation for two identical cracks.

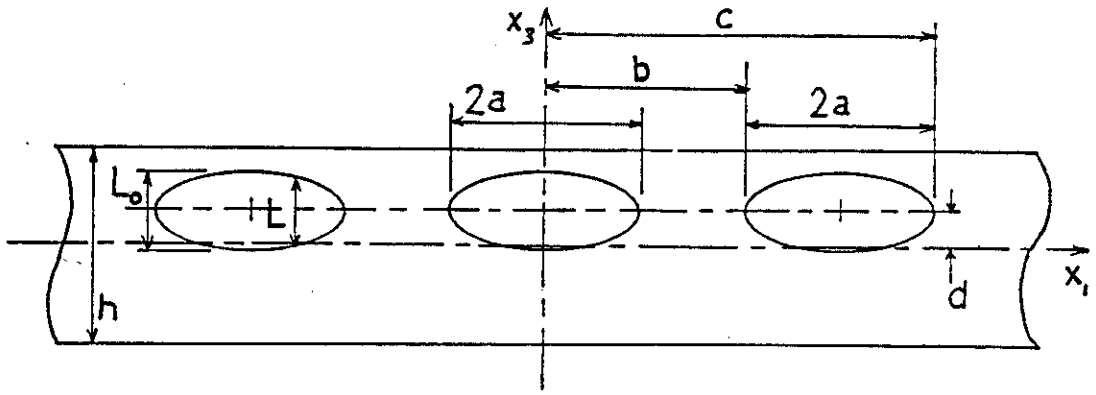

Figure 6. Geometry and notation for three identical cracks.

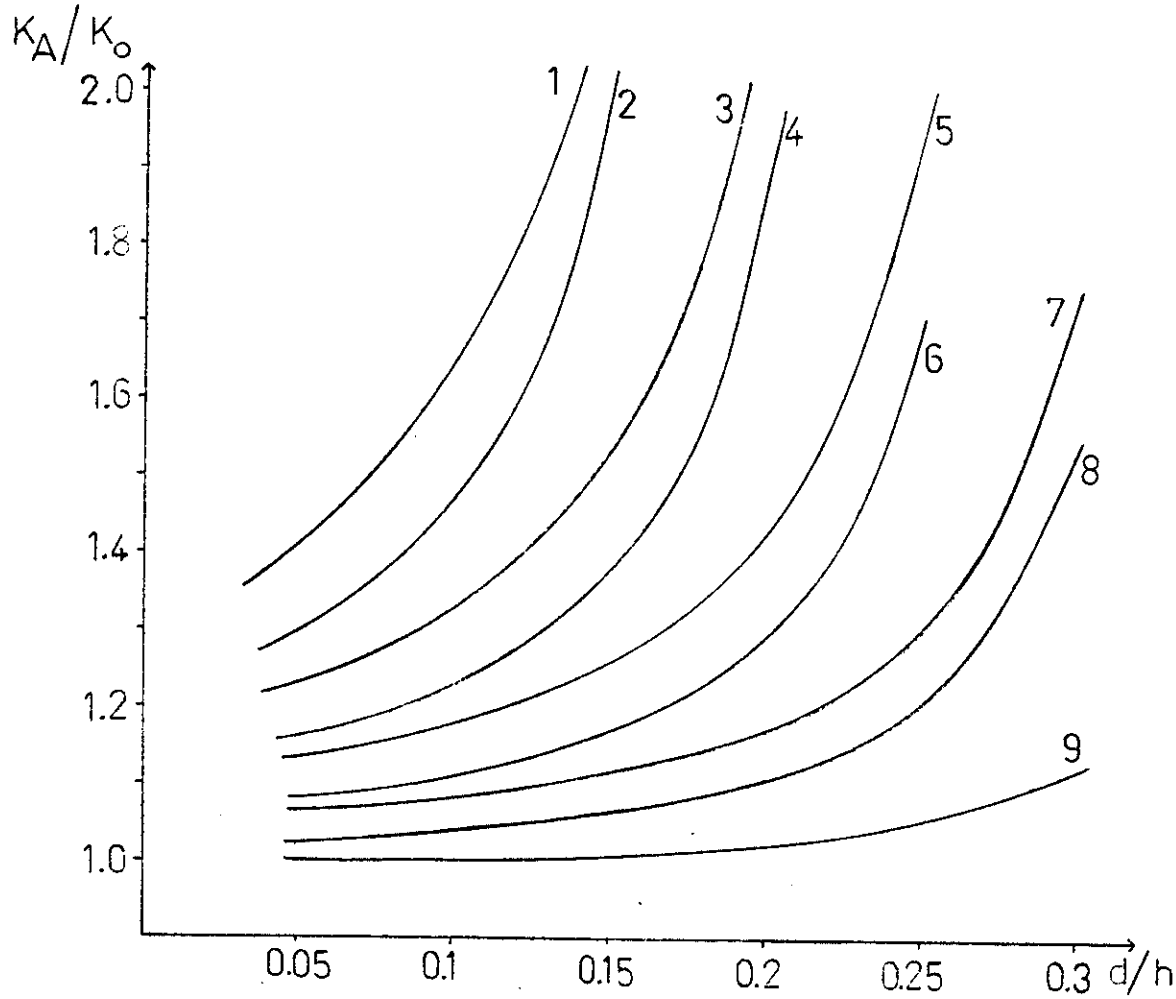

1: $L_o/h=0.65$, $a/L_o=7$,
2: $L_o/h=0.65$, $a/L_o=3$,
3: $L_o/h=0.55$, $a/L_o=7$,
4: $L_o/h=0.55$, $a/L_o=3$,
5: $L_o/h=0.45$, $a/L_o=7$,
6: $L_o/h=0.45$, $a/L_o=3$,
7: $L_o/h=0.35$, $a/L_o=7$,
8: $L_o/h=0.35$, $a/L_o=3$,
9: $L_o/h=0.25$, $a/L_o=3$.

Figure 7. Effect of d/h ratio on the normalized stress intensity factors calculated at the midsection of various internal elliptic cracks under pure tension.

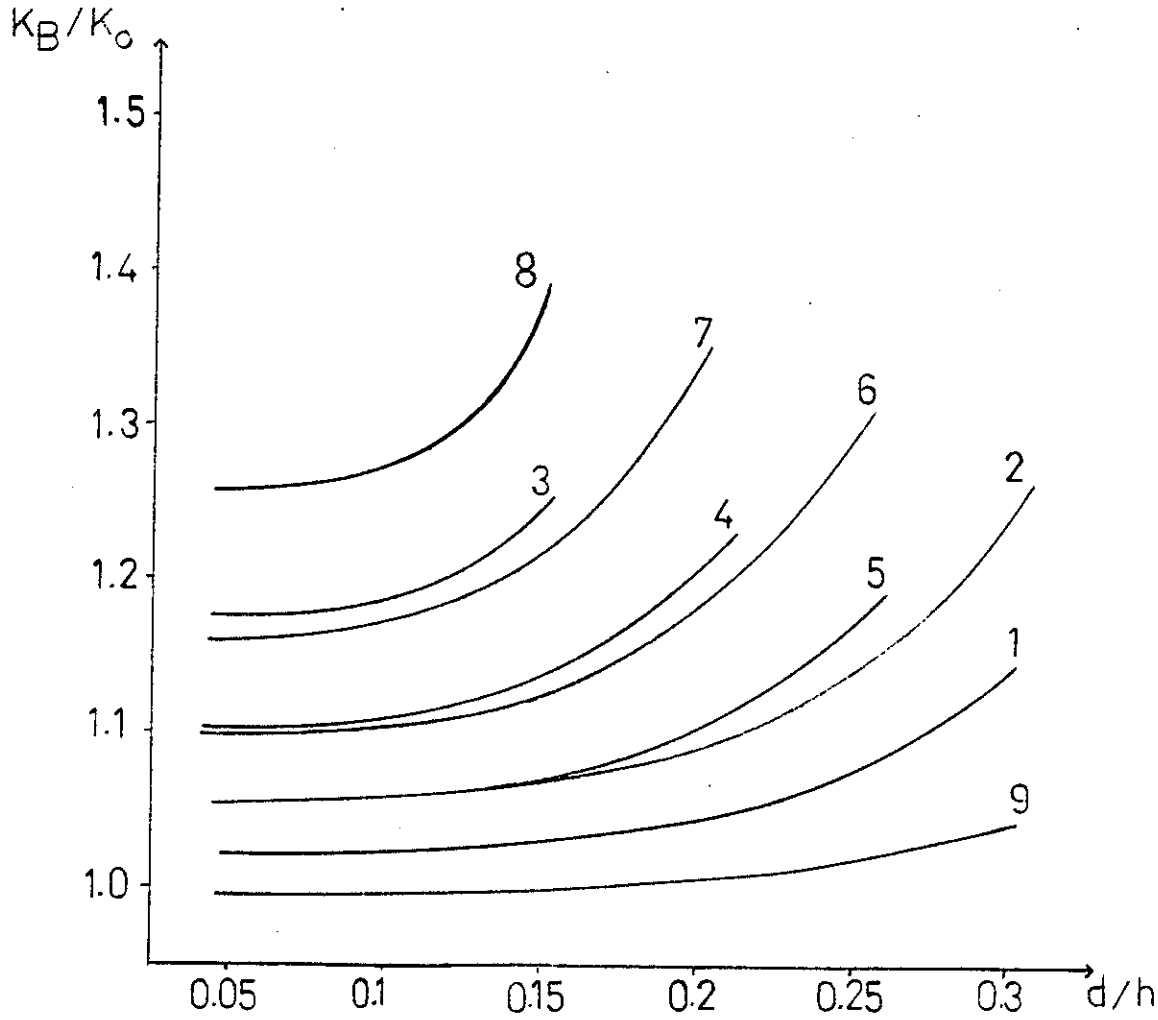

1: $L_o/h=0.35$, $a/L_o=3$,
2: $L_o/h=0.35$, $a/L_o=7$,
3: $L_o/h=0.65$, $a/L_o=3$,
4: $L_o/h=0.55$, $a/L_o=3$,
5: $L_o/h=0.45$, $a/L_o=3$,
6: $L_o/h=0.45$, $a/L_o=7$,
7: $L_o/h=0.55$, $a/L_o=7$,
8: $L_o/h=0.65$, $a/L_o=7$,
9: $L_o/h=0.25$, $a/L_o=3$.

Figure 8. Effect of d/h ratio on the normalized stress intensity factors calculated at the midsection of various internal elliptic cracks under pure tension.

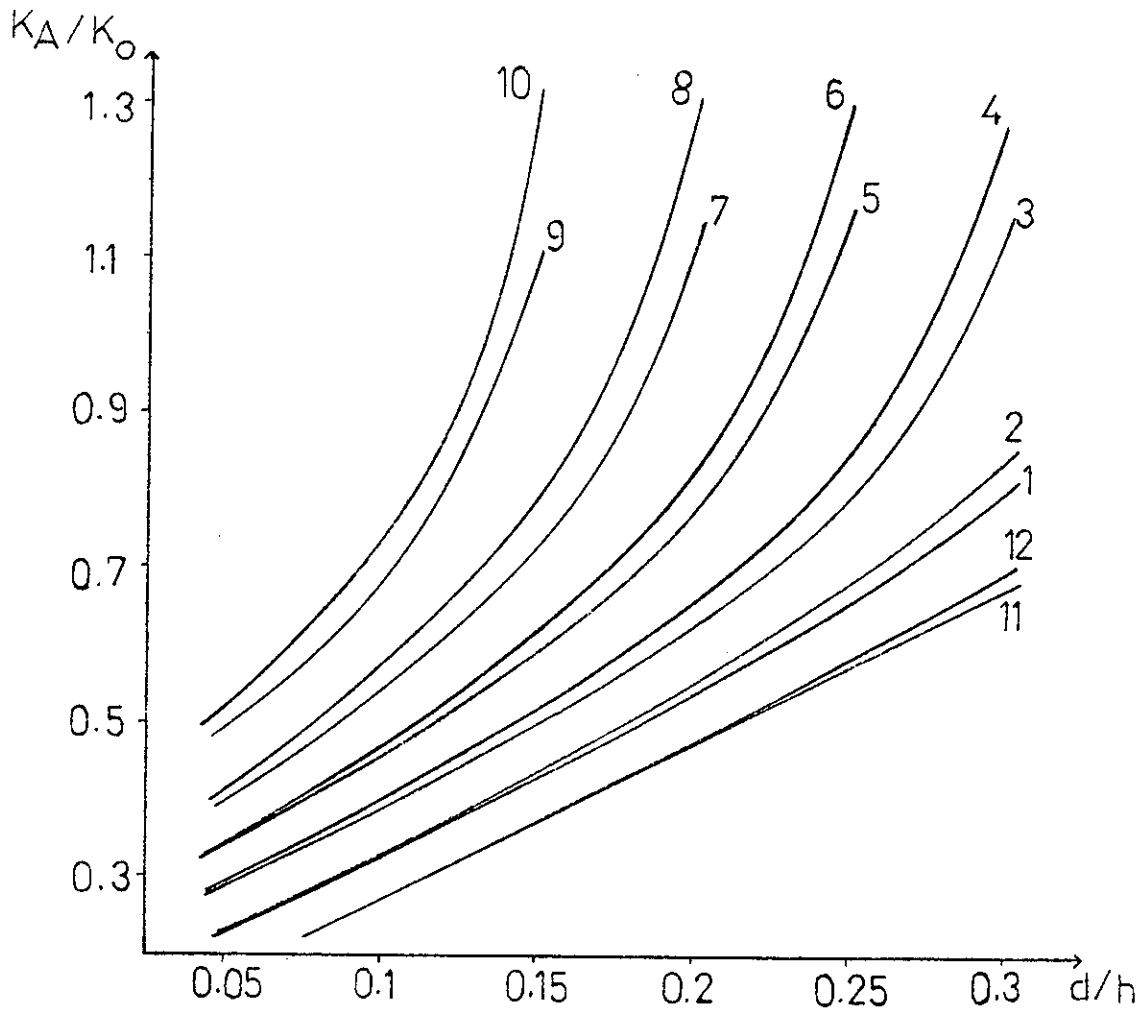

1: $L_o/h=0.25$, $a/L_o=3$,
2: $L_o/h=0.25$, $a/L_o=7$,
3: $L_o/h=0.35$, $a/L_o=3$,
4: $L_o/h=0.35$, $a/L_o=7$,
5: $L_o/h=0.45$, $a/L_o=3$,
6: $L_o/h=0.45$, $a/L_o=7$,
7: $L_o/h=0.55$, $a/L_o=3$,
8: $L_o/h=0.55$, $a/L_o=7$,
9: $L_o/h=0.65$, $a/L_o=3$,
10: $L_o/h=0.65$, $a/L_o=7$,
11: $L_o/h=0.15$, $a/L_o=3$,
12: $L_o/h=0.15$, $a/L_o=7$.

Figure 9. Effect of d/h ratio on the normalized stress intensity factors calculated at the midsection of various internal elliptic cracks under pure bending.

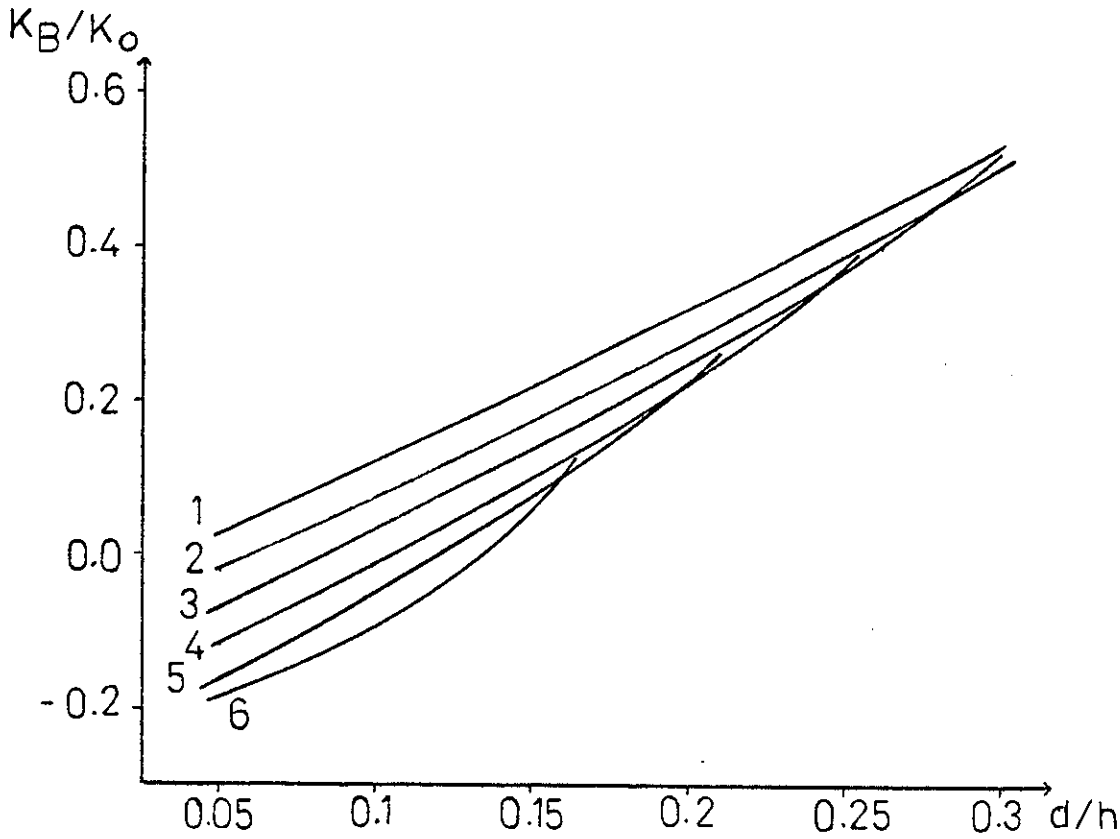

1: $L_o/h=0.15$, $a/L_o=3$,
2: $L_o/h=0.25$, $a/L_o=3$,
3: $L_o/h=0.35$, $a/L_o=3$,
4: $L_o/h=0.45$, $a/L_o=3$,
5: $L_o/h=0.55$, $a/L_o=3$,
6: $L_o/h=0.65$, $a/L_o=3$,

Figure 10. Effect of d/h ratio on the normalized stress intensity factors calculated at the midsection of various internal elliptic cracks under pure bending.

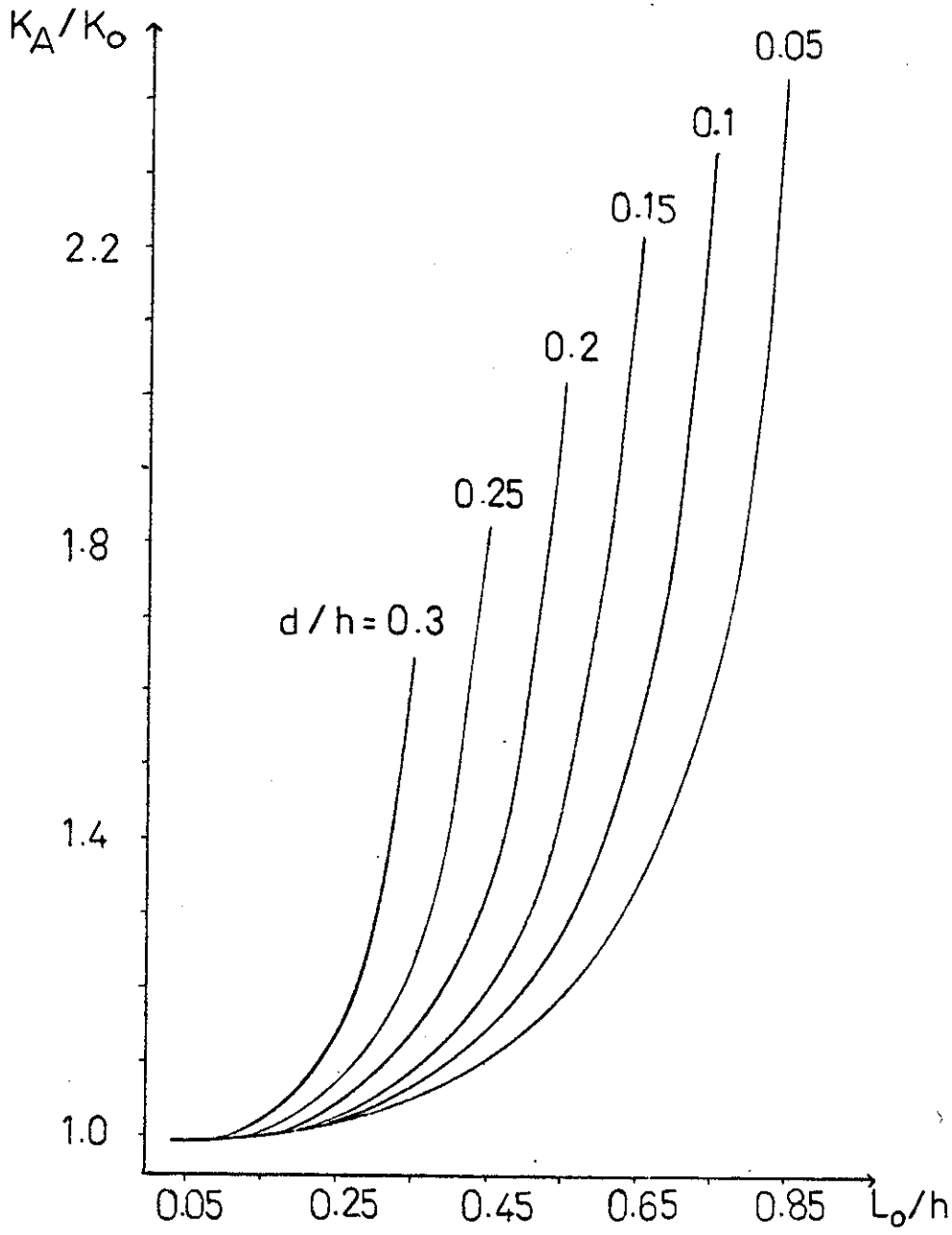

Figure 11. Effect of L_o/h ratio on the normalized stress intensity factors calculated at the midsection of internal elliptic cracks with $a/L_o=4$ and different d/h ratios under pure tension.

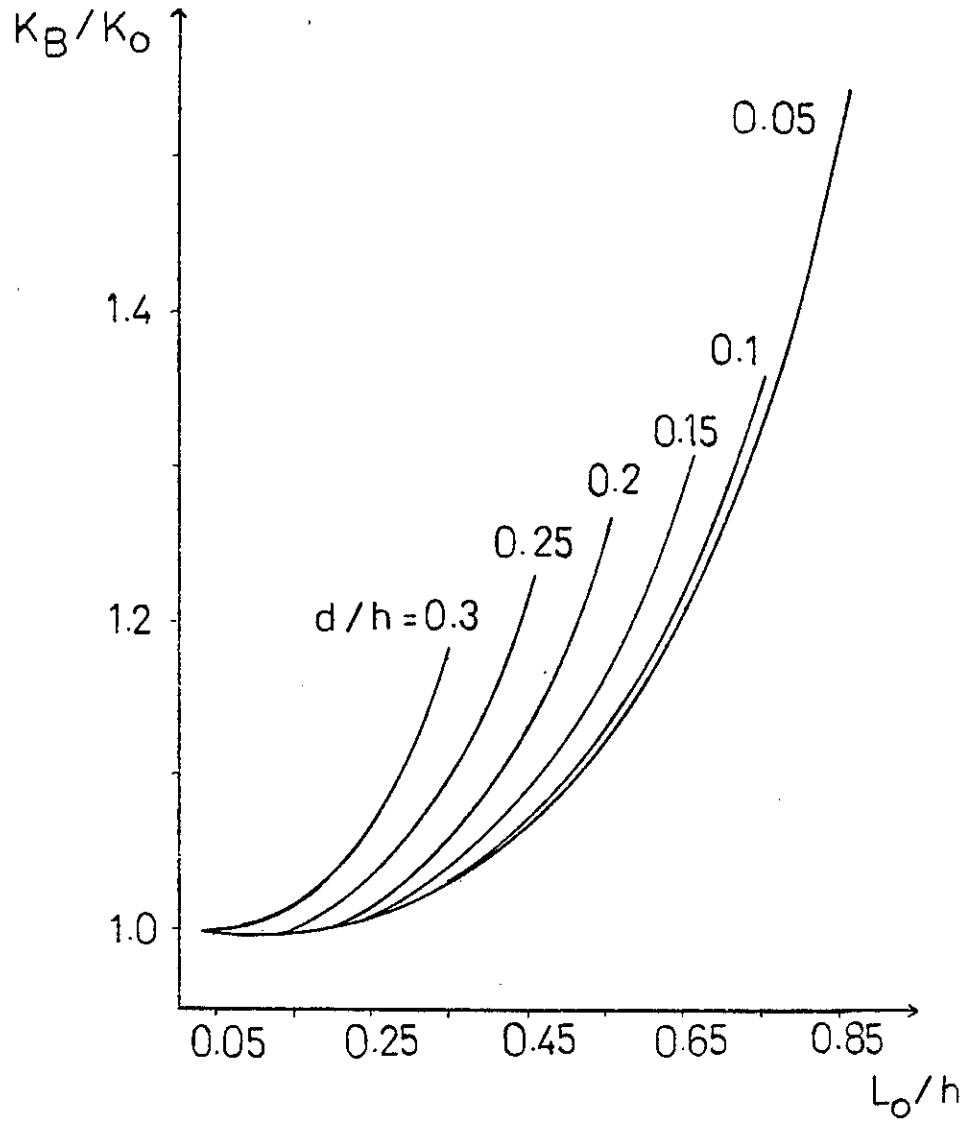

Figure 12. Effect of L_o/h ratio on the normalized stress intensity factors calculated at the midsection of internal elliptic cracks with $a/L_o=4$ and different d/h ratios under pure tension.

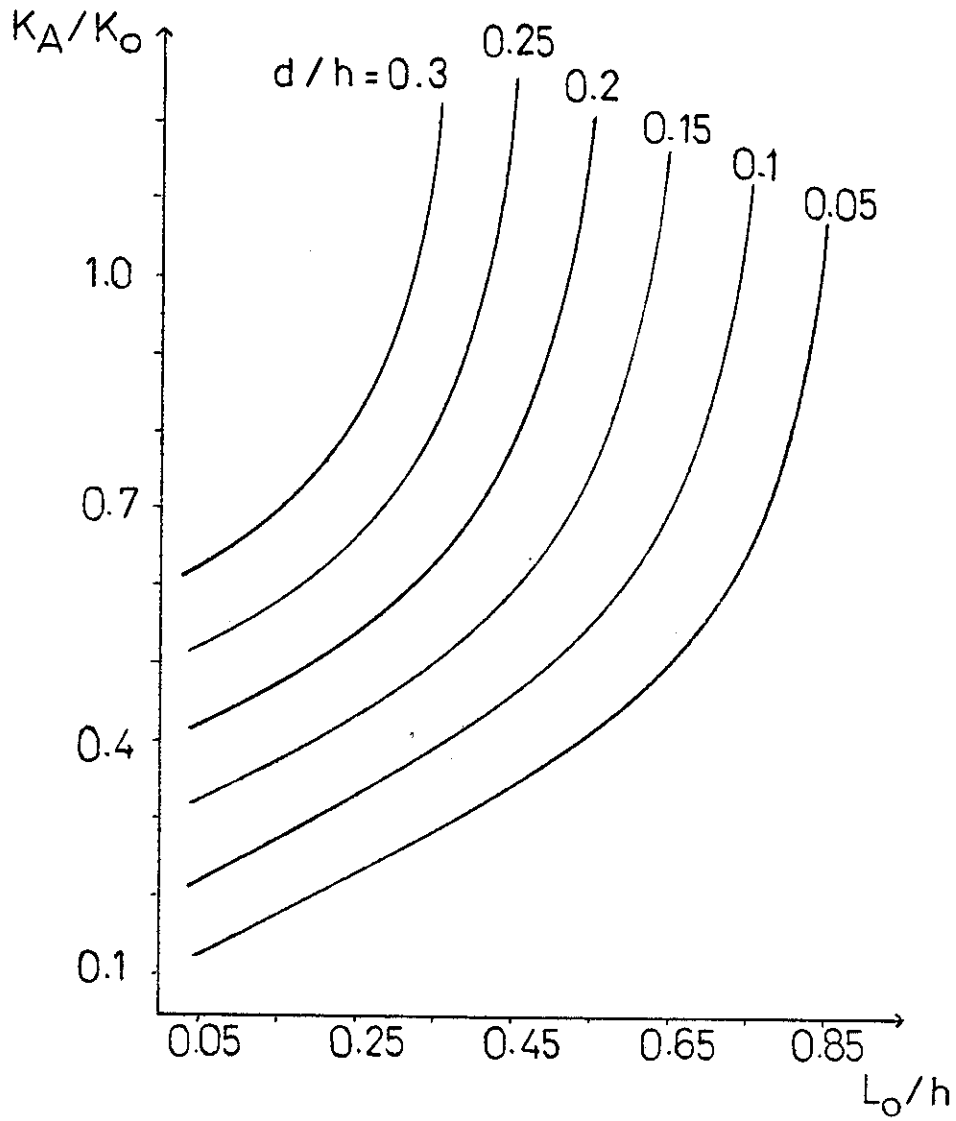

Figure 13. Effect of L_o/h ratio on the normalized stress intensity factors calculated at the midsection of internal elliptic cracks with $a/L_o=4$ and different d/h ratios under pure bending.

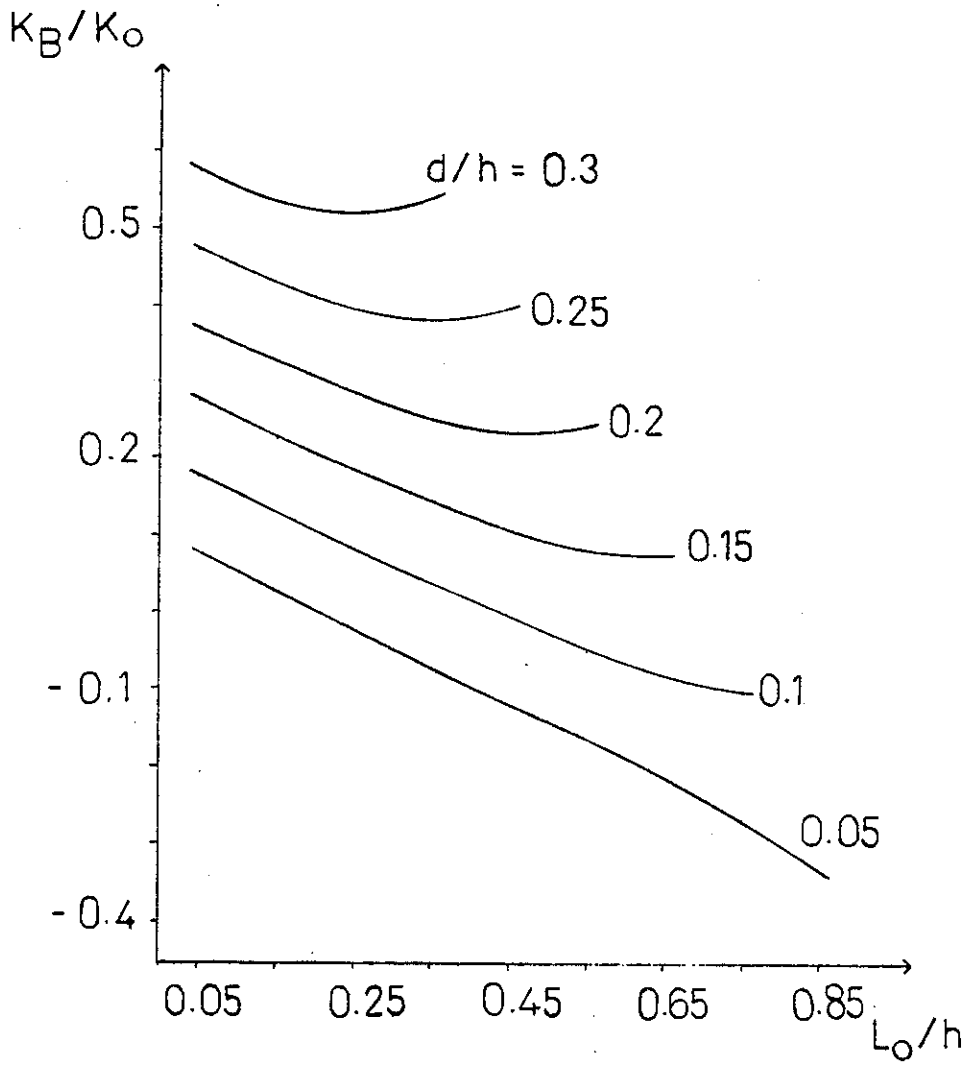

Figure 14. Effect of L_o/h ratio on the normalized stress intensity factors calculated at the midsection of internal elliptic cracks with $a/L_o=4$ and different d/h ratios under pure bending.

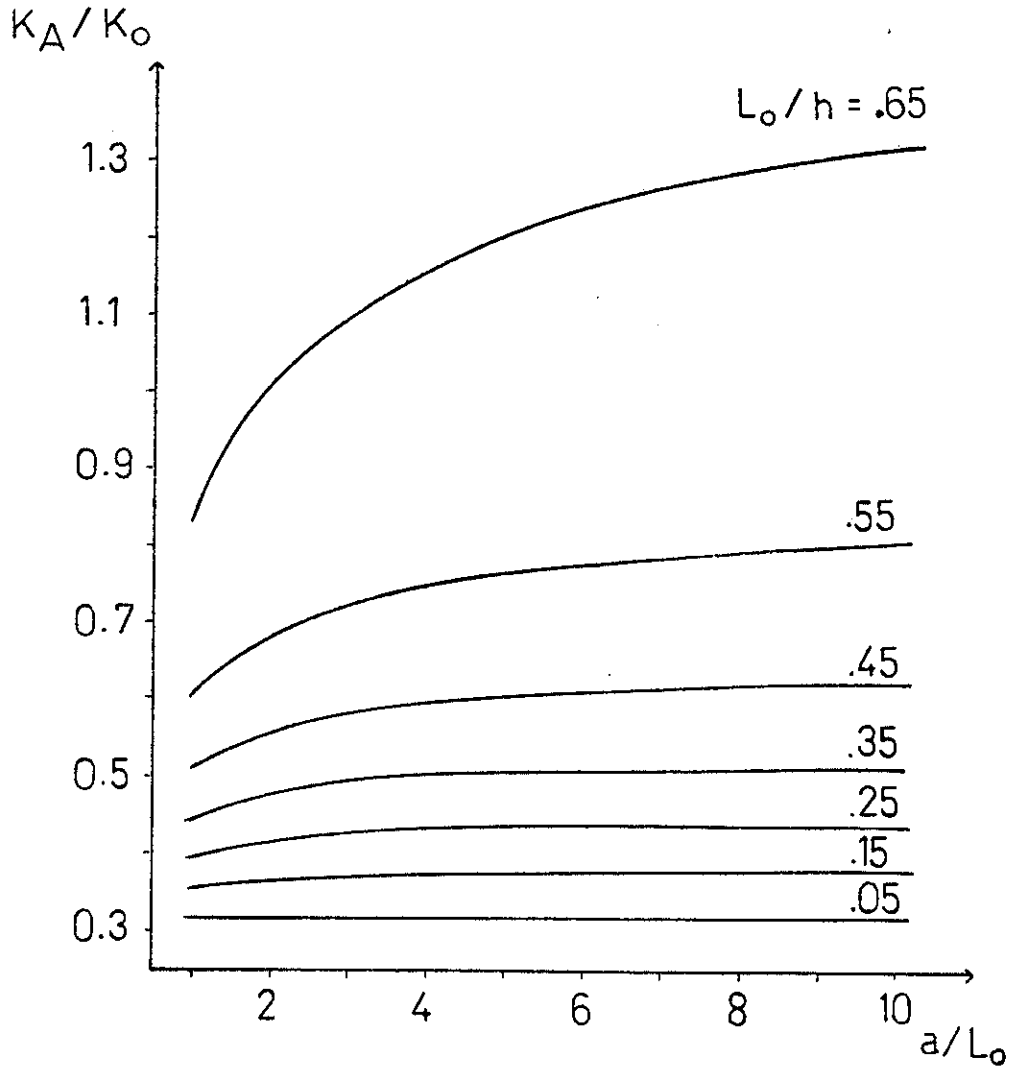

Figure 15. Effect of a/L_o ratio on the normalized stress intensity factors calculated at the midsection of internal elliptic cracks with d/h=0.15 and different L_o/h ratios under pure bending.

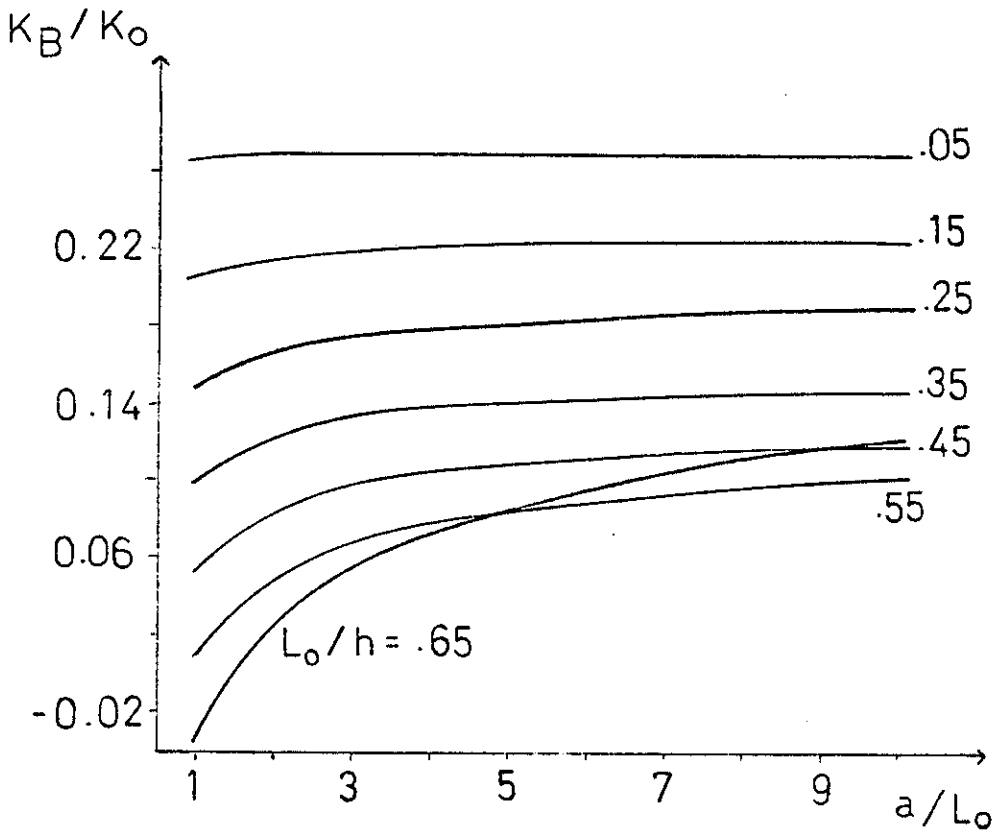

Figure 16. Effect of a/L_o ratio on the normalized stress intensity factors calculated at the midsection of internal elliptic cracks with d/h=0.15 and different L_o/h ratios under pure bending.

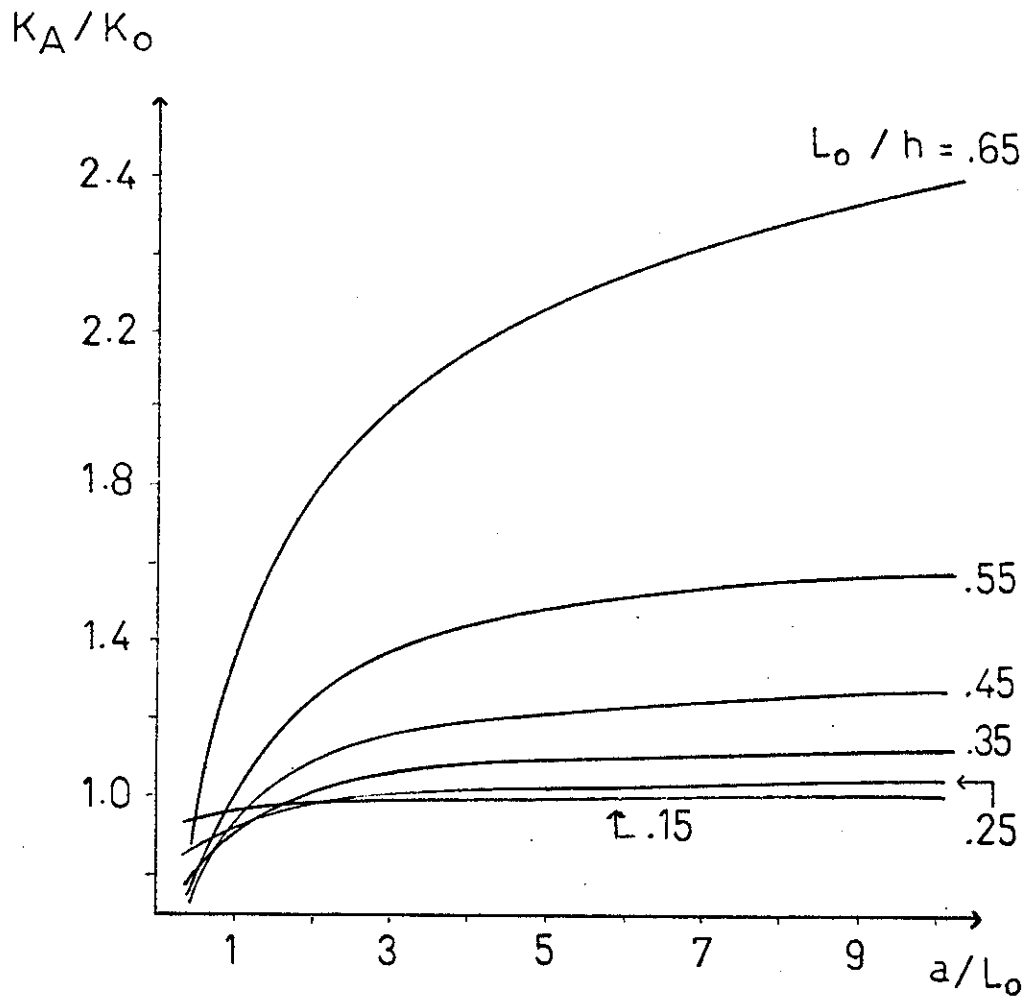

Figure 17. Effect of a/L_o ratio on the normalized stress intensity factors calculated at the midsection of internal elliptic cracks with $d/h=0.15$ and different L_o/h ratios under pure tension.

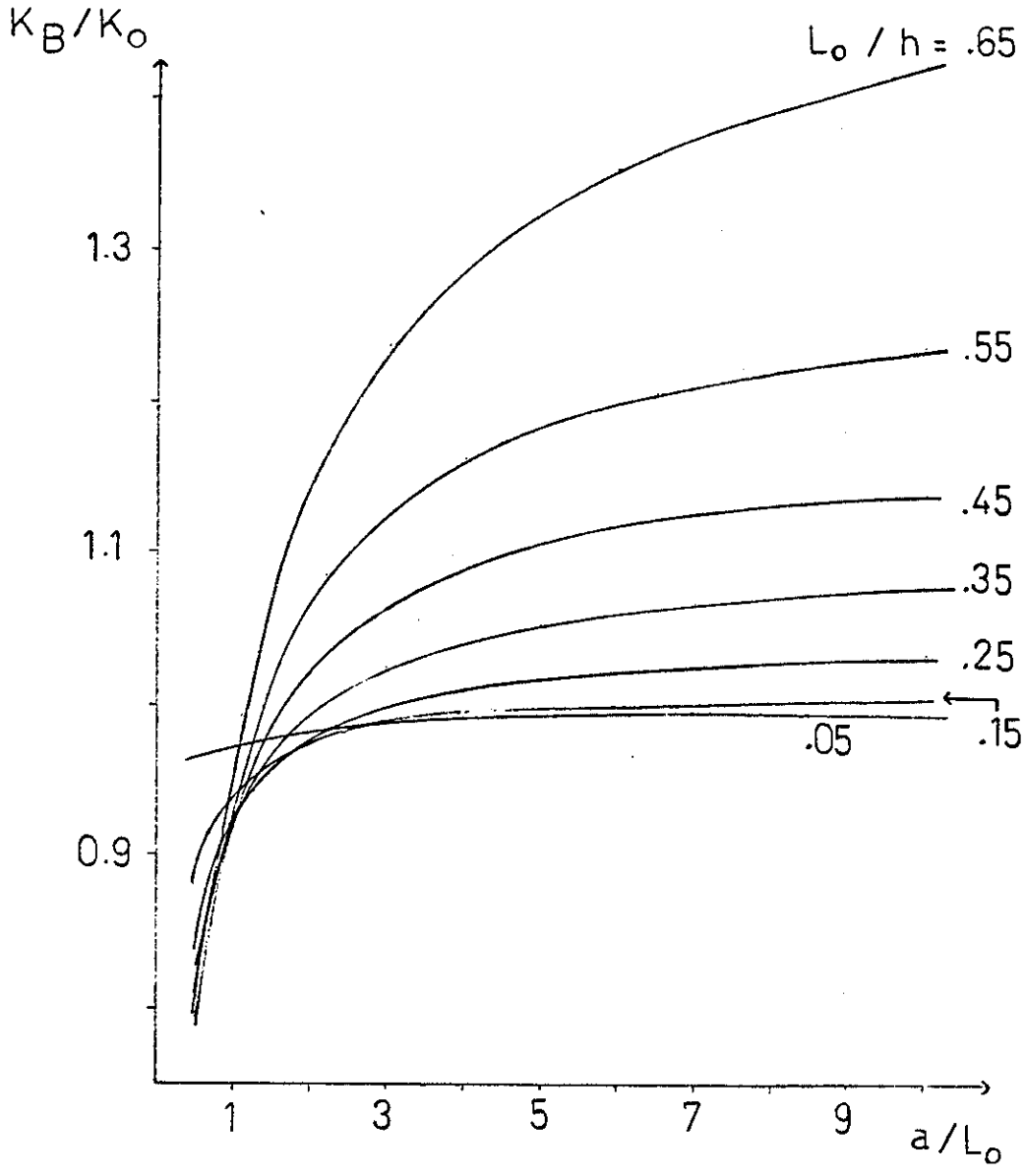

Figure 18. Effect of a/L_o ratio on the normalized stress intensity factors calculated at the midsection of internal elliptic cracks with d/h=0.15 and different L_o/h ratios under pure tension.

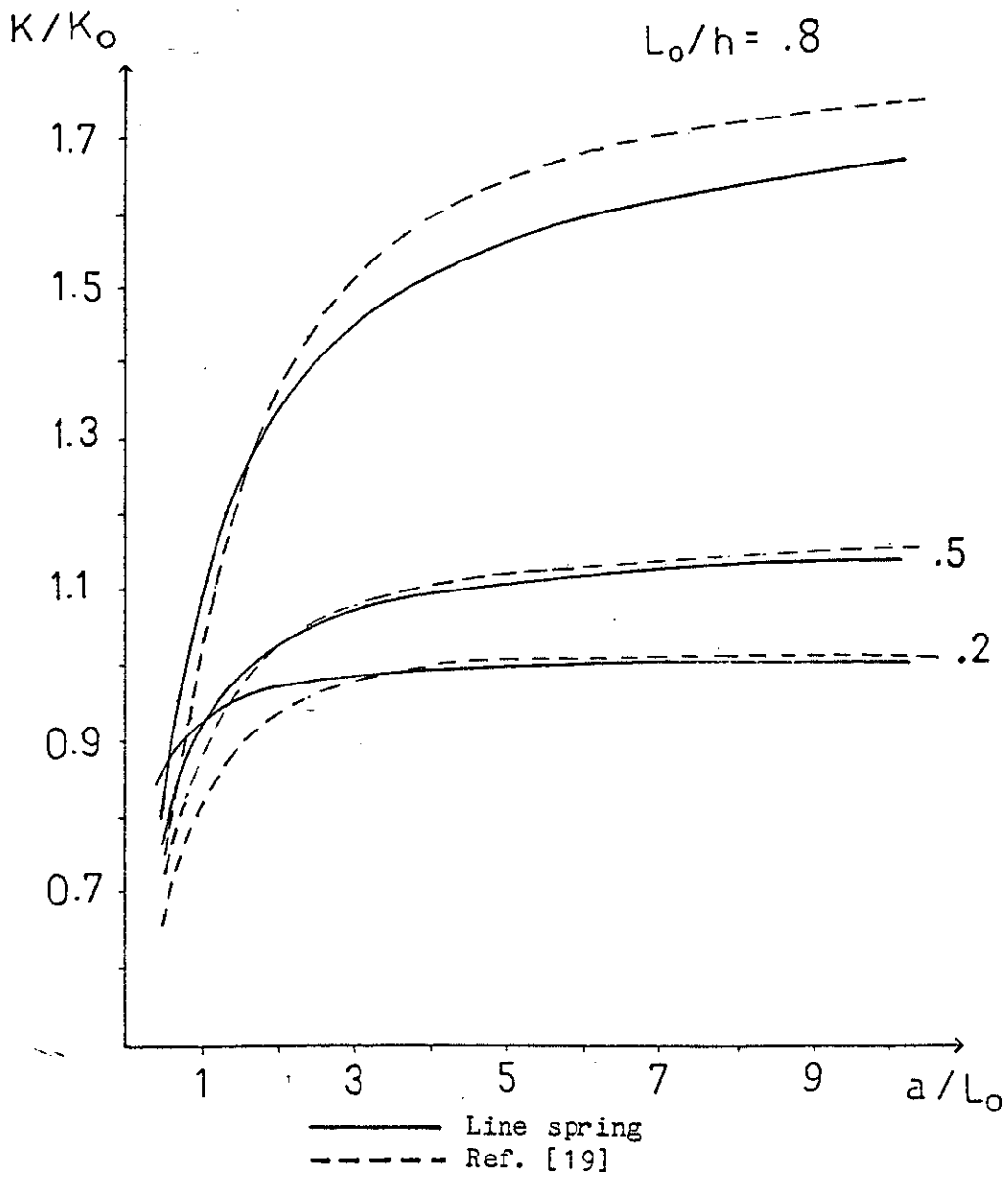

Figure 19. Comparison of the normalized stress intensity factors calculated in this study at x=0 for an internal planar elliptic crack in a plate under uniform tension and with the corresponding values given in Ref.[19].

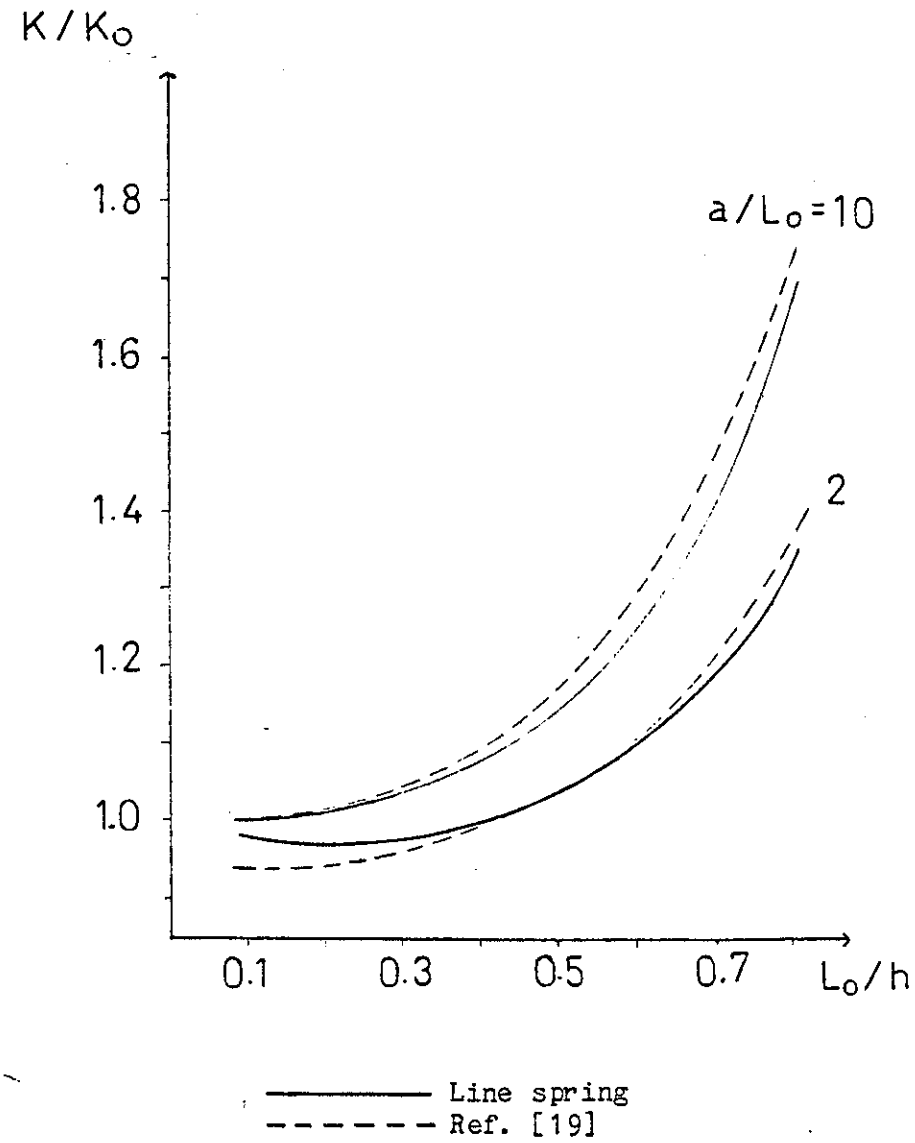

Figure 20. Comparison of the normalized stress intensity factors calculated in this study at x=0 for an internal planar elliptic crack in a plate under uniform tension and with the corresponding values given in Ref.[19].

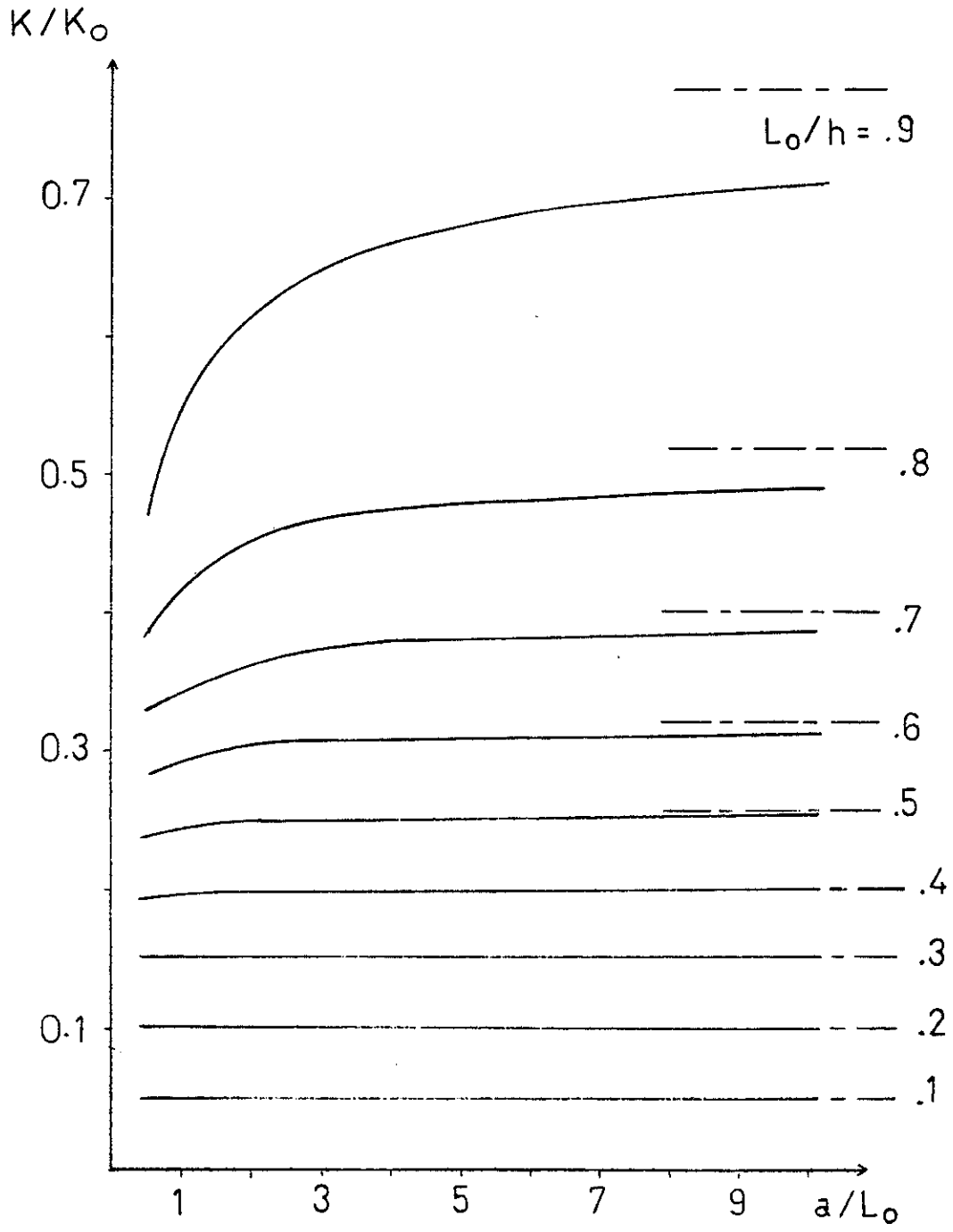

Figure 21. Normalized stress intensity fators calculated at the midsection of a symmetrically located (d/h=0) internal planar elliptic crack in a plate under uniform bending.

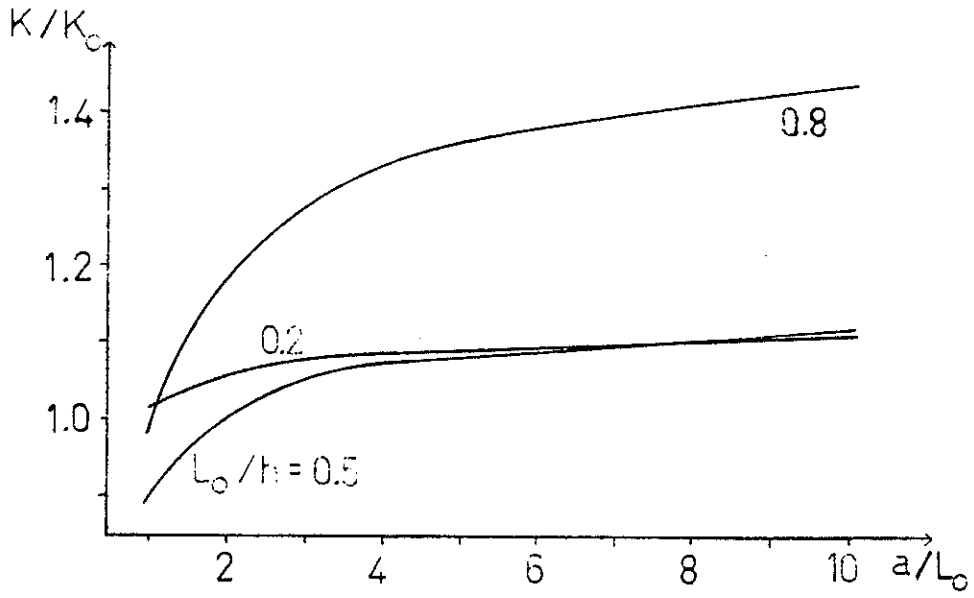

Figure 22. Normalized stress intensity factors calculated at the midsection of two opposite planar elliptic edge cracks in a plate under uniform tension.

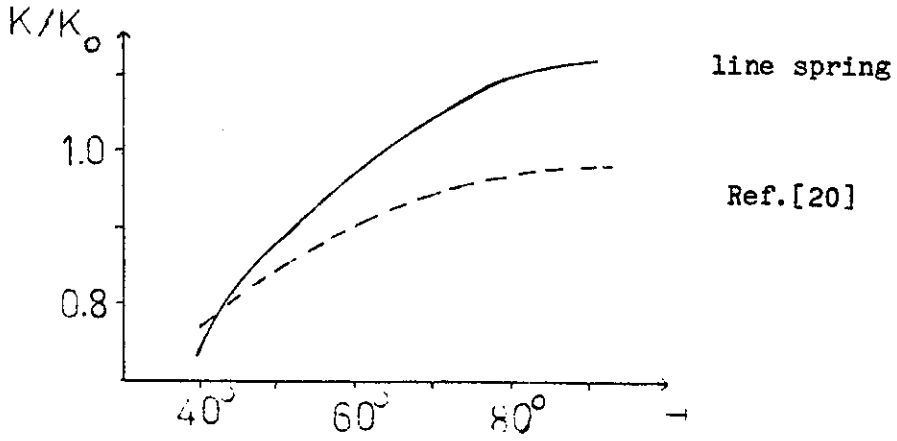

Figure 23. Comparison of the stress intensity factors calculated in this study at the midsection of a symmetrically located internal(d/h=0) planar elliptic crack in a plate under uniform tension with the corresponding results given in [20]. $L_o/h=.57$, $a/L_o=1.25$, $x=\cos\theta$.

REFERENCES

1. F. Delale and F. Erdogan, "Line Spring Model for Surface Cracks in a Reissner Plate", Int. J. Eng. Sci., Vol.19, 1981, pp.1331 .

2. F. Delale and F. Erdogan, "Transverse Shear Effect in a Circumferentially Cracked Cylindrical Shell", Quart. Appl. Math., Vol.37, 1979, pp.239 .

3. J. R. Rice and N. Levy, "The Part-Through Surface Crack in an Elastic Plate", J. of Appl. Mech., Trans. ASME, Vol.39, 1972, pp.185 .

4. F. Erdogan, "Mixed Boundary-Value Problems in Mechanics: Addendum", Mechanics Today, S. Nemat-Nasser(ed), Vol.4, pp.199 .

5. F. W. Smith and D. R. Sorensen, "The Semi-Elliptical Surface Crack - A Solution by the Alternating Method", Int. J. of Fracture, Vol.12, 1976, pp.47 .

6. R. C. Shah and A. S. Kobayashi, "On the Surface Flaw Problem", The Surface Crack: Physical Problems and Computational Solutions, ed. J. L. Swedlow, 1972, pp.79 .

7. J. Heliot, R. C. Labbens, A. Pellisier-Tannon, "Semi Elliptic Cracks in a Cylinder Subjected to Stress Gradients", Fracture Mechanics, ASTM, STP 677, 1979, pp.341 .

8. I. S. Raju, J. C. Newman, Jr., "Stress-Intensity Factors for a Wide Range of Semi-Elliptical Surface Cracks in Finite-Thickness Plates", J. of Eng. Fracture Mechanics, Vol.11, 1979, pp. 817 .

9. J. C. Newman, Jr., "A Review and Assessment of the Stress-Intensity Factors for Surface Cracks", NASA Technical Memorandum 78805, Nov. 1978.

10. S. N. Atluri, K. Kathiresan, A. S. Kobayashi, M. Nakayaki, "Inner Surface Cracks in an Internally Pressurized Cylinder Analyzed by a Three-Dimensional Displacement-Hybrid Finite Element Method", ASME, Part III, New York, 1977, pp.527 .

11. F. Delale and F. Erdogan, "The Effect of Transverse Shear in a Cracked Plate Under Skewsymmetric Loading", J. Appl. Mech., Trans. ASME, Vol.46 .

12. D. M. Parks, "The Inelastic Line Spring: Estimates of Elastic-Plastic Fracture Parameters for Surface Cracked Plates and Shells", ASME, Paper 80-C2/PVP-109, 1980.

13. D. M. Parks, "Inelastic Analysis of Surface Flaws Using the Line Spring Model", Proceedings of the 5'th Int. Conf. on Fracture, Cannes, France, 1981.

14. F. Delale and F. Erdogan, "Application of the Line Spring Model to a Cylindrical Shell Containing a Circumferential or an Axial Part-Through Crack", J. Appl. Mech., Trans. ASME, Vol.49, 1982, pp.97 .

15. F. Erdogan and H. Boduroglu, "Surface Cracks in a Plate of Finite Width Under Extension or Bending", Theoretical and Applied Fracture Mechanics, Vol.1, 1985(to appear).

16. F. Erdogan and O. S. Yahsi, "A Cylindrical Shell With a Stress-Free End Which Contains an Axial Part-Through or Through Crack", Project Report, NASA NGR 39-007-011, Lehigh University, Dec. 1983.

17. F. Erdogan and O. S. Yahsi, "A Pressurized Cylindrical Shell With a Fixed End Which Contains an Axial Part-Through or Through Crack", Project Report, NASA NGR 39-007-011, Lehigh University, Dec. 1983.

18. F. Erdogan and G. D. Gupta, "The Problem of Edge Cracks in an Infinite Strip", J. Appl. Mechanics, Trans. ASME, 1974, pp.1001 .

19. J. C. Newman, Jr. and I. S. Raju, "Stress Intensity Factor Equations for Cracks in Three-Dimensional Finite Bodies", ASTM STP-791, 1983, pp. 238 .

20. T. Nishioka and S. N. Atluri, "Analytical Solution for Embedded Elliptic Cracks, and Finite Element Alternating Method for Elliptical Surface Cracks, Subjected to Arbitrary Loadings", Engineering Fracture Mechanics, Vol.17, 1983, pp.247 .

APPENDIX I

The dimensionless quantities used in the formulation:

$$x = \frac{x_1}{a_i} , \qquad y = \frac{x_2}{a_i} , \qquad z = \frac{x_3}{a_i} ,$$

$$u = \frac{u_1}{a_i} , \qquad v = \frac{u_2}{a_i} , \qquad w = \frac{u_3}{a_i} ,$$

$$\beta_x = \beta_1 , \qquad \beta_y = \beta_2$$

$$\lambda^4 = 12 (1 - \nu^2) \frac{a_i^2}{h^2} , \qquad \kappa = \frac{h^2}{5 (1 - \nu) a_i^2} ,$$

$$p = \left[\frac{2}{\kappa(1-\nu)}\right]^{1/2} ,$$

$$R_1 = \frac{a_i(1 - \nu^2)}{2\pi h \lambda^4} , \qquad R_2 = \frac{3 + \nu}{1 + \nu} ,$$

$$R_3 = \frac{4\kappa (1 - \nu)}{(1 + \nu)} , \qquad R_4 = \frac{4}{1 + \nu} .$$

APPENDIX II

Procedure for finding coefficients of the shape functions (g_t and g_b) are as follows. Loading should be seperated as pure tension and pure bending. For pure tension case

$$m = 0 \quad .$$

By using (8), (9) and (10a)

$$K(s) = \sqrt{h}\,\sigma\, g_t(s) \quad ,$$

$$K(s) = \sqrt{h}\,\sigma\,\sqrt{\pi s}\sum_{i=1}^{n} b_i(s)^{2(i-1)} \quad ,$$

$$K(s) = \sigma\sqrt{\pi L(x_1)}\sum_{i=1}^{n} b_i(s)^{2(i-1)} \quad ,$$

$$\frac{K(s)}{\sigma\sqrt{\pi L(x_1)}} = \sum_{i=1}^{n} b_i(s)^{2(i-1)} \quad .$$

Values of the left handside can easily be found for a wide range of s values in related literature, which enables us to create n equations with b_i's as the n unknowns. Solution of this system is the coefficient of corresponding shape function.

Same procedure is followed under pure bending to find c_i's.

APPENDIX III

Solution of the Integral Equations

i- Gauss-Chebyshev Closed Type Integration Formula

The solution of the integral equation which only has the Cauchy type singularity

$$\frac{1}{\pi}\int_{-1}^{1}\frac{\phi(t)}{t-x}\,dt + \int_{-1}^{1} k(x,t)\,\phi(t)\,dt = f(x) \quad , \quad -1 < x < 1 \quad ,$$

may be expressed as

$$\phi(t) = (1 - t^2)^{-1/2} g(t)$$

$$K(x,t) = \frac{1}{\pi}\,\frac{1}{t-x} + k(x,t)$$

$$\frac{\pi}{n-1}\left[\frac{1}{2}K(x_j,t_1)g(t_1) + \sum_{i=2}^{n-1} K(x_j,t_i)g(t_i) + \frac{1}{2}K(x_j,t_n)g(t_n)\right]$$

$$= f(x_j) \quad , \quad j = 1, \ldots\ldots, (n-1)$$

$$t_i = \cos\left[\frac{i-1}{n-1}\pi\right] \quad , \quad i = 1, \ldots\ldots, n$$

$$x_j = \cos\left[\frac{2j-1}{2n-2}\pi\right] , \quad j = 1, \ldots\ldots , (n-1)$$

and the additional condition

$$\int_{-1}^{1} \Phi(t)\, dt = A ,$$

becomes

$$\frac{\pi}{n-1}\left[\frac{1}{2}g(t_1) + \sum_{i=2}^{n-1} g(t_i) + \frac{1}{2}g(t_n)\right] = A$$

One may find the detailed derivation of the formula in [4].

When there is a system of integral equations with more than one unknown functions to be solved, the above procedure can be used by applying the formula to each integration seperately. For example

$$\frac{1}{\pi}\int_{-1}^{1}\frac{\Phi_1(t)}{t-x}\,dt + \int_{-1}^{1} k_{11}(x,t)\Phi_1(t)\,dt + \int_{-1}^{1} k_{12}(x,t)\Phi_2(t)\,dt = f_1(x) ,$$

$$\int_{-1}^{1} k_{21}(x,t)\Phi_1(t)\,dt + \int_{-1}^{1} k_{22}(x,t)\Phi_2(t)\,dt + \frac{1}{\pi}\int_{-1}^{1}\frac{\Phi_2(t)}{t-x}\,dt = f_2(x) ,$$

$$\int_{-1}^{1} \Phi_1(t)\, dt = A_1 , \qquad \int_{-1}^{1} \Phi_2(t)\, dt = A_2 , \qquad -1 < x < 1$$

can be solved as

$$\Phi_1(t) = (1 - t^2)^{-1/2} g_1(t) ,$$

$$\Phi_2(s) = (1 - s^2)^{-1/2} g_2(s) ,$$

s has been introduced to define different collocation points for each functions.

$$K_{11}(x,t) = \frac{1}{\pi} \frac{1}{t-x} + k_{11}(x,t) ,$$

$$K_{12}(x,s) = k_{12}(x,s) ,$$

$$K_{21}(x,s) = k_{21}(x,s) ,$$

$$K_{22}(x,s) = \frac{1}{\pi} \frac{1}{s-x} + k_{22}(x,s) ,$$

$$\frac{\pi}{n_1-1}\left[\frac{1}{2}K_{11}(x_j,t_1)g_1(t_1)+\sum_{i=2}^{n_1-1}K_{11}(x_j,t_i)g_1(t_i)+\frac{1}{2}K_{11}(x_j,t_{n1})g_1(t_{n1})\right]$$

$$+\frac{\pi}{n_2-1}\left[\frac{1}{2}K_{12}(x_j,s_1)g_2(s_1)+\sum_{i=2}^{n_2-1}K_{12}(x_j,s_i)g_2(s_i)\right.$$

$$\left.+\frac{1}{2}K_{12}(x_j,s_{n2})g_2(s_{n2})\right]=f_2(x_j)\ ,$$

$$x_j=\cos\left[\frac{2j-1}{2n_1-2}\pi\right]\ ,\qquad j=1,\ .....\ ,(n_1-1)$$

$$\frac{\pi}{n_1-1}\left[\frac{1}{2}K_{21}(x_j,t_1)g_1(t_1)+\sum_{i=2}^{n_1-1}K_{21}(x_j,t_i)g_1(t_i)+\frac{1}{2}K_{21}(x_j,t_{n1})g_1(t_{n1})\right]$$

$$+\frac{\pi}{n_2-1}\left[\frac{1}{2}K_{22}(x_j,s_1)g_2(s_1)+\sum_{i=2}^{n_2-1}K_{22}(x_j,s_i)g_2(s_i)\right.$$

$$\left.+\frac{1}{2}K_{22}(x_j,s_{n2})g_2(s_{n2})\right]=f_2(x_j)$$

$$X_j=\cos\left[\frac{2j-1}{2n_2-2}\pi\right]\ ,\qquad j=1,\ .....\ ,(n_2-1)$$

$$\frac{\pi}{n_1-1}\left[\frac{1}{2}g_1(t_1)+\sum_{i=2}^{n_1-1}g_1(t_i)+\frac{1}{2}g_1(t_{n1})\right]=A_1\ ,$$

$$\frac{\pi}{n_2-1}\left[\frac{1}{2}g_2(s_1)+\sum_{i=2}^{n_2-1}g_2(s_i)+\frac{1}{2}g_2(s_{n2})\right]=A_2\ ,$$

$$t_i = \cos\left[\frac{i-1}{n_1-1}\pi\right] , \qquad i = 1, \ldots\ldots , n_1$$

$$s_i = \cos\left[\frac{i-1}{n_2-1}\pi\right] , \qquad i = 1, \ldots\ldots , n_2$$

Above solution can also be used for any number of unknown functions in the same manner.

ii- Order of Singularity in the Integral Equation

At first glance, it seems that (31) has singularities other than Cauchy type. But if we take a closer look to the equation, we will see that modified Bessel function of the second kind has the following property for relatively small values of the argument.

$$K_r(x) \sim 2^{r-1}(r-1)!x^{-r} \quad ,$$

$$K_2(x) \sim 2\, x^{-2} \quad .$$

By using above property, we can say that

$$\lim_{(t-x)\to 0} K_2(p|t-x|) = \frac{2}{p^2(t-x)^2} = \frac{K(1-p)}{(t-x)^2}$$

which gives

$$\lim_{(t-x)\to 0} \left[\frac{4}{1+\nu} \frac{1}{t-x} K_2(p|t-x|) - \frac{4k(1-\nu)}{1+\nu} \frac{1}{(t-x)^3} \right] = 0 \quad .$$

This proves that (31) has only Cauchy type singularity and can be solved by Gauss-Chebyshev closed type integration formula.

Integrals on the interval (-1 , x) can be written on (-1 , +1) by redifining the kernels by the use of a step function H(y) as follows:

$$\int_{-1}^{x} f(t)\, dt = \int_{-1}^{1} H(x-t)\, f(t)\, dt$$

where,

$$H(y) = \begin{cases} 0 & \text{if} \quad y < 0 \\ 1 & \text{if} \quad y \geq 0 \ . \end{cases}$$

APPENDIX IV

Numerical Integration

Gauss-Chebyshev closed type integration formula is used for numerical integration purposes. Any integral in the interval (-1 , +1) can be expressed as,

$$\int_{-1}^{1} \frac{f(x)\,dx}{\sqrt{1-x^2}} = \frac{\pi}{n-1}\left[\frac{1}{2}f(x_1) + \sum_{i=2}^{n-1} f(x_i) + \frac{1}{2}f(x_n)\right]$$

If an integration in the interval (-1 , x) is desired, above formula can again be used by multiplying the integrand with the H function defined in Appendix III.

Number of points (n) in the integration should be much higher than the number of points used in the solution of integral equations if one desires to evaluate the stress intensity factor or the crack front at any point accurately. Values of the functions to be integrated at any point can be found by interpolating the function between the two surrounding known values found from the solution of integral equations.

APPENDIX C

THE CRACK-INCLUSION INTERACTION PROBLEM

by

Liu Xue-Hui and F. Erdogan

Lehigh University, Bethlehem, PA

ABSTRACT

In this study the general plane elastostatic problem of interaction between a crack and an inclusion is considered. The Green's functions for a pair of dislocations and a pair of concentrated body forces are used to generate the crack and the inclusion. The integral equations of the problem is obtained for a line crack and an elastic line inclusion having an arbitrary relative orientation and size. The nature of stress singularity around the end points of rigid and elastic inclusions is described. A question of specific interest which is studied is the nature of stress singularity around the point of intersection of the crack and the inclusion. Three special cases of this intersection problem which have been studied are a crack and an inclusion which are collinear and have a common end point, a crack perpendicular to an inclusion with a common end point (the L configuration), and a crack perpendicular to an inclusion terminating at its midpoint (the T configuration). The problem is solved for an arbitrary uniform stress state away from the crack-inclusion region. First, the non-intersecting crack-inclusion problem is considered for various relative size, orientation, and stiffness parameters and the stress intensity factors at the ends of the inclusion and the crack are calculated. Then for the crack-inclusion intersection case special stress intensity factors are defined and are calculated again for various values of the parameters defining the relative size and orientation of the crack and the inclusion and the stiffness of the inclusion.

1. Introduction

In studying the fracture of multi-phase materials, structures composed of bonded dissimilar solids, and welded joints it is necessary to take into account the effect of the imperfections in the medium. Generally such imperfections are in the form of either geometric discontinuities or material inhomogeneities. For example, in welded joints various shapes of voids, cracks, notches and regions of lack of fusion may be mentioned as examples for the former and variety of inclusions for the latter. From the viewpoint of fracture mechanics two important classes of imperfections are the planar flaws which may be idealized as cracks and relatively thin inhomogeneities which may be idealized as flat inclusions with "sharp" boundaries. In both cases the edges of the defects are lines of stress singularity and, consequently, regions of potential crack initiation and propagation.

The technical literature on cracks, voids and inclusions which exist in the material separately is quite extensive. However, the problems concerning the interaction of cracks, voids and inclusions do not seem to be as widely studied (see, for example, [1] for the results of crack-circular inclusion or void interaction problem and for some references). In this paper the relatively simple problem of an elastic plane containing a crack and an arbitrarily oriented flat elastic inclusion is considered. Of special interest is the examination of the asymptotic stress field in the neighborhood of inclusion ends and the problems of intersecting cracks and inclusions. The basic dislocation and concentrated force solutions are used to formulate the problem [2]. Hence, the formulation can easily be extended to study problems involving multiple cracks and inclusions.

2. Integral Equations of the Problem

The geometry of the crack-inclusion interaction problem under consideration is shown in Figure 1. It is assumed that the medium is under a state of plane strain or generalized plane stress and the in-plane dimensions of the medium are large compared to the lengths of and the distance between the crack and the inclusion so that the effect of the remote boundaries on the

perturbed stress state may be neglected. Thus, the Green's functions for the concentrated forces and dislocations in an infinite plane may be used to formulate the problem. It is further assumed that the inclusion is sufficiently "thin" so that its bending stiffness may also be neglected.

Referring to Figure 1 we consider the stresses and displacements due to a pair of edge dislocations on the x axis, a pair of concentrated forces on the line θ=constant and the applied loads acting on the medium away from the crack-inclusion region. Let the subscripts d, p and a designate these three stress and deformation states, i.e., let σ_{dij}, σ_{pij} and σ_{aij}, $(i,j) = (x,y)$ or $(i,j) = (r,\theta)$, be the stress components due to dislocations, concentrated forces, and applied loads, respectively. The total stress state in the elastic plane may, therefore, be expressed as

$$\sigma_{ij}(x,y) = \sigma_{dij}(x,y) + \sigma_{pij}(x,y) + \sigma_{aij}(x,y), \quad (i,j = x,y) \tag{1}$$

Let us now assume that the dislocations are distributed along $a<x<b$, $y=0$ forming a crack. If $g(x)$ and $h(x)$ refer to the dislocation densities defined by

$$\frac{\partial}{\partial x}\left[u_y(x,+0) - u_y(x,-0)\right] = g(x) \ , \ a < x < b \ ,$$

$$\frac{\partial}{\partial x}\left[u_x(x,+0) - u_x(x,-0)\right] = h(x) \ , \ a < x < b \ , \tag{2a,b}$$

the corresponding stress components at a point (x,y) in the plane may be expressed as

$$\sigma_{dxx}(x,y) = \int_a^b \left[G_{xx}(x,y,t)g(t) + H_{xx}(x,y,t)h(t)\right]dt \ ,$$

$$\sigma_{dyy}(x,y) = \int_a^b \left[G_{yy}(x,y,t)g(t) + H_{yy}(x,y,t)h(t)\right]dt \ , \tag{3a-c}$$

$$\sigma_{dxy}(x,y) = \int_a^b \left[G_{xy}(x,y,t)g(t) + H_{xy}(x,y,t)h(t)\right]dt \ ,$$

where

$$G_{xx} = \frac{2\mu}{\pi(\kappa+1)} \cdot \frac{(t-x)[(t-x)^2 - y^2]}{[(t-x)^2 + y^2]^2} ,$$

$$G_{yy} = \frac{2\mu}{\pi(\kappa+1)} \cdot \frac{(t-x)[3y^2 + (t-x)^2]}{[(t-x)^2 + y^2]^2} ,$$

$$G_{xy} = \frac{2\mu}{\pi(\kappa+1)} \cdot \frac{y[y^2 - (t-x)^2]}{[(t-x)^2 + y^2]^2} ,$$

$$H_{xx} = \frac{2\mu}{\pi(\kappa+1)} \cdot \frac{y[y^2 + 3(t-x)^2]}{[(t-x)^2 + y^2]^2} , \qquad (4a\text{-}f)$$

$$H_{yy} = \frac{2\mu}{\pi(\kappa+1)} \cdot \frac{y[y^2 - (t-x)^2]}{[(t-x)^2 + y^2]^2} ,$$

$$H_{xy} = \frac{2\mu}{\pi(\kappa+1)} \cdot \frac{(t-x)[(t-x)^2 - y^2]}{[(t-x)^2 + y^2]^2} .$$

In (4) μ and κ are the elastic constants of the medium, μ the shear modulus, $\kappa = 3-4\nu$ for plane strain and $\kappa = (3-\nu)/(1+\nu)$ for plane stress ν being the Poisson's ratio.

Similarly, from the concentrated force solution as given, for example, in [2] the stress components $\sigma_{pij} = S_{ij}$ due to a pair of forces P_x and P_y acting at the point (x_o, y_o) may be written as

$$S_{xx}(x,y,x_o,y_o) = \frac{1}{2\pi(\kappa+1)} \frac{(A_1+A_2)P_x + (B_1+B_2)P_y}{[(x-x_o)^2 + (y-y_o)^2]^2} ,$$

$$S_{yy}(x,y,x_o,y_o) = \frac{1}{2\pi(\kappa+1)} \frac{(A_1-A_2)P_x + (B_1-B_2)P_y}{[(x-x_o)^2 + (y-y_o)^2]^2} , \qquad (5a\text{-}c)$$

$$S_{xy}(x,y,x_o,y_o) = \frac{1}{2\pi(\kappa+1)} \frac{A_3P_x + B_3P_y}{[(x-x_o)^2 + (y-y_o)^2]^2} ,$$

$$A_1 = -2(x-x_o)[(x-x_o)^2 + (y-y_o)^2]$$

$$A_2 = -\kappa(x-x_o)[(x-x_o)^2 + (y-y_o)^2] - (x-x_o)[(x-x_o)^2 - (y-y_o)^2] + 2(y-y_o)^2(x-x_o)$$

$$B_1 = -2(y-y_o)[(x-x_o)^2 + (y-y_o)^2]$$

$$B_2 = +\kappa(y-y_o)[(x-x_o)^2+ (y-y_o)^2]-(y-y_o)[(x-x_o)^2-(y-y_o)^2]-2(x-x_o)^2(y-y_o)$$

$$A_3 = -\kappa(y-y_o)[(x-x_o)^2+(y-y_o)^2]-(y-y_o)[(x-x_o)^2-(y-y_o)^2]-2(x-x_o)^2(y-y_o)$$

$$B_3 = -\kappa(x-x_o)[(x-x_o)^2+(y-y_o)^2]+(x-x_o)[(x-x_o)^2-(y-y_o)^2]-2(y-y_o)^2(x-x_o)$$

(6a-f)

If the inclusion is located along the line $c < r < d$, θ = constant, and if its bending stiffness is neglected, then the following conditions are valid:

$$u_r(r,\theta+0) = u_r(r,\theta-0),\ u_\theta(r,\theta+0) = u_\theta(r,\theta-0)\ ,$$

$$-P_\theta(r,\theta) = \sigma_{\theta\theta}(r,\theta+0) - \sigma_{\theta\theta}(r,\theta-0) = 0\ , \qquad (7a\text{-}d)$$

$$-P_r(r,\theta) = -p(r) = \sigma_{r\theta}(r,\theta+0) - \sigma_{r\theta}(r,\theta-0)\ ,\ (c<r<d).$$

Thus, to formulate the problem it is sufficient to consider only the radial component $P_r=p$ of the concentrated force. For $P_\theta=0$ and $P_r=p$ observing that

$$P_x = p\cos\theta\ ,\ P_y = p\sin\theta\ , \qquad (8a,b)$$

and substituting $x_o = r_o\cos\theta$, $y_o = r_o\sin\theta$, by using the kernels S_{ij} given by (5) the stress components σ_{pij} are found to be

$$\sigma_{pxx}(x,y) = \frac{1}{2\pi(\kappa+1)}\int_c^d \frac{(A_1'+A_2')\cos\theta+(B_1'+B_2')\sin\theta}{[(x-r_o\cos\theta)^2+(y-r_o\sin\theta)^2]^2}\,p(r_o)dr_o\ ,$$

$$\sigma_{pyy}(x,y) = \frac{1}{2\pi(\kappa+1)}\int_c^d \frac{(A_1'-A_2')\cos\theta+(B_1'-B_2')\sin\theta}{[(x-r_o\cos\theta)^2+(y-r_o\sin\theta)^2]^2}\,p(r_o)dr_o\ , \qquad (9a\text{-}c)$$

$$\sigma_{pxy}(x,y) = \frac{1}{2\pi(\kappa+1)}\int_c^d \frac{A_3'\cos\theta + B_3'\sin\theta}{[(x-r_o\cos\theta)^2+(y-r_o\sin\theta)^2]^2}\,p(r_o)dr_o\ ,$$

where the functions A_i', B_i', (i=1,2,3) are obtained from (6) by substituting $x_o = r_o\cos\theta$ and $y_o = r_o\sin\theta$, e.g.,

$$A_1'(x,y,r_o) = -2(x-r_o\cos\theta)[(x-r_o\cos\theta)^2 + (y-r_o\sin\theta)^2] \ . \qquad (10)$$

Since the stresses σ_{aij} due to the applied loads are known, from (1), (3) and (9) it is seen that once the functions g(x), h(x) and p(r) are determined the problem is solved. These unknown functions may be determined by expressing the stress boundary conditions on the crack surfaces and the displacement compatibility condition along the inclusion, namely

$$\sigma_{yy}(x,0) = \sigma_{dyy}(x,0) + \sigma_{pyy}(x,0) + \sigma_{ayy}(x,0) = 0 \ , \quad (a<x<b),$$

$$\sigma_{xy}(x,0) = \sigma_{dxy}(x,0) + \sigma_{pxy}(x,0) + \sigma_{axy}(x,0) = 0 \ , \quad (a<x<b), \qquad (11a\text{-}c)$$

$$\varepsilon_{rr}(r,\theta) = \varepsilon_{drr}(r,\theta) + \varepsilon_{prr}(r,\theta) + \varepsilon_{arr}(r,\theta) = \varepsilon_i(r), \ (c<r<d)$$

where $\varepsilon_i(r)$ is the (longitudinal) strain in the inclusion. If, for example, the stress state away from the crack inclusion region is given by σ_{ij}^{∞}, (i,j) = (x,y), then the applied quantities in (11) may be expressed as

$$\sigma_{ayy}(x,0) = \sigma_{yy}^{\infty} \ , \ \sigma_{axy}(x,0) = \sigma_{xy}^{\infty} \ ,$$

$$\varepsilon_{arr}(r,\theta) = \frac{1+\kappa}{8\mu}\left[\sigma_{xx}^{\infty}\left(\cos^2\theta - \frac{3-\kappa}{1+\kappa}\sin^2\theta\right)\right.$$

$$\left. + \sigma_{yy}^{\infty}\left(\sin^2\theta - \frac{3-\kappa}{1+\kappa}\cos^2\theta\right) + \frac{4}{1+\kappa}\sigma_{xy}^{\infty}\sin 2\theta\right] . \qquad (12a\text{-}c)$$

We now note that if p(r) is the body force acting on the elastic medium then -p(r) would be the force acting on the inclusion distributed along its length. Thus, the strain in the inclusion may be obtained as

$$\varepsilon_i(r) = -\frac{1+\kappa_s}{8\mu_s A_s}\int_r^d p(r_o)dr_o \qquad (13)$$

where μ_s and κ_s are the elastic constants, and A_s is the cross-sectional area of the inclusion corresponding to unit thickness of the medium in z-direction. From the expression of ε_{rr} given by the Hooke's law

$$\varepsilon_{rr} = \frac{1+\kappa}{8\mu}\left(\sigma_{rr} - \frac{3-\kappa}{1+\kappa}\sigma_{\theta\theta}\right) , \tag{14}$$

from (9) and the corresponding stress transformation it can be shown that

$$\varepsilon_{prr}(r,\theta) = \frac{\kappa}{2\pi(1+\kappa)\mu}\int_c^d \frac{p(r_o)}{r_o - r}\, dr_o . \tag{15}$$

Similarly, from (3), (4) and (14) we find

$$\varepsilon_{drr}(r,\theta) = \frac{1+\kappa}{8\mu}\int_a^b [G_\varepsilon(r,t)g(t) + H_\varepsilon(r,t)h(t)]dt \tag{16}$$

where

$$\begin{aligned} G(r,t) = \frac{2\mu}{\pi(1+\kappa)}\frac{1}{R^4}\{&\cos^2\theta - \frac{3-\kappa}{1+\kappa}\sin^2\theta)(t - r\cos\theta) \times \\ &\times[(t-r\cos\theta)^2 - r^2\sin^2\theta] + (\sin^2\theta - \frac{3-\kappa}{1+\kappa}\cos^2\theta) \times \\ &\times(t-r\cos\theta)[3r^2\sin^2\theta + (t-r\cos\theta)^2] \\ &+ \frac{4}{1+\kappa}\sin 2\theta\; r\sin\theta[r^2\sin^2\theta - (t-r\cos\theta)^2]\} , \end{aligned} \tag{17}$$

$$\begin{aligned} H_\varepsilon(r,t) = \frac{2\mu}{\pi(1+\kappa)}\frac{1}{R^4}\{&(\cos^2\theta - \frac{3-\kappa}{1+\kappa}\sin^2\theta)r\sin\theta[r^2\sin^2\theta \\ &+ 3(t-r\cos\theta)^2] + (\sin^2\theta - \frac{3-\kappa}{1+\kappa}\cos^2\theta)r\sin\theta \times \\ &\times[r^2\sin^2\theta - (t-r^2\cos^2\theta)^2] + \frac{4}{1+\kappa}\sin 2\theta \times \\ &\times(t-r\cos\theta)[(t-r\cos\theta)^2 - r^2\sin^2\theta] , \end{aligned} \tag{18}$$

$$R^2 = (t - r\cos\theta)^2 + r^2\sin^2\theta \quad . \tag{19}$$

Finally, by substituting from (3), (4), (9), (12), (13), (15) and (16) into (11), the integral equations of the problem may be obtained as follows:

$$\frac{1}{\pi}\int_a^b \frac{g(t)dt}{t-x} + \frac{1}{4\pi\mu}\int_c^d \frac{(A_1'-A_2')\cos\theta+(B_1'-B_2')\sin\theta}{[(x-r_o\cos\theta)^2+(r_o\sin\theta)^2]^2}\, p(r_o)dr_o = -\frac{1+\kappa}{2\mu}\sigma_{yy}^{\infty} ,$$

$$(a<x<b) ,$$

$$\frac{1}{\pi}\int_a^b \frac{h(t)dt}{t-x} + \frac{1}{4\pi\mu}\int_c^d \frac{(A_3'\cos\theta+B_3'\sin\theta)p(r_o)}{[(x-r_o\cos\theta)^2+(r_o\sin\theta)^2]^2}\, dr_o = -\frac{1+\kappa}{2\mu}\sigma_{xy}^{\infty} ,$$

$$(a<x<b) ,$$

$$\frac{c_o}{\pi}\int_a^b G_\varepsilon(r,t)g(t)dt + \frac{c_o}{\pi}\int_a^b H_\varepsilon(r,t)h(t)dt + \frac{1}{\pi}\int_c^d \frac{p(r_o)}{r_o-r}\, dr_o$$

$$+ \frac{\gamma c_o}{\pi}\int_c^d H(r_o-r)p(r_o)dr_o = -\frac{c_o}{\pi}[(\cos^2\theta - \frac{3-\kappa}{1+\kappa}\sin^2\theta)\sigma_{xx}^{\infty}$$

$$+ (\sin^2\theta - \frac{3-\kappa}{1+\kappa}\cos^2\theta)\sigma_{yy}^{\infty} + \frac{4}{1+\kappa}\sigma_{xy}^{\infty}\sin 2\theta], \quad (c<r<d) , \qquad (20a\text{-}c)$$

where

$$c_o = \frac{\pi(1+\kappa)^2}{4\kappa} , \quad \gamma = \frac{\mu(1+\kappa_s)}{A_s\mu_s(1+\kappa)} . \qquad (21a,b)$$

From the definition of g and h given by (2) it follows that

$$\int_a^b g(t)dt = 0 , \quad \int_a^b h(t)dt = 0 . \qquad (22a,b)$$

Also, the static equilibrium of the inclusion requires that

$$\int_c^d p(r)dr = 0 . \qquad (23)$$

Thus, the system of singular integral equations must be solved under the conditions (22) and (23). From the function-theoretic examination of the integral equations (20) it can be shown that the unknown functions g, h and p are of the following form [2]:

$$g(t) = \frac{F_1(t)}{(b-t)^{\frac{1}{2}}(t-a)^{\frac{1}{2}}}, \quad h(t) = \frac{F_2(t)}{(b-t)^{\frac{1}{2}}(t-a)^{\frac{1}{2}}}, \quad p(r) = \frac{F_3(r)}{(d-r)^{\frac{1}{2}}(r-c)^{\frac{1}{2}}}, \tag{24a-c}$$

where F_1, F_2 and F_3 are bounded functions. The solution of (20) subject to (22) and (23) may easily be obtained by using the numerical method described in [3].

3. Stress Singularities

After solving (20) the Modes I and II stress intensity factors k_1 and k_2 at the crack tips x=a and x=b, y=0 which are defined by

$$k_1(a) = \lim_{x\to a} \sqrt{2(a-x)}\, \sigma_{yy}(x,0), \quad k_1(b) = \lim_{x\to b} \sqrt{2(x-b)}\, \sigma_{yy}(x,0),$$

$$k_2(a) = \lim_{x\to a} \sqrt{2(a-x)}\, \sigma_{xy}(x,0), \quad k_2(b) = \lim_{x\to b} \sqrt{2(x-b)}\, \sigma_{xy}(x,0), \tag{25a-d}$$

may be obtained as follows:

$$k_1(a) = \frac{2\mu}{1+\kappa} \lim_{x\to a} \sqrt{2(x-a)}\, g(x), \quad k_1(b) = -\frac{2\mu}{1+\kappa} \lim_{x\to b} \sqrt{2(b-x)}\, g(x),$$

$$k_2(a) = \frac{2\mu}{1+\kappa} \lim_{x\to a} \sqrt{2(x-a)}\, h(x), \quad k_2(b) = -\frac{2\mu}{1+\kappa} \lim_{x\to b} \sqrt{2(b-x)}\, h(x). \tag{26a-d}$$

The constants k_1 and k_2 are related to the asymptotic stress fields near the crack tips through the well-known expressions (see, for example, [4] and [5]). However, not so well-known is the asymptotic behavior of the stress fields near the inclusions having sharp edges. From (24c) and (7d) it is seen that the shear stress $\sigma_{r\theta}$ has a square-root singularity at the

tip of the inclusion. However, if one is interested in crack initiation around such singular points, one needs to know the direction and the magnitude of the maximum local cleavage stress. This, in turn, requires the investigation of the complete asymptotic stress field near the singular points. By using the basic form of the solution of the related density functions given by (24) and going back to the original stress expressions, the asymptotic stress fields may be developed by following the general techniques described in, for example, [6] or [7].

In an elastic medium containing an elastic line inclusion under plane strain or generalized plane stress conditions, the asymptotic analysis gives the near tip stress field as follows [7](*):

$$\sigma_{yy}(r,\theta) \cong \frac{k_1}{\sqrt{2r}} \cos\frac{\theta}{2} ,$$

$$\sigma_{xx}(r,\theta) \cong -\frac{3+\kappa}{\kappa-1} \frac{k_1}{\sqrt{2r}} \cos\frac{\theta}{2} ,$$

$$\sigma_{xy}(r,\theta) \cong -\frac{\kappa+1}{\kappa-1} \frac{k_1}{\sqrt{2r}} \sin\frac{\theta}{2} , \qquad (27a\text{-}c)$$

where x,y and r,θ are the standard rectangular and polar coordinates, the origin of coordinate axes is at the inclusion tip and the inclusion lies along the negative x axis or along $\theta=\pi$, $r>0$. Equations (27) suggest that similar to crack problems one may define a (Mode I) "stress intensity factor" in terms of the (tensile) cleavage stress as follows:

$$k_1 = \lim_{r\to 0} \sqrt{2r}\, \sigma_{yy}(r,0) . \qquad (28)$$

From (7) by observing that (at the right end of the inclusion)

$$\sigma_{xy}(r,+\pi) - \sigma_{xy}(r,-\pi) = -p(r) , \qquad (29)$$

(*) Note the misprints in (4.6) of [7].

in terms of the function $p(x)$ k_1 may be expressed as

$$k_1 = -\lim_{r\to 0} \frac{1}{2}\frac{\kappa-1}{\kappa+1}\sqrt{2r}\, p(r) \ . \tag{30}$$

It should be noted that in the case of flexible elastic line inclusions there is no antisymmetric singular stress field. For example, in a plane under pure shear (σ^{∞}_{xy}) parallel to the inclusion, the perturbed stress field is zero. Physically this of course follows from the fact that the normal strain (ε_{xx}) parallel to the plane of shear is zero.

Similarly, for a rigid line inclusion (i.e., for an inclusion having infinite bending as well as tensile stiffness) it can be shown that for small values of r the asymptotic stress field is given by

$$\sigma_{yy}(r,\theta) \cong \frac{1}{\sqrt{2r}}\left(k_1 \cos\frac{\theta}{2} + \frac{\kappa+1}{\kappa-1} k_2 \sin\frac{\theta}{2}\right) ,$$

$$\sigma_{xx}(r,\theta) \cong \frac{1}{\sqrt{2r}}\left(-\frac{3+\kappa}{\kappa-1} k_1 \cos\frac{\theta}{2} + \frac{3-\kappa}{\kappa-1} k_2 \sin\frac{\theta}{2}\right) , \tag{31a-c}$$

$$\sigma_{xy}(r,\theta) \cong \frac{1}{\sqrt{2r}}\left(-\frac{\kappa+1}{\kappa-1} k_1 \sin\frac{\theta}{2} + k_2 \cos\frac{\theta}{2}\right) \ .$$

Again, the stress intensity factors k_1 and k_2 are defined in terms of the tensile and shear cleavage stresses at $\theta=0$ plane as follows:

$$k_1 = \lim_{r\to 0} \sqrt{2r}\, \sigma_{yy}(r,0) \ , \ k_2 = \lim_{r\to 0} \sqrt{2r}\, \sigma_{xy}(r,0) \ . \tag{32a,b}$$

As in the crack problems, the antiplane shear component of the asymptotic stress field around flat elastic and rigid inclusions is uncoupled. Defining a Mode III stress intensity factor by

$$k_3 = \lim_{r\to 0} \sqrt{2r}\, \sigma_{xz}(r,0) \ , \tag{33}$$

the asymptotic stress field may be expressed as

$$\sigma_{xz}(r,\theta) \cong \frac{k_3}{\sqrt{2r}} \cos\frac{\theta}{2} ,$$

$$\sigma_{yz}(r,\theta) \cong \frac{k_3}{\sqrt{2r}} \sin\frac{\theta}{2} , \qquad (34a,b)$$

where again the inclusion lies along $\theta=\pi$ plane(*).

4. Crack-Inclusion Intersection

Analytically as well as from a practical viewpoint intersection of cracks and inclusions presents some interesting problems. In these problems the point of intersection is a point of irregular singularity with a power other than 1/2. Even though the general intersection problems for an arbitrary value of θ may be treated in a relatively straightforward manner, in this paper only some special cases will be considered.

4.1 The case of $\theta = \frac{\pi}{2}$, a = 0, c = 0

In this case the system of singular integral equations (20) becomes

$$\frac{1}{\pi}\int_0^b \frac{g(t)}{t-x}\,dt + \frac{1}{\pi}\int_0^d \left[\frac{c_1 t}{x^2+t^2} - \frac{c_2 t x^2}{(x^2+t^2)^2}\right]p(t)dt = f_1(x) , \quad (0<x<b) ,$$

$$\frac{1}{\pi}\int_0^b \frac{h(t)}{t-x}\,dt + \frac{1}{\pi}\int_0^d \left[\frac{c_2 x^3}{(x^2+t^2)^2} - \frac{c_1 x}{x^2+t^2}\right]p(t)dt = f_2(x) , \quad (0<x<b) ,$$

(*) Note that in this case if the remote stress is decomposed into σ^{∞}_{xz} and σ^{∞}_{yz}, the perturbed stress field due to σ^{∞}_{yz} would be zero. For the cleavage plane θ the shear cleavage stress may be written as $\sigma_{\theta_0}(r,\theta)=\sigma_{xz}\sin\theta-\sigma_{yz}\cos\theta= -(k_3/\sqrt{2r})\sin(\theta/2)$, $\theta_0 = \theta+\pi/2$, indicating that $\theta=\mp\pi/2$ is the maximum cleavage planes.

$$\frac{1}{\pi}\int_0^b \left[\frac{c_3 t}{t^2+r^2} + \frac{c_4 t r^2}{(t^2+r^2)^2}\right] g(t)dt + \frac{1}{\pi}\int_0^b \left[\frac{c_3 r}{t^2+r^2} - \frac{c_4 r t^2}{(t^2+r^2)^2}\right] h(t)dt$$

$$+ \frac{1}{\pi}\int_0^d \frac{p(t)}{t-r}\,dt + \frac{c_5}{\pi}\int_0^d H(t-r)p(t)dt = f_3(r)\ ,\ (0<r<d), \qquad (35a\text{-}c)$$

where

$$c_1 = \frac{3+\kappa}{4\mu}\ ,\ c_2 = \frac{1}{\mu}\ ,\ c_3 = \frac{\mu(\kappa-1)}{\kappa}\ ,$$

$$c_4 = \frac{4\mu}{\kappa}\ ,\ c_5 = \frac{\pi(1+\kappa)(1+\kappa_s)\mu}{4A_s\kappa\mu_s}\ , \qquad (36)$$

and f_1, f_2 and f_3 are known input functions (see, for example, the right hand side of (20)). Note that aside from the simple Cauchy kernels, (35) has kernels which become unbounded as the variables (t,x,r) approach the point of irregular singularity (x=0=t=r). Thus, defining the unknown functions by

$$g(t) = \frac{F_1(t)}{t^\alpha(b-t)^{\beta_1}}\ ,\ h(t) = \frac{F_2(t)}{t^\alpha(b-t)^{\beta_2}}\ ,\ p(t) = \frac{F_3(t)}{t^\alpha(c-t)^{\beta_3}}\ ,$$

$$0<\mathrm{Re}(\alpha,\beta_k)<1,\ (k=1,2,3)\ , \qquad (37a\text{-}c)$$

and by using the function-theoretic technique described in [3], the characteristic equations for β_1, β_2, β_3 and α may be obtained as follows:

$$\cot\pi\beta_k = 0\ ,\ (k = 1,2,3) \qquad (38)$$

$$b_1\cos^2\pi\alpha - (b_2+8\alpha-b_3\alpha^2)\cos^2\frac{\pi\alpha}{2}$$

$$-(b_4-b_5\alpha+b_3\alpha^2)\sin^2\frac{\pi\alpha}{2} = 0\ , \qquad (39)$$

where

$$b_1 = 8\kappa/(1+\kappa) \ , \ b_2 = 2(3+\kappa)(\kappa-1)/(\kappa+1) \ ,$$

$$b_3 = 8/(\kappa+1) \ , \ b_4 = 2(3-\kappa) \ , \ b_5 = 16/(1+\kappa) \ . \qquad (40)$$

Note that the properties of the inclusion (as expressed by the constant c_5 in (36)) enter the integral equations (35) only through a Fredholm kernel and, therefore, have no influence on the singular behavior of the solution, and α is dependent on κ or on the Poisson's ratio of the medium only. From (38) it is seen that the acceptable roots are $\beta_k = 0.5$, (k = 1,2,3). The numerical examination of (39) indicates that in this special case of $\theta = \frac{\pi}{2}$ we have $0.5<\alpha<1$, meaning that the stress state at r=0=x has a stronger singularity than the conventional crack tip singularity of $1/\sqrt{r}$. This may be due to the fact that in this problem two singular stress fields are combined at r=0. Also, it turns out that for $0<\nu\leq.5$ the characteristic equation (39) has two roots in $0<Re(\alpha)<1$ and both are real. These roots are given in Table 1 for various values of the Poisson's ratio.

Table 1. Powers of stress singularity α for a crack and an inclusion: a = 0, c = 0, $\theta = \pi/2$ (Fig. 1).

ν	plane strain		plane stress	
	α_1	α_2	α_1	α_2
0.0	0.63627093	0	0.63627093	0
0.1	0.64489401	0.09571474	0.64408581	0.08990596
0.2	0.65405762	0.14825371	0.65095281	0.13249000
0.3	0.66352760	0.18953334	0.65695651	0.16176440
0.4	0.67270080	0.22567265	0.66217253	0.18404447
0.5	0.67996342	0.26027940	0.66666667	0.20196313

The stress intensity factors at the crack tip x=b, y=0 and at the end of the inclusion x=0, y=d may be obtained by using the relations (26) and (30). At the singular point x=0, y=0 the following useful stress intensity factors are defined;

$$k_1(0) = \lim_{x\to-0} \sqrt{2}\, x^{\alpha}\, \sigma_{yy}(-0,0) \ ,$$

$$k_2(0) = \lim_{x\to-0} \sqrt{2}\, x^{\alpha}\, \sigma_{xy}(-0,0) \ , \qquad (41a,b)$$

for the crack, and

$$k_1(0) = \lim_{y\to+0} \frac{\sqrt{2}}{2}\, y^{\alpha}\, p(0,+0) \qquad (42)$$

for the inclusion.

4.2 The Special Case of $\theta = \frac{\pi}{2}$, $c = -d$, $a = 0$.

In this case the problem is further simplified by assuming "symmetric" external loads (for example, $\sigma_{xy}^{\infty}=0$ in (20)). Thus, the plane of the crack is a plane of symmetry, $h(x) = 0$, and (20) would reduce to

$$\frac{1}{\pi}\int_0^b \frac{g(t)}{t-x}\,dt + \frac{2}{\pi}\int_0^d \left[\frac{c_1 t}{t^2+x^2} - \frac{c_2 t x^2}{(t^2+x^2)^2}\right]p(t)dt = f_1(x), \ (0<x<b) \ ,$$

$$\frac{1}{\pi}\int_0^b \left[\frac{c_3 t}{t^2+y^2} + \frac{c_4 t y^2}{(t^2+y^2)^2}\right]g(t)dt + \frac{1}{\pi}\int_0^d \left[\frac{1}{t-y} + \frac{1}{t+y}\right.$$

$$\left. + c_5 H(t-y)\right]p(t)dt = f_3(y) \ , \ (0<y<d) \ , \qquad (43a,b)$$

where, again the input functions f_1 and f_3 are known and, for example, are given in (20) (with $\sigma_{xy}^{\infty} = 0$) and the constants $c_1,\ldots,c_5$ are defined by (36).

By defining

$$g(t) = \frac{G_1(t)}{t^{\alpha}(b-t)^{\beta_1}} \ , \ p(t) = \frac{G_2(t)}{t^{\alpha}(d-t)^{\beta_2}} \ , \ 0<\mathrm{Re}(\alpha,\beta_1,\beta_2)<1 \qquad (44)$$

from (43) it may be shown that

$$\cot\beta_k = 0 \ , \ (k=1,2) \ , \qquad (45)$$

$$\cos\pi\alpha-(c_3 + \frac{1}{2} c_4\alpha)(c_1 - \frac{1}{2} c_2\alpha) = 0 \ . \qquad (46)$$

From (45) it is seen that $\beta_k = 0.5$. A close examination of (46) shows that it has only one root for which $0<Re(\alpha)<1$. Furthermore, this root turns out to be real and highly dependent on the Poisson's ratio (see Table 2). The characteristic equation (46) and the roots given in Table 2 are identical to those found in [8] where an infinitely long stringer in cracked plate was considered.

Table 2. Power of stress singularity α at the crack-inclusion intersection for $\theta=\pi/2$, c=-d, a=0 and for symmetric loading.

ν	α	
	plane strain	plane stress
0	0	0
0.1	0.10964561	0.10263043
0.2	0.17432137	0.15468088
0.3	0.22678790	0.19132495
0.4	0.27392547	0.21972274
0.5	0.31955800	0.24288552

In this problem, too, the stress intensity factors for the crack and the inclusion may be defined as in (41) and (42).

4.3 The Special Case of $\theta=\pi$, a=0, c=0

In this case the crack and the inclusion are on the x axis and occupy (y=0, 0<x<b) and (y=0, -d<x<0), respectively. Restricting our attention again to the symmetric loading for which h(x) = 0 and observing that for the variables along the inclusion $r = -x$, $r_o = -t$, $p(r_o) = -p_x(t)$, the integral equations of the problem may be expressed as

$$\frac{1}{\pi}\int_0^b \frac{g(t)}{t-x}\,dt - \frac{1}{\pi}\frac{\kappa-1}{4\mu}\int_{-d}^{0}\frac{p_x(t)}{t-x}\,dt = f_1(x)\ ,\ (0<x<b)$$

$$\frac{c_3}{\pi}\int_0^b \frac{g(t)}{t-x}\,dt + \frac{1}{\pi}\int_{-d}^{0}\frac{p_x(t)}{t-x}\,dt - \frac{c_5}{\pi}\int_{-d}^{x} p_x(t)dt = f_3(x),\ (-d<x<0) \qquad (47a,b)$$

where the constants c_3 and c_5 are defined by (36) and the known functions f_1 and f_3 are given by the right hand sides of (20a) and (20c) (with $\sigma_{xy}^{\infty}=0$). If we now let

$$g(t) = \frac{H_1(t)}{t^{\alpha}(b-t)^{\beta_1}}\ ,\ p_x(t) = \frac{H_2(t)}{(-t)^{\alpha}(t+d)^{\beta_2}}\ ,\ 0<\mathrm{Re}(\alpha,\beta_1,\beta_2)<1\ , \qquad (48)$$

from (47) the characteristic equations for α, β_1 and β_2 may be obtained as follows:

$$\cot\pi\beta_k = 0\ ,\ (k = 1,2)\ , \qquad (49)$$

$$\cos 2\pi\alpha = -\left(\frac{\kappa-1}{2\sqrt{\kappa}}\right)^2\ . \qquad (50)$$

Equation (49) again gives $\beta_1 = \beta_2 = 0.5$. From (50) it may easily be seen that α is complex and its value for which $0<\mathrm{Re}(\alpha)<1$ is found to be

$$\alpha = \frac{1}{2} + i\left(\frac{\log\kappa}{2\pi}\right)\ . \qquad (51)$$

This value of α turns out to be identical to the power of singularity for a perfectly rough rigid stamp with a sharp corner pressed against an elastic half plane having κ as an elastic constant [2] (e.g., $\kappa = 3-4\nu$ for the plane strain case). At first this result may be somewhat unexpected. However, upon closer examination of the problem first, from (47b) it may be seen that the elasticity of the inclusion (i.e., the term containing the constant c_5) has no effect on the nature of the stress singularity. Thus, if one assumes the inclusion to be inextensible, for the symmetric problem under consideration it can be shown that the conditions in the neighborhood of the

crack tip x=0, y=0, for example, for y<0, are identical to the conditions around the corner of the stamp in the elastic half plane occupying y<0. It, therefore, appears that for the elastic inclusion collinear with a crack, the stress state around the common end point would have the standard complex singularity found in the rigid stamp problem.

5. The Results

The crack-inclusion problem described in previous sections is solved for a uniform stress state σ_{ij}^{∞}, (i,j=x,y), away from the crack-inclusion region. For simplicity the results are obtained by assuming one stress component (σ_{xx}^{∞} or σ_{yy}^{∞} or σ_{xy}^{∞}) to be nonzero at a time. The solution for a more general loading may then be obtained by superposition. Even though the stress state everywhere in the plane can be calculated after solving the integral equations (e.g., (20)) and determining the density functions g, h, and p, only the stress intensity factors are given in this section. For nonintersecting cracks and inclusions the stress intensity factors defined by (26) and (28) are normalized as follows:

$$k_i'(x_j) = \frac{k_i(x_j)}{\sigma_a^{\infty}\sqrt{(b-a)/2}} \quad , \quad (i=(1,2);\ x_j=(a,b);\ \sigma_a^{\infty}=(\sigma_{yy}^{\infty},\sigma_{xx}^{\infty},\sigma_{xy}^{\infty})), \tag{52}$$

for the crack and

$$k_1'(r_j) = \frac{k_1(r_j)}{k_o} \ , \ k_o = \frac{1-\kappa}{2(1+\kappa)}\ \sigma_a^{\infty}\ \sqrt{(d-c)/2} \ ,$$

$$(r_j = (c,d) \ , \ \sigma_a^{\infty} = (\sigma_{yy}^{\infty},\ \sigma_{xx}^{\infty},\ \sigma_{xy}^{\infty})) \tag{53}$$

for the inclusion.

Referring to Figure 1, for c=a, d=b, and (b/a)=5 the effect of the angle θ on the stress intensity factors is shown in Table 3. These results are given for two values of the stiffness parameter γ defined by (21), namely γ=0 (the inextensible inclusion) and γ=10.

Table 3. Normalized stress intensity factors in a plane containing a crack and an inclusion subjected to a uniform stress state σ^{∞}_{ij} away from the crack-inclusion region (c=a,d=b,a=b/5,Fig. 1).

γ	k'	θ						
		1°	30°	60°	90°	120°	150°	180°
		(a) $\sigma^{\infty}_{yy} \neq 0$, $\sigma^{\infty}_{xx} = 0$, $\sigma^{\infty}_{xy} = 0$						
0	$k_1'(a)$	.8905	1.0083	1.0298	1.0049	.9912	1.0001	1.0076
	$k_2'(a)$	-.2152	-.0098	-.0661	-.0830	-.0367	.0004	.0000
	$k_1'(b)$	1.0221	.9967	.9570	.9617	.9857	1.0001	1.0033
	$k_2'(b)$	.4327	-.0065	-.0002	.0007	-.0001	.0001	.0000
	$k_1'(c)$	.9570	-.3273	-1.1324	-1.3970	-.8879	-.0310	.3850
	$k_1'(d)$	.8012	.1552	-.6989	-1.1134	-.7336	.0428	.4320
10	$k_1'(a)$	.9691	.9999	1.0016	.9988	.9978	1.0000	1.0014
	$k_2'(a)$	-.0517	-.0047	-.0136	-.0153	-.0066	.0001	.0000
	$k_1'(b)$	.9862	.9997	.9919	.9928	.9973	1.0000	1.0006
	$k_2'(b)$	.0742	-.0020	.0001	.0005	.0002	.0000	.0000
	$k_1'(c)$	.2619	-.1277	-.3979	-.4735	-.2989	-.0220	.1106
	$k_1'(d)$	-.0269	.1001	-.1848	-.3269	-.2177	.0171	.1354
		(b) $\sigma^{\infty}_{xx} \neq 0$, $\sigma^{\infty}_{yy} = 0$, $\sigma^{\infty}_{xy} = 0$						
0	$k_1'(a)$	.1237	.0704	-.0034	-.0034	.0008	-.0117	-.0203
	$k_2'(a)$	.2355	.0122	.0052	.0310	.0036	-.0161	.0000
	$k_1'(b)$	-.0806	-.0365	.0036	.0142	.0014	-.0072	-.0086
	$k_2'(b)$	-.5321	-.0140	.0001	.0001	.0000	-.0003	.0000
	$k_1'(c)$	-1.1068	-.6949	.0766	.4620	.0774	-.6988	-1.0877
	$k_1'(d)$	-1.4785	-.6941	.0772	.4644	.0776	-.6994	-.0884
10	$k_1'(a)$	.0385	.0106	-.0005	-.0001	.0002	-.0023	-.0038
	$k_2'(a)$	.0587	.0004	.0010	.0056	.0006	.0029	.0000
	$k_1'(b)$	-.0252	-.0068	.0007	.0026	.0003	-.0013	-.0016
	$k_2'(b)$	-.1128	-.0030	.0000	.0000	.0000	.0000	.0000
	$k_1'(c)$	-.3440	-.2152	.0239	.1432	.0239	-.2151	-.3346
	$k_1'(d)$	-.3885	-.2154	.0239	.1434	.0239	-.2151	-.3347

Table 3 - cont.

γ	k'	θ						
		1°	30°	60°	90°	120°	150°	180°
		(c) $\sigma^{\infty}_{yy} \neq 0$, $\sigma^{\infty}_{xx} = 0$, $\sigma^{\infty}_{xy} = 0$						
0	$k'_1(a)$	.1289	.1428	.0669	.0028	.0134	.0223	0.0000
	$k'_2(a)$	1.0849	1.0180	.9054	.9950	1.0599	1.0304	1.0000
	$k'_1(b)$	.1641	-.0754	-.0670	-.0021	0.0231	.0136	0.0000
	$k'_2(b)$	1.4055	.9685	.9974	.9995	1.0005	1.0005	1.0000
	$k'_1(c)$	-1.0246	-1.6348	-1.3085	.0533	1.3767	1.3606	0.0000
	$k'_1(d)$	2.0539	-1.3808	-1.4661	-.1076	1.2735	.3117	.0000
10	$k'_1(a)$	.0858	.0198	.0100	.0010	.0032	.0043	.0000
	$k'_2(a)$	1.0527	.9967	.9826	.9992	1.0108	1.0054	1.0000
	$k'_1(b)$	.1044	-.0140	-.0121	-.0003	.0043	.0025	.0000
	$k'_2(b)$	1.1662	.9929	.9994	.9998	.9999	1.0000	1.0000
	$k'_1(c)$	-.6916	-.5492	-.3731	.0557	.4513	-.4316	.0000
	$k'_1(d)$	1.1639	-.4179	-.4533	-.0342	.3912	-.4029	.0000

Some sample results for an inclusion collinear with a crack (i.e, for $\theta=0$) are given in Table 4. Note that for this configuration under the

Table 4. Normalized stress intensity factors for an inclusion collinear with a crack. Relative dimensions: $\theta=0$, d-c = b-a, c = b+s. Applied loads: σ^{∞}_{ij}, (i,j=x,y) (Fig. 1).

σ^{∞}_{ij}	k'	s = (b-a)/100		s = (b-a)/2	
		γ = 0	γ = 10	γ = 0	γ = 10
σ^{∞}_{xx}	$k_1'(a)$	-0.0202	-0.0040	-0.0019	-0.0004
	$k_1'(b)$	-0.1338	-0.0300	-0.0027	-0.0005
	$k_1'(c)$	-1.0482	-0.3296	-1.0889	-0.3347
	$k_1'(d)$	-1.0845	-0.3345	-1.0889	-0.3347
σ^{∞}_{yy}	$k_1'(a)$	1.0047	1.0006	1.0008	1.0002
	$k_1'(b)$	1.0200	0.9987	1.0011	1.0002
	$k_1'(c)$	-0.0861	-0.1571	0.4559	0.1397
	$k_1'(d)$	0.3841	0.1273	0.4590	0.1413

loads shown in the table, that is, for σ^{∞}_{yy} and σ^{∞}_{xx}, because of symmetry the Mode II stress intensity factors $k_2(a)$ and $k_2(b)$ are zero. Also, for the shear loading σ^{∞}_{xy} it is found that $k_2'(a) = 1$, $k_2'(b) = 1$ and $k_1(a) = k_1(b) = k_1(c) = k_1(d) = 0$. This follows from the fact that in the cracked plane under pure shear σ^{∞}_{xy} the strain component $\varepsilon_{xx}(x,0)$ is zero and hence an inextensible inclusion on the x axis would have no effect on the stress distribution.

Another special configuration is an inclusion parallel to the crack for which Table 5 shows some sample results. In the two special configurations considered in Tables 4 and 5 the effect of the crack-inclusion interaction on the stress intensity factors does not seem to be very significant.

The results for an elastic medium for which xz plane is a plane of symmetry with respect to the crack-inclusion geometry as well as the

Table 5. Normalized stress intensity factors in a plane containing an inclusion parallel and equal in length to a crack, both symmetrically located with respect to the y axis. The crack is along the x axis and H is the distance between the crack and the inclusion in y direction (Fig. 1).

σ^{∞}_{ij}	k'	H = b-a		H = 10(b-a)	
		γ = 0	γ = 10	γ = 0	γ = 10
σ^{∞}_{xx}	$k'_1(a)=k'_1(b)$	-0.0182	-0.0070	-0.0007	-0.0002
	$k'_2(a)=-k'_2(b)$	0.0281	-0.0011	0.0006	0.0000
	$k'_1(c)=k'_1(d)$	-1.0834	-1.0887	-0.0683	-0.0683
σ^{∞}_{yy}	$k'_1(a)=k'_1(b)$	1.0063	1.0028	1.0004	1.0001
	$k'_2(a)=-k'_2(b)$	-0.0060	0.0004	-0.0001	0.0000
	$k'_1(c)=k'_1(d)$	0.3917	0.4387	0.0411	0.0276
σ^{∞}_{xy}	$k'_1(a)=-k'_1(b)$	-0.0042	0.0000	-0.0002	0.0000
	$k'_2(a)=k'_2(b)$	0.9965	1.0000	0.9998	1.0000
	$k'_1(c)$	-0.1131	0.0033	-0.0123	0.0004
	$k'_1(d)$	0.1129	-0.0052	0.0123	-0.0006

applied loads are given in Figures 2-12. In this example the crack is perpendicular to the inclusion and the external load is a uniform tension parallel or perpendicular to the crack and away from the crack-inclusion region (see the insert in the figures). The results shown in the figures are self-explanatory. However, the solution also has some unusual features among which, for example, one may mention the tendency of the crack tip stress intensity factors k'(a) and k'(b) to "peaking" as γ decreases and as d/ℓ increases (where 2d and 2ℓ are the lengths of the inclusion and the crack, respectively and $\gamma = 0$ corresponds to an inextensible inclusion).

The results for the limiting case of the crack touching the inclusion are given in Figures 8-12. In this case at the singular point x=0, y=0 the stress intensity factor $k_1(a)$ and the normalized stress intensity factor $k_1'(a)$ are defined by

$$k_1(a) = \lim_{x\to 0^-} \sqrt{2}\, x^{\alpha}\sigma_{yy}(x,0) \ , \ (x < 0) \ , \tag{54}$$

$$k_1'(a) = k(a)/\sigma_{ij}^{\infty}\sqrt{\ell} \ , \ (i=(x,y);\ \ell=b/2) \tag{55}$$

where the power of singularity α is given in Table 2. The results shown in Figures 8-12 are obtained for $\nu = 0.3$.

The stress intensity factors for the other symmetric crack inclusion problem, namely for the problem in which y axis is the line of symmetry with regard to loading and geometry are given in Figures 13-28. In this problem $a=-\ell$, $b=\ell$, $d>c>0$ and the external load is either σ_{yy}^{∞} or σ_{xx}^{∞} (see the insert in Figure 13). Note that the figures show the crack tip stress intensity factors at $x=a=-\ell$ and $k_1(b)=k_1(a)$, $k_2(b)=-k_2(a)$. Generally the magnitude of $k_1(a)$ and $k_2(a)$ seem to increase with increasing length and stiffness of the inclusion (i.e., with increasing $(d-c)/2\ell$ and decreasing $\gamma = \mu(1+\kappa_s)/A_s\mu_s(1+\kappa)$, where μ_s is the shear modulus of the inclusion). Also, as expected, $k_1(c)$ and $k_1(d)$ describing the intensity of the stress field at inclusion ends tend to increase as the stiffness of the inclusion increases. However, their dependence on the relative length parameters is somewhat more complicated (see, for example, Figure 16 for change in behavior of the variation of $k_1(d)$ at $(d-c)/2\ell=5$). Figures 13-20 show the effect

of the inclusion length for constant crack length 2ℓ and constant distance c (Figure 13). The effect of the distance c for constant inclusion and crack lengths is shown in Figures 13-28.

The results of the nonsymmetric problem showing the effect of the relative location of the inclusion are shown in Table 6. Referring to Figure 1, in these calculations it is assumed that $\theta = \frac{\pi}{2}$, $d-c = 2\ell$, $c/2\ell = 0.1$ and $a/2\ell$ is variable.

Finally, the stress intensity factors for the crack-inclusion intersection problem considered in Section 4.1 are given in Figures 29-43. The normalized stress intensity factors shown in these figures are defined by (see (41), (52) and (53))

$$k'_{1B} = \frac{1}{\sigma^{\infty}_{ij}\sqrt{\ell}} \lim_{x\to b} \sqrt{2(x-b)}\, \sigma_{yy}(x,0) ,$$

$$k'_{2B} = \frac{1}{\sigma^{\infty}_{ij}\sqrt{\ell}} \lim_{x\to b} \sqrt{2(x-b)}\, \sigma_{xy}(x,0) ,$$

$$k'_{1A} = \frac{1}{\sigma^{\infty}_{ij}\sqrt{\ell}} \lim_{x\to -0} \sqrt{2}\, x^{\alpha}\, \sigma_{yy}(-0,0) ,$$

$$k'_{2A} = \frac{1}{\sigma^{\infty}_{ij}\sqrt{\ell}} \lim_{x\to -0} \sqrt{2}\, x^{\alpha}\, {}_{xy}(-0,0) , \qquad (56)$$

$$k'_{1D} = \frac{1}{k_o} \lim_{y\to d} \sqrt{2(y-d)}\, \sigma_{xx}(0,y) ,$$

$$k_o = \frac{1-\kappa}{2(1+\kappa)}\, \sigma^{\infty}_{ij}\, \sqrt{d/2} \quad .$$

In this case too, generally the magnitude of the stress intensity factors increases with increasing length and stiffness of the inclusion. However, since the crack and the inclusion are located in each other's "shadow", the relative dimensions seem to have considerable influence on the variation as well as the magnitude of the stress intensity factors.

Table 6. The effect of the relative location of inclusion on the stress intensity factors; $\theta = \pi/2$, $(d-c)/2\ell = 1$, $c/2\ell = 0.1$ (Figure 1).

σ^{∞}_{ij}	$\frac{a}{2\ell}$	$k_1'(a)$	$k_2'(a)$	$k_1'(b)$	$k_2'(b)$	$k_1'(c)$	$k_1'(d)$
σ^{∞}_{xx}	0.1	-0.0202	0.0490	0.0161	0.0003	0.4450	0.4471
	0.0	-0.1033	0.0425	0.0133	0.0039	0.4192	0.4402
	-0.1	-0.0849	-0.0044	0.0076	0.0081	0.3538	0.4285
	-0.3	-0.0349	-0.0308	0.0023	0.0060	0.3348	0.4163
	-0.5	-0.0363	-0.0114	-0.0363	0.0114	0.3195	0.4109
σ^{∞}_{yy}	+0.1	1.0458	-0.1396	0.9545	0.0012	-1.5217	-1.0543
	0.0	1.2652	-0.1090	0.9667	-0.0078	-1.2922	-0.9497
	-0.1	1.1548	0.0064	0.9865	-0.0150	-0.5345	-0.8136
	-0.3	1.0448	0.0294	1.0013	-0.0102	-0.2308	-0.6378
	-0.5	1.0313	0.0129	1.0313	-0.0129	-0.1959	-0.5801
σ^{∞}_{xy}	0.1	0.0098	0.9905	-0.0033	0.9992	0.1050	-0.1338
	0.0	0.0493	0.9796	-0.0065	0.9983	-0.1734	-0.1675
	-0.1	0.0463	1.0019	-0.0041	0.9960	-0.1054	-0.1648
	-0.3	0.0123	1.0066	-0.0007	0.9971	-0.0236	-0.0977
	-0.5	0	1	0	1	0	0

References

1. F. Erdogan and G.D. Gupta, "The Inclusion Problem with a Crack Crossing the Boundary", Int. J. of Fracture, Vol. 11, pp. 13-27, 1975.

2. I.N. Muskhelishvili, Some Basic Problems of the Mathematical Theory of Elasticity, Noordhoff, Groningen, The Netherlands, 1953.

3. F. Erdogan, "Mixed Boundary Value Problems in Mechanics", Mechanics Today, Vol. 4, S. Nemat-Nasser, ed. pp. 1-86, Pergamon Press Inc., 1978.

4. G.R. Irwin, "Analysis of Stresses and Strains Near the End of a Crack Traversing a Plate", J. Appl. Mech., Vol. 24, Trans. ASME, pp. 361-364, 1957.

5. M.L. Williams, "On the Stress Distribution at the Base of a Stationary Crack", J. Appl. Mech., Vol. 24, Trans. ASME, pp. 109-114, 1957.

6. F. Delale and F. Erdogan, "Transverse Shear Effect in a Circumferentially Cracked Cylindrical Shell", Quarterly of Applied Mathematics, Vol. 37, pp. 239-258, 1979.

7. F. Erdogan and G.D. Gupta, "Stresses near a Flat Inclusion in Bonded Dissimilar Materials", Int. J. Solids Structures, Vol. 8, pp. 533-547, 1972.

8. O.S. Yahsi and F. Erdogan, "A Note on the Cracked Plates Reinforced by a Line Stiffener", Engineering Fracture Mechanics, (to appear) 1984.

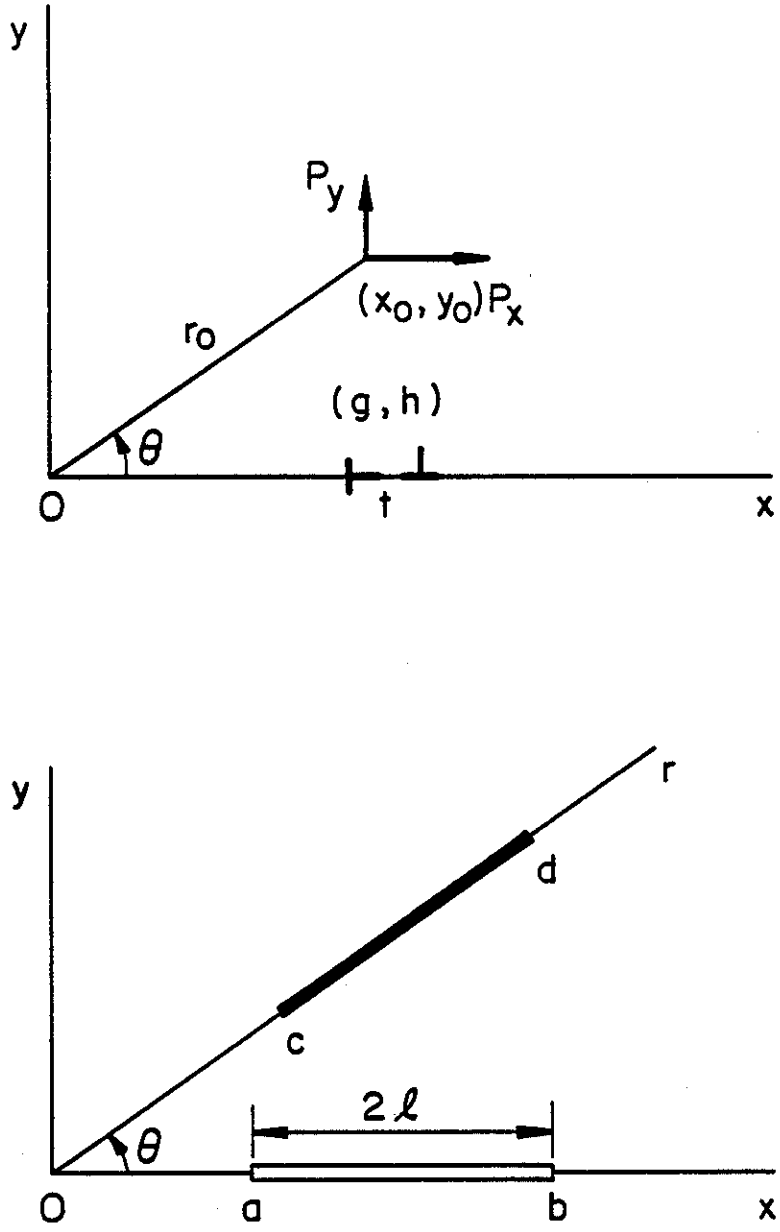

Figure 1. The geometry and notation for the crack-inclusion problem.

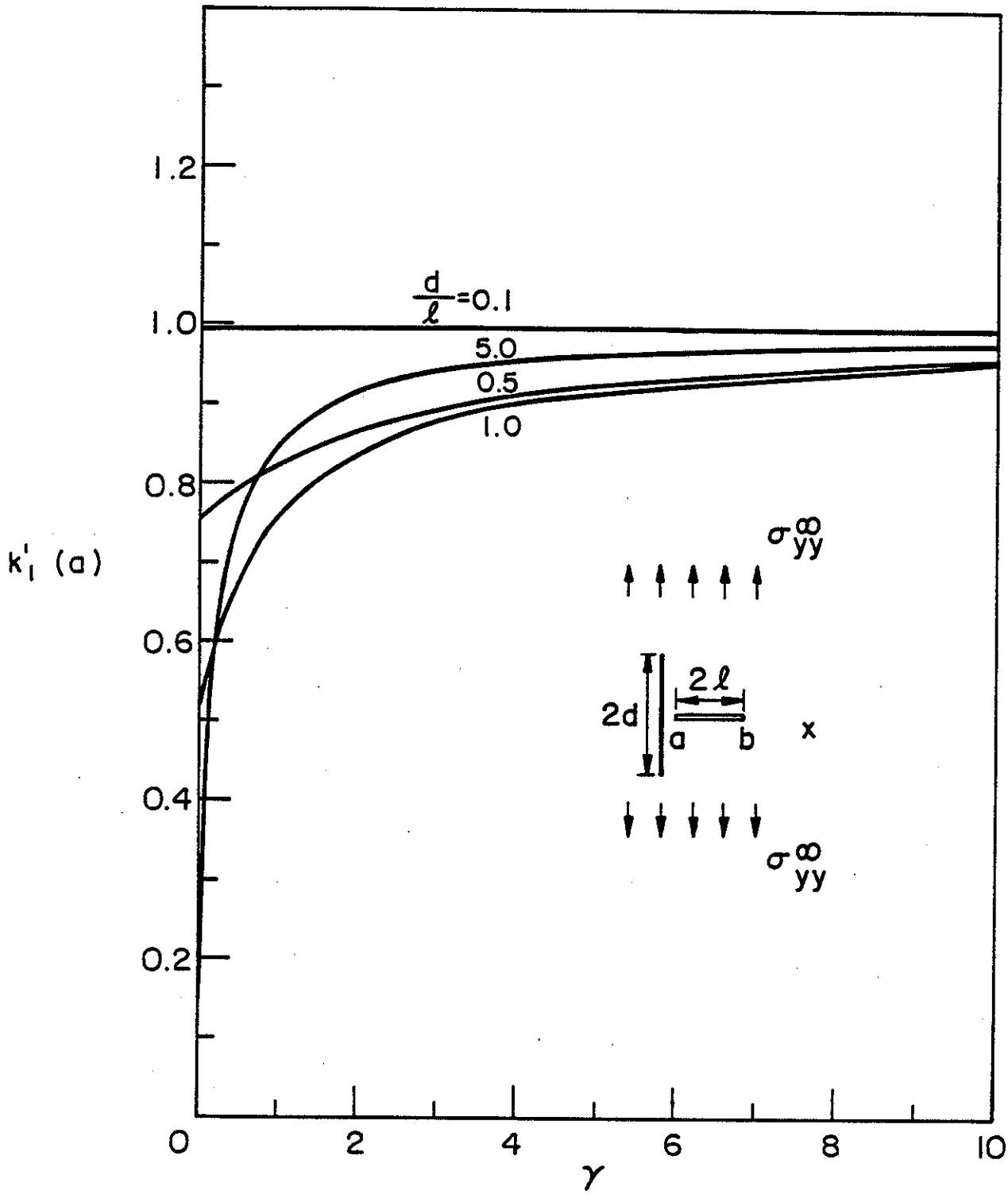

Figure 2. The effect of the stiffness and the relative length of the inclusion on the normalized stress intensity factor $k_I'(a)$; $\sigma_{yy}^{\infty} \neq 0$, $\sigma_{xx}^{\infty} = 0$, $\sigma_{xy}^{\infty} = 0$; $a/\ell = 0.5$, $\nu = 0.3$.

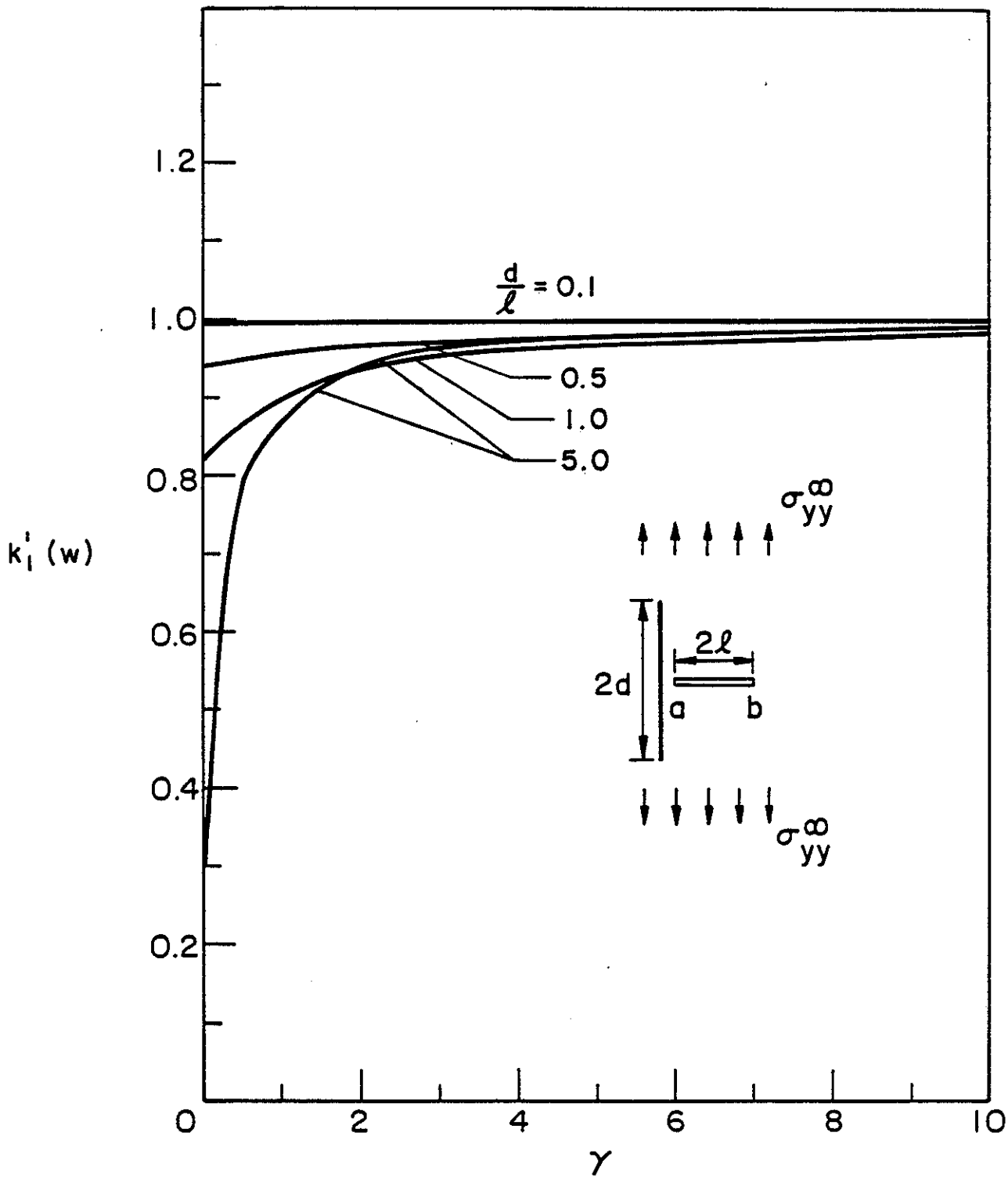

Figure 3. Normalized stress intensity factor $k_1'(b)$; $\sigma^{\infty}_{yy} \neq 0$, $\sigma^{\infty}_{xx} = 0 = \sigma^{\infty}_{xy}$, $a/\ell = 0.5$, $\nu = 0.3$.

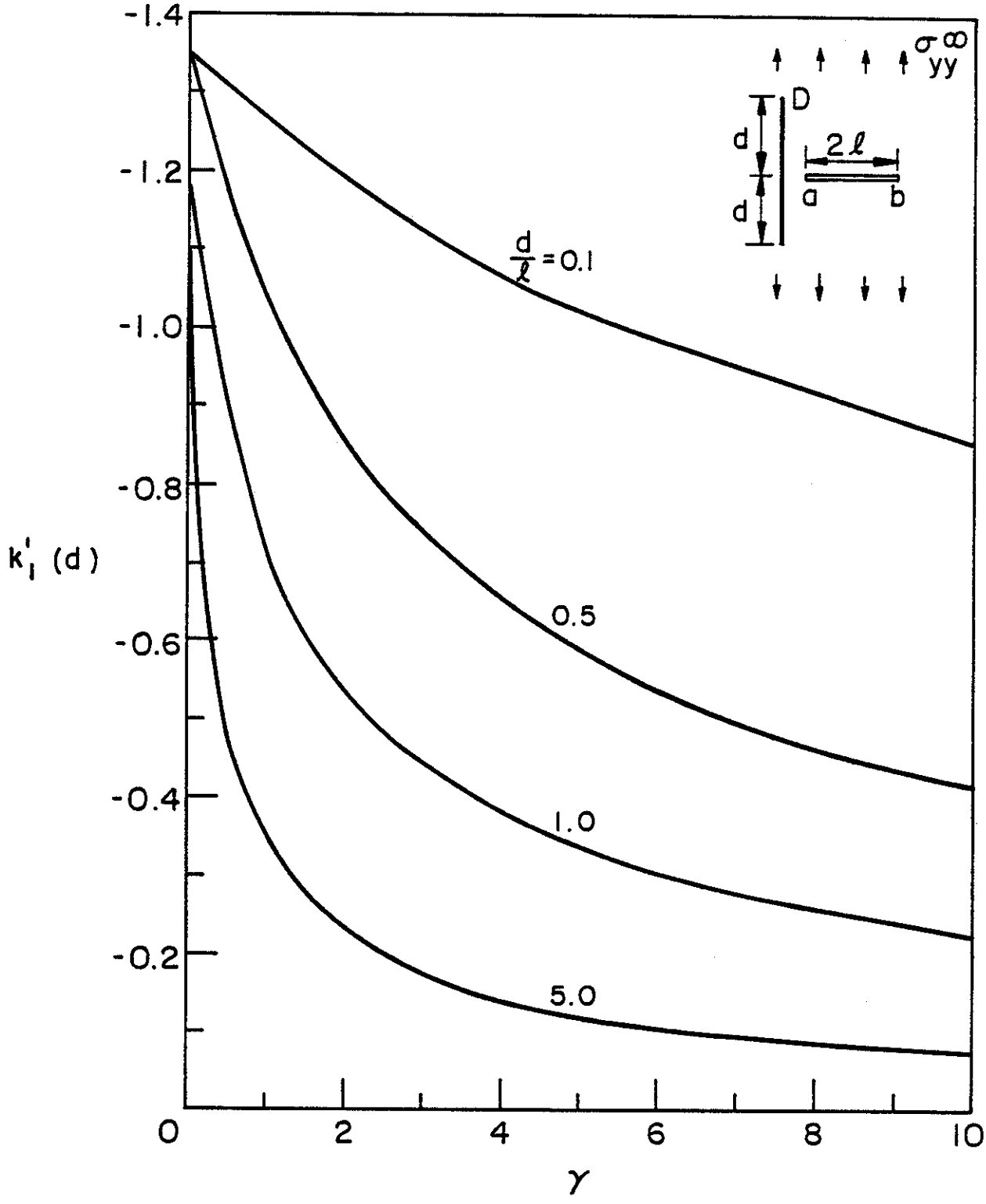

Figure 4. Normalized stress intensity factor at the inclusion end y=d; $\sigma_{yy}^{\infty} \neq 0$, $\sigma_{xx}^{\infty} = \sigma_{xy}^{\infty} = 0$, $a/\ell = 0.5$, $\nu = 0.3$.

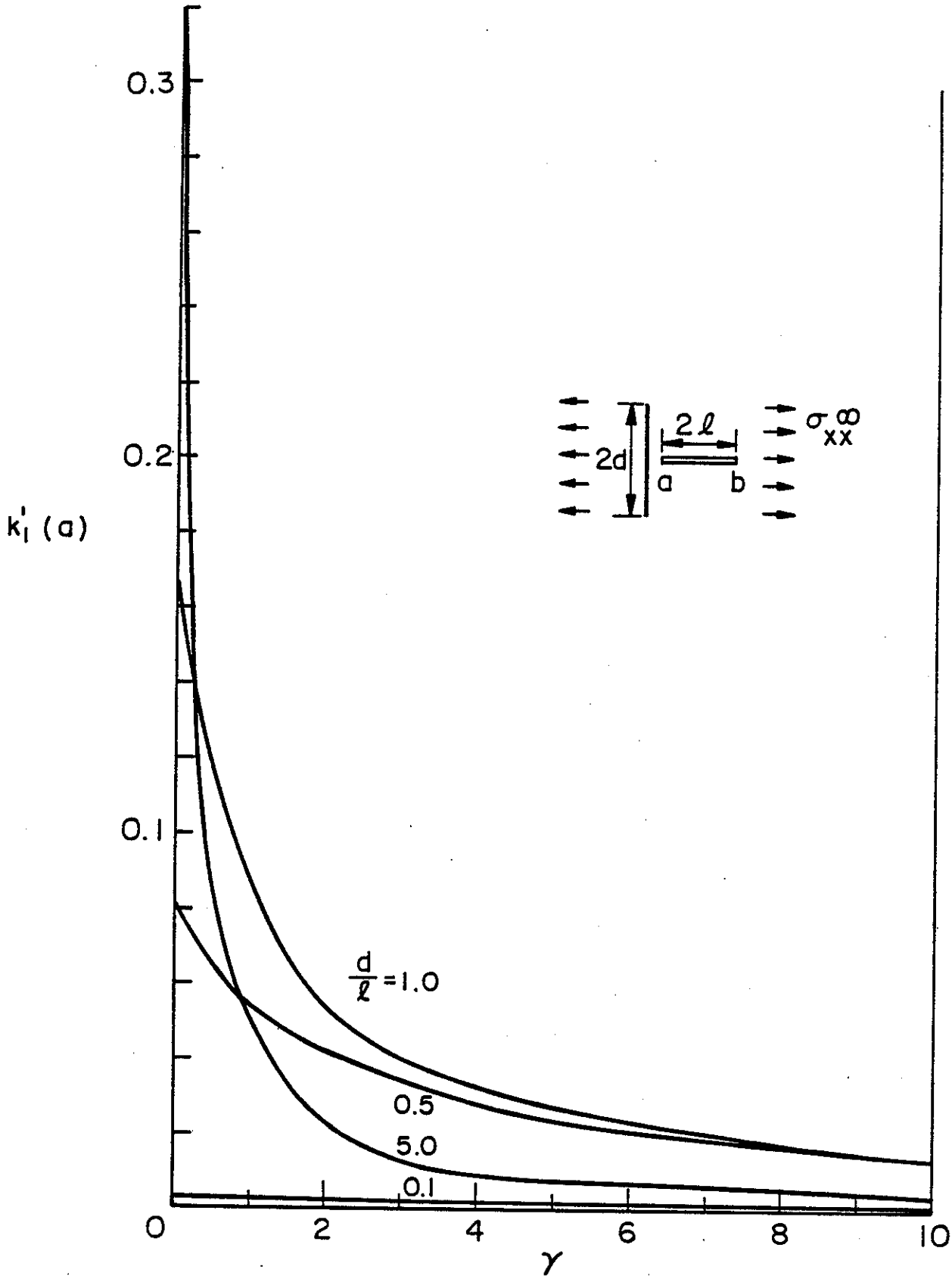

Figure 5. Normalized stress intensity factor at the crack tip x=a; $\sigma_{xx}^{\infty} \neq 0$, $\sigma_{yy}^{\infty} = \sigma_{xy}^{\infty} = 0$, $a/\ell = 0.5$, $\nu = 0.3$.

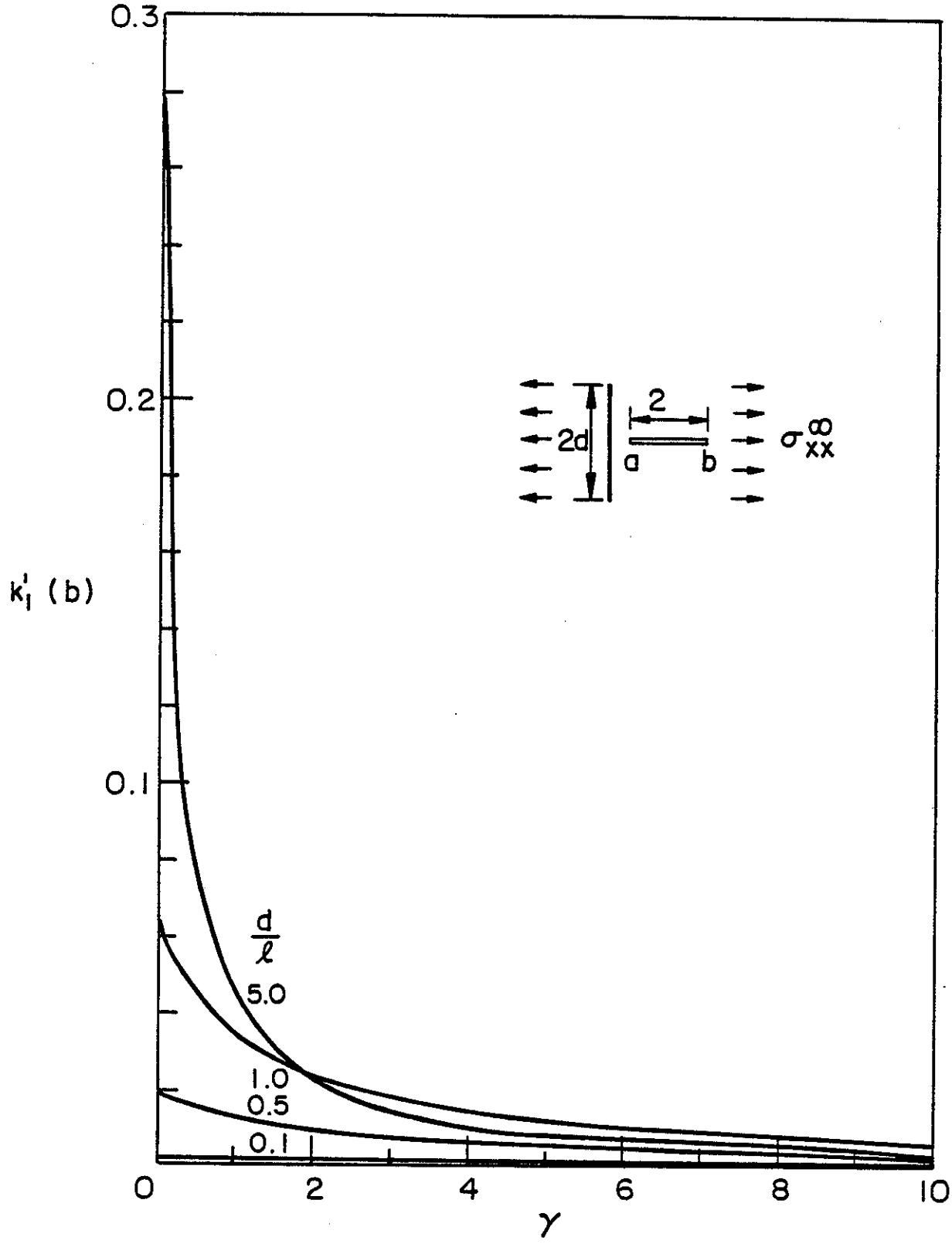

Figure 6. Normalized stress intensity factor at the crack tip x=b; $\sigma_{xx}^{\infty} \neq 0$, $\sigma_{yy}^{\infty} = \sigma_{xy}^{\infty} = 0$, $a/\ell = 0.5$, $\nu = 0.3$.

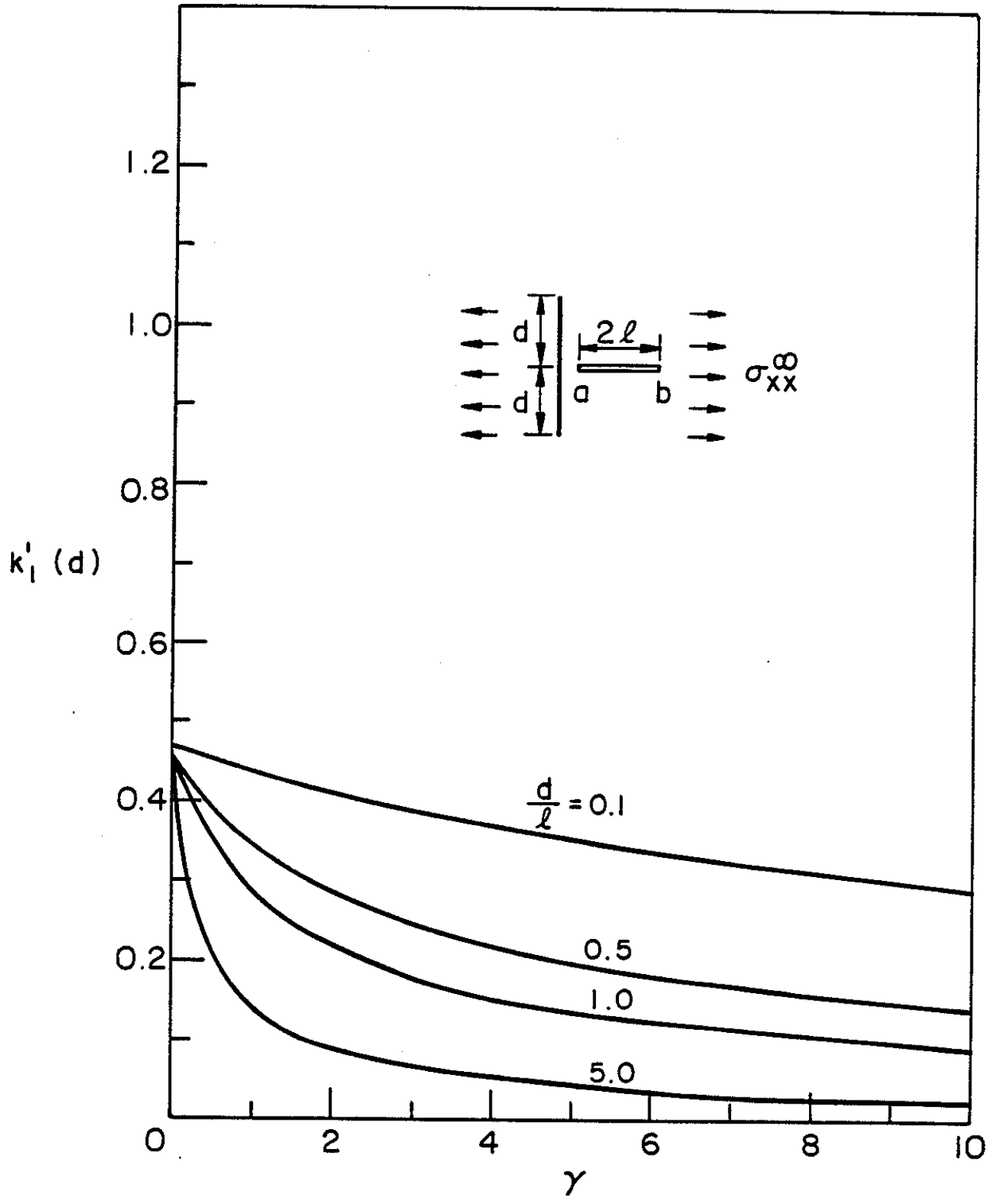

Figure 7. Normalized stress intensity factor at the inclusion end y=d; $\sigma_{xx}^{\infty} \neq 0$, $\sigma_{yy}^{\infty} = \sigma_{xy}^{\infty} = 0$, $a/\ell = 0.5$, $\nu = 0.3$.

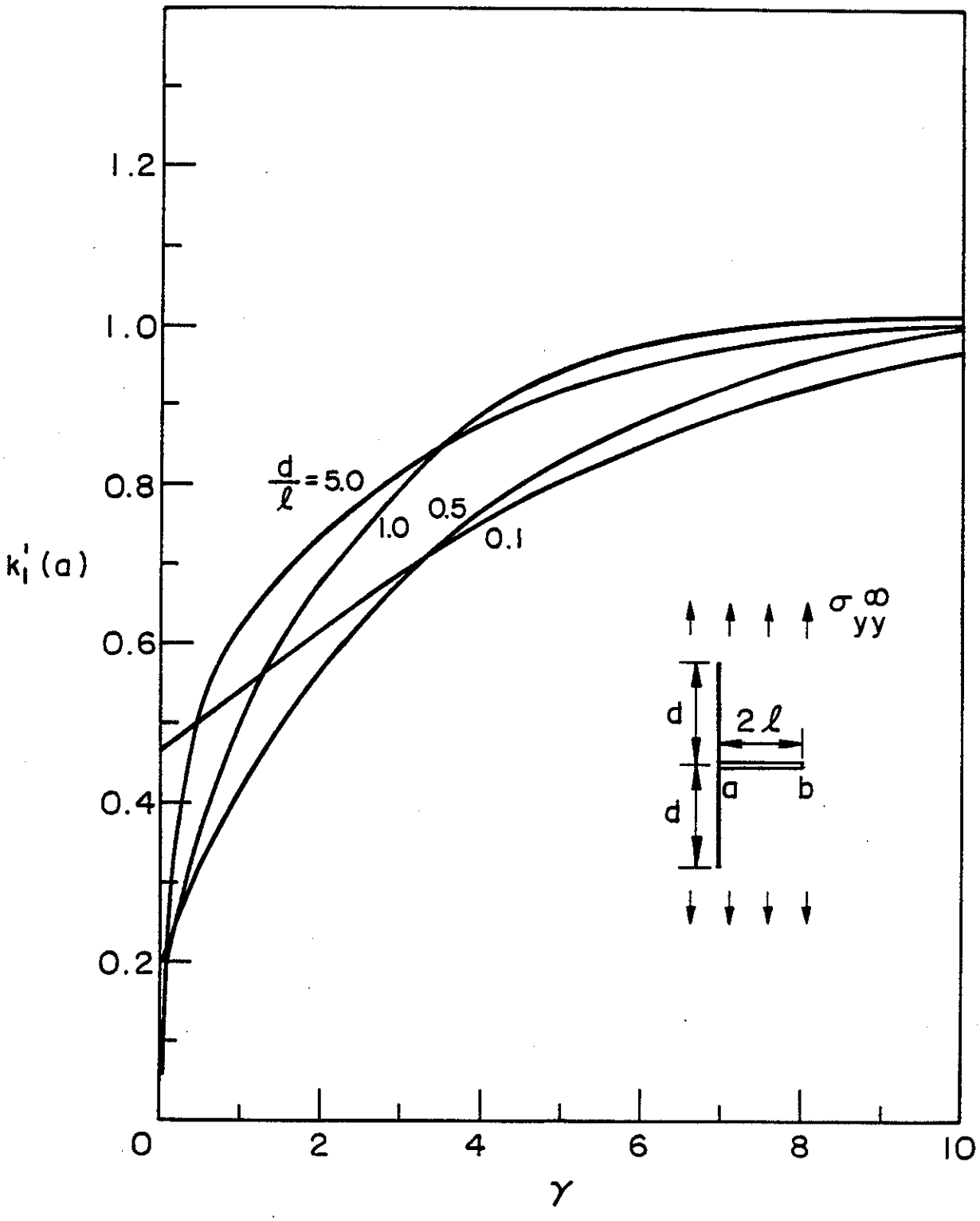

Figure 8. Normalized stress intensity factor at the crack tip x=a=0, $\sigma_{yy}^{\infty} \neq 0$, $\sigma_{xx}^{\infty} = \sigma_{xy}^{\infty} = 0$, $\nu = 0.3$.

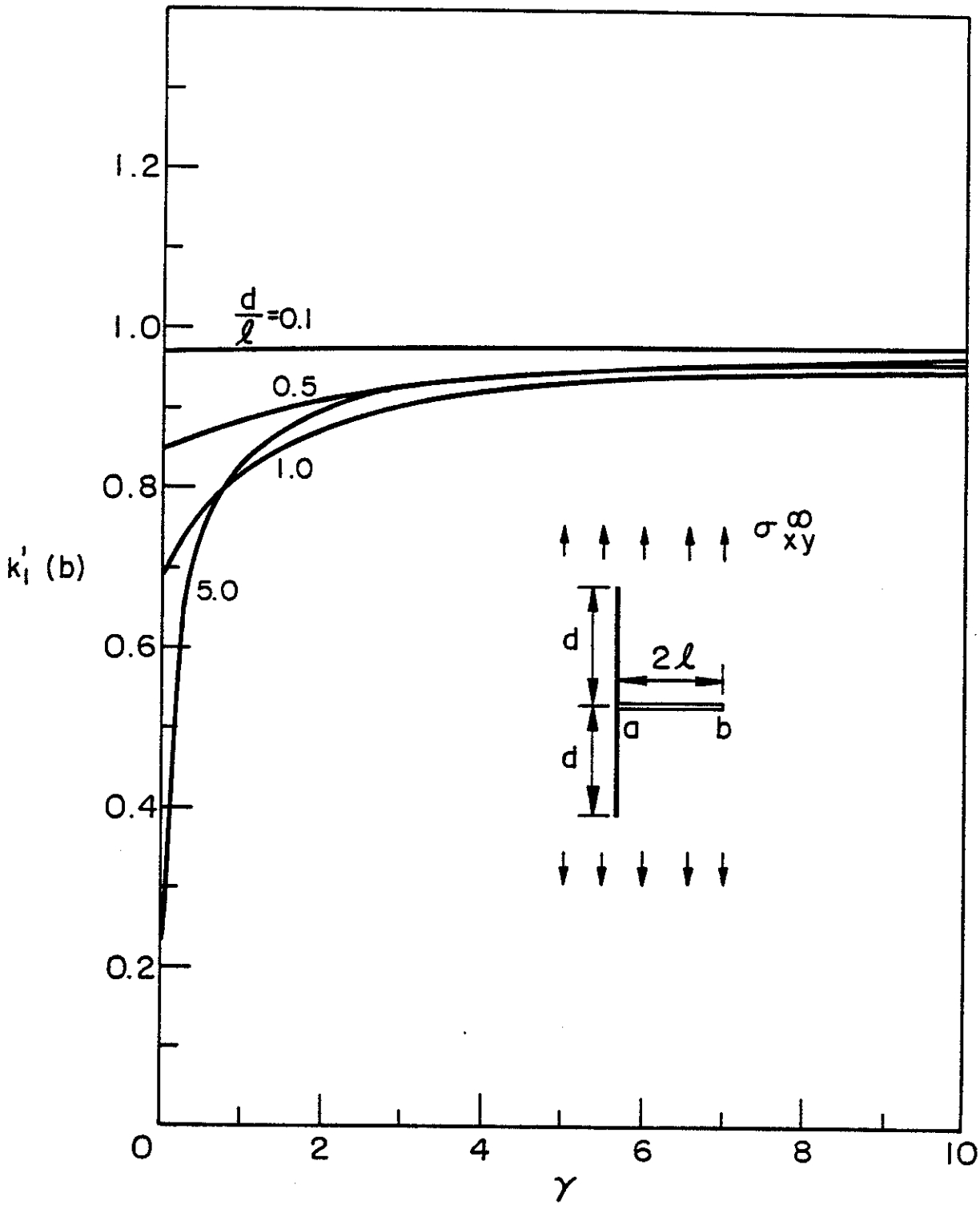

Figure 9. Normalized stress intensity factor at the crack tip x=b, $\sigma^{\infty}_{yy} \neq 0$, $\sigma^{\infty}_{xx} = \sigma^{\infty}_{xy} = 0$, $\nu = 0.3$, a = 0.

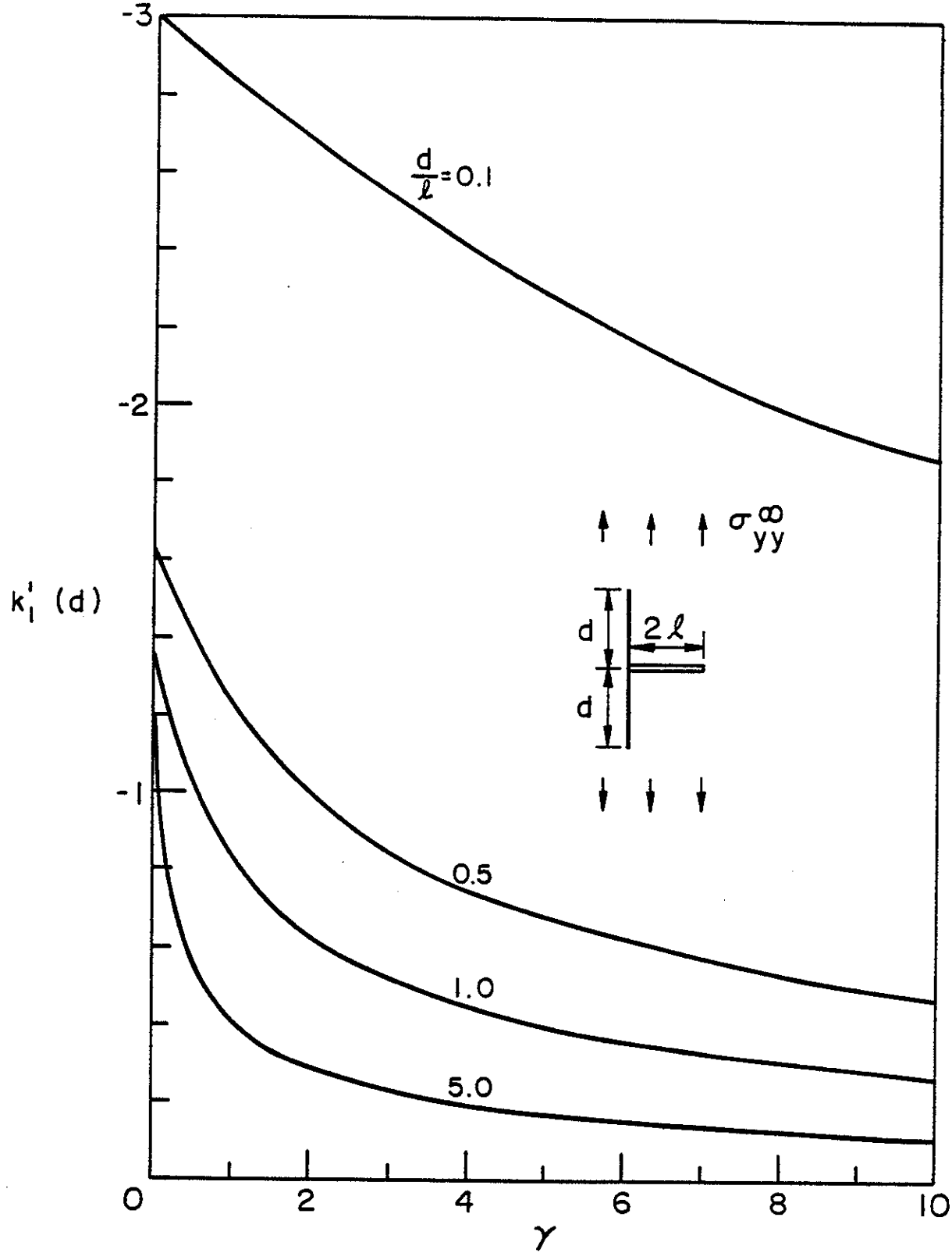

Figure 10. Normalized stress intensity factor at the inclusion end y=d, $\sigma_{yy}^{\infty} \neq 0$, $\sigma_{xx}^{\infty} = \sigma_{xy}^{\infty} = 0$, $\nu = 0.3$, $a = 0$.

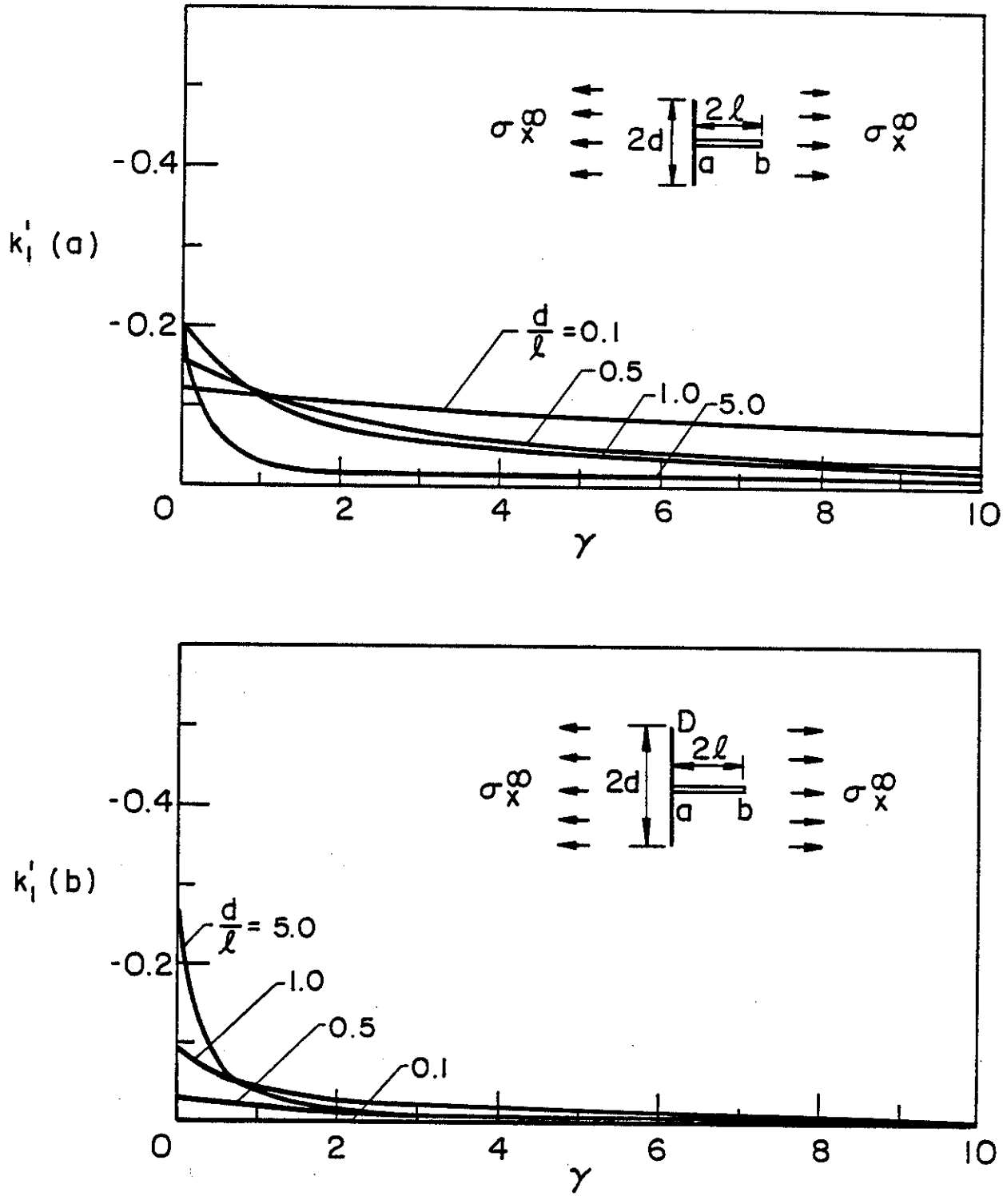

Figure 11. Normalized stress intensity factors at the crack tips x=a=0 and x=b; $\sigma_{xx}^\infty \neq 0$, $\sigma_{yy}^\infty = \sigma_{xy}^\infty = 0$, a = 0, ν = 0.3.

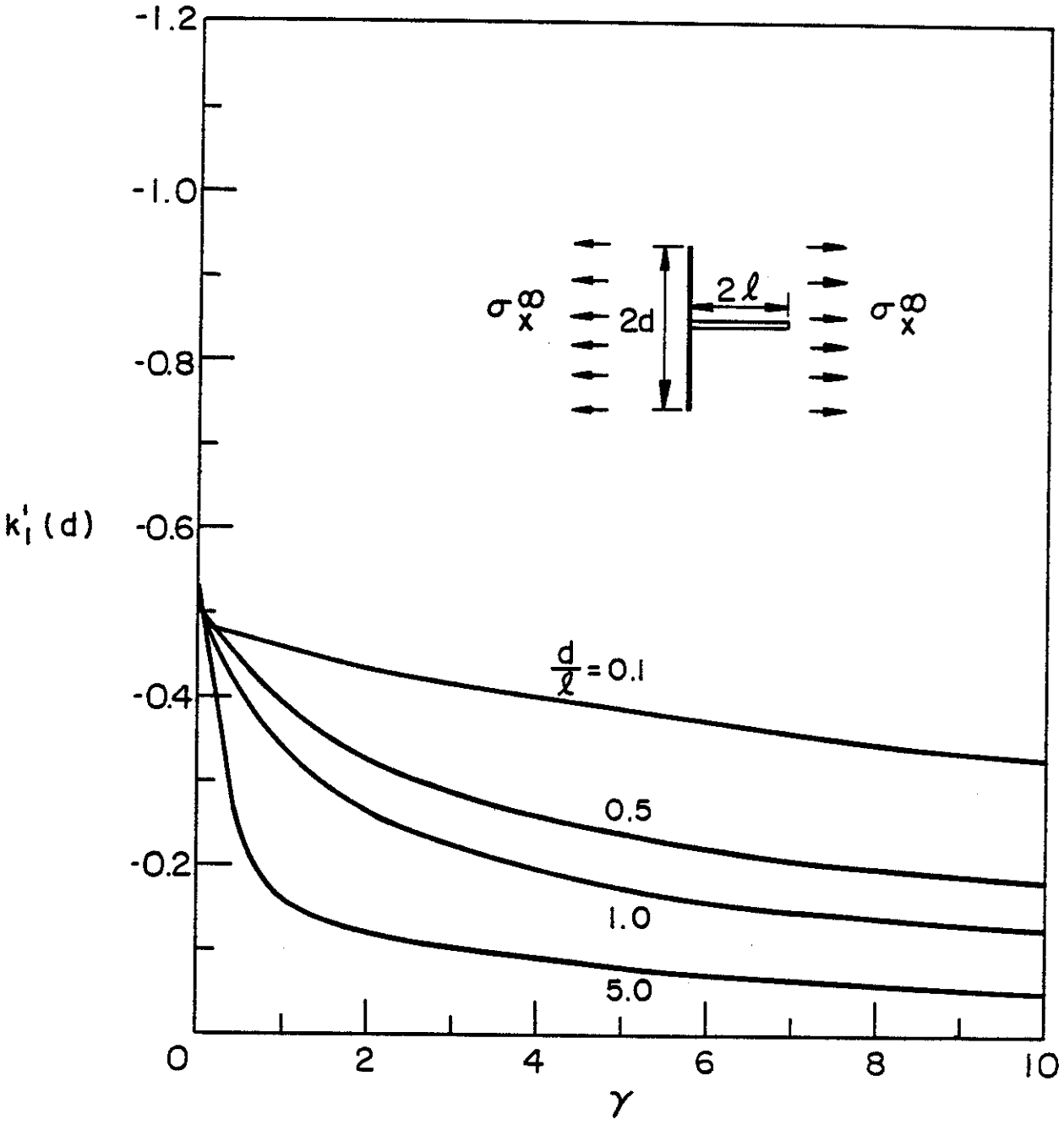

Figure 12. Normalized stress intensity factor at the inclusion end y=d; $\sigma_{xx}^\infty \neq 0$, $\sigma_{yy}^\infty = \sigma_{xy}^\infty = 0$, a = 0, $\nu = 0.3$.

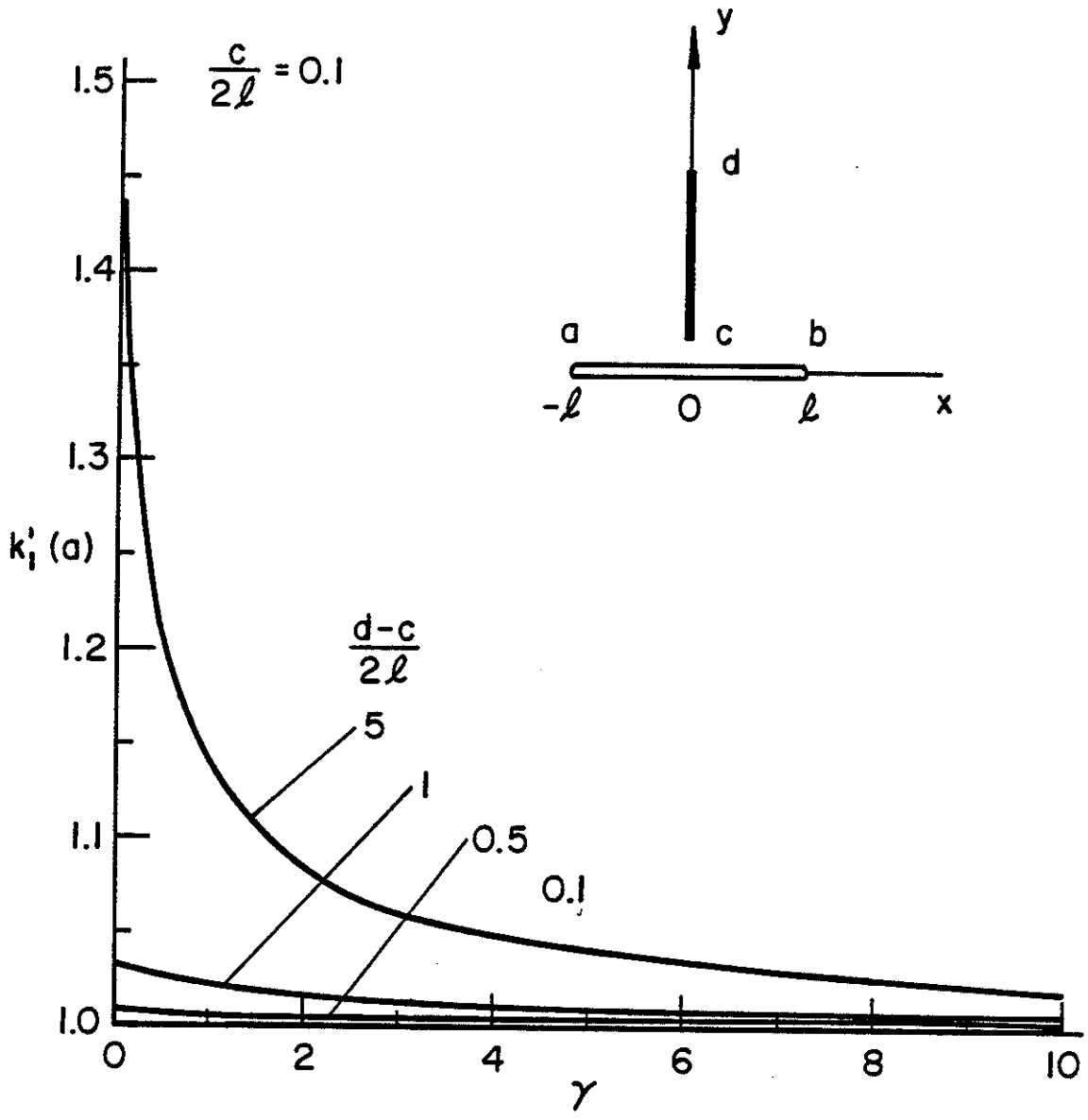

Figure 13. Mode I stress intensity factor at the crack tip $x=a=-\ell$; $\sigma^{\infty}_{yy} \neq 0$, $\sigma^{\infty}_{xx} = 0$, $\sigma^{\infty}_{xy} = 0$, $\theta = \pi/2$, $c = 0.2\ell$, $b = \ell$, $\nu = 0.3$.

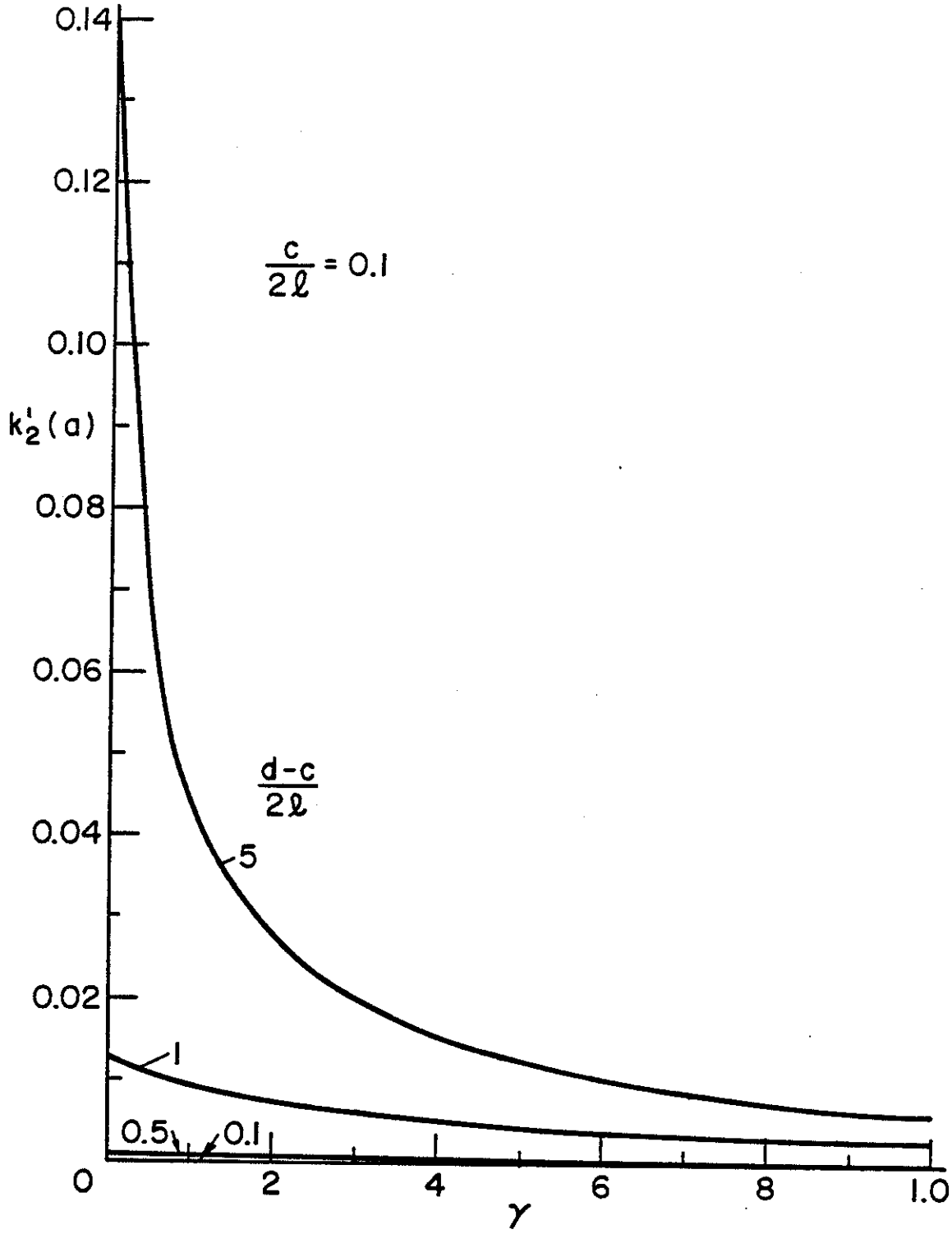

Figure 14. Mode II stress intensity factor at the crack tip $x=a=-\ell$; $\sigma_{yy}^{\infty} \neq 0$, $\sigma_{xx}^{\infty} = \sigma_{xy}^{\infty} = 0$, $\theta = \pi/2$, $c = 0.2\ell$, $b = \ell$, $\nu = 0.3$.

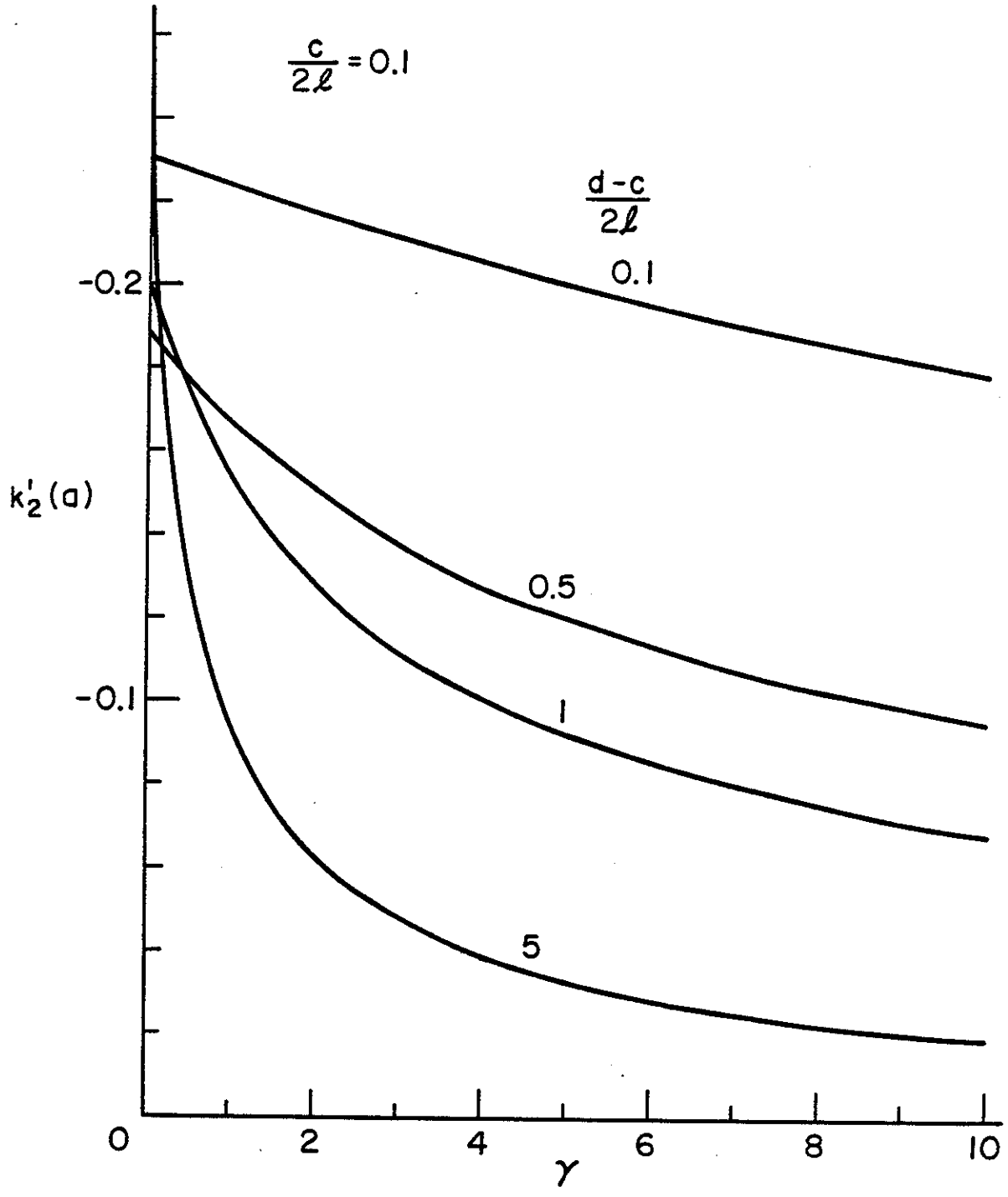

Figure 15. Stress intensity factor at the inclusion end y=c; $\sigma^{\infty}_{yy} \neq 0$, $\sigma^{\infty}_{xx} = \sigma^{\infty}_{xy} = 0$, $\theta = \pi/2$, $c = 0.2\ell$, $\nu = 0.3$, $b = \ell$.

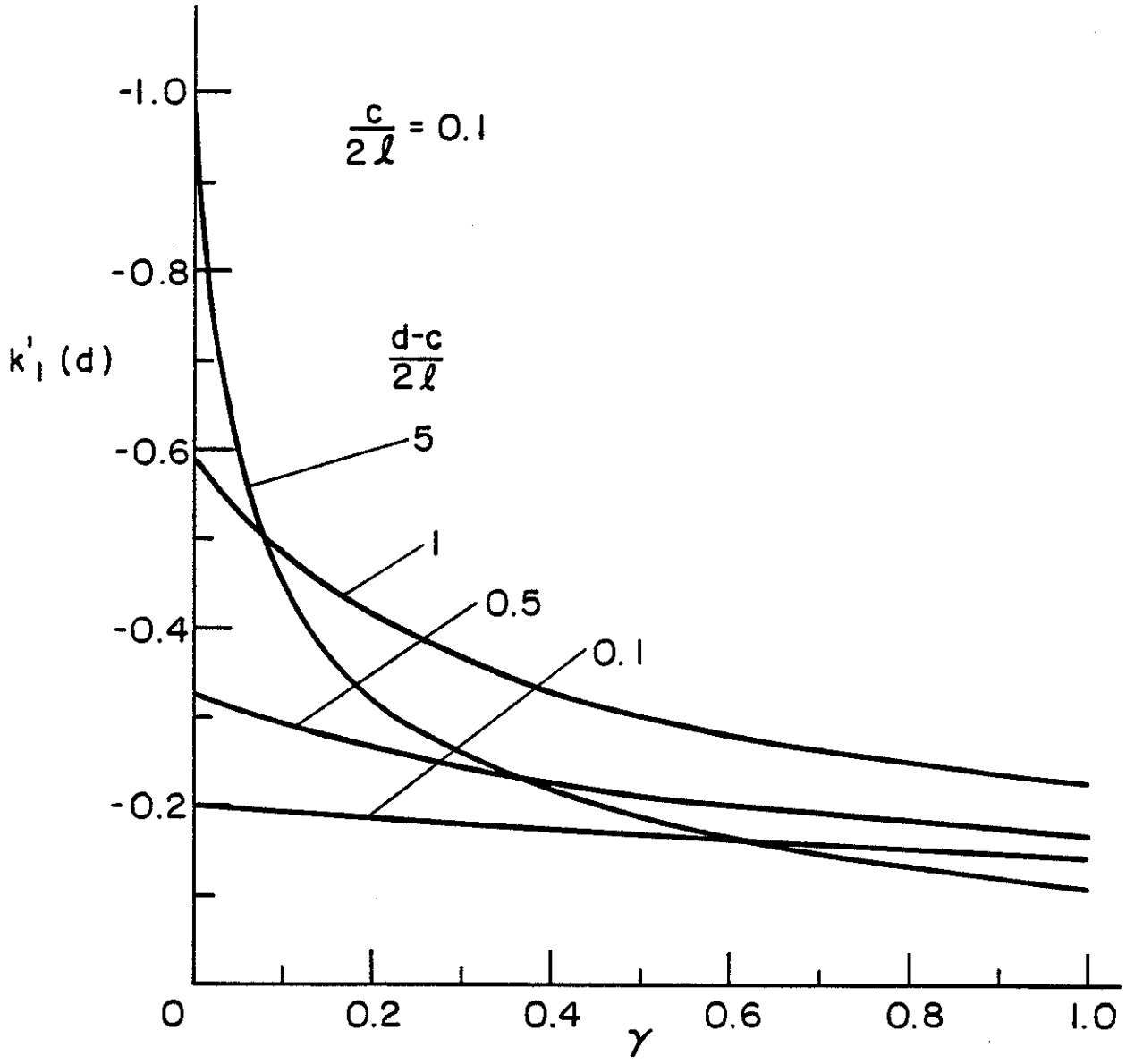

Figure 16. Stress intensity factor at the inclusion end y=d; $\sigma^{\infty}_{yy} \neq 0$, $\sigma^{\infty}_{xx} = \sigma^{\infty}_{xy} = 0$, $\nu = 0.3$, $\theta = \pi/2$, $c = 0.2\ell$, $b = \ell = -a$.

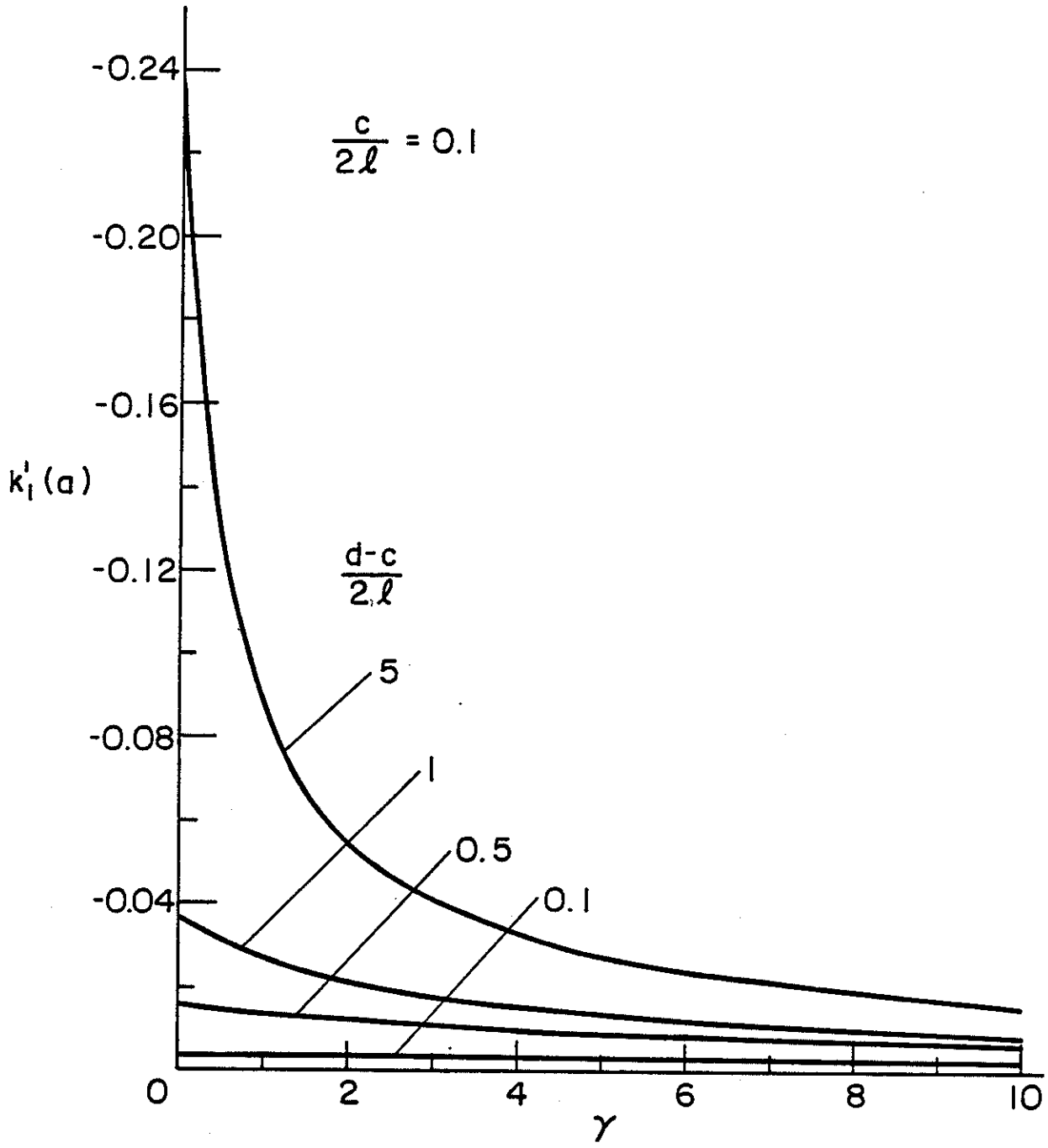

Figure 17. Mode I stress intensity factor at the crack tip $x=a=-\ell$; $\sigma_{xx}^{\infty} \neq 0$, $\sigma_{yy}^{\infty} = \sigma_{xy}^{\infty} = 0$, $\theta = \pi/2$, $\nu = 0.3$, $c = 0.2\ell$, $b = \ell$.

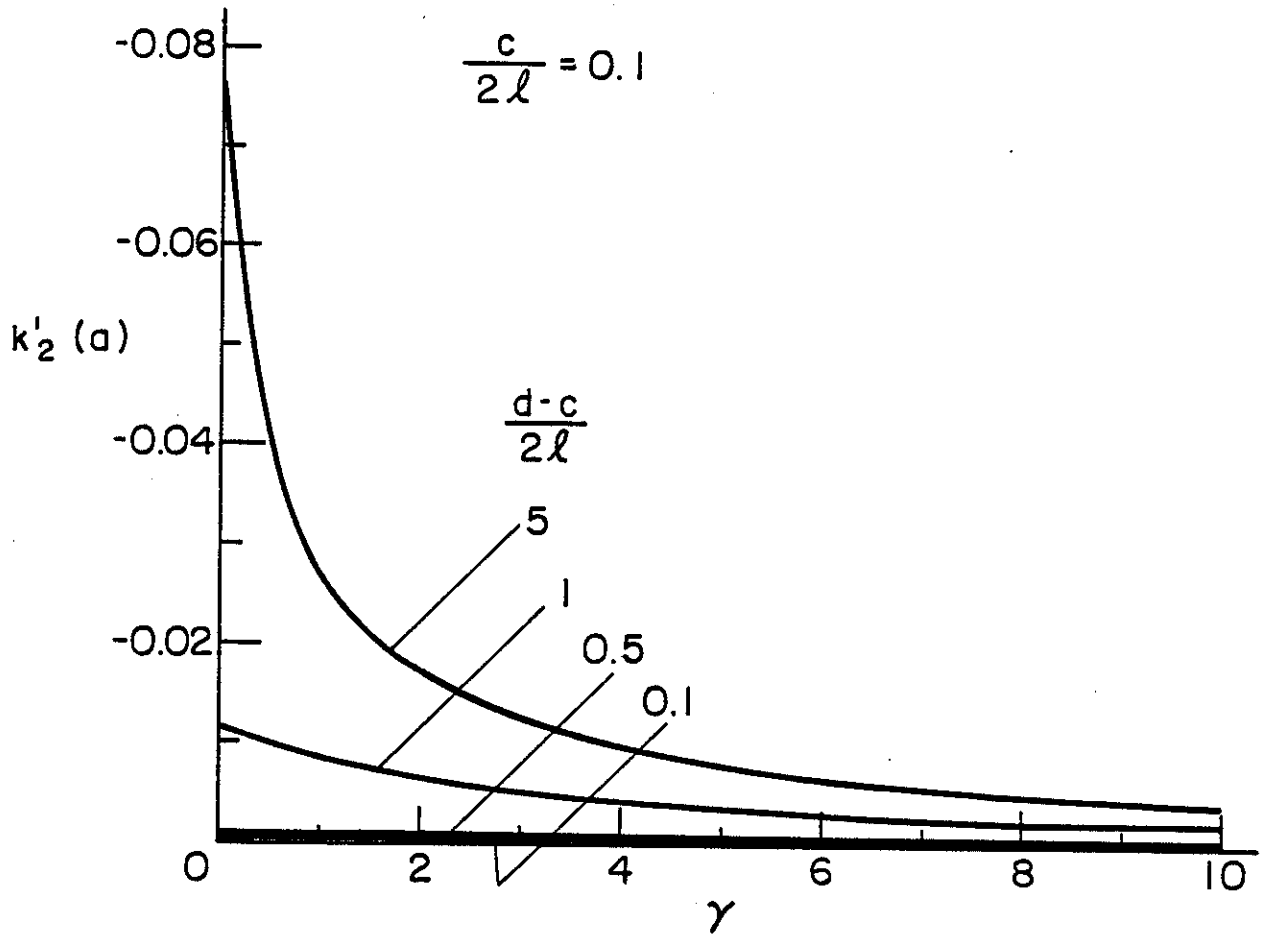

Figure 18. Mode II stress intensity factor at the crack tip $x=a=-\ell$; $\sigma^{\infty}_{xx} \neq 0$, $\sigma^{\infty}_{yy} = \sigma^{\infty}_{xy} = 0$, $\nu = 0.3$, $\theta = \pi/2$, $c = 0.2\ell$, $b = \ell$.

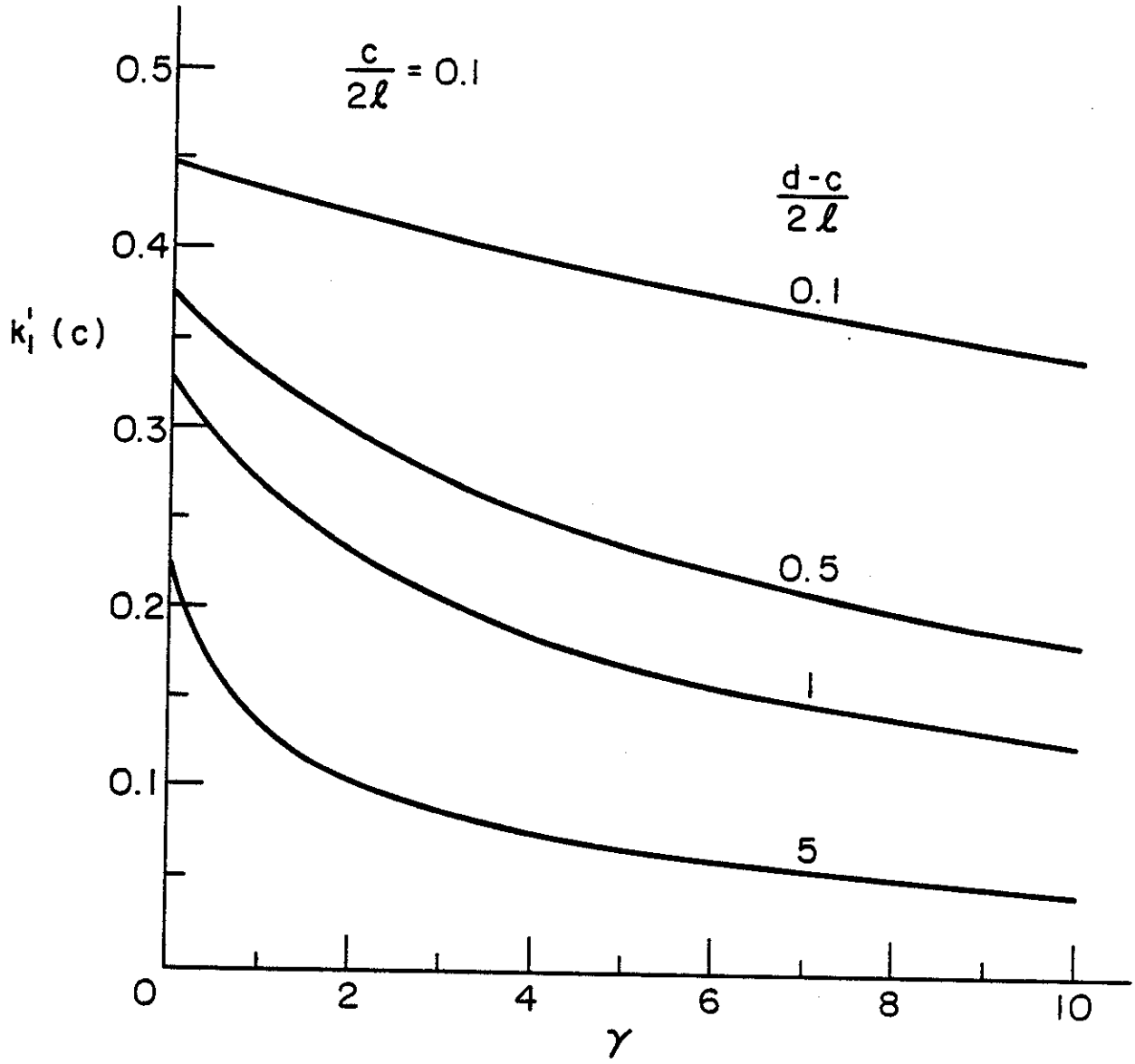

Figure 19. Stress intensity factor at the inclusion end y = c; $\sigma^{\infty}_{xx} \neq 0$, $\sigma^{\infty}_{yy} = \sigma^{\infty}_{xy} = 0$, $\nu = 0.3$, $c = 0.2\ell$, $\theta = \pi/2$, $b = \ell = -a$.

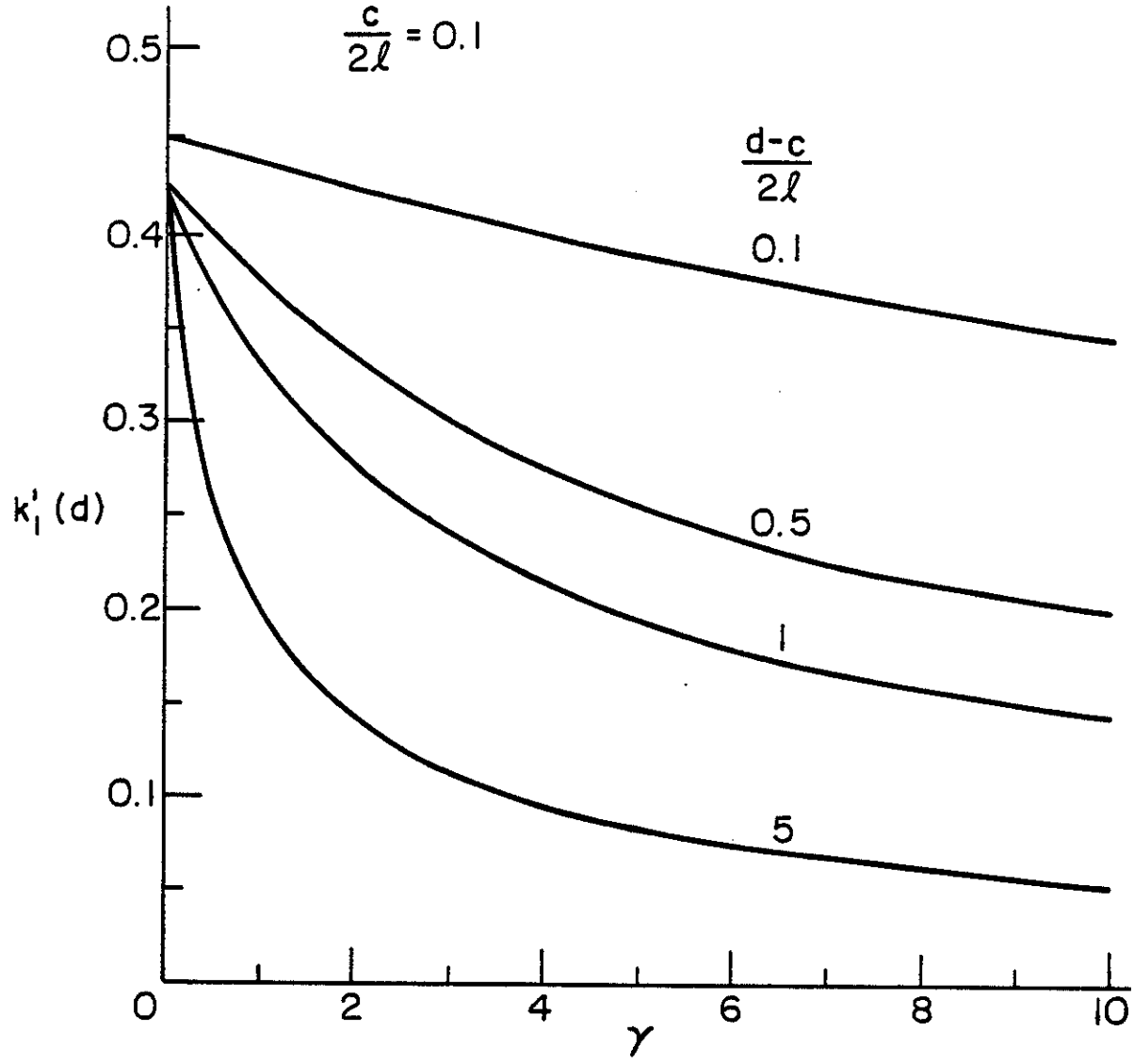

Figure 20. Stress intensity factor at the inclusion end y = d; $\sigma^{\infty}_{xx} \neq 0$, $\sigma^{\infty}_{yy} = \sigma^{\infty}_{xy} = 0$, $\nu = 0.3$, $\theta = \pi/2$, $c = 0.2\ell$, $b = \ell = -a$.

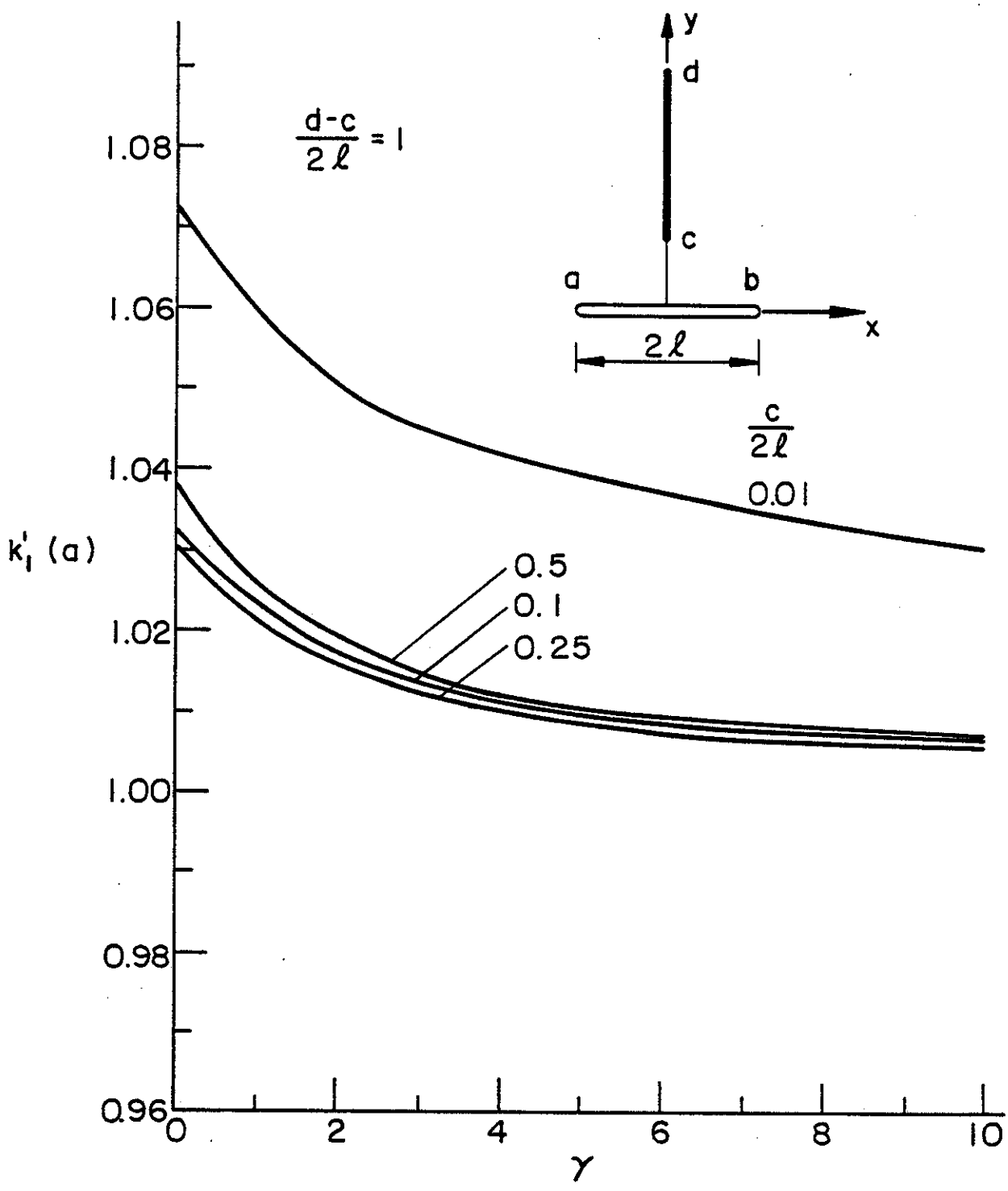

Figure 21. Mode I stress intensity factor at the crack tip $x = a = -\ell$; $\sigma^{\infty}_{yy} \neq 0$, $\sigma^{\infty}_{xx} = \sigma^{\infty}_{xy} = 0$, $\theta = \pi/2$, $\nu = 0.3$, $d-c = 2\ell$, $b = \ell$.

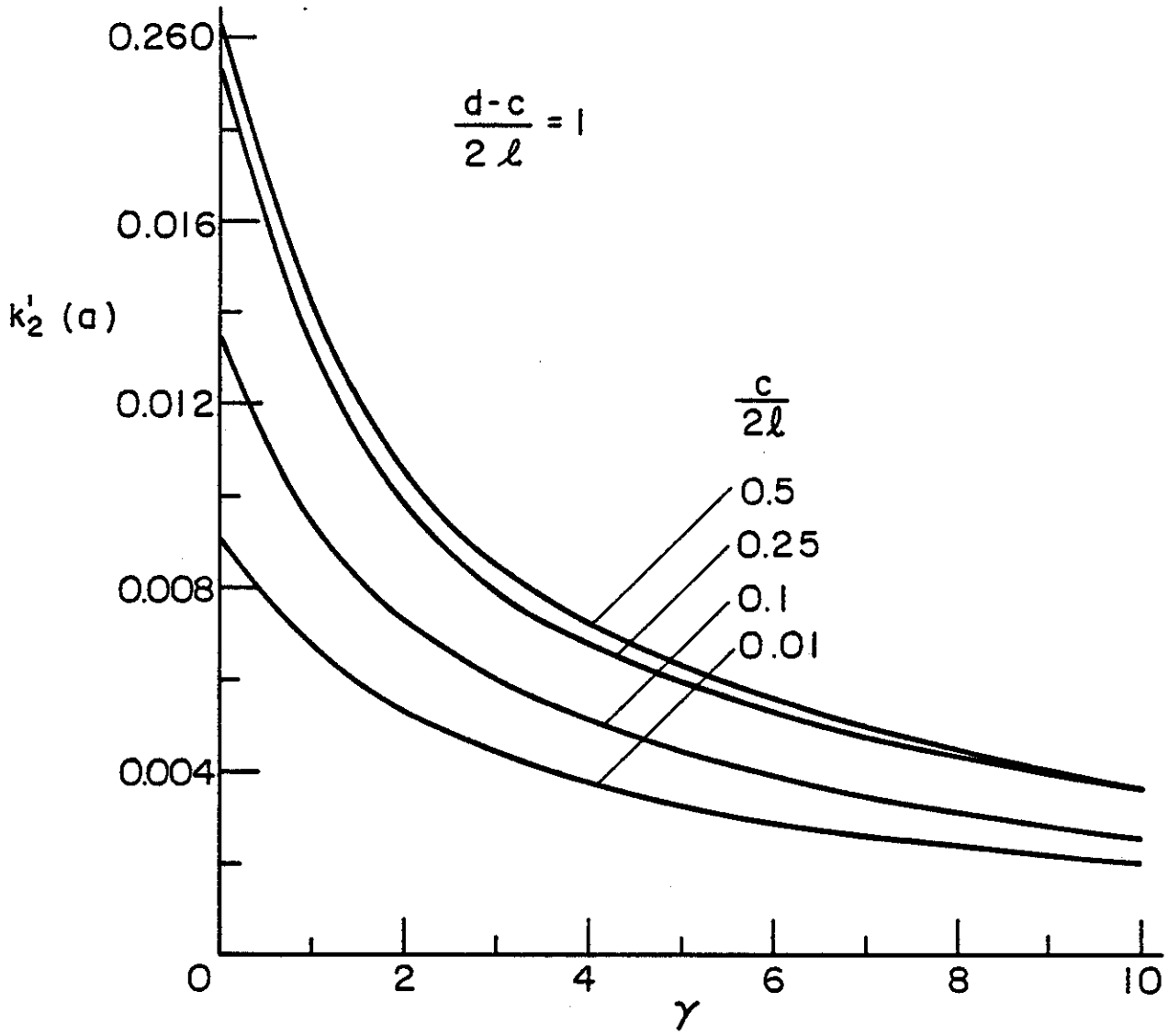

Figure 22. Mode II stress intensity factor at the crack tip $x = a = -\ell$; $\sigma^{\infty}_{yy} \neq 0$, $\sigma^{\infty}_{xx} = \sigma^{\infty}_{xy} = 0$, $\nu = 0.3$, $\theta = \pi/2$, $d-c = 2\ell$, $b = \ell$.

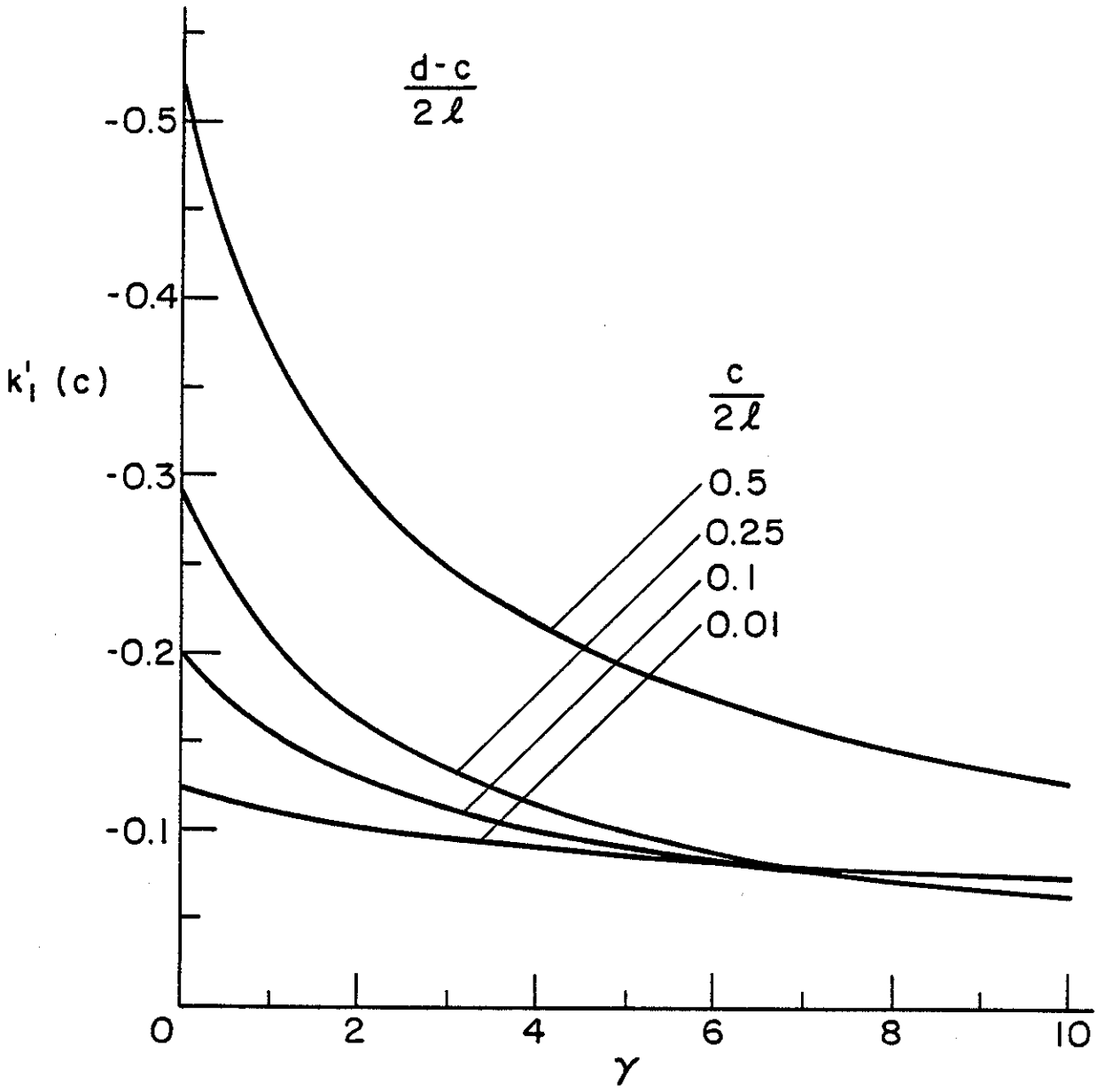

Figure 23. Stress intensity factor at the inclusion end y = c; $\sigma^{\infty}_{yy} \neq 0$, $\sigma^{\infty}_{xx} = \sigma^{\infty}_{xy} = 0$, $\nu = 0.3$, $\theta = \pi/2$, d-c = 2ℓ, b = ℓ = -a.

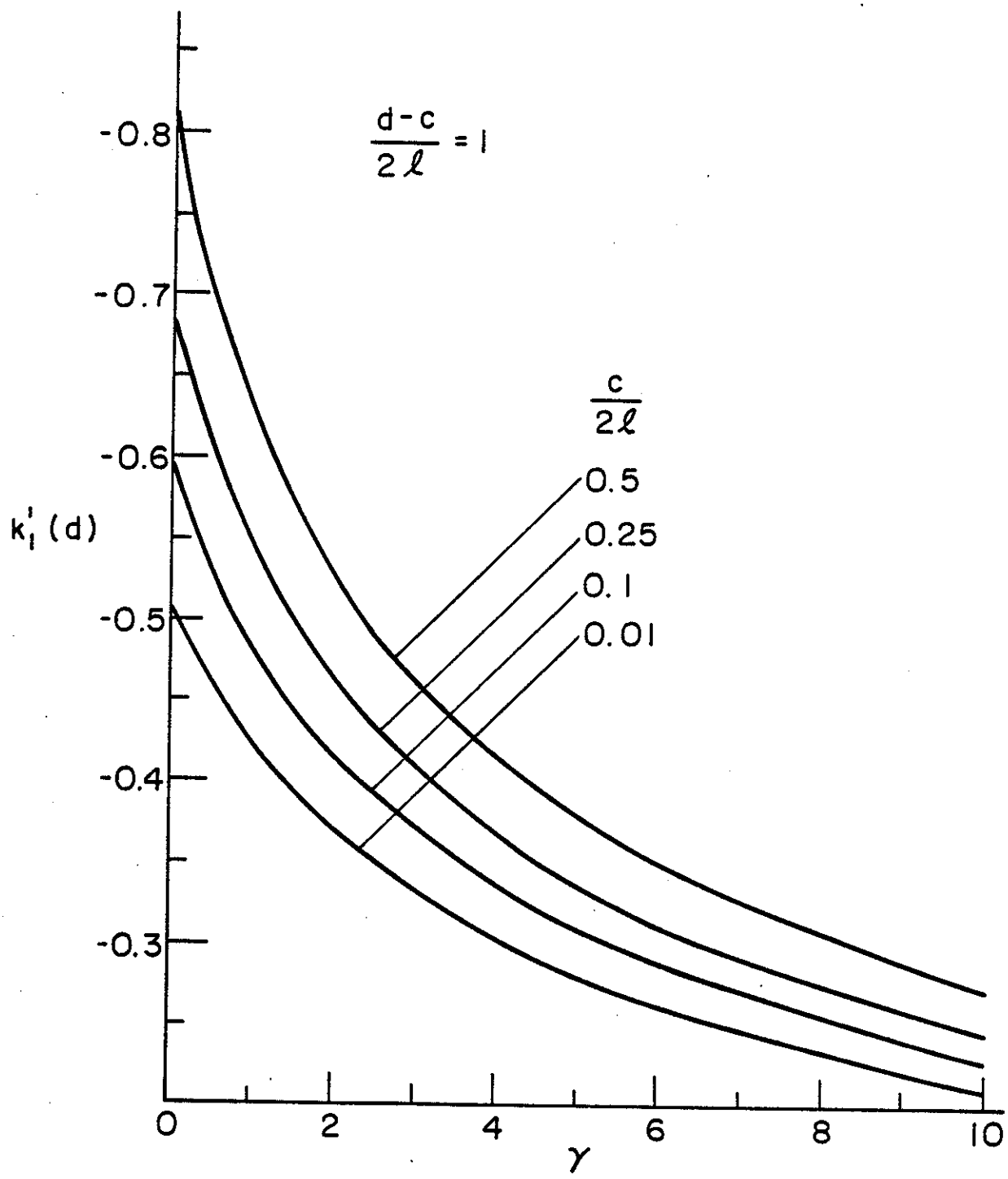

Figure 24. Stress intensity factor at the inclusion end y=d; $\sigma_{yy}^{\infty} \neq 0$, $\sigma_{xx}^{\infty} = \sigma_{xy}^{\infty} = 0$, $\nu = 0.3$, $\theta = \pi/2$, d-c = 2ℓ, b = ℓ = -a.

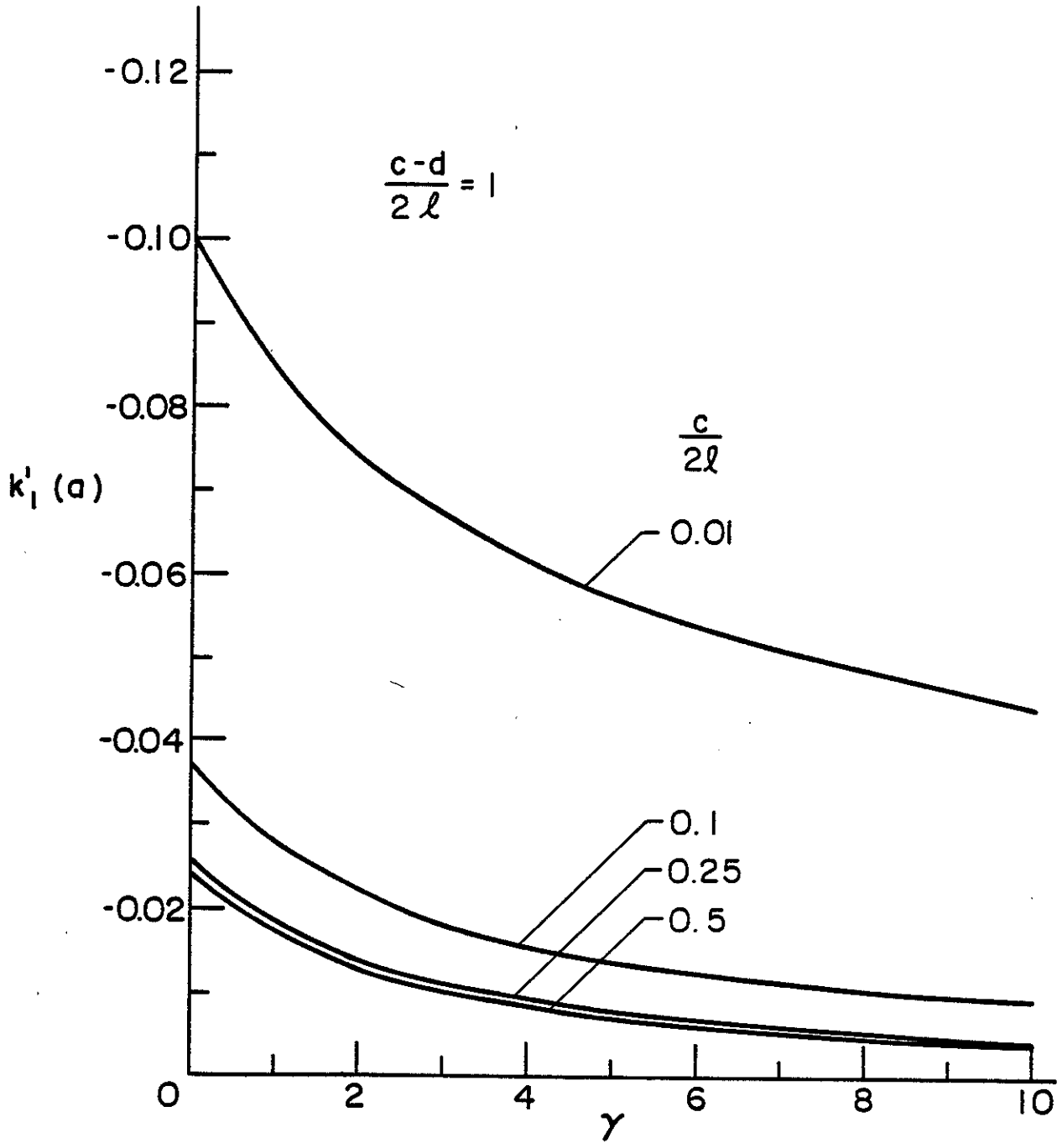

Figure 25. Mode I stress intensity factor at the crack tip x = a = -ℓ; $\sigma^{\infty}_{xx} \neq 0$, $\sigma^{\infty}_{yy} = \sigma^{\infty}_{xy} = 0$, $\nu = 0.3$, $\theta = \pi/2$, b = ℓ, d-c = 2 ℓ

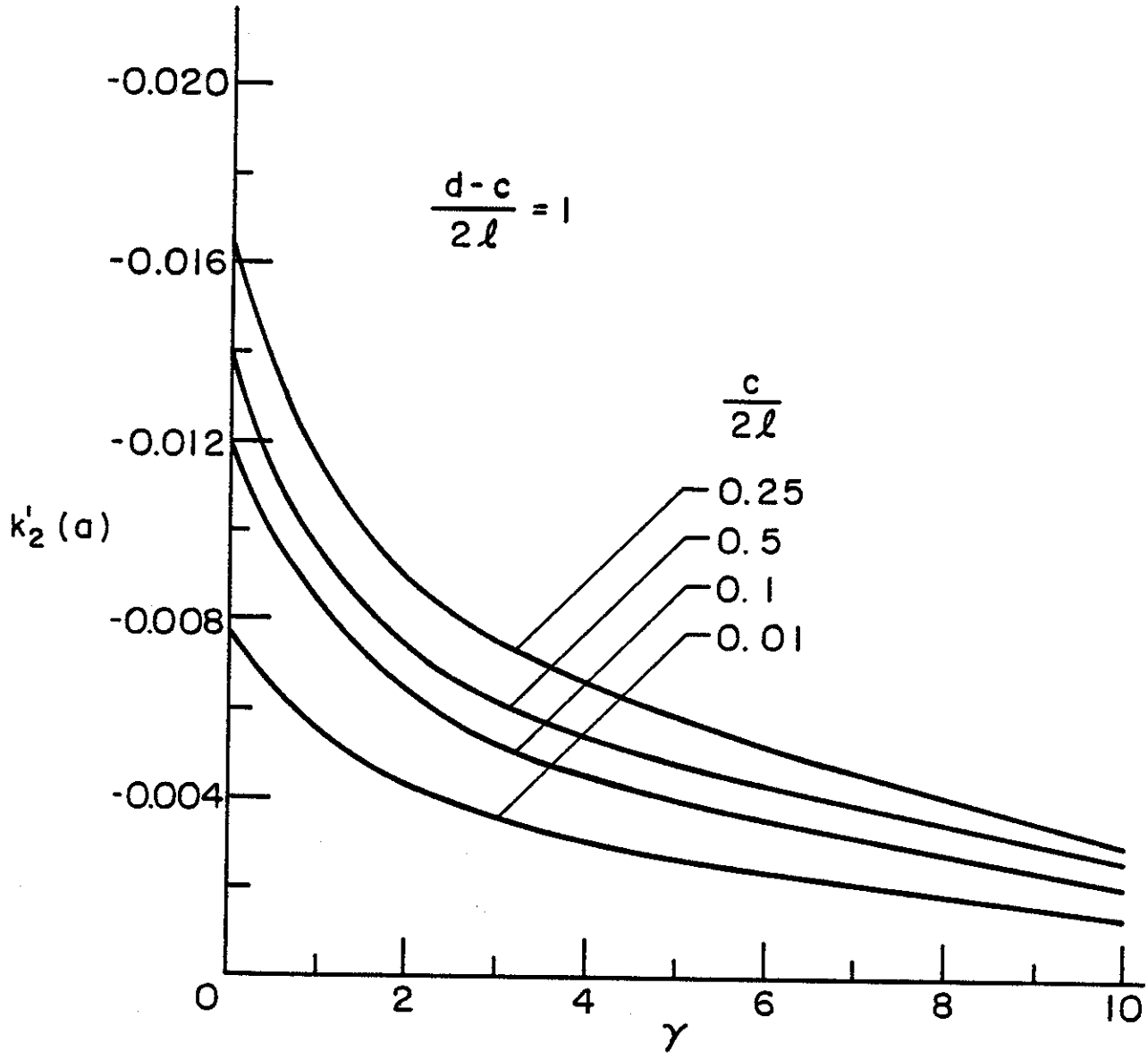

Figure 26. Mode II stress intensity factor at the crack tip $x = a = -\ell$; $\sigma_{xx}^{\infty} \neq 0$, $\sigma_{yy}^{\infty} = \sigma_{xy}^{\infty} = 0$, $\nu = 0.3$, $\theta = \pi/2$, $d-c = 2\ell$, $b = \ell$.

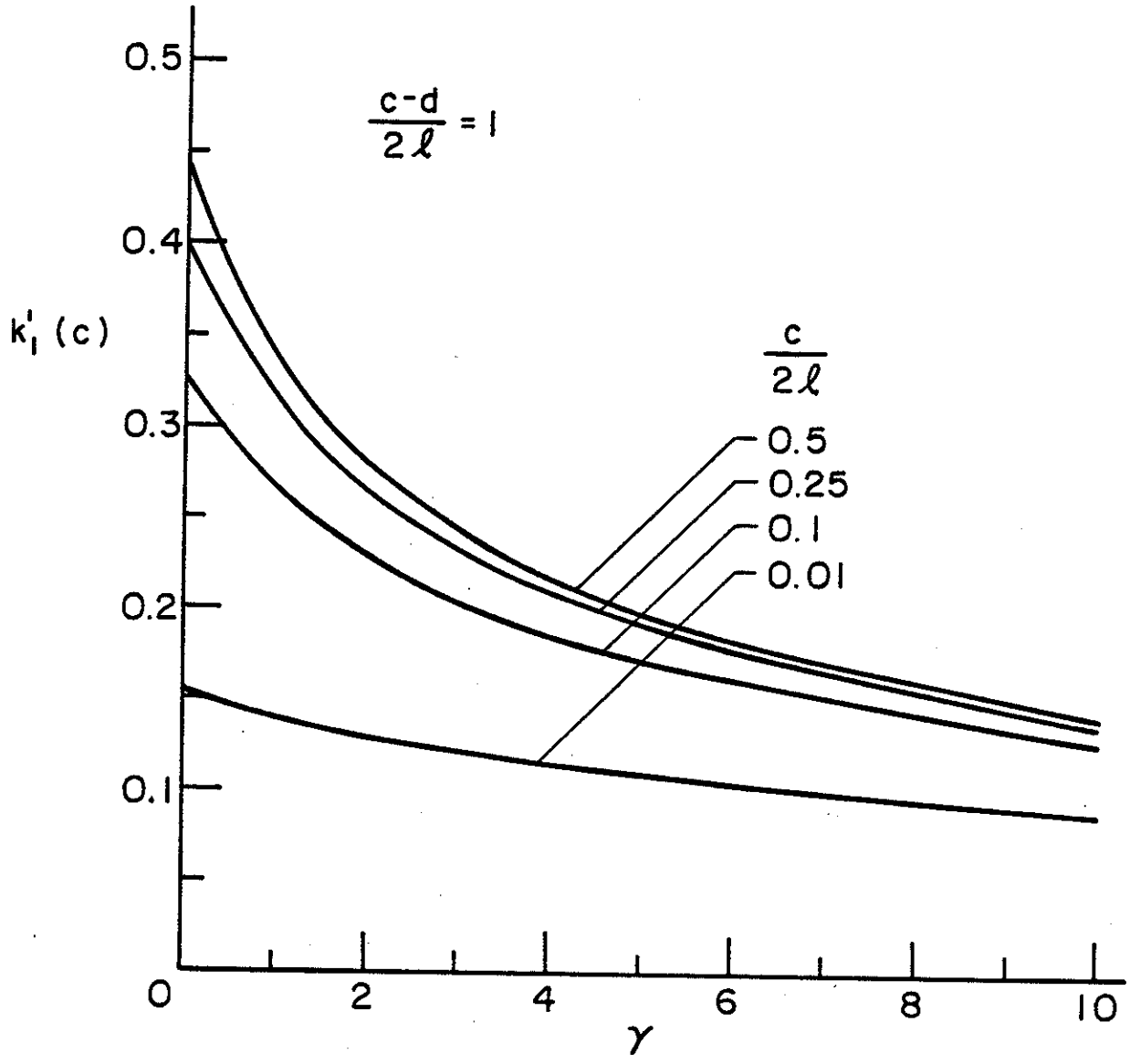

Figure 27. Stress intensity factor at the inclusion end y = c; $\sigma_{xx}^{\infty} \neq 0$, $\sigma_{yy}^{\infty} = \sigma_{xy}^{\infty} = 0$, $\nu = 0.3$, $\theta = \pi/2$, d-c = 2ℓ, b = ℓ = -a.

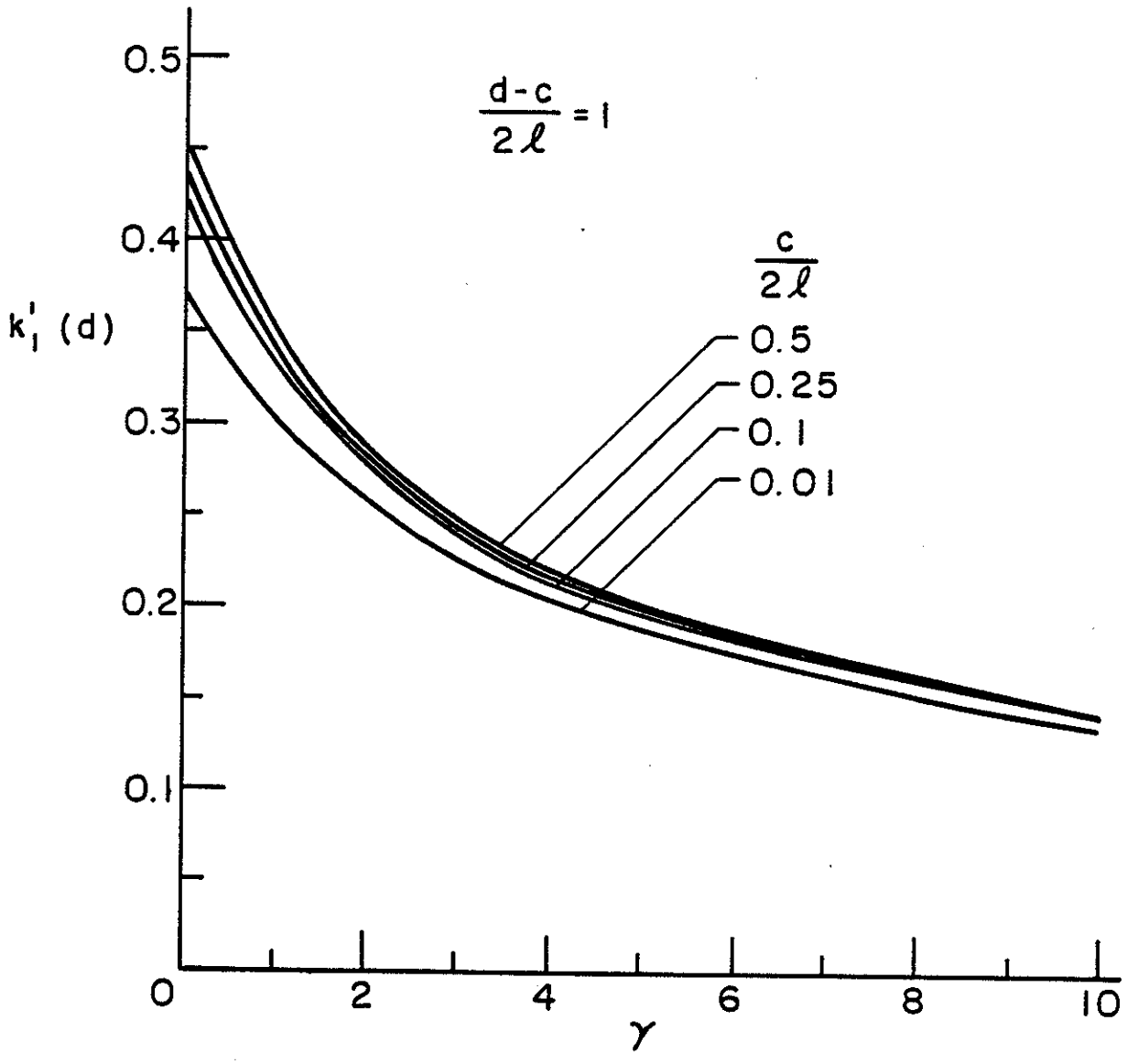

Figure 28. Stress intensity factor at the inclusion end y = d; $\sigma_{xx}^{\infty} \neq 0$, $\sigma_{yy}^{\infty} = \sigma_{xy}^{\infty} = 0$, $\nu = 0.3$, $\theta = \pi/2$, d-c = 2ℓ, b = ℓ = -a.

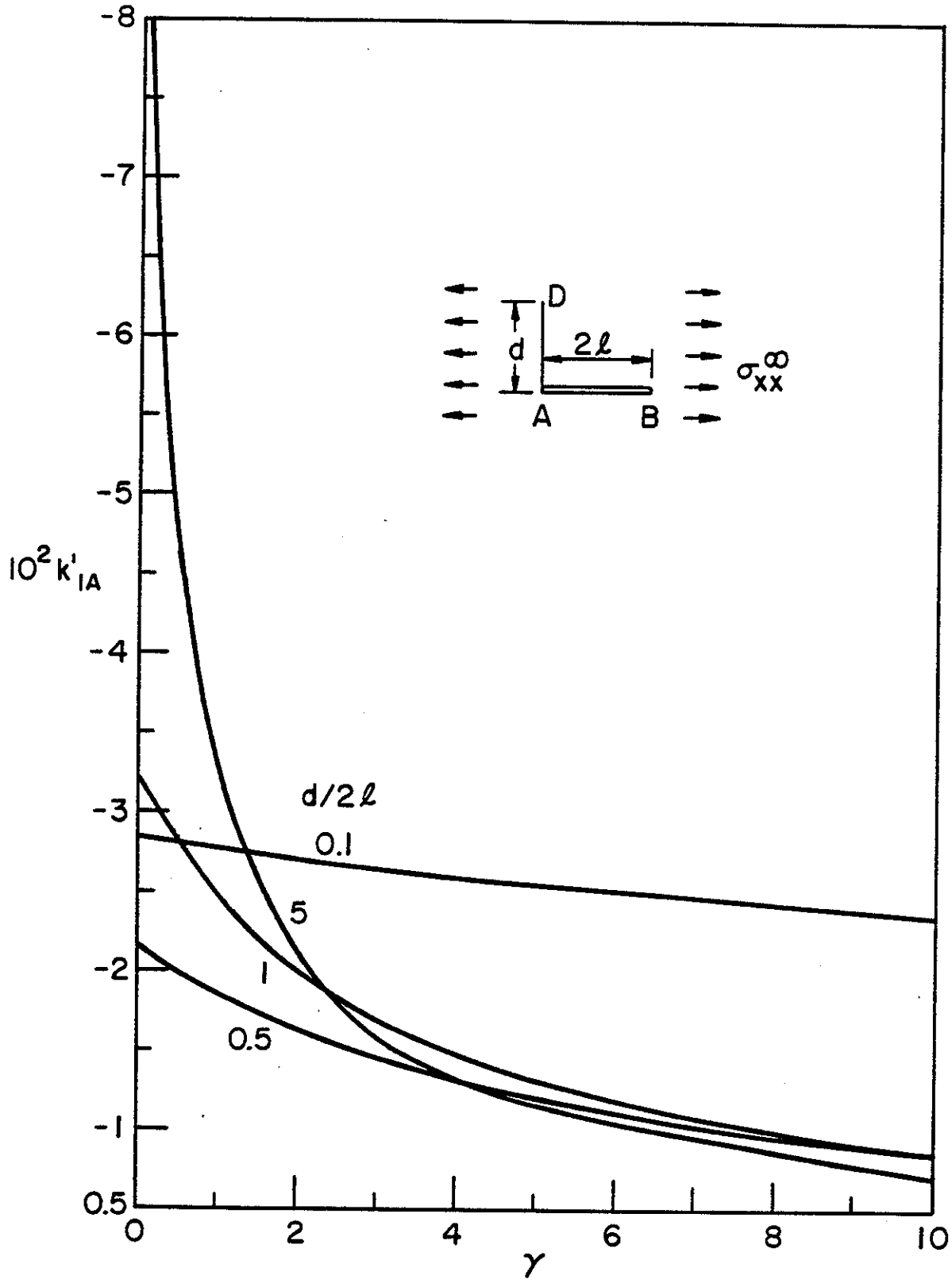

Figure 29. Normalized stress intensity factor for the inclusion-crack intersection problem for which $\theta = \pi/2$, $a = 0$, $b = 2\ell$, $c = 0$, $d/2\ell$ and γ variables. k'_{IA} for $\sigma^{\infty}_{xx} \neq 0$, $\sigma^{\infty}_{xy} = 0$, $\sigma^{\infty}_{yy} = 0$.

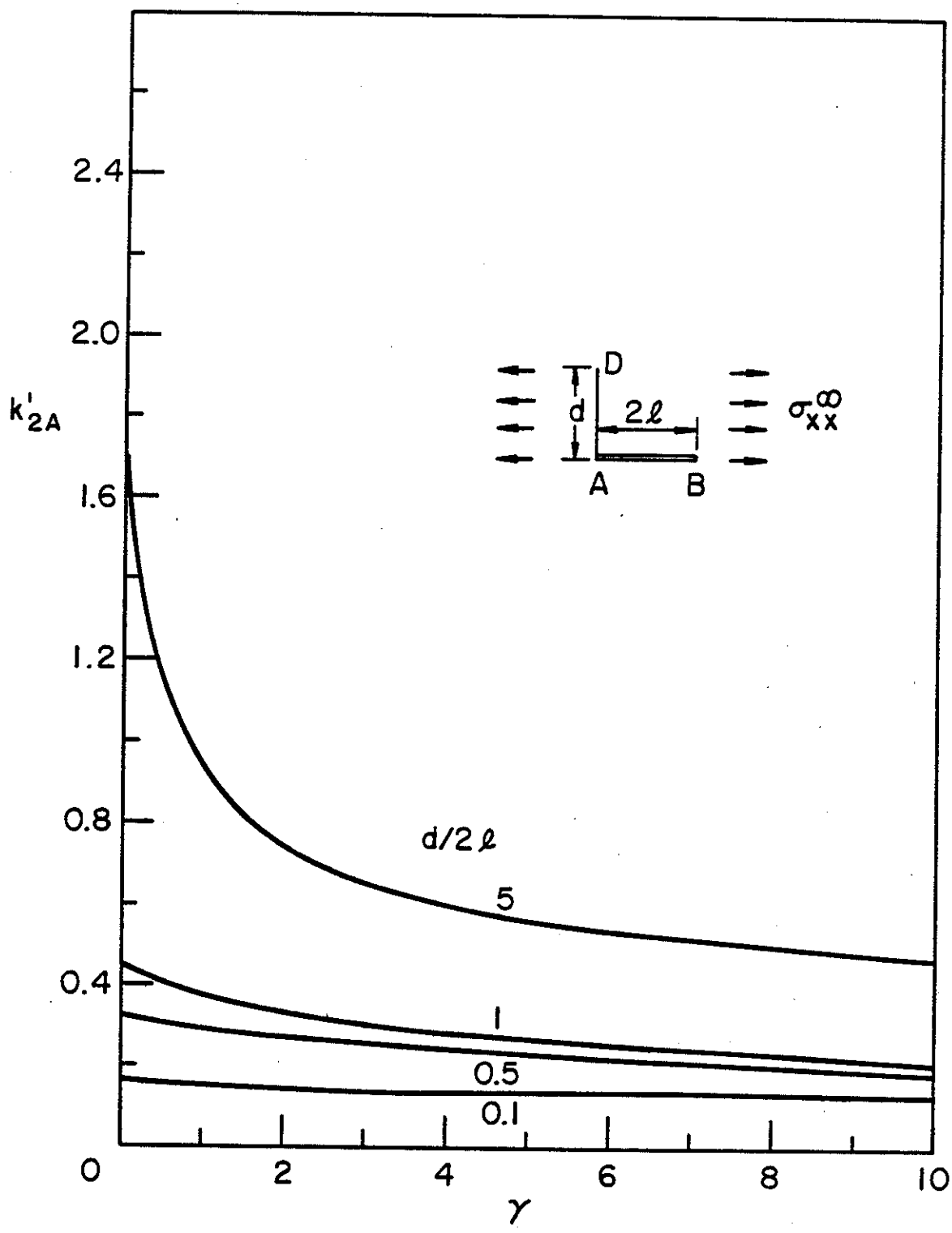

Figure 30. Normalized stress intensity factor for the inclusion-crack intersection problem for which $\theta = \pi/2$, $a = 0$, $b = 2\ell$, $c = 0$, $d/2\ell$ and γ variables. k_{2A}, $\sigma^{\infty}_{xx} = 0$, $\sigma^{\infty}_{xy} = \sigma^{\infty}_{yy} = 0$.

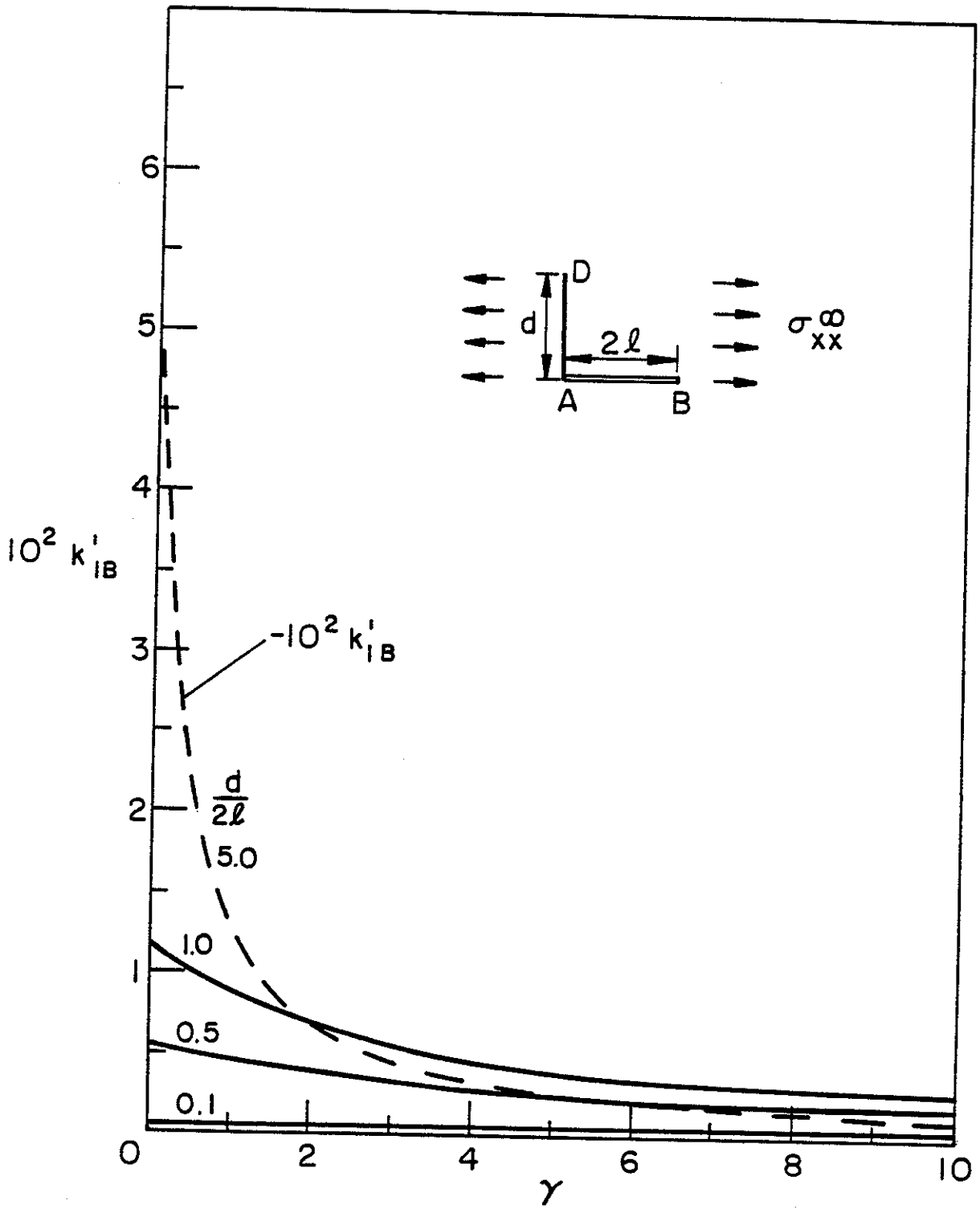

Figure 31. Normalized stress intensity factor for the inclusion-crack intersection problem for which $\theta = \pi/2$, $a = 0$, $b = 2\ell$, $c = 0$, $d/2\ell$ and γ variables. k'_{IB}, $\sigma^{\infty}_{xx} \neq 0$.

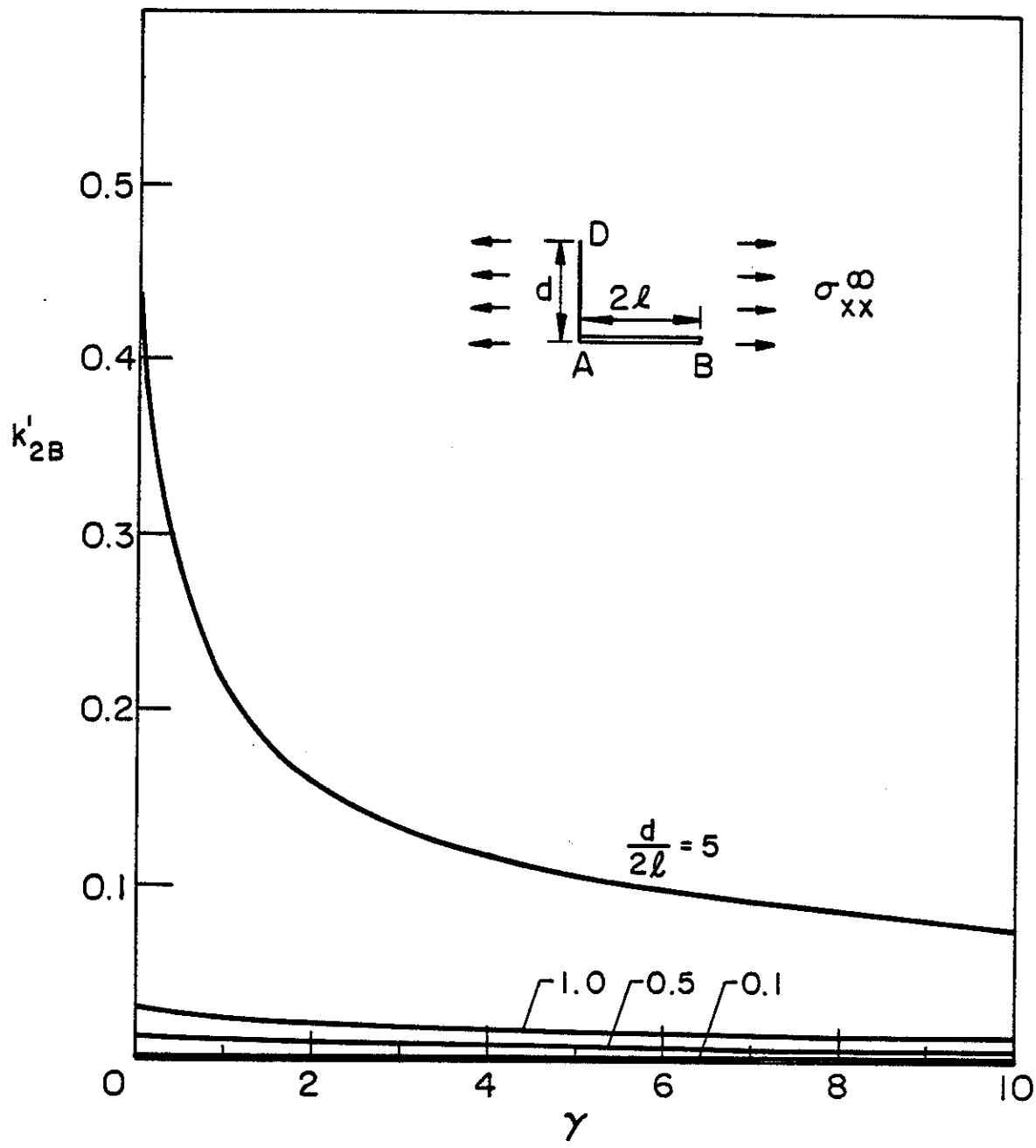

Figure 32. Normalized stress intensity factor for the inclusion-crack intersection problem for which $\theta = \pi/2$, $a = 0$, $b = 2\ell$, $c = 0$, $d/2\ell$ and γ variables. k_{2B} , $\sigma^{\infty}_{xx} \neq 0$.

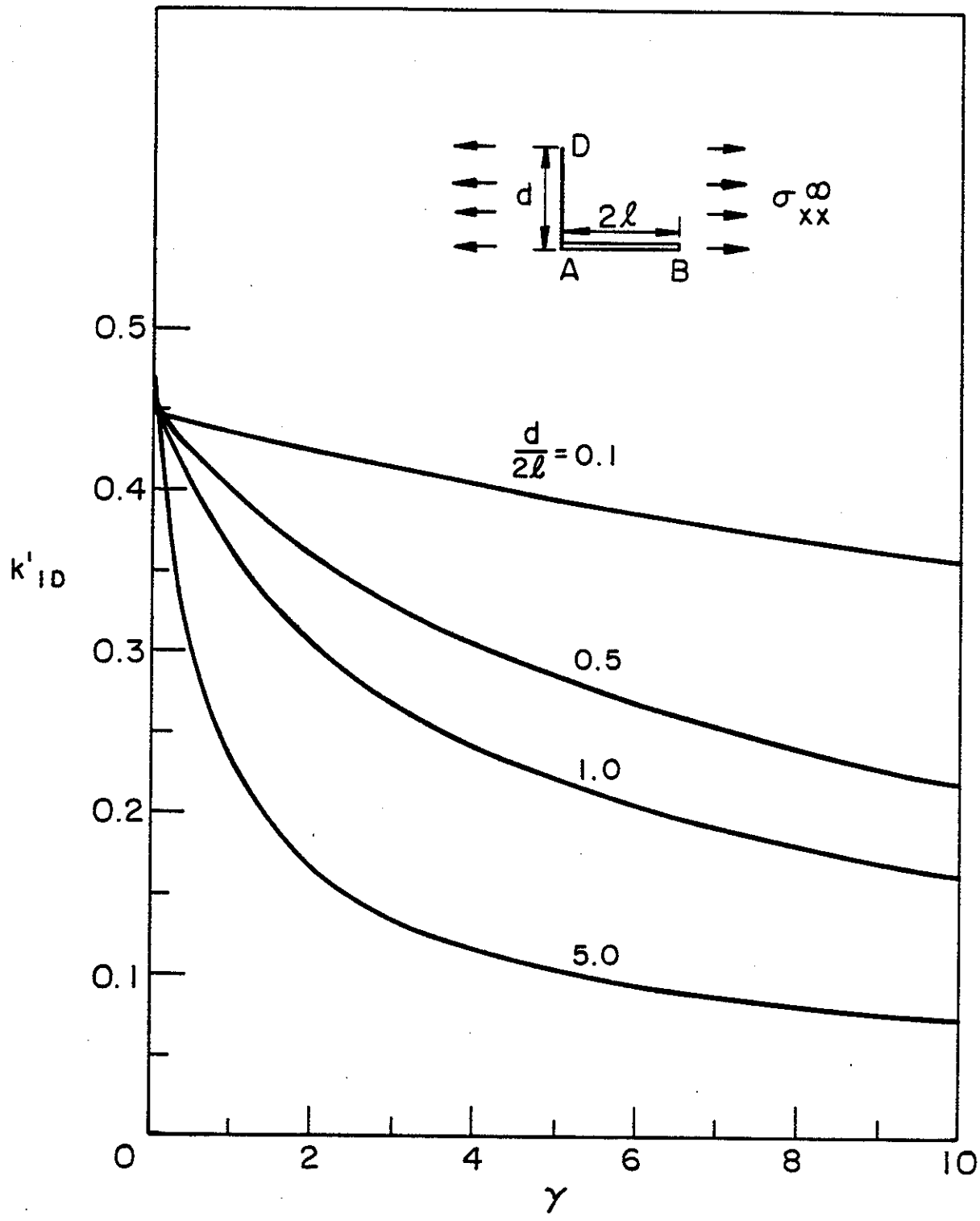

Figure 33. Normalized stress intensity factor for the inclusion-crack intersection problem for which $\theta = \pi/2$, a = 0, b = 2ℓ, c = 0, $d/2\ell$ and γ variables. k_{ID} , $\sigma^{\infty}_{xx} = 0$.

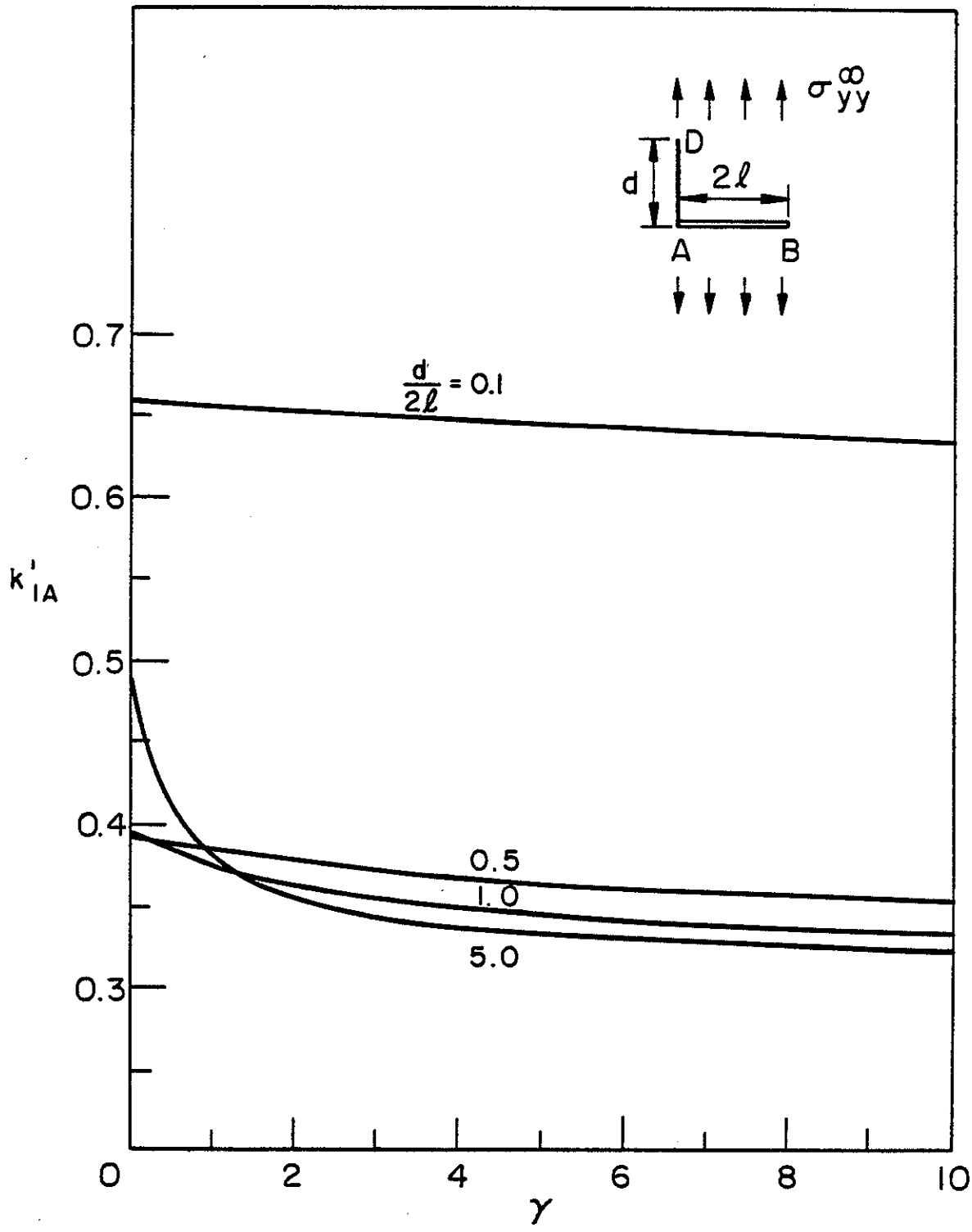

Figure 34. Normalized stress intensity factor for the inclusion-crack intersection problem for which $\theta = \pi/2$, $a = 0$, $b = 2\ell$, $c = 0$, $d/2\ell$ and γ variables. k'_{IA}, $\sigma^{\infty}_{yy} \neq 0$.

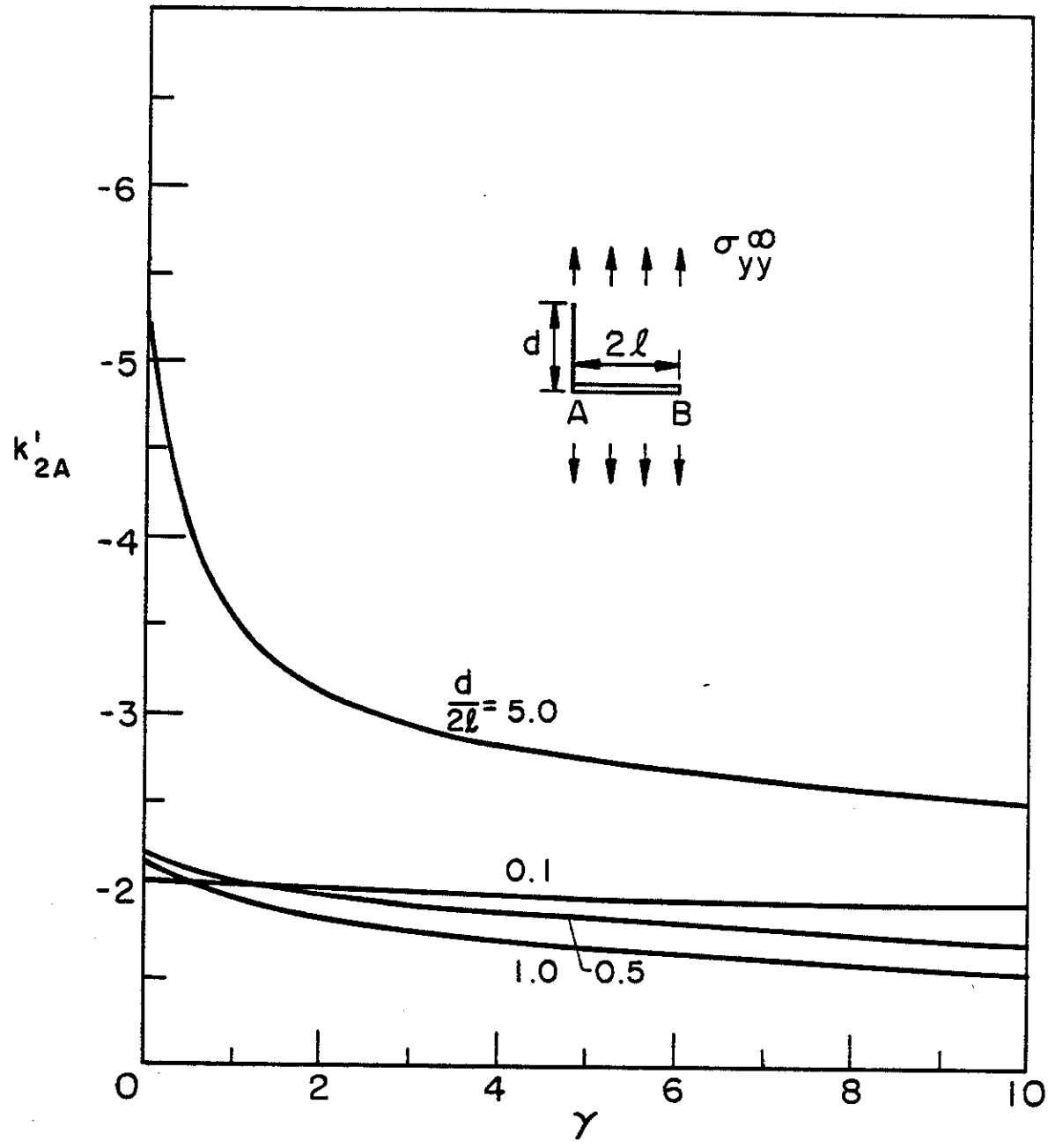

Figure 35. Normalized stress intensity factor for the inclusion-crack intersection problem for which $\theta = \pi/2$, a = 0, b = 2ℓ, c = 0, d/2ℓ and γ variables. k_{2A} , $\sigma^{\infty}_{yy} \neq 0$.

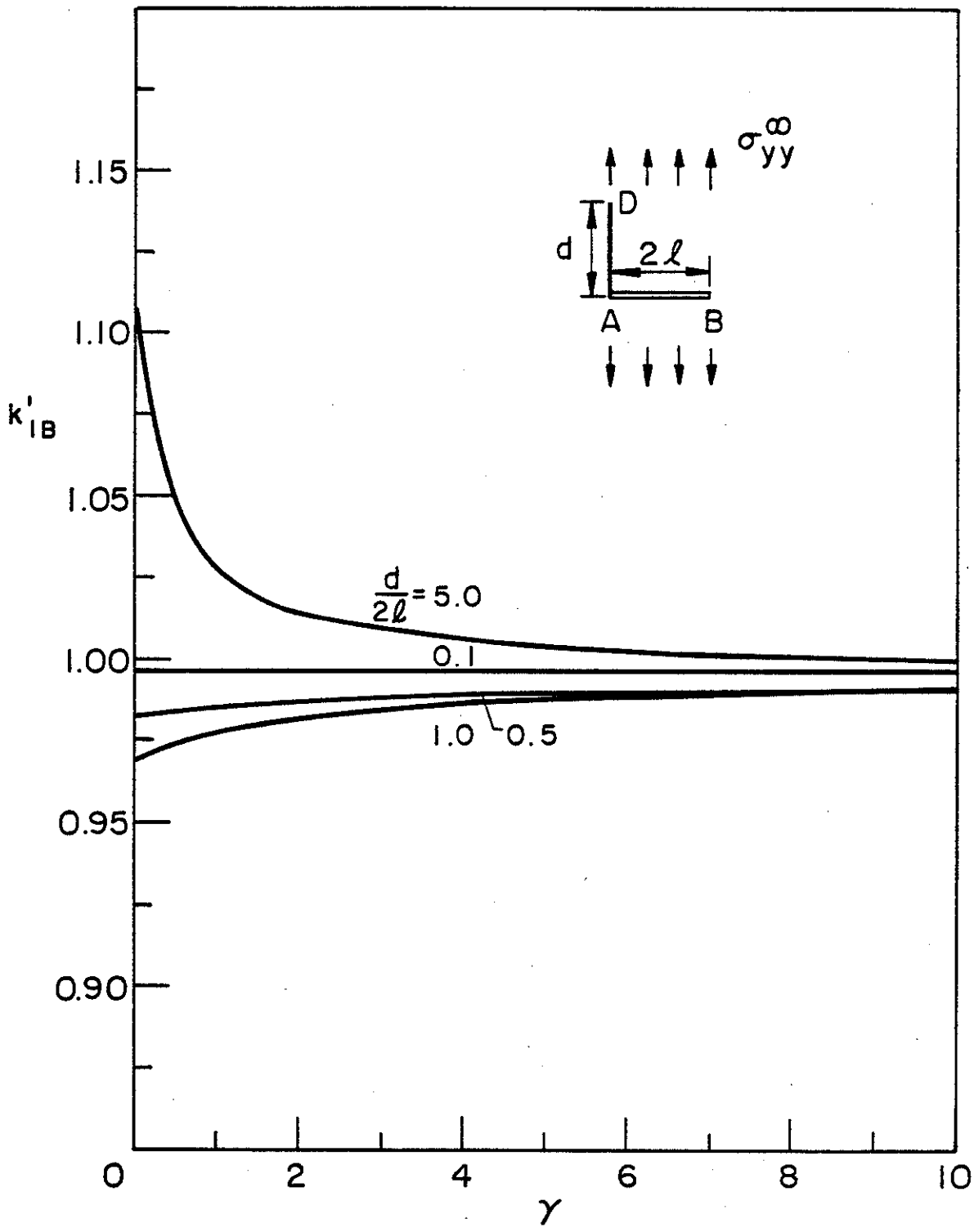

Figure 36. Normalized stress intensity factor for the inclusion-crack intersection problem for which $\theta = \pi/2$, a = 0, b = 2ℓ, c = 0, d/2ℓ and γ variables. k'_{IB} , $\sigma^{\infty}_{yy} \neq 0$.

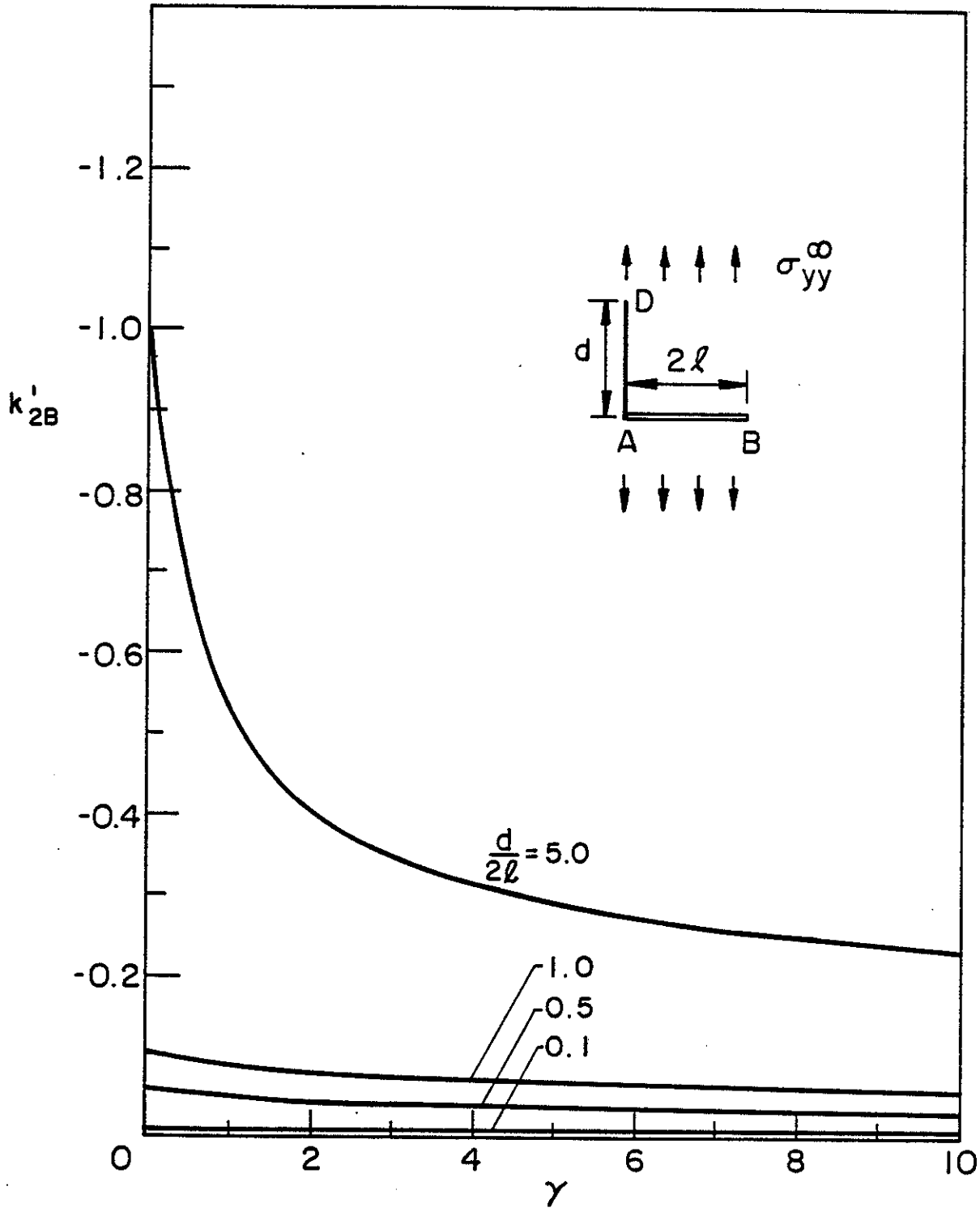

Figure 37. Normalized stress intensity factor for the inclusion-crack intersection problem for which $\theta = \pi/2$, a = 0, b = 2ℓ, c = 0, $d/2\ell$ and γ variables. k_{2B} , $\sigma^{\infty}_{yy} \neq 0$.

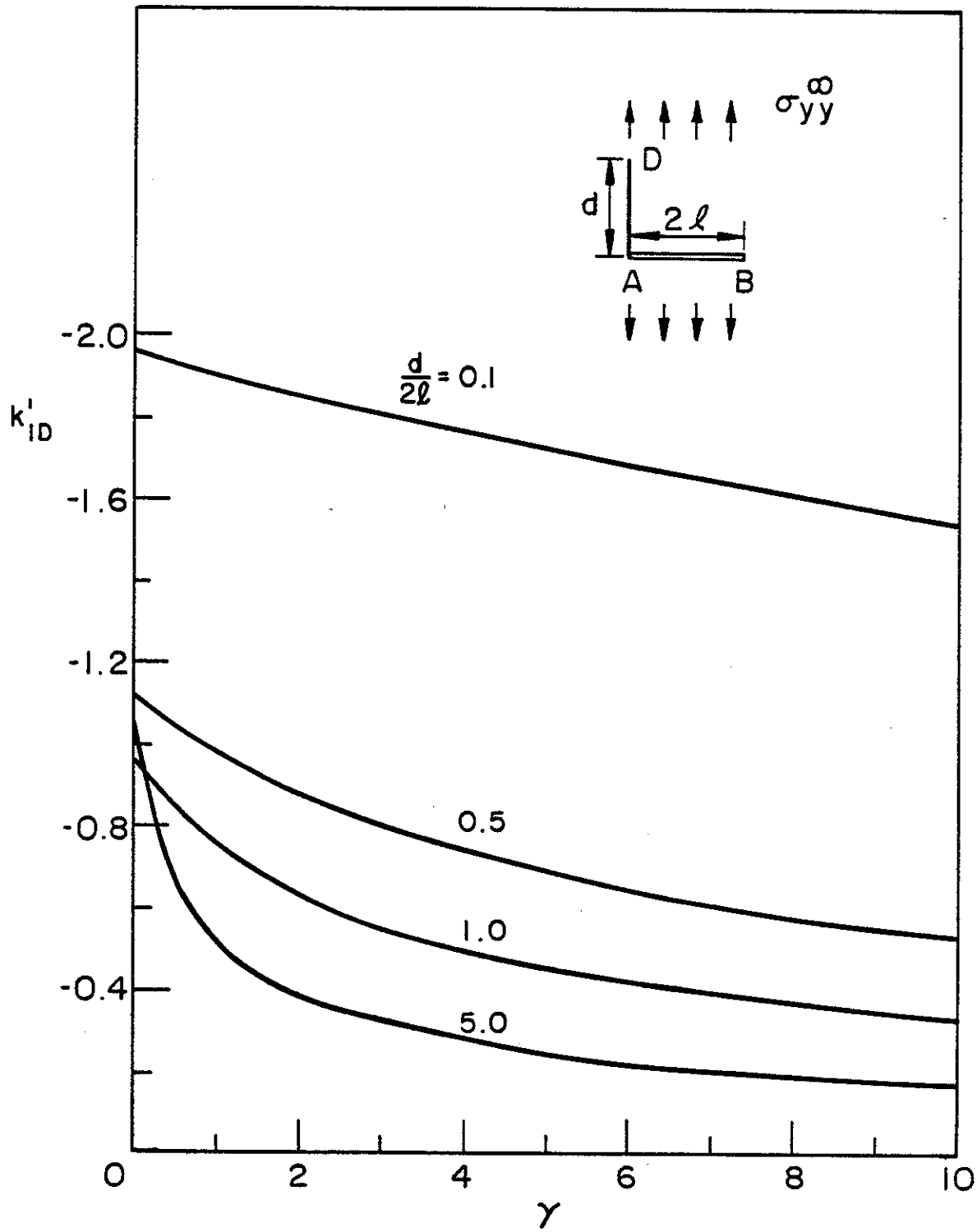

Figure 38. Normalized stress intensity factor for the inclusion-crack intersection problem for which $\theta = \pi/2$, $a = 0$, $b = 2\ell$, $c = 0$, $d/2\ell$ and γ variables. k_{ID}, $\sigma_{yy}^{\infty} \neq 0$.

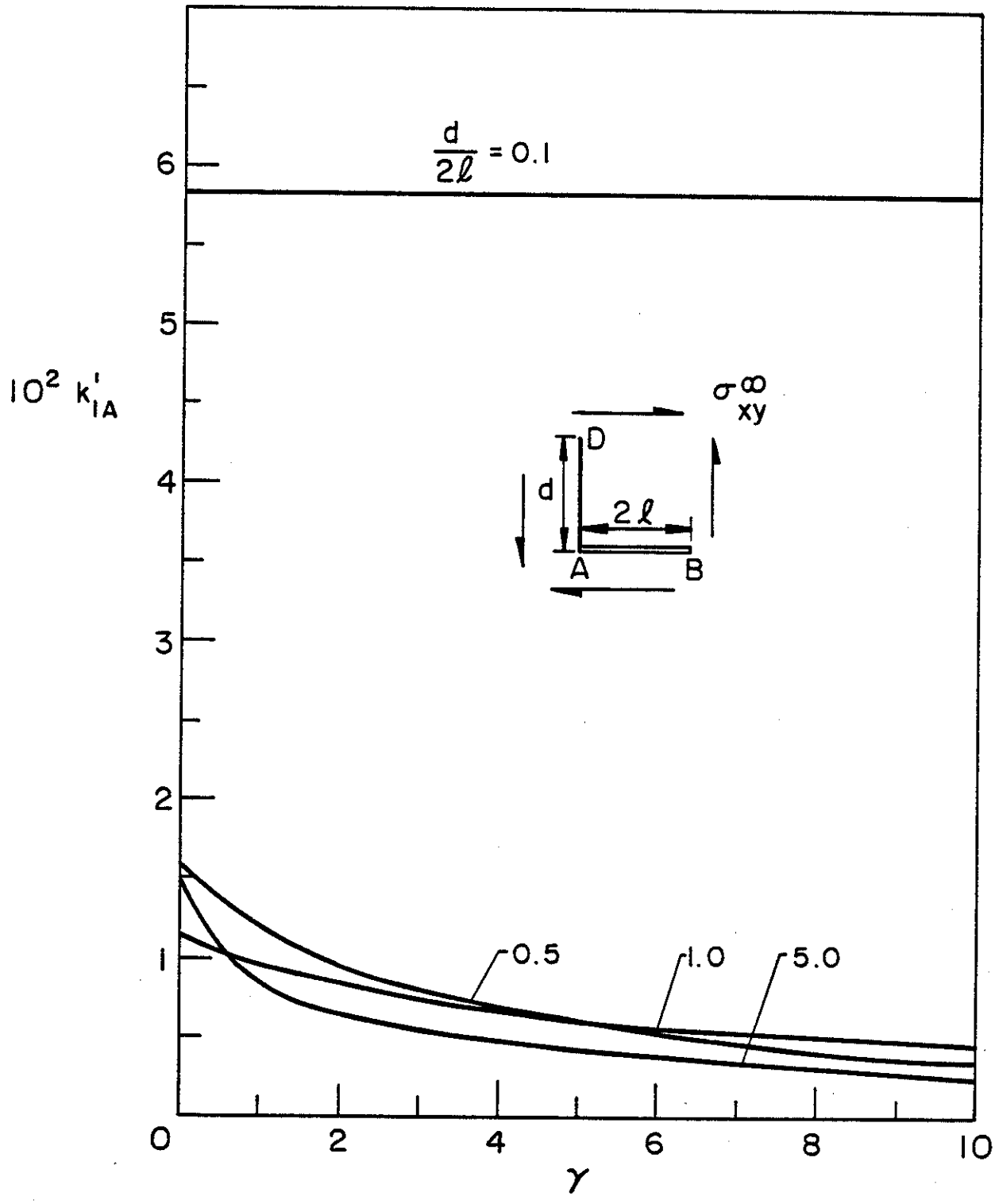

Figure 39. Normalized stress intensity factor for the inclusion-crack intersection problem for which $\theta = \pi/2$, $a = 0$, $b = 2\ell$, $c = 0$, $d/2\ell$ and γ variables. k_{IA} , $\sigma^{\infty}_{xy} \neq 0$.

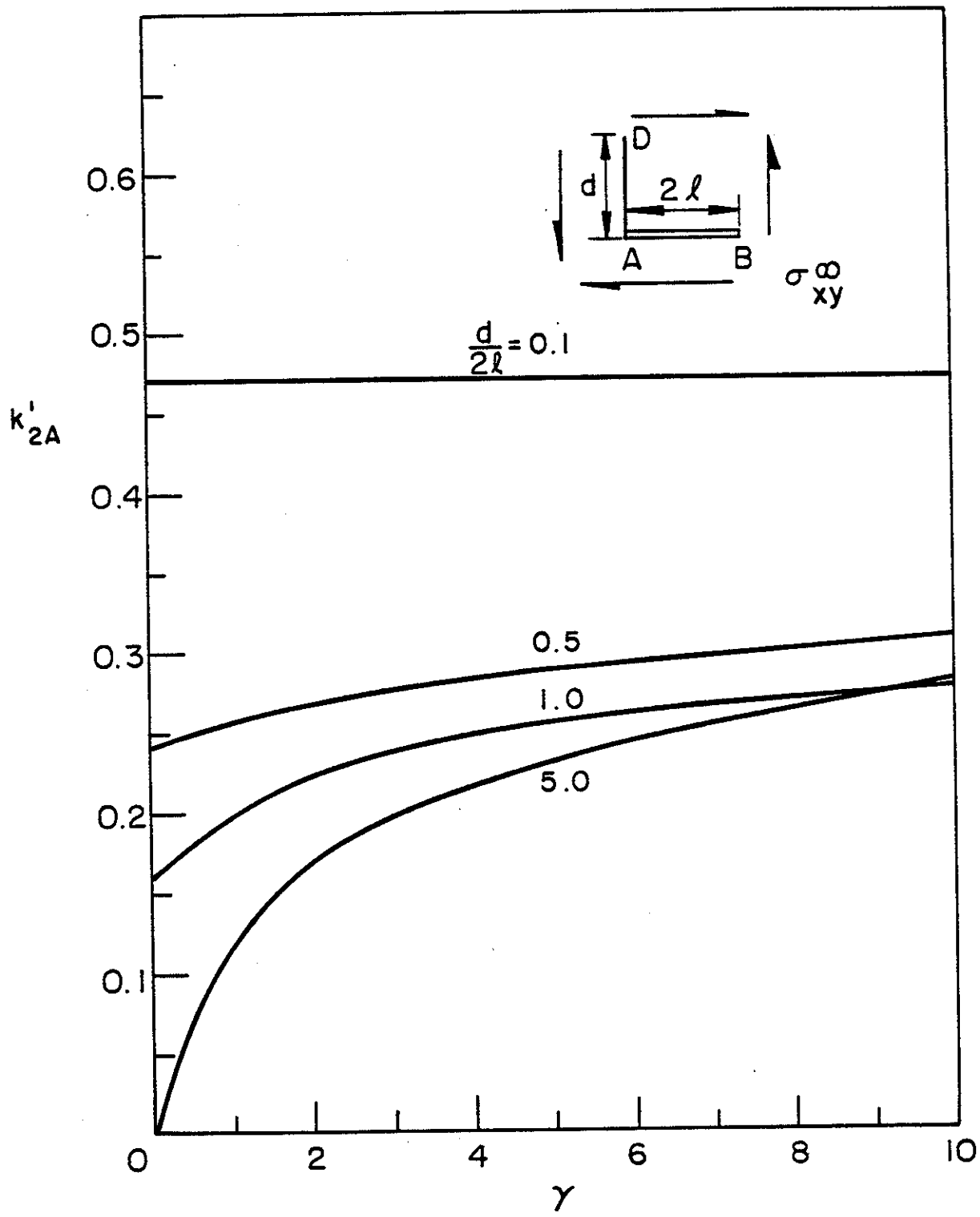

Figure 40. Normalized stress intensity factor for the inclusion-crack intersection problem for which $\theta = \pi/2$, a = 0, b = 2ℓ, c = 0, d/2ℓ and γ variables. k_{2A} , $\sigma^{\infty}_{xy} \neq 0$.

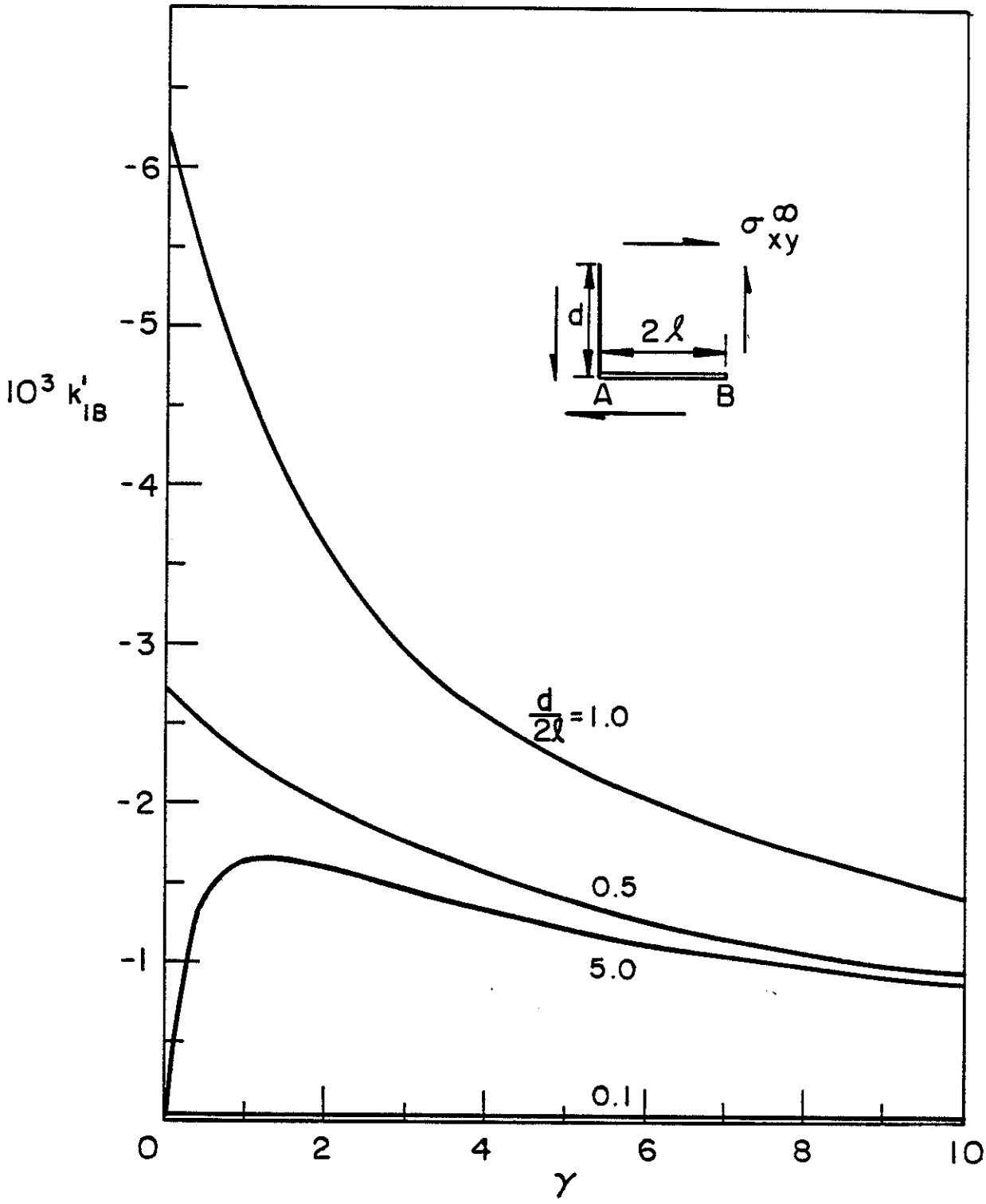

Figure 41. Normalized stress intensity factor for the inclusion-crack intersection problem for which $\theta = \pi/2$, a = 0, b = 2ℓ, c = 0, $d/2\ell$ and γ variables. k'_{IB}, $\sigma^{\infty}_{xy} \neq 0$.

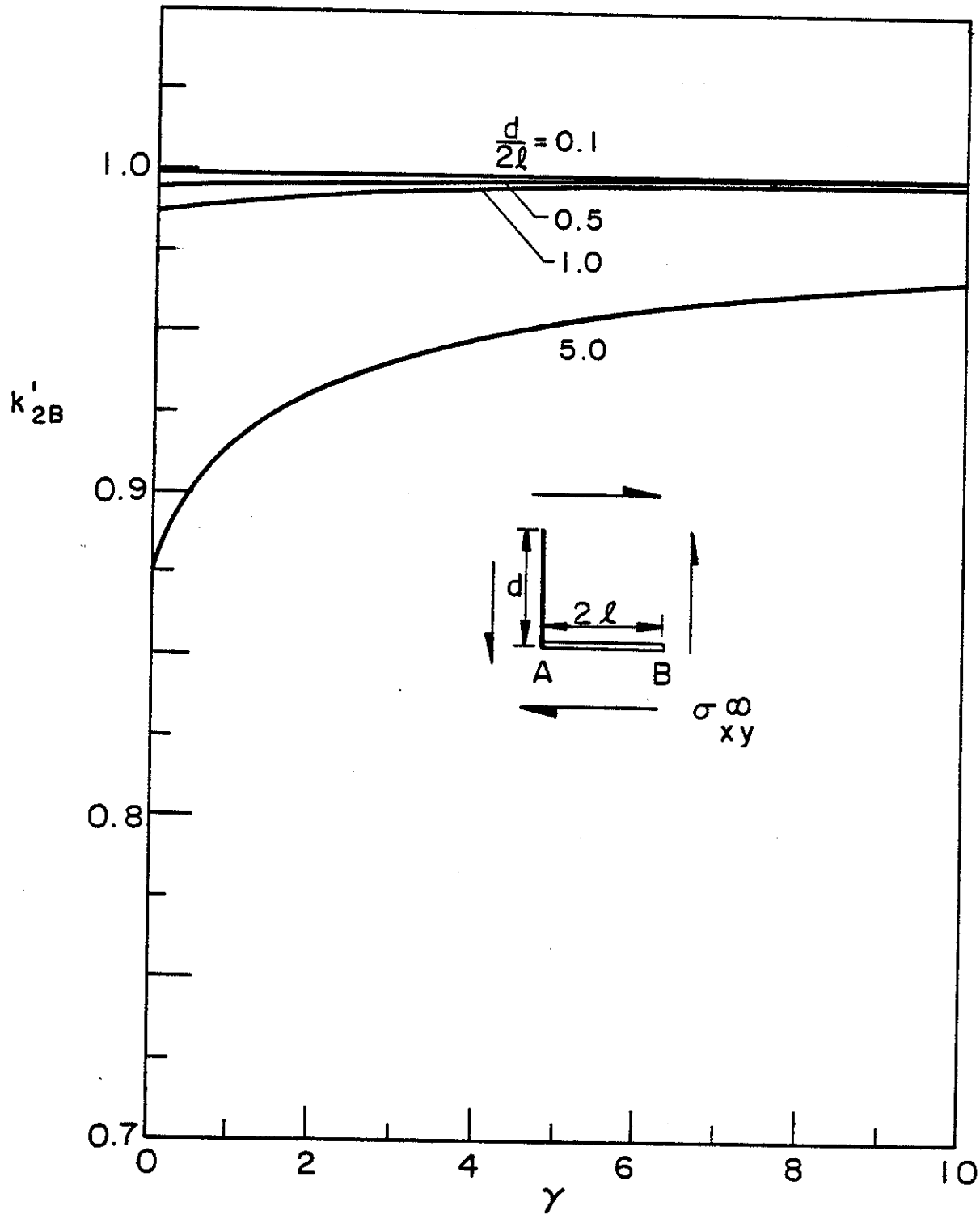

Figure 42. Normalized stress intensity factor for the inclusion-crack intersection problem for which $\theta = \pi/2$, a = 0, b = 2ℓ, c = 0, d/2ℓ and γ variables. k_{2B} , $\sigma^{\infty}_{xy} \neq 0$.

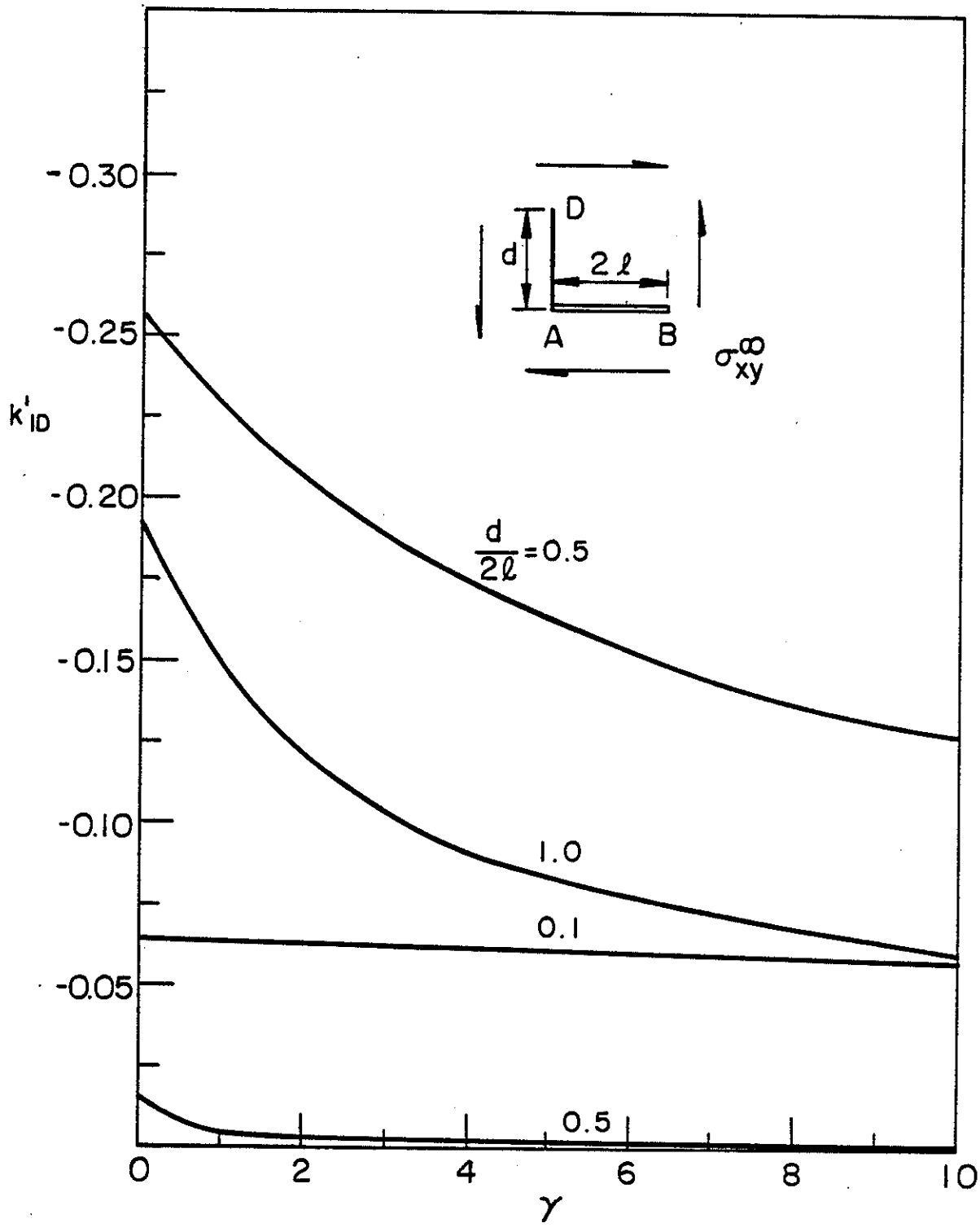

Figure 43. Normalized stress intensity factor for the inclusion-crack intersection problem for which $\theta = \pi/2$, $a = 0$, $b = 2\ell$, $c = 0$, $d/2\ell$ and γ variables. k_{ID} , $\sigma^{\infty}_{xy} \neq 0$.

APPENDIX D

FURTHER RESULTS ON CRACK-INCLUSION INTERACTION PROBLEM

Liu Xue-Hui and F. Erdogan

1. Introduction

The general formulation of the crack-inclusion interaction problem was given in Appendix C of this report. The general problem considered in Appendix C is described in Fig. 1. The inclusion-crack intersection problems studied in Appendix C included the cases of the common end points (i.e., a=0, c=0, Fig. 1) and the crack terminating at the inclusion. The intersection problem in which the inclusion end terminates at the crack was not studied. The special case of 90 degree angle of intersection is shown in Fig. 2 and is studied in this report.

2. The Formulation

The formulation of the problem is identical to that given in [1], except that in this case we have to consider two separate cracks along (-a<x<0, y=0) and (0<x<b, y=0). The reason for this is that at (x=0, y=+0) the stress state is expected to be singular with a power different than 1/2 and (-a,0), (0,b) and (0,d) must be treated as three separate lines of displacement or stress discontinuity. To formulate the problem we define the following unknown functions:

$$\frac{\partial}{\partial x}[u_y(x,+0)-u_y(x,-0)] = g_1(x) \ , \ 0<x<b \ ,$$

$$\frac{\partial}{\partial x}[u_x(x,+0)-u_x(x,-0)] = h_1(x) \ , \ 0<x<b \ ,$$

$$\frac{\partial}{\partial x}[u_y(x,+0)-u_y(x,-0)] = g_2(x) \ , \ -a<x<0 \ , \qquad (1a\text{-}e)$$

$$\frac{\partial}{\partial x}[u_x(x,+0)-u_x(x,-0)] = h_2(x) \ , \ -a<x<0$$

$p(y)$: distributed body force simulating the inclusion, $0<y<d$.

The Green's functions for the dislocations g and h and the concentrated body force p were given in [1]. The integral equations for the unknown functions defined in (1) are obtained from the boundary conditions on the crack surfaces and the displacement compatibility condition along the stiffener. These conditions may be expressed as (Fig. 2)

$$\sigma_{1dyy}(x,0) + \sigma_{2dyy}(x,0) + \sigma_{pyy}(x,0) + \sigma_{ayy}(x,0) = 0, \quad 0<x<b ,$$

$$\sigma_{1dxy}(x,0) + \sigma_{2dxy}(x,0) + \sigma_{pxy}(x,0) + \sigma_{axy}(x,0) = 0, \quad 0<x<b ,$$

$$\sigma_{1dyy}(x,0) + \sigma_{2dyy}(x,0) + \sigma_{pyy}(x,0) + \sigma_{ayy}(x,0) = 0, \quad -a<x<0 , \qquad (2a\text{-}e)$$

$$\sigma_{1dxy}(x,0) + \sigma_{2dxy}(x,0) + \sigma_{pxy}(x,0) + \sigma_{axy}(x,0) = 0, \quad -a<x<0 ,$$

$$\varepsilon_{1dyy}(0,y) + \varepsilon_{2dyy}(0,y) + \varepsilon_{pyy}(0,y) + \varepsilon_{ayy}(0,y) = \varepsilon_s(y), \quad 0<y<d,$$

where σ_{idyy}, σ_{idxy} and ε_{idyy} are the relevant stress and strain components due to the dislocation pairs g_i and h_i (i=1,2), σ_{pyy}, σ_{pxy} and ε_{pyy} are due to the concentrated body force p, σ_{ayy}, σ_{axy} and ε_{ayy} are the applied stress and strain components and $\varepsilon_s(y)$ is the strain in the inclusion. If the stress state away from the crack-inclusion region is given by σ^{∞}_{ij}, (i,j=x,y), then the applied stress and strain components are

$$\sigma_{ayy}(x,0) = \sigma^{\infty}_{yy} , \quad \sigma_{axy}(x,0) = \sigma^{\infty}_{xy} ,$$

$$\varepsilon_{ayy}(0,y) = \frac{1+\kappa}{8\mu}\left[-\frac{3-\kappa}{1+\kappa}\sigma^{\infty}_{xx} + \sigma^{\infty}_{yy}\right] , \qquad (3a\text{-}c)$$

where μ is the shear modulus and $\kappa=3-4\nu$ for plane strain and $\kappa=(3-\nu)/(1+\nu)$ for plane stress. By observing that the inclusion is under a longitudinal distributed force -p(y), the strain in the inclusion may be expressed as

$$\varepsilon_s(y) = -\frac{1+\kappa_s}{8\mu_s A_s}\int_y^d p(r)dr \qquad (4)$$

where κ_s and μ_s are the elastic constants and A_s is the cross-sectional area of the inclusion per unit thickness in z direction. The expressions for all the remaining terms are given in [1]. Thus, by using the kernels developed in [1], the system of equations (2) may be expressed as follows:

$$\frac{2\mu}{\pi(\kappa+1)}\left(\int_0^b \frac{g_1(t)dt}{t-x}+\int_{-a}^0 \frac{g_2(t)dt}{t-x}\right)-\frac{1}{2\pi(1+\kappa)}\int_0^d\left[\frac{(2+\kappa)t}{t^2+x^2}-\frac{t(3x^2-t^2)}{(t^2+x^2)^2}\right]p(t)dt$$

$$=-\sigma_{yy}^{\infty}\ ,\quad 0<x<b\ , \tag{5}$$

$$\frac{2\mu}{\pi(\kappa+1)}\left(\int_0^b \frac{h_1(t)dt}{t-x}+\int_{-a}^0 \frac{h_2(t)dt}{t-x}\right)-\frac{1}{2\pi(1+\kappa)}\int_0^d\left[\frac{\kappa x}{t^2+x^2}+\frac{x(3t^2-x^2)}{(t^2+x^2)^2}\right]p(t)dt$$

$$=-\sigma_{xy}^{\infty}\ ,\quad 0<x<b\ , \tag{6}$$

$$\frac{2\mu}{\pi(\kappa+1)}\left(\int_0^b \frac{g_1(t)dt}{t-x}+\int_{-a}^0 \frac{g_2(t)dt}{t-x}\right)-\frac{1}{2\pi(1+\kappa)}\int_0^d\left[\frac{(2+\kappa)t}{t^2+x^2}-\frac{t(3x^2-t^2)}{(t^2+x^2)^2}\right]p(t)dt$$

$$=-\sigma_{yy}^{\infty}\ ,\quad -a<x<0\ , \tag{7}$$

$$\frac{2\mu}{\pi(\kappa+1)}\left(\int_0^b \frac{h_1(t)dt}{t-x}+\int_{-a}^0 \frac{h_2(t)dt}{t-x}\right)-\frac{1}{2\pi(1+\kappa)}\int_0^d\left[\frac{\kappa x}{t^2+x^2}+\frac{x(3t^2-x^2)}{(t^2+x^2)^2}\right]p(t)dt$$

$$=-\sigma_{xy}^{\infty}\ ,\quad -a<x<0\ , \tag{8}$$

$$\frac{1}{\pi}\int_0^b \frac{t(t^2+3y^2)-\frac{3-\kappa}{1+\kappa}t(t^2-y^2)}{(t^2+y^2)^2}g_1(t)dt+\frac{1}{\pi}\int_0^b \frac{y(y^2-t^2)-\frac{3-\kappa}{1+\kappa}y(3t^2+y^2)}{(t^2+y^2)^2}h_1(t)dt$$

$$+\frac{1}{\pi}\int_{-a}^0 \frac{t(t^2+3y^2)-\frac{3-\kappa}{1+\kappa}t(t^2-y^2)}{(t^2+y^2)^2}g_2(t)dt+\frac{1}{\pi}\int_{-a}^0 \frac{y(y^2-t^2)-\frac{3-\kappa}{1+\kappa}y(3t^2+y^2)}{(t^2+y^2)^2}h_2(t)dt$$

$$+\frac{\kappa+3+\frac{3-\kappa}{1+\kappa}(\kappa-1)}{4\mu}\frac{1}{\pi}\int_0^d \frac{p(t)dt}{t-y}=-\frac{(1+\kappa)E}{2\mu A_s E_s}\int_0^y p(t)dt+\frac{1+\kappa}{2\mu}\left(\frac{3-\kappa}{1+\kappa}\sigma_{xx}^{\infty}-\sigma_{yy}^{\infty}\right)\ ,$$

$$0<y<d\ , \tag{9}$$

The integral equations (5)-(9) must be solved under the following single-valuedness and equilibrium conditions:

$$\int_{-a}^{o} g_2(t)dt + \int_{o}^{b} g_1(t)dt = 0 \ , \tag{10}$$

$$\int_{-a}^{o} h_2(t)dt + \int_{o}^{b} h_1(t)dt = 0 \ , \tag{11}$$

$$\int_{o}^{d} p(t)dt = 0 \ . \tag{12}$$

From Fig. 2 it is clear that the end points x=b, x=-a and y=d are points of stress singularity with standard 1/2 power [1]. However, the nature of the singularity at x=y=0 is not known and does not appear to have been studied before. To study this and to solve the problem described by equations (5)-(12) we express the unknown functions as follows:

$$g_1(t) = \frac{F_1(t)}{t^{\alpha}(b-t)^{\beta_1}} \ , \ h_1(t) = \frac{F_2(t)}{t^{\alpha}(b-t)^{\beta_2}} \ , \ (0<t<b) \ ,$$

$$g_2(t) = \frac{F_3(t)}{(-t)^{\alpha}(t+a)^{\beta_3}} \ , \ h_2(t) = \frac{F_4(t)}{(-t)^{\alpha}(t+a)^{\beta_4}} \ , \ (-a<t<0) \ ,$$

$$p(t) = \frac{\mu F_5(t)}{t^{\alpha}(d-t)^{\beta_5}} \ , \ (0<t<d) \ . \tag{13a-e}$$

where $F_1,\ldots,F_5$ are unknown bounded functions and

$$0<\mathrm{Re}(\alpha,\beta_k)<1 \ , \ (k = 1,\ldots,5) \ . \tag{14}$$

By substituting now from (13) into (5)-(9) and by using the function theoretic method (see, for example, [28])to perform the asymptotic analysis near the crack and inclusion tips (x=b, y=0), (x=-a, y=0) and (y=d, x=0) we first obtain the following standard characteristic equations:

$$\cot\pi\beta_k = 0 \quad , (k = 1,2,3,4,5) \tag{15}$$

giving $\beta_k = 1/2$, $(k=1,\ldots,5)$. Similarly, the asymptotic analysis around the singular point $(x=0, y=0)$ yields

$$\frac{F_1(0)}{b^{\beta_1}} \frac{\cot\pi\alpha}{x^\alpha} - \frac{F_3(0)}{a^{\beta_3}} \frac{1}{x^\alpha \sin\pi\alpha} + \frac{F_5(0)}{d^{\beta_5}} \frac{c_1 - \alpha/2}{2x^\alpha \sin\frac{\pi\alpha}{2}} = R_1(x) \ ,$$

$$\frac{F_2(0)}{b^{\beta_2}} \frac{\cot\pi\alpha}{x^\alpha} - \frac{F_4(0)}{a^{\beta_4}} \frac{1}{x^\alpha \sin\pi\alpha} + \frac{F_5(0)}{d^{\beta_5}} \frac{c_2 - (1-\alpha)/2}{2x^\alpha \cos\frac{\pi\alpha}{2}} = R_2(x) \ ,$$

$$\frac{F_1(0)}{b^{\beta_1}} \frac{1}{x^\alpha \sin\pi\alpha} - \frac{F_3(0)}{a^{\beta_3}} \frac{\cot\pi\alpha}{x^\alpha} + \frac{F_5(0)}{d^{\beta_5}} \frac{c_1 - \alpha/2}{2x^\alpha \sin\frac{\pi\alpha}{2}} = R_3(x) \ ,$$

$$\frac{F_2(0)}{b^{\beta_2}} \frac{1}{x^\alpha \sin\pi\alpha} - \frac{F_4(0)}{a^{\beta_4}} \frac{\cot\pi\alpha}{x^\alpha} - \frac{F_5(0)}{d^{\beta_5}} \frac{c_2 - (1-\alpha)/2}{2x^\alpha \cos\frac{\pi\alpha}{2}} = R_4(x) \ ,$$

$$\frac{F_1(0)}{b^{\beta_1}} \frac{c_3 + c_4\alpha/2}{2y^\alpha \sin\frac{\pi\alpha}{2}} + \frac{F_2(0)}{b^{\beta_2}} \frac{c_3 - c_4(1-\alpha)/2}{2y^\alpha \cos\frac{\pi\alpha}{2}} - \frac{F_3(0)}{a^{\beta_3}} \frac{c_3 + c_4\alpha/2}{2y^\alpha \sin\frac{\pi\alpha}{2}}$$

$$+ \frac{F_4(0)}{a^{\beta_4}} \frac{c_3 - c_4(1-\alpha)/2}{2y^\alpha \cos\frac{\pi\alpha}{2}} + \frac{F_5(0)}{d^{\beta_5}} \frac{c_5 \cot\pi\alpha}{y^\alpha} = R_5(x) \ , \tag{16a-e}$$

where the functions $R_1,\ldots,R_5$ represent all the bounded terms near and at $(x=0,y=0)$ and the constants c_i are given by

$$c_1 = (\kappa+3)/4 \ , \ c_2 = (\kappa-1)/4 \ , \ c_3 = 2(\kappa-1)/(\kappa+1) \ ,$$

$$c_4 = 8/(\kappa+1) \ , \ c_5 = 2\kappa/(\kappa+1) \ . \tag{17}$$

If we now multiply both sides of (16a-d) by x^α and (16e) by y^α and let $x=0$, $y=0$ we obtain a system of five linear homogeneous algebraic equations in $F_1(0),\ldots,F_5(0)$. Since $F_1(0),\ldots,F_5(0)$ are nonzero, the determinant of the

coefficients of this algebraic system must be zero, giving the following characteristic equation to determine the power of singularity α

$$\{c_5(2\cos^2\frac{\pi\alpha}{2}-1) + [c_2-(1-\alpha)/2][c_3-c_4(1-\alpha)/2]$$
$$- (c_1-\alpha/2)(c_3+c_4\alpha/2)\}(1-\cos^2\frac{\pi\alpha}{2})\cos^2\frac{\pi\alpha}{2} = 0 \ . \qquad (18)$$

From (18) and (17) it may be observed that α is a function of κ and hence, for a given value of the Poisson's ratio ν, would have slightly different values for plane strain and plane stress cases. The values of α obtained from (18) are given in Table B1. Around the point (x=0, y=+0) the stress state has the behavior

$$\sigma_{ij} \cong \frac{1}{r^\alpha} \ , \ (r^2 = x^2+y^2) \ . \qquad (19)$$

Table 1. The power α of stress singularity at (x=0, y=+0).

ν	α	
	Plane Strain	Plane Stress
0	0	0
0.1	0.1329561	0.1237571
0.2	0.2189266	0.1926872
0.3	0.2888271	0.2416508
0.4	0.3500900	0.2794708
0.5	0.4053884	0.3100165

From Table 1 it may be seen that the stress singularity for the plane strain case is somewhat stronger than that for the plane stress case.

3. The Stress Intensity Factors

The system of singular integral equations (5)-(9) is solved by normalizing the intervals (0,b), (-a,0) and (0,d) and by using Gauss-Jacobi integration formulas [2]. The normalization is accomplished by defining

$$t = \frac{b}{2}(r+1)\ ,\ x = \frac{b}{2}(s+1)\ ,\ (0<(x,t)<b,\ -1<(r,s)<1)\ ;$$

$$t = \frac{a}{2}(r-1)\ ,\ x = \frac{a}{2}(s-1)\ ,\ (-a<(x,t)<0,\ -1<(r,s)<1)\ ;$$

$$t = \frac{d}{2}(r+1)\ ,\ y = \frac{d}{2}(s+1)\ ,\ (0<(y,t)<d,\ -1<(r,s)<1);$$

$$g_1(t) = G_1(r)w_1(r)\ ,\ h_1(t) = G_2(r)w_1(r)\ ,\ w_1(r) = (1+r)^{-\alpha}(1-r)^{-1/2}\ ,$$

$$g_2(t) = G_3(r)w_2(r)\ ,\ h_2(t) = G_4(r)w_2(r)\ ,\ w_2(r) = (1-r)^{-\alpha}(1+r)^{-1/2}\ ,$$

$$p(t) = G_5(r)w_3(r)\ ,\ w_3(r) = (1+r)^{-\alpha}(1-r)^{-1/2},\ (-1<r<1)\ . \qquad (20)$$

With (20) the stress intensity factors at the singular points may be defined and evaluated as follows:

$$k_1(b) = \lim_{x\to b}\sqrt{2(x-b)}\ \sigma_{yy}(x,0) = -\frac{2\mu}{1+\kappa}\frac{\sqrt{b}}{2^{\alpha}}G_1(1)\ , \qquad (21)$$

$$k_2(b) = \lim_{x\to a}\sqrt{2(x-b)}\ \sigma_{xy}(x,0) = -\frac{2\mu}{1+\kappa}\frac{\sqrt{b}}{2^{\alpha}}G_2(1)\ , \qquad (22)$$

$$k_1(-a) = \lim_{x\to -b}\sqrt{-2(x+a)}\ \sigma_{yy}(x,0) = \frac{2\mu}{1+\kappa}\frac{\sqrt{a}}{2^{\alpha}}G_3(-1)\ , \qquad (23)$$

$$k_2(-a) = \lim_{x\to -b}\sqrt{-2(x+a)}\ \sigma_{xy}(x,0) = \frac{2\mu}{1+\kappa}\frac{\sqrt{a}}{2^{\alpha}}G_4(-1)\ , \qquad (24)$$

$$k_1(d) = \lim_{y\to d+0} \sqrt{2(y-d)}\,\sigma_{xx}(0,y) = -\lim_{y\to d-0} \frac{1}{2}\frac{\kappa-1}{\kappa+1}\sqrt{2(d-y)}p(y)$$

$$= -\frac{\kappa-1}{2(\kappa+1)}\frac{\sqrt{d}}{2^{\alpha}}G_5(1) \quad . \quad (*) \qquad (25)$$

At the singular point (x=0, y=+0) we define the stress intensity factors in terms of the tensile and shear cleavage stresses as follows:

$$k_{xx}(0) = \lim_{y\to 0} \sqrt{2}\; y^{\alpha}\,\sigma_{xx}(0,y) \quad , \qquad (26)$$

$$k_{xy}(0) = \lim_{y\to 0} \sqrt{2}\, y^{\alpha}\,\sigma_{xy}(+0,y) \quad . \qquad (27)$$

From (26) and the solution of the problem k_1 may be found as follows:

$$k_{xx}(0) = \frac{2\mu}{\kappa+1}\frac{1}{2^{\alpha}}\left[\frac{(1-\alpha)a^{\alpha}G_1(-1)}{2\sin\frac{\pi\alpha}{2}} + \frac{(2-\alpha)a^{\alpha}G_2(-1)}{2\cos\frac{\pi\alpha}{2}} - \frac{(1-\alpha)b^{\alpha}G_3(1)}{2\sin\frac{\pi\alpha}{2}}\right.$$

$$\left. + \frac{(2-\alpha)b^{\alpha}G_4(1)}{2\cos\frac{\pi\alpha}{2}}\right] - \frac{\kappa-1}{2(\kappa+1)}\frac{1}{2^{\alpha}}\frac{d^{\alpha}G_5(-1)}{\sin\pi\alpha} \quad . \qquad (28)$$

Also, from the general local equilibrium condition

$$\sigma_{xy}(+0,y) - \sigma_{xy}(-0,y) + p(y) = 0 \qquad (29)$$

and from $|\sigma^{+}_{xy}| = |\sigma^{-}_{xy}|$ we obtain

$$k_{xy}(0) = -\lim_{y\to 0}\frac{\sqrt{2}}{2}y^{\alpha}p(y) = -\left(\frac{d}{2}\right)^{\alpha}\frac{G_5(-1)}{2} \quad . \qquad (30)$$

(*) See Appendix C

4. The Results

The only solution which was not discussed in [1] is the crack-inclusion intersection problem shown in Fig. 2. Particularly important in this case is the stress state around the point of intersection (x=0, y=+0) as it relates to the initiation of a branching crack at this point. In calculating the results it is assumed that away from the crack inclusion region the medium is subjected to a uniform stress state given by σ^{∞}_{xx}, σ^{∞}_{yy}, σ^{∞}_{xy}. Since the superposition is valid, the problem is solved by taking one of these three stress components nonzero at a time. The results are shown in Figures 3- 12. At the crack tips the figures show the normalized Mode I and Mode II stress intensity factors defined by

$$k_1'(a) = \frac{k_1(a)}{\sigma^{\infty}_{ij}\sqrt{a/2}} , \quad k_2'(a) = \frac{k_2(a)}{\sigma^{\infty}_{ij}\sqrt{a/2}} , \quad k_1'(b) = \frac{k_1(b)}{\sigma^{\infty}_{ij}\sqrt{b/2}} ,$$

$$k_2'(b) = \frac{k_2(b)}{\sigma^{\infty}_{ij}\sqrt{b/2}} , \quad (i,j=x,y) . \qquad (31a\text{-}d)$$

At the inclusion tip (x=0, y=d) we define [1]

$$k_1'(d) = k_1(d)/k_o , \quad k_o = \frac{1-\kappa}{2(1+\kappa)}\,\sigma^{\infty}_{ij}\sqrt{d}/2^{\alpha} , \quad (i,j=x,y) . \qquad (32a\text{-}b)$$

The tensile and shear stress intensity factors at (x=0, y=+0) are normalized as follows:

$$k'_{xx}(0) = k_{xx}(0)/(\sigma^{\infty}_{ij}\sqrt{d/2}) , \quad k'_{xy}(0) = 2k_{xy}(0)/(\sigma^{\infty}_{ij}\sqrt{d/2}) , \quad (i,j=x,y). \ (*) \qquad (33a,b)$$

Figure 3 shows the normalized Mode I stress intensity factors at the crack tips for a uniform stress σ^{∞}_{yy} away from the crack-inclusion region. Note

(*) Note the factor of 2 in (33b); k'_{xy} is the "stress intensity factor" corresponding to p(y) at y=0 (see Eqs. 29 and 30).

that as the crack tip approaches the crack-inclusion intersection point (x=0, y=0) the corresponding stress intensity factor becomes unbounded (see, also, the results given in [1]). For this loading condition the Mode II stress intensity factors are very small and, hence, are not presented. Figure 4 shows the Mode II stress intensity factors at the crack tip for the pure shear loading σ^{∞}_{xy} which are nearly identical to those shown in Fig. 3. Similarly, for the shear loading the Mode I stress intensity factors are very small and, therefore, are not presented. The normalized stress intensity factor at the inclusion tip (x=0, y=d) is shown in Fig. 5 for the three uniform applied stresses σ^{∞}_{xx}, σ^{∞}_{yy} and σ^{∞}_{xy}. In the results shown in figures 3- 12 it is assumed that the medium is under plane strain condition, the Poisson's ratio of the plane is 0.3 and, unless stated otherwise, the stiffness parameter

$$\gamma = \frac{\mu(1+\kappa_s)}{A_s\mu_s(1+\kappa)} \tag{34}$$

has a value of 0.1. The effect of γ on $k_1(d)$ is shown in Fig. 6.

The effect of the relative location (a/b) of the inclusion on the stress intensity factors $k_{xx}(0)$ and $k_{xy}(0)$ at crack-inclusion intersection point (x=0, y=+0) is shown in Figures 7 and 8. Figures 9 and 10 show the effect of the stiffness parameter γ on $k_{xx}(0)$ and $k_{xy}(0)$. The effect of the inclusion length d on the stress intensity factors is shown in Figures 11 and 12.

REFERENCES

1. Appendix C of this report.

2. F. Erdogan, "Mixed Boundary Value Problems in Mechanics", Mechanics Today, S. Nemat-Nasser, ed., Vol. 4, p.1, Pergamon Press, Oxford, 1978.

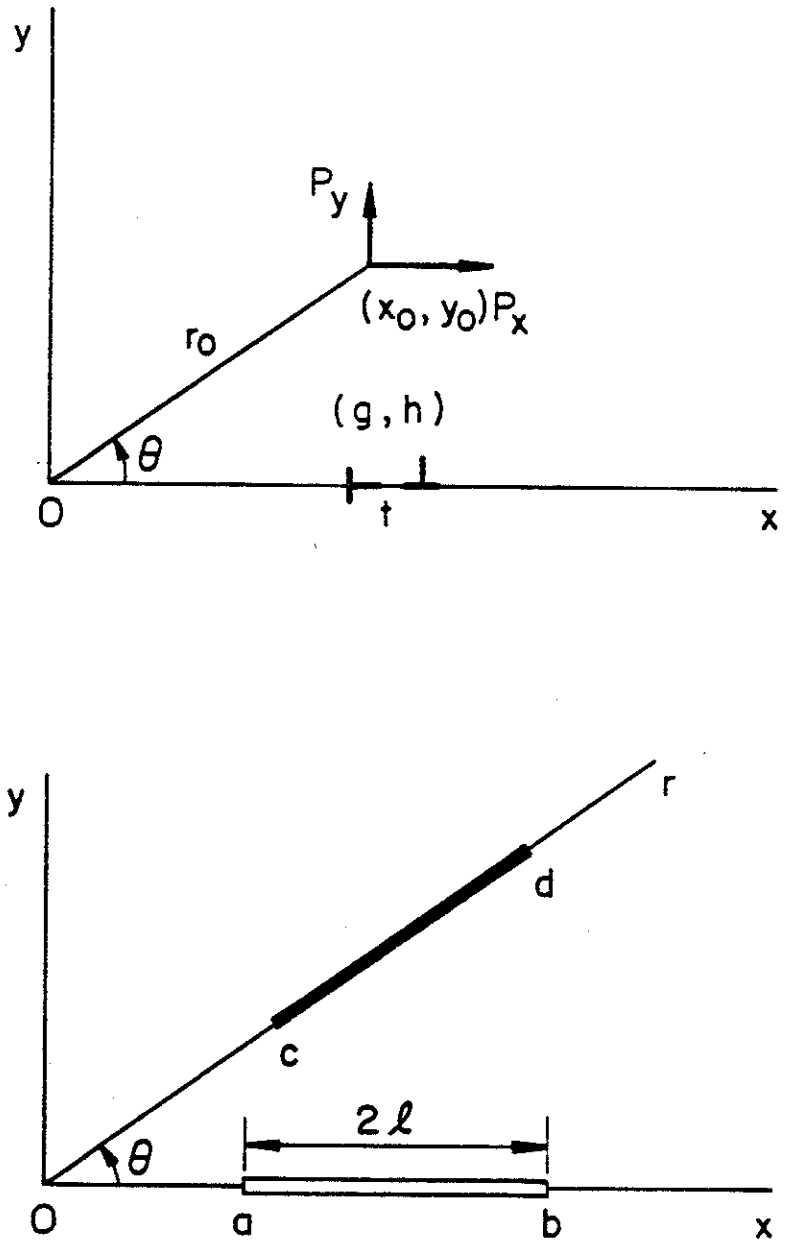

Figure 1. The geometry and notation for the crack-inclusion problem.

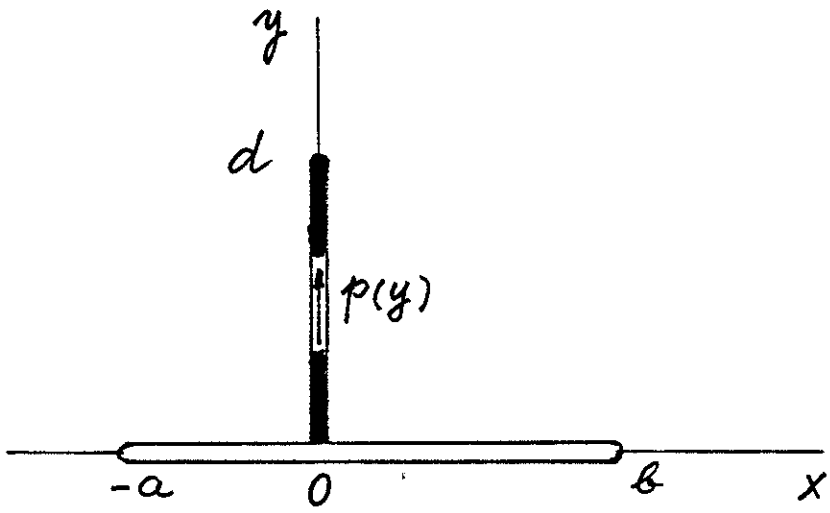

Figure 2. The crack-inclusion geometry.

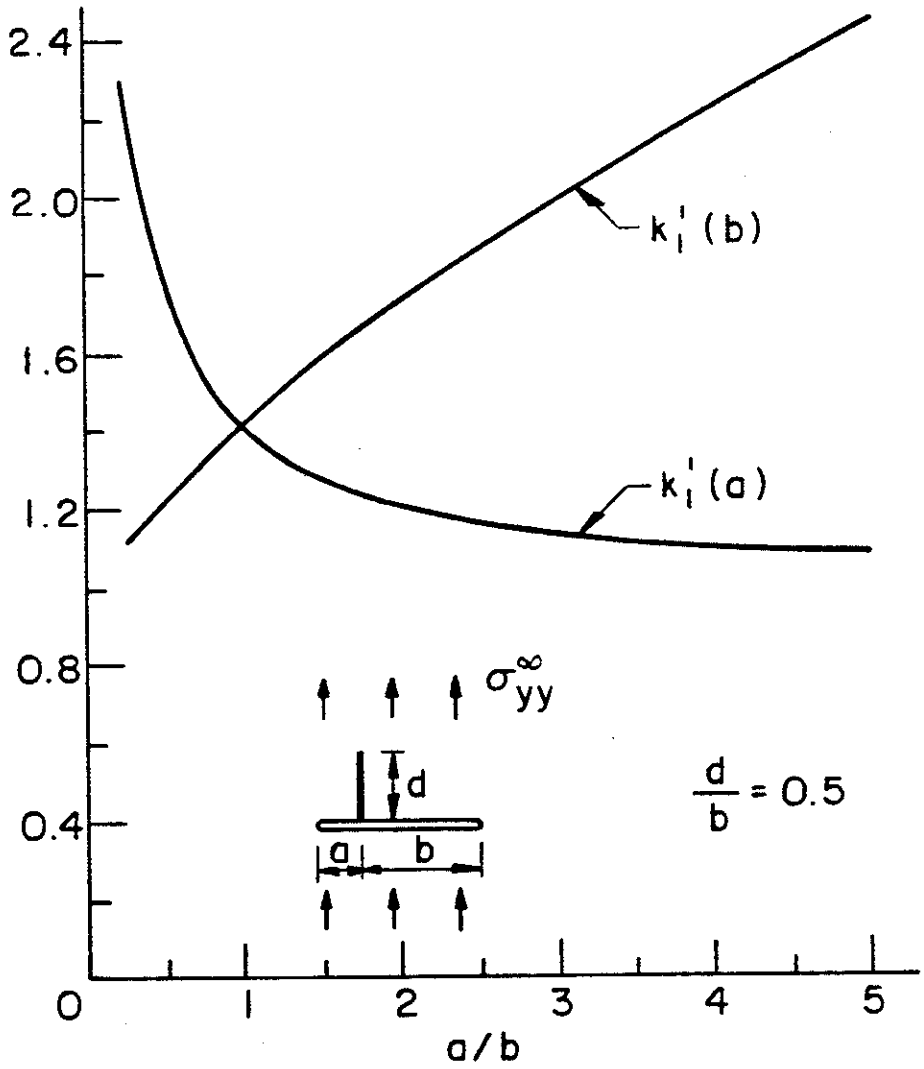

Figure 3. Normalized Mode I stress intensity factors at the crack tip, ν=0.3, γ=0.1.

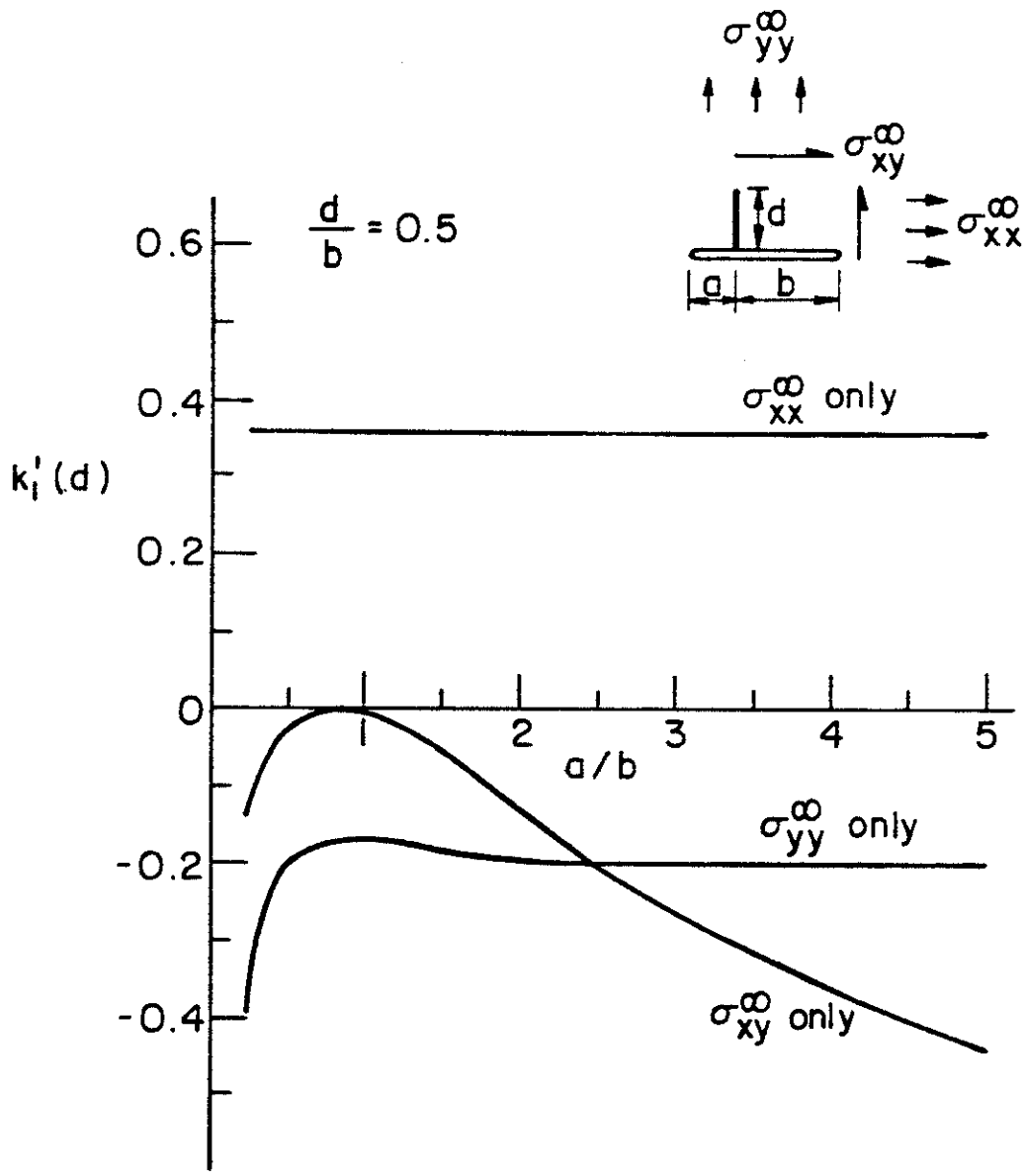

Figure 5. Normalized stress intensity factor at the inclusion end, ν=0.3, γ=0.1.

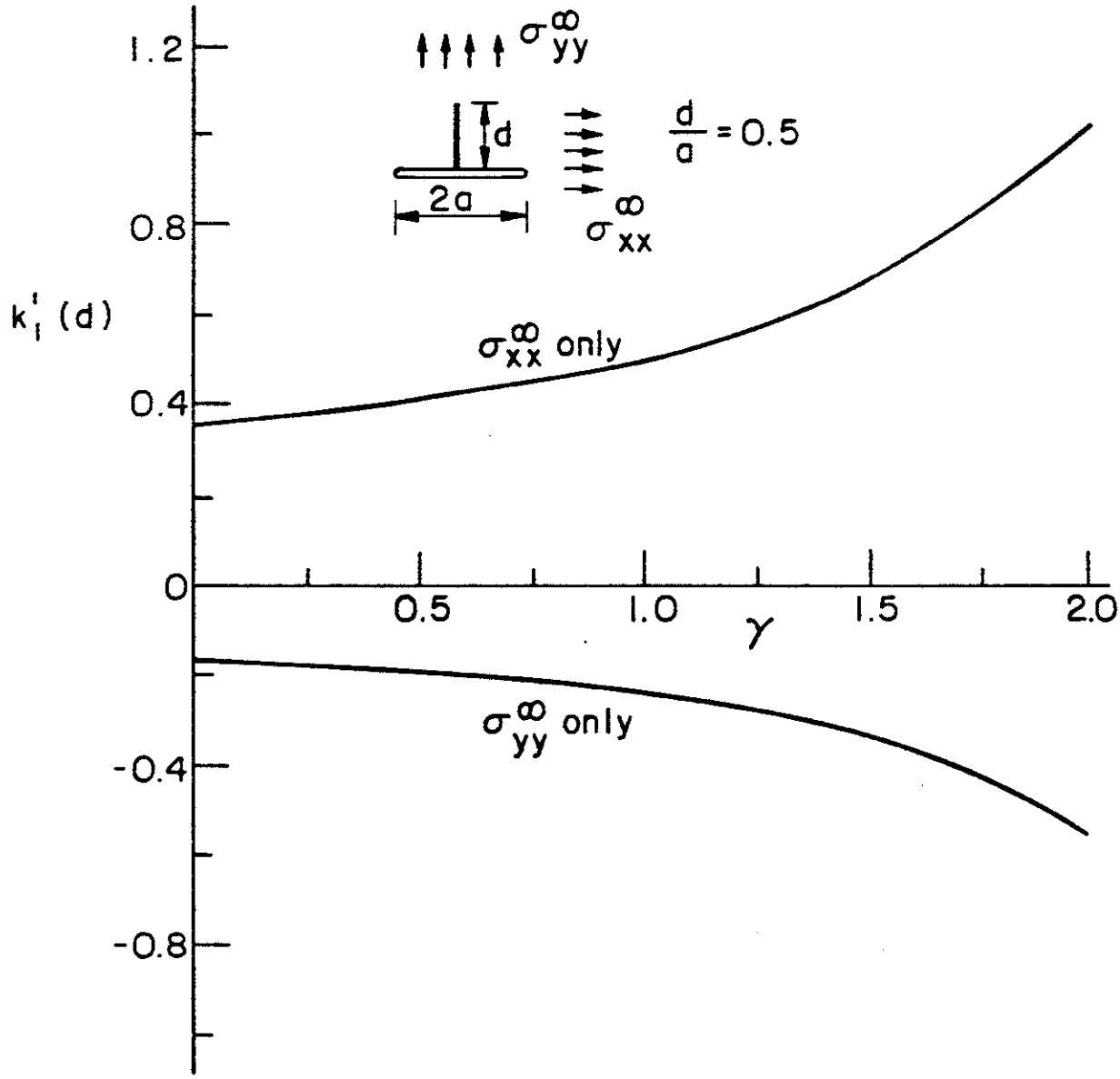

Figure 6. The effect of the stiffness parameter γ on the stress intensity factor at the inclusion end, ν=0, b=a.

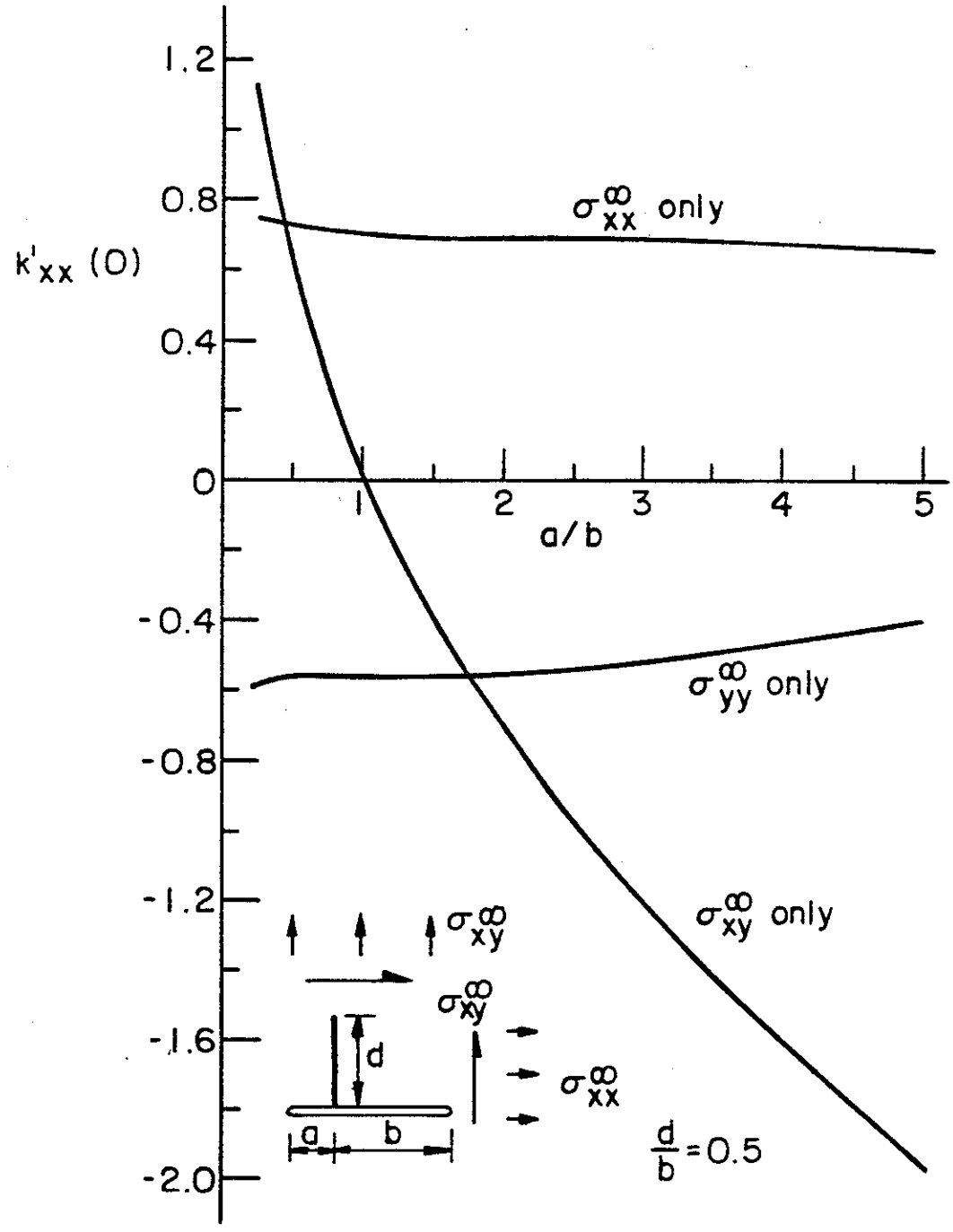

Figure 7. "Tensile" component $k_{xx}(0)$ of the stress intensity factor at the crack-inclusion intersection point, ν=0.3, γ=0.1.

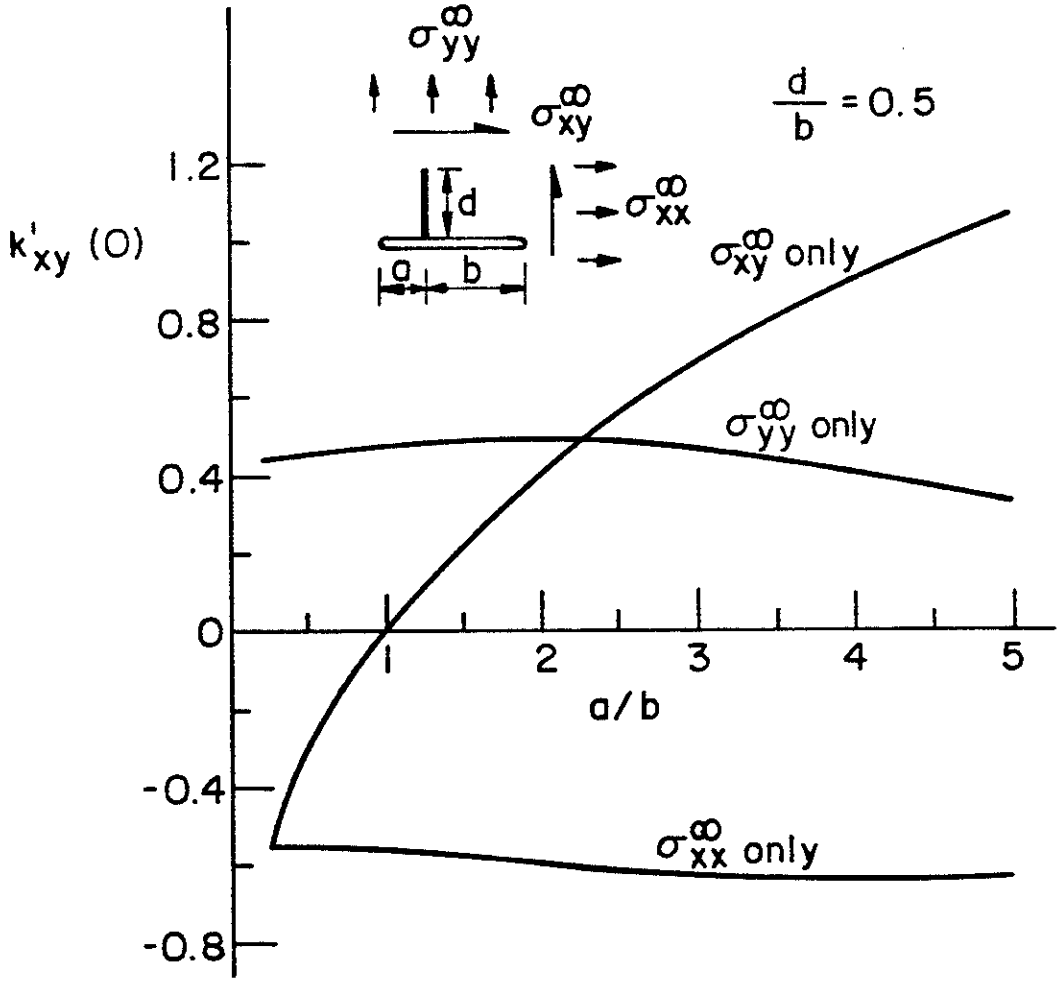

Figure 8. "Shear" component $k_{xy}(0)$ of the stress intensity factor at the crack-inclusion intersection point, ν=0.3, γ=0.1.

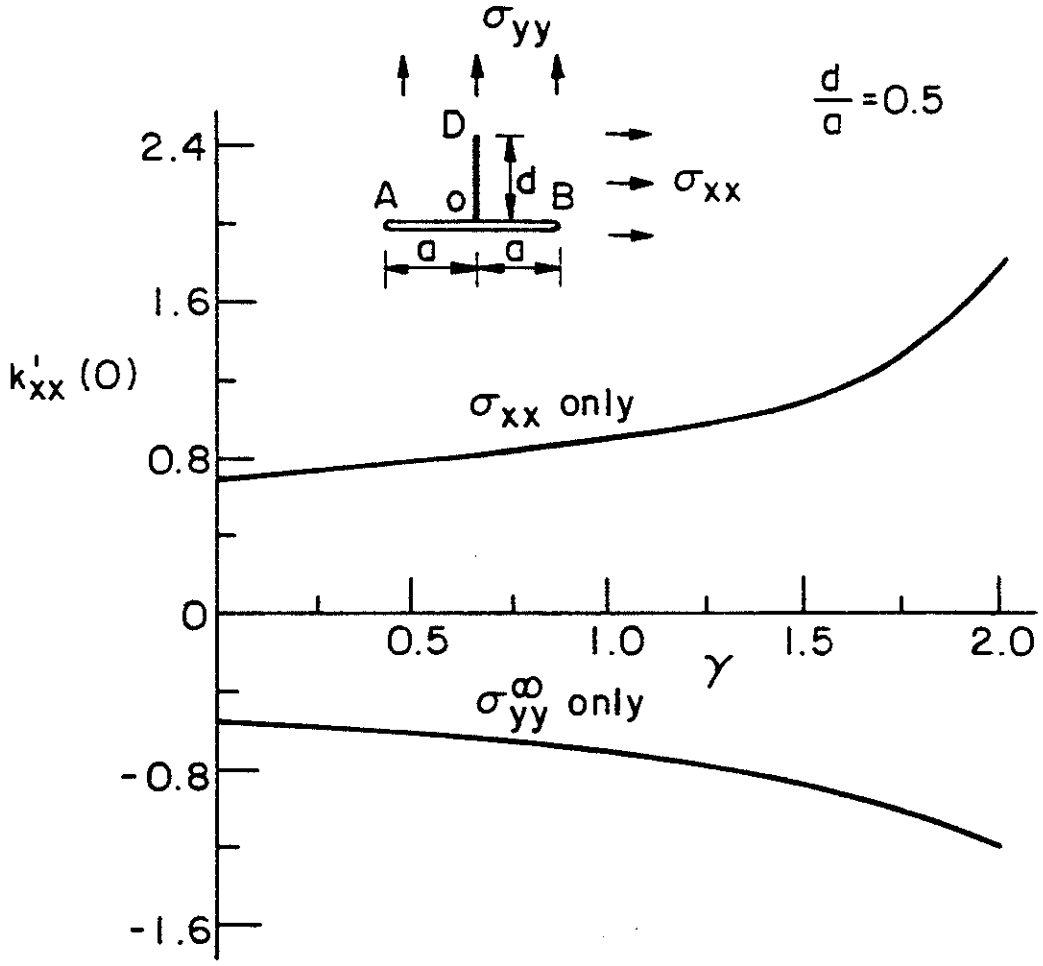

Figure 9. The effect of stiffness ratio γ on $k_{xx}(0)$, ν=0.3, a=b=2d.

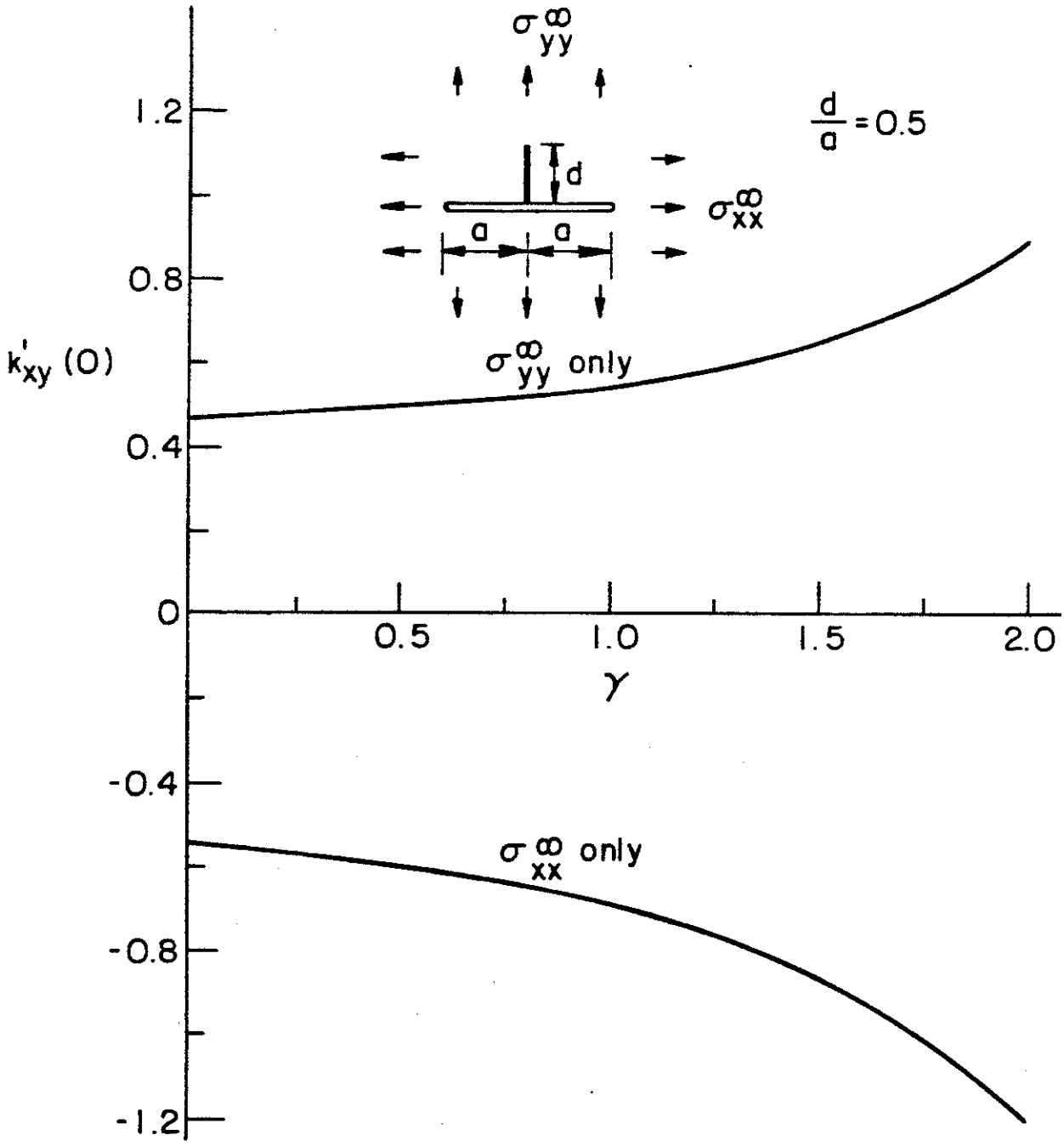

Figure 10. The effect of γ on $k_{xy}(0)$, ν=0.3, a=b=2d.

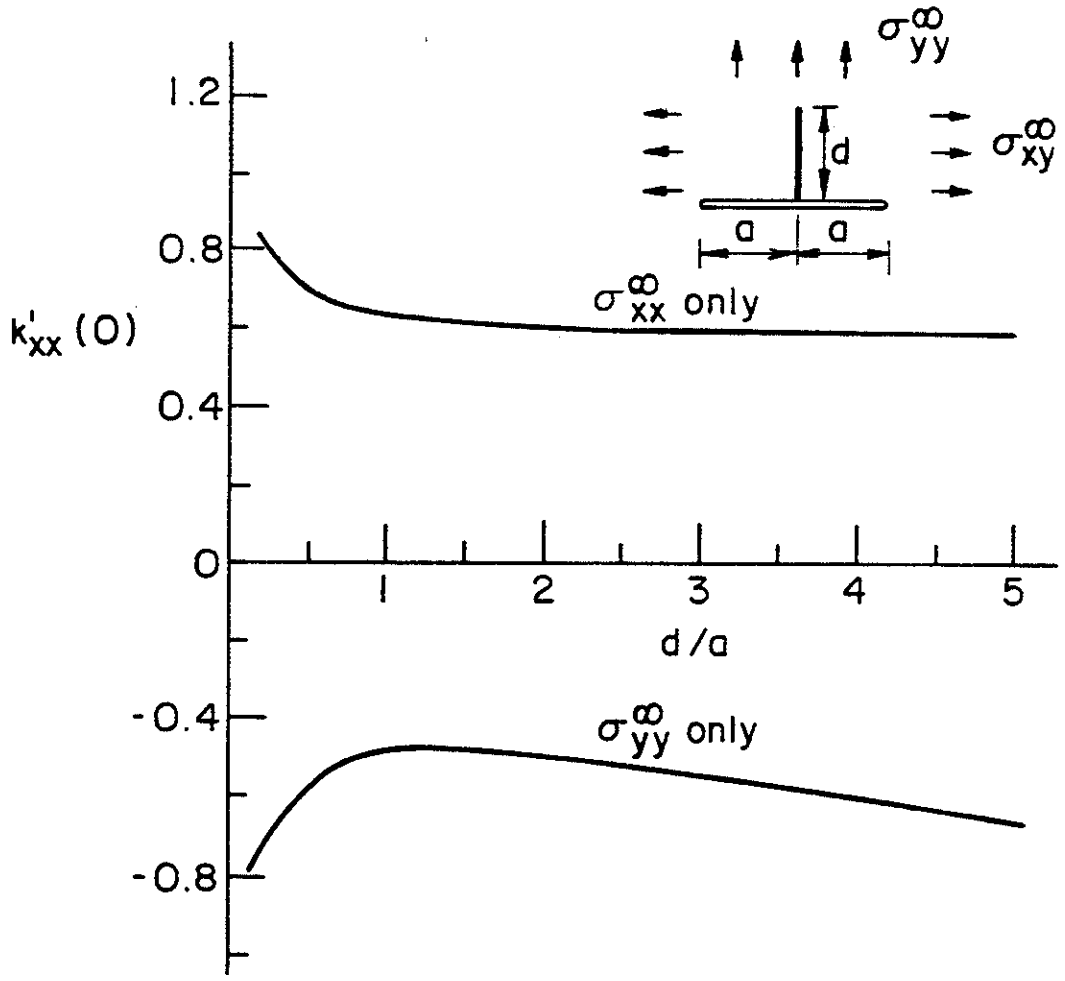

Figure 11. The effect of the inclusion length d on $k_{xx}(0)$, ν=0.3, γ=0.1, a=b.

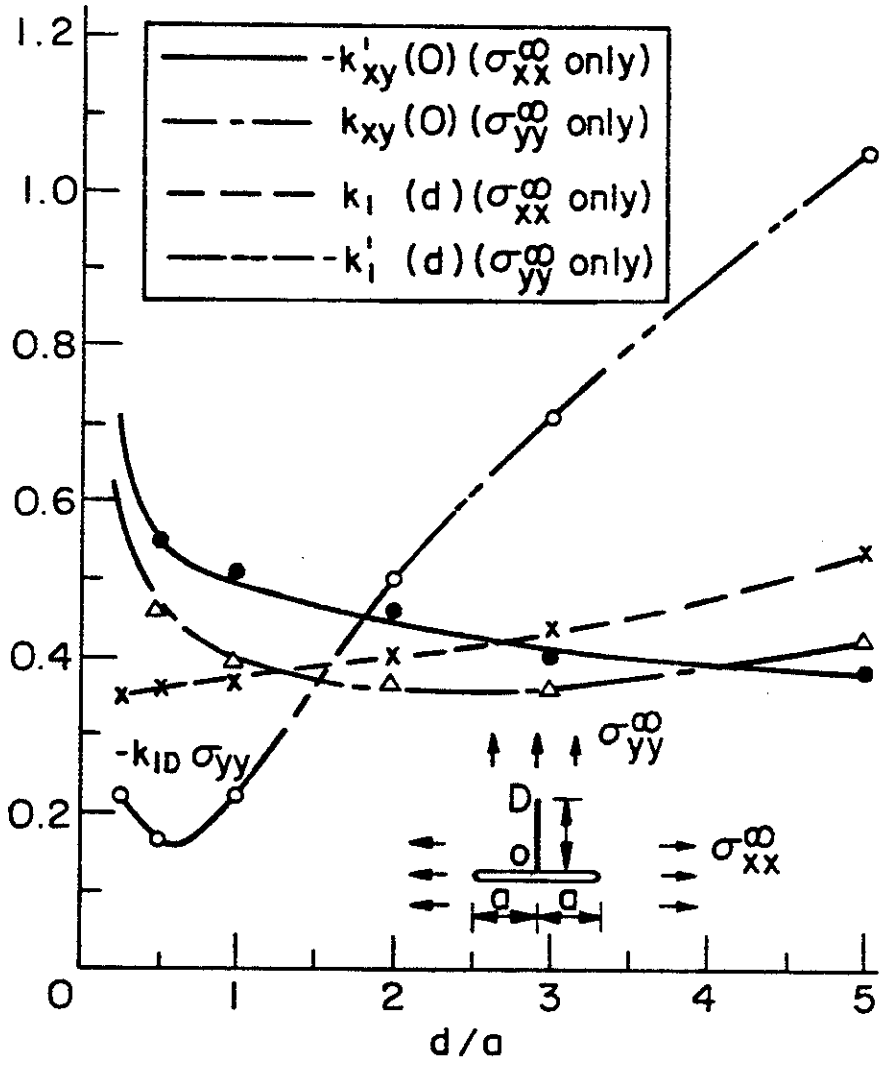

Figure 12. The effect of the inclusion length d on the stress intensity factors at the inclusion ends (x=0, y=d) and (x=0, y=+0), ν=0.3, γ=0.1.

APPENDIX E

A CYLINDRICAL SHELL WITH AN ARBITRARILY ORIENTED CRACK

O.S. Yahsi and F. Erdogan

Lehigh University, Bethlehem, PA.

ABSTRACT

In this paper the general problem of a shallow shell with constant curvatures is considered. It is assumed that the shell contains an arbitrailiy oriented through crack and the material is specially orthotropic. The nonsymmetric problem is solved for arbitrary self-equilibrating crack surface tractions, which, added to an appropriate solution for an uncracked shell, would give the result for a cracked shell under most general loading conditions. The problem is reduced to a system of five singular integral equations in a set of unknown functions representing relative displacements and rotations on the crack surfaces. The stress state around the crack tip is asymptotically analyzed and it is shown that the results are identical to those obtained from the two-dimensional in-plane and anti-plane elasticity solutions. The numerical results are given for a cylindrical shell containing an arbitrarily oriented through crack. Some sample results showing the effect of the Poisson's ratio and the material orthotropy are also presented.

1. Introduction

Because of their potential applications to the strength and failure analysis of such structurally important elements as pressure vessels, pipes, and a great variety of aerospace and hydrospace components, in recent past the crack problems in shells have attracted considerable attention. Typical solutions obtained by using the classical shallow shell theory may be found, for example, in [1]-[4]. In a Mode I type of shell problem (that is, in a shell for which the geometry and the loading are symmetric with respect to the plane of the crack), particularly for membrane loading, the solution based on the classical theory seems to be adequate. However, in skewsymmetric or nonsymmetric problems, because of the Kirchhoff assumption regarding the

transverse shear and the twisting moment, in the classical solution it is not possible to separate Mode II and Mode III (i.e., respectively in-plane and anti-plane shear) stress states around the crack tips. In this case a singularity of the form $r^{-\frac{1}{2}}$ in Mode II stress state automatically implies $r^{-\frac{3}{2}}$ singularity in Mode III. For flat plates such drawbacks of the classical theory was pointed out in [5] where it was found that the asymptotic results obtained from plate bending and two-dimensional elasticity could be brought in agreement provided one uses a sixth order plate theory (e.g., that of Reissner's [6]).

In the crack problems for shells even though the membrane and bending results are coupled, the asymptotic behavior of the membrane and bending stresses around the crack tips should be identical to those given by respectively the plane stress and plate bending solutions. This was shown to be the case for the classical shell results (see, for example, the review article [7]). Recent studies using a Reissner-type shell theory [8], [9] shows that similar agreement is also obtained between shell results and those given by the plane elasticity and a sixth order plate bending theory [10]-[13].

Because of the high likelihood of Mode I type fracture most of the previous studies of crack problems in shells were on the symmetrically loaded structures in which the crack is located in one of the principal planes of curvature. The advantage of this crack geometry is that one can always formulate the problem for one half of the shell only as a symmetric or an antisymmetric problem and reduce the number of unknowns. However, in such structural components as pipes and pipe elbows, if, in addition to internal pressure and bending the external loads include also torsion, then the most likely orientation of the crack initiation and propagation would be along a helix rather than a principal plane of curvature. In this case, the problem would have no symmetry and all five stress intensity factors associated with the five membrane, bending, and transverse shear resultants on the crack surfaces would be coupled. Consequently, the related mixed boundary value problem would reduce to a system of five pairs of dual integral equations or five singular integral equations.

In this paper we consider the simplest and yet, from a practical viewpoint, perhaps the most important such problem, namely a cylindrical shell containing a through crack along an arbitrary direction with respect to the axis of the cylinder. In formulating the problem it is assumed that the regular solution of the shell without the crack for the given applied loads is obtained and the problem is reduced to a perturbation problem in which the self-equilibrating crack surface tractions are the only external loads.

2. The Basic Equations

The problem under consideration is described in Fig. 1. As in [11]-[13] the material is assumed to be specially orthotropic, that is the elastic constants defined by

$$\varepsilon_{11} = \frac{1}{E_1}(\sigma_{11}-\nu_1\sigma_{22}) \ , \ \varepsilon_{22} = \frac{1}{E_2}(\sigma_{22}-\nu_2\sigma_{11}) \ ,$$

$$\varepsilon_{12} = \sigma_{12}/2G_{12} \ , \ \nu_1/E_1 = \nu_2/E_2 \tag{2.1}$$

satisfy the following factorization condition(*) [12]

$$G_{12} = \frac{\sqrt{E_1E_2}}{2(1+\sqrt{\nu_1\nu_2})} \ . \tag{2.2}$$

Defining the following "effective" material constants

$$E = \sqrt{E_1E_2} \ , \ \nu = \sqrt{\nu_1\nu_2} \ , \ B = \frac{5G}{6} \ , \ G = \frac{E}{2(1+\nu)} \ , \ c = (E_1/E_2)^{\frac{1}{4}}, \tag{2.3}$$

(*) The results given in [12] show that the effect of material orthotropy on the stress intensity factors can be quite significant. In practice the material may be orthotropic because it is either a composite laminate or a rolled sheet metal alloy. Orthotropic materials are also anisotropic with regard to their resistance to fracture and crack propagation. Hence, in a cylindrical shell if the axes of orthotropy do not coincide with the axial and circumferential directions, the solution of the general inclined crack problem becomes all the more important. The solution is also necessary to analyze the weld defects and cracks initiated in the weak cleavage plane of the rolled sheet in spirally welded pipes.

equations (2.1) may be written as

$$\varepsilon_{11} = \frac{1}{E}\left(\frac{\sigma_{11}}{c^2} - \nu\sigma_{22}\right) , \quad \varepsilon_{22} = \frac{1}{E}\left(c^2\sigma_{22} - \nu\sigma_{11}\right) , \quad \varepsilon_{12} = \frac{\sigma_{12}}{2G} . \tag{2.4}$$

The derivation of the differential equations for a specially orthotropic shallow shell based on a transverse shear theory [8], [9] may be found in [11]-[13] and will not be repeated in this paper. Referring to Appendix A for notation and to [11]-[13] for details, in terms of a stress function ϕ and the z-component of the displacement w the problem may be formulated as follows:

$$\nabla^4\phi - \frac{1}{\lambda^2}\left(\lambda_1^2\frac{\partial^2}{\partial y^2} - 2\lambda_{12}^2\frac{\partial^2}{\partial x\partial y} + \lambda_2^2\frac{\partial^2}{\partial x^2}\right)w = 0 , \tag{2.5}$$

$$\nabla^4 w + \lambda^2(1-\kappa\nabla^2)\left(\lambda_1^2\frac{\partial^2}{\partial y^2} - 2\lambda_{12}^2\frac{\partial^2}{\partial x\partial y} + \lambda_2^2\frac{\partial^2}{\partial x^2}\right)\phi = \lambda^4(1-\kappa\nabla^2)\left(\frac{q}{h}\right) , \tag{2.6}$$

$$\kappa\nabla^2\psi - \psi - w = 0 , \tag{2.7}$$

$$\frac{\kappa(1-\nu)}{2}\nabla^2\Omega - \Omega = 0 . \tag{2.8}$$

The shell parameters λ_1, λ_2, λ_{12}, λ, and κ are defined in Appendix A, $q(x,y)$ is the transverse loading, and the curvatures are given by

$$\frac{1}{R_1} = -\frac{\partial^2 Z}{\partial x_1^2} , \quad \frac{1}{R_2} = -\frac{\partial^2 Z}{\partial x_2^2} , \quad \frac{1}{R_{12}} = -\frac{\partial^2 Z}{\partial x_1\partial x_2} , \tag{2.9}$$

where $Z = Z(x_1, x_2)$ is the equation of the middle surface of the shell. The functions ψ and Ω are related to the components of the rotation vector by

$$\beta_x = \frac{\partial\psi}{\partial x} + \kappa\frac{1-\nu}{2}\frac{\partial\Omega}{\partial y} , \quad \beta_y = \frac{\partial\psi}{\partial y} - \kappa\frac{1-\nu}{2}\frac{\partial\Omega}{\partial x} . \tag{2.10}$$

The normalized membrane, moment, and transverse shear resultants are given by

$$N_{xx} = \frac{\partial^2\phi}{\partial y^2} \ , \ N_{yy} = \frac{\partial^2\phi}{\partial x^2} \ , \ N_{xy} = - \frac{\partial^2\phi}{\partial x \partial y} \ ; \tag{2.11}$$

$$M_{xx} = \frac{a}{h\lambda^4} \left(\frac{\partial \beta_x}{\partial x} + \nu \frac{\partial \beta_y}{\partial y}\right) \ , \ M_{yy} = \frac{a}{h\lambda^4} \left(\nu \frac{\partial \beta_x}{\partial x} + \frac{\partial \beta_y}{\partial y}\right) \ ,$$

$$M_{xy} = \frac{a}{h\lambda^4} \frac{1-\nu}{2} \left(\frac{\partial \beta_x}{\partial y} + \frac{\partial \beta_y}{\partial x}\right) \ ; \tag{2.12}$$

$$V_x = \frac{\partial w}{\partial x} + \beta_x \ , \ V_y = \frac{\partial w}{\partial y} + \beta_y \ . \tag{2.13}$$

3. General Solution of Differential Equations

Eliminating ϕ in (2.5) and (2.6) one obtains an eighth order differential equation for $w(x,y)$. If the solution of this differential equation is expressed as

$$w(x,y) = \frac{1}{2\pi} \int_{-\infty}^{\infty} f(x,\alpha) e^{-iy\alpha} d\alpha \ , \ f(x,\alpha) = R(\alpha) e^{mx} \ , \tag{3.1}$$

the characteristic equation for m is found to be

$$\begin{aligned} D(m) = {} & m^8 - (4\alpha^2 + \kappa\lambda_2^4) m^6 - 4\kappa\lambda_{12}^2\lambda_2^2 \alpha i m^5 \\ & + [6\alpha^4 + \kappa(4\lambda_{12}^4 + 2\lambda_1^2\lambda_2^2 + \lambda_2^4)\alpha^2 + \lambda_2^4] m^4 \\ & + 4\lambda_{12}^2 [\lambda_2^2 + \kappa(\lambda_1^2 + \lambda_2^2)\alpha^2] \alpha i m^3 \\ & - [4\alpha^4 + \kappa\alpha^2(4\lambda_{12}^4 + 2\lambda_1^2\lambda_2^2 + \lambda_1^4) + 4\lambda_{12}^4 + 2\lambda_1^2\lambda_2^2] \alpha^2 m^2 \\ & - 4\lambda_1^2\lambda_{12}^2 (1 + \kappa\alpha^2) \alpha^3 i m + \alpha^4 (\alpha^4 + \kappa\lambda_1^4\alpha^2 + \lambda_1^4) = 0 \ . \end{aligned} \tag{3.2}$$

In (3.2), by substituting $m = is$ it may be seen that

$$D(is) = \sum_{0}^{8} a_k(\alpha)s^k = 0 \ , \tag{3.3}$$

where the coefficients a_k are real and, hence, the complex roots are in conjugate form. Since $Re(m_j) = Im(s_j)$, $(j=1,\ldots,8)$, by ordering the roots m_j of (3.2) properly it may be shown that they have the following property:

$$Re(m_{j+4}) = -Re(m_j) \ , \ Re(m_j) < 0 \ , \ (j=1,\ldots,4) \ . \tag{3.4}$$

Considering now the regularity conditions at $x=\mp\infty$ from (3.1) and (3.4) it follows that

$$f(x,\alpha) = \begin{cases} \sum_{1}^{4} R_j(\alpha)e^{m_j x} & , \ x > 0 \ , \\ \sum_{5}^{8} R_j(\alpha)e^{m_j x} & , \ x < 0 \ . \end{cases} \tag{3.5}$$

Similarly, if we let

$$\phi(x,y) = \frac{1}{2\pi}\int_{-\infty}^{\infty} g(x,\alpha)e^{-iy\alpha}\, d\alpha, \tag{3.6}$$

from (2.5), (3.1) and (3.5) we obtain

$$g(x,\alpha) = \begin{cases} \sum_{1}^{4} R_j(\alpha)K_j(\alpha)e^{m_j x} & , \ x > 0 \ , \\ \sum_{5}^{8} R_j(\alpha)K_j(\alpha)e^{m_j x} & , \ x < 0 \ , \end{cases} \tag{3.7}$$

where

$$K_j(\alpha) = \frac{(\lambda_2^2-\lambda_1^2)\alpha^2 + \lambda_2^2 p_j + 2\lambda_{12}^2 \alpha m_j i}{\lambda^2 p_j^2} \ , \ p_j = m_j^2 - \alpha^2 \ . \tag{3.8}$$

Also, by assuming that

$$\omega(x,y) = \frac{1}{2\pi}\int_{-\infty}^{\infty} h(x,\alpha)e^{-i\alpha y}\,d\alpha\ , \tag{3.9}$$

$$\psi(x,y) = \frac{1}{2\pi}\int_{-\infty}^{\infty} \theta(x,\alpha)e^{-i\alpha y}\,d\alpha\ , \tag{3.10}$$

from (2.7), (2.8), (3.1) and (3.5) we find

$$h(x,\alpha) = \begin{cases} A_1(\alpha)e^{r_1 x} & ,\quad x > 0 \\ A_2(\alpha)e^{r_2 x} & ,\quad x < 0 \end{cases}\ , \tag{3.11}$$

$$r_1 = -r_2 = -\left[\alpha^2 + \frac{2}{\kappa(1-\nu)}\right]^{\frac{1}{2}}\ , \tag{3.12}$$

$$\theta(x,\alpha) = \begin{cases} \sum_{1}^{4} \dfrac{R_j(\alpha)}{\kappa p_j - 1} e^{m_j x} & ,\quad x > 0 \\ \sum_{5}^{8} \dfrac{R_j(\alpha)}{\kappa p_j - 1} e^{m_j x} & ,\quad x < 0 \end{cases}\ . \tag{3.13}$$

The expressions for the stress, moment, and transverse shear resultants may be obtained by substituting from the solution given above into (2.10)-(2.13). The results are given in Appendix B.

Since the problem has no symmetry, the preceding analysis would give its solution for the half regions $x>0$ and $x<0$ separately, and since each half would have five boundary conditions at $x=0$, ten unknown functions are needed to account for these conditions. Quite apart from the crack problem, $R_1,\ldots,R_8$, A_1, and A_2 are the ten unknowns which may be used to solve the two half shell problems. In the crack problem following are the continuity and boundary conditions which must be satisfied at $x=0$:

$$N_{xx}(+0,y) = N_{xx}(-0,y)\ ,\ -\infty<y<\infty\ , \tag{3.14}$$

$$M_{xx}(+0,y) = M_{xx}(-0,y)\ ,\ -\infty<y<\infty\ , \tag{3.15}$$

$$N_{xy}(+0,y) = N_{xy}(-0,y) \ , \quad -\infty<y<\infty \ , \tag{3.16}$$

$$M_{xy}(+0,y) = M_{xy}(-0,y) \ , \quad -\infty<y<\infty \ , \tag{3.17}$$

$$V_x(+0,y) = V_x(-0,y) \ , \quad -\infty<y<\infty \ ; \tag{3.18}$$

$$\left.\begin{aligned} &N_{xx}(+0,y) = F_1(y) \ , \ |y|<\sqrt{c} \ , \\ &u(+0,y) - u(-0,y) = 0 \ , \ |y|>\sqrt{c} \ , \end{aligned}\right\} \tag{3.19}$$

$$\left.\begin{aligned} &M_{xx}(+0,y) = F_2(y), \ |y|<\sqrt{c} \ , \\ &\beta_x(+0,y) - \beta_x(-0,y) = 0 \ , \ |y|>\sqrt{c} \ , \end{aligned}\right\} \tag{3.20}$$

$$\left.\begin{aligned} &N_{xy}(+0,y) = F_3(y) \ , \ |y|<\sqrt{c} \ , \\ &v(+0,y) - v(-0,y) = 0, \ |y|>\sqrt{c} \ , \end{aligned}\right\} \tag{3.21}$$

$$\left.\begin{aligned} &M_{xy}(+0,y) = F_4(y) \ , \ |y|<\sqrt{c} \ , \\ &\beta_y(+0,y) - \beta_y(-0,y) = 0 \ , \ |y|>\sqrt{c} \ , \end{aligned}\right\} \tag{3.22}$$

$$\left.\begin{aligned} &V_x(+0,y) = F_5(y) \ , \ |y|<\sqrt{c} \ , \\ &w(+0,y) - w(-0,y) = 0, \ |y|>\sqrt{c} \ , \end{aligned}\right\} \tag{3.23}$$

where $F_1,\ldots,F_5$ are the known crack surface loads in the perturbation problem under consideration.

From the expressions of the stress, moment, and the transverse shear resultants given in Appendix B, it may be seen that the homogeneous relations (3.14)-(3.18) can be used to eliminate five of the ten unknown functions $R_1,\ldots,R_8$, A_1, and A_2. The remaining five may then be obtained from the mixed boundary conditions (3.19)-(3.23). The problem may be reduced to a

system of five dual integral equations by obtaining expressions for the displacements and rotations similar to that given in Appendix B and then by substituting into (3.19)-(3.13). However, in the problem under consideration this procedure would be extremely lengthy. A somewhat more convenient approach is the reduction of the mixed boundary conditions directly to a system of integral equations. From the nature of the mixed conditions it is clear that the integral equations will be singular. In order to avoid strong singularities in the resulting integral equations it is necessary that the new unknown functions be selected as the derivatives of the "displacement" quantities rather than the displacements and rotations. Of the "displacements" which appear in the mixed boundary conditions β_x, β_y, and w may readily be expressed in terms of R_j and A_k, (j=1,...,8; k=1,2) by using the solution given in this section. To find u and v we use the basic strain-displacement relations for the shallow shells, namely

$$\varepsilon_{ij} = \frac{1}{2}\left[u_{i,j} + u_{j,i} + Z_{,i}\, u_{3,j} + Z_{,j}\, u_{3,i}\right], \quad (i,j=1,2) \ . \tag{3.24}$$

From (3.24) it can be shown that

$$\frac{\partial u_1}{\partial x_2^2} = 2\,\frac{\partial \varepsilon_{12}}{\partial x_2} - \frac{\partial \varepsilon_{22}}{\partial x_1} - \frac{\partial Z}{\partial x_1}\frac{\partial^2 u_3}{\partial x_2^2} - \frac{\partial^2 Z}{\partial x_2^2}\frac{\partial u_3}{\partial x_1} \ . \tag{3.25}$$

By substituting from (2.4), (2.9) and Appendix B into (3.25) we obtain

$$\frac{\partial u}{\partial y} = 2(1+\nu)N_{xy} - \int \frac{\partial N_{yy}}{\partial x}\,dy + \nu \int \frac{\partial N_{xx}}{\partial x}\,dy$$

$$+ \int\left[\left(\frac{\lambda_1}{\lambda}\right)^2 x + \left(\frac{\lambda_{12}}{\lambda}\right)^2 y\right]\frac{\partial^2 w}{\partial y^2}\,dy + \left(\frac{\lambda_2}{\lambda}\right)^2 \int \frac{\partial w}{\partial x}\,dy \ . \tag{3.26}$$

From (3.19)-(3.23) it is seen that the y-derivatives of the relative crack surface displacements and rotations are the natural choice for the new unknown functions. However, (3.26) suggests that for the in-plane displacements u and v such a choice would require very complicated analysis. In fact, in the present problem it is not feasible to express the functions

R_j and A_k in terms of the new unknowns in the desired form if they are selected as the derivatives of u^+-u^- and v^+-v^-. We thus define the new unknown functions as follows:

$$G_1(y) = \lim_{x\to+0} \left[\frac{\partial u}{\partial y} - \left(\frac{\lambda_{12}}{\lambda}\right)^2 \int y \frac{\partial^2 w}{\partial y^2}\, dy\right]$$

$$- \lim_{x\to-0} \left[\frac{\partial u}{\partial y} - \left(\frac{\lambda_{12}}{\lambda}\right)^2 \int y \frac{\partial^2 w}{\partial y^2}\, dy\right] , \tag{3.27}$$

$$G_2(y) = \lim_{x\to+0} \frac{\partial \beta_x}{\partial y} - \lim_{x\to-0} \frac{\partial \beta_x}{\partial y} , \tag{3.28}$$

$$G_3(y) = \lim_{x\to+0} \left[\frac{\partial v}{\partial y} - \left(\frac{\lambda_2}{\lambda}\right)^2 y \frac{\partial w}{\partial y}\right] - \lim_{x\to-0} \left[\frac{\partial v}{\partial y} - \left(\frac{\lambda_2}{\lambda}\right)^2 y \frac{\partial w}{\partial y}\right] , \tag{3.29}$$

$$G_4(y) = \lim_{x\to+0} \frac{\partial \beta_y}{\partial y} - \lim_{x\to-0} \frac{\partial \beta_y}{\partial y} , \tag{3.30}$$

$$G_5(y) = \lim_{x\to+0} \frac{\partial w}{\partial y} - \lim_{x\to-0} \frac{\partial w}{\partial y} . \tag{3.31}$$

By using now the solution given in this section and the results of Appendix B, the auxiliary functions $G_1,\ldots,G_5$ may be expressed in terms of $R_1,\ldots,R_8$, A_1, and A_2 as follows:

$$G_1(y) = \frac{1}{2\pi} \int_{-\infty}^{\infty} \frac{i}{\alpha} \left[\sum_1^4 \left(\frac{\lambda_2^2}{\lambda^2} - K_j p_j\right) m_j R_j(\alpha) \right.$$

$$\left. - \sum_5^8 \left(\frac{\lambda_2^2}{\lambda^2} - K_j p_j\right) m_j R_j(\alpha) \right] e^{-i\alpha y}\, d\alpha , \tag{3.32}$$

$$G_2(y) = \frac{1}{2\pi}\int_{-\infty}^{\infty}\{-i\alpha[\sum_1^4 \frac{m_j R_j(\alpha)}{\kappa p_j - 1} - \sum_5^8 \frac{m_j R_j(\alpha)}{\kappa p_j - 1}]$$

$$- \frac{\alpha^2\kappa(1-\nu)}{2}[A_1(\alpha)-A_2(\alpha)]\}e^{-i\alpha y}\,d\alpha\,, \tag{3.33}$$

$$G_3(y) = \frac{1}{2\pi}\int_{-\infty}^{\infty}\{\sum_1^4 K_j R_j[p_j+(1+\nu)\alpha^2] - \sum_5^8 K_j R_j[p_j+(1+\nu)\alpha^2]\}e^{-i\alpha y}\,d\alpha\,, \tag{3.34}$$

$$G_4(y) = -\frac{1}{2\pi}\int_{-\infty}^{\infty}[\alpha^2(\sum_1^4 \frac{R_j}{\kappa p_j - 1} - \sum_5^8 \frac{R_j}{\kappa p_j - 1})$$

$$- \frac{\kappa(1-\nu)}{2}\alpha\, i\,(r_1A_1 - r_2A_2)]e^{-i\alpha y}\,d\alpha\,, \tag{3.35}$$

$$G_5(y) = -\frac{1}{2\pi}\int_{-\infty}^{\infty} i\alpha[\sum_1^4 R_j - \sum_5^8 R_j]e^{-i\alpha y}\,d\alpha\,. \tag{3.36}$$

Also, by substituting from Appendix B into (3.14)-(3.18) and inverting the Fourier integrals we find

$$\sum_1^4 K_j R_j - \sum_5^8 K_j R_j = 0\,, \tag{3.37}$$

$$\sum_1^4 \frac{p_j+(1-\nu)\,\alpha^2}{\kappa p_j - 1} R_j - \sum_5^8 \frac{p_j+(1-\nu)\alpha^2}{\kappa p_j - 1} R_j$$

$$- \frac{\kappa}{2}(1-\nu)^2\, i\,\alpha\,(r_1A_1 - r_2A_2) = 0\,, \tag{3.38}$$

$$\sum_1^4 m_j K_j R_j - \sum_5^8 m_j K_j R_j = 0\,, \tag{3.39}$$

$$i\alpha \sum_{1}^{4} \frac{m_j R_j}{\kappa p_j - 1} - i\alpha \sum_{5}^{8} \frac{m_j R_j}{\kappa p_j - 1}$$

$$+ \frac{\kappa}{4}(1-\nu)(\alpha^2+r_1^2)(A_1-A_2) = 0 \quad , \tag{3.40}$$

$$\sum_{1}^{4} \frac{m_j p_j R_j}{\kappa p_j - 1} - \sum_{5}^{8} \frac{m_j p_j R_j}{\kappa p_j - 1} - \frac{i}{2}\alpha(1-\nu)(A_1-A_2) = 0 \ . \tag{3.41}$$

From (3.32)-(3.41) it then follows that

$$-\frac{i}{\alpha}\left(\sum_{1}^{4} m_j p_j K_j R_j - \sum_{5}^{8} m_j p_j K_j R_j\right) = q_1(\alpha) - \left(\frac{\lambda_2}{\lambda\alpha}\right)^2 q_2(\alpha) \ , \tag{3.42}$$

$$(A_1-A_2)/2 = q_2(\alpha) \ , \tag{3.43}$$

$$\sum_{1}^{4} p_j K_j R_j - \sum_{5}^{8} p_j K_j R_j = q_3(\alpha) \quad , \tag{3.44}$$

$$\sum_{1}^{4} \frac{p_j R_j}{\kappa p_j - 1} - \sum_{5}^{8} \frac{p_j R_j}{\kappa p_j - 1} = (1-\nu) q_4(\alpha) \ , \tag{3.45}$$

$$-i\alpha\left(\sum_{1}^{4} R_j - \sum_{5}^{8} R_j\right) = q_5(\alpha) \ , \tag{3.46}$$

where

$$q_j(\alpha) = \int_{-\sqrt{c}}^{\sqrt{c}} G_j(t) e^{i\alpha t}\, dt \ , \ (j=1,\ldots,5) \ . \tag{3.47}$$

In defining q_j by (3.47) it is assumed that $G_j(y) = 0$ for $|y| > \sqrt{c}$. From (3.37)-(3.46) the unknown functions $R_1,\ldots,R_8$, A_1, and A_2 may be obtained as follows:

$$R_j(\alpha) = \sum_{k=1}^{5} i\, B_{jk}(\alpha) q_k(\alpha) \ , \ (j=1,\ldots,8) \ , \tag{3.48}$$

$$A_j(\alpha) = \sum_{k=1}^{5} C_{jk}(\alpha) q_k(\alpha) \ , \ (j=1,2) \ ; \tag{3.49}$$

where B_{jk} and C_{jk} are known functions of α.

4. The Integral Equations

The relations to determine the functions $G_1,\ldots,G_5$ necessary to complete the solution of the problem are obtained by substituting from (3.47)-(3.49) and Appendix B into the mixed boundary conditions (3.19)-(3.23). From the definitions of $G_1,\ldots,G_5$ as given by (3.27)-(3.31) it is seen that they are related to the derivatives of the crack surface displacements and rotations. Thus, in addition to requiring that $G_j(y) = 0$ for $|y| > \sqrt{c}$, $(j=1,\ldots,5)$, further conditions must be imposed on these functions in order to insure the continuity of displacements and rotations in the shell for $x=0$, $|y| > \sqrt{c}$ (see (3.19)-(3.23)). That is, $G_1,\ldots,G_5$ must be such that

$$\int_{-\sqrt{c}}^{\sqrt{c}} \frac{\partial}{\partial y}\left[\omega_j(+0,y) - \omega_j(-0,y)\right]dy = 0 \quad , \tag{4.1}$$

where ω_j, $(j=1,\ldots,5)$ represents the displacements and rotations u, v, w, β_x, and β_y. From (3.27)-(3.31) the single-valuedness conditions of the form (4.1) may now be expressed as

$$\int_{-\sqrt{c}}^{\sqrt{c}} \left[G_1(t)+\left(\frac{\lambda_{12}}{\lambda}\right)^2 tG_5(t)\right]dt - \left(\frac{\lambda_{12}}{\lambda}\right)^2 \int_{-\sqrt{c}}^{\sqrt{c}} dt \int_{-\sqrt{c}}^{t} G_5(y)dy = 0 \ , \tag{4.2}$$

$$\int_{-\sqrt{c}}^{\sqrt{c}} G_2(t)dt = 0 \quad , \tag{4.3}$$

$$\int_{-\sqrt{c}}^{\sqrt{c}} \left[G_3(t) + \left(\frac{\lambda_2}{\lambda}\right)^2 t\, G_5(t)\right]dt = 0 \quad , \tag{4.4}$$

$$\int_{-\sqrt{c}}^{\sqrt{c}} G_4(t)dt = 0 \quad , \tag{4.5}$$

$$\int_{-\sqrt{c}}^{\sqrt{c}} G_5(t)dt = 0 \quad . \tag{4.6}$$

With the requirements that $G_j(y)$ be zero for $|y| > \sqrt{c}$ and the conditions (4.2)-(4.6) be satisfied, the second part of the mixed boundary conditions (3.19)-(3.23) relating to the displacements and rotations has thus been taken care of. The first part of (3.19)-(3.23) relating to crack surface loading would then give the integral equations to determine $G_1,\ldots,G_5$ which may be expressed as

$$\lim_{x\to+0} -\frac{1}{2\pi}\int_{-\infty}^{\infty}\alpha^2\sum_1^4 K_jR_je^{m_jx-i\alpha y}\,d\alpha = F_1(y),\ |y|<\sqrt{c}\ , \tag{4.7}$$

$$\lim_{x\to+0}\frac{1}{2\pi}\frac{a}{h\lambda^4}\int_{-\infty}^{\infty}\Big[\sum_1^4\frac{p_j+(1-\nu)\alpha^2}{\kappa p_j-1}R_j\,e^{m_jx}$$

$$-\frac{\kappa}{2}(1-\nu)^2\,i\alpha A_1r_1e^{r_1x}\Big]e^{-i\alpha y}d\alpha = F_2(y),\ |y|<\sqrt{c}\ , \tag{4.8}$$

$$\lim_{x\to+0}\frac{i}{2\pi}\int_{-\infty}^{\infty}\alpha\sum_1^4 m_jK_jR_je^{m_jx-i\alpha y}d\alpha = F_3(y),\ |y|<c\ , \tag{4.9}$$

$$\lim_{x\to+0}\frac{1}{2\pi}\frac{a(1-\nu)}{h\lambda^4}\int_{-\infty}^{\infty}\Big[i\alpha\sum_1^4\frac{m_jR_j}{\kappa p_j-1}e^{m_jx}$$

$$+\frac{\kappa}{2}(1-\nu)(\alpha^2+r_1^2)A_1e^{r_1x}\Big]e^{-i\alpha y}\,d\alpha = -F_4(y),\ |y|<\sqrt{c}\ , \tag{4.10}$$

$$\lim_{x\to+0}\frac{1}{2\pi}\int_{-\infty}^{\infty}\Big[\sum_1^4\frac{\kappa p_jm_jR_j}{\kappa p_j-1}e^{m_jx}$$

$$-\frac{\kappa}{2}(1-\nu)\alpha iA_1e^{r_1x}\Big]e^{-i\alpha y}d\alpha = F_5(y),\ |y|<\sqrt{c}\ . \tag{4.11}$$

By substituting now from (3.47)-(3.49) into (4.7)-(4.11) and by changing the order of integrations we obtain a system of integral equations for $G_1,\ldots,G_5$ of the following form:

$$\lim_{x\to+0}\int_{-\sqrt{c}}^{\sqrt{c}}\sum_{1}^{5}G_j(t)dt\int_{-\infty}^{\infty}V_{kj}(x,\alpha)e^{i(t-y)}d\alpha = F_k(y),\ (k=1,\ldots,5),\ |y|<\sqrt{c} \tag{4.12}$$

where $V_{kj}(x,\alpha)$, $(k,j=1,\ldots,5)$ are known functions. The dependence of V_{kj} on α is primarily through $r_1(\alpha)$, $r_2(\alpha)$ and the roots $m_j(\alpha)$, $(j=1,\ldots,8)$ of the characteristic equation (3.2) and is therefore very complicated. However, the functions V_{kj} depend on x only through the exponential damping terms $\exp(m_j x)$, $(j=1,\ldots,4)$ and $\exp(r_1 x)$ which simplifies the asymptotic analysis of the kernels in (4.12) quite considerably. To examine the singular behavior of the kernels given by the inner integrals in (4.12) the asymptotic analysis of the functions $V_{kj}(x,\alpha)$ for large values of $|\alpha|$ is needed. First, from (3.2) and (3.12) it can be shown that for large values of $|\alpha|$ the characteristic roots m_j and r_j have the following asymptotic values:

$$m_j(\alpha) = -|\alpha|\left(1 + \frac{p_j}{2\alpha^2} - \frac{p_j^2}{8\alpha^4} + \ldots\right),\ (j=1,\ldots,4), \tag{4.13}$$

$$m_j(\alpha) = |\alpha|\left(1 + \frac{p_j}{2\alpha^2} - \frac{p_j^2}{8\alpha^4} + \ldots\right),\ (j=5,\ldots,8), \tag{4.14}$$

$$r_1(\alpha) = -|\alpha|\left(1 + \frac{1}{\kappa(1-\nu)\alpha^2} - \ldots\right), \tag{4.15}$$

$$r_2(\alpha) = |\alpha|\left(1 + \frac{1}{\kappa(1-\nu)\alpha^2} - \ldots\right), \tag{4.16}$$

where $p_j = m_j^2 - \alpha^2$. Then, observing that the coefficients B_{jk} and C_{jk} which appear in the expressions of R_j and A_j (see (3.48) and (3.49)) depend on α through m_j, $(j=1,\ldots,8)$, and r_k, $(k=1,2)$ only, the asymptotic expansion of $V_{kj}(x,\alpha)$ for large values of $|\alpha|$ may be obtained by using (4.13)-(4.14). Consider, for example, the integral equation (4.7). By using the asymptotic values found for $m_j(\alpha)$ and (3.37), (3.39), and (3.42) it can be shown that for large values of $|\alpha|$ we have

$$\sum_{1}^{4}K_j R_j(\alpha) \cong -\frac{\mathrm{sign}(\alpha)}{4i\alpha^2}q_1(\alpha)\ . \tag{4.17}$$

By adding and subtracting the asymptotic value to and from the integrand, (4.7) may be written as

$$\lim_{x\to+0}\{-\frac{1}{2\pi}\int_{-\infty}^{\infty}[\alpha^2\sum_{1}^{4}K_jR_je^{m_jx}+\frac{\text{sign}(\alpha)}{4i}q_1(\alpha)e^{-|\alpha|x}]e^{-i\alpha y}\,d\alpha$$

$$+\frac{1}{2\pi}\int_{-\infty}^{\infty}\frac{\text{sign}(\alpha)}{4i}e^{-|\alpha|x}\,d\alpha\int_{-\sqrt{c}}^{\sqrt{c}}G_1(t)e^{i\alpha(t-y)}dt\}=F_1(y),\quad |y|<\sqrt{c}\ . \tag{4.18}$$

By changing the order of integration, evaluating the resulting inner integral, and then going to limit, the second integral in (4.18) may be expressed as

$$\lim_{x\to+0}\frac{1}{2\pi}\int_{-\sqrt{c}}^{\sqrt{c}}G_1(t)dt\,\frac{1}{2}\int_{o}^{\infty}e^{-\alpha x}\sin\alpha(t-y)d\alpha$$

$$=\lim_{x\to+0}\frac{1}{4\pi}\int_{-\sqrt{c}}^{\sqrt{c}}\frac{(t-y)G_1(t)}{(t-y)^2+x^2}\,dt=\frac{1}{4\pi}\int_{-\sqrt{c}}^{\sqrt{c}}\frac{G_1(t)}{t-y}\,dt\ . \tag{4.19}$$

The first integral in (4.18) is uniformly convergent, and hence, the limit can be put under the integral sign. By substituting now from (3.47), (3.48) and (4.19) into (4.18) we obtain

$$\int_{-\sqrt{c}}^{\sqrt{c}}[\frac{G_1(t)}{t-y}+\sum_{1}^{5}k_{1j}(y,t)G_j(t)]dt=4\pi F_1(y),\quad |y|<\sqrt{c}\ , \tag{4.20}$$

where the kernels $k_{1j}(y,t)$ are known functions which are bounded for all values y and t in the closed interval $[-\sqrt{c},\sqrt{c}]$.

Similarly, the integral equations (4.8)-(4.11) can be reduced to

$$\int_{-\sqrt{c}}^{\sqrt{c}}[\frac{1-\nu^2}{\lambda^4}\frac{G_2(t)}{t-y}+\sum_{1}^{5}k_{2j}(y,t)G_j(t)]dt=4\pi\frac{h}{a}F_2(y),\quad |y|<\sqrt{c}\ , \tag{4.21}$$

$$\int_{-\sqrt{c}}^{\sqrt{c}}[\frac{G_3(t)}{t-y}+\sum_{1}^{5}k_{3j}(y,t)G_j(t)]dt=4\pi F_3(y),\quad |y|<\sqrt{c}\ , \tag{4.22}$$

$$\int_{-\sqrt{c}}^{\sqrt{c}} \left[\frac{1-\nu^2}{\lambda^4}\frac{G_4(t)}{t-y} + \sum_1^5 k_{4j}(y,t)G_j(t)\right]dt = 4\pi \frac{h}{a} F_4(y), \quad |y|<\sqrt{c} , \tag{4.23}$$

$$\int_{-\sqrt{c}}^{\sqrt{c}} \left[\frac{G_5(t)}{t-y} + \sum_1^5 k_{5j}(y,t)G_j(t)\right]dt = 4\pi F_5(y), \quad |y|<\sqrt{c} . \tag{4.24}$$

The expressions of the Fredholm kernels, $k_{ij}(y,t)$, $(i,j=1,\ldots,5)$, are given in Appendix C. The details of the analysis may be found in [14]. The system of singular integral equations (4.20)-(4.24) must be solved under the additional conditions (4.2)-(4.6). They may be solved in a straightforward manner by using the Gaussian integration technique (see, for example, [15]). The major work in this problem is the evaluation of the Fredholm kernels $k_{ij}(y,t)$, $(i,j=1,\ldots,5)$ which are given in terms of Fourier integrals. To improve the accuracy the asymptotic parts of all integrands are separated and the related integrals are evaluated in closed form. The details of this analysis may also be found in [14].

5. Asymptotic Stress Field Around the Crack Tips, Stress Intensity Factors

For the numerical solution of the system of singular integral equations (4.20)-(4.24) the interval $(-\sqrt{c}, \sqrt{c})$ is normalized by defining

$$\tau = t/\sqrt{c} , \quad \eta = y/\sqrt{c} , \quad \xi = x/\sqrt{c} ,$$

$$H_j(\tau) = G_j(\tau\sqrt{c}), (j = 1,\ldots,5) , \quad -1<\tau<1 . \tag{5.1}$$

We now observe that the index of the system of singular integral equations is +1 and its solution is of the following form:

$$H_j(\tau) = h_j(\tau)/(1-\tau^2)^{\frac{1}{2}} , \quad (-1<\tau<1) , \quad (j=1,\ldots,5) , \tag{5.2}$$

where $h_1,\ldots,h_5$ are unknown bounded functions. The membrane, bending, and transverse shear resultants may be obtained by substituting from (5.1),

(5.2), and (4.47)-(4.49) into the expressions given in Appendix B. The asymptotic behavior of the stress field around the crack tip could then be obtained by using the asymptotic expansions of m_j and r_k, (j=1,...,8; k=1,2) given in (4.13)-(4.16) and the following asymptotic relation [16]

$$\int_{-1}^{1} \frac{h(\tau)}{\sqrt{1-\tau^2}} e^{i\alpha\tau}\, d\tau = \left(\frac{\pi}{2|\alpha|}\right)^{\frac{1}{2}} \{h(1)\exp[i(\alpha - \frac{\pi\alpha}{4|\alpha|})]$$

$$+ h(-1)\exp[-i(\alpha - \frac{\pi\alpha}{4|\alpha|})] + O(\frac{1}{|\alpha|})\} \ , \ (|\alpha|\to\infty) \ , \qquad (5.3)$$

giving

$$N_{xx} \cong \xi \frac{h_3(1)}{4\sqrt{2\pi}} \int_0^\infty \sqrt{\alpha}\, e^{-\alpha|\xi|} \cos[\alpha(1-\eta) - \tfrac{\pi}{4}]d\alpha$$

$$+ \frac{h_1(1)}{4\sqrt{2\pi}} \int_0^\infty \frac{1}{\sqrt{\alpha}} (1+\alpha|\xi|)e^{-\alpha|\xi|} \sin[\alpha(1-\eta) - \tfrac{\pi}{4}]d\alpha, \qquad (5.4)$$

$$N_{yy} \cong \frac{h_3(1)}{2\sqrt{2\pi}} \int_0^\infty \frac{e^{-\alpha|\xi|}}{\sqrt{\alpha}} \cos[\alpha(1-\eta) - \tfrac{\pi}{4}]d\alpha$$

$$+ \frac{h_1(1)}{4\sqrt{2\pi}} \int_0^\infty \frac{1}{\sqrt{\alpha}} (1-\alpha|\xi|e^{-\alpha|\xi|} \sin[\alpha(1-\eta) - \tfrac{\pi}{4}]d\alpha \ , \qquad (5.5)$$

$$N_{xy} \cong \frac{h_3(1)}{4\sqrt{2\pi}} \int_0^\infty \frac{1}{\sqrt{\alpha}} (1-\alpha|\xi|)e^{-\alpha|\xi|} \sin[\alpha(1-\eta) - \tfrac{\pi}{4}]d\alpha$$

$$+ \frac{h_1(1)}{4\sqrt{2\pi}} \int_0^\infty \xi\sqrt{\alpha}\, e^{-\alpha|\xi|} \cos[\alpha(1-\eta) - \tfrac{\pi}{4}]d\alpha \ , \qquad (5.6)$$

$$M_{xx} = \frac{h}{12a}\frac{\xi h_4(1)}{4\sqrt{2\pi}}\int_0^\infty \sqrt{\alpha}\, e^{-\alpha|\xi|}\cos[\alpha(1-\eta) - \tfrac{\pi}{4}]d\alpha$$

$$+ \frac{h}{12a}\frac{h_2(1)}{4\sqrt{2\pi}}\int_0^\infty \frac{1}{\sqrt{\alpha}}(1+\alpha|\xi|)e^{-\alpha|\xi|}\sin[\alpha(1-\eta) - \tfrac{\pi}{4}]d\alpha, \qquad (5.7)$$

$$M_{yy} = \frac{h}{12a}\frac{h_4(1)}{2\sqrt{2\pi}}\int_0^\infty \frac{e^{-\alpha|\xi|}}{\sqrt{\alpha}}\cos[\alpha(1-\eta) - \tfrac{\pi}{4}]d\alpha$$

$$+ \frac{h}{12a}\frac{h_2(1)}{4\sqrt{2\pi}}\int_0^\infty \frac{1}{\sqrt{\alpha}}(1-\alpha|\xi|)e^{-\alpha|\xi|}\sin[\alpha(1-\eta) - \tfrac{\pi}{4}]d\alpha, \qquad (5.8)$$

$$M_{xy} \cong \frac{1}{12}\frac{h}{a}\frac{h_4(1)}{4\sqrt{2\pi}}\int_0^\infty \frac{1}{\sqrt{\alpha}}(1-\alpha|\xi|)e^{-\alpha|\xi|}\sin[\alpha(1-\eta) - \tfrac{\pi}{4}]d\alpha$$

$$+ \frac{1}{12}\frac{h}{a}\frac{h_2(1)}{4\sqrt{2\pi}}\int_0^\infty \sqrt{\alpha}|\xi|e^{-\alpha|\xi|}\cos[\alpha(1-\eta) - \tfrac{\pi}{4}]d\alpha \quad , \qquad (5.9)$$

$$V_x \cong \frac{h_5(1)}{2\sqrt{2\pi}}\int_0^\infty \frac{e^{-\alpha|\xi|}}{\sqrt{\alpha}}\sin[\alpha(1-\eta) - \tfrac{\pi}{4}]d\alpha \quad , \qquad (5.10)$$

$$V_y \cong \frac{h_5(1)}{2\sqrt{2\pi}}\int_0^\infty \frac{e^{-\alpha|\xi|}}{\sqrt{\alpha}}\cos[\alpha(1-\eta) - \tfrac{\pi}{4}]d\alpha \quad . \qquad (5.11)$$

Defining the new coordinates r, θ in η, ξ plane by

$$\xi = r\sin\theta \ , \quad n-1 = r\cos\theta \ , \qquad (5.12)$$

and using the relation [16]

$$\int_0^\infty z^{\mu-1} e^{-sz} \begin{Bmatrix}\sin\\ \cos\end{Bmatrix}(rz)dz = \frac{\Gamma(\mu)}{(s^2+r^2)^{\mu/2}} \begin{Bmatrix}\sin\\ \cos\end{Bmatrix}(\mu \tan^{-1}\frac{r}{s})$$

$$(s>0 \ , \ \mu>0) \ , \qquad (5.13)$$

equations (5.4)-(5.11) can be reduced to the following form

$$N_{xx} \cong -\frac{h_3(1)}{4\sqrt{2r}}\left[-\frac{1}{4}\sin\frac{\theta}{2}+\frac{1}{4}\sin\frac{5\theta}{2}\right]-\frac{h_1(1)}{4\sqrt{2r}}\left[\frac{5}{4}\cos\frac{\theta}{2}-\frac{1}{4}\cos\frac{5\theta}{2}\right], \tag{5.14}$$

$$N_{yy} \cong -\frac{h_3(1)}{4\sqrt{2r}}\left[-\frac{7}{4}\sin\frac{\theta}{2}-\frac{1}{4}\sin\frac{5\theta}{2}\right]-\frac{h_1(1)}{4\sqrt{2r}}\left[\frac{3}{4}\cos\frac{\theta}{2}+\frac{1}{4}\cos\frac{5\theta}{2}\right], \tag{5.15}$$

$$N_{xy} \cong -\frac{h_3(1)}{4\sqrt{2r}}\left[\frac{3}{4}\cos\frac{\theta}{2}+\frac{1}{4}\cos\frac{5\theta}{2}\right]-\frac{h_1(1)}{4\sqrt{2r}}\left[-\frac{1}{4}\sin\frac{\theta}{2}+\frac{1}{4}\sin\frac{5\theta}{2}\right], \tag{5.16}$$

$$M_{xx} \cong -\frac{h_4(1)}{4\sqrt{2r}}\frac{h}{12a}\left[-\frac{1}{4}\sin\frac{\theta}{2}+\frac{1}{4}\sin\frac{5\theta}{2}\right]-\frac{h_2(1)}{4\sqrt{2r}}\frac{h}{12a}\left[\frac{5}{4}\cos\frac{\theta}{2}-\frac{1}{4}\cos\frac{5\theta}{2}\right], \tag{5.17}$$

$$M_{yy} \cong -\frac{h_4(1)}{4\sqrt{2r}}\frac{h}{12a}\left[-\frac{7}{4}\sin\frac{\theta}{2}-\frac{1}{4}\sin\frac{5\theta}{2}\right]-\frac{h_2(1)}{4\sqrt{2r}}\frac{h}{12a}\left[\frac{3}{4}\cos\frac{\theta}{2}+\frac{1}{4}\cos\frac{5\theta}{2}\right], \tag{5.18}$$

$$M_{xy} \cong -\frac{h_4(1)}{4\sqrt{2r}}\frac{h}{12a}\left[\frac{3}{4}\cos\frac{\theta}{2}+\frac{1}{4}\cos\frac{5\theta}{2}\right]-\frac{h_2(1)}{4\sqrt{2r}}\frac{h}{12a}\left[-\frac{1}{4}\sin\frac{\theta}{2}+\frac{1}{4}\sin\frac{5\theta}{2}\right], \tag{5.19}$$

$$V_x \cong -\frac{h_5(1)}{2\sqrt{2r}}\cos\frac{\theta}{2}, \tag{5.20}$$

$$V_y \cong \frac{h_5(1)}{2\sqrt{2r}}\sin\frac{\theta}{2}. \tag{5.21}$$

By observing that the membrane and bending components of the stresses are given by (see Appendix A)

$$\sigma_{ij}^{m} = N_{ij}, \sigma_{ij}^{b} = \frac{12az}{h}M_{ij} \quad (i,j=x,y) \tag{5.22}$$

from equations (5.14)-(5.19) for the leading terms of the combined in-plane stresses $\sigma_{ij} = \sigma_{ij}^{m} + \sigma_{ij}^{b}$, (i,j=x,y) one obtains

$$\sigma_{xx} \cong -\frac{h_3(1)+zh_4(1)}{4\sqrt{2r}}\left[-\frac{1}{4}\sin\frac{\theta}{2}+\frac{1}{4}\sin\frac{5\theta}{2}\right]$$

$$-\frac{h_1(1)+zh_2(1)}{4\sqrt{2r}}\left[\frac{5}{4}\cos\frac{\theta}{2}-\frac{1}{4}\cos\frac{5\theta}{2}\right], \tag{5.23}$$

$$\sigma_{yy} \cong -\frac{h_3(1)+zh_4(1)}{4\sqrt{2r}}\left[-\frac{7}{4}\sin\frac{\theta}{2}-\frac{1}{4}\sin\frac{5\theta}{2}\right]$$

$$-\frac{h_1(1)+zh_2(1)}{4\sqrt{2r}}\left[\frac{3}{4}\cos\frac{\theta}{2}+\frac{1}{4}\cos\frac{5\theta}{2}\right], \tag{5.24}$$

$$\sigma_{xy} \cong -\frac{h_3(1)+zh_4(1)}{4\sqrt{2r}}\left[\frac{3}{4}\cos\frac{\theta}{2}+\frac{1}{4}\cos\frac{5\theta}{2}\right]$$

$$-\frac{h_1(1)+zh_2(1)}{4\sqrt{2r}}\left[-\frac{1}{4}\sin\frac{\theta}{2}+\frac{1}{4}\sin\frac{5\theta}{2}\right]. \tag{5.25}$$

Similarly, for the transverse shear stresses from

$$\sigma_{iz} = \frac{3}{2}V_i\left[1-\left(\frac{az}{h/2}\right)^2\right], \ (i = x,y), \tag{5.26}$$

we obtain

$$\sigma_{xz} \cong -\frac{3}{2}\frac{h_5(1)}{2\sqrt{2r}}\cos\frac{\theta}{2}\left[1-\left(\frac{az}{h/2}\right)^2\right], \tag{5.27}$$

$$\sigma_{yz} \cong -\frac{3}{2}\frac{h_5(1)}{2\sqrt{2r}}\sin\frac{\theta}{2}\left[1-\left(\frac{az}{h/2}\right)^2\right]. \tag{5.28}$$

Note that for the isotropic materials c=1 and the asymptotic stress fields (5.23)-(5.25) and (5.27)-(5.28) found from the shell solution are identical to those given by respectively the in-plane and the anti-plane elasticity solution of a two-dimensional crack problem. If we now define the Modes I, II, and III stress intensity factors (for a crack along $x_1=0$, $-a<x_2<a$) by

$$k_j(x_3) = \lim_{x_2 \to a} \sqrt{2(x_2-a)}\, \sigma_{1j}(0,x_2,x_3) \ , \ (j=1,2,3) \ , \tag{5.29}$$

from (5.23)-(5.25) and (5.27) and Appendix A we obtain

$$k_1(x_3) = - \frac{cE}{4} \sqrt{a} \left[h_1(1) + \frac{x_3}{a} h_2(1)\right] \ , \tag{5.30}$$

$$k_2(x_3) = - \frac{E\sqrt{a}}{4} \left[h_3(1) + \frac{x_3}{a} h_4(1)\right] \ , \tag{5.31}$$

$$k_3(x_3) = - \frac{3}{4} B\sqrt{a}\sqrt{c}\, h_5(1)\left[1 - \left(\frac{x_3}{h/2}\right)^2\right] \ . \tag{5.32}$$

6. The Results and Discussion

The main interest in this study is in evaluating the stress intensity factors in shells for various crack geometries and loading conditions. For each crack geometry the problem is solved by assuming only one of the five possible crack surface loadings to be nonzero at a time. For a general loading the result may then be obtained by superposition. From (5.30) and (5.31) it is seen that the in-plane stress intensity factors k_1 and k_2 have a "membrane" and a "bending" component, and h_1 and h_3 are related to the membrane and h_2 and h_4 are related to the bending stresses. For simplicity, the related stress intensity factors are defined separately. The calculated results are normalized with respect to a standard stress intensity factor $\sigma_j\sqrt{a}$ where σ_j stands for any one of the following five nominal ("membrane", "bending", in-plane "shear", "twisting", and "transverse shear") stresses:

$$\sigma_m = N_{11}/h \ , \ \sigma_b = 6M_{11}/h^2 \ , \ \sigma_s = N_{12}/h \ ,$$

$$\sigma_t = 6M_{12}/h^2 \ , \ \sigma_v = (3/2)V_1/h \ , \tag{6.1 a-e}$$

where crack lies in x_2x_3 plane and N_{11}, M_{11}, N_{12}, M_{12}, and V_1 are (a measure or amplitude of) the crack surface tractions.

The normalized stress intensity factors are then defined and calculated in terms of $h_i(1)$, (i=1,...,5) as follows:

$$k_{mj} = \frac{k_1(0)}{\sigma_j\sqrt{a}} = -\frac{cE}{4\sigma_j} h_1(1) , \tag{6.2}$$

$$k_{bj} = \frac{k_1(h/2)-k_1(0)}{\sigma_j\sqrt{a}} = -\frac{cE}{4\sigma_j}\frac{h}{2a} h_2(1) , \tag{6.3}$$

$$k_{sj} = \frac{k_2(0)}{\sigma_j\sqrt{a}} = -\frac{E}{4\sigma_j} h_3(1) , \tag{6.4}$$

$$k_{tj} = \frac{k_2(h/2)-k_2(0)}{\sigma_j\sqrt{a}} = -\frac{E}{4\sigma_j}\frac{h}{2a} h_4(1) , \tag{6.5}$$

$$k_{vj} = \frac{k_3(0)}{\sigma_j\sqrt{a}} = -\frac{3}{4}\frac{B}{\sigma_j}\sqrt{c}\, h_5(1) , \quad (j=m,b,s,t,v) , \tag{6.6}$$

where for each individual loading σ_j is given by (6.1). In the case of uniform crack surface loads N_{11}, M_{11}, N_{12}, M_{12}, and V_1, referring to (3.19)-(3.23), Appendix A, and (6.1) the input functions of the system of integral equations (4.20)-(4.24) are given by

$$F_1(y) = \frac{\sigma_m}{cE} , \; F_2(y) = \frac{\sigma_b}{6cE} , \; F_3(y) = \frac{\sigma_s}{E} , \; F_4(y) = \frac{\sigma_t}{6E} ,$$

$$F_5(y) = \frac{2}{3}\frac{\sigma_v}{B\sqrt{c}} . \tag{6.7}$$

Even though the formulation given in this paper is valid for any shell with constant curvatures $1/R_1$, $1/R_2$, and $1/R_{12}$, the results are obtained for the practical problem of a cylindrical shell containing an arbitrarily oriented crack only (Fig. 1). The crack is assumed to be in a plane defined by the angle β shown in Fig. 1. For the shallow cylindrical shell the curvatures referred to x_1, x_2 axes shown in the figure and defined by (2.9)

Table 1. Stress intensity factor ratios in an isotropic cylindrical shell containing an inclined crack under uniform membrane loading N_{11}, $\nu = 0.3$, $\beta = 45°$.

	a/h \ h/R	1	2	3	5	10
k_{mm}	1/5	1.097	1.302	1.544	2.030	3.486
	1/10	1.049	1.167	1.321	1.665	2.516
	1/15	1.033	1.116	1.230	1.501	2.199
	1/25	1.020	1.072	1.148	1.341	1.886
	1/50	1.010	1.037	1.079	1.194	1.563
	1/100	1.005	1.019	1.041	1.106	1.337
	1/200	1.002	1.010	1.021	1.056	1.192
k_{bm}	1/5	0.084	0.122	0.100	-0.069	-0.761
	1/10	0.058	0.108	0.126	0.079	-0.299
	1/15	0.046	0.093	0.121	0.118	-0.125
	1/25	0.032	0.073	0.104	0.132	0.023
	1/50	0.020	0.049	0.076	0.117	0.120
	1/100	0.012	0.031	0.051	0.089	0.139
	1/200	0.007	0.019	0.033	0.062	0.120
k_{sm}	1/5	-0.036	-0.108	-0.190	-0.333	-0.517
	1/10	-0.018	-0.060	-0.113	-0.227	-0.424
	1/15	-0.012	-0.041	-0.081	-0.173	-0.365
	1/25	-0.007	-0.025	-0.052	-0.119	-0.289
	1/50	-0.004	-0.013	-0.028	-0.068	-0.192
	1/100	-0.002	-0.007	-0.014	-0.037	-0.117
	1/200	-0.001	-0.003	-0.007	-0.019	-0.067
k_{tm}	1/5	0.012	-0.029	-0.119	-0.432	-4.232
	1/10	0.010	-0.008	-0.053	-0.219	-1.853
	1/15	0.008	-0.002	-0.031	-0.144	-1.244
	1/25	0.006	0.002	-0.015	-0.082	-0.757
	1/50	0.004	0.003	-0.004	-0.036	-0.379
	1/100	0.003	0.003	0.000	-0.015	-0.186
	1/200	0.002	0.002	0.001	-0.006	-0.090
k_{vm}	1/5	-0.051	-0.139	-0.261	-0.609	-2.630
	1/10	-0.026	-0.070	-0.131	-0.302	-1.117
	1/15	-0.018	-0.047	-0.088	-0.201	-0.736
	1/25	-0.011	-0.029	-0.053	-0.121	-0.441
	1/50	-0.005	-0.015	-0.028	-0.062	-0.221
	1/100	-0.003	-0.008	-0.014	-0.032	-0.111
	1/200	-0.001	-0.004	-0.008	-0.017	-0.056

may be expressed as

$$\frac{1}{R_1} = \frac{\sin^2\beta}{R} , \frac{1}{R_2} = \frac{\cos^2\beta}{R} , \frac{1}{R_{12}} = - \frac{\sin\beta\cos\beta}{R} . \qquad (6.8)$$

Some numerical results obtained for an isotropic cylinder are shown in Figures 2-11. Figures 2-6 show the primary stress intensity factor ratios k_{mm}, k_{bb}, k_{ss}, k_{tt}, and k_{vv} for a cylinder having a crack inclinced 45° with respect to the axis. The unusual results here are those found for k_{tt} and k_{vv}. Under a twisting moment M_{12} uniformly distributed along the crack, the Mode II stress intensity factor ratio k_{tt} appears to be nearly independent of the shell curvature 1/R but highly dependent on a/h. Fig. 6 shows that the monotonic variation of the stress intensity factor ratios with a/h and h/R observed in Figures 2-5 and in previous shell solutions is not valid for k_{vv}. This seems to be the case for all values of β varying from zero to ninety degrees.

The effect of β on the primary stress intensity ratios k_{mm}, k_{bb}, k_{ss}, k_{tt}, and k_{vv} is shown in Figures 7-11. Extensive results giving all stress intensity ratios k_{ij} (i,j=m,b,s,t,v) for β=0, 15°, 30°, 45°, 60°, 75°, 90° and for varying h/R and a/h may be found in [14]. Table 1 shows some sample results regarding the secondary stress intensity ratios in a cylinder with a 45° crack under torsion (i.e., N_{11} = constant and all other crack surface tractions zero).

The stress intensity factors given in Figures 2-11 and in Table 1 are obtained for the Poisson's ratio ν = 0.3. Some sample results showing the effect of ν on the stress intensity factors are given in Table 2. It is seen that this effect is not really significant.

It should be noted that the Poisson's ratio ν in isotropic shells and $\nu = \sqrt{\nu_1\nu_2}$ and the stiffness ratio $c = (E_1/E_2)^{\frac{1}{4}}$ in specially orthotropic shells appear in the expressions of the kernels of the integral equations. Thus, to investigate the effect of the material orthotropy on the stress intensity factors both ν and c must be varied. However, as seen from Table 2 the influence of ν is rather insignificant. Therefore, to study the effect of the material orthotropy it may be sufficient to vary c only.

Table 2. The effect of Poisson's ratio on the stress intensity factor ratios in an isotropic cylindrical shell containing an inclined crack, $\beta=45°$, $a/h=2$, $h/R=1/10$.

k \ ν	0.0	0.1	0.2	0.3	0.4	0.5
k_{mm}	1.166	1.167	1.167	1.167	1.166	1.164
k_{bm}	0.063	0.077	0.092	0.108	0.124	0.140
k_{sm}	-0.058	-0.059	-0.059	-0.060	-0.060	-0.059
k_{tm}	-0.009	-0.008	-0.008	-0.008	-0.008	-0.008
k_{vm}	-0.075	-0.073	-0.072	-0.070	-0.069	-0.067
k_{mb}	0.018	0.023	0.028	0.034	0.039	0.045
k_{bb}	0.605	0.617	0.626	0.632	0.634	0.631
k_{sb}	-0.016	-0.018	-0.019	-0.021	-0.024	-0.026
k_{tb}	-0.005	-0.005	-0.006	-0.006	-0.006	-0.006
k_{vb}	0.004	0.003	0.003	0.003	0.003	0.003
k_{ms}	-0.058	-0.059	-0.059	-0.060	-0.060	-0.060
k_{bs}	-0.054	-0.059	-0.064	-0.069	-0.074	-0.080
k_{ss}	1.059	1.059	1.059	1.059	1.058	1.057
k_{ts}	0.007	0.007	0.008	0.008	0.009	0.010
k_{vs}	0.133	0.131	0.129	0.128	0.126	0.124
k_{mt}	0.005	0.005	0.005	0.004	0.004	0.003
k_{bt}	-0.005	-0.005	-0.006	-0.006	-0.006	-0.006
k_{st}	-0.007	-0.007	-0.007	-0.006	-0.006	-0.005
k_{tt}	0.309	0.325	0.339	0.353	0.366	0.379
k_{vt}	-0.095	-0.094	-0.093	-0.091	-0.090	-0.088
k_{mv}	-0.223	-0.244	-0.266	-0.287	-0.308	-0.330
k_{bv}	-0.004	0.001	0.007	0.014	0.022	0.032
k_{sv}	-0.174	-0.187	-0.200	-0.213	-0.226	-0.238
k_{tv}	1.138	1.166	1.191	1.213	1.233	1.250
k_{vv}	2.304	2.287	2.272	2.258	2.244	2.231

Table 3. The effect of material orthotropy on the stress intensity factor ratios in a cylindrical shell containing an inclined crack; β=45, a/h=3, h/r=1/10.

k \ E_1/E_2	0.037	1.000	26.667
k_{mm}	1.127	1.321	1.984
k_{bm}	0.078	0.126	0.125
k_{sm}	-0.056	-0.113	-0.181
k_{tm}	-0.010	-0.053	-0.179
k_{vm}	-0.074	-0.131	-0.263
k_{mb}	0.024	0.044	0.050
k_{bb}	0.569	0.567	0.534
k_{sb}	-0.011	-0.026	-0.028
k_{tb}	-0.004	-0.005	-0.002
k_{vb}	0.004	0.007	0.012
k_{ms}	-0.057	-0.115	-0.189
k_{bs}	-0.031	-0.073	-0.079
k_{ss}	1.082	1.111	1.205
k_{ts}	0.019	0.068	0.179
k_{vs}	0.238	0.228	0.331
k_{mt}	0.005	0.004	0.003
k_{bt}	-0.004	-0.006	-0.005
k_{st}	-0.010	-0.006	-0.005
k_{tt}	0.314	0.273	0.189
k_{vt}	-0.095	-0.093	-0.087
k_{mv}	-0.166	-0.577	-1.100
k_{bv}	-0.009	0.030	0.090
k_{sv}	-0.277	-0.491	-0.872
k_{tv}	1.033	1.888	2.724
k_{vv}	2.089	2.671	3.573

For a strongly orthotropic material (graphite-epoxy composite) this effect is shown in Table 3. The axes of material orthotropy are along 45° directions with respect to the cylinder axis and the crack is located along one or the other axis of orthotropy. The Poisson's ratio is $\nu = \sqrt{\nu_1 \nu_2} = 0.037$ for the orthotropic shells and $\nu = 0.3$ for the isotropic results included for the purpose of comparison. The table shows that the effect of material orthotropy on the stress intensity factors could be very significant.

The quantity which is of some interest in certain fracture studies is the rate of internally released or externally added energy per unit fracture area created as a result of crack propagation. If U is the work of the external loads, V the total strain energy, and A the fracture surface, then in a quasistatic problem the rate of energy available for fracture would be d(U-V)/dA. For elastic problems this energy rate is known to be the same for "fixed grip" and "fixed load" conditions. It can therefore be calculated as the crack closure energy under fixed grip conditions. Under these conditions, dU = 0 and for a crack going from x_2=a to x_2=a+da, dV may be expressed as

$$dV = -\int_{-h/2}^{h/2} \int_{o}^{da} \frac{1}{2} \sum_{j=1}^{3} \sigma_{1j}(0,x_2,x_3)[u_j(+0,x_2-da,x_3) - u_j(-0,x_2-da,x_3)]dx_2 dx_3 \tag{6.9}$$

where the minus sign is due to the fact that during the "release" of the crack surfaces in $a<x_2<a+da$, $-h/2<x_3<h/2$ the tractions and displacements are in opposite directions (consequently, the total strain energy of the shell decrease). For small values of da we now observe that

$$\sigma_{1j}(0,x_2,x_3) = \frac{k_j(x_3)}{\sqrt{2(x_2-a)}}, \quad (j=1,2,3) \tag{6.10}$$

$$u_j(+0,x_2-da,x_3)-u_j(-0,x_2-da,x_3) = \frac{4k_j(x_3)}{E}\sqrt{2(a+da-x_2)}, \quad (j=1,2) \tag{6.11}$$

$$u_3(+0,x_2-da,x_3)-u_3(-0,x_2-da,x_3) = \frac{k_3(x_3)}{G}\sqrt{2(a+da-x_2)}, \tag{6.12}$$

where k_1, k_2, and k_3 are the Modes I, II, and III stress intensity factors around the crack border x_2=a.

Referring to the definitions of the stress intensity ratios k_{ij} (i,j=m,b,s,t,v), given by (6.2)-(6.6) we can define the "membrane", "bending", "shear", "twisting" and the "transverse shear" components of the stress intensity factors at the crack tip x_2=a as follows:

$$k_i = \sum_j k_{ij}\sigma_j\sqrt{a} \ , \ (i,j = m,b,s,t,v) \ . \tag{6.13}$$

From (5.30)-(5.32), (6.2)-(6.6), and (6.13) the stress intensity factors may then be expressed as

$$k_1(x_3) = k_m + k_b \left(\frac{x_3}{h/2}\right) \ , \tag{6.14}$$

$$k_2(x_3) = k_s + k_t \left(\frac{x_3}{h/2}\right) \ , \tag{6.15}$$

$$k_3(x_3) = k_v\left[1 - \left(\frac{x_3}{h/2}\right)^2\right] \ . \tag{6.16}$$

By substituting from (6.10)-(6.12) and (6.14)-(6.16) into (6.9) we obtain

$$dV = -\frac{\pi}{E}\left[k_m^2 + \frac{k_b^2}{3} + k_s^2 + \frac{k_t^2}{3} + \frac{4(1+\nu)}{15}k_v^2\right]hda. \tag{6.17}$$

Observing that hda = dA, for the rate of externally added or internally released energy (at one crack tip x_2=a, per unit shell thickness, per unit crack extension in the plane of the original crack) we find

$$\frac{d}{dA}(U-V) = \frac{\pi}{E}\left[k_m^2 + \frac{k_b^2}{3} + k_s^2 + \frac{k_t^2}{3} + \frac{4(1+\nu)}{15}k_v^2\right] \ . \tag{6.18}$$

Finally it is again worthwhile to remember that <u>all</u> shell theories are, to varying degrees, approximations of the three dimensional elasticity. Therefore, even if the "shallowness" assumption is satisfied, the theory used in this paper and the results given are only approximate. Strictly speaking, the crack problems considered in plates and shells are three-dimensional elasticity problems. Such problems in their simplest form do

not seem to be as yet analytically tractable. However, from a structural viewpoint, the shell solutions can be useful in the sense that the "plane stress" crack solutions are, that is, the results should be interpreted and used in a certain thickness-average sense. Since the shell theories are quite numerous, there is always the question as to what theory to use in the crack problem. Clearly there is no unique answer for this question. However, one could try to establish some guidelines and set certain minimum requirements. In crack problems the most important information (from an application viewpoint) is imbedded in the asymptotic solution of the problem around the crack tips. The first requirement then is that the asymptotic results found from the shell solution must be compatible with that of the in-plane and anti-plane elasticity solutions of the crack problem. This means that the stresses around the crack tips must have the standard square root singularity and their angular distribution must be identical to that given by the related two-dimensional elasticity solutions.

In crack problems since one is interested in the behavior of the solution very near the crack tip, it is natural to assume that all local length parameters would have some influence on the results which are of interest. In a general shallow shell there are five local length parameters, namely three radii of curvature, R_1, R_2, R_{12}, the crack length 2a, and the thickness h. A particular shell theory to be suitable for crack problems should therefore contain four dimensionless (independent) length parameters.

Again, since it is desired that the shell theory give a reasonably accurate solution near the crack tip, it would be necessary that the theory should accommodate all the stress boundary conditions on the crack surfaces separately.

Reissner's transverse shear theory, which has been used in this paper, seems to be the simplest theory which satisfy all these requirements. Aside from a certain degree of confidence one may have in its results,an advantage of such a compatible theory, is that it makes it possible to carry out calculations such as that of energy release rate (see (6.18)) routinely. This, of course, is primarily due to the fact that the asymptotic results (5.23)-(5.25) and (5.27)-(5.28) are identical to that of the corresponding

elasticity solutions. However, since a higher order shell theory does not necessarily imply higher accuracy in (certain calculated) results, there are still unresolved questions. Are the results of the crack problems obtained from the Reissner's shell theory, for example, more reliable than that given by the classical shell theory? For the stress intensity factors we think the answer is yes. The reason for this is largely the fact that the classical theory satisfies none of the requirements listed above. Could one improve the solution further by considering "higher order" theories which may take into account additional features of deformations and stresses (such as, for example, the stretch in thickness direction)? Even if one can solve such problems with the same degree of numerical accuracy as the problems based on simpler shell theories, it would be difficult to know which solution is more reliable. In our view, therefore, it would be very difficult to justify the use of a more complex theory than Reissner's in solving the crack problem in shells unless one has a demonstrable reason for it.

References

1. E.S. Folias, "An axial crack in a pressurized cylindrical shell", Int. J. of Fracture Mechanics, Vol. 1, pp. 104-113, 1965.

2. L.G. Copley and J.L. Sanders, Jr., "A longitudinal crack in a cylindrical shell under internal pressure", Int. J. of Fracture Mechanics, Vol. 5, pp. 117-131, 1969.

3. F. Erdogan and J.J. Kibler, "Cylindrical and spherical shells with cracks", Int. J. of Fracture Mechanics, Vol. 5, pp. 229-237, 1969.

4. J.G. Simmonds, M.R. Bradley, and J.W. Nicholson, "Stress intensity factors for arbitrarily oriented cracks in shallow shells", J. Appl. Mech., Vol. 45, Trans. ASME, pp. 135-141, 1978.

5. J.K. Knowles and N.M. Wang, "On the bending of an elastic plate containing a crack", J. Math. and Physics. Vol. 39, pp. 223-236, 1960.

6. E. Reissner, "On bending of elastic plates", Quart. Appl. Math., Vol. 5, pp. 55-68, 1947.

7. F. Erdogan, "Crack problems in cylindrical and spherical shells", Plates and Shells with Cracks, G.C. Sih, ed., Noordhoff Int. Publ. Leyden, pp. 161-199, 1977.

8. E. Reissner and F.Y.M. Wan, "On the equations of linear shallow shell theory", Studies in Applied Mathematics, Vol. 48, pp. 132-145, 1969.

9. P.M. Naghdi, "Note on the equations of shallow elastic shells", Quart. Appl. Mathematics, Vol. 14, pp. 331-333, 1956.

10. G.C.Sih and H.C. Hagendorf, "A new theory of spherical shells with cracks", Thin Shell Structures: Theory, Experiment and Design, Y.C. Fung, and E.E. Sechler, eds., Prentice Hall, Englewood Cliffs, N.Z., 1974.

11. S. Krenk, "Influence of transverse shear on an axial crack in a cylindrical shell", Int. J. of Fracture Mechanics, Vol. 14, pp. 123-143, 1978.

12. F. Delale and F. Erdogan, "Effect of transverse shear and material orthotropy in a cracked spherical cap", Int. J. Solids, Structures, Vol. 15, pp. 907-926, 1979.

13. F. Delale and F. Erdogan, "Transverse shear effect in a circumferentially cracked cylindrical shell", Quart. Appl. Mathematics, Vol. 37, pp. 239-258, 1979.

14. O.S. Yahsi, "Effect of Transverse Shear and Material Orthotropy in a Cylindrical Shell Containing an Arbitrarily Oriented Crack", Ph.D. Dissertation, Lehigh University, 1981.

15. F. Erdogan, "Mixed boundary value problems", Mechanics Today, S. Nemat-Nasser, ed. Vol. 4, pp. 1-86, Pergamon Press, Oxford, 1978.

16. I.S. Gradshteyn and I.M. Ryzhik, Tables of Integrals Series and Products, Academic Press, Inc., New York, 1965.

Appendix A

Dimensionless and normalized quantities used in the analysis,

$$x = x_1/a\sqrt{c} \ , \ y = x_2\sqrt{c}/a \ , \ z = x_3/a \ ; \tag{A.1}$$

$$u = u_1\sqrt{c}/a \ , \ v = u_2/a\sqrt{c} \ , \ w = u_3/a \ ; \tag{A.2}$$

$$\beta_x = \beta_1 \sqrt{c} \ , \ \beta_y = \beta_2/\sqrt{c} \ ; \tag{A.3}$$

$$\phi(x,y) = F(x_1,x_2)/Eha^2; \tag{A.4}$$

$$\sigma_{xx} = \frac{\sigma_{11}}{Ec} \ , \ \sigma_{yy} = \frac{c\sigma_{22}}{E} \ , \ \sigma_{xy} = \frac{\sigma_{12}}{E} \ , \ \sigma_{xz} = \frac{\sigma_{13}}{B\sqrt{c}} \ , \ \sigma_{yz} = \frac{\sqrt{c}\ \sigma_{23}}{B} \ ; \tag{A.5}$$

$$N_{xx} = N_{11}/Ehc \ , \ N_{yy} = cN_{22}/Eh \ , \ N_{xy} = N_{12}/Eh \ ; \tag{A.6}$$

$$M_{xx} = M_{11}/Ech^2 \ , \ M_{yy} = cM_{22}/Eh^2 \ , \ M_{xy} = M_{12}/Eh^2 \ ; \tag{A.7}$$

$$V_x = V_1/Bh\sqrt{c} \ , \ V_y = V_2\sqrt{c}/Bh \ ; \tag{A.8}$$

$$\lambda_1^4 = 12(1-\nu^2)\ \frac{c^2a^4}{h^2R_1^2} \ , \ \lambda_2^4 = 12(1-\nu^2)\ \frac{a^4}{c^2h^2R_2^2} \ ,$$

$$\lambda_{12}^4 = 12(1-\nu^2)\ \frac{a^4}{h^2R_{12}^2} \ , \ \lambda^4 = 12(1-\nu^2)\ \frac{a^2}{h^2} \ , \ \kappa = E/B\lambda^4 \ ; \tag{A.9}$$

$$E = \sqrt{E_1/E_2} \ , \ \nu = \sqrt{\nu_1\nu_2} \ , \ (\nu_1/E_1 = \nu_2/E_2) \ , \ c^4 = \frac{E_1}{E_2} \ , \ B = \frac{5E}{12(1+\nu)} \ . \tag{A.10}$$

Appendix B

The stress, moment, and transverse shear resultants.

$$N_{xx}(x,y) = \begin{cases} -\frac{1}{2\pi}\int_{-\infty}^{\infty}\alpha^2 \sum_{j=1}^{4} K_j R_j(\alpha) e^{m_j x} e^{-i\alpha y} d\alpha & x > 0, \\ -\frac{1}{2\pi}\int_{-\infty}^{\infty}\alpha^2 \sum_{j=5}^{8} K_j R_j(\alpha) e^{m_j x} e^{-i\alpha y} d\alpha & x < 0, \end{cases} \tag{B.1}$$

$$M_{xx}(x,y) = \begin{cases} \frac{1}{2\pi}\frac{a}{h\lambda^4}\int_{-\infty}^{\infty}\sum_{j=1}^{4}\frac{(1-\nu)\alpha^2+p_j}{\kappa p_{j-1}} R_j(\alpha) e^{m_j x} e^{-i\alpha y} d\alpha \\ -\frac{1}{2\pi}\frac{a}{h\lambda^4}\frac{\kappa(1-\nu)^2}{2}\int_{-\infty}^{\infty} iA_1(\alpha)\alpha r_1 e^{r_1 x} e^{-i\alpha y} d\alpha \quad x>0, \\ \frac{1}{2\pi}\frac{a}{h\lambda^4}\int_{-\infty}^{\infty}\sum_{j=5}^{8}\frac{(1-\nu)\alpha^2+p_j}{\kappa p_{j-1}} R_j(\alpha) e^{m_j x} e^{-i\alpha y} d\alpha \\ -\frac{1}{2\pi}\frac{a}{h\lambda^4}\frac{\kappa(1-\nu)^2}{2}\int_{-\infty}^{\infty} i\, A_2(\alpha)\alpha r_2 e^{r_2 x} e^{-i\alpha y} d\alpha \end{cases}$$

$x<0$. (B.2)

$$N_{xy}(x,y) = \begin{cases} \frac{i}{2\pi}\int_{-\infty}^{\infty}\alpha \sum_{j=1}^{4} R_j(\alpha) K_j m_j e^{m_j x} e^{-i\alpha y} d\alpha & x>0\ , \\ \frac{i}{2\pi}\int_{-\infty}^{\infty}\alpha \sum_{j=5}^{8} R_j(\alpha) K_j m_j e^{m_j x} e^{-i\alpha y} d\alpha & x\ 0. \end{cases} \tag{B.3}$$

$$M_{xy}(x,y) = \begin{cases} -\frac{1}{2\pi}\frac{(1-\nu)a}{h\lambda^4}\int_{-\infty}^{\infty} i\alpha \sum_{j=1}^{4} \frac{m_j R_j(\alpha)}{\kappa p_j - 1} e^{m_j x} e^{-i\alpha y} d\alpha \\ \quad -\frac{1}{2\pi}\frac{a\kappa}{h\lambda^4}\frac{(1-\nu)^2}{4}\int_{-\infty}^{\infty}(\alpha^2+r_1^2)A_1(\alpha)e^{r_1 x}e^{-i\alpha y}d\alpha, \quad x>0, \\ -\frac{1}{2\pi}\frac{(1-\nu)a}{h\lambda^4}\int_{-\infty}^{\infty} i\alpha \sum_{j=5}^{8} \frac{m_j R_j(\alpha)}{\kappa p_j - 1} e^{m_j x} e^{-i\alpha y} d\alpha \\ \quad -\frac{1}{2\pi}\frac{a\kappa}{h\lambda^4}\frac{(1-\nu)^2}{4}\int_{-\infty}^{\infty}(\alpha^2+r_2^2)A_2(\alpha)e^{r_2 x}e^{-i\alpha y}d\alpha, \quad x<0 . \end{cases} \quad (B.4)$$

$$V_x(x,y) = \begin{cases} \frac{1}{2\pi}\int_{-\infty}^{\infty} \sum_{j=1}^{4} \frac{\kappa p_j R_j(\alpha) m_j}{\kappa p_j - 1} e^{m_j x} e^{-i\alpha y} d\alpha \\ \quad -\frac{1}{2\pi}\frac{\kappa(1-\nu)}{2}\int_{-\infty}^{\infty} iA_1(\alpha)\alpha\, e^{r_1 x}e^{-i\alpha y}d\alpha, \quad x>0, \\ \frac{1}{2\pi}\int_{-\infty}^{\infty} \sum_{j=5}^{8} \frac{\kappa p_j R_j(\alpha) m_j}{\kappa p_j - 1} e^{m_j x} e^{-i\alpha y}\, d\alpha \\ \quad -\frac{1}{2\pi}\frac{\kappa(1-\nu)}{2}\int_{-\infty}^{\infty} iA_2(\alpha)\alpha\, e^{r_2 x}e^{-i\alpha y}d\alpha, x<0 . \end{cases} \quad (B.5)$$

$$N_{yy}(x,y) = \begin{cases} \frac{1}{2\pi}\int_{-\infty}^{\infty} \sum_{j=1}^{4} R_j K_j m_j^2 e^{m_j x} e^{-i\alpha y}\, d\alpha, & x>0, \\ \frac{1}{2\pi}\int_{-\infty}^{\infty} \sum_{j=5}^{8} R_j K_j m_j^2 e^{m_j x} e^{-i\alpha y} d\alpha, & x<0 . \end{cases} \tag{B.6}$$

$$M_{yy}(x,y) = \begin{cases} \frac{1}{2\pi}\frac{a}{h\lambda^4}\int_{-\infty}^{\infty} \sum_{j=1}^{4} \frac{\nu p_j-(1-\nu)\alpha^2}{\kappa p_j-1} R_j e^{m_j x} e^{-i\alpha y} d\alpha \\ + \frac{1}{2\pi}\frac{a}{h\lambda^4}\frac{\kappa(1-\nu)^2}{2}\int_{\infty}^{\infty} i A_1(\alpha)\alpha r_1 e^{r_1 x} e^{-i\alpha y} d\alpha, & x>0, \\ \frac{1}{2\pi}\frac{a}{h\lambda^4}\int_{-\infty}^{\infty} \sum_{j=5}^{8} \frac{\nu p_j-(1-\nu)\alpha^2}{\kappa p_j-1} R_j e^{m_j x} e^{-i\alpha y} d\alpha \\ + \frac{1}{2\pi}\frac{a}{h\lambda^4}\frac{\kappa(1-\nu)^2}{2}\int_{-\infty}^{\infty} i A_2(\alpha)\alpha r_2 e^{r_2 x} e^{-i\alpha y} d\alpha, & x<0. \end{cases} \tag{B.7}$$

$$V_y(x,y) = \begin{cases} -\frac{1}{2\pi}\int_{-\infty}^{\infty} i\alpha \sum_{j=1}^{4} \frac{\kappa p_j}{\kappa p_j-1} R_j e^{m_j x} e^{-i\alpha y} d\alpha \\ -\frac{1}{2\pi}\int_{-\infty}^{\infty} \frac{\kappa(1-\nu)}{2} A_1(\alpha) r_1 e^{r_1 x} e^{-i\alpha y} d\alpha, & x>0, \\ -\frac{1}{2\pi}\int_{-\infty}^{\infty} i\alpha \sum_{j=5}^{8} \frac{\kappa p_j}{\kappa p_j-1} R_j e^{m_j x} e^{-i\alpha y} d\alpha \\ -\frac{1}{2\pi}\int_{-\infty}^{\infty} \frac{\kappa(1-\nu)}{2} A_2(\alpha) r_2 e^{r_2 x} e^{-i\alpha y} d\alpha, & x<0 . \end{cases} \tag{B.8}$$

APPENDIX C

The Kernels of Integral Equations:

$$k_{11}(\sqrt{c}\,\tau,\sqrt{c}\,\eta) = \int_0^\infty [2\alpha^2 \mathrm{Re}(\sum_{j=1}^{8} K_j B_{j1}) - 1]\sin\alpha\sqrt{c}(\tau-\eta)d\alpha$$

$$+ 2\int_0^\infty \alpha^2 \mathrm{Im}(\sum_{j=1}^{8} K_j B_{j1})\cos\alpha\sqrt{c}(\tau-\eta)d\alpha\ , \qquad (C.1)$$

$$k_{12}(\sqrt{c}\,\tau,\sqrt{c}\,\eta) = 2\int_0^\infty \alpha^2 \mathrm{Re}[\sum_{j=1}^{8} K_j B_{j2}]\sin\alpha\sqrt{c}(\tau-\eta)d\alpha$$

$$+ 2\int_0^\infty \alpha^2 \mathrm{Im}[\sum_{j=1}^{8} K_j B_{j2}]\cos\alpha\sqrt{c}(\tau-\eta)d\alpha\ , \qquad (C.2)$$

$$k_{13}(\sqrt{c}\,\tau,\sqrt{c}\,\eta) = 2\int_0^\infty \alpha^2 \mathrm{Re}[\sum_{j=1}^{8} K_j B_{j3}]\sin\alpha\sqrt{c}(\tau-\eta)d\alpha$$

$$+ 2\int_0^\infty \alpha^2 \mathrm{Im}[\sum_{j=1}^{8} K_j B_{j3}]\cos\alpha\sqrt{c}(\tau-\eta)d\alpha\,, \qquad (C.3)$$

$$k_{14}(\sqrt{c}\,\tau,\sqrt{c}\,\eta) = 2\int_0^\infty \alpha^2 \mathrm{Re}[\sum_{j=1}^{8} K_j B_{j4}]\sin\alpha\sqrt{c}(\tau-\eta)d\alpha$$

$$+ 2\int_0^\infty \alpha^2 \mathrm{Im}[\sum_{j=1}^{8} K_j B_{j4}]\cos\alpha\sqrt{c}(\tau-\eta)d\alpha\,, \qquad (C.4)$$

$$k_{15}(\sqrt{c}\,\tau,\sqrt{c}\,\eta) = 2\int_0^\infty \alpha^2 \mathrm{Re}[\sum_{j=1}^{8} K_j B_{j5}]\sin\alpha\sqrt{c}(\tau-\eta)d\alpha$$

$$+ 2\int_0^\infty \alpha^2 \mathrm{Im}[\sum_{j=1}^{8} K_j B_{j5}]\cos\alpha\sqrt{c}(\tau-\eta)d\alpha \quad , \qquad (C.5)$$

$$k_{21}(\sqrt{c}\,\tau,\sqrt{c}\,\eta) = -\frac{2}{\lambda^4}\int_0^\infty \mathrm{Re}[\sum_{j=1}^{8} \frac{p_j+(1-\nu)\alpha^2}{\kappa p_j - 1} B_{j1}]\sin\alpha\sqrt{c}(\tau-\eta)d\alpha$$

$$-\frac{2}{\lambda^4}\int_0^\infty \mathrm{Im}[\sum_{j=1}^{8} \frac{p_j+(1-\nu)\alpha^2}{\kappa p_j - 1} B_{j1}]\cos\alpha\sqrt{c}(\tau-\eta)d\alpha \, , \qquad (C.6)$$

$$k_{22}(\sqrt{c}\,\tau,\sqrt{c}\,\eta) = \int_0^\infty \{-\frac{2}{\lambda^4}\mathrm{Re}[\sum_{j=1}^{8} \frac{p_j+(1-\nu)\alpha^2}{\kappa p_j - 1} B_{j2}] + \frac{2k(1-\nu)^2\alpha r_1}{\lambda^4} - \frac{1-\nu^2}{\lambda^4}\}$$

$$\times \sin\alpha\sqrt{c}(\tau-\eta)d\alpha$$

$$-\frac{2}{\lambda^4}\int_0^\infty \mathrm{Im}[\sum_{j=1}^{8} \frac{p_j+(1-\nu)\alpha^2}{\kappa p_j - 1} B_{j2}]\cos\alpha\sqrt{c}(\tau-\eta)d\alpha \, , \qquad (C.7)$$

$$k_{23}(\sqrt{c}\,\tau,\sqrt{c}\,\eta) = -\frac{2}{\lambda^4}\int_0^\infty \mathrm{Re}[\sum_{j=1}^{8} \frac{p_j+(1-\nu)\alpha^2}{\kappa p_j - 1} B_{j3}]\sin\alpha\sqrt{c}(\tau-\eta)d\alpha$$

$$-\frac{2}{\lambda^4}\int_0^\infty \mathrm{Im}[\sum_{j=1}^{8} \frac{p_j+(1-\nu)\alpha^2}{\kappa p_j - 1} B_{j3}]\cos\alpha\sqrt{c}(\tau-\eta)d\alpha \, , \qquad (C.8)$$

$$k_{24}(\sqrt{c}\,\tau,\sqrt{c}\,\eta) = -\frac{2}{\lambda^4}\int_0^\infty \mathrm{Re}\Big[\sum_{j=1}^{8}\frac{p_j+(1-\nu)\alpha^2}{\kappa p_j-1}B_{j4}\Big]\sin\alpha\sqrt{c}(\tau-\eta)d\alpha$$

$$-\frac{2}{\lambda^4}\int_0^\infty \mathrm{Im}\Big[\sum_{j=1}^{8}\frac{p_j+(1-\nu)\alpha^2}{\kappa p_j-1}B_{j4}\Big]\cos\alpha\sqrt{c}(\tau-\eta)d\alpha\ , \qquad (C.9)$$

$$k_{25}(\sqrt{c}\,\tau,\sqrt{c}\,\eta) = -\frac{2}{\lambda^4}\int_0^\infty \mathrm{Re}\Big[\sum_{j=1}^{8}\frac{p_j+(1-\nu)\alpha^2}{\kappa p_j-1}B_{j5}\Big]\sin\alpha\sqrt{c}(\tau-\eta)d\alpha$$

$$-\frac{2}{\lambda^4}\int_0^\infty \mathrm{Im}\Big[\sum_{j=1}^{8}\frac{p_j+(1-\nu)\alpha^2}{\kappa p_j-1}B_{j5}\Big]\cos\alpha\sqrt{c}(\tau-\eta)d\alpha, \qquad (C.10)$$

$$k_{31}(\sqrt{c}\,\tau,\sqrt{c}\,\eta) = -2\int_0^\infty \alpha\ \mathrm{Re}\Big[\sum_{j=1}^{8}K_j m_j B_{j1}\Big]\cos\alpha\sqrt{c}(\tau-\eta)d\alpha$$

$$+2\int_0^\infty \alpha\ \mathrm{Im}\Big[\sum_{j=1}^{8}K_j m_j B_{j1}\Big]\sin\alpha\sqrt{c}(\tau-\eta)d\alpha\ , \qquad (C.11)$$

$$k_{32}(\sqrt{c}\,\tau,\sqrt{c}\,\eta) = -2\int_0^\infty \alpha\ \mathrm{Re}\Big[\sum_{1}^{8}K_j m_j B_{j2}\Big]\cos\alpha\sqrt{c}(\tau-\eta)d\alpha$$

$$+2\int_0^\infty \alpha\ \mathrm{Im}\Big[\sum_{1}^{8}K_j m_j B_{j2}\Big]\sin\alpha\sqrt{c}(\tau-\eta)d\alpha\,, \qquad (C.12)$$

$$k_{33}(\sqrt{c}\,\tau,\sqrt{c}\,\eta) = -2\int_0^\infty \alpha\ \mathrm{Re}\Big[\sum_{j=1}^{8} K_j m_j B_{j3}\Big]\cos\alpha\sqrt{c}(\tau-\eta)d\alpha$$

$$+\int_0^\infty \{2\alpha\,\mathrm{Im}\Big[\sum_{j=1}^{8} K_j m_j B_{j3}\Big]-1\}\sin\alpha\sqrt{c}(\tau-\eta)d\alpha, \qquad (C.13)$$

$$k_{34}(\sqrt{c}\,\tau,\sqrt{c}\,\eta) = -2\int_0^\infty \alpha\ \mathrm{Re}\Big[\sum_{j=1}^{8} K_j m_j B_{j4}\Big]\cos\alpha\sqrt{c}(\tau-\eta)d\alpha$$

$$+2\int_0^\infty \alpha\ \mathrm{Im}\Big[\sum_{j=1}^{8} K_j m_j B_{j4}\Big]\sin\alpha\sqrt{c}(\tau-\eta)d\alpha, \qquad (C.14)$$

$$k_{35}(\sqrt{c}\,\tau,\sqrt{c}\,\eta) = -2\int_0^\infty \alpha\ \mathrm{Re}\Big[\sum_{j=1}^{8} K_j m_j B_{j5}\Big]\cos\alpha\sqrt{c}(\tau-\eta)d\alpha$$

$$+2\int_0^\infty \alpha\ \mathrm{Im}\Big[\sum_{j=1}^{8} K_j m_j B_{j5}\Big]\sin\alpha\sqrt{c}(\tau-\eta)d\alpha, \qquad (C.15)$$

$$k_{41}(\sqrt{c}\,\tau,\sqrt{c}\,\eta) = \frac{2(1-\nu)}{\lambda^4}\int_0^\infty \alpha\ \mathrm{Re}\Big[\sum_{j=1}^{8} \frac{m_j}{\kappa p_j - 1} B_{j1}\Big]\cos\alpha\sqrt{c}(\tau-\eta)d\alpha$$

$$-\frac{2(1-\nu)}{\lambda^4}\int_0^\infty \alpha\ \mathrm{Im}\Big[\sum_{j=1}^{8} \frac{m_j}{p_j - 1} B_{j1}\Big]\sin\alpha\sqrt{c}(\tau-\eta)d\alpha, \qquad (C.16)$$

$$k_{42}(\sqrt{c}\,\tau,\sqrt{c}\,\eta) = \frac{2(1-\nu)}{\lambda^4}\int_0^\infty \alpha\ \mathrm{Re}\Big[\sum_{j=1}^{8}\frac{m_j}{\kappa p_j - 1}B_{j2}\Big]\cos\alpha\sqrt{c}(\tau-\eta)d\alpha$$

$$-\frac{2(1-\nu)}{\lambda^4}\int_0^\infty \alpha\ \mathrm{Im}\Big[\sum_{j=1}^{8}\frac{m_j}{\kappa p_j - 1}B_{j2}\Big]\sin\alpha\sqrt{c}(\tau-\eta)d\alpha\,, \quad (C.17)$$

$$k_{43}(\sqrt{c}\,\tau,\sqrt{c}\,\eta) = \frac{2(1-)}{\lambda^4}\int_0^\infty \alpha\ \mathrm{Re}\Big[\sum_{j=1}^{8}\frac{m_j}{\kappa p_j - 1}B_{j3}\Big]\cos\alpha\sqrt{c}(\tau-\eta)d\alpha$$

$$-\frac{2(1-\nu)}{\lambda^4}\int_0^\infty \alpha\ \mathrm{Im}\Big[\sum_{j=1}^{8}\frac{m_j}{\kappa p_j - 1}B_{j3}\Big]\sin\alpha\sqrt{c}(\tau-\eta)d\alpha\,, \quad (C.18)$$

$$k_{44}(\sqrt{c}\,\tau,\sqrt{c}\,\eta) = \frac{2(1-\nu)}{\lambda^4}\int_0^\infty \alpha\ \mathrm{Re}\Big[\sum_{j=1}^{8}\frac{m_j}{\kappa p_j - 1}B_{j4}\Big]\cos\alpha\sqrt{c}(\tau-\eta)d\alpha$$

$$-\int_0^\infty \Big\{\frac{2(1-\nu)}{\lambda^4}\alpha\ \mathrm{Im}\Big[\sum_{j=1}^{8}\frac{m_j}{\kappa p_j - 1}B_{j4}\Big] + \frac{1-\nu^2}{\lambda^4} + \frac{1+\alpha^2\kappa(1-\nu)}{\alpha r_1\lambda^4}(\alpha^2+r_1^{\,2})$$

$$x(1-\nu)\Big\}\sin\alpha\sqrt{c}(\tau-\eta)d\alpha\,, \quad (C.19)$$

$$k_{45}(\sqrt{c}\,\tau,\sqrt{c}\,\eta) = \frac{2(1-\nu)}{\lambda^4}\int_0^\infty \alpha\ \mathrm{Re}\Big[\sum_{j=1}^{8}\frac{m_j}{\kappa p_j - 1}B_{j5}\Big]\cos\alpha\sqrt{c}(\tau-\eta)d\alpha$$

$$-\frac{2(1-\nu)}{\lambda^4}\int_0^\infty \alpha\ \mathrm{Im}\Big[\sum_{j=1}^{8}\frac{m_j}{\kappa p_j - 1}B_{j5}\Big]\sin\alpha\sqrt{c}(\tau-\eta)d\alpha$$

$$+\frac{(1-\nu)}{\lambda^4}\int_0^\infty \frac{\alpha^2+r_1^{\,2}}{r_1}\cos\alpha\sqrt{c}(\tau-\eta)d\alpha\,, \quad (C.20)$$

$$k_{51}(\sqrt{c}\,\tau,\sqrt{c}\,\eta) = -\int_0^\infty \mathrm{Re}\Big[\sum_{j=1}^{8} \frac{\kappa p_j m_j}{\kappa p_j - 1} B_{j1}\Big]\sin\alpha\sqrt{c}(\tau-\eta)d\alpha$$

$$-\int_0^\infty \mathrm{Im}\Big[\sum_{j=1}^{8} \frac{\kappa p_j m_j}{\kappa p_j - 1} B_{j1}\Big]\cos\alpha\sqrt{c}(\tau-\eta)d\alpha\,, \qquad (C.21)$$

$$k_{52}(\sqrt{c}\,\tau,\sqrt{c}\,\eta) = -\int_0^\infty \mathrm{Re}\Big[\sum_{j=1}^{8} \frac{\kappa p_j m_j}{\kappa p_j - 1} B_{j2}\Big]\sin\alpha\sqrt{c}(\tau-\eta)d\alpha$$

$$-\int_0^\infty \mathrm{Im}\Big[\sum_{j=1}^{8} \frac{\kappa p_j m_j}{\kappa p_j - 1} B_{j2}\Big]\cos\alpha\sqrt{c}(\tau-\eta)d\alpha \qquad (C.22)$$

$$k_{53}(\sqrt{c}\,\tau,\sqrt{c}\,\eta) = -\int_0^\infty \mathrm{Re}\Big[\sum_{j=1}^{8} \frac{\kappa p_j m_j}{\kappa p_j - 1} B_{j3}\Big]\sin\alpha\sqrt{c}(\tau-\eta)d\alpha$$

$$-\int_0^\infty \mathrm{Im}\Big[\sum_{j=1}^{8} \frac{\kappa p_j m_j}{\kappa p_j - 1} B_{j3}\Big]\cos\alpha\sqrt{c}(\tau-\eta)d\alpha\,, \qquad (C.23)$$

$$k_{54}(\sqrt{c}\,\tau,\sqrt{c}\,\eta) = -\int_0^\infty \mathrm{Re}\Big[\sum_{j=1}^{8} \frac{\kappa p_j m_j}{\kappa p_j - 1} B_{j4}\Big]\sin\alpha\sqrt{c}(\tau-\eta)d\alpha$$

$$-\int_0^\infty \mathrm{Im}\Big[\sum_{j=1}^{8} \frac{\kappa p_j m_j}{\kappa p_j - 1} B_{j4}\Big]\cos\alpha\sqrt{c}(\tau-\eta)d\alpha$$

$$-\int_0^\infty \frac{1+\alpha^2\kappa(1-\nu)}{r_1}\cos\alpha\sqrt{c}(\tau-\eta)d\alpha\,, \qquad (C.24)$$

$$k_{55}(\sqrt{c}\,\tau,\sqrt{c}\,\eta) = -\int_0^\infty \{\mathrm{Re}[\sum_{j=1}^{8} \frac{\kappa p_j m_j}{\kappa p_j - 1} B_{j5}] + (\frac{\alpha}{r_1} + 1)\}\sin\alpha\sqrt{c}(\tau-\eta)d\alpha$$

$$-\int_0^\infty \mathrm{Im}[\sum_{j=1}^{8} \frac{\kappa p_j m_j}{\kappa p_j - 1} B_{j5}]\cos\alpha\sqrt{c}(\tau-\eta)d\alpha\ , \qquad (C.25)$$

In the expressions given above $B_{jk}(\alpha)$, (j=1,...,8; k=1,...,5) are the coefficients given in (3.48) which are obtained by solving the linear algebraic equations (3.37)-(3.46) for the unknowns $R_1,\ldots,R_8$, A_1, and A_2.

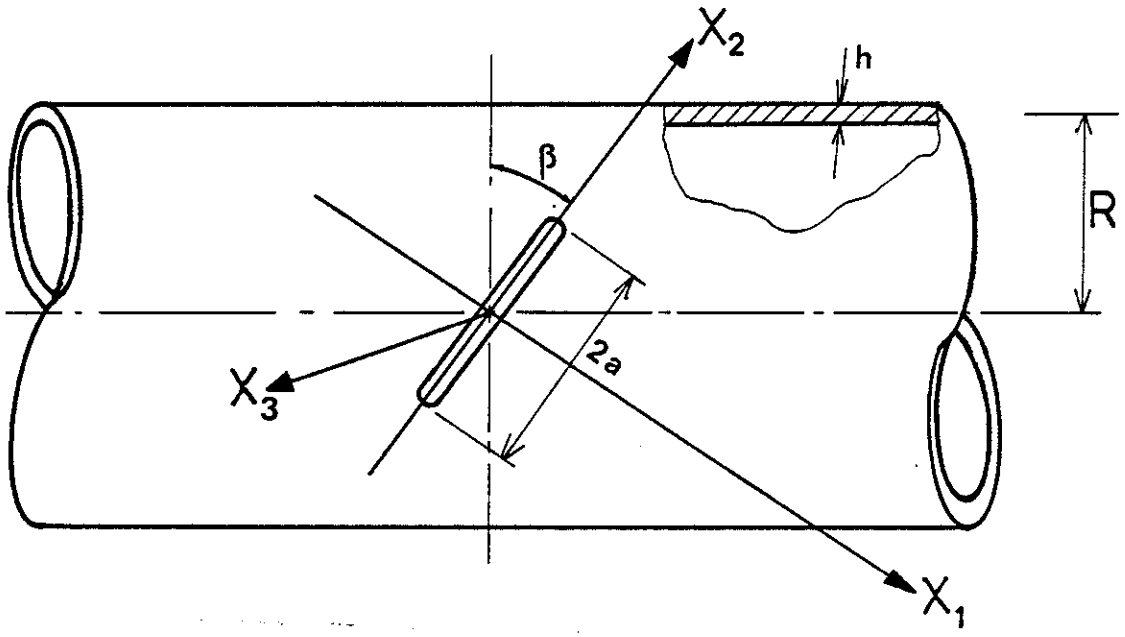

Figure 1. Geometry of a cylindrical shell containing an inclined crack.

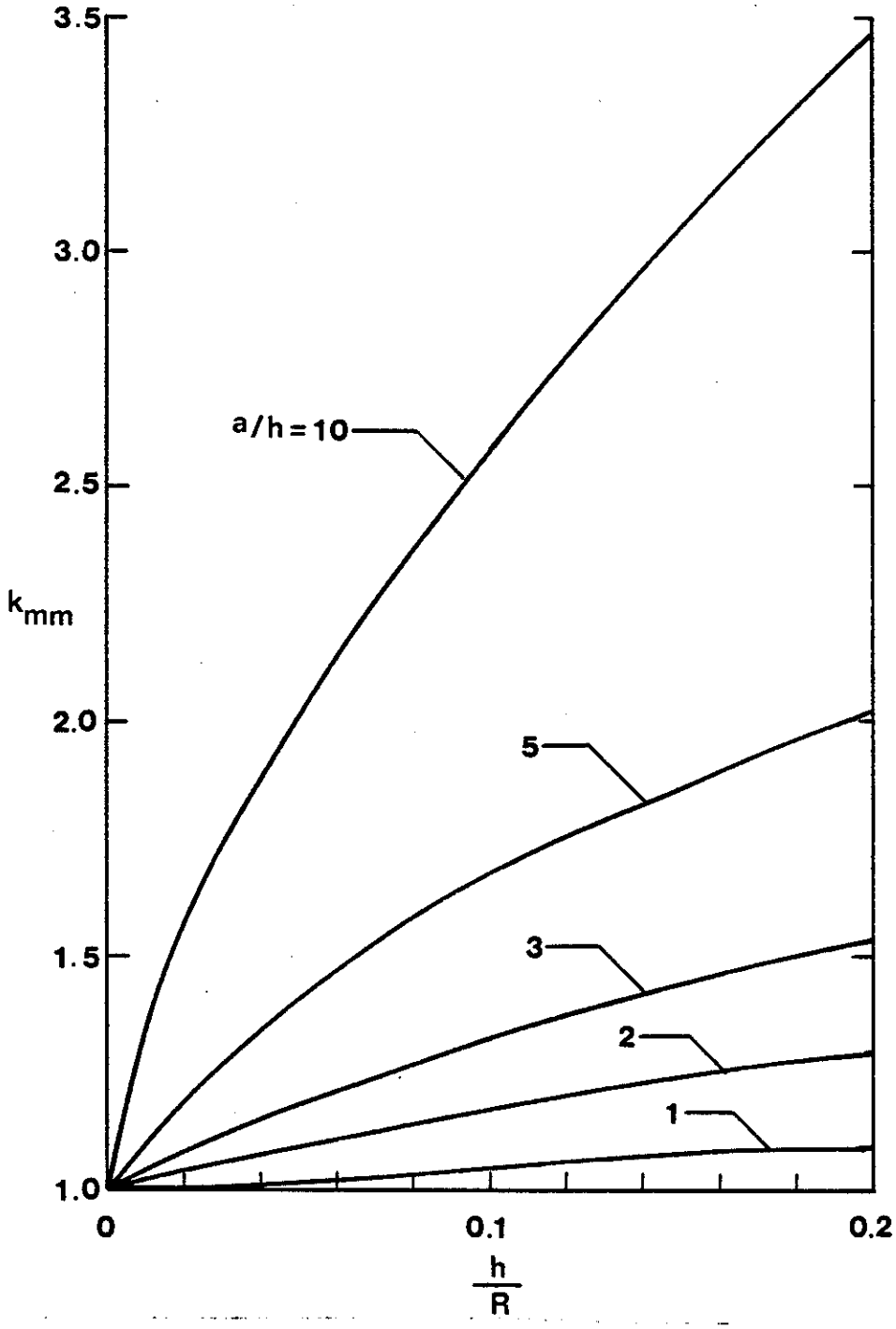

Figure 2. Stress intensity factor ratio k_{mm} in an isotropic cylindrical shell containing an inclined crack under uniform membrane loading N_{11}; $\beta=45°$, $\nu=0.3$.

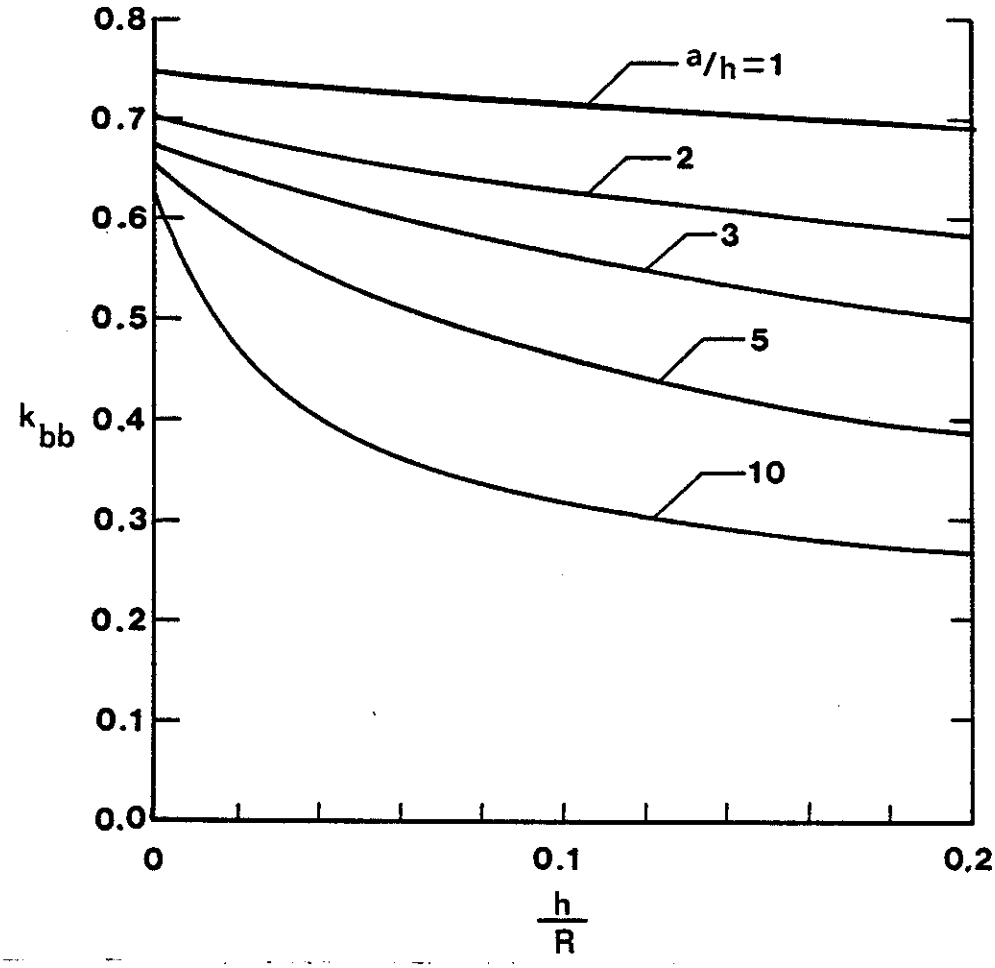

Figure 3. Stress intensity factor ratio k_{bb} in an isotropic cylindrical shell containing an inclined crack under uniform bending moment M_{11}; $\beta=45°$, $\nu=0.3$.

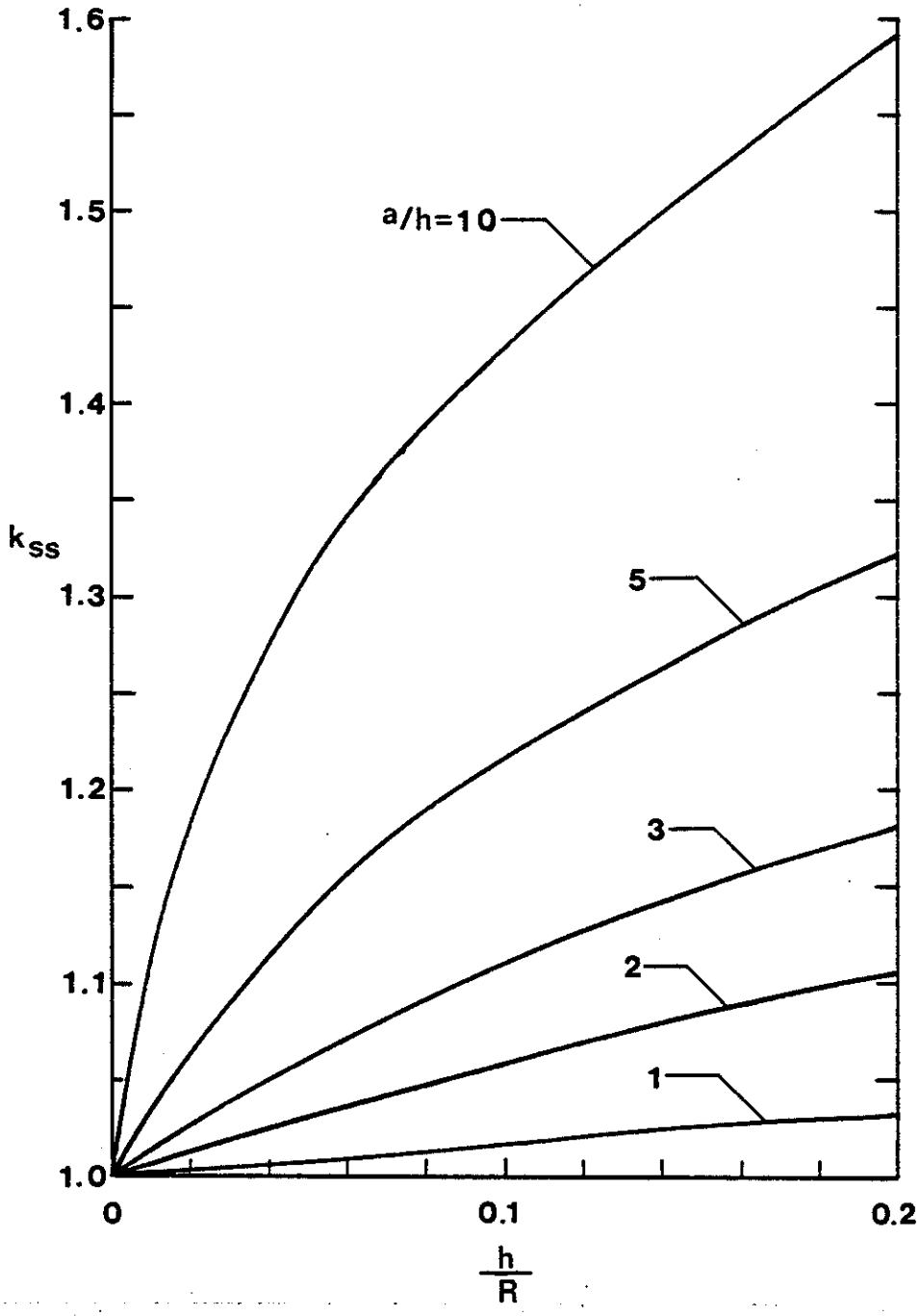

Figure 4. Stress intensity factor ratio k_{ss} in an isotropic cylindrical shell containing an inclined crack under uniform in-plane shear loading N_{12}; β=45°, ν=0.3.

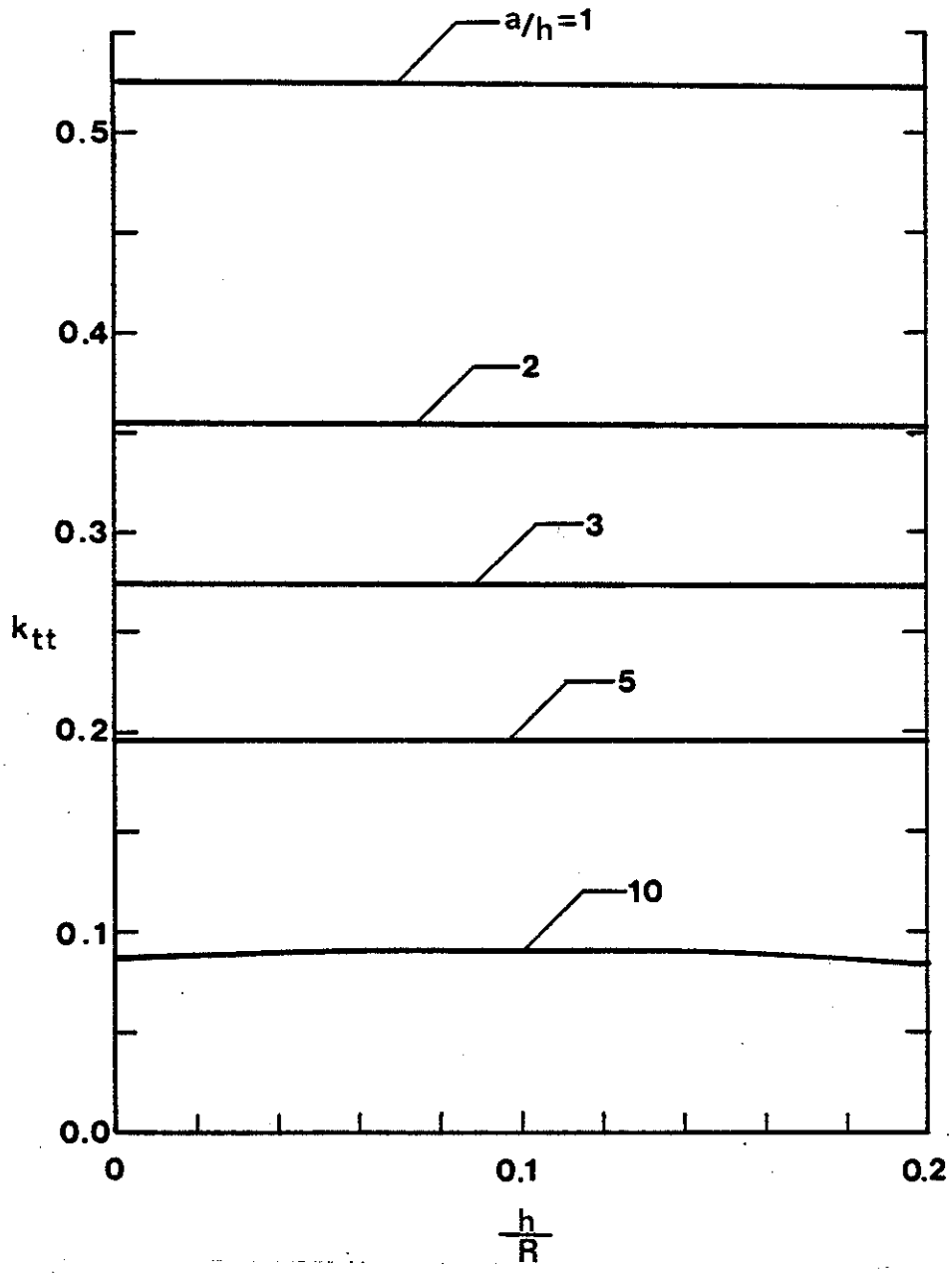

Figure 5. Stress intensity factor ratio k_{tt} in an isotropic cylindrical shell containing an inclined crack under uniform twisting moment M_{12}; $\beta=45°$, $\nu=0.3$.

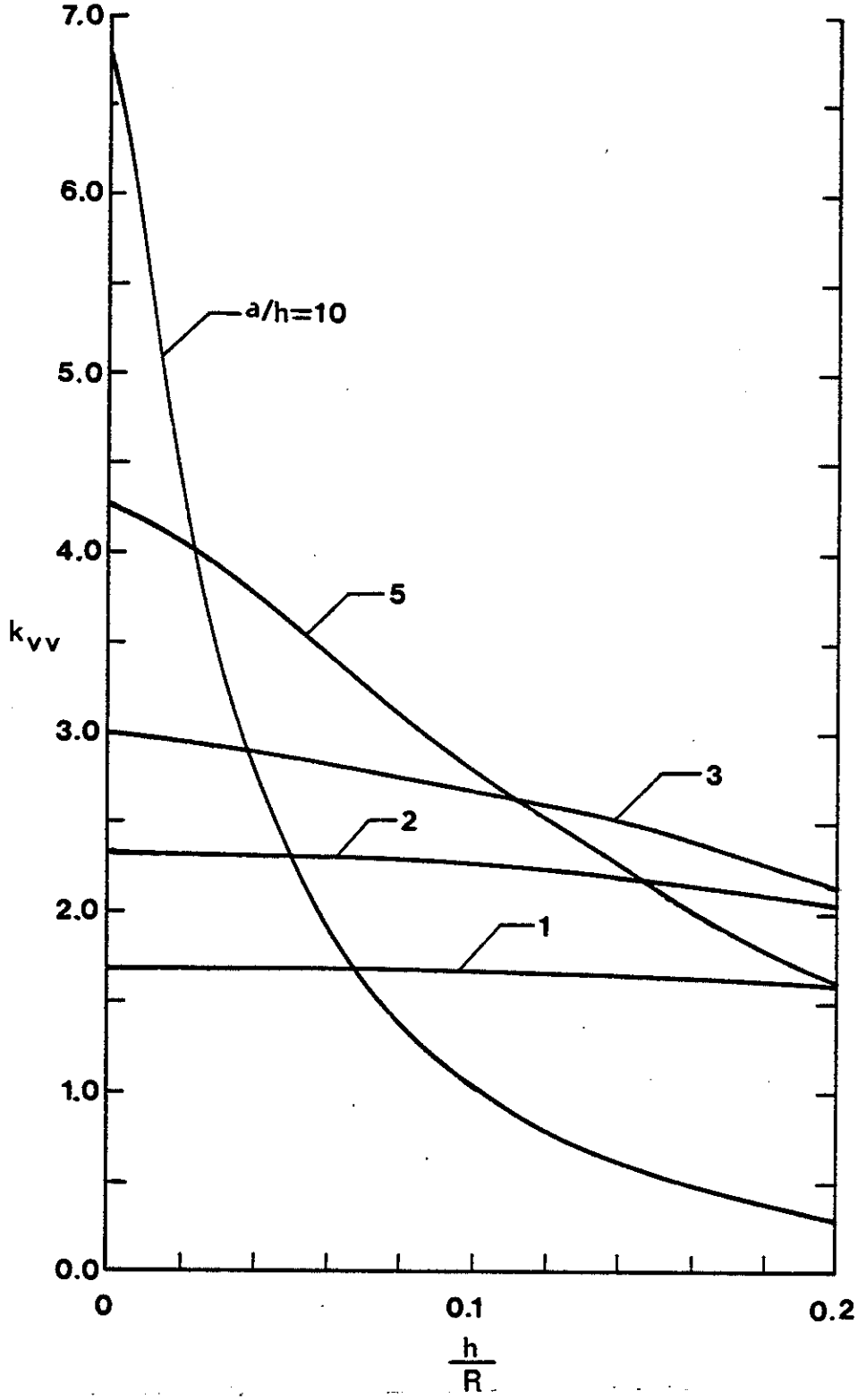

Figure 6. Stress intensity factor ratio k_{VV} in an isotropic cylindrical shell containing an inclined crack under uniform transverse shear loading V_1; $\beta=45°$, $\nu=0.3$.

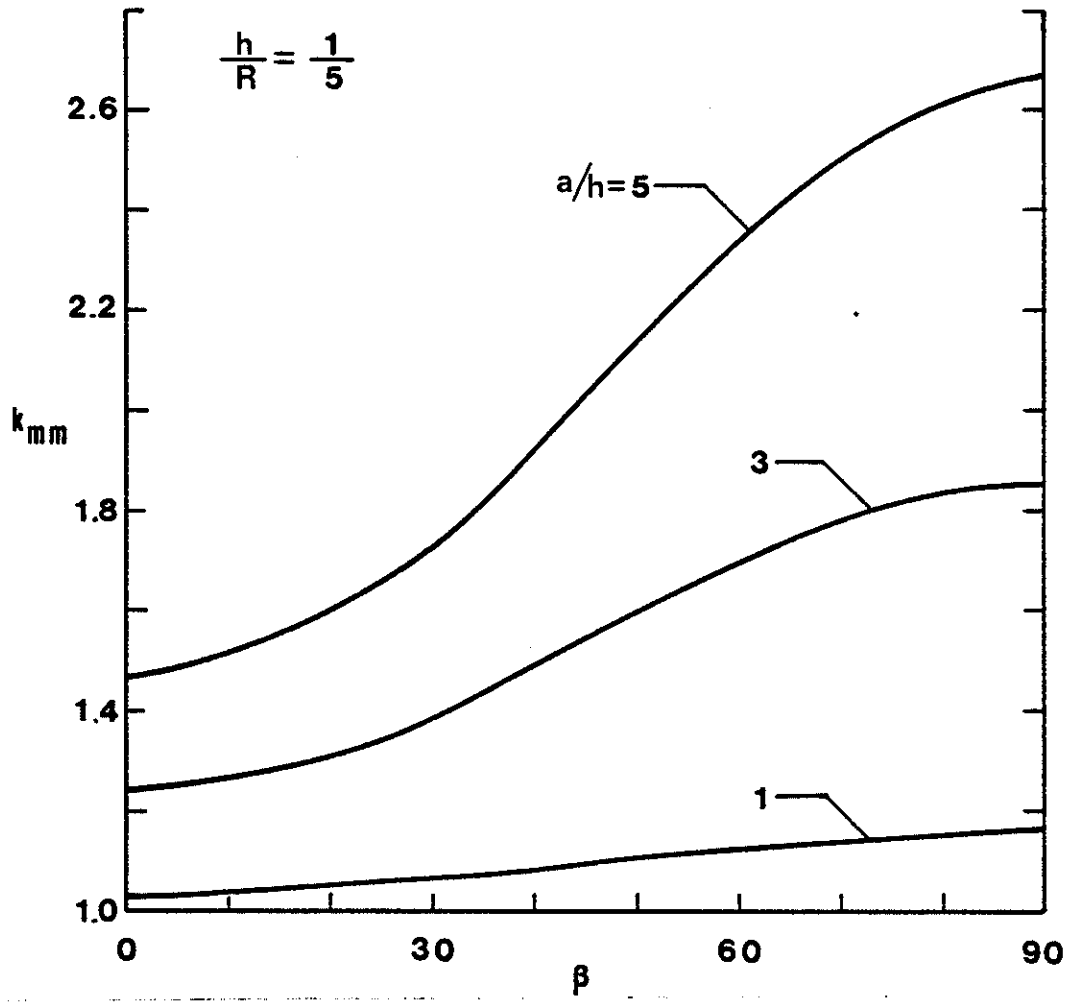

Figure 7. Stress intensity factor ratio k_{mm} in an isotropic cylindrical shell containing an inclined crack under uniform membrane loading N_{11}; ν=0.3, h/R=1/5.

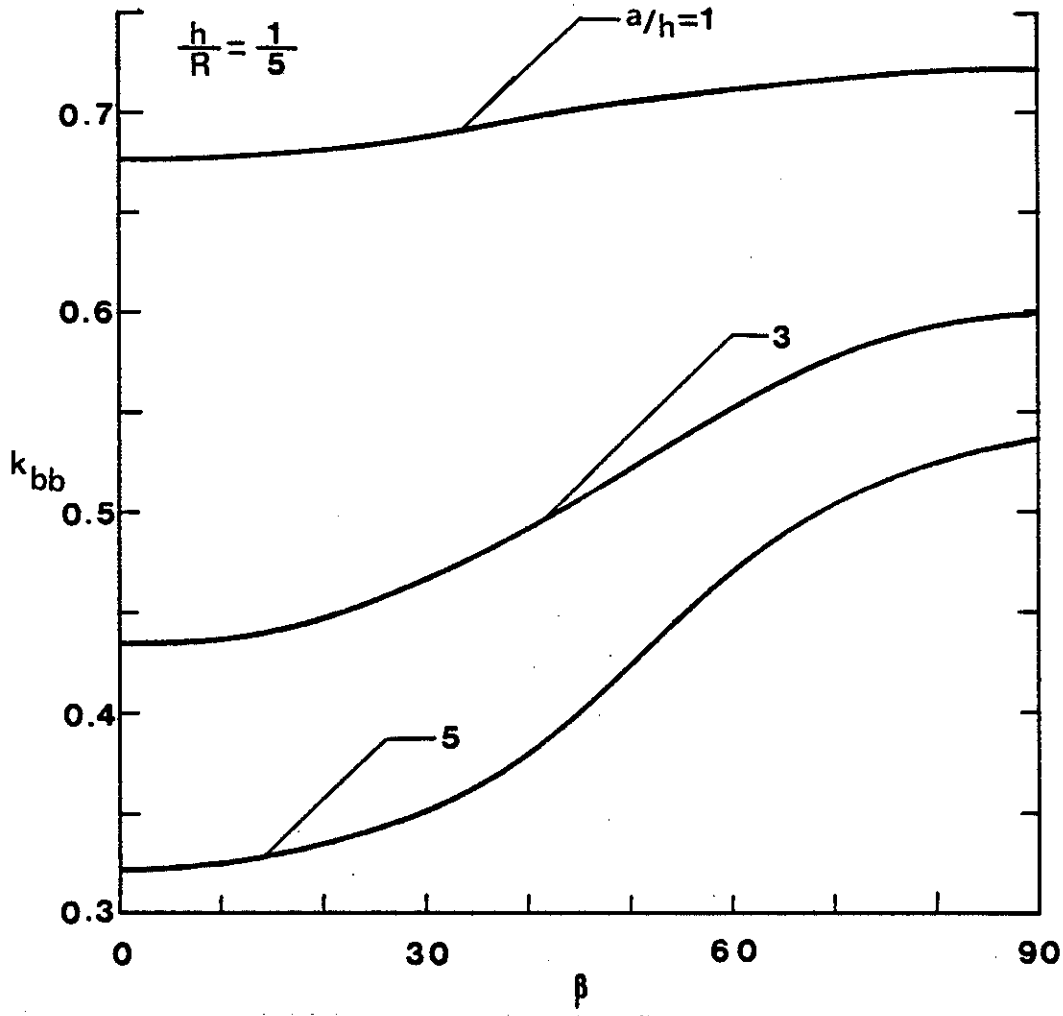

Figure 8. Stress intensity factor ratio k_{bb} in an isotropic cylindrical shell containing an inclined crack under uniform bending moment M_{11}; ν=0.3, h/R=1/5.

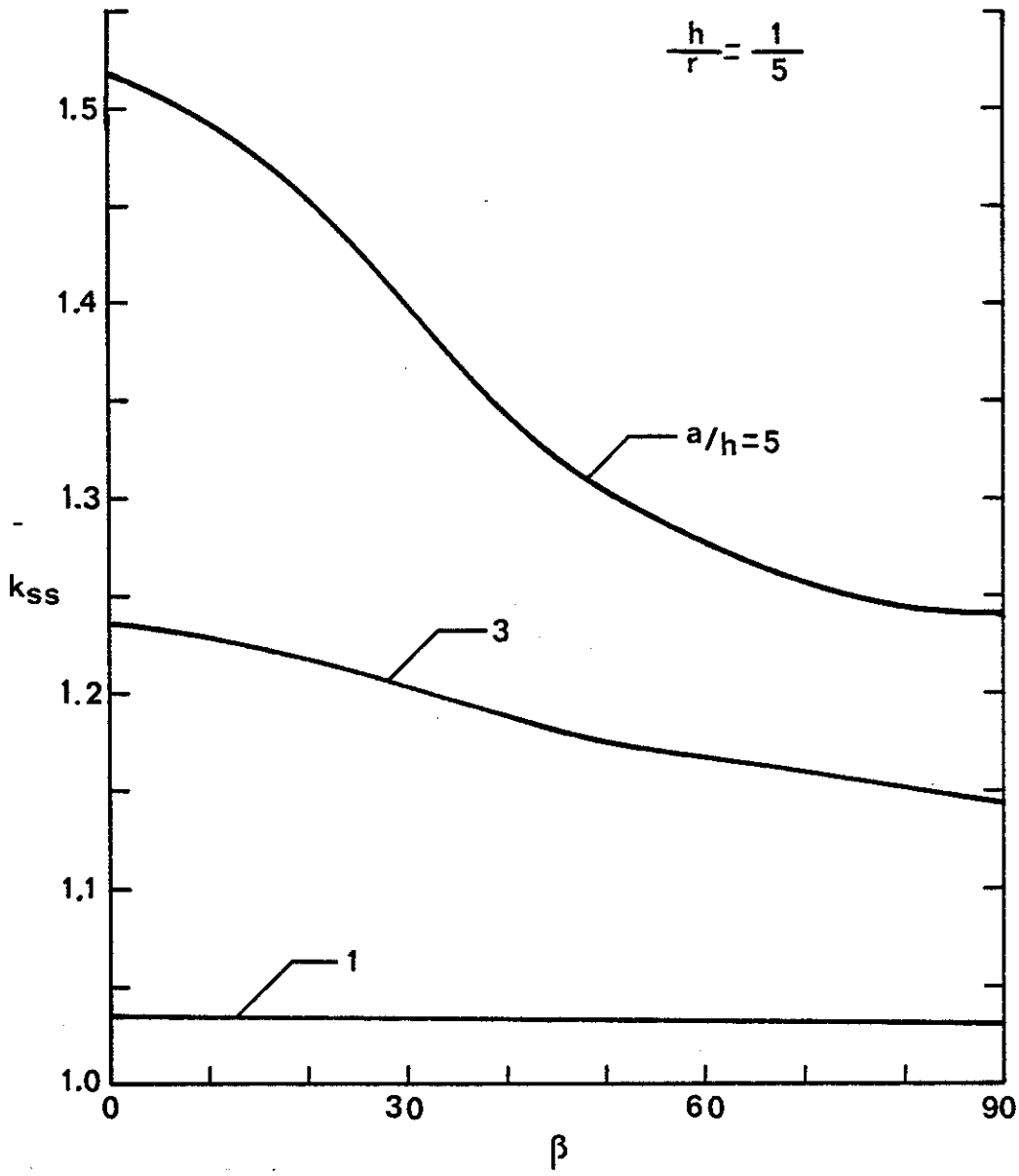

Figure 9. Stress intensity factor ratio k_{ss} in an isotropic cylindrical shell containing an inclined crack under uniform in-plane shear loading N_{12}; ν=0.3, h/R=1/5.

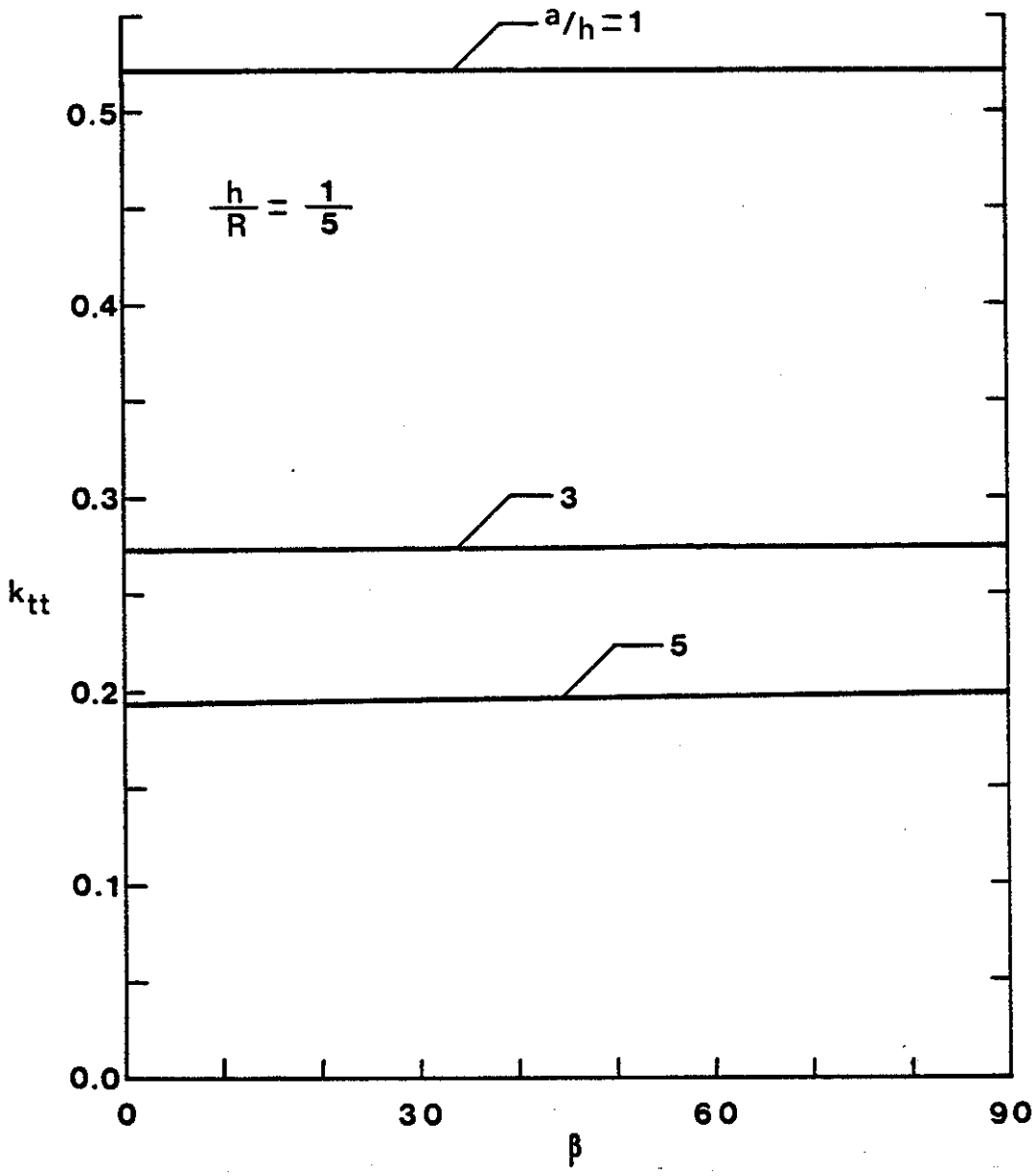

Figure 10. Stress intensity factor ratio k_{tt} in an isotropic cylindrical shell containing an inclined crack under uniform twisting moment M_{12}; ν=0.3, h/R=1/5.

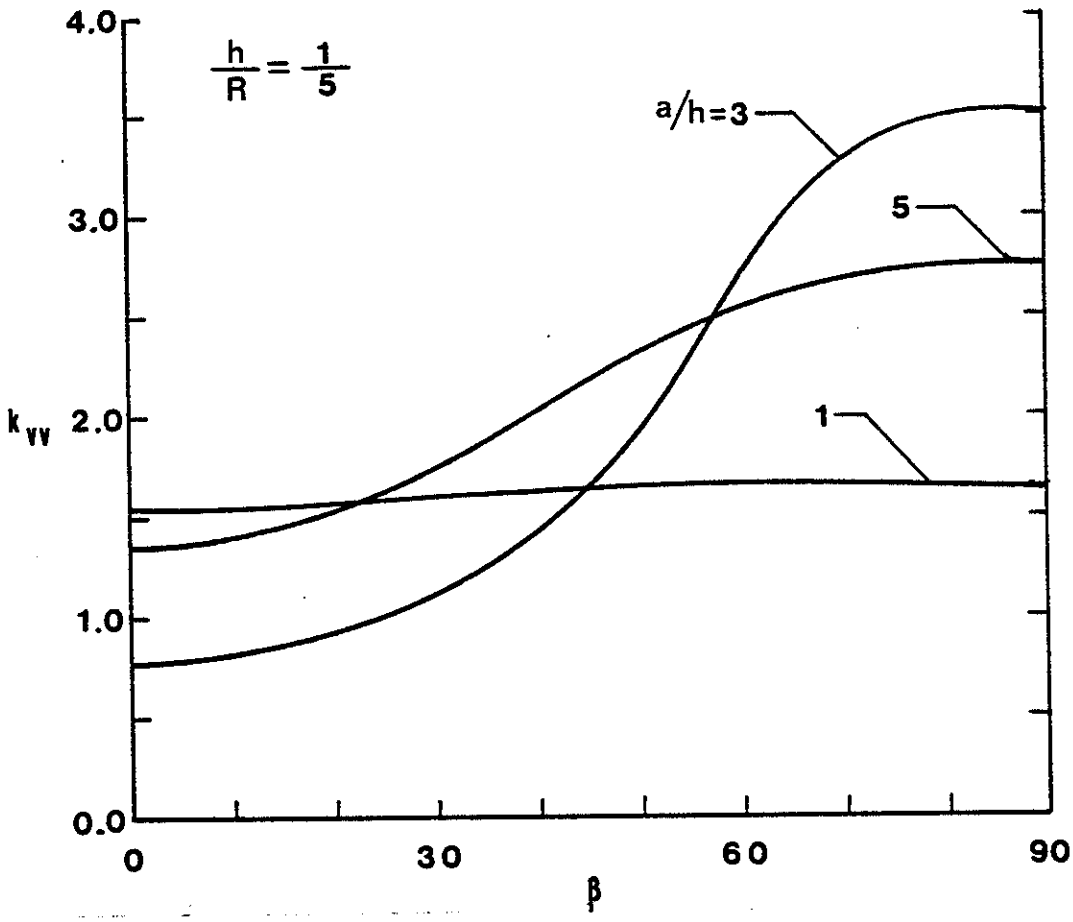

Figure 11. Stress intensity factor ratio k_{VV} in an isotropic cylindrical shell containing an inclined crack under uniform transverse shear loading V_1; ν=0.3, h/R=1/5.